

AD_____

AWARD NUMBER: DAMD17-02-1-0706

TITLE: TARGET (Translational Approaches for the Reversal, Genetic Evaluation and Treatment) of Lung Cancer

PRINCIPAL INVESTIGATOR: Waun Ki Hong, M.D.
Fadlo R. Khuri, M.D.

CONTRACTING ORGANIZATION: University of Texas
M.D. Anderson Cancer Center
Houston, Texas 77030

REPORT DATE: September 2006

TYPE OF REPORT: Final

PREPARED FOR: U.S. Army Medical Research and Materiel Command
Fort Detrick, Maryland 21702-5012

DISTRIBUTION STATEMENT: Approved for Public Release;
Distribution Unlimited

The views, opinions and/or findings contained in this report are those of the author(s) and should not be construed as an official Department of the Army position, policy or decision unless so designated by other documentation.

REPORT DOCUMENTATION PAGE				Form Approved OMB No. 0704-0188	
Public reporting burden for this collection of information is estimated to average 1 hour per response, including the time for reviewing instructions, searching existing data sources, gathering and maintaining the data needed, and completing and reviewing this collection of information. Send comments regarding this burden estimate or any other aspect of this collection of information, including suggestions for reducing this burden to Department of Defense, Washington Headquarters Services, Directorate for Information Operations and Reports (0704-0188), 1215 Jefferson Davis Highway, Suite 1204, Arlington, VA 22202-4302. Respondents should be aware that notwithstanding any other provision of law, no person shall be subject to any penalty for failing to comply with a collection of information if it does not display a currently valid OMB control number. PLEASE DO NOT RETURN YOUR FORM TO THE ABOVE ADDRESS.					
1. REPORT DATE (DD-MM-YYYY) 01-09-2006		2. REPORT TYPE Final		3. DATES COVERED (From - To) 1 Sep 2002 – 31 Aug 2006	
4. TITLE AND SUBTITLE TARGET (Translational Approaches for the Reversal, Genetic Evaluation and Treatment) of Lung Cancer				5a. CONTRACT NUMBER	
				5b. GRANT NUMBER DAMD17-02-1-0706	
				5c. PROGRAM ELEMENT NUMBER	
6. AUTHOR(S) Waun Ki Hong, M.D. and Fadlo R. Khuri, M.D. E-Mail: whong@mdanderson.org				5d. PROJECT NUMBER	
				5e. TASK NUMBER	
				5f. WORK UNIT NUMBER	
7. PERFORMING ORGANIZATION NAME(S) AND ADDRESS(ES) University of Texas, M.D. Anderson Cancer Center Houston, Texas 77030				8. PERFORMING ORGANIZATION REPORT NUMBER	
9. SPONSORING / MONITORING AGENCY NAME(S) AND ADDRESS(ES) U.S. Army Medical Research and Materiel Command Fort Detrick, Maryland 21702-5012				10. SPONSOR/MONITOR'S ACRONYM(S)	
				11. SPONSOR/MONITOR'S REPORT NUMBER(S)	
12. DISTRIBUTION / AVAILABILITY STATEMENT Approved for Public Release; Distribution Unlimited					
13. SUPPLEMENTARY NOTES					
14. ABSTRACT TARGET is focused on a series of projects designed to obtain data in the preclinical and clinical settings to help us further understand the epidemiology of lung cancer, the molecular biology, genetics and epigenetics of lung cancer in the context of tobacco-damaged aerodigestive tract tissue, and the anti-cancer activity of several promising new agents, and various treatment and drug delivery approaches in models of lung cancer and other aerodigestive tract tumors.					
15. SUBJECT TERMS lung cancer, genetic markers, molecular epidemiology					
16. SECURITY CLASSIFICATION OF:			17. LIMITATION OF ABSTRACT	18. NUMBER OF PAGES	19a. NAME OF RESPONSIBLE PERSON
a. REPORT	b. ABSTRACT	c. THIS PAGE			USAMRMC
U	U	U	UU	347	19b. TELEPHONE NUMBER (include area code)

TABLE OF CONTENTS

INTRODUCTION	4
Project 1	4
Project 2	9
Project 3	19
Project 4	26
Project 5	35
Project 6	46
Project 7	53
Project 8	68
Project 9	69
Project 10	71
Core B Biostatistics and Data Management	74
KEY RESEARCH ACCOMPLISHMENTS	75
REPORTABLE OUTCOMES/BIBLIOGRAPHY	79
CONCLUSIONS	84
REFERENCES	86
LIST OF PERSONNEL RECEIVING PAY FROM THE RESEARCH EFFORT	87
APPENDIX	89
I. Project 5 - Raw data	90
II. Project 5 - Figures	111
III. Publications	

INTRODUCTION

Lung cancer is the most deadly cancer in the world and the leading cause of cancer-related mortality in both men and women. In 2006, there will be an estimated 174,470 new cases of lung cancer and 162,460 deaths in the United States, which are more deaths than those predicted for breast, prostate, and colorectal cancers combined (Jemal et al., 2006). The 5-year overall survival rate of patients with lung cancer is extremely poor at less than 16% compared to 7% in 1970s (Jemal et al., 2006). Progress in conventional treatment options (surgery, radiation, and chemotherapy) has been minimal, reaching a ceiling in the cure of lung cancer. Therefore, new therapeutic approaches are desperately needed to improve patient survival with lung cancer.

Understanding of the biology of lung cancer from different perspectives is the basis for development of new therapeutic modalities for lung cancer. In 2002, we developed the **TARGET** (Translational Approaches for the Reversal, Genetic Evaluation and Treatment of Lung Cancer) Program with ten diverse seed projects designed to obtain data in both preclinical and clinical settings to help understand the epidemiology, molecular biology, genetics and epigenetics of lung cancer in the context of tobacco-damaged aerodigestive tract tissues, anti-tumor activities of promising therapeutic agents, and the development of orthotopic murine human lung cancer models to test the effects of anti-angiogenesis and chemotherapeutic agents. Specific aims are:

- To understand the epidemiology of lung cancer to accurately identify patients most likely to develop cancer by identifying genetic susceptibility markers related to DNA repair capacity in lung cancer using both surrogate and target tissues;
- To study the genetic instability induced by tobacco related carcinogens and the effects of chemoprevention on its reversal;
- To identify and characterize novel biomarkers for early diagnosis of lung cancer.
- To investigate prognostic roles of hypermethylation of death-associated protein (DAP) kinase and p16;
- To evaluate the effects of epigenetic approaches on DNA methylation, histone deacetylation, and growth of non-small cell lung cancer (NSCLC) cell lines;
- To understand the molecular mechanisms of the tumor suppressor gene *FUS1* on a global scale;
- To develop orthotopic and metastatic lung cancer models in mice and examine the effects of anti-angiogenic and chemotherapeutic agents using the models to identify optimal therapeutic combinations in lung cancer patients.

To achieve the objectives, we proposed the ten research projects, and Administrative and Biostatistics and Data Management Cores for three years with one-year extension.

The final report summarizes work conducted over the entire research period, highlights key research accomplishments and reportable outcomes with a bibliography of all publications and meeting abstracts derived from **TARGET**, and includes a list of personnel receiving pay from the research effort.

BODY OF PROGRESS REPORT

Project 1: Molecular Epidemiology of Lung Cancer

(Project Leader: Margaret Spitz, M.D., M.P.H.)

The current approach to risk assessment is multi-tiered, beginning with the least invasive approach, lymphocyte analysis, and proceeding to the most invasive approach, analysis of target tissue, e.g. lung tissue. We now have an extensive set of data on phenotypic and genotypic markers of susceptibility as predictors of lung cancer risk. However, we do not know how well these data that are

derived from surrogate tissue (lymphocytes) reflect events at the level of the target tissue. Therefore, the logical next step in risk assessment is to correlate these surrogate phenotype/genotype data with tissue specific analyses from bronchial epithelial cells, bronchial washings, and tumor tissue. Our long-term goal is to determine if these lymphocyte markers are an adequate reflection of genetic events in the target organs and/or tissues. This finding will have substantial implications for future large-scale population-based molecular epidemiology studies, as well as for identification of high-risk subgroups for preventive interventions.

Summary of Research Findings:

Specific Aim 1: Create a specimen and data resource.

We planned to enroll a consecutive series of 100 lung cancer cases of any histology, age, gender and ethnicity, undergoing thoracotomy for definitive therapy. These patients will have detailed epidemiologic risk assessments including tobacco exposure, dietary intake and family history. Blood samples, bronchial washings and bronchial biopsies will be obtained on each patient.

Findings: We have consented 178 patients since receiving DoD approval in May 2004. 158 of these patients have completed surgical resections to date. For 131 patients we have both bronchial brushings and blood. 67 (51%) participants are female and 64 (49%) are male. 125 (95%) participants are white, 4 (3%). 19 are less than 55 years of age, as shown in Table 1.

Specific Aim 2: Surrogate risk markers

We will perform a panel of genotypic (select polymorphisms in DNA repair genes) and functional (DNA repair capacity, mutagen sensitivity, and COMET) assays of genetic susceptibility on peripheral lymphocyte DNA from the 100 patients identified in Specific Aim 1.

Findings: We have genotyped for selected polymorphisms in DNA repair genes and performed functional assays (DNA repair capacity, mutagen sensitivity, COMET) on peripheral lymphocyte DNA from the patients identified in Specific Aim 1.

Mutagen benzo[a]pyrene diol epoxide (BPDE)-induced mutagen sensitivity in lymphocytes (a measure of overall genetic instability) was significantly positively associated with 3p deletions in lymphocytes on FISH analysis ($p=0.0066$) as well as 3p aberrations ($p=0.0024$) and borderline significantly associated with FISH 10q aberrations ($p=0.0570$) in lymphocytes (Table 2).

Race/Ethnicity	Male		Female		Total	
	N	%	N	%	N	%
White	63	(99)	62	(93)	125	(95)
Black	0	(0)	4	(6)	4	(3)
Asian	1	(1)	1	(1)	2	(2)
Total	64	(49)	67	(51)	131	(100)

Age	Male		Female		Total	
	N	%	N	%	N	%
35-45	1	(1)	2	(3)	3	(2)
46-55	6	(9)	10	(15)	16	(12)
56-65	22	(35)	23	(34)	45	(35)
66-75	25	(39)	22	(33)	47	(36)
75+	10	(16)	10	(15)	20	(15)
Total	64	(49)	67	(51)	131	(100)

Table 1: A distribution of studied subjects

Table 2 Correlations between Mutagen Sensitivity and Loci Specific Genetic Instability in Lymphocytes

<i>BPDE-sensitivity</i>	<i>bp3pdel</i>	<i>bp10qdel</i>	<i>bp3paber</i>	<i>bp10qaber</i>
<i>N</i>	67	67	66	67
<i>Corr coefficient</i>	0.3289	0.2077	0.3679	0.2337
<i>P-value</i>	0.0066	0.0917	0.0024	0.0570

Abbreviations: bp3pdel: BPDE-induced 3p deletion; bp3paber: BPDE-induced 3p aberrations; bp10qdel: BPDE-induced 10q deletion; bp10qaber: BPDE-induced 10q aberrations; Correlation coefficient was obtained from Spearman's correlation coefficient test.

Specific Aim 3: Target markers

To determine the genetic susceptibility profile in target tissue, we will establish bronchial epithelial cell cultures from fresh tumor specimens at thoracotomy of the 100 lung cancer patients from Specific Aim 1 and perform, in parallel, phenotypic DNA repair capacity and mutagen challenge assays.

Findings: Table 3 summarizes FISH studies completed to date and the actual values for the FISH studies in the bronchial brushes and touch preparations as well as the lymphocytes.

Dr. Peter Koo has received 63 bronchial epithelial samples and successfully cultured 50 that have been shared with the labs of Drs. Xifeng Wu and Qingyi Wei. We tested all functional assays on commercially available cells. For the DNA repair assay, we inoculated the frozen cells in 24-well culture plate and did transfection with BPDE-damaged luciferase plasmid into these passage 2 cells, and obtained a dose response curve for DNA repair capacity (DRC). We also established dose response curves for both the BPDE and gamma radiation comet assay experiments and selected the best dose for each. DNA repair capacity data are available on 41 of these samples with a mean (SD) of 14.8 (10.2).

Table 3 FISH data in Target Tissue

variable	N	Mean(SD)	Range
cep3/3p-BB/NT(%Del)	129	2.07(1.75)	0.0-8.0
cep3/3p-BB/T(%Del)	133	5.32(3.92)	0.0-30.0
cep3/3p-TP/T(%Del)	110	15.26(9.31)	3.0-53.0
cep3/3p-TP/AB(%Del)	72	4.25(2.94)	0.0-16.0
cep3/3p-TP/NT(%Del)	99	3.22(2.84)	0.0-14.0
cep10/10q-BB/NT(%Del)	127	1.20(1.31)	0.0-6.0
cep10/10q-BB/T(%Del)	132	3.81(1.98)	0.0-11.0
cep10/10q-TP/T(%Del)	109	10.61(6.52)	2.0-29.0
cep10/10q-TP/AB(%Del)	73	4.21(2.50)	1.0-14.0
cep10/10q-TP/NT(%Del)	97	2.20(1.96)	0.0-9.0
cep3p-bpde(%Del)	111	2.02(0.56)	0.8-4.2
cep10q-bpde(%Del)	113	1.61(0.51)	0.6-3.2

Abbreviations: BBT, bronchial brushings on tumor side; BBN, bronchial brushings on normal side; TT, tumor tissue; NT, adjacent normal tissue

There was no evidence of correlation between DRC of the target cells and lymphocyte DRC from the same subjects ($P=0.3187$), data not shown.

Specific Aim 4: Assess concordance of findings in paired samples

We will compare, using FISH analyses, the rate of concordance of DNA deletions at 3p21.3 and 10q22 loci in cells obtained from bronchial washings and peripheral lymphocyte cultures of the same patients.

Findings: There is a significant correlation between BPDE-induced mutagen sensitivity as assessed in the lymphocytes and 3p and 10 q aberrations in bronchial brushing epithelial cells from the non-tumor side and uninvolved lung tissue, but not with the tumor tissue (Table 4).

Table 4 Correlation of Mutagen Sensitivity and 3p and 10 Q in target tissue

BPDE-sens	3p					10q				
	PBLs	BBN	TT	NT	AT	PBLs	BBT	BBN	TT	NT
N	106	87	79	71	51	108	89	84	78	69
Corr. Coef	0.308	0.0477	0.1844	0.2913	0.398	0.1657	0.119	0.2344	0.0522	0.2905
P-value	0.0013	0.6608	0.1038	0.0137	0.0038	0.0866	0.2665	0.0319	0.6499	0.0155

Abbreviations: BBT, bronchial brushings on tumor side; BBN, bronchial brushings on normal side; TT, tumor tissue; NT, adjacent normal tissue; Correlation coefficients were obtained from Spearman's correlation coefficient test.

We have also correlated FISH data with smoking phenotype data (Table 5). No significant correlations were noted. However, 3p deletions and 10q deletions in bronchial brushes from either normal and tumor side of bronchial brushes and tumor preps were strongly correlated.

Table 5 Concordance of FISH data and smoking data

	Packyr		cep3pBBNT		cep3pBBT		cep3pTPT		cep3pTPAB		cep3pTPNT	
	Corr. Coef.	P value	Corr. Coef.	P value	Corr. Coef.	P value	Corr. Coef.	P value	Corr. Coef.	P value	Corr. Coef.	P value
Packyr	1		0.1618	0.1626	0.117	0.3014	0.1725	0.1629	0.1053		0.1434	
cep3pBBNT	0.1618	0.1626	1		0.4978	<0.0001	0.2352	0.0152	0.0481	-0.0268	0.7941	
cep3pBBT	0.117	0.3014	0.4978	<0.0001	1		0.3662	0.0001	0.1258	0.1894	0.0604	
cep3pTPT	0.1725	0.1629	0.2352	0.0152	0.3662	0.0001	1		0.5421	0.4727	<0.001	
cep3pTPAB	0.1053	0.5014	0.0481	0.6902	0.1258	0.2922	0.5421	<0.001	1	0.559	<0.001	
cep3pTPNT	0.1912	0.1434	-0.0268	0.7941	0.1894	0.0604	0.4727	<0.001	0.559	1		
cep10qBBNT	0.046	0.6932	0.308	0.0005	0.2621	0.003	0.0489	0.6236	0.0023	0.0963	0.3509	
cep10qBBT	0.1626	0.1522	0.2302	0.0089	0.4953	<0.001	0.2421	0.0116	0.1659	0.2556	0.0111	
cep10qTPT	0.009	0.9428	0.0957	0.3315	0.0085	0.9302	0.1903	0.0485	0.0852	0.1089	0.2856	
cep10qTPAB	0.0868	0.5708	0.1147	0.3375	-0.0492	0.6794	0.3333	0.004	0.373	0.1834	0.1258	
cep10qTPNT	0.0665	0.6169	0.1631	0.1143	0.1287	0.2115	0.1844	0.0722	0.3265	0.2543	0.0129	

variable	packyr	Ppackyr	cep10qBBNT	cep10qBBT	cep10qBBT	cep10qBBT	cep10qTPT	cep10qTPT	cep10qTPAB	cep10qTPNT	cep10qTPNT
	Corr. Coef.	P value	Corr. Coef.	P value	Corr. Coef.	P value	Corr. Coef.	P value	Corr. Coef.	Corr. Coef.	P value
Packyr	1		0.046	0.6932	0.1626	0.1522	0.009	0.9428	0.0868	0.0665	0.6169
cep3pBBNT	0.1618	0.1626	0.308	0.0005	0.2302	0.0089	0.0957	0.3315	0.1147	0.1631	0.1143
cep3pBBT	0.117	0.3014	0.2621	0.003	0.4953	<0.001	0.0085	0.9302	-0.0492	0.1287	0.2115
cep3pTPT	0.1725	0.1629	0.0489	0.6236	0.2421	0.0116	0.1903	0.0485	0.3333	0.1844	0.0722
cep3pTPAB	0.1053	0.5014	0.0023	0.9848	0.1659	0.1637	0.0852	0.4766	0.373	0.3265	0.0055
cep3pTPNT	0.1912	0.1434	0.0963	0.3509	0.2556	0.0111	0.1089	0.2856	0.1834	0.2543	0.0129
cep10qBBNT	0.046	0.6932	1		0.4267	<0.001	0.1069	0.2802	0.0914	0.3128	0.0019
cep10qBBT	0.1626	0.1522	0.4267	<0.001	1		0.1041	0.2812	-0.0452	0.1499	0.1428
cep10qTPT	0.009	0.9428	0.1069	0.2802	0.1041	0.2812	1		0.4556	0.3096	0.002
cep10qTPAB	0.0868	0.5708	0.0914	0.4453	-0.0452	0.704	0.4556	0.0001	1	0.3675	0.0015
cep10qTPNT	0.0665	0.6169	0.3128	0.0019	0.1499	0.1428	0.3096	0.002	0.3675	1	

Abbreviations: bp3pdel: BPDE-induced 3p deletion; bp3paber: BPDE-induced 3p aberrations; bp10qdel: BPDE-induced 10q deletion; bp10qaber: BPDE-induced 10q aberrations; Correlation coefficient was obtained from Spearman's correlation coefficient test.

There was also no correlation between lymphocytes and epithelial cells of the same patients assayed by DNA repair capacity (DRC) and the comet assay (Table 6). Taken together, we have put these

findings in 3 manuscripts, in which 2 were submitted and 1 in preparation as detailed in Reportable Outcomes.

Table 6. Correlation between lymphocytes and epithelial cells (data of comet and DRC)

Variable	N	DRC_epithel(coeff.)	Pvalue	N(DRC_LYM)	DRC_LYM(coeff.)	Pvalue
Olive tail moment	24	-0.222	0.296	29	0.001	0.994
BPDE tail moment	24	-0.014	0.949	29	0.078	0.689
DRC_epithelial	25	1.000		25	-0.144	0.491
DRC_Lymphocyte	25	-0.144	0.491	30	1.000	

spearman test for correlation.

In addition to the work proposed in the original grant, a small portion of the fund was used to support our ongoing and highly related studies, which resulted in 5 peer-reviewed publications as listed in Reportable Outcomes.

Key Research Accomplishments:

- Consented 178 patients. Exceeded target enrollment of 100 patients (131) with both bronchial brushings and blood.
- There is a significant correlation between latent genetic instability as measured by BPDE-induced mutagen sensitivity in the lymphocytes and 3p and 10q aberrations by FISH assay in bronchial brushing epithelial cells from the non-tumor side and uninvolved lung tissue, but not with the tumor tissue of the same patients.
- DNA repair capacity data are available on 41 epithelial samples with a mean (SD) of 14.8 (10.2). There was no evidence of correlation between DRC of the cells and lymphocyte DRC from the same subjects ($P=0.3187$).
- BPDE sensitivity in lymphocytes (a measure of overall genetic instability) was significantly positively associated with 3p deletions in lymphocytes on FISH analysis ($p=0.0066$) as well as 3p aberrations ($p=0.0024$) and borderline significantly associated with FISH 10q aberrations ($p=0.0570$) in lymphocytes.
- 3p deletions and 10q deletions in bronchial brushes from either normal or tumor side of bronchial brushes and tumor preps were strongly correlated.
- In a subset of the cases, there was no correlation between lymphocyte markers and those in epithelial cells. However, the complete data set has yet to be analyzed.

Reportable Outcomes

Articles in peer-reviewed journals:

1. Barkan GA, Caraway NP, Jiang F, Zaidi TM, Fernandez R, Vaporciyan A, Morice R, Zhou X, Bekele BN, Katz R. Comparison of molecular abnormalities in bronchial brushings and tumor touch preparations. *Cancer Cytopathology* 105: 35-43, 2005.
2. El-Zein R, Schabath MB, Etzel CJ, Lopez MS, Franklin JD, Spitz MR. Cytokinesis-Blocked Micronucleus Assay as a Novel Biomarker for Lung Cancer Risk. *Cancer Res* 66: 6449-56, 2006.
3. Gu J, Berman DM, Lu C, Wistuba II, Roth JA, Frazier M, Spitz MR, Wu XF. Aberrant Promoter Methylation Profile and Association with Survival in Patients with Non-Small Cell Lung Cancer. *Clin Cancer Res* (in press), 2006.

4. Gu J, Spitz MR, Wu X. Polymorphisms of STK15 (Aurora-A) gene and lung cancer risk. *Carcinogenesis* (in press), 2006.
5. Lin X, Gu J, Lu C, Spitz MR, Wu X. Expression of telomere-associated proteins as prognostic markers for overall survival in patients with non-small cell lung cancer. *Clin Cancer Res* (in press), 2006.

Manuscripts in progress:

1. Lin X, Wu X, Katz R, Shao L, Koo P, Spitz MR. Correlations of genetic instability markers in surrogate and target tissues in lung cancer patients (in preparation).
2. Schabath MB, Wei Q, Greisinger AJ, Etzel CJ, Spitz MR. DNA repair capacity and prior respiratory disease jointly modify lung cancer risk. *Cancer Res* (submitted) 2006.
3. Wu X, Lin J, Etzel CJ, Schabath MB, Gorlova OY, Zhang Q, Dong Q, Amos CI, Spitz MR. Interplay between mutagen sensitivity and epidemiological factors in lung cancer risk. *Am J Hum Genet* (submitted) 2006.

Meeting Abstracts:

1. Etzel CJ, Zhang Q, Schabath M, Dong Q, Wu XF, Wei QY, Spitz MR. Building a comprehensive quantitative risk assessment model for lung cancer. *Proc AACR 46:#4051*, 2005.
2. Schabath MB, Wei Q, Xifeng Wu X, Spitz MR. Prior respiratory disease, DNA repair capacity, and inflammation-related genotypes modify lung cancer risk. *Proc AACR 47:#5663*, 2006.
3. Wang L, Shi Q, Guo Z, Qiao Y, Spitz MR, Wei Q. A novel assay to measure the capacity to repair N7-guanine site-specific DNA damage. *Proc AACR 47:#5661*, 2006.
4. Wu X, Huang M, Gu J, Amos C, Shao L, Zhang Q and Spitz M. DNA repair and cell cycle control pathways in lung cancer predisposition. *Proc AACR 47:#5662*, 2006.
5. Wu X, Lin J, Etzel C, Schabath M, Gorlova O, Zhang Q, Dong Q, Amos C and Spitz M. Interplay between mutagen sensitivity and epidemiological factors in modulating lung cancer risk. *Proc AACR 47:#435*, 2006.
6. Yang H, Spitz M, Liu J, Gu J, Lu C, Stewart D and Wu X. ATM haplotype-tagging SNPs predict non-small cell lung cancer risk. *Proc AACR 47:#445*, 2006.

Project-generated resources:

Our NCI-funded Lung SPORE project builds upon this specimen and data resource. The SPORE project is evaluating telomere length in peripheral blood lymphocytes and bronchial brushings from the same patients enrolled in our DOD project. We are also performing FISH studies on 3p and 10q in sputum as early detection markers.

Conclusion:

Mutagen sensitivity (a measure of overall genetic instability) unmasked by *in vitro* exposure to benzo-a-pyrene is a marker of constitutional genetic susceptibility and is correlated with genetic aberrations in bronchial epithelial cells and uninvolved lung tissue, but not the cancer tissue. Latent genetic instability in lymphocytes reflects generalized genetic instability in the normal, but not cancerous target tissue.

Project 2: Genetic Instability by Smoking Status

(Project leader: Walter Hittelman, Ph.D.)

Tobacco exposure is a major etiologic factor for lung cancer and risk increases with smoking intensity and duration. For lung cancer risk assessment, methodologies are required that can quantify accumulated lung damage hypothesized to lead to a mosaic of clonal outgrowths throughout the bronchial epithelium. Chromosome in situ hybridization is a useful technique we used to estimate the frequency of cells involved in clonal outgrowths. Now there is a need to verify these findings by independent methods and to develop more sensitive techniques for detection of clonal outgrowths in

small groups of cells, and to evaluate the effects of smoking cessation and /or chemopreventive intervention on clonal outgrowths. Therefore, we proposed this study.

Summary of Research Findings:

Specific Aim 2.1: To determine optimal conditions for detecting clonal changes using fluorescent inter-simple sequence repeat PCR (FISSR-PCR), standardize and validate FISSR-PCR for application to bronchial biopsy specimens

Our initial studies had suggested the inter-SSR PCR could be used to sensitively detect the presence of clonal outgrowths in small tissue specimens. The Aim was to improve the technology for use on tissue sections and to determine the sensitivity and reproducibility of this technique for detecting clonal and subclonal lung cell populations.

Findings: To make our analyses more amenable to quantification, we explored the use of fluorescence-labeled primers and then visualization and quantification of the PCR-derived bands on gels using the ABI 377 sequencer. A typical output of a run is shown in Figure 1 where reference markers are included to better carry out size determinations of the detected band peaks. The gels are scanned during the run and each lane's results can be plotted as a line plot.

We next set out to optimize the conditions of the inter-SSR-PCR reaction to best visualize the DNA fingerprints. Once the reaction conditions had been optimized, we determined the reproducibility of the system by carrying out parallel PCR reactions on the same DNA samples, carrying out parallel analyses on separate DNA extractions, and then carrying out parallel runs on the ABI sequencer. As shown in Figure 2, we concluded that inter-SSR-PCR was reproducible for the analysis of DNA changes, at least on cells grown *in vitro*.

Now that we had optimized the Inter-SSR PCR reaction for ABI 377 sequencer analysis, we wanted to determine whether this fingerprinting technique could detect cumulative clonal changes in lung cells as they progressed toward a malignant phenotype. For this purpose, we utilized a series of cell lines originally developed by Klein-Szanto whereby normal human bronchial epithelial cells were immortalized with SV40 (BEAS2B cells), allowed to grow in rat tracheal lining (1799 cells), and then treated with tobacco smoke condensate to generate non-tumorigenic (1198) and tumorigenic (11701) lines. As shown in Figure 3 and Table 1, inter-SSR PCR analysis of these cell lines demonstrated cumulative band changes as cells progressed toward the malignant phenotype.

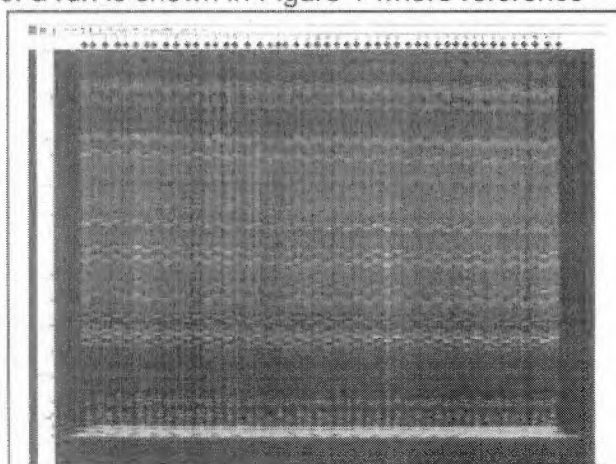


Figure 1: Illustration of typical output of a gel run of PCR products on the ABI 377 sequencer. The blue products are from the PCR reaction and the red products are the size references.

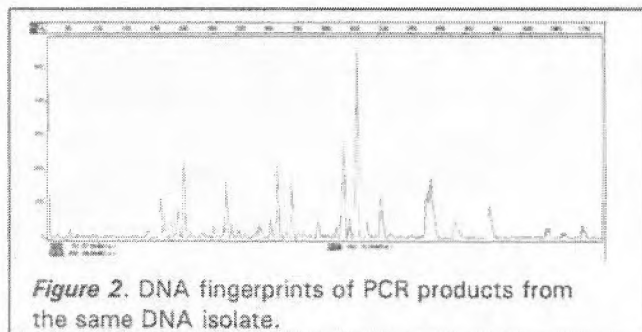
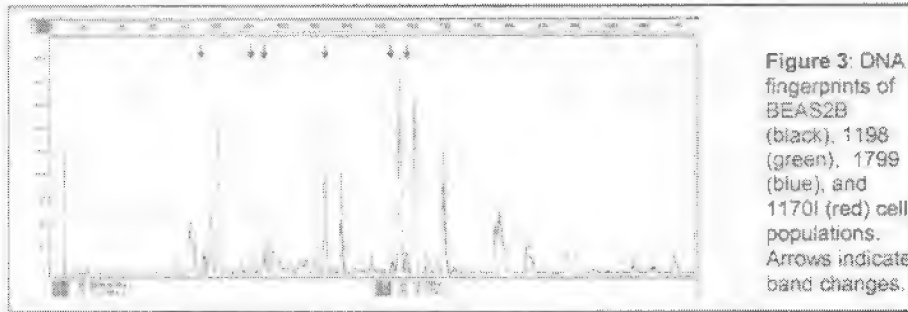


Figure 2. DNA fingerprints of PCR products from the same DNA isolate.



Cell Lines	Fam(CA) _n RG		Hex(CA) _n RY		Total
	Total # of bands	Result (# diff bands)	Total # of bands	Result (# diff bands)	
Beas 2B	51	0	21	0	0
1799	50	7	20	2	9
1198	51	6	20	4	10
1170I	50	7	20	5	12

Table 1: DNA fingerprint band changes during progression of lung cell lines from immortalized BEAS2B cells to 1170I tumorigenic cells.

To determine the sensitivity of Inter-SSR PCR for detecting subclonal variants, we subcloned the BEAS2B line into monoclonal outgrowths. We then chose two clones that differed in two bands (Figure 4) and then we mixed their DNAs in different ratios prior to FISSR PCR analysis. As shown in Figures 4 and 5, subclonal variants occupying 20%-25% of the population could be detected by this approach. Next, we performed a similar analysis mixing subclones of 1170 cell populations at various proportions and then performed inter-SSR PCR analysis to determine our ability to detect the presence of subclones within the population. As shown in Figure 6, where the heights of the peaks were plotted as a function of the relative dilutions of the two cell lines, we again estimated that a subclonal population could be detected by FISSR-PCR if it occupied around 20% of the total population.

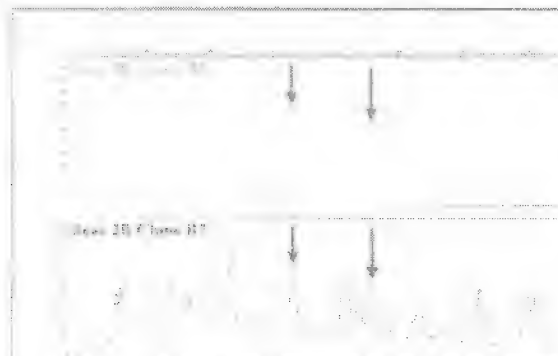


Figure 4: DNA fingerprints of two BEAS2B subclones with differing bands.

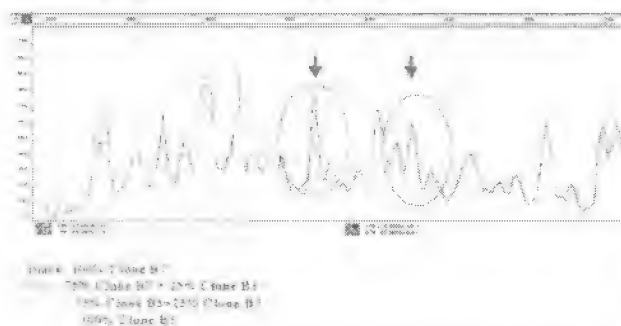


Figure 5: DNA fingerprints of mixtures of BEAS2B clones in different proportions.

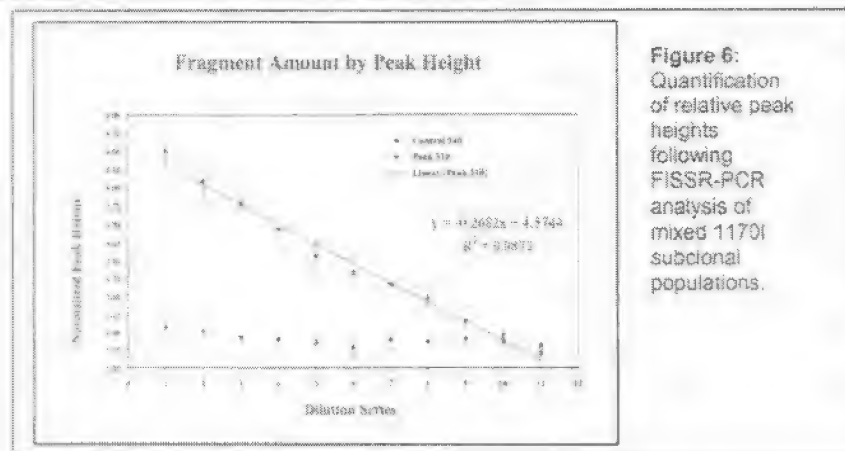


Figure 6:
Quantification
of relative peak
heights
following
FISSR-PCR
analysis of
mixed 1170I
subclonal
populations.

Since our long-term goal is to better understand how genetic instability leads to subclonal outgrowths in lung tissue, we were interested in comparing the degree of subclonal variation in immortal BEAS2B cells and tumorigenic 1170I cells. To this end, we isolated monoclonal fractions from each cell line and carried out inter-SSR PCR on each clonal outgrowth. As shown in Tables 2 and 3, both cell lines

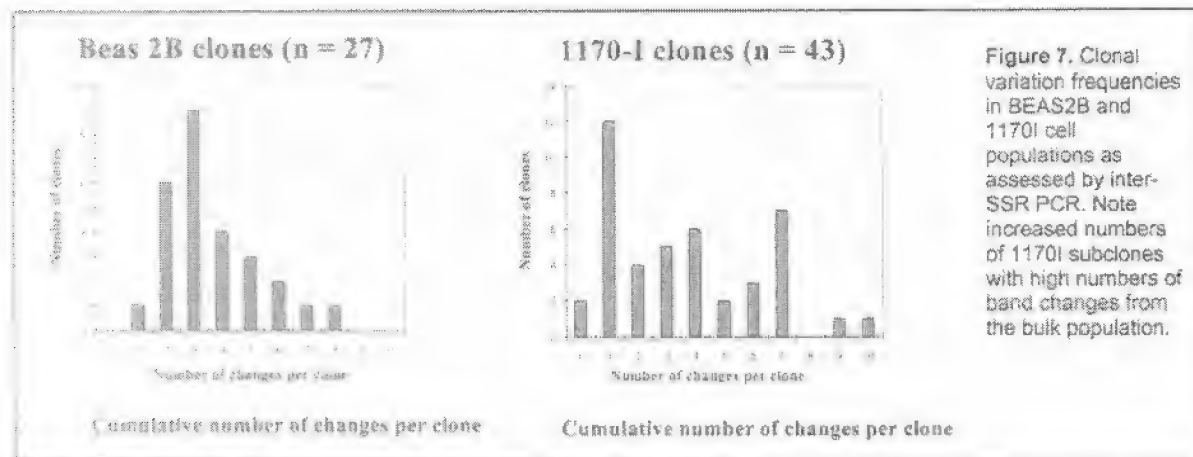
Dilution Series	Fam-CALRG		Hex-CALRY		Subclonal Outgrowth
	Peak 1 (bp)	Peak 2 (bp)	Peak 1 (bp)	Peak 2 (bp)	
1	220, 240				1
2		260			2
3		260			3
4		260			4
5		260			5
6		260			6
7		260			7
8		260			8
9		260			9
10		260			10
11		260			11
12		260			12
13		260			13
14		260			14
15		260			15
16		260			16
17		260			17
18		260			18
19		260			19
20		260			20
21		260			21
22		260			22
23		260			23
24		260			24
25		260			25
26		260			26
27		260			27
28		260			28
29		260			29
30		260			30
31		260			31
32		260			32
33		260			33
34		260			34
35		260			35
36		260			36
37		260			37
38		260			38
39		260			39
40		260			40
41		260			41
42		260			42
43		260			43
44		260			44

Table 2: Subclonal changes in BEAS2B cells

Dilution Series	Fam-CALRG		Hex-CALRY		Subclonal Outgrowth
	Peak 1 (bp)	Peak 2 (bp)	Peak 1 (bp)	Peak 2 (bp)	
1	220, 240				1
2		260			2
3		260			3
4		260			4
5		260			5
6		260			6
7		260			7
8		260			8
9		260			9
10		260			10
11		260			11
12		260			12
13		260			13
14		260			14
15		260			15
16		260			16
17		260			17
18		260			18
19		260			19
20		260			20
21		260			21
22		260			22
23		260			23
24		260			24
25		260			25
26		260			26
27		260			27
28		260			28
29		260			29
30		260			30
31		260			31
32		260			32
33		260			33
34		260			34
35		260			35
36		260			36
37		260			37
38		260			38
39		260			39
40		260			40
41		260			41
42		260			42
43		260			43
44		260			44

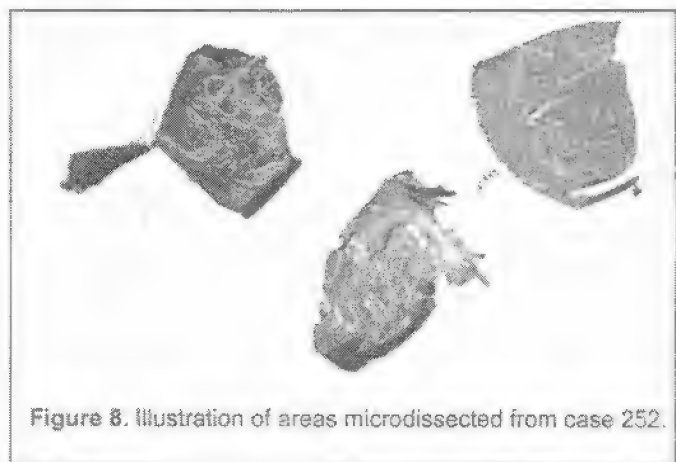
Table 3: Subclonal changes in 1170I cells

showed the presence of subclonal populations. However, as shown in Figure 7, the tumorigenic 1170I cell population had a higher level of clonal variation than did the immortal BEAS2B cell line. Interestingly, a significant fraction of the subclones from each cell line exhibited common individual bands that were not evident in the bulk population, suggesting some clonal selection in the setting of monoclonal outgrowth in multiwell cultures. A repeat study where monoclonal outgrowths were generated and analyzed by inter-SSR PCR showed a similar phenomenon, however the particular bands selected appeared different from the first study suggesting that the culture conditions can influence which subclones in the population are selected.



We next initiated studies to determine our ability to carry out FISSR-PCR on cells microdissected from paraffin-embedded specimens. The first studies were carried out on cell culture pellets that have been formalin-fixed and embedded in paraffin. During the course of these experiments, we found that the use of paraffin-embedded specimens limited our ability to carry out analyses on very small amounts of microdissected material due to limitations in DNA extraction from the paraffin-embedded material, limitations in the size of the PCR products to about 500 base pairs due to formalin-induced DNA cross links, and interference of detergent used in the DNA extraction with the fluorescence signal detection. We therefore decided to optimize the conditions for FISSR-PCR reactions for use on frozen material. We focused on three initial components of the analysis. First, in collaboration with Dr. Ignacio Wistuba, we compared the laser capture microdissection technique with needle dissection and found that both techniques were suitable. Second, we optimized the DNA extraction methodology from the frozen tissue material, with or without phenol extraction and ethanol precipitation and examined the effect of column purification of the DNA. Third, we optimized the PCR reaction by examining different PCR systems, including the effect of hot start PCR, different DNA polymerases, different PCR buffer systems, and different PCR temperatures.

Once the conditions for FISSR-PCR analyses were developed for frozen material, in collaboration with Dr. Ignacio Wistuba, we obtained human lung samples from lung tumor resection cases and microdissected out multiple areas from the tumor specimens, including tumor, stromal, and apparently normal epithelial regions. For example, for human lung sample case 252, we microdissected eight regions from different parts of the resection specimen, including three tumor regions, four normal epithelial regions, and one stromal region (Figure 8) as well as a lymphocytic region.



We carried out an analysis of 16 lung cancer cases where we characterized the degree of clonal variation between different regions of the tumor resection specimen, including lung tumor regions (1-12 regions per case; mean 3.1), normal bronchial epithelial regions (1-10 regions per case; mean 4.0), and stromal regions (1-8 regions per case; mean 2.1). We used three primer sets for these studies, including a Fam-(CA)⁸RG primer, a Fam-(CA)⁸RY primer, and a FAM-(AGC)⁴Y primer. All reactions were carried out in triplicate to ensure reproducibility. Only those peaks where all triplicate profiles consistently showed changes at least 50% of peak height were counted as DNA band changes. The utilization of three primer sets permitted analysis of between 224 and 328 different

bands. Figure 9 provides an example of a comparison between a bronchial epithelial region (blue, mauve, and turquoise lines) and a stromal standard for the case (red, peach, and yellow lines). As shown in this figure, two band changes were evident in the bronchial epithelium compared to the stromal region.

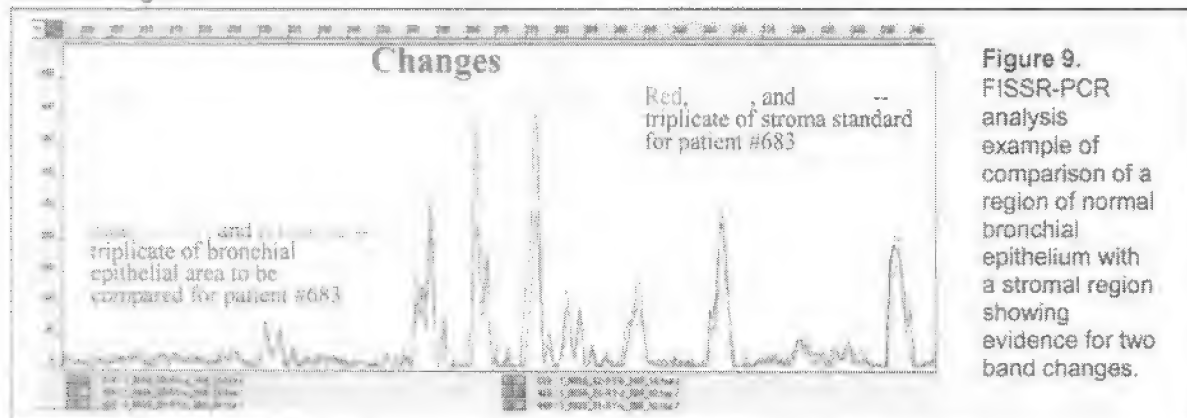


Figure 9.
 FISSR-PCR
 analysis
 example of
 a region of
 normal
 bronchial
 epithelium
 with a
 stromal
 region
 showing
 evidence for
 two band
 changes.

The clinical and demographic characteristics of the 16 lung cancer cases whose tumor resections were examined by FISSR-PCR analysis are shown in Table 4. 15 of the 16 cases were adenocarcinoma and the remaining case was squamous cell carcinoma. As might be expected for studies based on surgical resection specimens, 12 of the 16 cases were pathological stage I tumors. With regard to smoking status, 9 cases involved former smokers, 5 cases involved current smokers, and two cases involved never smokers.

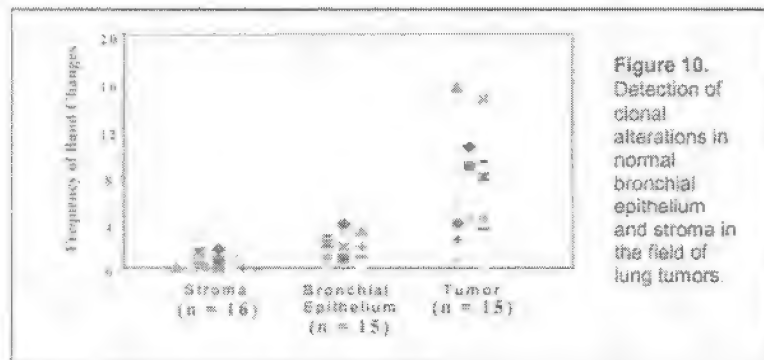
All regions dissected from the lung cancer specimens showed band alterations based on one standard pattern seen in an associated stromal region. As shown in Figure 10, the

Patient and Tumor Characteristics			
Total patient		N=16	(%)
Gender	Male	10	62.5
	Female	6	37.5
Age		59.9(40 - 79)	
Tumor Type	Adenocarcinoma	15	93.8
	Squamous	1	6.2
Pathological stage	I	12	75.0
	III	4	25.0
Metastasis		None	
Smoking status	Never	2	12.5
	Former	9	56.25
	Current	5	31.25

Note: most patient samples were analyzed after abstract submission and all the data are included in this poster

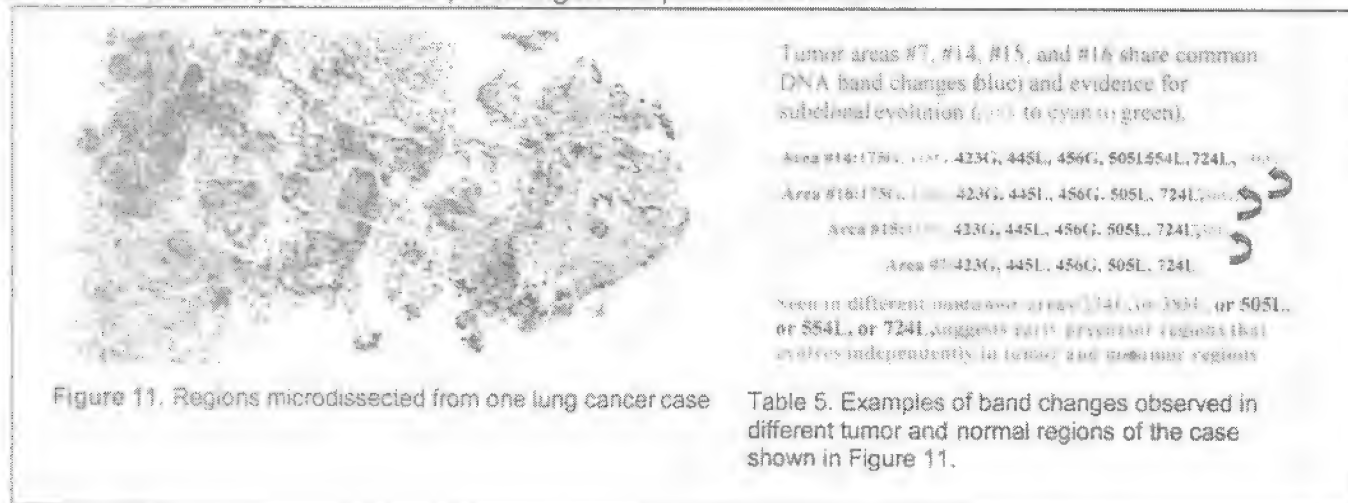
Table 4: Patient and tumor characteristics of the 16 cases examined by FISSR-PCR.

tumor regions showed the highest extent of clonal alteration compared to the stromal regions (median 6.03 band changes for 15 tumor region cases analyzed). Nevertheless, the degree of clonal change varied between tumor cases. Of importance, significant levels of clonal change were also apparent in regions dissected from normal appearing bronchial epithelium in the lung cancer specimens, albeit at lower levels than that observed in the tumor regions (median, 1.89 band changes). Again, the



degree of clonal change in normal appearing bronchial epithelium differed between cancer cases. Of interest, and somewhat surprisingly, small levels of clonal alterations were also detected in the stromal regions in some lung cancer cases (median, 0.43). While the levels of clonal alteration in the stroma were generally small compared to that found in the bronchial epithelium and in the tumor regions, it was still detectable at fairly high levels in some cases.

An example of the changes observed in one lung tumor specimen is illustrated in Figure 11 and Table 5. In this case, as shown in Figure 3, 16 separate tumor regions and 3 normal regions were microdissected and subjected to FISSR-PCR analysis. The frequency of band changes in this case for the tumor regions was 14.6 while that in the normal regions was 1.6. Of interest, not all tumor regions showed identical band changes. While each region might have shown some common changes, there were also differences in specific band changes from region to region, suggesting both clonal evolution and subclonal variation within the lung tumor specimen. Also of interest, some of the normal regions contained identical individual band changes also found in the tumor, suggesting a possible precursor to product relationship. On the other hand, other normal regions showed no common changes with the tumor specimen suggesting a different premalignant pathway from that associated with the specific multistep tumorigenesis pattern in the tumor.



In general, the data shown in Figure 10 suggested that there might be some relationship between the degrees of clonal alteration in the tumor regions with that in the bronchial epithelial regions in the tumor specimen. When compared on a case-by-case basis, however, while there was a trend for concordance of the degree of clonal change in the tumor and bronchial epithelial regions, the relationship was not strictly monotonic (Figure 12). Similarly, while lung tumor specimens from former smokers showed a slightly higher median frequency of clonal changes when compared to current

smokers, there was a high degree of overlap in clonal alteration frequencies between the two groups (Figure 13).



Figure 12. Correlation of the degree of clonal alterations apparent in the tumor regions compared to the bronchial epithelium

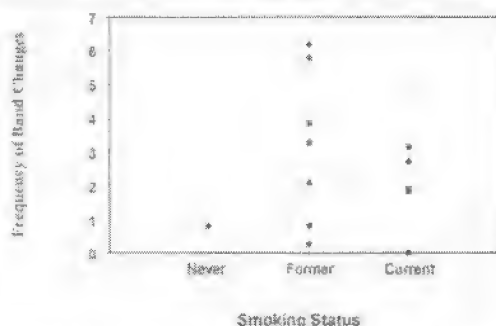


Figure 13. Relationship between smoking status and the frequency of clonal alterations detected in the tumor regions.

Taken together, these studies suggest that FISSR-PCR together with microdissection is sufficiently sensitive to quantify clonal and subclonal changes in lung tissues, including tumor, normal bronchial epithelium, and even stromal regions. These data provide validation of our prior studies utilizing both premature chromosome condensation and in situ hybridization, and that of others using LOH analysis, that lung tumorigenesis represents a field process where tobacco exposure can create genetic changes throughout the exposed lung tissue leading to the presence of multifocal clonal outgrowths.

The levels of clonal alteration found in the bronchial epithelium tend to be less than that found in the adjacent tumors. Nevertheless, there was weak concordance between the levels of clonal alteration in the tumor and in the normal bronchial epithelium, providing support for a strength component to the field effect. This finding is important in the setting of estimating risk of individuals without cancer since it suggests that random biopsies can still provide quantitative information for the tissue field as a whole. The studies in former smokers further support our prior in situ hybridization data suggesting that, despite smoking cessation, clonal outgrowths remain in the exposed tissue and contribute to evolve toward the development of malignancy. Studies are currently ongoing in other projects to better understand the mechanisms that drive clonal outgrowth and continued genomic instability in lung tissues of former smokers.

Specific Aim 2.2: Determine whether smoking status influences changes in clonal frequency and determine whether chemopreventive intervention has differential impact on clonal outgrowths in current and former smokers

With the FISSR-PCR technique for the analysis of the degree of clonal alterations in microdissected tissue specimens, we initiated the next set of studies to examine and compare the degree of clonal alterations in the bronchial epithelium of current and former smokers who are at increased risk for lung cancer in association with their history of tobacco smoke exposure.

Findings: As described above, we found that the FISSR-PCR assay is much more robust when frozen tissue is utilized. Therefore, we identified a series of frozen bronchial biopsies from a group of individuals who participated previously in our 4HPR chemoprevention trial. We chose two groups for further study based on the presence of high or low clonal alterations based on chromosome in situ hybridization studies on paraffin-embedded specimens.

We carried out FISSR-PCR analyses for 16 cases that had participated in the 4-HPR clinical trial that involved current smokers without cancer. The clinical characteristics and demographic information of the participants are shown in Table 6. As illustrated in Figure 14, multiple regions (i.e., 1-4 areas each) of bronchial epithelium and stroma were microdissected, and purified genomic DNA was

analyzed by FISSR-PCR using three sets of primers ((CA)₈RG, (CA)₈RY, and (AGC)₄Y), providing a maximum of 350 informative DNA bands of varying lengths. As shown in Table 7, overall, we detected from 0 to 55 total band changes per microdissected epithelial region (median = 1.5 per 100 DNA bands). Different regions within the same bronchial biopsies showed both common and distinct DNA band changes, suggesting subclonal variations even within a single biopsy.

Total patient		N=16	(%)
Gender	Male	9	56
	Female	7	43
Age		49.9 (36 – 61)	
Smoking Status	Current	16	100
Smoking years		30.8 (15 – 50)	
Pack per Day		14 (10 – 25)	
Histology	Normal	2	12.5
	Basal cell hyperplasia	12	75.0
	Squamous metaplasia	2	12.5

Case 95-23	
E = epithelium S = stroma	

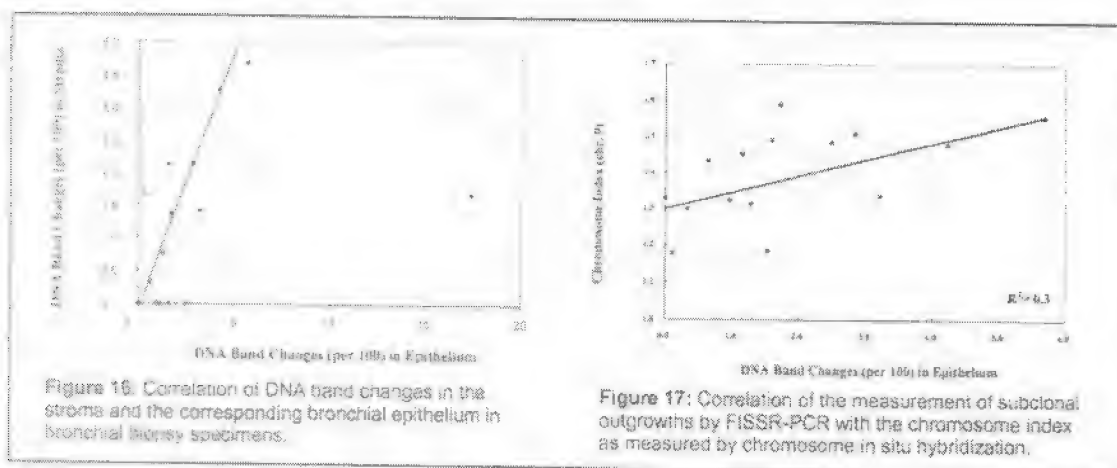
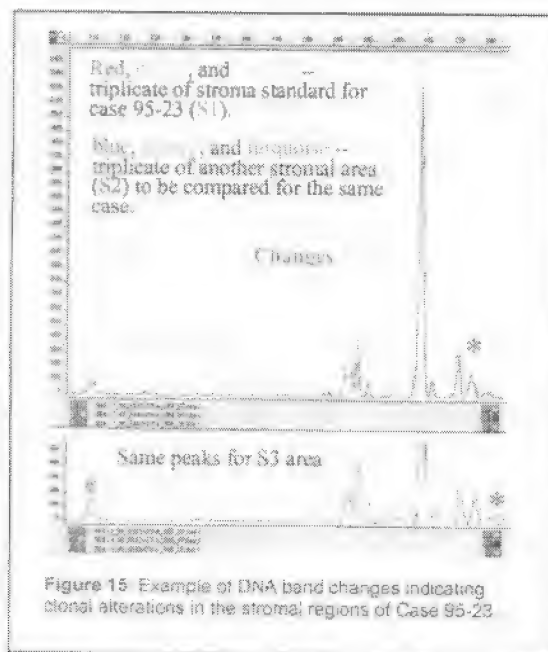
Table 6: Clinical characteristics and demographic information of the 16 participants from the 4HPR chemoprevention trial.

Figure 14: Example of epithelial and stromal regions microdissected for FISSR-PCR analysis.

Table 7: Evidence for clonal and subclonal changes in biopsies of former smokers without cancer by FISSR-PCR and chromosome in situ hybridization

Number of areas dissected per patient:		
	Average	Range
• Stroma	2.1	1 - 3
• Bronchial Epithelial	1.7	1 - 4
PCR Primer Sets: 3 *		
Total DNA bands/3 primers:		299 - 350
Changes/100 bands by FISSR-PCR		
	Median	Range
• Stromal	1.0	0 - 3.7
• Bronchial Epithelial	1.5	0 - 12.4
Chi. Index ²	1.42	1.17 - 1.59

As illustrated in Figure 15, we also detected from 0-20 total band changes per microdissected stromal region (median = 1.0 per 100 DNA bands), suggesting the presence of clonal outgrowths even in the stroma. Interestingly, as shown in Figure 16, bronchial biopsies with high clonal frequencies in the epithelial component also tended to show increased clonal change in the associated stroma ($p=0.04$, two-tailed chi square). Importantly, bronchial biopsies from individuals showing high clonal changes by FISSR-PCR also showed evidence of high clonal change by CISH ($R^2 = 0.3$) (Figure 17).



Taken together, these studies confirm out prior observations using different technologies that clonal genetic changes are present in the bronchial epithelium of current and former smokers. Moreover, subclonal outgrowths can also be detected in the stromal component underlying the epithelium. The degree of clonal changes in the stroma correlates positively with that found in the associated epithelium, suggesting a possible active role of the stromal component in epithelial clonal outgrowth and progression toward cancer. The levels of clonal and subclonal outgrowth measured by FISSR-PCR correlated with the degree of genetic change as measured by chromosome in situ hybridization.

Key Research Accomplishments

- Developed the sensitive and highly reproducible FISSR-PCR technique and applied it to detect clonal and subclonal outgrowths in microdissected epithelium and stroma from frozen tissue sections of resected lung tumors and of bronchial biopsies obtained during chemoprevention studies.
- Demonstrated increased genetic instability and increased clonal/subclonal heterogeneity in an *in vitro* model of bronchial epithelial cell populations at different stages of lung tumorigenesis.

- Demonstrated that the stroma underlying genetically altered bronchial epithelium also exhibits clonal and subclonal outgrowths. The degree of clonal change in the stroma appeared to be related to the degree of clonal/subclonal change in the bronchial epithelium.
- Demonstrated the presence of clonal/subclonal changes in the bronchial epithelium and underlying stroma of current and former smokers at increased risk for lung cancer development. The degree of clonal/subclonal change detected was related to the degree of genetic instability measured in biopsies of the same subjects by chromosome in situ hybridization.

Reportable Outcomes

Meeting Abstracts:

1. Hittelman W N, Wang G, Koo JSP, Lu, T. The spatial distribution and etiology of genetic instability in organotypic bronchial epithelial cell cultures. Proc. AACR 46:3527, 2005.
2. Lu T, Hittelman WN. Assessment of subclonal evolution in human bronchial epithelial cell lines progressing toward malignancy by fluorescence inter-simple sequence repeat PCR. Proc AACR 44:894, 2003.
3. Lu T, Hittelman WN. Improvement and application of fluorescence inter-simple sequence repeat polymorphism chain reaction for the study of subclonal growths in lung epithelial cell populations. Chest 125 (Suppl. 5):110-111S, 2004.
4. Lu T, Hittelman WN. Quantitative fluorescence inter-simple sequence repeat PCR for subclonal analysis of bronchial cell populations. Proc AACR 45, 2004.
5. Lu T, Wistuba II, Hittelman WN. Detection of clonal and subclonal outgrowths in the upper aerodigestive tract of current and former smokers with lung cancer. Proc AACR 46:#2230, 2005.
6. Lu T, Wistuba II, Hittelman WN. Existence of clonal and subclonal outgrowths in the bronchial epithelium and stroma of current smokers. Proc AACR 47:#462, 2006.

Conclusion

The FISSR-PCR studies confirm the in situ hybridization results and show that this technology is useful for quantifying the extent of clonal and subclonal outgrowths in the bronchial epithelium, and also demonstrated that the stroma underlying the damaged bronchial epithelium could undergo clonal change and evolution, suggesting that the stroma may play a significant role in lung tumorigenesis.

Project 3: Epithelial Biomarkers of Lung Cancer: Evaluation of Airway Secretions to Study Lung Carcinogenesis

(Project Leader: Ja Seok Koo, Ph.D.)

Most patients with lung cancer are diagnosed in late stages due to the limit of current standard screening tools. Population screening methods, such as sputum cytology and chest x-ray, have failed to show reduced lung cancer mortality. Therefore, advanced and non-invasive screening tools are urgently needed to detect lung cancer at an early stage. The objectives of this study are to develop novel biomarkers for early diagnosis of lung cancer using easily accessible samples (sputum and bronchial washing) and to generate a better understanding of lung cancer development and progression.

Summary of Research Findings:

Specific Aim 1: Identify proteins whose secretion or release is different in squamous metaplastic tracheobronchial epithelial cells as compared to normal mucous epithelial cells

Phenotypes of the cultures of primary normal human tracheobronchial epithelial (NHTBE) cells are dependent on retinoic acid (RA) when the cultures are maintained in air-liquid interface (ALI) culture method. Cultures maintained in RA-sufficient media generate a fully-differentiated mucociliary

bronchial epithelium mimicking *in vivo* tracheobronchial epithelium, in contrast the cultures become squamous metaplasia in RA-deficient media. To identify proteins whose secretion or release is different in squamous metaplastic tracheobronchial epithelial cells as compared to normal mucous epithelial cells, apical surface liquid (ASL) from the NHTBE cell cultures grown in RA-sufficient (mucous) or RA-deficient (squamous) media were collected by apical washing with PBS. Protein profiles of the ASL from the squamous metaplastic NHTBE cultures were analyzed by two dimensional polyacrylamide gel electrophoresis (2-D PAGE). Initial identification of protein spots on the 2-D PAGE was performed by matrix assisted laser desorption/ionization-time of flight-mass spectrometry (MALDI-TOF) and nanoelectrospray-tandem mass spectrometry (nES-MS/MS) analysis in collaboration with the Proteomics Core Facility in our institution.

Findings: Squamous-cell carcinoma (SCC) in the lung originates from bronchial epithelial cells that acquire increasingly abnormal phenotypes. However, there are no known biomarkers that are clinically efficient for the early detection of premalignant lesions and lung cancer. Here, we sought to identify secreted molecules produced from squamous bronchial epithelial cells cultured by organotypic culture methods. We analyzed protein expression patterns in apical surface fluid (ASF) from aberrantly differentiated squamous metaplastic normal human tracheobronchial epithelial (NHTBE) and mucous NHTBE cells. Comparative two-dimensional PAGE analysis revealed that 174 unique proteins in the ASF of squamous NHTBE cells compared to normal mucociliary differentiated NHTBE cells. Among them, 64 well-separated protein spots were identified using liquid chromatography-tandem mass spectrometry, revealing 22 different proteins in the ASF from squamous NHTBE cells. Expression of 6 of these proteins (SCCA1, SCCA2, S100A8, S100A9, annexin I, and annexin II) in the squamous NHTBE cells was further confirmed with immunoblot analysis. Notably, SCCA1 and SCCA2 were verified as being uniquely expressed in squamous metaplastic NHTBE cells but not in normal mucous NHTBE or adenocarcinoma cells. Moreover, SCCA1 and SCCA2 expression increased in *in vitro* lung carcinogenesis model cell lines with increasing malignancy.

In summary, we identified proteins that are uniquely secreted from squamous metaplastic primary human bronchial epithelial cells cultured by the organotypic air-liquid interface method. These ASF proteins may be used to detect abnormal lesions in the lung without collecting invasive biopsy specimens. A manuscript is in peer-review in *Cancer Research* (Koo et al., 2006).

Specific Aim 2: Identify and characterize abnormal proteins secreted by lung squamous cell carcinomas

This aim was proposed to test whether the panel of proteins identified from Specific Aim 1 is abnormally overexpressed in only premalignant squamous metaplasia or remains overexpressed in cancer cells.

Findings: As we presented in the 2005 annual report, expression of SCCA1 and 2 was progressively increased in transformed/tumorigenic cell lines and only detected in squamous cell carcinomas but not in adenocarcinomas as determined in resected lung tumor specimens (Koo et al, 2006).

Specific Aim 2 was completed and part of the data was published in the manuscript (Koo et al, 2006) and another part of the data was published in *Mol Genet Genomics* (Koo et al, 2005). (See Appendix-Publications).

Specific Aim 3: Evaluate the efficacy of these differently-secreted proteins to serve as novel biomarkers using readily-accessible clinical specimens

Findings: To evaluate the efficacy of the putative biomarkers identified in Specific Aims 1 and 2, particularly SCCA1, SCCA2, S100A8, Annexin I, Annexin II, and maspin in clinical samples, immunoblot analysis was performed using 120 bronchial washing specimens collected through the

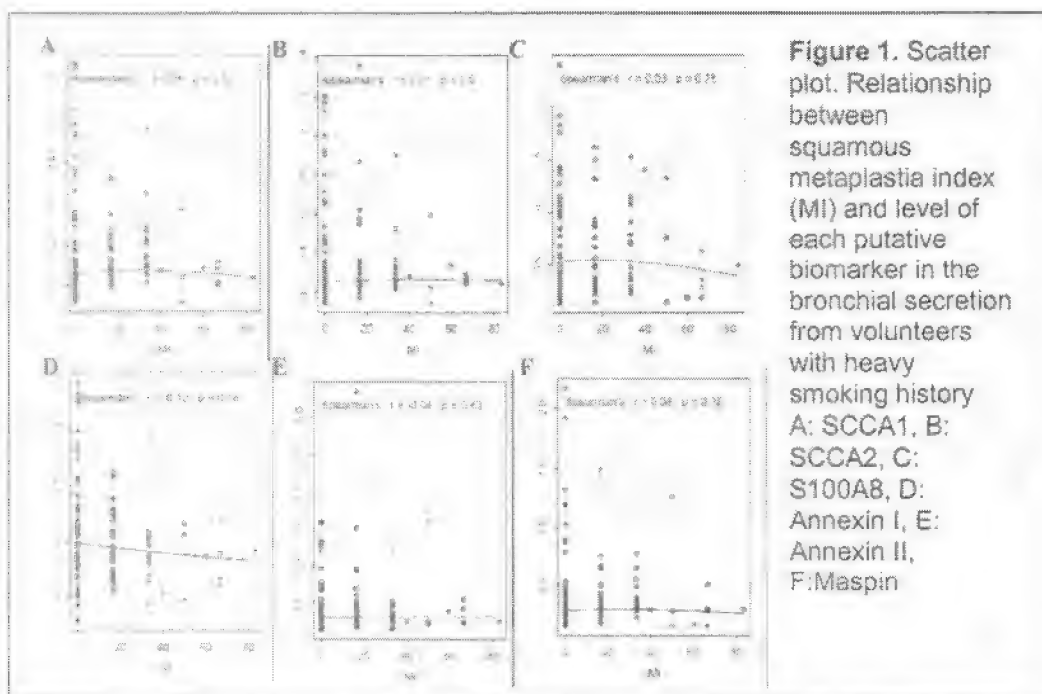
Lung P01 clinical trial (PI: Dr. Waun Ki Hong). Clinical characteristics of the volunteers are described in Table 1. The bronchial washing samples were centrifuged at 500 x g for 5 min at 4°C to pellet exfoliated cells and cellular debris. The supernatant were transferred to new tubes and protein concentrations were determined using a Bicinchoninic Acid (BCA) protein assay kit (Pierce, Rockford, IL). Bronchial washings containing total 50 µg of protein were transferred onto nitrocellulose membrane by dot-blot apparatus. The blotted membrane was subjected for immune detection using specific antibodies against proteins listed above.

Table 1. Clinical Characteristics of the Volunteers.

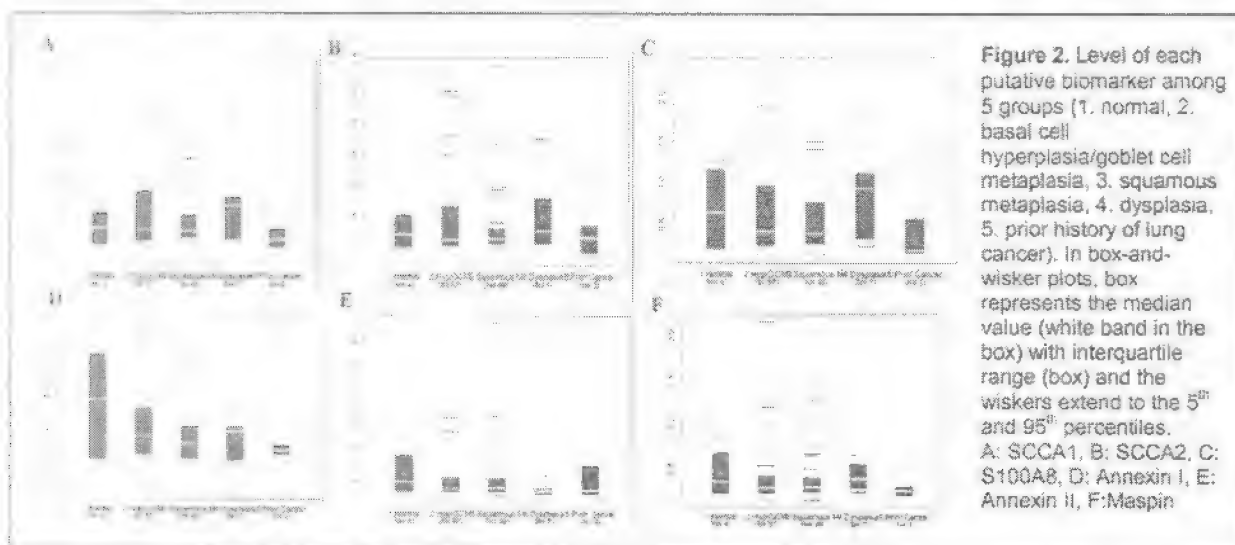
Variables	Number of patients (%)
Median age (range)	54 years (32-73)
Sex	
Male	60 (50%)
Female	60 (50%)
Smoking Status	
Current	94
Former	26
Pack-year of smoking	
Median (range)	41 years (20-86)
Histology*	
Normal	4
BCH/GBM†	57
Squamous metaplasia(SQ)	49
Dysplasia	7
Previous History of lung Cancer	3
Median Index of SQ metaplasia	0% (0%-83.33%)

* The worst histologic grade of eight piece of biopsy. † BCH/GBM: Basal cell hyperplasia/Goblet and basal cell metaplasia.

To determine whether any of the markers identified through previous aims can be used for detection of morphological abnormalities in the bronchial mucosa, we compared the level of these biomarkers' expression (as determined by dot-blot analysis) with histology of endobronchial biopsy. As shown in Figure 1, Spearman's analysis showed no statistically significant correlation between expression of each marker and morphologic abnormalities as represented by metaplasia index (MI).

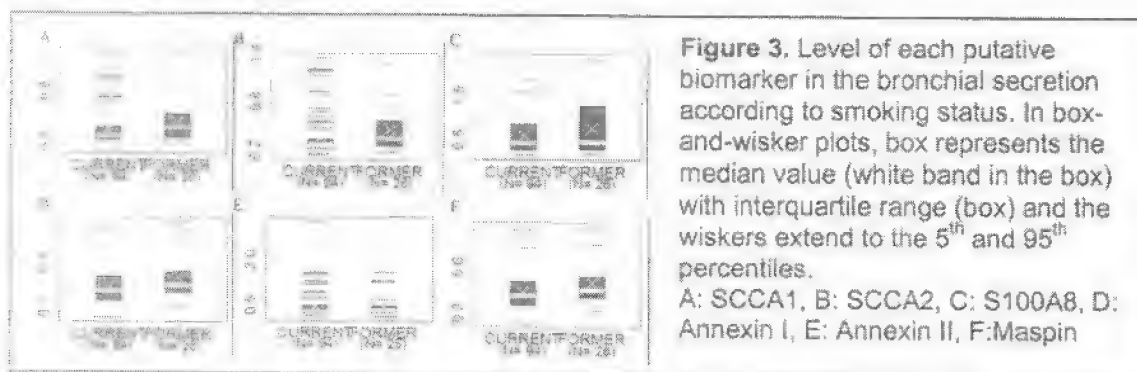


To further determine whether these markers are associated with a particular type of abnormal histomorphology of the bronchial mucosa, we compared the level of each putative biomarker in the bronchial lavage with 5 groups (1. normal, 2. BCH/GBM, 3. squamous metaplasia, 4. dysplasia, 5. group with prior history of lung cancer) categorized by the risk of lung cancer development on the basis of endobronchial biopsy histology. As shown in Figure 2, no statistically significant differences in the expression of each marker were found among 5 groups. However, the small population in the groups with basal cell hyperplasia/goblet cell metaplasia or with squamous metaplasia showed very high levels of marker expression in bronchial lavage specimen.



We also compared differences in histology or each biomarker levels of bronchial lavage specimen between current smoker and former smoker. Interestingly, we found that current smoker has lower SCCA1 ($P=0.01$) and SCCA2 expression ($P=0.005$) and higher frequency of basal cell hyperplasia with goblet cell metaplasia ($P<0.0001$) (Fig. 3). This result suggests that relative proportion of SCCA1

and SCCA2 protein in bronchial secretion is decreased due to the relative increase of mucous goblet cells in the bronchial trees.



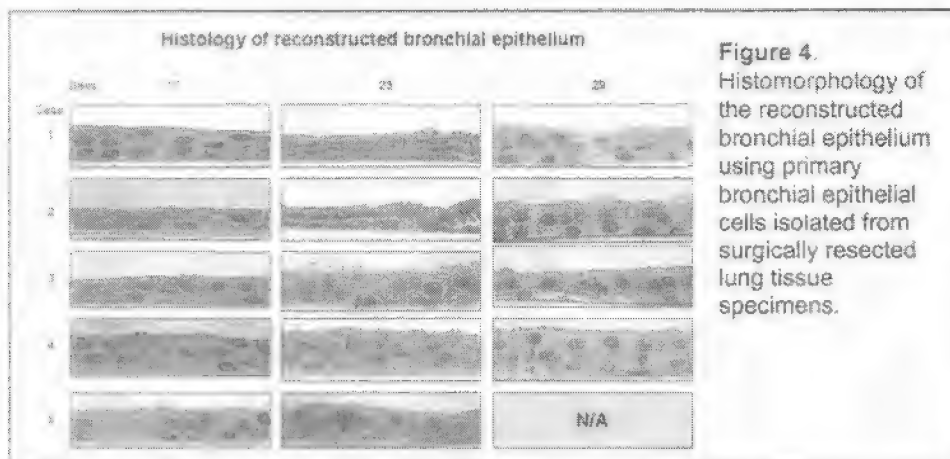
In conclusion, expression levels of biomarkers, SCCA1, SCCA2, Annexin I, Annexin II, S100A8, and Maspin in bronchial lavage are not directly correlated with histological appearance of bronchial mucosa in heavy smokers, indicating there is much discrepancy between morphological changes in the bronchial mucosa and secretory protein changes.

Specific Aim 4: Establish primary bronchial epithelial cells in culture and evaluate the expression of candidate biomarkers in bronchial epithelium of lung cancer patients.

We proposed to investigate the expression and regulation of the biomarkers in bronchial epithelial cells in cultures and to address whether the molecular alterations are persistent during the development and differentiation of bronchial epithelium of the lung cancer patients. The source for epithelial cells is from bronchial biopsy tissues collected from 100 newly diagnosed, and previously untreated lung cancer patients who are undergoing surgery at M. D. Anderson Cancer Center, as described in Project 1 (PI: Margaret Spitz) of **TARGET**.

Findings: We have obtained 64 surgically-removed lung tissues from 64 different patients. Bronchial epithelial cells were successfully isolated from 55 tissue specimens and stored in liquid nitrogen. Nine cases were not successful to isolate epithelial cells. Six cases were lost due to contamination and three cases were lost due to incubator problem. The cells of 50 cases were distributed to Dr. Spitz's laboratory for their proposed studies in Project 1 of **TARGET**.

We successfully reconstructed bronchial epithelial structure using primary bronchial epithelial cells isolated from lung cancer patients using organotypic air-liquid interface culture method. Typical histology of the *in vivo* reconstructed bronchial epithelium was shown in Figure 4. Histologic evaluation of 17, 23, and 29-days-old bronchial epithelial cell cultures showed no obvious bias in growth, histologic abnormalities, or mucociliary differentiation. However, a tendency of loose polarity of the cultures was observed in some cases.



To determine whether bronchial epithelial cells from lung cancer patients abnormally express biomarkers identified from the previous aims, we compared expression levels of SCCA1, SCCA2, annexin I, and annexin II by dot-blot analysis of apical secretions collected from organotypic cultures of bronchial epithelial cells from 6 different lung cancer patients. As shown in Figure 5, although they generate mucociliary morphology, certain cultures produced high levels of SCCA1 and Annexin 2 (case #1 and #4). Interestingly, these two cases showed very high percentage of 3p22.1 deletion in the tumor cells as determined by FISH analysis (see Figure 5 and Table 2). Moreover, the epithelial cells secreted higher levels of SCCA1, and Annexin 2 showed correspondingly lower DNA repair capacity than the cells secret lower (or undetectable) levels of the markers (DNA repair assay was performed in Project 1 of **TARGET-PI**: Dr. Spitz). This result suggests that concurrently overexpressed SCCA1 and Annexin 2 in the secretions from the epithelial cells may serve as surrogate markers for lower DNA repair capacity and high percentage of 3p loss of heterozygosity in bronchial epithelial cells.

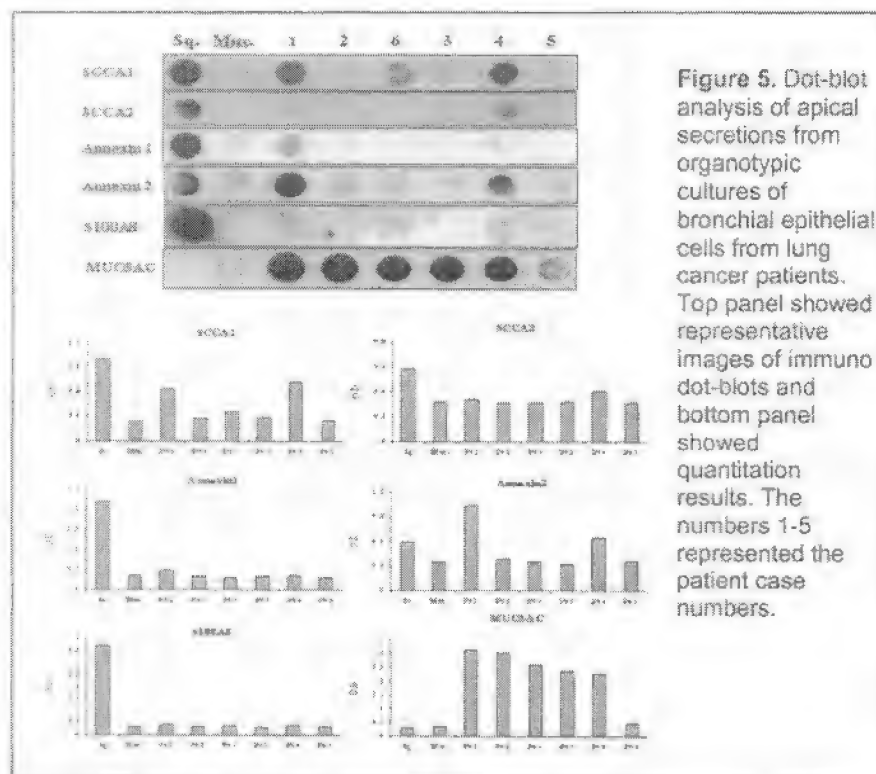


Table 2. Correlation of the expression levels of SCCA1 and Annexin 2 with DNA repair capacity and deletion of 3p22.1 in tumor.

Case #	SCCA1 (O.D.)	Ann 2 (O.D.)	DNA Repair Capacity	Control cep3/3p (%Del)	cep3/3p- TBB (%Del)	cep3/3p- NBB (%Del)	cep3/3p- TTP (% Del)	cep3/3p- NTP (% Del)	cep3/3p- TAB (% Del)
1	0.888	0.819	9.1	3	18	3	35	8	3
2	1.064	0.864	25.0	3	6	1	9	3	7
3	0.507	0.394	n/a	3	5	2	n/a	3	n/a
4	0.882	0.849	7.4	3	1	0	46	7	10
5	0.386	0.367	16.4	1	11	4	11	n/a	n/a

Abbreviations

Control cep3/3p (%Del)	deletions of 3p22.1 from control bronchial wash
cep3/3p-TBB (%Del)	deletions of 3p22.1 from bronch brush tumor side
cep3/3p-NBB (%Del)	deletions of 3p22.1 from bronch brush normal side
cep3/3p-TTP (% Del)	deletions of 3p22.1 from tumor
cep3/3p-NTP (% Del)	deletions of 3p22.1 from normal lung
cep3/3p-TAB (% Del)	deletions of 3p22.1 from bronchus adjacent to tumor

* The same abbreviations apply to the 10q probe.
 * n/a: data is not available

* Case numbers match with cases in Figures 4 and

Whether these primary bronchial epithelial cells from lung cancer patients contain any molecular or genetic abnormalities is not known. In collaboration with Dr. Ruth Katz, FISH analysis of deletion status of 3p22.1 region was performed on the cells from primary tumor and adjacent areas. As shown in Table 2, case 1 and 4 showed higher frequency of loss of 3p22.1 in tumor and also normal side of the lung, consistent with the findings when using the organotypic cultured cells. Further molecular, cellular, and genetic characterization of these primary epithelial cells isolated from lung cancer patients may facilitate better insight into lung cancer development.

Key Research Accomplishments

- We identified 23 unique biomarkers over-represented in the secretions from metaplastic squamous bronchial epithelial cells using comparative 2D-PAGE analysis of the apical surface fluids (ASF) obtained from squamous metaplastic and normal mucociliary bronchial epithelial cells.
- We found that expression of the unique proteins SCCA1 and SCCA2 was progressively increased in transformed/tumorigenic cell lines and only detected in squamous cell carcinoma but not in adenocarcinoma cells.
- We found that expression levels of SCCA1, SCCA2, Annexin I, Annexin II, S100A8, and Maspin in bronchial lavage are not directly correlated with histological appearance of bronchial mucosa in heavy smokers.
- We identified that genes in the WNT pathway, apoptosis, and cell cycle are concurrently deregulated in non-small cell lung cancer cells as compared to organotypically cultured normal bronchial epithelial cells.
- We successfully generated bronchial epithelium recapitulating *in vivo* bronchial epithelium using primary bronchial epithelial cells isolated from surgically-resected lung tissue specimens.
- Organotypic culture of the primary epithelial cells isolated from patients with lung cancer showed no obvious bias in growth, histologic abnormalities, or mucociliary differentiation.
- We demonstrated that primary bronchial epithelial cells isolated from surgically resected lung tissue specimens can be used for determination of the genetic susceptibility in lung target tissues assayed in DNA repair capacity and mutagen sensitivity.
- Concurrently overexpressed SCCA1 and Annexin 2 in the secretions from the bronchial epithelial cells may serve as surrogate markers for lower DNA repair capacity and high percentage of 3p loss of heterozygosity in corresponding tumors.

Reportable Outcomes

Articles published or in progress:

1. Ju Z, Kapoor M, Newton K, Cheon K, Ramaswamy A, Lotan R, Strong LC, Koo JS. Global detection of molecular changes reveals concurrent alteration of several biological pathways in non-small cell lung cancer cells. *Mol Genet Genom* 274:141-54, 2005.
2. Kim SW, Cheon K, Kim CH, Yoon JH, Hawke D, Kobayashi R, Lotan R, Hong WK, and Koo JS. Proteomics-Based Identification of Proteins Secreted in Apical Surface Fluid of Squamous Metaplastic Human Tracheobronchial Epithelial Cells Cultured by Three-Dimensional Organotypic Air-Liquid Interface Method. *Cancer Res* (in review), 2006.
3. Lee WS, Jimenez CA, Cheon K, Ryu SH, Wistuba II, Liu D, Lee JJ, Lotan R, Hong WK, Morice R, and Koo JS. Evaluation of Secretory Proteins as Surrogate Markers of Metaplasia/Dysplasia of Lung Mucosa. (in preparation)

Abstracts:

1. Kim SW, Kim CH, Cheon K, Newton K, Hawke D, Kobayashi R, Koo JS. Identification of markers for squamous metaplasia of bronchial epithelial cells. *Proc AACR* 46, 2005.

Conclusion

We conclude that 1) Secreted proteins (secretome) from premalignant or malignant lung cells hold promise as potential biomarkers to detect early lung cancer; 2) Expression levels of individual biomarkers identified in secretions from metaplastic squamous cells in bronchial lavage are not directly correlated with histological appearance of bronchial mucosa; 3) Primary bronchial epithelial cells isolated from bronchial mucosa of patients (64 cases) with lung cancer will be useful resources to understand the mechanisms of lung carcinogenesis, particularly molecular abnormalities in epithelial cells adjacent to tumor. In addition, they may have potential value to determine sensitivity or resistance to therapy by performing treatment simulation *in vitro*.

Project 4: Prognostic Role of Promoter Hypermethylation of Death-Associated Protein (DAP) Kinase and p16 Genes in Early-Stage Non-Small Cell Lung Cancer

(Project Leader: Charles Lu, M.D., Co-Leader: Li Mao, M.D.)

Specific Aim 1: To examine the relationship between hypermethylation of the death-associated protein (DAP) kinase gene promoter and disease-free, disease-specific, and overall survival in completely resected, early-stage NSCLC.

Specific Aim 2: To examine the relationship between hypermethylation of the p16 gene promoter and disease-free, disease-specific, and overall survival in completely resected, early-stage NSCLC.

Specific Aim 3: To examine the relationship between hypermethylation of the p16 gene promoter and history of tobacco smoke exposure in early-stage NSCLC.

Specific Aim 4: To determine the independent prognostic significance of these two molecular biomarkers after adjusting for relevant clinicopathologic variables (T-stage, N-stage, age, gender, histology, type of surgery, performance status, weight loss, smoking status).

The goal of this research proposal is to determine the prognostic importance of promoter hypermethylation of selected candidate genes in patients with early-stage, resected NSCLC who have been followed as part of a clinical research database. This study will create a high-quality database that includes clinical information in addition to surgical pathology specimens.

Summary of Research Findings for Specific Aims 1 - 4:

Subjects in this study are identified from a clinical research database of patients who have undergone surgical resection in the Department of Thoracic and Cardiovascular Surgery (DTCS), The University of Texas M. D. Anderson Cancer Center (UTMDACC). This database was established in 1997, and includes all patients who undergo thoracic surgical resection at UTMDACC. Detailed demographic, clinical, and pathologic data are recorded using standardized data collection forms. Follow-up clinical information is also collected at each clinic visit. Patients with completely resected stages I or II NSCLC and not receiving post-operative adjuvant therapy (either chemotherapy or chest radiotherapy) are eligible for this study. The proposed sample size was 300 subjects.

A query of the DTCS clinical research database yielded an initial list of 559 patients who underwent surgery between January 1, 1997 and December 31, 2001. To date, the medical records of these 559 patients have been screened, and 362 (64.7%) eligible subjects have been identified. Our collaborator in the Department of Pathology (Dr. Ignacio Wistuba) has reviewed these screened patients to confirm tumor histology and to determine if sufficient surgical tissue samples (paraffin blocks) exist to perform the required hypermethylation assays. 282 paraffin blocks have been retrieved. 267 and 261 subjects have had DAP kinase and p16 promoter hypermethylation assays performed on their tumor specimens in the laboratory of Dr. Li Mao.

Subjects with available tumor tissue have been entered into the study database. We have conducted a thorough review of the clinical data for these subjects (gender, age, tumor histology, preoperative clinical variables - performance status, weight loss, smoking status), and have obtained updated follow-up information (date of disease recurrence, date of death/last follow-up, development of second primary tumors) from our institution's medical informatics department, the Social Security Death Index, and direct telephone inquiries. Patient characteristics are listed in Table 1.

Table 1: Descriptive statistics of patients' characteristics

Characteristics	Frequency	Characteristics	Frequency
Sex		Race	
male	154(54.6%)	white	255(90.4%)
female	128(45.4%)	black	13(4.6%)
		hispanic	7(2.5%)
		others	7(2.5%)
Smoking status			
never	66(23.4%)		
former	113(40.1%)		
current	103(36.5%)		
T stage		N stage	
1	146(51.8%)	0	234(83.0%)
2	129(45.7%)	1	48(17.0%)
3	7(2.5%)		
Pathological stage		Histology	
IA	135(47.9%)	Adenocarcinoma	171(60.6%)
IB	93(33.0%)	SCC	82(29.1%)
IIA	11(3.9%)	Large cell carcinoma	10(3.6%)
IIB	43(15.3%)	Adenosquamous	6(2.1%)
		BAC	8(2.8%)
		Sarcomatoid	3(1.1%)
		LCNEC	2(0.7%)
Grade		Weight loss ≥5%	
1	43(15.6%)	no	262(92.9%)
2	120(43.6%)	yes	20(7.1%)
3	112(40.7%)		
PS			
0	178(63.1%)		
1	103(36.5%)		
2	1(0.4%)		

Findings: We found that the recurrence rate of these patients with early stage NSCLC was 21.3% and the death rate was 38% (Table 2).

Table 2: Descriptive statistics of patients' recurrent and survival status			
Characteristics	Frequency	Characteristics	Frequency
Recurrent NSCLC		Survival Status	
no	222(78.7%)	Alive	175(62.0%)
yes	60(21.3%)	Death	107(38.0%)
local	26	Died of disease	46
distant	54	die of non-NSCLC (excluding SPT)	31
liver	6	die of SPT	9
bone	9	unknown	21
brain	13		
adrenal	3		
other	1		

The promoter methylation status of *DAP kinase* and *p16* was observed in 36.3% (97 of 267 cases) and 36.4% (95 of 261 cases) respectively. No significant statistical correlations were observed between *DAP kinase* methylation status and subject characteristics (Table 3). No significant statistical correlations were observed between *p16* methylation status and subject characteristics (Table 4), but a positive trend for increased *p16* methylation and grade ($p=0.084$) was observed. A higher frequency of *p16* methylation was observed in ever vs never smokers (39% vs 28%, $p=0.17$).

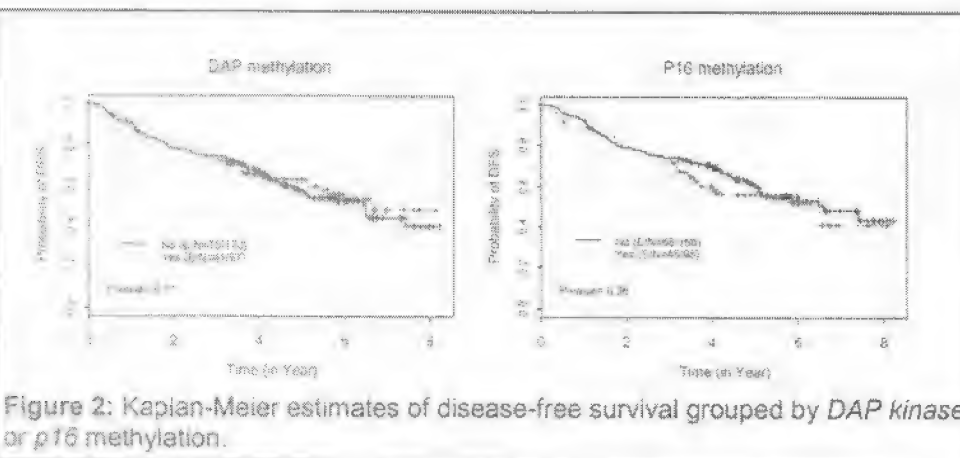
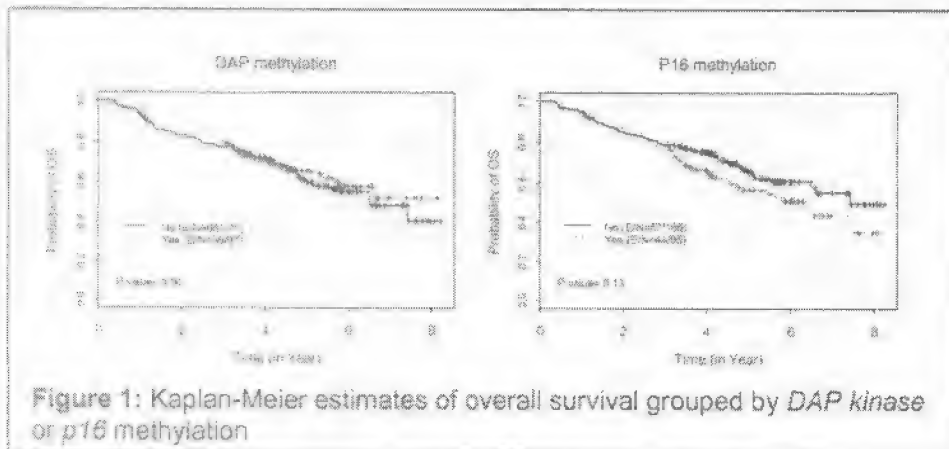
Table 3: Correlations between *DAP* kinase methylation and patients' characteristics

		DAPK methylation		p-value
		No methylation	methylation	
Age				0.33
	Mean \pm std	66.0 \pm 10.7	67.7 \pm 9.8	
	Median (min, max)	67(33, 90)	68(43, 90)	
Race				0.67
	non-white	18(69.2%)	8(30.8%)	
	white	152(63.1%)	89(36.9%)	
Sex				0.90
	female	93(64.1%)	52(35.9%)	
	male	77(63.1%)	45(36.9%)	
Smoking status				0.95
	never	38(63.3%)	22(36.7%)	
	former	69(62.7%)	41(37.3%)	
	current	63(65%)	34(35.1%)	
Histology				0.67
	adenocarcinoma	107(65.6%)	56(34.4%)	
	squamous	48(60%)	32(40%)	
	others	8(66.7%)	3(33.3%)	
Grade				0.27
	well	29(74.4%)	10(25.6%)	
	moderate	69(59.5%)	47(40.5%)	
	poor	67(63.8%)	38(36.2%)	
T stage				0.37
	T1	84(60.9%)	54(39.1%)	
	T2+T3	86(66.7%)	43(33.3%)	
N stage				0.50
	N0	143(64.7%)	78(35.3%)	
	N1	27(58.7%)	19(41.3%)	
Pathological stage				0.87
	IA+IB	137(64%)	77(36%)	
	IIA+IIB	33(62.3%)	20(37.7%)	
PS				0.12
	0	113(67.3%)	55(32.7%)	
	1+2	57(57.6%)	42(42.4%)	
Weight loss \geq5%				0.81
	no	158(64%)	89(36%)	
	yes	12(60%)	8(40%)	

Table 4: Correlations between p16 methylation and patients' characteristics

		p16 methylation		p-value
		No methylation	methylation	
Age				0.30
	Mean \pm std	66.1 \pm 10.2	67.1 \pm 10.6	
	Median (min, max)	67(40, 90)	68(33, 87)	
Race				0.27
	non-white	13(52%)	12(48%)	
	white	153(64.8%)	83(35.2%)	
Sex				0.99
	female	91(63.6%)	52(36.4%)	
	male	75(63.6%)	43(36.4%)	
Smoking status				0.32
	never	43(71.7%)	17(28.3%)	
	former	63(60%)	42(40%)	
	current	60(62.5%)	36(37.5%)	
Histology				0.35
	adenocarcinoma	108(67.5%)	52(32.5%)	
	squamous	45(58.4%)	32(41.6%)	
	others	5(55.6%)	4(44.4%)	
Grade				0.084
	well	31(79.5%)	8(20.5%)	
	moderate	68(60.7%)	44(39.3%)	
	poor	63(61.2%)	40(38.8%)	
T stage				0.80
	T1	87(64.4%)	48(35.6%)	
	T2+T3	79(62.7%)	47(37.3%)	
N stage				0.40
	N0	140(64.8%)	76(35.2%)	
	N1	26(57.8%)	19(42.2%)	
Pathological stage				0.33
	IA+IB	137(65.2%)	73(34.8%)	
	IIA+IIB	29(56.9%)	22(43.1%)	
PS				0.29
	0	109(66.1%)	56(33.9%)	
	1+2	57(59.4%)	39(40.6%)	
Weight loss \geq 5%				0.64
	no	152(63.1%)	89(36.9%)	
	yes	14(70%)	6(30%)	

Preliminary analyses did not show significant statistical correlations between methylation status and overall survival (*p16* $p=0.13$; *DAP kinase* $p=0.56$) (Figure 1) or disease-free survival (*p16* $p=0.36$; *DAP kinase* $p=0.71$) (Figure 2).



Univariate Cox regression analyses were performed to assess the relationship between patient characteristics and overall survival and disease-free survival (Tables 5 and 6). In multivariate analyses, only age and grade were significant predictors of overall survival (Table 7) and disease-free survival (Table 8).

Table 5: Univariate Cox proportional hazards regression models in estimating overall survival

Characteristics	Parameter estimate	Std. error	p-value	Hazard ratio
Age	0.06	0.01	<0.0001	1.06
Race (white vs. non-white)	0.18	0.37	0.63	1.19
Gender (female vs. male)	0.24	0.19	0.22	1.27
Smoke status				
Former vs. never	-0.07	0.25	0.79	0.94
Current vs. never	0.08	0.25	0.76	1.08
Histology				
Adenocarcinoma vs. others	-0.35	0.52	0.50	0.74
SCC vs. others	0.06	0.53	0.91	1.06
Grade				
Moderate vs. well	0.64	0.35	0.065	1.91
Poor vs. well	0.82	0.35	0.019	2.27
T stage (T2+T3 vs. T1)	0.32	0.19	0.10	1.38
N stage (N1+N2 vs. N0)	0.37	0.25	0.14	1.45
Pathological stage (IIA+IIB vs. IA+IB)	0.39	0.24	0.10	1.47
PS (2+1 vs. 0)	0.34	0.20	0.081	1.41
Weight loss ≥5% (yes vs. no)	0.57	0.33	0.087	1.77
DAP kinase methylation	-0.12	0.21	0.56	0.89
p16 methylation	0.31	0.20	0.13	1.36

Table 6: Univariate Cox proportional hazards regression models in estimating disease-free survival

Characteristics	Parameter estimate	Std. error	p-value	Hazard ratio
Age	0.05	0.01	<0.0001	1.05
Race (white vs. non-white)	0.21	0.35	0.55	1.23
Gender (female vs. male)	0.18	0.18	0.33	1.19
Smoke status				
Former vs. never	-0.03	0.24	0.91	0.97
Current vs. never	0.09	0.24	0.69	1.10
Histology				
Adenocarcinoma vs. others	-0.15	0.51	0.78	0.86
SCC vs. others	0.15	0.52	0.77	1.17
Grade				
Moderate vs. well	0.71	0.33	0.034	2.02
Poor vs. well	0.84	0.33	0.011	2.32
T stage (T2+T3 vs. T1)	0.46	0.18	0.013	1.58
N stage (N1+N2 vs. N0)	0.49	0.23	0.029	1.63
Pathological stage (IIA+IIB vs. IA+IB)	0.42	0.22	0.053	1.53
PS (2+1 vs. 0)	0.39	0.18	0.035	1.48
Weight loss ≥5% (yes vs. no)	0.49	0.32	0.13	1.63
DAP methylation	-0.07	0.19	0.71	0.93
P16 methylation	0.18	0.19	0.36	1.97

Table 7: Multivariate Cox proportional hazards regression models in estimating overall survival

Characteristics	Parameter estimate	Std. error	p-value	Hazard ratio
Age	0.07	0.01	<0.0001	1.07
Grade				
Moderate vs. poor	-0.40	0.22	0.069	0.67
Well vs. poor	-0.81	0.38	0.031	0.44

Table 8: Multivariate Cox proportional hazards regression models in estimating disease-free survival

Characteristics	Parameter estimate	Std. error	p-value	Hazard ratio
Age	0.06	0.01	<0.0001	1.06
Grade				
Moderate vs. poor	-0.34	0.20	0.093	0.71
Well vs. poor	-0.80	0.35	0.024	0.45

Key Research Accomplishments

- We did not observe significantly statistical correlations between *DAP kinase* methylation status and subject characteristics.
- We did not observe significantly statistical correlations between *p16* methylation status and subject characteristics, but a positive trend for increased *p16* methylation and grade ($p=0.084$) was observed.
- We observe a higher frequency of *p16* methylation in ever vs never smokers (39% vs 28%, $p=0.17$).
- We did not detect significantly statistical correlations between methylation status and overall survival (*p16* $p=0.13$; *DAP kinase* $p=0.56$) or disease-free survival (*p16* $p=0.36$; *DAP kinase* $p=0.71$).
- in multivariate analyses only age and grade were significant predictors of overall survival and disease-free survival.

Reportable Outcomes

Articles published or in progress:

1. Lu C, Soria JC, Tang X, Xu XC, Wang L, Mao L, Lotan R, Kemp B, Bekele BN, Feng L, Hong WK, Khuri FR. Prognostic Factors in Resected Stage I Non-Small Cell Lung Cancer (NSCLC): A Multivariate Analysis of Six Molecular Markers. *J Clin Oncol* 22: 4575-83, 2004.
2. Wei QY, Wang LE, Sturgis EM, Mao L. Expression of Nucleotide Excision Repair Proteins in Lymphocytes as a Marker of Susceptibility to Squamous Cell Carcinomas of the Head and Neck. *Cancer Epidem Biomarkers and Prev* 14:1961-6, 2005.
3. Lu C, Wistuba I, Zhou X, Bekele BN, Putnam JB, Jr., Correa A, Mao L. Prognostic role of promoter hypermethylation of death-associated protein (DAP) kinase and p 16 genes in early-stage non-small cell lung cancer. (in preparation)

Abstracts:

1. Lu C, Wistuba I, Zhou X, Bekele BN, Putnam JB, Jr, Correa A, Mao L. Prognostic role of promoter hypermethylation of death-associated protein (DAP) kinase and p 16 genes in early-stage non-small cell lung cancer. *Proc ASCO* 24:7216, 2006.

Conclusion

In this relatively large cohort of early-stage NSCLC patients, we did not detect significantly statistical correlations between *p16* and *DAP kinase* promoter methylation and clinical outcomes. Further subset analyses stratified by gender and histology will be performed. The prognostic role of these biomarkers in NSCLC remains unclear.

This project has produced a valuable clinical-pathological database. We have already begun a second study analyzing the prognostic role of the forkhead transcription factor FOXO3a in this patient population.

Project 5: An Epigenetic Approach to Lung Cancer Therapy

(Project Leader: Reuben Lotan, Ph.D.)

Loss of expression of tumor suppressor genes is one of the hallmarks of cancer development. It occurs after loss of heterozygosity and mutations in tumor suppressor genes. In addition, epigenetic silencing of several tumor suppressor genes can occur by aberrant methylation of CpG islands in gene promoter regions (Baylin et al, 2006) and by changes in chromatin structure resulting from alterations in histone acetylation state (Kelly et al, 2005). Nucleosomes containing unacetylated positively charged histones bind tightly to DNA producing a compact configuration, which inhibits transcription. A targeted approach to reverse the silencing of genes has been the use of the DNA methylation inhibitor, 5-aza-2'-deoxycytidine (5-AZA-CdR), and the histone deacetylase inhibitor suberoylanilide hydroxamic acid (SAHA). Each of these agents alone can reactivate the expression of certain silenced genes and their combination can reactivate a greater range of genes. Combination of the two epigenetic modulators has shown efficacy in the treatment of myeloid neoplasms (Gore et al, 2006).

The objective of this study was to assess the potential of epigenetic therapy against lung cancer. We hypothesized that combinations of the histone deacetylase inhibitor SAHA and the demethylating agent 5-aza-CdR have potential to act additively or synergistically to enhance cell death *in vitro* and *in vivo* and can be effective in the therapy of non-small cell lung cancers (NSCLC). To test this hypothesis, we pursued the following specific aims, and under each aim, we then summarized research achievements in the final report.

Specific Aim 1: To determine the ability of SAHA and 5-aza-CdR used as single agents and in combination to inhibit the growth and induce apoptosis in normal bronchial and small airway epithelial cells, immortalized, premalignant, transformed and tumorigenic lung cells and several established non-small cell lung cancer (NSCLC) cell lines *in vitro*.

Specific Aim 2: To explore the mechanisms underpinning possible interactions between SAHA and 5-aza-CdR, including analysis of differential gene expression between untreated cells and cells treated with SAHA alone, 5-aza-CdR alone, and the combination of the two agents using Affymetrix oligonucleotide microarrays.

Specific Aim 3: To determine the ability of SAHA, 5-aza-CdR, and their combinations to inhibit the growth of human NSCLC cells implanted subcutaneously in athymic nude mice.

Specific Aim 4: To investigate the mechanisms of the *in vivo* activity, especially those related to inhibition of cell growth and induction of apoptosis.

Summary of Research Findings:

Specific Aim 1: To determine the ability of SAHA and 5-aza-CdR used as single agents and in combination to inhibit the growth and induce apoptosis in normal bronchial and small airway epithelial cells, immortalized, premalignant, transformed

and tumorigenic lung cells and several established non-small cell lung cancer (NSCLC) cell lines *in vitro*.

We investigated the effects of 5-AZA-CdR and SAHA (see structures in Figure1) and their combinations on the *in vitro* growth of human NSCLC cell lines listed in Table 1.

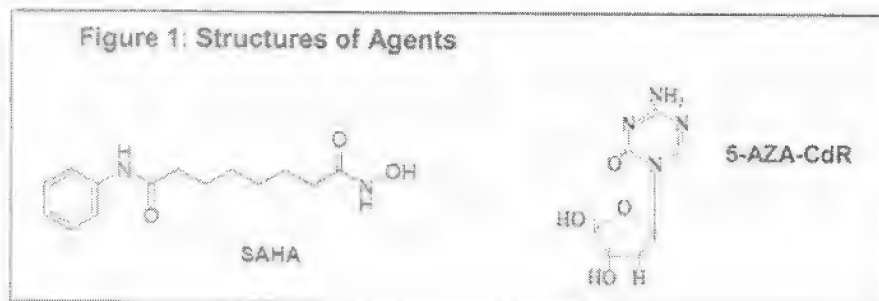


Table 1: Cells used in this study and their sensitivity to 5-AZA-CdR and SAHA

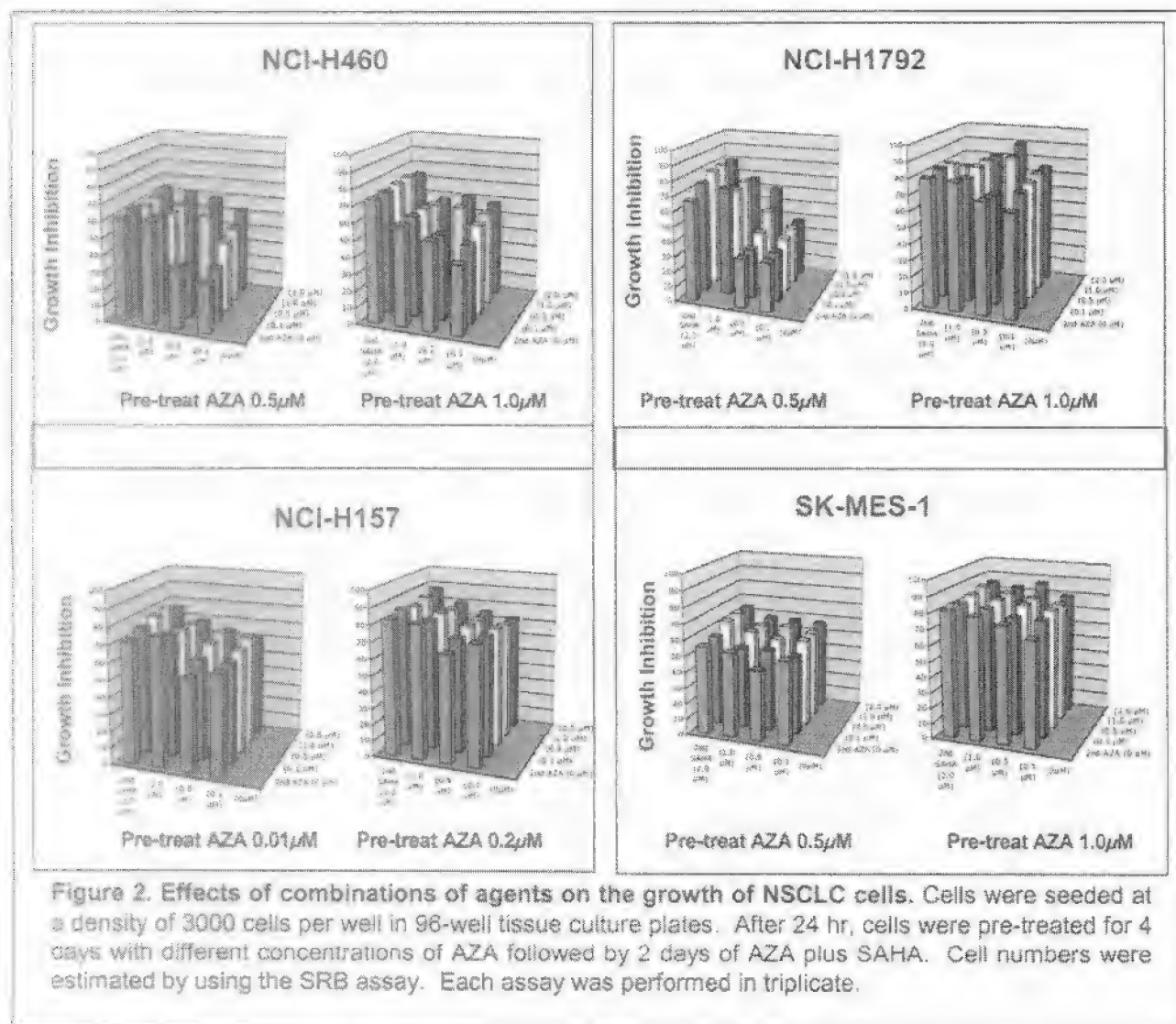
Cell line	Description	IC ₅₀ (μM)*	
		5-AZA-CdR	SAHA
NCI-H460	Large cell carcinoma, pleural fluid	3.2	0.6
NCI-H157	Squamous cell carcinoma, pleural effusion	0.42	1.0
NCI-H1792	Adenocarcinoma, pleural effusion	1.7	2.0
SK-MES-1	Squamous cell carcinoma, pleural effusion	0.6	1.5
11701	Tumorigenic derived from immortalized human bronchial epithelial cells after exposure to cigarette smoke condensate <i>in vivo</i>	0.5	0.8
1198	Transformed human bronchial epithelial cells	0.5	1.0
1799	Immortalized human bronchial epithelial cells	1.0	0.5
BEAS-2B	Human bronchial epithelial cells immortalized with adenovirus 12-SV40 large T antigen	1.75	1.0
NHBE	Normal human bronchial epithelial cells	0.8	0.6
SAEC	Small airway epithelial cells	6.0	>6.0

* 5-AZA-CdR and SAHA were added to cell culture medium at the doses between 0.1 and 6.0 μM. The sulforhodamine B assay was used to detect inhibition of cell growth. Concentrations required for 50% growth inhibition (IC₅₀) of each agent alone were determined from dose-response curves.

Findings: We found that the two agents inhibited the growth of all cell lines albeit with differential potencies. The IC₅₀ for 5-AZA-CdR ranged from 0.42 to 6 μM whereas that of SAHA ranged from 0.5 to >6 μM. The normal SAEC cells were the least sensitive (Table 1).

For combination studies, we pre-treated the cells with low concentrations of 5-AZA-CdR (between

0.01 and 1 μ M) depending on the sensitivity of individual cell lines and then treated with AZA alone (0.1, 0.5, 1 and 2 μ M) or combined with SAHA (0.1, 0.5, 1 and 2 μ M) (Figures 2-4). 5-AZA-CdR and SAHA in combination produced a greater inhibition of cell growth than either agent alone (Figure 2).



The malignant H1792 cells showed marked effects of the combination of agents whereas the other cell lines were not more sensitive to the combination than to each agent alone. It is noteworthy that the cells were sensitive to 5-AZA-CdR alone and that the experimental design required that the cells be pretreated with 5-AZA-CdR for 4 days because this agent needs to be incorporated into DNA to be able to inhibit the enzyme DNA methyltransferase.

We then analyzed the effects of AZA and SAHA on premalignant lung cells that were represented by immortalized cells (BEAS-2B and 1799, the transformed cells (1198) and their tumorigenic derivative 1170-1 (Table 1). These cells have an inactivated p53 signaling as the large T antigen of SV40 virus used for immortalization binds to p53 and inactivates it. Although NSCLC is not caused by viral transformation, many NSCLCs have aberrant p53 signaling due to p53 mutations or inactivation.

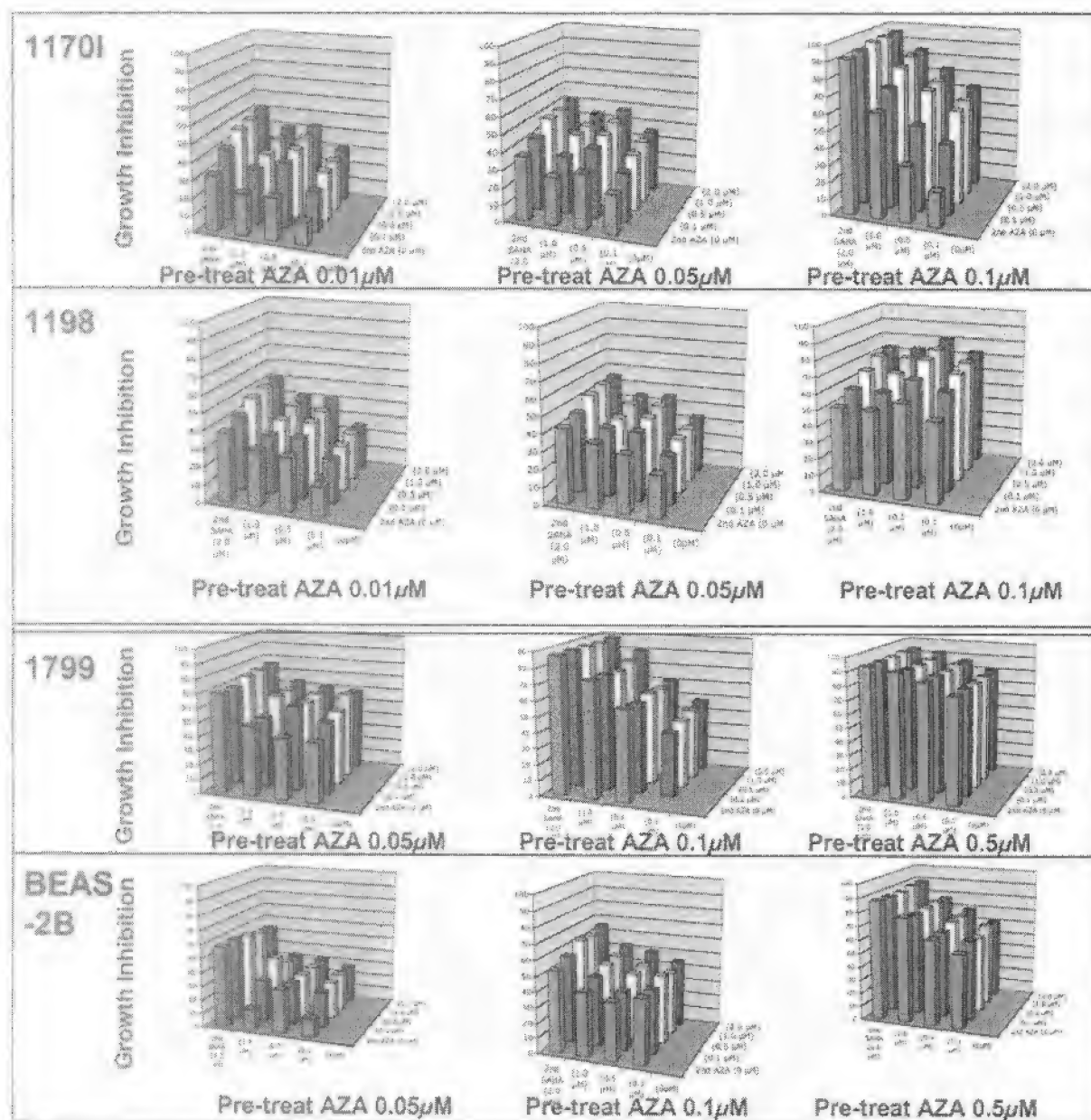


Figure 3. Effects of combinations of agents on the growth of premalignant cells. The experiments were conducted as in Figure 2 above but with premalignant cells rather than NSCLC cells.

As shown in Figure 3, among the human bronchial epithelial cell-derived premalignant cells and their tumorigenic derivative, both the transformed 1198 and the malignant 1170-I showed the greatest sensitivity to the combination of AZA and SAHA compared to each of the agents alone. The immortalized cells showed almost no enhancement of response by the combination.

Specific Aim 2: To explore the mechanisms underpinning possible interactions between SAHA and 5-aza-CdR including analysis of differential gene expression between untreated cells and cells treated with SAHA alone, 5-aza-CdR alone and their combination using Affymetrix oligonucleotide microarrays.

To explore the mechanisms by which SAHA exerts its growth inhibitory effects, we analyzed changes in cell growth and apoptosis and the level of different proteins implicated in cell death. We determined effects of SAHA on cell growth and apoptosis in 10 cancer cell lines compared to premalignant (Leuk1) and normal oral (NOK) cells. Apoptosis induction was assessed using DNA fragmentation, TUNEL, and ELISA. Mechanisms of apoptosis were analyzed after coincubation with pan-caspase and specific caspase and Fas inhibitors and after small interfering RNA (siRNA) transfection.

Findings: Results have been summarized in a manuscript (Gillenwater et al, 2006) that we intend to submit for publication. The manuscript and related figures are attached in **Appendices III and II** respectively. Here we only summarize the findings and refer to figures and tables in the manuscript

SAHA inhibits the growth of human HNSCC cells while sparing premalignant and normal oral cells. As shown in Figure 1, SAHA inhibited growth of all 10 cancer cell lines in a concentration-dependent manner, with an estimated IC_{50} ranging from 1.35 to 7.7 μ M after a 3-day treatment. In comparison, SAHA had a more limited effect on the growth of an immortalized leukoplakia cell line (Leuk1) and normal human oral gingival keratinocyte (NOK) cells. The inhibition of growth of HNSCC cell lines 17B and 22B was both dose- and time-dependent between 1 and 4 days (Fig. 1D and 1E).

SAHA selectively induces cell-cycle arrest and apoptosis in HNSCC cells. We next examined the effects of SAHA on two sensitive HNSCC cell lines, 17B and 22B. We detected an increase in the proportion of HNSCC cells in the G2 cell cycle phase after treatment with 4 μ M SAHA for 24 hours, suggesting that cell cycle inhibition may contribute to the overall decrease in cell numbers after exposure to SAHA. In comparison, very little, if any, cell cycle arrest was detected in Leuk1 and NOK cells (Fig. 2A). Because several HDAC inhibitors induce apoptosis *in vitro* in various cancer cell lines, we next examined whether SAHA induced apoptosis in HNSCC cell lines 17B and 22B, and Leuk1 and NOK cells. Using a TUNEL-flow cytometry analysis, we detected an increase in apoptotic cell population in 17B and 22B cell lines from less than 2% in untreated cells to about 60% in cells treated for 24 hr with 4 μ M SAHA. In contrast, only minor increase in apoptosis was observed in the Leuk1 or NOK cells treated under the same conditions (Figure 2B). SAHA also induced DNA fragmentation, a hallmark of apoptosis, in both HNSCC cancer lines (Fig. 2C).

SAHA increases acetylation of histones H3 and H4 in HNSCC cells, Leuk1 and NOK cells. To determine whether SAHA induced accumulation of acetylated histones in HNSCC cells at concentrations that induced growth inhibition and apoptosis, we cultured four cell lines with 4 μ M SAHA for various periods of time and evaluated for the presence of acetylated H3 and H4 using Western blotting with acetylated histone-specific antibodies. We detected a time dependent increase in acetylated H3 and H4 in all four cell lines, 17B, 22B, Leuk1 and NOK cells beginning at 3 hr (Fig. 3A, 3B).

SAHA induces expression of p21^{WAF1} mRNA and protein. The cell cycle kinase inhibitor p21^{WAF1} is induced in various transformed cells by HDAC inhibitors such as SAHA and may play a role in the growth inhibition observed after *in vitro* treatment with these agents. We detected increased expression of p21^{WAF1} mRNA (Fig. 3C) and p21^{WAF1} protein (Fig. 3D) in HNSCC cell lines 17B and 22B after treatment with 4 μ M SAHA. In the 17B cells p21^{WAF1} protein level peaked at 15 hours and then declined, whereas in the 22B cells, maximal p21^{WAF1} protein expression was seen at 24 hours. In comparison, both Leuk1 and NOK cells had a higher constitutive level of p21^{WAF1} mRNA than the malignant cells yet their protein level was low. Nonetheless, incubation with 4 μ M SAHA had small effect on p21^{WAF1} mRNA but increased the level of p21^{WAF1} protein in Leuk1 by 24 hours and NOK cells by 3 hours (Fig. 3E,F).

SAHA induces apoptosis via the mitochondrial (intrinsic) pathway in HNSCC cells. Apoptosis can be initiated via the mitochondrial (intrinsic) pathway that functions through caspase-9, or via the

death-receptor (extrinsic) pathway that acts through caspase-8. The release of cytochrome C from the mitochondria initiates caspase activation, thus triggering the important intrinsic apoptotic pathway frequently induced by cytotoxic agents. We next examined the effects of incubating 17B and 22B cells with 4 μ M SAHA on several key aspects of apoptosis initiation via the intrinsic pathway, such as cytochrome C release, activation of caspases and cleavage of protein substrates. As shown in Figure 4A, SAHA triggered a rapid release of cytochrome C into the cytosol in 17B and 22B HNSCC cells. This was followed by activation of caspase-9 within 15 hours, as demonstrated by the decreased expression of procaspase-9 by Western blotting of total protein extracts in Figure 4B. Next, we observed a time-dependent activation of the effector caspase-3 within 15 hours, as demonstrated by decrease in procaspase-3 and appearance of the cleaved form of the caspase substrate PARP (Fig. 4B).

Activation of the caspase cascade is required for SAHA-induced apoptosis. We examined the effect of SAHA on apoptosis induction in the presence of a caspase inhibitor to determine whether activation of the caspase cascade is necessary for SAHA to induce apoptosis in HNSCC cells. As shown in Figure 4C, the pan-caspase inhibitor Z-VAD-FMK suppressed SAHA-induced apoptosis in 17B and 22B cells. This indicates that activation of the caspase cascade is required for SAHA to induce apoptosis in these HNSCC cell lines. However, a specific caspase-9 inhibitor only partially blocked the induction of apoptosis (Fig 4D), indicating that alternative caspase cascades also play a role in SAHA-induced apoptosis. As shown in Figure 4D, a specific inhibitor of caspase-8 also blocked the induction of apoptosis in HNSCC cells by SAHA, indicating a role for the extrinsic apoptosis pathway.

SAHA activates the death receptor (extrinsic) apoptosis pathway. The death receptor (extrinsic) apoptosis pathway involves binding of a ligand to one of the TNF family of death receptors, activation of caspase-8, followed by caspase-3 activation. However, the intrinsic and the extrinsic pathways are linked through the ability of caspase 8 to cleave BID, which in turn leads to cytochrome C release from the mitochondria. To explore whether incubation of HNSCC cells in SAHA would also activate the death receptor pathway, we evaluated the expression of Fas(CD95) and FasL(CD95L), DR4, DR5, and tumor necrosis factor-related apoptosis-inducing ligand (TRAIL) before and after exposure to SAHA for various time periods. As shown in Figure 5A, there was little if any expression of Fas and FasL in untreated 17B and 22B cells, but after incubation with SAHA, there was a time-dependent increase in expression of both molecules. In both HNSCC cell lines, the expression of Fas and FasL increased by 3 hours, but in the 17B cells, expression peaked at 15 hours, whereas in the 22B cells, expression was strongest at 24 hours. SAHA also activated caspase-8 and cleaved BID by 15 hours in both HNSCC cell lines (Fig. 5C), demonstrating activation of the extrinsic apoptosis pathway by this agent. In contrast, untreated Leuk1 and NOK cells expressed both Fas and FasL, and SAHA did not change the level of constitutive expression (Fig. 5A). SAHA did not alter the expression levels of DR4 and DR5, and increased TRAIL only marginally after 24 hrs (Fig. 5D).

To determine whether activation of Fas was required for SAHA to induce apoptosis, we incubated 17B and 22B cells with SAHA in the presence of soluble Fas to compete for FasL. As shown in Figure 5E, competitive inhibition with soluble Fas was able to block the induction of apoptosis in these cells by SAHA. This suggests that activation of Fas is required for SAHA to induce apoptosis in HNSCC cells.

Partial silencing of caspases 8 and 9 reduces SAHA-induced apoptosis. Caspase-9, caspase-8, and Fas expressions were also blocked by transfecting specific siRNAs into 22B cells, and then analyzing whether SAHA could still induce apoptosis in these cells. siRNA transfection was effective in blocking activation of caspase-9 (Fig. 6A) and caspase-8 (Fig. 6B) in SAHA-treated cells. As shown in Figure 6C, this effect also decreased the ability of SAHA to induce apoptosis in 22B cells by 84% and 78%, respectively. Furthermore, transfection of Fas siRNA alone also reduced the ability of SAHA to induce apoptosis in 22B HNSCC cells by 63% (Fig. 6C).

Inhibition of Fas activation limits SAHA-induced inhibition of anchorage-dependent colony formation. To determine whether blocking SAHA-induced apoptosis by the different siRNAs described above could also protect the cells from growth inhibition, we analyzed the ability of 22 B cells to form colonies in the presence and absence of SAHA after siRNA transfection. As demonstrated in Figure 6D, SAHA inhibited colony formation by about 98%, whereas selective interference with caspase-9 and caspase-8 decreased the inhibitory effect of SAHA to 45% and 43%, respectively. Interference with Fas signaling also decreased the ability of SAHA to suppress colony formation in 22B HNSCC cells to 61%, whereas non-specific siRNA decreased the effect of SAHA by less than 10%, further supporting the contributions of both apoptosis pathways in mediating the effects of SAHA on growth inhibition as well as apoptosis induction in HNSCC cells.

Effects of another HDAC inhibitor, valproic acid, on cell growth and apoptosis.

In addition to studying the effects of SAHA in proposed originally, we also investigated the effects of another HDAC inhibitor, valproic acid. The results of this study are summarized in the finished manuscript (Zhong et al, 2006) attached in **Appendix III – Publications**.

Background: Valproic acid (VPA), a commonly used anti-seizure medication, is an HDAC inhibitor that is currently being evaluated in clinical trials in myeloid malignancies in combination with decitabine. To determine whether VPA has potential clinical applications for chemoprevention and therapy in patients with head and neck squamous cell carcinoma (HNSCC), we analyzed the effect of VPA on growth and apoptosis of HNSCC cell lines. The results are summarized below and refer to figures in the manuscript (Zhong et al, 2006) attached in **Appendix III – Publications**.

Findings: VPA suppressed the growth of all 9 cell lines with IC_{50} ranging from 1.73 mM to 15.17 mM after a 3-day treatment (Fig. 1). Subsequent mechanistic studies focused on the most sensitive cell line, 17B. Cell cycle analysis revealed an increased percentage of cells in sub-G1 and in G2 after 16 hours incubation with VPA in a dose-dependent manner (data not shown). TUNEL apoptosis assays demonstrated that a 16-hr exposure to VPA at concentrations of 2.5, 5 and 10 mM resulted in 15%, 22.1% and 37.5% apoptotic cells, respectively. DNA laddering observed in agarose gels confirmed the induction of apoptosis (Fig. 2). Northern and Western blot analyses were performed to study the expression of key genes in growth arrest and apoptosis pathways. VPA increased nuclear content of acetylated histones H3 and H4. The levels of p53 mRNA and protein decreased, while the levels of p21/WAF1 increased after treatment with VPA, suggesting that VPA exerted the growth inhibition effect through a p21-dependent, but p53-independent pathway (Fig. 3). The protein levels of pro-caspases 3, 6 and 9 decreased, accompanied by simultaneous increased levels of cleaved caspases 3 and 9, and cleaved PARP (Fig. 4), and addition of the caspase inhibitor Z-VAD-FMK to VPA-treated 17B cells abolished VPA-induced apoptosis, indicating that VPA acts through a cascade of caspases (Fig. 5). VPA treatment did not change the protein levels of Fas, Bax, Bcl-2 or caspase 8, but further analysis of the extrinsic apoptosis pathway revealed increased DR5, FADD, caspase 10 and decreased pro-caspase 2, suggesting activation of this pathway (Fig. 6). Interestingly, although levels of TRAIL decreased, partial blockage of DR5 and FADD using siRNA transfection markedly diminished the ability of VPA to induce apoptosis in 17B cells, suggesting an important role for DR5-mediated signaling (Fig. 7). Indeed, treatment of the cells with a combination of exogenous TRAIL and VPA augmented the apoptosis inducing effect of the HDAC inhibitor (Fig. 8). Further, treatment with both 5-aza-CdR and VPA synergistically increased apoptosis, suggesting a possible role for combinations of these agents.

siRNA inhibition on DNMT1 expression and cell growth of NSCLC A549 cells. The inhibition of 5-AZA-CdR on DNA methyltransferase (DNMT) requires its incorporation into DNA that greatly limits its inhibitory effect and application. The newly emerging siRNA agents show powerful inhibitory effects on many target genes, which encourages us to test effects of DNMT-specific siRNA on expression of

DNMT and cell growth. The results have been published in *International Journal of Oncology* (Oridate et al, 2005), and are summarized below.

Findings: Transfection of DNMT1 siRNA decreased DNMT1 protein levels specifically and effectively in A549 cells. This decrease was accompanied by suppression of cell proliferation and colony-forming ability. The mechanism of this inhibition may be related to the increased levels of the cyclin-dependent kinase inhibitor p21. These results suggest that the siRNA approach can be used to disrupt DNMT1 activity and cancer cell growth.

Effects of SAHA and 5-AZA-CdR alone and combined on gene expression. We used Affymetrix gene expression microarray to evaluate the effects of the epigenetic modulators on gene expression. The analysis involved treating the cells with SAHA (4 μ M), 5-AZA-CdR (1 μ M) for 3 days or with SAHA (4 μ M) for 1 day or with 5-AZA-CdR (1 μ M) for 3 days followed by 1-day treatment with the combination of 5-AZA-CdR (1 μ M) plus SAHA (4 μ M). RNA samples isolated from these treated cells were subjected to microarray analysis using the commercial Human Affymetrix U133A chip.

Findings: The analysis was performed by the Bioinformatics Core and is summarized in Appendix 1, Tables 2-7. In brief, Table 2 lists genes showing over 2-fold increased expression after treatment with SAHA (4 μ M; 24hr); Table 3 lists genes showing over 2-fold decreased expression after treatment with SAHA (4 μ M; 24hr); Table 4 shows genes having over 2-fold increased expression after treatment with 5-AZA-CdR (1 μ M; 4days); Table 5 shows genes having over 2-fold decreased expression after treatment with 5-AZA-CdR (1 μ M; 4days); Table 6 lists genes showing over 2-fold increased expression after treatment with 5-AZA-CdR (1 μ M 4days) and SAHA (4 μ M last 24 hrs of the 5-AZA-CdR treatment) compared to untreated control cells; Table 7 lists genes showing over 2-fold decreased expression after treatment with 5-AZA-CdR (1 μ M 4days) and SAHA (4 μ M last 24 hrs of the 5-AZA-CdR treatment).

Overall, 5-AZA-CdR modulated the expression of 750 genes; SAHA modulated the expression of 1135 genes while their combination affected the expression of 1595 genes. There were genes that were modulated by 5-AZA-CdR alone or SAHA alone and not by the other or the combination. Each agent alone also modulated about 30% of the genes modulated by the combination of agents. Functional mining of the data using the Ingenuity program revealed that 5-AZA-CdR alone increased the expression of genes involved in canonical pathways including fatty acid biosynthesis, antigen presentation pathway, cell cycle: G2/M DNA damage checkpoint, interferon signaling in decreasing order of fold increase; whereas analysis according to functional network showed modulation of genes related to cancer, cell death, cell movement, cell cycle, DNA replication, recombination and repair, cell-to-cell signaling, and drug metabolism. A similar analysis of the effects of SAHA alone revealed modulation of canonical pathways including fatty acid biosynthesis, cell cycle G2/M DNA damage checkpoint, antigen presentation pathway, hypoxia signaling, and sonic hedgehog signaling. In relation to functional network modulation, SAHA affected genes related to cell cycle, cell assembly and organization, cancer, cell growth and proliferation, cell death, cell movement, inflammatory disease, molecular transport and cell-to-cell interactions. As mentioned above, many of these same genes were also modulated by the combination of 5-AZA-CdR and SAHA. However, there were subsets of genes that were regulated by the combination of the two agents but not by each agent alone. These included genes involved in oxidative phosphorylation, ERK/MAPK signaling, VEGF signaling, PPAR signaling, IL-6 signaling, EGF signaling, p38 MAPK signaling, IGF-1 signaling, integrin signaling, and NF- κ B signaling.

We have not completed this task yet. In the near future we should validate some of the microarray findings using quantitative polymerase chain reaction and Western blotting, and we will pursue some functional studies using siRNA library screening.

Specific Aim 3: To determine the ability of SAHA, 5-aza-CdR and their combinations to inhibit the growth of human NSCLC xenografts in athymic nude mice.

We performed the *in vivo* experiments to assess the ability of SAHA and 5-AZA-CdR to exert anti-tumor effects against human lung cancer xenograft in an *in vivo* mouse model. Sixty eight of 4-week-old athymic nu/nu female mice (Harlan, Inc. Indianapolis, IN) were injected s.c. bilaterally with 1×10^6 non-small cell lung cancer cells of cell line H157ASRARbeta in 0.1 ml of PBS. The mice were maintained without any treatment until tumors reached a volume of $\sim 100 \text{ mm}^3$. As shown in Table 8, tumor-bearing mice were divided into eight groups (8 to 10 mice/group) for the treatment study. For administration to mice, SAHA was dissolved and diluted in a vehicle of DMSO. Each group of mice received 25, 50, or 100 mg/kg SAHA daily as a single agent and combined with a fixed 5-aza-CdR dose of 1 mg/kg by i.p. injection. A control group of 8 animals was injected with vehicle only (DMSO). The injection volume was kept constant at $1 \mu\text{l}/\text{gram}$ body weight. The mice were weighed three times during the experimental period to assess toxicity of the treatments, and the tumors were measured every three days using calipers. The treatment period was planned for 21 days, when the vehicle-treated group of mice was expected to develop tumors with about 1 cm diameter requiring that the animals be sacrificed. Tumor volume was calculated from the two-dimensional caliper measurements using the following formula: Tumor volume = length x (width)² x $\pi/6$.

Table 8. The mice were randomized into 8 groups of 8 mice each (see below).

Group 1	Group 2	Group 3	Group 4	Group 5	Group 6	Group 7	Group 8
Control	5-aza-CdR	SAHA	SAHA	SAHA	SAHA	SAHA	SAHA
DMSO	1mg/kg	25mg/kg	50mg/kg	100mg/kg	25mg/kg	50mg/kg	100mg/kg
Only	Only	Only	Only	Only	5-aza-CdH	5-aza-CdH	5-aza-CdH
8 mice	8 mice	8 mice	8 mice	10 mice	1 mg/kg	1 mg/kg	1 mg/kg
					8 mice	8 mice	10mice

Findings: As shown in Table 9, SAHA did not decrease the weight gain of the mice over the 12 days of the experiment even at the highest dose. In contrast, 5-aza-CdR caused loss of weight even at the lower dose and both doses caused nearly 50% mortality whether given alone or with SAHA. The weight of the tumors in the mice that survived until day 12 was much lower in the mice treated with the combination of the two agents than with each agent alone as seen in Figure 4, and the kinetics of tumor growth are slowed down in treated mice with the greatest effects observed in double-treated mice, which also lost considerable body weight (Fig. 5).

Table 9: Effects of SAHA alone, 5-aza-CdR alone and their combination administration on the body weights and survival of the RAR-βASH 157 Abs (12) Human NSCLC bearing mice.

Treatment	Initial body weight (g) ^a	5 days Treated body Weight (g)	10 days Treated Weight (g)	Final body weight (g) Day 12	Death [days (D) of treatment]
Vehicle (DMSO)	19.33 ± 1.32 (n = 8)	19.89 ± 1.11 (n = 8)	21.36 ± 1.28 (n = 8)	21.59 ± 1.12 (n = 8)	0
25 mg/kg SAHA	18.48 ± 1.39 (n = 8)	18.91 ± 1.43 (n = 8)	19.16 ± 2.00 (n = 8)	20.33 ± 1.79 (n = 8)	0
50 mg/kg SAHA	19.59 ± 0.83 (n = 10)	19.94 ± 1.04 (n = 8)	20.10 ± 1.44 (n = 10)	20.38 ± 1.43 (n = 8)	0
100 mg/kg SAHA	19.33 ± 2.11 (n = 10)	19.71 ± 1.83 (n = 10)	19.91 ± 1.96 (n = 10)	20.61 ± 2.06 (n = 10)	0
1mg/kg 5-aza-CdR Only	18.63 ± 1.65 (n = 8)	17.69 ± 2.68 (n = 8)	17.73 ± 3.51 (n = 7)	15.65 ± 2.96 (n = 4)	1 (D10) ^b 3 (D11) ^b 4 (D12) ^b
25mg/kg SAHA 1mg/kg 5-aza-CdR	18.59 ± 2.18 (n = 8)	16.84 ± 1.66 (n = 8)	15.22 ± 2.26 (n = 5)	13.64 ± 1.10 (n = 4)	3 (D10) ^b 1 (D11) ^b 4 (D12) ^b
50mg/kg SAHA 1mg/kg 5-aza-CdR	18.59 ± 2.18 (n = 8)	16.84 ± 1.66 (n = 8)	15.76 ± 1.25 (n = 4)	14.58 ± 0.51 (n = 4)	4 (D10) ^b 2 (D11) ^b 2 (D12) ^b

100 mg/kg SAHA 1mg/kg 5-aza-CdR	18.65 ± 1.36 (n = 10)	16.68 ± 1.65 (n = 10)	15. ± 1.68 (n = 9)	12.95 ± 0.7 (n = 5)	1 (D10) ^a 4 (D11) ^b 5 (D12) ^b
------------------------------------	-----------------------	-----------------------	--------------------	---------------------	--

^a All values are presented as the mean ± SE for the surviving animals (n) in each treatment group. Initial and final body weights refer to the weight of the mice at the start of SAHA treatment and the end of the experiment, respectively. ^b Mice that died in this dose group showed marked weight loss for 1–2 days before death.

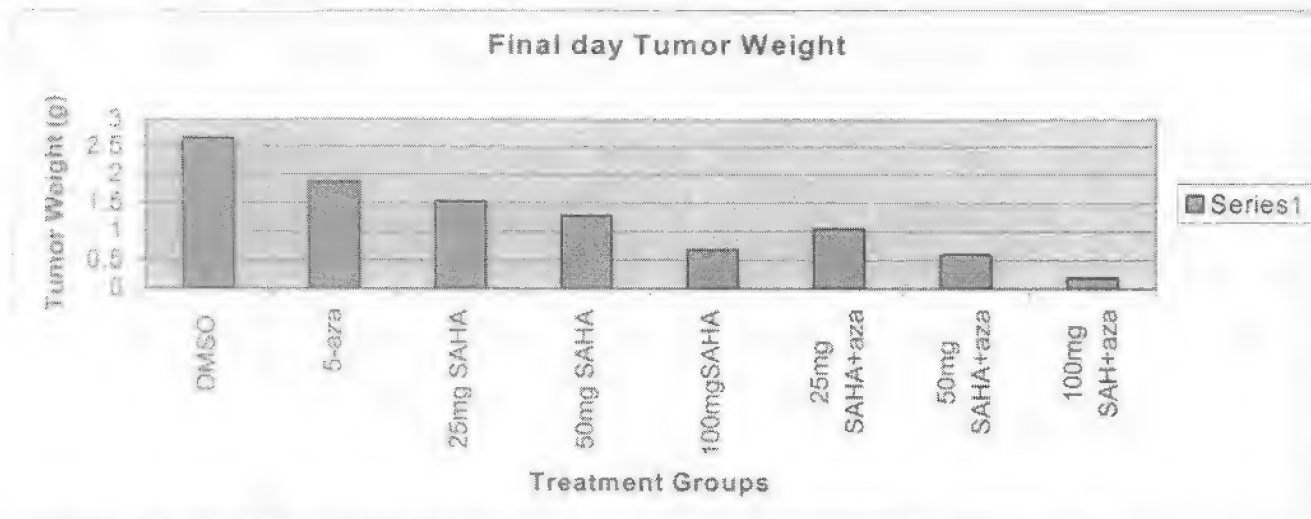
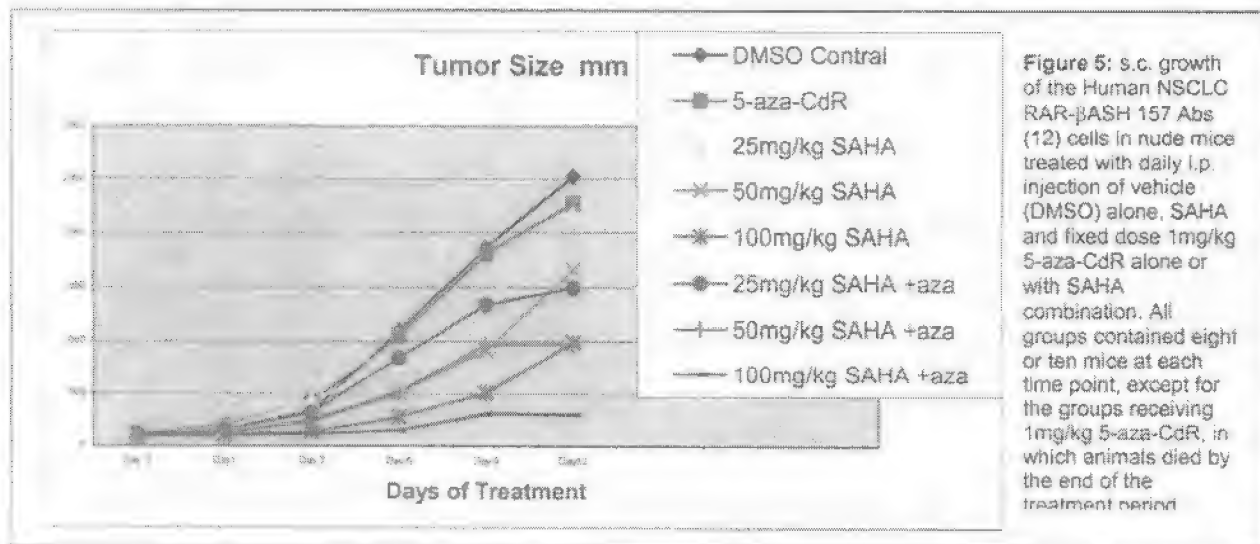


Figure 4: The final day tumor weight for groups DMSO and SAHA (25, 50 and 100mg/kg). The tumors from groups 1mg/kg 5-aza-CdR only and combination with SAHA (25, 50 and 100mg/kg) are weighted at the day (day 10, day 11 and day12) the mice died.



Key Research Accomplishments:

- We found that 5-AZA-CdR, SAHA, and valproic acid were able to inhibit the growth of premalignant and malignant lung epithelial cells and head and neck SCCs in a dose dependent fashion. Normal oral epithelial cells were much less sensitive; in some of the cell lines, 5-AZA-CdR and SAHA acted synergistically.
- Both SAHA and valproic acid inhibited the growth by G2 arrest and also induced apoptosis in HNSCC cell lines.
- We found that siRNA-mediated gene silencing of DNMT can be applied to inhibit the growth of lung cancer cells.

- SAHA inhibited histone deacetylase in normal, precancerous and cancerous cells, but inhibited growth in only the cancer cells.
- Inhibition of cell proliferation by which SAHA and valproic acid may involve the induction of p21; The induction of apoptosis by SAHA and valproic acid includes activation of the mitochondrial pathway (activation of caspase 9 and caspase 3); SAHA also activated Fas death receptor mediated apoptosis pathway, which involves caspase 8.
- SAHA, 5-aza-CdR and their combinations inhibited the growth of human NSCLC cells implanted subcutaneously in athymic nude mice, demonstrating antitumor activities of SAHA and 5-aza-CdR alone and in combination.
- We discovered subsets of genes and network that are modulated by SAHA and 5-aza-CdR and by their combination.

Reportable Outcomes

Articles published or in progress:

1. Ondate N, Lotan R. Suppression of DNA methyltransferase 1 levels in head and neck squamous carcinoma cells using small interfering RNA results in growth inhibition and increase in Cdk inhibitor p21. *Int. J. Oncology*, 26: 757-761, 2005.
2. Gillenwater AM, Zhong M, Lotan R. Induction of apoptosis in head and neck squamous carcinoma cells by the histone deacetylase inhibitor SAHA is mediated by both mitochondrial and Fas (CD95) signaling. (ready for submission)
3. Fujimoto JY, Men T, Lee JJ, Kong M, Ayers GD, Hong WK, Lotan R. Additive and synergistic effects of 5-aza-2'-deoxycytidine and suberoylanilide hydroxamic acid (SAHA) on human lung carcinoma cells in vitro and in vivo. (in preparation)
4. Zhong M, Gillenwater A, Lotan R. Valproic acid induces growth inhibition and apoptosis in head and neck squamous carcinoma cell lines. (in preparation)

Meeting Abstracts:

1. Fujimoto JY, Hong WK, Lotan R. Antineoplastic action of 5-aza-2'-deoxycytidine and suberoylanilide hydroxamic acid (SAHA) on human lung carcinoma cells. *Proc AACR 46: #1820*, 2005.
2. Zhong M, Gillenwater A, Lotan R. Valproic acid induces growth inhibition and apoptosis in head and neck squamous carcinoma cell lines. *Proc AACR 47: #5494*, 2006.

Conclusions

Our data demonstrate that the epigenetic modulators 5-aza-CdR, SAHA, and valproic acid exert growth inhibitory and apoptosis-inducing activity in HNSCC cells and premalignant and malignant lung epithelial cells *in vitro*, and SAHA and 5-aza-CdR are also active *in vivo* especially in combination. These results strongly support that this combination should be investigated further for therapeutic use in patients with this malignancy.

References

1. Baylin SB, Ohm JE. Epigenetic gene silencing in cancer - a mechanism for early oncogenic pathway addiction? *Nat Rev Cancer*. 2006;6:107-16.
2. Kelly WK, Marks PA. Drug insight: Histone deacetylase inhibitors--development of the new targeted anticancer agent suberoylanilide hydroxamic acid. *Nat Clin Pract Oncol*. 2005;2:150-7
3. Gore SD, Baylin S, Sugar E, Carraway H, Miller CB, Carducci M, Grever M, Galm O, Dausess T, Karp JE, Rudek MA, Zhao M, Smith BD, Manning J, Jiemjit A, Dover G, Mays A, Zwiebel J, Murgu A, Weng LJ, Herman JG. Combined DNA methyltransferase and histone deacetylase inhibition in the treatment of myeloid neoplasms. *Cancer Res*. 2006;66:6361-9.

Project 6: The Role of the Farnesyl Transferase Inhibitor SCH66336 in Treatment of Carcinoma of the Lung and Aerodigestive Tract

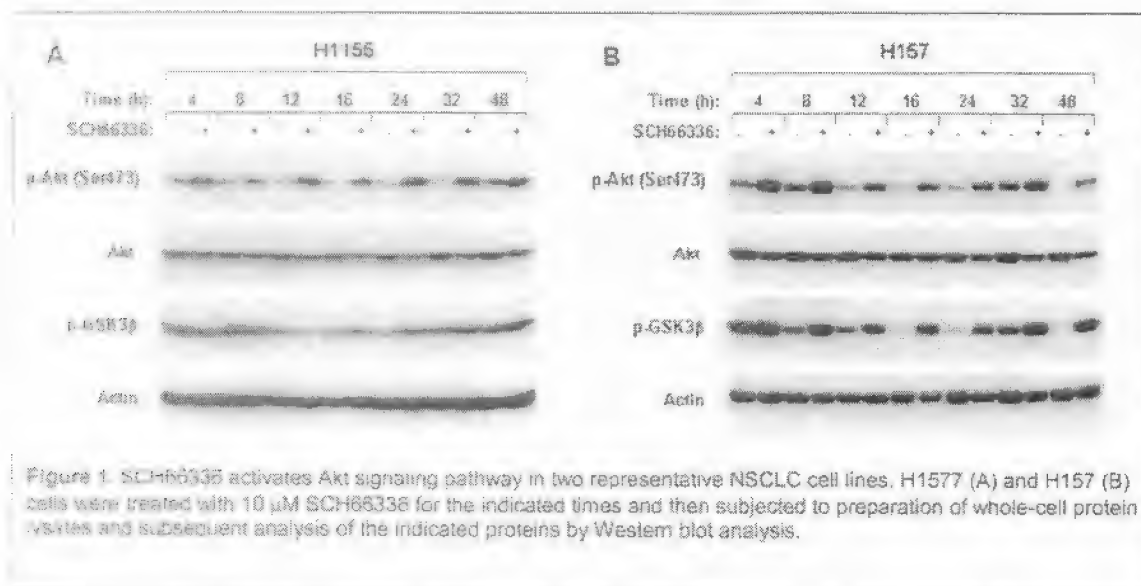
(Project leader: Fadlo Khuri, M.D.; Co-Leader: Shi-Young Sun, Ph.D.)

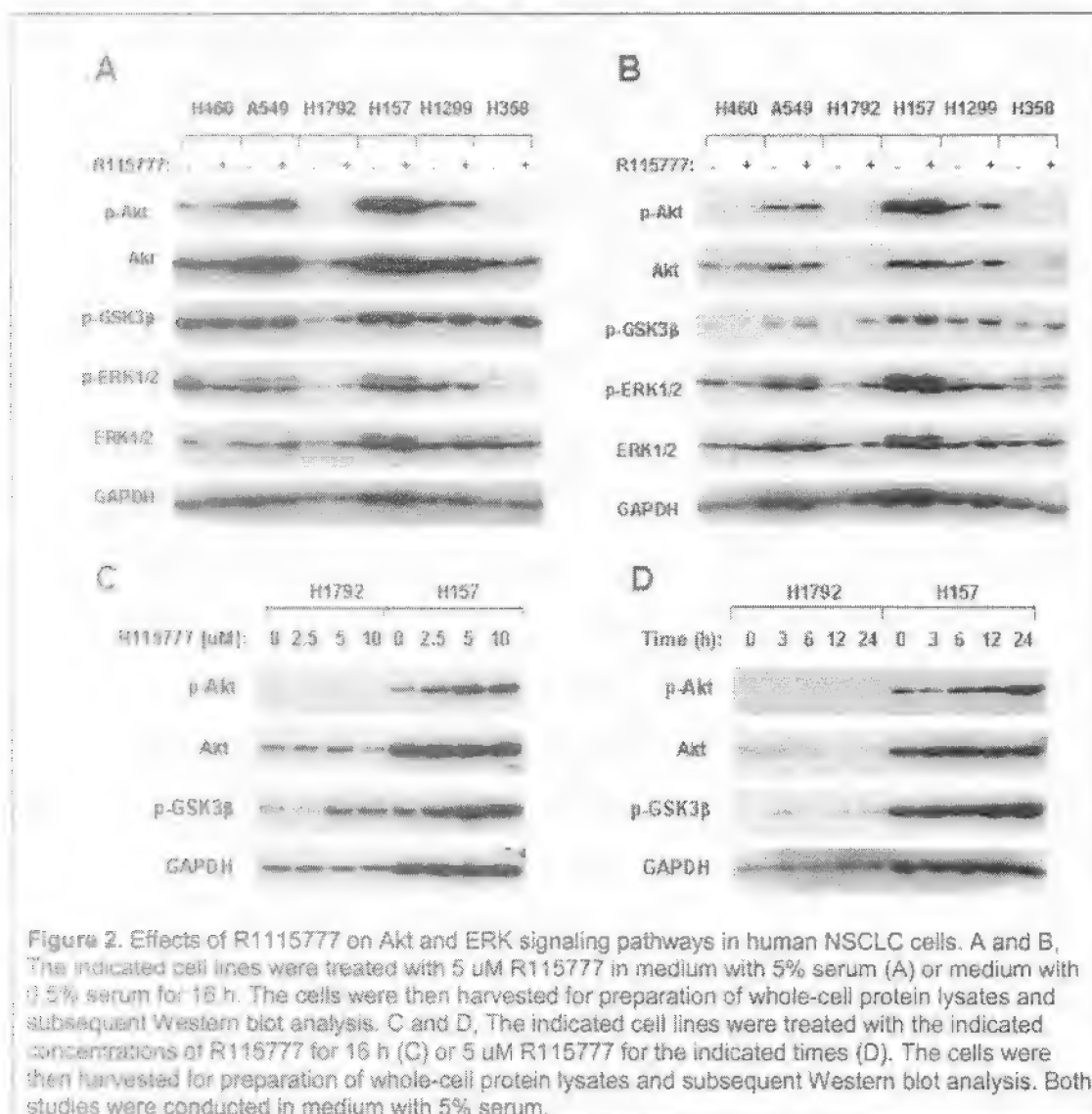
The RAS oncoprotein is an important transforming protein in many cancers, acting through several pathways downstream of RAS, effecting multiple downstream molecules including the raf-MAP kinase pathways, the PI3 kinase pathway, and by promoting angiogenesis and inhibiting apoptosis. In order to be activated, RAS requires farnesylation to be tethered to the cytoplasmic side of the plasma membrane and remain constitutively activated. The goal of the project is to investigate the molecular mechanisms through which the farnesyl transferase inhibitors (e.g., SCH66336) act in the lung and aerodigestive tract carcinomas.

Summary of Research Findings:

Specific Aim 1: To evaluate effects of SCH66336 on Ras downstream signaling and apoptosis and angiogenesis in lung and head and neck squamous cell carcinoma cells

Findings: We examined the effects of SCH66336 on Akt and Raf/ERK signaling pathways in a panel of human NSCLC cells and found that SCH66336 did not decrease the levels of p-Akt, Akt, Raf-1, p-ERK1/ERK2, and ERK1/ERK2. In at least two of the cell lines, we found that SCH66336 in fact increased p-Akt and p-GSK3 β (a well-known substrate of Akt) levels in a dose- and time-dependent manner (Fig. 1). We also examined the effects of another FTI called R115777 on these signaling pathways. Interestingly, we found that this FTI did not decrease the levels of p-Akt, Akt, Raf-1, p-ERK1/ERK2, and ERK1/ERK2 either. Like SCH66336, R115777 actually increased p-Akt and p-GSK3 β levels in some NSCLC cell lines (Fig. 2). These results suggest that inhibition of protein farnesylation in some NSCLC cell lines activates Akt survival signaling pathway. Detailed findings have been published in *Cancer Biology & Therapy* (Sun et al, 2004). We are currently investigating whether FTI-induced Akt activation leads to cell resistance to FTIs.





Specific Aim 2: To evaluate effects of SCH66336 on protein expression in lung and head and neck cancer cell lines and determine roles of affected proteins as biomarkers and effectors of response to treatment with SCH66336

We proposed to evaluate the effects of SCH66336 on protein expression in both lung and head and neck cancer cell lines by identifying proteins whose expression is altered by treatment with SCH66336 and determining the role of these proteins as biomarkers and effectors of response to treatment with farnesyl transferase inhibitors.

Findings:

FTIs modulate the expression of DR5 that contributes to FTI-induced apoptosis. The expression of death receptor 5 (DR5) is inducible by certain therapeutic agents and its activation by overexpression or ligation with its ligand triggers apoptosis. Our study showed that SCH66336 activated caspase-8 and its downstream caspases, whereas the caspase-8 specific inhibitor Z-IETD-FMK or small interfering RNA (siRNA) abrogated SCH66336-induced apoptosis. Moreover, SCH66336 increased both total levels of DR5 expression and cell surface distribution of DR5 in human NSCLC cells as well as other types of cancer cell lines. The combination of SCH66336 with its ligand tumor necrosis factor-related apoptosis-inducing ligand (TRAIL) further enhanced induction of

apoptosis. Overexpression of a dominant-negative FADD mutant or silencing of DR5 expression using a siRNA attenuated SCH66336-induced apoptosis. These results indicate a critical role of DR5-mediated extrinsic apoptotic pathway in SCH66336-induced apoptosis. Moreover, the potencies of FTIs on DR5 induction are associated with their abilities to inhibit protein farnesylation and to induce apoptosis. Collectively, we conclude that FTIs, particularly SCH66336, induce DR5 expression leading to a caspase-8-mediated apoptosis and enhancement of TRAIL-induced apoptosis. These effects may be related to their farnesylation inhibitory activity. Some of the findings have been published in *Cancer Research* (Sun et al, 2005). The rest of the work was submitted to *Oncogene* for publication (Sun et al, 2006).

Related to this finding, we discovered that another FTI R115777 also upregulated DR5 expression and enhanced TRAIL-induced apoptosis in human NSCLC cells. Silencing of DR5 expression abrogated R115777-induced enhancement of TRAIL-induced apoptosis, suggesting that R115777 enhances TRAIL-induced apoptosis through DR5 upregulation. Additional experiments showed that R115777 also increased DR5 mRNA levels, suggesting that R115777 increases DR5 expression at the transcriptional level. Collectively, we have identified DR5 as a protein that is regulated by FTIs and plays an important role in mediating FTI-induced apoptosis. A manuscript has been completed and is undergoing review by Johnson & Johnson (Qiu et al, 2006).

FTIs modulate c-FLIP expression. Moreover, we found that FTIs increased the levels of c-FLIP, a protein that inhibits death receptor-mediated apoptosis, in some NSCLC cell lines, particularly those with Akt activation upon FTI treatment. However, FTIs decreased FLIP levels in other NSCLC cell lines. It seems that cells exhibiting increased FLIP upon FTI treatment were generally less sensitive to FTI-induced apoptosis than those with decreased FLIP on FTI treatment. The impact of FLIP modulation on FTI-induced apoptosis in human NSCLC cells is under study now. Nevertheless, FLIP as another protein modulated by FTIs, further supports the importance of death receptor-mediated extrinsic apoptotic pathway in FTI-induced apoptosis.

FTIs modulate CHOP/GADD153 expression that mediates FTI-induced DR5 expression. One of our important findings is that FTIs upregulate the expression of death receptor 5 (DR5), which contributes to FTI-mediated apoptosis in human lung cancer cells. To demonstrate the mechanism by which FTIs induce DR5 expression, we determined whether FTIs increased the activity of DR5 promoter. Indeed, we found that both SCH66336 (Lonafarnib, LNF) and R115777 enhanced DR5 promoter activity, indicating that FTIs upregulate DR5 expression at the transcriptional levels. Using deletion strategy, we generated reporter constructs with different lengths of DR5 promoter region to narrow down the possible region that FTIs work on. By transient transfection and luciferase activity assay, we identified the region between -373 and -240 critical for SCH66336 transactivation of DR5 promoter because reporter construct with 240 bp DR5 promoter region lost luciferase activity upon SCH66336 treatment (Figs. 3A and 3B). It has been documented that the transcription factor CHOP (GADD153) mediates DR5 transactivation in response to certain cancer therapeutic agents. Coincidentally, we found that CHOP binding site locates in this region (between -373 and -240). To demonstrate the role of CHOP in FTI-induced DR5 expression, we obtained reported constructs with wild-type CHOP binding site (w), mutant CHOP binding site (CHOPm), mutant Elk-1 binding site (Elk-1m), and mutant NF- κ B binding site (NF- κ Bm), respectively. In the luciferase assay, we found that only CHOPm reported construct did not show any luciferase activity upon treatment with SCH66336, indicating that CHOP binding site indeed is responsible for SCH66336-mediated DR5 transactivation (Figs. 3C and 3D).

Next, we examined whether FTIs modulated the expression of CHOP. By western blot analysis, we found that SCH66336 increased the levels of CHOP protein in a time-dependent manner, which was accompanied with DR5 upregulation. The upregulation of both CHOP and DR5 expression started at 3 h post SCH66336 treatment and was sustained up to 24 h. We detected cleavage of caspase-8,

caspase-3 and PARP at 12 h after SCH66336 treatment (Fig. 4). Thus, we conclude that CHOP induction, like DR5 upregulation, is an early event ahead of caspase activation in cells exposed to SCH66336. Since both DR5 and CHOP expression are regulated by JNK activation, we then examined modulatory effects of SCH66336 on the expression of CHOP and DR5 in the presence of the JNK inhibitor SP600125. SP600125, at concentrations that abolished SCH66336-induced increase in c-Jun phosphorylation, failed to inhibit SCH66336-induced CHOP expression, but partially diminished SCH66336's effect on DR5 induction in both H1792 and H157 cells (Fig. 5). These results indicate that JNK activation partially participates in SCH66336-induced DR5 expression, but not in CHOP upregulation.

At last, we determined whether SCH66336 upregulates DR5 expression through a CHOP-dependent mechanism. To this end, we silenced CHOP expression using CHOP siRNA and then examined its impact on SCH66336-induced DR5 expression. SCH66336 could induce DR5 expression in cells transfected with control siRNA. However, in cells transfected with CHOP siRNA, CHOP induction was blocked and accordingly DR5 induction was substantially inhibited upon exposure to SCH66336 (Fig. 5). In agreement, we found that SCH66336-induced increase in cell surface DR5 was also diminished. Therefore, these results indicate that CHOP mediates SCH66336-induced DR5 upregulation.

This work is close to completion and is being summarized in a manuscript once we finish all experiments (Zou et al, 2006).

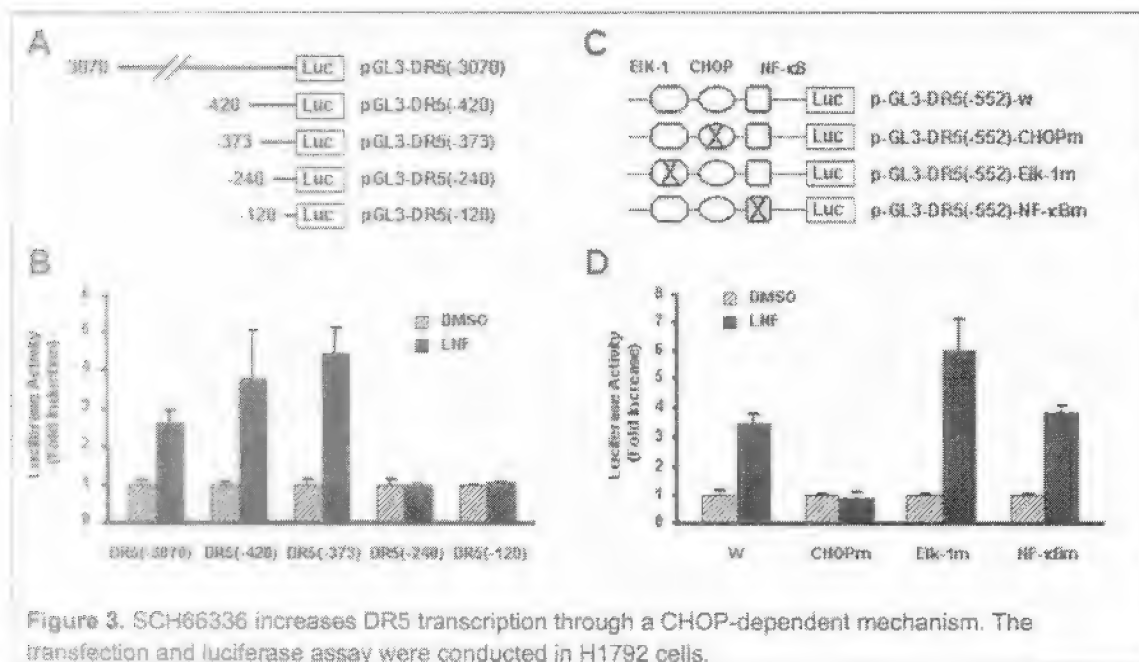
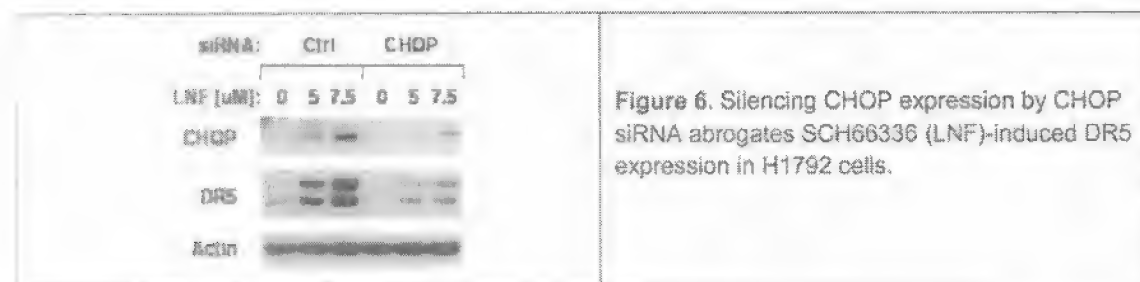
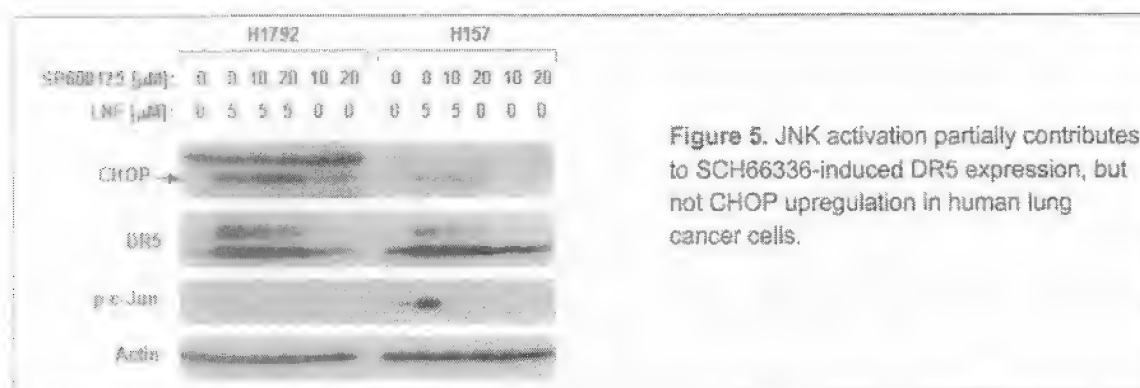
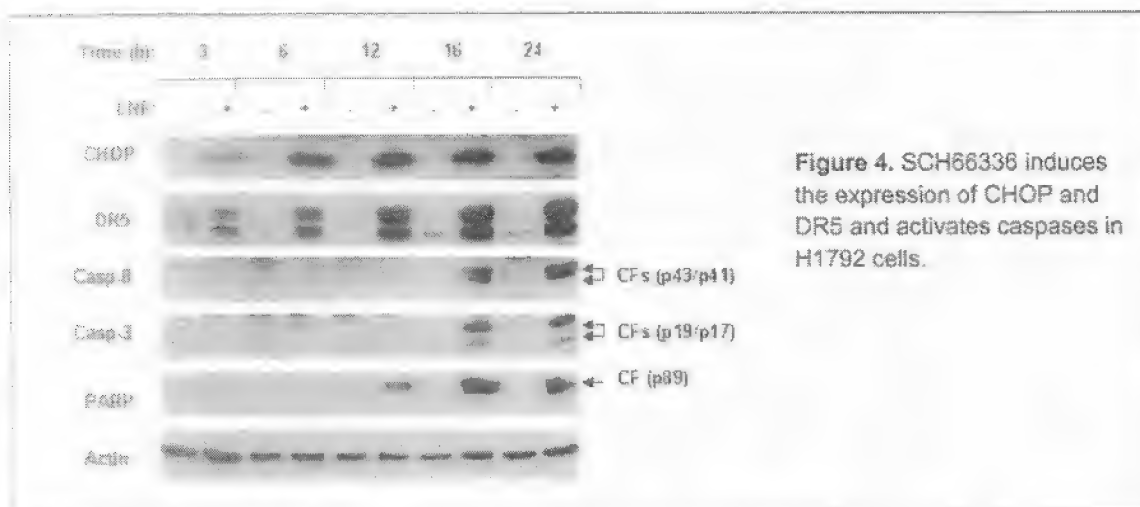


Figure 3. SCH66336 increases DR5 transcription through a CHOP-dependent mechanism. The transfection and luciferase assay were conducted in H1792 cells.



FTIs augment TRAIL-induced apoptosis. Based on our important findings, we hypothesized that FTIs would be able to enhance TRAIL (tumor necrosis factor-related apoptosis-inducing ligand)-induced apoptosis. Indeed, we found that both SCH66336 and R115777, when combined with TRAIL, exhibited augmented apoptosis-inducing effects in human lung cancer cells lines (Fig. 7). This effect was associated with DR5 upregulation because silencing of DR5 expression attenuated induction of apoptosis by the combination of a FTI and TRAIL (Fig. 8). Since a single agent FTI has limited activity in clinical trials, combination of a FTI with other agents may improve FTIs' efficacy. From this point of view, our findings may have immediate translational significance, particularly when TRAIL is currently being tested in phase I trials.

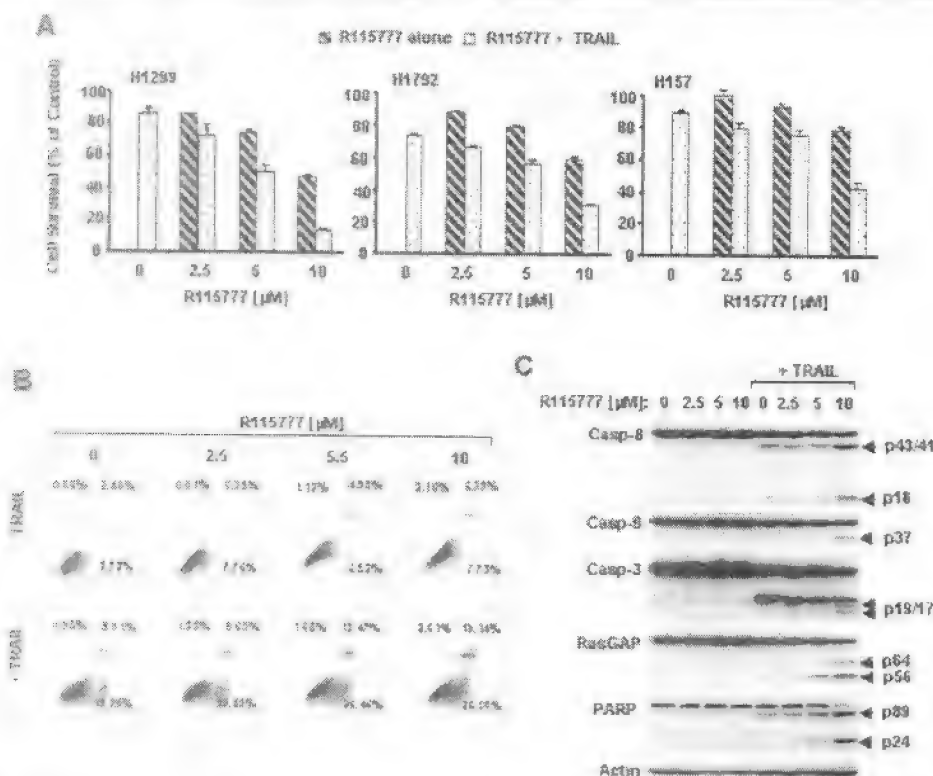


Figure 7. R115777 enhances TRAIL-induced apoptotic cell death in human lung cancer cells. A, cell survival evaluated by SRB assay; B, Apoptosis evaluated by Annexin V staining; and C, Caspase activation by Western blot analysis.

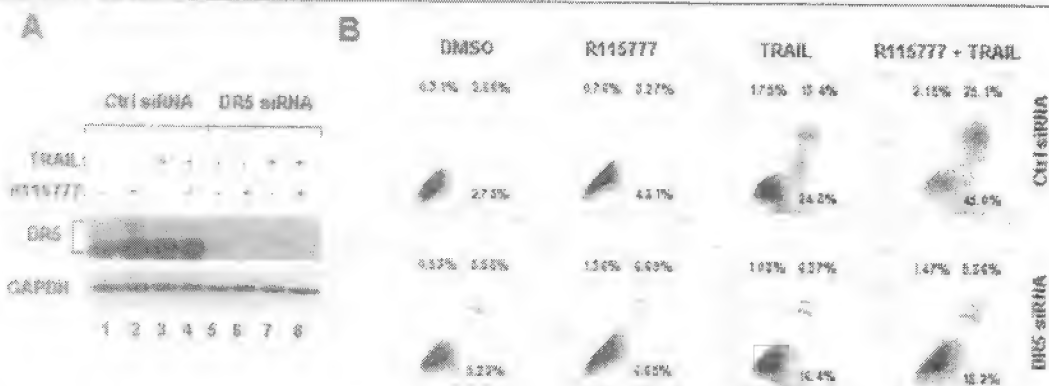


Figure 8. Silencing of DR5 expression abrogates augmented induction of apoptosis by R115777 and TRAIL combination. A, DR5 expression evaluated by Western blot analysis. B, Apoptosis measured by Annexin V staining.

Specific Aim 3: To evaluate the efficacy of SCH66336 as an inhibitor of growth and an inducer of apoptosis in an orthotopic model of head and neck squamous cell carcinoma

Since SCH66336 (lonafarnib) and other farnesyl transferase inhibitors (R115777/Tipifarnib) failed to demonstrate either single agent efficacy in lung or aerodigestive cancers as a single agent in the clinic, or efficacy in combination chemotherapy in the front-line treatment of non-small cell lung cancer (Adjei et al, 2003), we thus decided to change our future focus on the efficacy of the combination of

FTIs with other agents such as PI3K inhibitors or Akt inhibitors in animal models of lung and aerodigestive cancers. We hypothesize that blockage of Akt activation induced by FTIs can enhance the FTI's anticancer efficacy.

Specific Aim 4: To investigate mechanisms of farnesyl transferase inhibitor-induced apoptosis in combination with retinoids such as 4-HPR or taxanes such as docetaxel and paclitaxel in non-small cell lung cancer and squamous head and neck cancer cell lines

Findings: In collaboration with Dr. Giannakakou's group at Winship Cancer Institute, we showed that the FTI SCH66336 affected the microtubule cytoskeleton resulting in microtubule bundle formation, increased microtubule stabilization and acetylation, and suppression of microtubule dynamics. Notably, treatment with the combination of low doses of SCH66336 with paclitaxel markedly enhanced tubulin acetylation (a marker of microtubule stability) as compared with either drug alone. This synergistic effect correlated with FT inhibition and was accompanied by a synergistic increase in mitotic arrest and cell death. Mechanistically, we showed that the combination of SCH66336 and paclitaxel inhibited the *in vitro* deacetylating activity of the only known tubulin deacetylase, histone deacetylase 6 (HDAC6). In addition, the SCH66336/taxane combination was synergistic only in cell lines expressing the wild-type HDAC6, but not a catalytic-mutant HDAC6, revealing that functional HDAC6 is required for the synergy of SCH66336 with taxanes. Furthermore, tubacin, a specific HDAC6 inhibitor, synergistically enhanced tubulin acetylation in combination with paclitaxel, similar to the combination of SCH66336 and paclitaxel. Taken together, these data suggest a relationship between FT inhibition, HDAC6 function, and cell death, providing insight into the putative molecular basis of the SCH66336/taxane synergistic antiproliferative combination.

In addition, we conducted a phase I study of farnesyl transferase inhibitor (FTI) SCH66336 with paclitaxel in solid tumors to establish the maximum tolerated dose of lonafarnib, a novel farnesyltransferase inhibitor, in combination with paclitaxel in patients with solid tumors and to characterize the safety, tolerability, dose-limiting toxicity, and pharmacokinetics of this combination regimen. We conclude that when combined with paclitaxel, the recommended dose of lonafarnib for Phase II trials is 100 mg p.o. twice daily with 175 mg/m² of paclitaxel i.v. every 3 weeks. Additional studies of lonafarnib in combination regimens appear warranted, particularly in patients with non-small cell lung cancer. The study was published in *Clinical Cancer Research* (Khuri et al, 2004).

Key Research Accomplishments

- FTIs including SCH66336 and R115777 induce growth arrest and apoptosis independent of Akt and Raf/ERK signaling pathways in human NSCLC cells, and in some NSCLC cell lines, SCH66336 and R115777 instead activate Akt surviving pathways, which may lead to FTI resistance.
- FTIs increase DR5 expression through a CHOP-dependent mechanism that contributes to SCH66336-induced apoptosis and enhances TRAIL-induced apoptosis. Our findings 1) suggest that both DR5 and CHOP can be tested as predictive biomarkers for FTI-based cancer therapy, and 2) warrant the future clinical testing of the combination of a FTI with TRAIL for therapy of human cancer including lung cancer.
- FTIs modulate the expression of FLIP either by decreasing or increasing its expression depending on cell lines.
- The functional HDAC6 is required for the synergy of SCH66336 with taxanes

Reportable Outcomes

Articles published or in progress:

1. Khuri FR, Glisson BS, Kim ES, Meyers ML, Herbst RS, Thall PF, Munden RF, Statkevich YP, Bangert S, Thompson E, Cascino M, Shin DM, Papadimitrakopoulou V, Kurie JM, Kies MS, Lee

1. JS, Fossella FV, Hong WK. Phase I study of farnesyl transferase inhibitor (FTI) SCH66336 with paclitaxel in solid tumors. *Clinical Cancer Research*, 10:2968-76, 2004.
2. Sun S-Y, Zhou Z, Wang R, Khuri FR. The farnesyltransferase inhibitor Lonafarnib induces growth arrest or apoptosis of human lung cancer cells without downregulation of Akt. *Cancer Biology and Therapy*. 3:1092-8, 2004.
3. Sun SY, Liu X, Zou W, Yue P, Zhou Z, Marcus AI, Khuri FR. Activation of the death receptor 5-mediated extrinsic apoptotic pathway contributes to farnesyltransferase inhibitor-induced apoptosis in human lung cancer cells. *Oncogene* (submitted), 2006.
4. Qiu Y, Liu X, Yue P, Lonial S, Khuri RK, Sun SY. The farnesyltransferase inhibitor R115777 upregulates DR5 expression and enhances TRAIL-induced apoptosis in human lung cancer cells. (Manuscript completed and undergoing review by Johnson & Johnson).
5. Zou W, Yue P, Khuri FR, Sun SY. The farnesyltransferase inhibitor Lonafarnib induces DR5 expression through a CHOP/GADD153-dependent mechanism. (in preparation)

Project-generated grants:

NCI Lung Cancer Program Project Grant (P01): "Targeting cell signaling in lung cancer to enhance therapeutic efficacy." PI: Fadlo R. Khuri. Duration: 04/01/06 -03/31/11.

Conclusion

We conclude that farnesyl transferase inhibitors SCH66336 and R115777 induce apoptosis by increasing DR5 expression and TRAIL-induced apoptosis, independent of downregulating Akt and Raf/ERK pathways, and DR5, c-FLIP, and CHOP are FTI-regulated proteins. The synergistic effect of SCH66336 with taxanes required the functional HDAC6.

Project 7: Mechanisms and Therapeutic Applications of the Tumor Suppressor Gene *FUS1* in Lung Cancer

(Project Leader: Lin Ji, Ph.D., Co-Leader: Rajagopal Ramesh, Ph.D.)

Lung cancer is the leading cause of cancer-related death in the world. Tumor suppressor genes (TSGs) play a major role in the pathogenesis of human cancers. Genetic alterations and allelic losses on the short arm of chromosome 3 (3p) are the most frequent and earliest cancer abnormalities detected in human lung cancers. The novel *FUS1* TSG was one of the candidate TSGs identified in a 120-kb homozygous-deletion region in human chromosome 3p21.3. In this project, the overall goal is to develop non-viral plasmid vectors and liposome-mediated therapeutic tumor suppressor gene delivery for molecular therapy for lung cancer.

Summary of Research Findings:

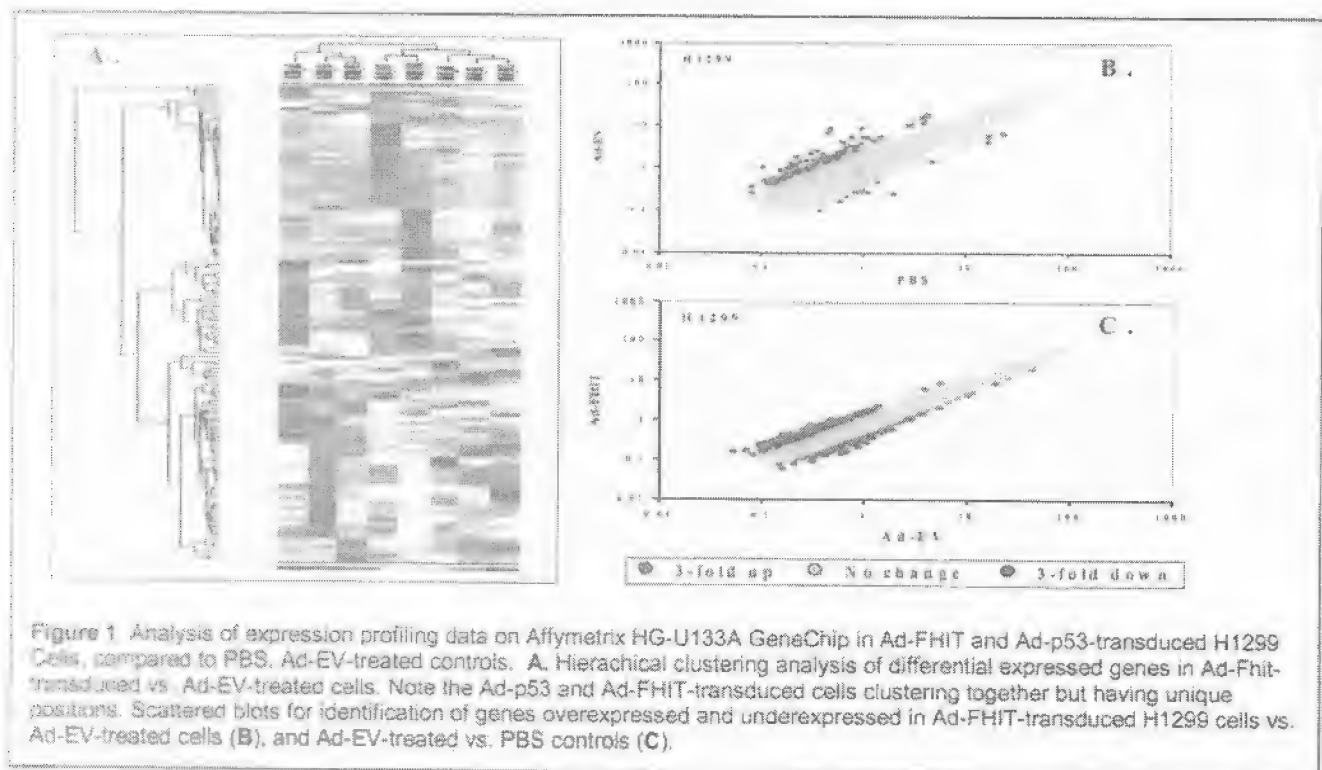
Specific Aim 7.1: To determine the global molecular changes and cellular responses to *FUS1*-mediated tumor-suppressor activities in human NSCLC cells by high throughput gene and protein expression profiling.

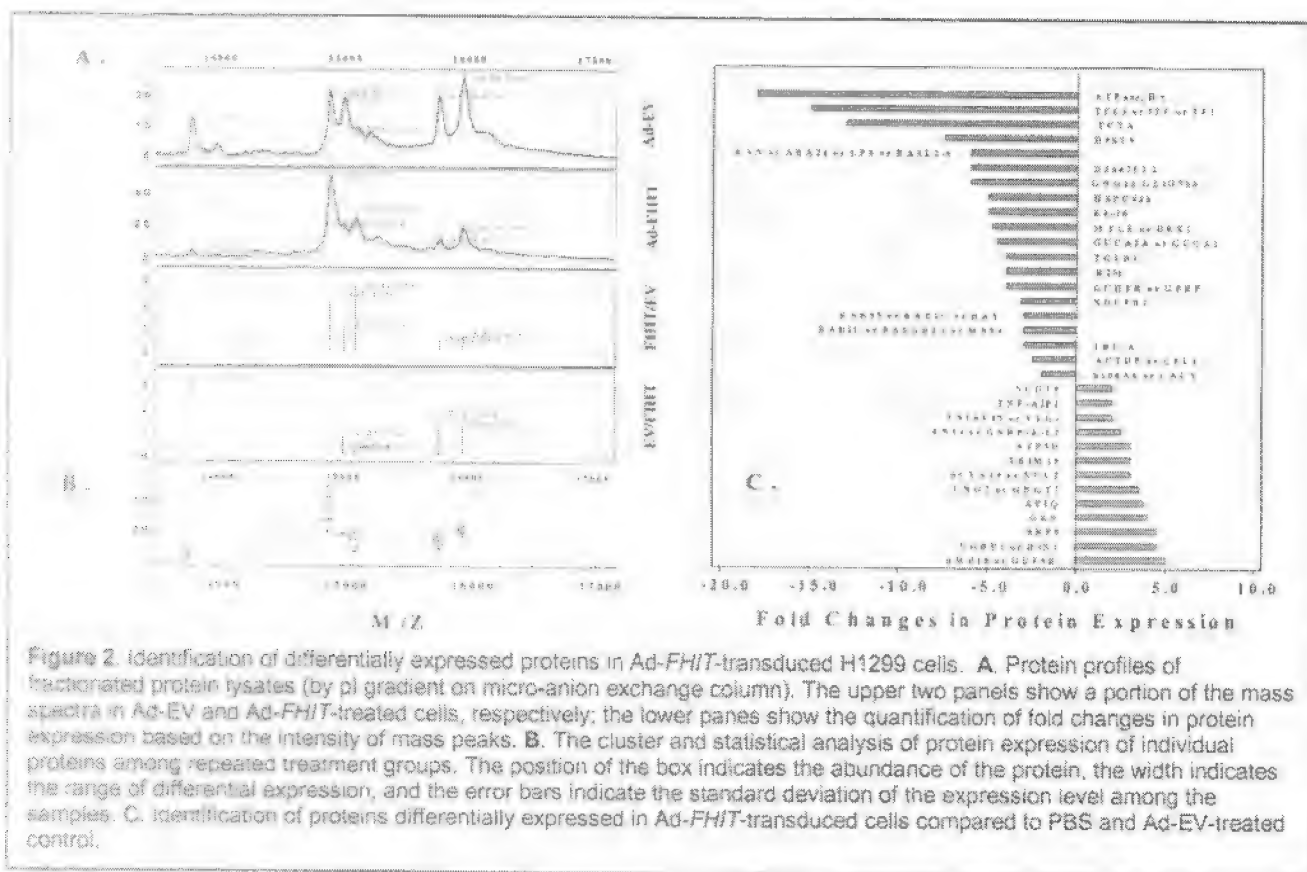
The advanced technologies of functional genomics—DNA microarrays and ProteinChip arrays—and a novel, inducible expression system are used to determine the gene and protein expression patterns mediated by overexpression of *FUS1* in Ad-*FUS1*-transduced NSCLC cells or by expression of *FUS1* at a physiological level. The specific targets of *FUS1* will be identified by comparison of the gene and protein expression profiles, and proteins of interest will be isolated. Since *FUS1* is a newly identified novel 3p21.3 tumor suppressor gene, and biological function and molecular mechanism of *FUS1*-mediated tumor suppressor activities are unknown, we first used the well-studied p53 and a novel FHIT tumor suppressor gene (located at 3p14.2 region)-mediated tumor as a model system for the development and validation of the technology.

7.1.1. Profiling technology development using Ad-FHIT-transduced NSCLC Cells as a Model System. We used a complementary gene and protein expression profiling with DNA microarray and ProteinChip technologies to quantitatively monitor cellular changes in gene and protein expression and discover the molecular targets of the novel FHIT TSG in non-small cell lung carcinoma (NSCLC) cells. We performed gene expression profiling analysis, using the Affymetrix HG-U133A GeneChips, in Ad-FHIT-transduced NSCLC H1299 and A549 cells, compared with those of PBS-treated mock and empty vector (Ad-EV) or Ad-LacZ-treated negative controls.

Findings: A comparative analysis of the gene and protein expression profiling revealed several unique cellular targets and signaling pathways involved in FHIT tumor suppressing activity, including the significantly down-regulated expression of proteins in the Ras/Rho GTPase super-family, the cytoskeleton- and tubulin-forming components, and the growth factors and the up-regulated protein mediators in cell death and apoptosis pathways (Fig. 1 and Fig. 2). Our data demonstrated that the complementary gene and protein expression technology is a powerful tool for generation of hypothesis and for identification of specific cellular targets and signaling pathways mediated by a specific gene product in a complex biological network.

Next, we developed a novel two- dimensional liquid chromatography (2D-LC) method for the fractionation and separation of crude protein lysates and for protein profiling and identification using a ProteinChip Array-based surface enhanced laser deposition/ionization time of flight mass spectrometry (SELDI-TOF-MS). For the 1st D-LC, cell lysates were fractionated based on the pI values of proteins by FPLC with a chroma focusing Mono-P column. The pI-fractionated samples were either directly applied protein profiling on CM10 and Q10 ProteinChip arrays by SELDI-MS or subjected to the 2nd D-LC, using a Non-porous reverse phase (NP-RP) column by HPLC, for further protein separation and identification.

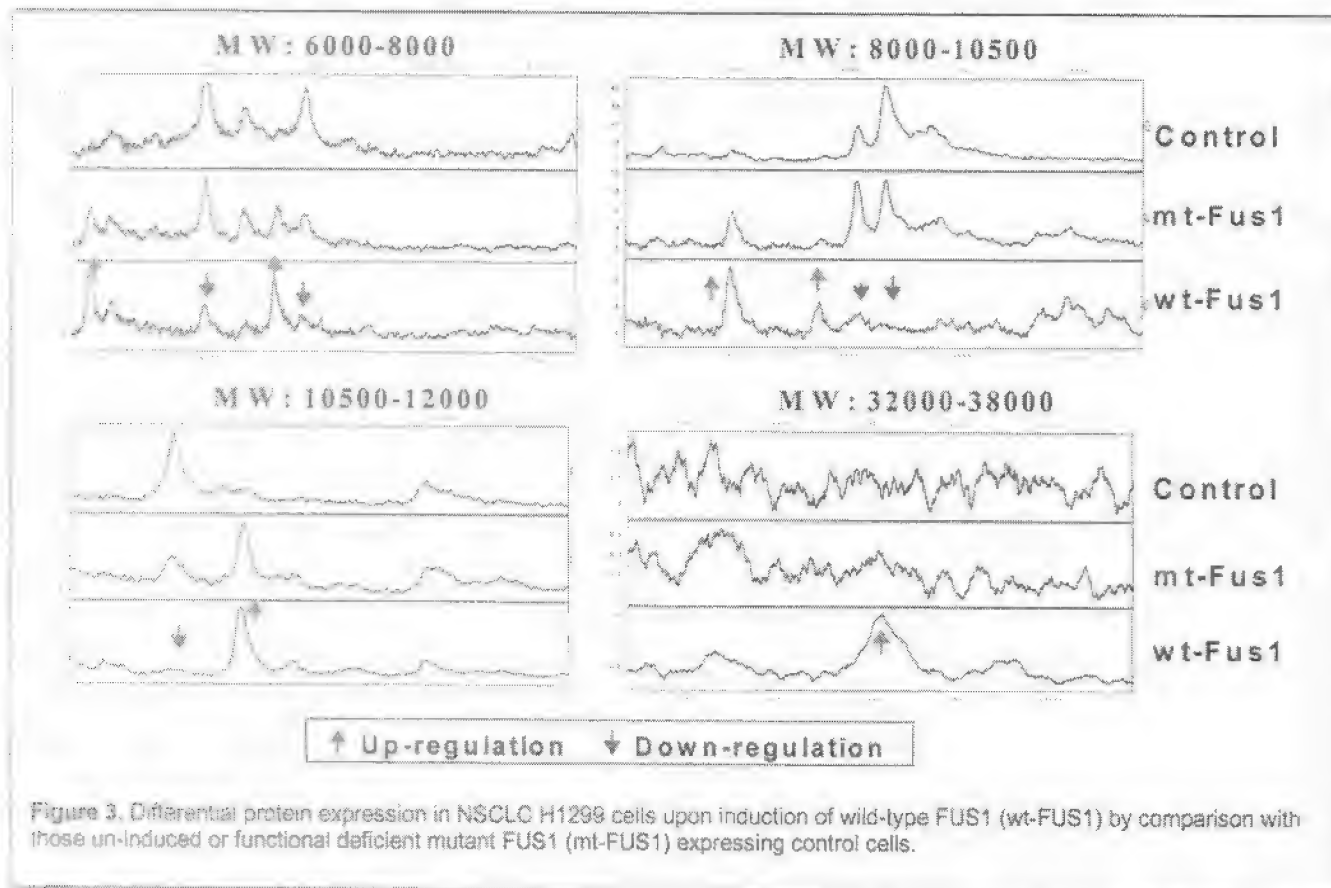




7.1.2. Gene and Protein Expression Profiling in FUS1 expressing NSCLC Cells. We used DNA microarrays and ProteinChip arrays and an inducible-FUS1 expression system to determine the gene and protein expression patterns mediated by induction of *FUS1* in NSCLC cells at either a therapeutic or physiological level. For this purpose, we have established FUS1-stable transfectants of NSCLC cell lines, which allow us to measure gene and protein expression changes mediated by FUS1 expression under physiological condition.

Findings: The specific targets of FUS1 were identified by comparison of the gene and protein expression profiles, and proteins of interest were isolated. From protein expression profiles, we have been able to detect more than 50 protein peaks that represent the differentially expressed protein species in response to the activation of FUS1 protein in these lung cancer cells. Some examples of protein profiles are shown in Figure 3.

We have also performed gene expression profiling simultaneously on RNA samples prepared from the same inducible FUS1-expression NSCLC cells as used for protein profiling. We used new Illumina Sentrix BeadChips (Illumina Inc., San Diego) for whole-genome expression profiling of multiple samples on a single chip. The Illumina BeadChip holds six whole-genome human samples on one chip, interrogating approximately 48,000 transcripts in each sample from the estimated 30,000 genes in the human genome. Expression of about 210 genes was found to be significantly modulated by the activation of FUS1 in these FUS1-deficient NSCLC cells. We are now in a process to systematically analyze these FUS1-targeted cellular proteins and genes using an integrated bioinformatics tools and biological pathway finding software to elucidate the FUS1-activated biological pathways.



Specific Aim 7.2: To elucidate the molecular mechanism of FUS1 in lung cancer pathogenesis by determining the expression and subcellular localization of the FUS1 protein in human normal lung tissue and tumor samples at various stages of development.

7.2.1. Inactivation of FUS1 in Human Lung Cancer Cells and Primary Tumors. We proposed to use both conventional tissue sections and available tissue arrays to examine the FUS1 expression and cellular localization by immunohistochemical analysis with anti-FUS1 antibodies.

Findings: In our preliminary studies, we examined 40 primary lung cancers and found that mutation of the FUS1 gene was infrequent and there were only a few nonsense mutations and a C-terminal deletion mutation that arose from aberrant mRNA splicing. In addition, we found no evidence for FUS1 promoter region methylation. FUS1 expression has been detected in various normal human tissues, including brain, heart, pancreas, prostate, kidney, and lung, based on quantifying Expressed Sequence Tags (ESTs) in Unigene clusters, as summarized in GeneCards. Although endogenous Fus1 expression could be detected in normal human bronchial epithelial cells and fibroblast cells (WI-38) by immunoblot analysis, and FUS1 mRNA transcription could be seen on Northern blots of RNAs prepared from lung cancer cell lines, we could not detect endogenous Fus1 protein in these lung cancer cell lines on immunoblots using the affinity-purified, anti-Fus1 peptide antibodies developed.

Furthermore, we performed immunohistochemical staining on a set of paired normal lung and lung cancer tissue sections. We found that normal lung epithelial cells express Fus1, but many lung cancer cells (15 out of 20, >70%) did not. We also found that even in those tumor samples with FUS1-positive staining, the staining was not uniformly detectable in all tumor cells. Based on both the lung cancer growth-suppressing properties of the Fus1 protein *in vitro* and in animal models and the observed loss of protein expression in primary tumors and tumor-derived cell lines, we hypothesized

that FUS1 would have to act as a TSG in a haploid sufficient manner (since most primary lung cancers experienced allelic loss in this 3p21.3 region), and that both loss of expression and deficient posttranslational modification of Fus1 protein might lead to loss of its tumor suppression function and lung cancer development.

Since mutation of FUS1 is infrequent and no evidence has been found for methylation or mutation of the FUS1 promoter region in lung cancers, other factors such as haploid sufficiency, low expression, abnormal products arising from aberrant mRNA splicing, and posttranslational modification of Fus1 may play important roles in lung tumorigenesis. We used ACPA analysis with SELDI-TOF-MS to evaluate the protein expression and myristoylation status in primary lung tumor and uninvolved normal lung tissue samples. Molecular analysis of tumors and their precursor lesions requires the isolation of specific cell subpopulations (normal, preneoplastic, and tumors) from a composite background of multiple cell types in tumor-tissue biopsies. This was accomplished with laser-captured microdissection (LCM) technology. To evaluate Fus1 protein expression and posttranslational modifications in human lung tumors and noninvolved tissues, we used LCM combined with appropriate tissue-preparation methods to separate and enrich tumor or noninvolved normal cells, and the resulting separated cell populations (about 500 - 1000 cells) were used for the Fus1-specific ACPA analysis by SELDI-TOF-MS. We found that only myristoylated protein species could be detected in normal cells (13 out of 15, $P = 0.0003$ by a Nonparametric 2x2 contingency table, McNemar Chi-square test), but both the unmyristoylated and myristoylated Fus1 protein were detected in tumor cells (5 out of 15 samples, $P = 0.0442$) as indicated by the precise mass of Fus1 protein on the mass spectra. The mixed status of Fus1 protein in the tumor cells may be a reflection of the tumor-cell molecular heterogeneity. In some tumor samples (7 out of 15 samples, $P = 0.0030$), neither form of Fus1 proteins could be captured, consistent with the immunohistochemical analysis in these tumor and normal tissue samples. The remaining three samples tested were un-resolvable due to the ambiguous spectra (spectra not shown). The difference in the observed Fus1 protein myristoylation status between the normal and the tumor cell populations is significant as indicated by a Nonparametric McNemar Marginal Homogeneity test for the equality of categorical responses from two paired and dependent populations ($P < 0.001$) (Fig. 4).

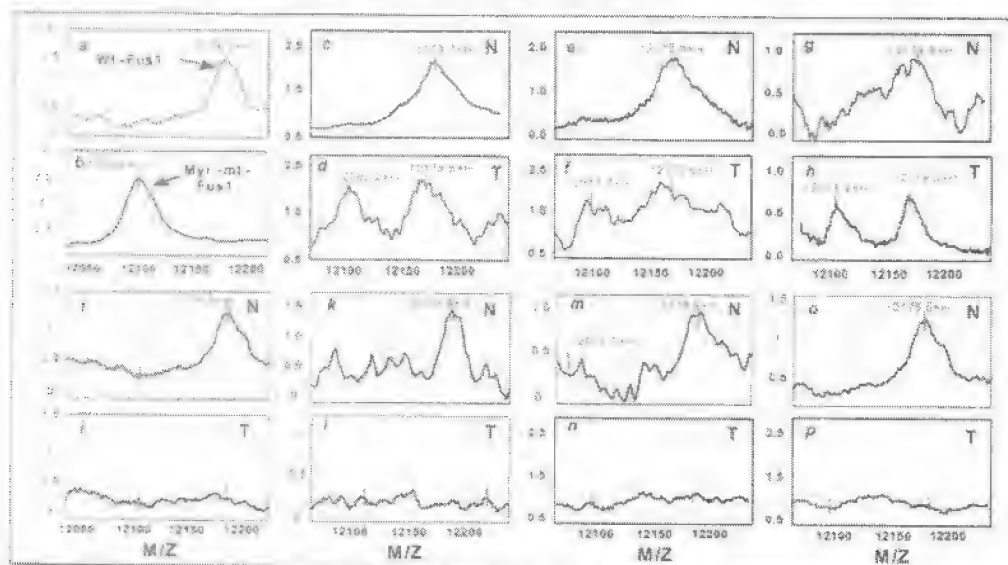
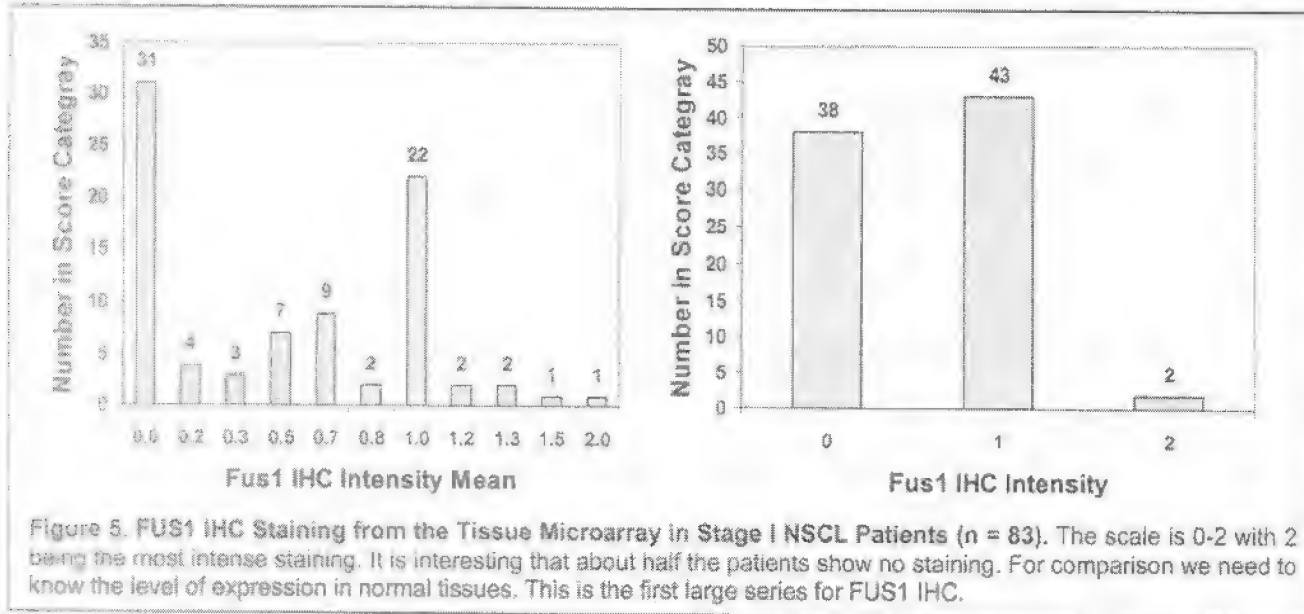


Figure 4. Detection of status Fus1 protein expression and posttranslational modification in LCM-enriched human primary lung tumor (T) and adjacent noninvolved normal (N) cells by ACPA with SELDI-TOF-Mass Spectrometry. The myristoylated Fus1 proteins specifically and precisely detected as a peak with mass of 12174 Da and the unmyristoylated Fus1 with a mass of 12024 Da.

We analyzed FUS1 protein expression on a tissue microarray in primary lung cancer samples in stage I NSCLC patients (Fig. 5). We found that about 45% of these lung tumors showed a complete loss of FUS1 expression, 52% exhibited a marginal low level expression, and only 2 of 83 tumors showed a normal level of FUS1 expression. These results suggest a role of FUS1 as a potential tumor suppressor and in lung cancer development due to the inactivation of FUS1 in primary lung cancer possibly by a mechanism of haploid sufficiency in human chromosome 3p21.3 region.



7.2.2. Study of Molecular Mechanism of FUS1 Tumor Suppressing Function

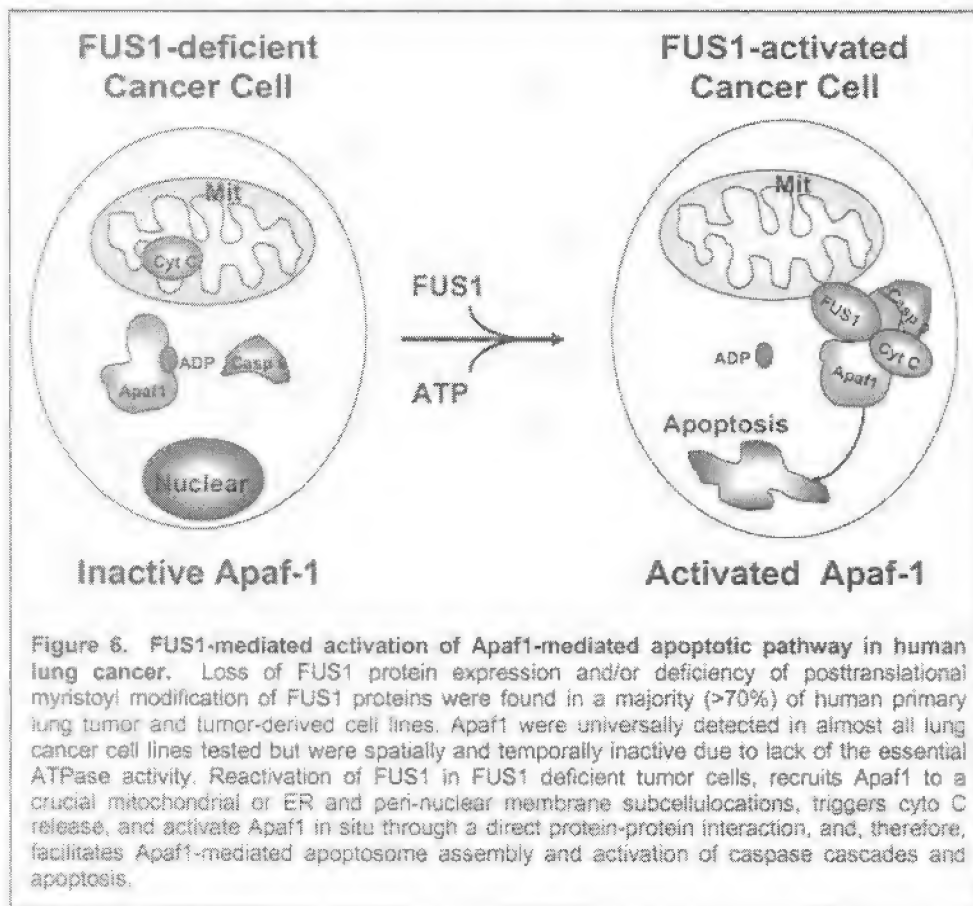
Findings:

a) Posttranslational Myristoylation of FUS1 protein is required for its tumor suppressing function: To study the molecular mechanisms of FUS1 tumor suppressing activities, we used a SELDI-Mass spectrometry analysis on an anti-Fus1-antibody-capture ProteinChip array and identified wild-type Fus1 as an N-myristoylated protein. Loss of expression or a defect of myristoylation of the Fus1 protein was observed in human primary lung cancer and cancer cell lines. A myristoylation-deficient mutant of the Fus1 protein abrogated its ability to inhibit tumor cell-induced clonogenicity *in vitro*, to induce apoptosis in lung tumor cells, and to suppress the growth of tumor xenografts and lung metastases *in vivo*, and rendered it susceptible to rapid proteasome-dependent degradation. Our results show that myristoylation is required for Fus1-mediated tumor-suppressing activity, and suggest a novel mechanism for the inactivation of TSGs in lung cancer and a role for deficient posttranslational modification in TSG-mediated carcinogenesis. Detailed findings were published in Cancer Research (Uno et al, 2004).

b) Interaction of FUS1 and Apaf-1 proteins plays an important role in Apaf-1-mediated mitochondrial apoptosis pathway: We have previously demonstrated that restoration of the wild-type (wt)-FUS1 by recombinant adenoviral vector- or DOTAP-cholesterol (DC)-nanoparticle-mediated gene transfer in 3p21.3-deficient non-small cell lung carcinoma (NSCLC) cells significantly suppressed tumor cell growth by induction of apoptosis and alteration of cell cycle kinetics *in vitro* and *in vivo*. However, the molecular mechanism and signaling pathway involved in the FUS1-mediated apoptosis remained largely unknown. In this study, we aimed to identify the potential cellular targets of FUS1 protein to have an insight into the mechanism of FUS1 function. We have found that FUS1 protein directly interacts with the apoptotic protease-activating factor 1 (Apaf-1) and functions as a key mediator in Apaf-1-mediated apoptosis signaling pathway. Apaf-1 protein expression is universally detected in various lung cancer cell lines but most of them lack FUS1 protein expression. Activation of wt-FUS1 protein in

FUS1-deficient cancer cells recruits cytoplasmic Apaf-1 proteins to the critical mitochondria and perinuclear membranes for apoptosome assembly and apoptosis induction. The apaf-1 protein appeared to be inactive in the FUS1-deficient tumor cells as demonstrated by the lack of the ATPase activity that is essential for the formation of the Apaf1-apoptosome and the activation of caspase-9. Induced or enforced expression of the endogenous or the exogenous FUS1 proteins activates Apaf-1 by induction of its ATPase activity in situ through FUS1-Apaf1 protein interaction, triggers release of

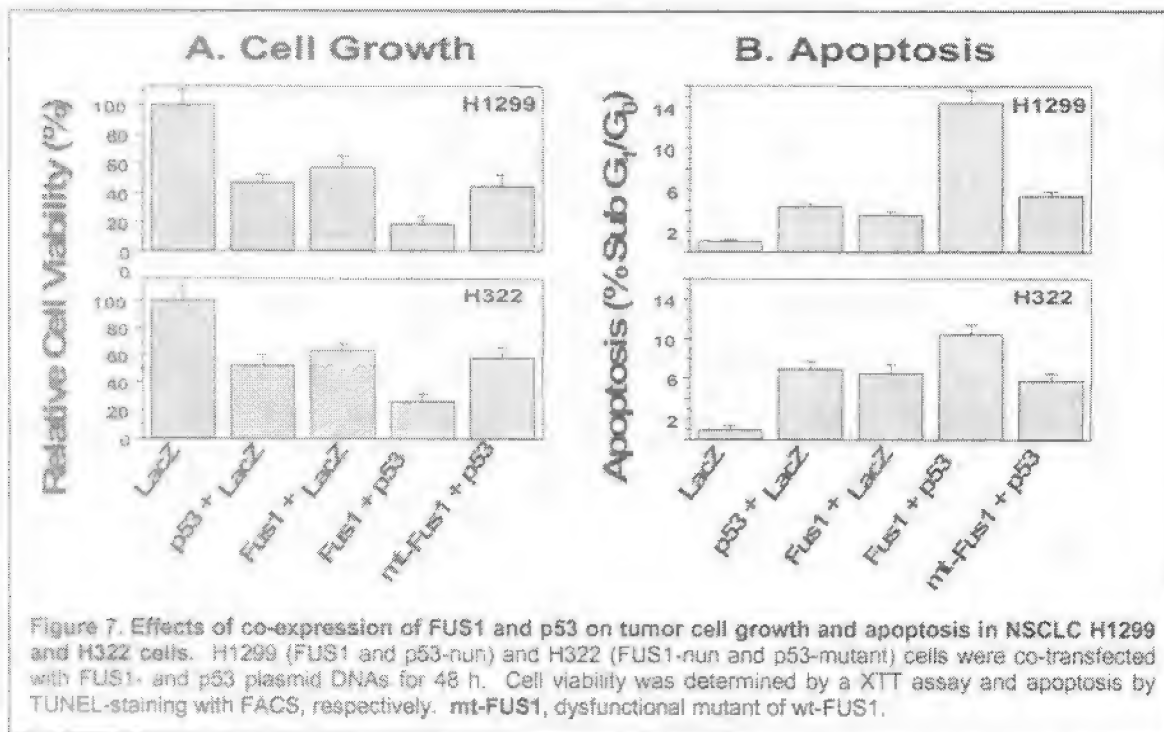
Cytochrome C, activates caspases 9 and 2, and induces apoptosis. These findings are summarized in Figure 6 and detailed in a manuscript submitted for publication in *Nature* (pending revision).



Specific Aim 7.3: To quantitatively evaluate interactions of the FUS1 gene with other 3p21.3 TSGs for their tumor-suppressing activities *in vitro* and *in vivo*.

7.3.1. Synergistic inhibition of NSCLC growth by co-treatment with FUS1- and p53-nanoparticles. We noticed that the tumor suppression function of FUS1 as well as several other potential 3p21.3 TSGs were directly or indirectly dependent of p53 activity (Nishizaki et al, 2004). In this study, we evaluated the combined effects of FUS1 and p53 on tumor cell growth and apoptosis induction in NSCLC cells co-transfected with FUS1- and p53-nanoparticles and explored molecular mechanisms of their mutual actions *in vitro*.

Findings: We found that coexpression of p53 and wild-type Fus1 (wt-Fus1), but not its NH2-myristoylation site mutant (mut-Fus1), synergistically inhibited cell proliferation and induced apoptosis in human NSCLC cells. We also found that the combination expression of wt-Fus1 and p53 enhanced the sensitivities of NSCLC cells to g-radiation and cisplatin treatment (Fig. 7). Furthermore, we found that the synergistic tumor suppression by Fus1 and p53 is implicated in Fus1-mediated augmentation of APAF-1 expression, accumulation of p53 protein, and inactivation of MDM2 in NSCLC cells. Our results therefore revealed a novel molecular mechanism involving Fus1-mediated tumor suppression function and its interaction with other cellular components in the pathways regulating p53 activity. Our findings showed that gene therapy by synergistic tumor suppressors such as Fus1 and p53 in combination with chemotherapy or radiotherapy may be an effective therapeutic strategy for NSCLC and other cancers.



7.3.2. Co-expression of FUS1 and p53 by nanoparticle-mediated gene transfer and treatment with cisplatin enhanced chemotherapeutic efficacy in NSCLC cells. Chemotherapy that is given sequentially or concurrently with external radiation therapy has emerged as a standard for the treatment of locally advanced NSCLC. However, no information is available on the interaction of FUS1 gene transfer with chemotherapy or radiotherapy for their anti-tumor functions in lung cancer. We have evaluated the combined effects of over-expressed FUS1, or FUS1 plus p53, with DNA-damaging agents cisplatin (CDDP) and γ -radiation on anti-tumor activities in human NSCLC cells and explored molecular mechanisms of their mutual actions *in vitro*.

Findings: We found that enforced expression of FUS1, or FUS1 plus p53, enhanced the sensitivities of NSCLC cells to these DNA-damaging agents, and that coexpression of p53 with wild type FUS1 (wt-FUS1), but not its dysfunctional myristoylation-deficient mutant (mut-FUS1), significantly enhanced sensitivities of NSCLC cells to treatment with CDDP or radiation. Moreover, we found that the observed enhancement of chemosensitivity and radiosensitivity by FUS1, or FUS1 plus p53, is associated with FUS1-mediated down-regulation of Mdm2 expression and the resultant accumulation of p53 protein, as well as the up-regulation of Apaf-1 expression in NSCLC cells.

Specific Aim 7.4: To determine the dose-limiting toxicity and biodistribution of the FUS1-lipoplex in a murine model and in a non-human primate model and to evaluate the therapeutic effect of the FUS1-lipoplex in local, solid tumors and experimental metastatic lung tumors.

7.4.1. Construction of plasmid DNA expression vector. We have recently developed a plasmid DNA expression vector system for expressing high levels of transgene in human cells. This vector system consists of a mammalian gene-expression cassette driven by a CMV minimum promoter with an E1 enhancer at the 3' end and a BGH-poly A signal sequence at the 5' end to ensure the efficient expression of the transgene *in vivo*. The kanamycin-resistance gene was chosen as the selectable marker to avoid development of antibiotic-resistance in patients. A minimum pMB1 origin of replication (*ori*) sequence is used to drive high-copy replication and production of the plasmid in the bacterial host strain DH5a. The plasmid backbone is minimal to ensure a higher yield of plasmid DNA production and a higher concentration of recombinant plasmid DNA per plasmid DNA preparation. In the present proposal we intend to use this plasmid DNA vector (pLJ143/KGB) to evaluate the toxicity and therapeutic efficacy of 3p21.3 genes. Production and purification of the plasmid DNA was carried out using standard published techniques.

Findings: Using this plasmid vector we assessed the expression of FUS1 *in vitro* in human lung tumor cells (H1299). The expression of the FUS1 protein in lung tumor cells was confirmed by western blot assay after transfection with DOTAP:cholesterol (DOTAP:Chol) liposome. Transfection of cells with lipoplex resulted in a strong FUS1 specific band (14.3 kD), whereas mock transfection with PBS resulted in undetectable FUS1 protein expression. FUS1 protein expression was observed at 24 and 48 hours after transfection. These results demonstrated that the plasmid DNA vector is efficient in expressing the transgene.

7.4.2. Suppression of Tumor Growth by Intratumoral Delivery of FUS1-lipoplex. To test whether delivery of TSGs (FUS1, and p53) complexed to DOTAP:Chol-liposome (FUS1-lipoplex) resulted in tumor suppression *in vivo*, preliminary therapeutic studies were conducted. Human lung cancer xenografts were established in nude mice by inoculating H1299 tumor cells subcutaneously into the dorsal flanks of nude mice.

Findings: In comparison with treatments with PBS or DOTAP:Chol-CAT complex, treatment with DOTAP:Chol-FUS1 complex significantly suppressed growth of H1299 tumors ($P < 0.01$). Most PBS or DOTAP:Chol-CAT complex treated tumor-bearing mice were euthanized by day 25 because their tumors were necrotic or had exceeded 1.5 cm in diameter. The growth of the tumors treated with DOTAP:Chol-FUS1 complex was well suppressed until day 25 on the average, after which they began to regrow gradually. Immunohistochemical analysis of tumors by TUNEL staining 2 days after the last injection of DOTAP:Chol-FUS1 revealed tumor cell apoptosis (Figure. 8). No significant induction of apoptosis was observed in control tumors. Furthermore, no observable side effects were found in the mice treated with DOTAP:Chol-FUS1 complex (data not shown), suggesting that such treatment was well tolerated.

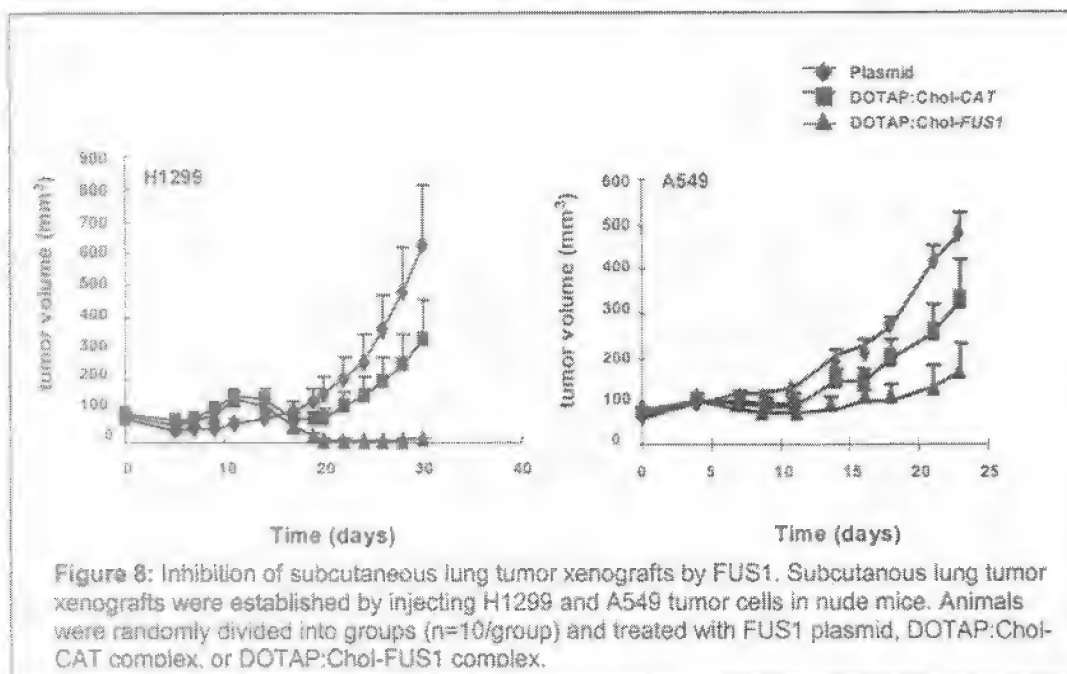


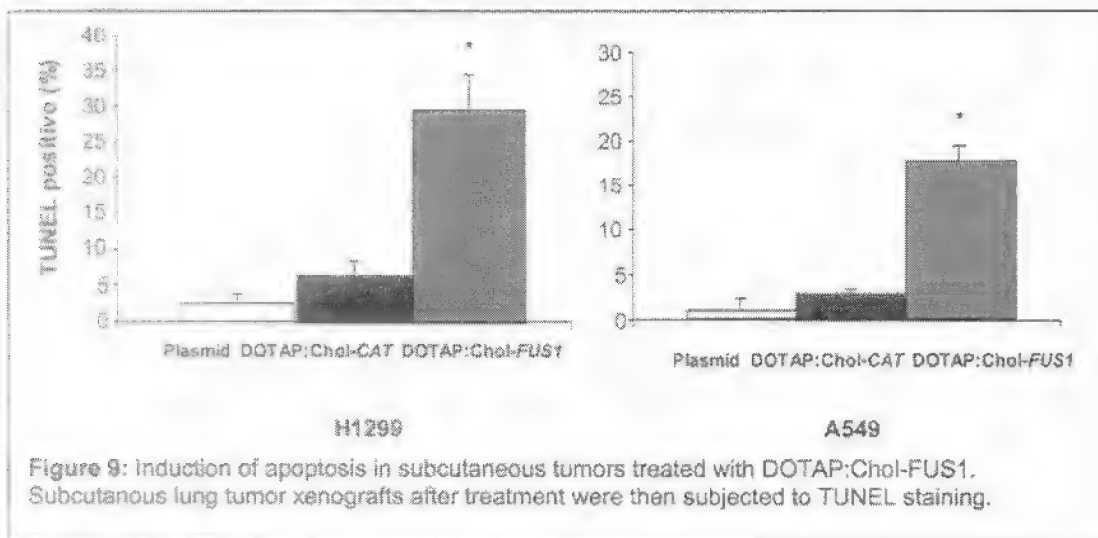
Figure 8: Inhibition of subcutaneous lung tumor xenografts by FUS1. Subcutaneous lung tumor xenografts were established by injecting H1299 and A549 tumor cells in nude mice. Animals were randomly divided into groups (n=10/group) and treated with FUS1 plasmid, DOTAP:Chol-CAT complex, or DOTAP:Chol-FUS1 complex.

Since the main aim of the present proposal is to develop and deliver therapeutic genes via the systemic route, we tested the therapeutic effect of FUS1 gene on experimental lung metastasis and animal survival. Preliminary studies were conducted in a nude mouse model bearing experimental A549 lung metastasis. Treatment with DOTAP:Chol-FUS1 resulted in a significant inhibition ($P = 0.01$) of tumor metastasis as indicated by the reduction in number of tumor nodules in the lungs. Animals treated with PBS, DOTAP:Chol.liposome alone, plasmid DNA alone, and DOTAP:Chol-CAT complex served as controls in these experiments. Correlating with these observations was the prolonged survival of lung tumor bearing animals (mean = 80 days; $P = 0.01$) treated with DOTAP:Chol-FUS1 complex (Fig. 8) compared to animals treated with PBS (mean = 47.8 days), treated with DOTAP:Chol. liposome (mean = 47.2 days), treated plasmid DNA (mean = 51.6 days), and treated with DOTAP:Chol-CAT complex (mean = 47.8 days). These preliminary results indicate the tumor suppressive function of FUS1 gene. Similarly, intravenous treatment subcutaneous H1299 tumor bearing nude mice with PEI-p53 complex demonstrated significant tumor suppression compared to control animals that were treated with PBS, and treated with PEI-b gal complex. These results demonstrate the feasibility of using these vectors for systemic therapy. However, further analyses are warranted, using other xenograft models as well as toxicity studies, prior to testing these vectors and genes in the clinic.

7.4.3 Intratumoral injection of FUS1-lipoplex induces apoptosis of human xenograft tumor. We tested the tumor suppressor function of FUS1 gene *in vivo* by direct intratumoral injection of DOTAP:Chol-FUS1 complex.

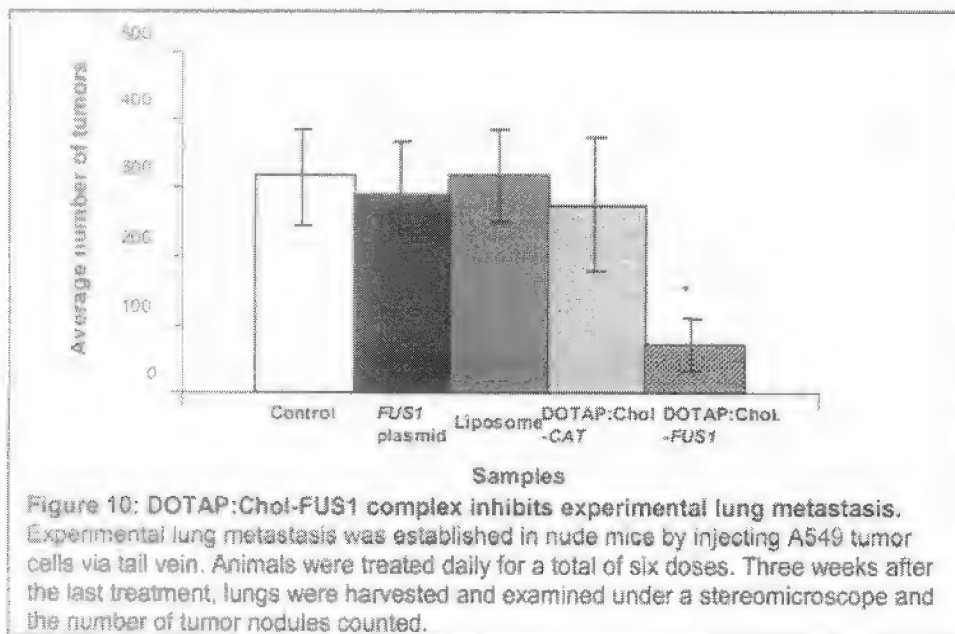
Findings: Treatment of subcutaneous lung tumor xenograft (H1299 and A549) for a total of six doses with DOTAP:Chol-FUS1 complex resulted in a significant suppression of tumor growth ($P = 0.005$ for H1299, and $P = 0.01$ for A549) compared to control animals that were treated with FUS1 plasmid DNA, and treated with DOTAP:Chol-CAT complex (Figure 9) That the tumor inhibition was due to FUS1 protein expression was demonstrated by immunohistochemical analysis. FUS1 protein expression was detected in the subcutaneous tumor tissues primarily localized to the cytoplasm as observed *in vitro* (data not shown). Expression was primarily observed in the tumor cells. However, expression in other cells intermixed with tumor cells was also observed. The subtype of cells staining positive for FUS1 in the tumor was not determined. Furthermore, tumors treated with DOTAP:Chol-FUS1 complex underwent significant apoptotic cell death as evidenced by TUNEL staining, compared

to tumors from those animals that were treated with plasmid DNA or DOTAP:Chol-CAT complex. (Fig. 9). Induction of apoptotic cell death was observed in both H1299 and A549 tumors.



7.4.4 Intravenous injection of DOTAP:Chol-FUS1 complex inhibits experimental lung metastasis. To test the tumor suppressor activity of *FUS1* on experimental lung metastases, lung tumors were established by injecting A549 tumor cells via tail vein.

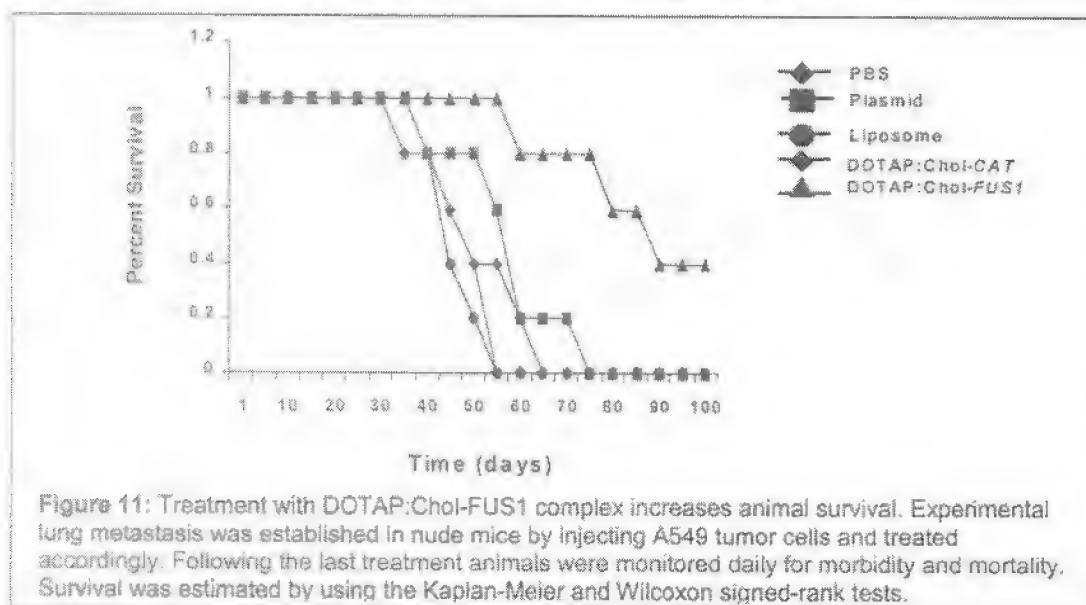
Findings: Intravenous treatments of these lung tumor-bearing animals with DOTAP:Chol-FUS1 complex resulted in a significant inhibition ($P = 0.001$) of lung metastases compared to control animals that were treated with PBS, treated with *FUS1* plasmid DNA, treated with liposome alone, and treated with DOTAP:Chol-CAT complex (Fig. 10). Animals treated with DOTAP:Chol-CAT complex demonstrated some tumor inhibition. The ability of DOTAP:Chol-CAT complex treatments to demonstrate some antitumor activity is not surprising and is attributed to non-specific antitumor activity. However, tumor inhibition was not significant compared to animals treated with PBS, treated with *FUS1* plasmid DNA and treated with liposome. These results show that the therapeutic effect observed in lung tumor-bearing animals when treated with DOTAP:Chol-wt*FUS1* is specific to wt *FUS1*.



7.4.5. Intravenous treatment of lung tumor bearing animals with DOTAP:Chol-FUS1 complex prolongs animal survival. We next evaluated the effect of DOTAP:Chol-FUS1 treatments on animal survival.

Findings: Treatment of experimental A549 lung tumor bearing animals with DOTAP:Chol-FUS1 complex resulted in a significant ($P = 0.01$) and prolonged survival (mean survival time = 80 days) (Fig. 11). In contrast, no significant survival was observed of animals that were treated with PBS (mean = 47.8), treated with FUS1 plasmid (mean = 51.6), treated with liposome (mean = 47.2), and treated with DOTAP:Chol-CAT complex (mean = 47.8). Furthermore, histopathological analysis of various organs demonstrated no significant treatment-related toxicity.

From the results of our preclinical studies it is evident that FUS1 functions as an effective tumor suppressor gene which when delivered intratumorally or intravenously effectively inhibits primary and disseminated lung tumor growth. These exciting results indicate the feasibility of using FUS1 complexed with DOTAP:Chol-liposome for treatment of lung cancer in the clinic.



7.4.6. Toxicity Study of Injected FUS1-Lipoplex. On the basis of results from recent studies (Templeton and Roberts et al, 1997; Templeton and Lasic et al, 1997) that have described efficient systemic delivery using a DOTAP:cholesterol lipid formulation, we conducted preliminary studies and have demonstrated the feasibility of *in vivo* gene delivery via systemic routes. Although the therapeutic efficacy was demonstrated in nude mouse model, the toxicity of the DNA-liposome complex that is relevant to determine the dose-limiting toxicity was not tested. For this purpose, we have initiated toxicity studies in mice (C3H) and in non-human primate (Cynomolgus monkeys; *Macaca fascicularis*). In this study a dose-related toxicity was studied at the M.D. Anderson Veterinary Facility in Bastrop, TX. The toxicology studies are being carried out under conditions regulated by the FDA for IND filing. Liposomes (20 mM DOTAP:cholesterol) were synthesized as described and mixed FUS1 plasmid DNA. A single 50 mg dose of lipoplex was intravenously injected into immunocompetent female C3H mice via the tail vein, and mice were monitored for toxicity, as determined by mortality and morbidity rates. Animals were also evaluated for liver enzyme profiles 24 and 48 hours after injection.

Findings: Preliminary results showed no signs of toxicity as none of the animals died. Liver enzyme profiles (OT/PT and AP) showed no significant differences in enzyme levels between treated and untreated animals. Preliminary toxicology results indicate an IC_{10} to be at 40 μ g of FUS1 DNA in mice.

Although monkey studies showed no significant morbidity, the concentration of DNA-inducing morbidity was similar to that in mice.

Summarily, these findings have been published in several articles (Ito et al, 2003, 2004; Ito and Ji et al, 2004; Gopalan et al, 2004) and used for a successful filing for an FDA approval for a Phase I clinical trial in late stage lung cancer patients using systemic treatment of the DOTAP:cholesterol:FUS1 DNA complexes.

Key Research Accomplishments:

- Developed novel vectors for Fus1-mediated and tumor-selected molecular cancer therapy and for non-invasive molecular imaging for monitoring therapeutic efficacy by systemic administration of FUS1-lipoplex nanoparticles.
- Evaluated the therapeutic efficacy of systemic administration of DOTAP:Cholesterol:FUS1 DNA (FUS1-lipoplex or FUS1-nanoparticle) on human lung cancer growth, metastases development, and animal survival. We found that treatment with FUS1-nanoparticle resulted in significant inhibition of lung tumor growth and metastases.
- Identified an apoptotic protease activating factor 1 (Apaf1) as the cellular target that directly interacts with Fus1 protein and found that Fus1 functioned as a key mediator in Apaf1-mediated mitochondrial apoptosis pathway by recruiting and directing cytoplasmic Apaf1 protein to a critical cellular location and activating it *in situ*, and by upregulating activity of other proapoptotic effectors such as p53 and downregulating anti-apoptotic mediators such as Bcl2 family proteins for the efficient induction of apoptosis.
- Studied the effects of Fus1 in combination with other tumor suppressor genes such as p53 and chemotherapeutic agents such as cisplatin, taxel, protein tyrosine kinase inhibitors on tumor cell proliferation and apoptosis *in vitro* and *in vivo*. Our results suggest that co-expression of FUS1 and p53 could synergistically inhibit lung cancer cell growth and wildtype Fus1 may play a critical role in modulating the sensitivity of tumor cells to the chemotherapeutic agents, especially, to DNA damaging agents, such as Cisplatin and ionizing radiation.
- Identified many cellular targets in FUS1-mediated tumor suppressor activities in lung cancer cells by a high throughput gene and protein expression profiling using technologies of gene microarrays and ProteinChip arrays.
- Evaluated the toxicity of systemic administration of FUS1-nanoparticles in mice and non-human primates (Monkey) in an AAALAC accredited GLP-grade facility and no signs of toxicity at these therapeutic dose levels were shown in those animal models.
- Based on these pre-clinical efficacy and toxicity studies, a Phase I clinical trial with systemic administration of FUS1-nanoparticle was designed and activated for treatment of advanced stage lung cancer patients at M. D. Anderson Cancer Center.

Reportable Outcomes

Articles published in peer-reviewed journals:

1. Gopalan B, Ito I, Branch CD, Clifton Stephens L, Roth JA, Ramesh R. Nanoparticle-based systemic gene therapy for lung cancer: molecular mechanisms and strategies to suppress nanoparticle-mediated inflammatory response. *Technol Cancer Res Treat* 3:647-657, 2004.
2. Ito I, Gopalan B, Mohiuddin I, Saeki T, Saito Y, Branch CD, Stephens LC, Yen N, Roth JA, Ramesh R. Increased uptake of liposomal-DNA complex by lung metastases following intravenous administration. *Mol Ther* 7:409-418, 2003.
3. Ito I, Saeki T, Mohiuddin I, Saito Y, Varporciyan A, Branch C, Roth JA, and Ramesh R. Persistent transgene expression following intravenous administration of a liposomal complex: role of IL-10 mediated immune suppression. *Mol Ther* 9:318-327, 2004.
4. Ji L, Minna JD, Roth JA. 3p21.3 Tumor Suppressor Cluster: Prospects for Translational Applications. (Review) *Future Oncology* 1:79-92, 2005.

5. Oida Y, Gopalan B, Miyahara R, Inoue S, Branch C, Mhashilkar AM, Roth JA, Chada S, and Ramesh R. Sulindac enhances Ad-mda7/IL-24 mediated apoptosis of human lung cancer cells. *Mol. Cancer Ther.* 4(2):291-304, 2005.
6. Uno F, Sasaki J, Nishizaki M, Carboni G, Xu K, Atkinson EN, Kondo M, Minna JD, Roth JA, Ji L. Myristoylation of the FUS1 protein required for tumor suppression in human lung cancer cells. *Cancer Res.* 64, 2969-2976, 2004.

Manuscripts in progress:

1. Futoshi Uno, Jilchiro Sasaki, Gitanjali Jayachandran, Kai Xu, John D. Minna, Jack A. Roth, Lin Ji. Activation of apoptosis by tumor suppressor FUS1 and Apaf-1 protein interaction. *Nature*, 2006 (pending revision).
2. Hiroyuki Kawashima, Futoshi Uno, Jonathan Kurie, John D. Minna, Jack A. Roth, Lin Ji. Synergistic inhibition of EGFR tyrosine kinase activity and NSCLC cell growth by combination treatment with FUS1-nanoparticle and gefitinib (in preparation).
3. Wuguo Deng, Futoshi Uno, John D. Minna, Jack A. Roth, Lin Ji. Synergistic tumor suppression by coexpression of FUS1 and p53 concurrences with FUS1-mediated down regulation of MDM2, accumulation of p53, and activation of Apaf1-dependent apoptotic pathway in human NSCLC cells (in preparation).
4. Hiroyuki Kawashima, Gitanjali Jayachandran, Wuguo Deng, Kai Xu, John D. Minna, Jack A. Roth, Lin Ji. Overcoming gefitinib resistance in NSCLC via inactivation of the PI3K/AKT signaling pathway by a combination of FUS1 nanoparticles and EGFR inhibitors (in preparation).
5. Guanglin Wu, Wuguo Deng, Gitanjali Jayachandran, John D. Minna, Jack A. Roth, Lin Ji. Interaction of the tumor suppressor FUS1 with PDGFR β inhibits PDGFR-mediated proliferation of human lung cancer cells (in preparation).

Meeting Abstracts:

1. Carboni GL, Shao J, Xu K, Gao B, Nishizaki M, Schmid RA, Minna JD, Roth JA, Ji L. Synergistic inhibition of tumor cell growth by CACNA2D2 and p53 via activation of DAPK pathway in lung cancer. American Association for Cancer Research (AACR), 94th Annual Meeting, Toronto, Ontario, Canada, April 5-9, 2003. *Proc. Am. Assoc. Cancer Res.*, 44:241-242, 2003.
2. Uno F, Sasaki J, Nishizaki M, Carboni G, Xu K, Minna JD, Roth JA, Ji L. Myristoylation of Fus1 protein is required for Fus1-mediated tumor suppressing activities in human lung cancer. American Association for Cancer Research (AACR), 94th Annual Meeting, Washington, District of Columbia, July 11-14, 2003. *Proc. Am. Assoc. Cancer Res.*, 44:75, 2003.
3. Jilchiro Sasaki, Futoshi Uno, John D. Minna, Jack A. Roth, Lin Ji. Enhanced Sensitivity of Tumor Cells to Chemotherapeutic Agents by Activation of FUS1 Tumor Suppressor Gene in Lung Cancer Cells. Proceedings of The 95th American Association for Cancer Research (AACR) Annual Meeting, Orlando, FL, March 27-31, 2004.
4. Futoshi Uno, Jilchiro Sasaki, Gitanjali Jayachandran, Kai Xu, John D. Minna, Jack A. Roth, Lin Ji. Activation of Apoptotic Signaling Pathway by Direct Interaction between Tumor Suppressor Fus1 and Apaf-1 proteins in Lung Cancer Cells Back to Search. Proceedings of The 95th American Association for Cancer Research (AACR) Annual Meeting, Orlando, FL, March 27-31, 2004 (AACR Scholar-in-Training Awards).
5. Hiroyuki Kawashima, Charles Lu, Jonathan Kurie, Sunil Chada, John D. Minna, Jack A. Roth, Lin Ji. Synergistic inhibition of EGFR tyrosine kinase and tumor cell growth in non-small cell lung cancer (NSCLC) by combination treatment with FUS1-nanoparticles and Gefitinib. ASCO Annual Meeting, Orlando, Florida, May 13-17, Abstract No: 7081, 2005.
6. Hiroyuki Kawashima, Futoshi Uno, Jonathan Kurie, John D. Minna, Jack A. Roth, Lin Ji. Synergistic inhibition of EGFR tyrosine kinase activity and NSCLC cell growth by combination treatment with FUS1-nanoparticle and gefitinib. American Association for Cancer Research (AACR), 96th Annual Meeting, Anaheim, CA, April 16-20, 2005. *Proc. Am. Assoc. Cancer Res.*, Vol. 46. #2707

7. Wuguo Deng, Futoshi Uno, John D Minna, Jack A. Roth, Lin Ji. Synergistic tumor suppression by coexpression of FUS1 and p53 concurrences with FUS1-mediated down regulation of MDM2, accumulation of p53, and activation of Apaf1-dependent apoptotic pathway in human NSCLC cells. American Association for Cancer Research (AACR), 96th Annual Meeting, Anaheim, CA, April 16-20, 2005. Proc. Am. Assoc. Cancer Res., Vol. 46. #3516
8. Gopalan, B., Branch, C.D., Stephens, L.C., Roth, J.A., Ramesh, R. A novel strategy for suppressing toxicity-mediated by systemic delivery of DNA-nanoparticles. Proc. Am. Assoc. Cancer Res., 46:788, abstract # 3345, 2005.
9. Hiroyuki Kawashima, Gitanjali Jayachandran, Wuguo Deng, Kai Xu, John D. Minna, Jack A. Roth, Lin Ji. Overcoming gefitinib resistance in NSCLC via inactivation of the PI3K/AKT signaling pathway by a combination of FUS1 nanoparticles and EGFR inhibitors. American Association for Cancer Research (AACR), 97th Annual Meeting, Washington DC, April 1-5, 2006. Proc. Am. Assoc. Cancer Res., Vol. 47. #5426.
10. Guanglin Wu, Wuguo Deng, Gitanjali Jayachandran, John D. Minna, Jack A. Roth, Lin Ji. Interaction of the tumor suppressor FUS1 with PDGFR β inhibits PDGFR-mediated proliferation of human lung cancer cells. American Association for Cancer Research (AACR), 97th Annual Meeting, Washington DC, April 1-5, 2006. Proc. Am. Assoc. Cancer Res., Vol. 47. #1460. (AACR Scholar-in-Training Awards).

Project-generated grants:

1. The grant titled "Systemic Non-Viral Gene Therapy for Lung Cancer" submitted to the Charolette Geyer Foundation has been funded. The preliminary data for this grant application was generated partly from studies conducted in Project 7 of TARGET.
2. NIH U01: Mouse Models of Human Cancers Consortium 4/1/2004-3/31/2009
Projects 2 and 5: Modeling Airway Lung Cancer and the Role of Inflammation
Project leader: Lin Ji, Ph.D.

Patents (Granted and Pending):

1. Ji, L., Roth, J.A. Detection of Expression and Posttranslational Modification of Fus1 Protein on ProteinChip Array by SELDI-TOF-MS. MDA04-107, 2004
2. Ji, L., Roth, J.A., Minna, J.D., and Lerman, M.I., Chromosome 3p21.3 genes as tumor suppressors. U.S. Patent, US-2004-0016006-A1; World Patent: WO 02/04511 A2
3. Jacki Lin, Ralph B. Arlinghaus, Lin Ji, Jack A. Roth, Inhibition of Abl Kinase by FUS1 Peptide, MDA05-048, January 25, 2005.
4. Lin Ji, Jack A. Roth, A Novel Therapeutic FUS1 (FP) and FP-Nanoparticle mediated Inhibition of PTK Activities and Tumor Cell Growth, MDA05-058, March 4, 2005
5. Gitanjali Jayachandran, Kevin Coombes, Jack Roth, and Lin Ji. High throughput serum phosphopeptide profiling for early detection, molecular classification, and diagnosis of lung cancer. MDA06-040, 2006

Conclusion

Our results revealed a novel molecular mechanism involving FUS1-mediated tumor suppression function *in vitro* and *in vivo*. We developed a novel DOTAP:Cholesterol:FUS1 plasmid DNA-nanoparticle for systemic treatment of lung cancer. Based on these pre-clinical efficacy and toxicity studies, a Phase I clinic trial with systemic administration of FUS1-nanoparticle has been opened for advanced stage lung cancer patients at M. D. Anderson Cancer Center.

References

1. Nishizaki, M., Sasaki, J., Fang, B., Atkinson, E.N., Minna, J.D., Roth, J., and Ji, L. Synergistic tumor suppression by coexpression of FHIT-mediated MDM2 inactivation and p53 stabilization in human NSCLC cells. Cancer Res 64 (16), 5632-5640, 2004.
2. Templeton NS, Roberts DD, Safer B. Efficient gene targeting in mouse embryonic stem cells. Gene Ther 4: 700-9, 1997.

3. Templeton NS, Lasic DD, Frederik PM, Strey HH, Roberts DD, Pavlakis GN. Improved DNA: Liposome complexes for increased systemic delivery and gene expression. *Nat Biotechnol* 5:647-52, 1997.

Project 8: Therapeutic Targeting of bcl-xl Expression in Non-Small Cell Lung Carcinoma
(Project leader: W Roy Smythe, M.D.)

Notes: In February 2004, Dr. Roy Smythe left M. D. Anderson to become Chairman of the Department of Surgery at Scott & White in Temple, TX. The balance of funds in his project was reallocated to Core A and Project 1. A summary of research findings follows.

The bcl-xl gene is a member of the bcl-2 family of genes that controls mitochondrial membrane potential and interacts with other members of this family to control apoptosis, or programmed cell death. When over-expressed, the bcl-xl protein leads to inhibition of apoptosis as well as decreased sensitivity to conventional treatments (i.e., chemotherapy and irradiation). Decreasing expression of this gene product by various means may conversely induce apoptosis in cancer cells and render them sensitive to more conventional available therapies.

Summary of Research Findings:

Specific Aim 1: Characterize *in vitro* effects of bcl-xl antisense on human NSCLC cells and evaluate such exposure as a prime for other pro-apoptotic therapies

Findings: We have evaluated a panel of bcl-xl antisense oligonucleotides (ASO) on the human non-small cell carcinoma cell lines A549 and H1299. We have identified one particular construct (ISIS 15999) that can decrease cell viability in a lipid delivery system by 60%-90%. We have also demonstrated the ability of this *in vitro* treatment to increase the apoptotic fraction of cells by more than 30%. This has also effectively sensitized these cell lines to cisplatin, with significant increases in both cell death and apoptosis over either monotherapy approach.

Due to a concern regarding the *in vivo* applicability of this antisense approach, we have been evaluating a siRNA approach for down-regulation of bcl-xl expression. We have designed and evaluated 5 separate siRNA double stranded constructs and have tested them on NSCLC lines *in vitro*. Two of these constructs effectively decreased bcl-xl expression at both protein (Western blot) and mRNA (real-time PCR) levels. The most promising construct was utilized to develop a hairpin loop plasmid delivery system. Both the siRNA double stranded and plasmid constructs are able to induce apoptotic cell death *in vitro*. Notably, the bcl-xl siRNA plasmid construct delivered with a lipid delivery system can sensitize NSCLC cells to cisplatin and decrease the amount of cisplatin required to kill 50% of these cells (IC50) by a full log.

Specific Aim 2: Develop an adenoviral vector capable of transferring an antisense bcl-xl gene construct

A full-length bcl-xl antisense adenoviral gene therapy vector (xl22) was developed (second generation replication deficient human type 5 construct). This has been confirmed by sequencing.

Specific Aim 3: Characterize the *in vitro* effects of bcl-xl antisense adenoviral vector exposure on human NSCLC cells and evaluate such exposure as a prime for other pro-apoptotic therapies

The bcl-xl antisense adenoviral vector (xl22) was evaluated *in vitro* in NSCLC cells and demonstrated to downregulate bcl-xl protein expression and induce apoptotic cell death.

Specific Aim 4: Characterize the therapeutic effects of bcl-xl antisense targeting with both ASO and adenoviral vectors in animal models of non-small cell lung carcinoma and evaluate such exposure as a prime for other pro-apoptotic therapies *in vivo*

We have demonstrated the ability of ASO to decrease intraperitoneal tumor burden in a xenograft model of mesothelioma (identical bcl-2 family expression pattern) by 30%-40%. Likewise, we have demonstrated that the xl22 construct can decrease tumor burden by more than 60%. We have recently demonstrated the ability to transfer the backbone siRNA plasmid system with a reporter gene (*E. Coli* beta galactosidase) utilizing a DOTAP:cholesterol delivery method into *in vivo* intraperitoneal xenograft tumor.

Key Research Accomplishments:

- Demonstrated that bcl-xl ASO and adenoviral construct (xl22) reduced bcl-xl expression and induced apoptosis in NSCLC lines, and sensitized the cell lines to cisplatin, with significant increases in both cell death and apoptosis over either monotherapy approach.
- Demonstrated that ASO and xl22 decreased intraperitoneal tumor burden by 30%-40% and > 60% respectively, in a xenograft model of mesothelioma.

Conclusion:

The bcl-2 antisense oligonucleotide (ASO) effectively blocked the bcl-2 expression *in vitro*, but the limitation of the *in vivo* applicability of this antisense approach may make it less advantageous than the newly emerged siRNA strategy for future use.

Project 9: Use of Perfluorocarbons (PFC) enhance Pulmonary Gene Transfer

(Project Leader: Ara Vaporciyan, M.D.)

Notes: This project didn't proceed well as originally proposed due to several reasons, mainly because the proposed animal study did not show any positive results, and after Dr. Vaporciyan decided to change the injection strategy and attempted to adopt the intravenous formulation of PFC, the company was unable to provide any of the material for this study because of its commitment to another party. Therefore, Dr. Vaporciyan decided to discontinue the study. The balance of funds for this project was reallocated to Core A in 2005.

Replication-deficient adenoviral vectors have demonstrated high-efficiency gene transfer in a wide variety of tissues. Hepatic clearance during intravenous administration as well as the host immune response to the viral antigens has limited its effectiveness. Based on our findings and a significant body of literature data, we hypothesized that the anti-inflammatory properties of PFC will limit the immune response, thereby improving transfer efficiency and duration of gene expression.

A brief summary of the work conducted for this Project is as follows.

Specific Aim 9.1: To determine the ability of perfluorocarbons to diminish the immune response, both innate and subsequent cellular and humoral responses, to intratracheal administration of adenoviral vector

We found that intratracheal administration of adenovirus in experimental mice allows transfection in the lung parenchyma only and the transfection efficiency was significantly increased when followed by intratracheal administration of perfluorocarbons (PFC). However, the second pulmonary transfection after repeated administration of adenovirus and then PFC was not successful.

This was either caused by interference of adenoviral transfection by the small amount of residual PFC or due to an enhanced immune response generated by the high expression after the first transfection.

To address the latter, we began experiments using a less immunogenic vector. In collaboration with Dr. Ramesh (Project 7) we had preliminary *in vitro* data demonstrating improved gene transfer into A549 lung cancer cell lines using liposomes (DOTAP:cholesterol lipid formulation mixed with β -gal plasmid DNA) in the presence of PFC. This enhanced gene transfer coupled with the decreased immunogenic properties of liposomes prompted us to attempt *in vivo* pulmonary gene delivery using liposomes with PFC.

Our initial attempts with liposomes administered intratracheally, with or without PFC, resulted in 100% mortality within 10 minutes secondary to respiratory distress. Further work with various ratios of DOTAP and cholesterol revealed that the lethal agent was the cholesterol. A new lipid formulation consisting only of DOTAP and β -gal plasmid DNA was created and administered safely. However, at 1 and 2 days post administration there was no β -gal expression regardless of the presence or absence of PFC. We have discontinued work with liposomal vectors *in vivo*.

Specific Aim 9.2: To determine the effects of perfluorocarbons on reduction and mechanical disruption of the humoral response, and subsequent effects on repeated gene transfer

Based on our preliminary *in vitro* data, PFC applied directly to lung cancer cell lines in culture can increase the transfection ability of both adenovirus and liposomal vectors. The well-characterized cell lines A549 and H460, when exposed to PFC for 30 minutes prior to transfection with adenoviral vector, had an increased expression of the vector by 90% and 41% respectively. The results using a liposomal vector showed an equally enhanced expression.

However, as mentioned above, when we intratracheally administered adenovirus followed by PFC to animals, they had a greatly diminished expression of the vector although the first injection generated a favorable expression. We found that the animal lung contained a significant amount of PFC even 21 days after the first injection. We speculated that the residual PFC in the lung might cause the poor transfection. Thus, we attempted to adopt another approach, hoping to prevent the accumulation of PFC within the alveolar compartment of the lung.

We exposed animals to PFC via an intravenous injection followed by intratracheal administration of adenoviral vector. Animals were initially injected intravenously with a 5ml/kg dose of PFC. However, the majority of the animals receiving this dose were unable to survive. Death ensued within 10 to 20 minutes of injection. Assays for lipopolysaccharide (LPS) revealed no detectable levels of LPS in the PFC source, indicating that a contaminated supply of PFC was not a cause of the animals' death. Repeated experiments using this dose resulted in the same outcome. Autopsy of the animals revealed a pale lung tissue. When this tissue was homogenized and the homogenate was allowed to settle, a definite layer of PFC could be seen. It was apparent that the PFC was unable to travel through the pulmonary capillary bed and was trapped in the lung limiting pulmonary blood flow and resulting in animal death. Therefore, a reduced dose of 1 ml/kg of PFC was utilized. These animals survived overnight but uniformly succumbed 12 hours after the injection. Autopsy of these animals identified a similar problem as seen in the higher-dosed animals.

There are fluorocarbon compounds of PFC specifically designed for intravenous injection. Use of these fluorocarbon PFCs may prevent death and allow enhanced transfection via the method described above. Attempts were made to contact a company that would provide the source for the intravenous formulation of PFC. Alliance Pharmaceuticals is an American corporation that did produce two forms of these fluorocarbon PFCs. The first agent was designed for liquid ventilation (named Liquivent) and the second was designed for intravenous injection as a blood replacement (named Oxygent). We had initially attempted to obtain Liquivent when we began our studies with PFC but Alliance Pharmaceuticals was unable to provide any Liquivent due to ongoing clinical trials exploring its role in liquid ventilation. They now no longer produce this product. We again attempted to contact

Alliance Pharmaceuticals to obtain the intravenous PFC product, Oxygent, however the company has entered into an agreement with a Chinese pharmaceutical company to produce and test this agent for blood conservation during surgery. As a result, they are unable to provide any of the material to our laboratory.

Specific Aim 9.3: To determine the ability of PFC to allow continued penetration of the pulmonary parenchyma in the setting of an animal model of severe emphysema

Specific Aim 9.4: To determine the ability of PFC-mediated gene transfer to effectively transduce a model of multifocal lung cancer

We declined to pursue Specific Aims 9.3 and 9.4 since Specific Aims 9.1 and 9.2 did not proceed as hoped

Key Research Accomplishments:

- Intratracheal administration of adenovirus allows transfection of the lung parenchyma only and is significantly increased when delivered in the presence of perfluorocarbon. Unfortunately, pulmonary transfection after repeated administration of adenovirus with perfluorocarbon intratracheally is not successful.
- We have explored DNA:Liposomal complexes with perfluorocarbon as well. Although *in vitro* studies were promising, any complex containing cholesterol administered intrathecally was lethal and complexes without cholesterol were unable to transfect lung tissue when administered intrathecally.

Project 10: Development of Novel Murine Models of Lung Cancer and Evaluation of Antiangiogenic Agents

(Project Leader: Roy Herbst, M.D., Ph.D., Co-Leader: Michael O'Reilly, M.D.)

Anti-angiogenic agents designed to inhibit tumor growth and prevent metastasis offer great therapeutic potential, but emerging data suggest limitations for their use as monotherapy in advanced malignancy, and anti-angiogenic therapy may require organ-specific development or optimization. Therefore, we propose to develop murine models of primary, recurrent, and metastatic human small and non-small cell lung cancer. We will then use the models to determine optimal effective combinations of anti-angiogenic and cytotoxic agents in these models of lung cancer. The goal of this project is to provide a rational basis for use of antiangiogenic agents with conventional and emerging modalities in the treatment of lung cancer.

Specific Aim 10.1: To develop and validate orthotopic and metastatic murine lung cancer models for testing the efficacy of anti-angiogenic agents alone and in combination with cytotoxic agents

Findings: We have developed and validated murine models of orthotopic and metastatic human lung cancer for testing the efficacy of antiangiogenic agents alone and in combination with cytotoxic chemotherapy. Our publications in *Clinical Cancer Research* (Onn et al, 2003) and *AACR abstract* (Isobe et al, 2004) describe the details of the study. Experimental murine models of primary human non-small cell and small cell lung cancer are now in place to study the biology and therapy of human lung cancer.

Specific Aim 10.2: To evaluate effects of anti-angiogenic agents alone and in combination with chemotherapeutic agents in orthotopic and metastatic murine models of human lung cancer

Findings: First, we tested an oral angiogenesis inhibitor ZD6474 that targets VEGFR2 and EGFR in the models. We found that ZD6474 resulted in the near complete suppression of malignant growth of established lung tumors and prevented pleural effusion formation and inhibited chest wall invasion in our orthotopic lung model. In contrast, systemic weekly therapy with Taxol had little or no effect on lung cancer progression. The detailed findings can be reviewed in the *AACR abstract* (Wu et al, 2004) and in *Clinical Cancer Research* (Onn et al, 2004). Additional manuscripts have been submitted to *Cancer Research* (Wu et al, 2006) and *Molecular Cancer Therapeutics* (Wu et al, 2006).

In addition, ZD6474 was effective against lung adenocarcinoma in our brain and bone metastatic models. The activity of ZD6474 was enhanced by combined therapy with Taxotere or Taxol in the brain metastatic models (lung adenocarcinoma), but Taxol antagonized ZD6474 activity in the bone metastatic model, suggesting that organ microenvironment influences response to combined antiangiogenic and cytotoxic therapies (Wu et al, AACR, 2004; Onn et al, 2004).

Specific Aim 10.3: To optimize combinations and sequences of anti-angiogenic therapy with chemotherapy or radiation therapy for treatment of lung cancer

Findings: As discussed above, we have tested and reported the results of the combination therapy of ZD6474 with Taxotere or Taxol in metastatic models. In addition, we also tested the efficacy of the combination of the targeted agent ZD6474 and radiation. We found that ZD6474 enhanced the therapeutic efficacy of irradiation in an orthotopic model of human non-small cell lung cancer. The findings were reported in the manuscript submitted to *Clinical Cancer Research* (Shibuya et al, 2006).

Specific Aim 10.4: To develop surrogate markers of response to therapy using immunohistochemical and gene expression analysis of tumor tissues

Previously, we reported that endothelial cell apoptosis preceded tumor cell apoptosis after ZD6474 treatment in the orthotopic human lung adenocarcinoma murine model, suggesting that the effect on the vasculature may be a useful surrogate for tumor response to ZD6474.

We will initiate soon a clinical trial that will study ZD6474 in untreated NSCLC patients. The mandatory tumor biopsies from this trial will be used to evaluate endothelial cell apoptosis and inhibition of VEGFR and EGFR receptor phosphorylation, which could be used as surrogate endpoints of ZD6474 effect. The study will be supported by a different funding mechanism.

Key Research Accomplishments

- Developed and validated murine models of orthotopic and metastatic human lung cancer
- Evaluated effects of ZD6474 alone and in combination with chemotherapeutic agents or radiation therapy using the orthotopic and metastatic lung cancer models.
- ZD6474 is a potent inhibitor of angiogenesis that is highly effective therapeutically in an orthotopic model of human lung cancer.
- Taxotere or Taxol enhanced the activity of ZD6474 in the brain metastatic models (lung adenocarcinoma), but Taxol antagonized ZD6474 activity in the bone metastatic model.

Reportable Outcomes

Articles in peer-reviewed journals:

1. Onn A, Isobe T, Itasaka S, Wu W, O'Reilly MS, Ki Hong W, Fidler IJ, Herbst RS. Development of an orthotopic model to study the biology and therapy of primary human lung cancer in nude mice. *Clin Cancer Res* 9:5532-39, 2003.
2. Onn A, Isobe T, Wu W, Itasaka S, Shintani T, Shibuya K, Kenji Y, O'Reilly MS, Fidler IJ, Herbst RS. Epidermal growth factor receptor tyrosine kinase inhibitor does not improve paclitaxel effect in an orthotopic mouse model of lung cancer. *Clin Cancer Res* 10:8613-9, 2004.

Manuscripts in progress:

1. Isobe T, Onn A, Wu W, Shintani T, Itasaka S, Shibuya K, O'Reilly MS, Herbst RS. Biology and therapy of human small cell lung cancer (SCLC) in novel orthotopic nude mouse models. (in preparation)
2. Itasaka S, Komaki R, Shibuya K, Shintani T, Bucana CD, Herbst RS, O'Reilly MS. Targeted therapy against VEGF and EGF receptor signaling with blocks angiogenesis and improves the therapeutic efficacy of chemotherapy in a mouse model of lung cancer brain metastasis. (in preparation)
3. Shibuya K, Ritsuko K, Shintani T, Itasaka S, Ryan A, Jürgensmeier JM, Milas L, Ang KK, Herbst RS, O'Reilly MS. Targeted therapy against VEGFR and EGFR with ZD6474 enhances the therapeutic efficacy of irradiation in an orthotopic model of human non-small cell lung cancer, *Clin Cancer Res* (submitted), 2006
4. Shintani T, Lewis VO, Komaki R, Ryan A, Herbst RS, O'Reilly MS. The anti-tumor and antiangiogenic effects of VEGFR and EGFR blockade are superior to EGFR blockade alone but are not enhanced by the addition of paclitaxel in a model of lung cancer bone metastasis. (in preparation)
5. Wu W, O'Reilly MS, Langley R, Tsan RZ, Baker CH, Bekele N, Tang XM, Onn A, Fidler IJ, Herbst RS. Expression of EGF/TGF- α by human lung cancer cells determines response to EGFR kinase inhibitors. *Cancer Res* (submitted), 2006.
6. Wu, Isobe T, Onn A, Itasaka S, Langley RR, Shintani T, Shibuya K, Komaki R, Ryan AJ, Fidler IJ, Herbst RS, O'Reilly MS. Targeted therapy of the tumor and vascular components of orthotopic human lung cancer by combined vascular endothelial growth factor and epidermal growth factor receptor signaling blockade. *Mol Cancer Ther* (submitted), 2006.

Meeting Abstracts:

1. Shibuya K, Komaki R, Shintani T, Wu W, Itasaka S, Isobe T, Ryan A, Herbst RS, O'Reilly MS. Combined blockade of VEGFR and EGFR with ZD6474 enhances the anti-tumor and anti-vascular effects of radiation therapy in an orthotopic mouse model of human lung cancer. *Proceedings of AACR: #5828*, 2005.
2. Shintani T, Lewis VO, Komaki R, Wu W, Ryan A, Herbst RS, O'Reilly MS. ZD6474 inhibits human lung cancer bone metastases in a murine model by targeting both the tumor and its vasculature. *Proceedings of AACR: # 5844*, 2005.
3. Isobe T, Onn A, Wu W, Shintani T, Itasaka S, Shibuya K, Hong WK, O'Reilly MS, Herbst RS. Biology and therapy of human small cell lung cancer (SCLC) in novel orthotopic nude mouse models. *Proceedings of AACR: #5136*, 2004.
4. Wu W, Onn A, Shintani T, Herbst RS, O'Reilly MS. ZD6474 enhances the anticancer efficacy of Paclitaxel in human Lung Cancer Models. *Angiogenesis* 7(Suppl 1):25, 2004.
5. Shibuya K, Komaki R, Wu W, Shintani T, Itasaka S, Isobe T, Ryan A, Herbst RS, O'Reilly MS.

- Targeted therapy against VEGFR and EGFR signaling with ZD6474 enhances the therapeutic efficacy of irradiation in an orthotopic mouse model of human non-small cell lung cancer. *Int'l J Radiation Oncol, Biology, Physics* 60(1 Suppl S):S149-50, 2004.
6. Wu W, Shintani T, O'Reilly MS, Herbst RS. Blocking VEGF and EGF receptor signaling with ZD6474 sensitizes human non-small cell lung cancer to chemotherapy with paclitaxel. *Europ J Cancer Suppl* 2(8 suppl):50, 2004.
 7. Wu W, Isobe T, Itasaka S, Shintani T, Langley RR, Onn A, Hansen JC, O'Reilly MS, Herbst RS. ZD6474, a small molecule targeting VEGF and EGF receptor signaling, inhibits lung angiogenesis and metastasis and improves survival in an orthotopic model of non-small cell lung cancer. *Proceedings of AACR*: # 4551, 2004.
 8. Wu W, Isobe T, Onn A, Shintani T, Itasaka S, Shibuya K, Langley RR, Hansen JC, Fidler IJ, Ryan AJ, Herbst RS, O'Reilly MS. Targeted therapy against VEGF and EGF receptor signaling with ZD6474 blocks angiogenesis and inhibits the growth and dissemination of orthotopic human lung cancer in mice. *Clin Cancer Res* 9(16 Pt 2):6143s, 2003.

Project-generated clinical trials:

Based on the preclinical findings from the **TARGET** projects, we have designed 2 clinical trials:

1. A phase II clinical trial with antiangiogenic agent ZD6474 in combination with chemotherapeutic agents in NSCLC patients (PI: Roy Herbst, M.D., Ph.D.)
2. A phase II randomized trial of treatment of malignant pleural effusion with ZD6474, a novel VEGFR and EGFR tyrosine kinase inhibitor (a part of **IMPACT**) (PI: Roy Herbst, M.D., Ph.D.)

Conclusion

We conclude that 1) the orthotopic murine model of lung cancer is a valuable tool to test the antiangiogenic agents and their combination with cytotoxic agents; 2) The model provides a rational basis for development of anti-angiogenic therapy with conventional and emerging modalities in the treatment of lung cancer; 3) ZD6474 is a potent inhibitor of angiogenesis that is highly effective therapeutically in an orthotopic model of human lung cancer. It will be prudent to develop clinical strategies for the combination of specific protein tyrosine kinase inhibitors that block both EGFR and VEGFR signaling.

Core B: Biostatistics & Data Management Core

(Core Director, J. Jack Lee, Ph.D.; Core Co-Director, B. Nebiyu Bekele, Ph.D.)

Core Goals:

- To provide the statistical design, sample size and power calculations for each project.
- To facilitate prospective data collection and quality control of data for animal experiments and basic science studies associated with the **TARGET** program.
- To provide all statistical data analysis including descriptive statistical analysis, hypothesis testing, estimation, modeling of prospectively generated data.
- To generate statistical reports for all projects.
- To collaborate and assist all project investigators in the publication of scientific results.

From the inception of the **TARGET** program, the Biostatistics and Data Management Core has worked actively with the project leaders in their research efforts, especially in the areas of biostatistical advice and consulting, the initial design of studies, and analysis of experimental results.

Key Research Accomplishments:

- In collaboration with Dr. Ruth Katz (Investigator in Project 1), the Core analyzed various data sets relating to the relationship between deletions of the 3p and 10q genes and overall survival for patients with NSCLC. The results were published in *Cancer* (Barkan et al, 2005).

- We also assisted Dr. Charlie Lu's project (Project 4). In collaboration with Dr. Lu, we have analyzed six molecular factors including DAP kinase potentially prognostic for overall survival of resectable Stage I NSCLC patients. The data were published in *Journal of Clinical Oncology* (Lu et al, 2004). Currently, we are analyzing the correlation between hypermethylation of DAP kinase and patient survival. A manuscript is in preparation (Lu et al, 2006)
- In addition, Dr. Jack Lee, in collaboration with Dr. Reuben Lotan (Project Leader of Project 5), evaluated the data of growth inhibitory and apoptosis effects of histone deacetylase inhibitor SAHA and demethylating agent, 5-aza-2-deoxycytidine, on lung cancer cell lines generated in Specific Aim 5.1. A manuscript is in preparation (Fujimoto et al., 2006).

Reportable Outcomes

Articles published or in progress:

1. Barkan GA, Caraway NP, Jiang F, Zaidi TM, Fernandez R, Vaporciyan A, Morice R, Zhou X, Bekele BN, Katz R. Comparison of molecular abnormalities in bronchial brushings and tumor touch preparations. *Cancer* 105: 35-43, 2005.
2. Lu C, Soria JC, Tang X, Xu XC, Wang L, Mao L, Lotan R, Kemp B, Bekele BN, Feng L, Hong WK, Khuri FR. "Prognostic Factors in Resected Stage I Non-Small Cell Lung Cancer (NSCLC): A Multivariate Analysis of Six Molecular Markers". *J Clin Oncol* 22: 4575-83, 2004.
3. Lu C, Wistuba I, Zhou X, Bekele BN, Putnam JB, Jr., Correa A, Mao L. Prognostic role of promoter hypermethylation of death-associated protein (DAP) kinase and p16 genes in early-stage non-small cell lung cancer (in preparation)
4. Fujimoto JY, Men T, Lee JJ, Kong M, Ayers GD, Hong WK, Lotan R. Additive and synergistic effects of 5-aza-2'-deoxycytidine and suberoylanilide hydroxamic acid (SAHA) on human lung carcinoma cells in vitro and in vivo (in preparation).

KEY RESEARCH ACCOMPLISHMENTS (IN SUMMARY)

Project 1: Molecular Epidemiology of Lung Cancer

- Consented 178 patients. Exceeded target enrollment of 100 patients (131) with both bronchial brushings and blood.
- There is a significant correlation between latent genetic instability as measured by BPDE-induced mutagen sensitivity in the lymphocytes and 3p and 10q aberrations by FISH assay in bronchial brushing epithelial cells from the non-tumor side and uninvolved lung tissue, but not with the tumor tissue of the same patients.
- DNA repair capacity data are available on 41 epithelial samples with a mean (SD) of 14.8 (10.2). There was no evidence of correlation between DRC of the cells and lymphocyte DRC from the same subjects ($P=0.3187$).
- BPDE sensitivity in lymphocytes (a measure of overall genetic instability) was significantly positively associated with 3p deletions in lymphocytes on FISH analysis ($p=0.0066$) as well as 3p aberrations ($p=0.0024$) and borderline significantly associated with FISH 10q aberrations ($p=0.0570$) in lymphocytes.
- 3p deletions and 10q deletions in bronchial brushes from either normal or tumor side of bronchial brushes and tumor preps were strongly correlated.
- In a subset of the cases, there was no correlation between lymphocyte markers and those in epithelial cells. However, the complete data set has yet to be analyzed.

Project 2: Genetic Instability by Smoking Status

- Developed the sensitive and highly reproducible FISSR-PCR technique and applied it to detect clonal and subclonal outgrowths in microdissected epithelium and stroma from frozen tissue

sections of resected lung tumors and of bronchial biopsies obtained during chemoprevention studies.

- Demonstrated increased genetic instability and increased clonal/subclonal heterogeneity in an *in vitro* model of bronchial epithelial cell populations at different stages of lung tumorigenesis.
- Demonstrated that the stroma underlying genetically altered bronchial epithelium also exhibits clonal and subclonal outgrowths. The degree of clonal change in the stroma appeared to be related to the degree of clonal/subclonal change in the bronchial epithelium.
- Demonstrated the presence of clonal/subclonal changes in the bronchial epithelium and underlying stroma of current and former smokers at increased risk for lung cancer development. The degree of clonal/subclonal change detected was related to the degree of genetic instability measured in biopsies of the same subjects by chromosome *in situ* hybridization.

Project 3: Epithelial Biomarkers of Lung Cancer: Evaluation of Airway Secretions to Study Lung Carcinogenesis

- We identified 23 unique biomarkers over-represented in the secretions from metaplastic squamous bronchial epithelial cells using comparative 2D-PAGE analysis of the apical surface fluids (ASF) obtained from squamous metaplastic and normal mucociliary bronchial epithelial cells.
- We found that expression of the unique proteins SCCA1 and SCCA2 was progressively increased in transformed/tumorigenic cell lines and only detected in squamous cell carcinoma but not in adenocarcinoma cells.
- We found that expression levels of SCCA1, SCCA2, Annexin I, Annexin II, S100A8, and Maspin in bronchial lavage are not directly correlated with histological appearance of bronchial mucosa in heavy smokers.
- We identified that genes in the WNT pathway, apoptosis, and cell cycle are concurrently deregulated in non-small cell lung cancer cells as compared to organotypically cultured normal bronchial epithelial cells.
- We successfully generated bronchial epithelium recapitulating *in vivo* bronchial epithelium using primary bronchial epithelial cells isolated from surgically-resected lung tissue specimens.
- Organotypic culture of the primary epithelial cells isolated from patients with lung cancer showed no obvious bias in growth, histologic abnormalities, or mucociliary differentiation.
- We demonstrated that primary bronchial epithelial cells isolated from surgically resected lung tissue specimens can be used for determination of the genetic susceptibility in lung target tissues assayed in DNA repair capacity and mutagen sensitivity.
- Concurrently overexpressed SCCA1 and Annexin 2 in the secretions from the bronchial epithelial cells may serve as surrogate markers for lower DNA repair capacity and high percentage of 3p loss of heterozygosity in corresponding tumors.

Project 4: Prognostic Role of Promoter Hypermethylation of Death-Associated Protein (DAP) Kinase and p16 in Early-Stage Non-Small Cell Lung Cancer

- We did not observe significant statistical correlations between *DAP kinase* methylation status and subject characteristics.
- We did not observe significant statistical correlations between *p16* methylation status and subject characteristics, but a positive trend for increased *p16* methylation and grade ($p=0.084$) was observed.
- We observe a higher frequency of *p16* methylation in ever vs never smokers (39% vs 28%, $p=0.17$).
- We did not detect significant statistical correlations between methylation status and overall survival (*p16* $p=0.13$; *DAP kinase* $p=0.56$) or disease-free survival (*p16* $p=0.36$; *DAP kinase* $p=0.71$).

- In multivariate analyses, only age and grade were significant predictors of overall survival and disease-free survival.

Project 5: An Epigenetic Approach to Lung Cancer Therapy

- We found that 5-AZA-CdR, SAHA, and valproic acid were able to inhibit the growth of premalignant and malignant lung epithelial cells and head and neck SCCs in a dose dependent fashion. Normal oral epithelial cells were much less sensitive; in some of the cell lines, 5-AZA-CdR and SAHA acted synergistically.
- Both SAHA and valproic acid inhibited the growth by G2 arrest and also induced apoptosis in HNSCC cell lines.
- We found that siRNA-mediated gene silencing of DNMT can be applied to inhibit the growth of lung cancer cells.
- SAHA inhibited histone deacetylase in normal, precancerous and cancerous cells, but inhibited growth in only the cancer cells.
- Inhibition of cell proliferation by which SAHA and valproic acid may involve the induction of p21; the induction of apoptosis by SAHA and valproic acid includes activation of the mitochondrial pathway (activation of caspase 9 and caspase 3); SAHA also activated Fas death receptor mediated apoptosis pathway, which involves caspase 8.
- SAHA, 5-aza-CdR and their combinations inhibited the growth of human NSCLC cells implanted subcutaneously in athymic nude mice, demonstrating anti-tumor activities of SAHA and 5-aza-CdR alone and in combination.
- We discovered subsets of genes and networks that are modulated by SAHA and 5-aza-CdR and by their combination.

Project 6: The Role of the Farnesyl Transferase Inhibitor SCH66336 in Treatment of Carcinoma of the Aerodigestive Tract

- FTIs including SCH66336 and R115777 induce growth arrest and apoptosis independent of Akt and Raf/ERK signaling pathways in human NSCLC cells, and in some NSCLC cell lines, SCH66336 and R115777 instead activate Akt surviving pathways, which may lead to FTI resistance.
- FTIs increase DR5 expression through CHOP-dependent mechanism that contributes to SCH66336-induced apoptosis and enhanced TRAIL-induced apoptosis. Our findings 1) suggest that both DR5 and CHOP can be tested as predictive biomarkers for FTI-based cancer therapy; and 2) warrant the future clinical testing of the combination of a FTI with TRAIL for therapy of human cancer including lung cancer.
- FTIs modulate the expression of FLIP either by decreasing or increasing its expression depending on cell lines.
- The functional HDAC6 is required for the synergy of SCH66336 with taxanes

Project 7: Mechanisms and Therapeutic Applications of the Tumor Suppressor Gene *FUS1* in Lung Cancer

- Developed novel vectors for Fus1-mediated and tumor-selected molecular cancer therapy and for non-invasive molecular imaging for monitoring therapeutic efficacy by systemic administration of FUS1-lipoplex nanoparticles.
- Evaluated the therapeutic efficacy of systemic administration of DOTAP:Cholesterol:FUS1 DNA (FUS1-lipoplex or FUS1-nanoparticle) on human lung cancer growth, metastases development, and animal survival. We found that treatment with FUS1-nanoparticle resulted in significant inhibition of lung tumor growth and metastases.
- Identified an apoptotic protease activating factor 1 (Apaf1) as the cellular target that directly interacts with Fus1 protein and found that Fus1 functioned as a key mediator in Apaf1-mediated mitochondrial apoptosis pathway by recruiting and directing cytoplasmic Apaf1

protein to a critical cellular location and activating it in situ, and by upregulating activity of other proapoptotic effectors such as p53 and downregulating anti-apoptotic mediators such as Bcl2 family proteins for the efficient induction of apoptosis.

- Studied the effects of Fus1 in combination with other tumor suppressor genes such as p53 and chemotherapeutic agents such as cisplatin, taxol, protein tyrosine kinase inhibitors on tumor cell proliferation and apoptosis *in vitro* and *in vivo*. Our results suggest that co-expression of FUS1 and p53 could synergistically inhibit lung cancer cell growth and wildtype Fus1 may play a critical role in modulating the sensitivity of tumor cells to the chemotherapeutic agents, especially, to DNA-damaging agents such as Cisplatin and ionizing radiation.
- Identified many cellular targets in FUS1-mediated tumor suppressor activities in lung cancer cells by a high throughput gene and protein expression profiling using technologies of gene microarrays and ProteinChip arrays.
- Evaluated the toxicity of systemic administration of FUS1-nanoparticles in mice and non-human primates (Monkey) in an AAALAC accredited GLP-grade facility and no signs of toxicity at these therapeutic dose levels were shown in these animal models.
- Based on these pre-clinical efficacy and toxicity studies, a Phase I clinical trial with systemic administration of FUS1-nanoparticle was designed and activated for treatment of advanced stage lung cancer patients at M. D. Anderson Cancer Center.

Project 8: Therapeutic Targeting of bcl-xl Expression in Non-Small Cell Lung Carcinoma

- Demonstrated that bcl-xl ASO and adenoviral construct (xl22) reduced bcl-xl expression and induced apoptosis in NSCLC lines, and sensitized the cell lines to cisplatin, with significant increases in both cell death and apoptosis over either monotherapy approach.
- Demonstrated that ASO and xl22 decreased intraperitoneal tumor burden in a xenograft model of mesothelioma by 30%–40% and more than 60%, respectively.

Project 9: Use of Perfluorocarbons (PFC) to Enhance Pulmonary Gene Transfer

- Intratracheal administration of adenovirus allows transfection of the lung parenchyma only and is significantly increased when delivered in the presence of perfluorocarbon. Unfortunately, pulmonary transfection after repeated administration of adenovirus with perfluorocarbon intratracheally is not successful.
- We have explored DNA:Liposomal complexes with perfluorocarbon as well. Although *in vitro* studies were promising, any complex containing cholesterol given intrathecally was lethal and complexes without cholesterol were unable to transfect lung tissue when administered intrathecally.

Project 10: Development of Novel Murine Models of Lung Cancer and Evaluation of Antiangiogenic Agents

- Developed and validated murine models of orthotopic and metastatic human lung cancer
- Evaluated effects of ZD6474 alone and in combination with chemotherapeutic agents or radiation therapy using the orthotopic and metastatic lung cancer models
- ZD6474 is a potent inhibitor of angiogenesis that is highly effective therapeutically in an orthotopic model of human lung cancer ZD6474.
- Taxotere or Taxol enhanced the activity of ZD6474 in the brain metastatic models (lung adenocarcinoma), but Taxol antagonized ZD6474 activity in the bone metastatic model.

Core B: Biostatistics & Data Management Core

- In collaboration with Dr. Ruth Katz (Investigator in Project 1), the Core analyzed various data sets relating to the relationship between deletions of the 3p and 10q genes and overall survival for patients with NSCLC. The results were published in *Cancer* (Barkan et al., 2005).

- We have also assisted Dr. Charlie Lu's project (Project 4). In collaboration with Dr. Lu, we have analyzed six molecular factors including DAP kinase potentially prognostic for overall survival of resectable Stage I NSCLC patients. The data were published in *Journal of Clinical Oncology* (Lu et al., 2004). Currently, we are in the process of analyzing the correlation between hypermethylation of DAP kinase and patient survival. A manuscript is in preparation for publication (Lu et al., 2006).
- In addition, Dr. Jack Lee, in collaboration with Dr. Reuben Lotan (Project leader of Project 5), evaluated the data of growth inhibitory and apoptosis effects of histone deacetylase inhibitor SAHA and demethylating agent, 5-aza-2-deoxycytidine on lung cancer cell lines generated in Specific Aim 5.1. A manuscript is in preparation for publication (Fujimoto et al., 2006).

REPORTABLE OUTCOMES (IN SUMMARY)

Articles in peer-reviewed journals:

1. Barkan GA, Caraway NP, Jiang F, Zaidi TM, Fernandez R, Vaporciyan A, Morice R, Zhou X, Bekele BN, Katz R. Comparison of molecular abnormalities in bronchial brushings and tumor touch preparations. *Cancer Cytopathology* 105: 35-43, 2005.
2. El-Zein R, Schabath MB, Etzel CJ, Lopez MS, Franklin JD, Spitz MR. Cytokinesis-Blocked Micronucleus Assay as a Novel Biomarker for Lung Cancer Risk. *Cancer Res* 66: 6449-56, 2006.
3. Gu J, Berman DM, Lu C, Wistuba II, Roth JA, Frazier M, Spitz MR, Wu XF. Aberrant Promoter Methylation Profile and Association with Survival in Patients with Non-Small Cell Lung Cancer. *Clin Cancer Res* (in press), 2006.
4. Gu J, Spitz MR, Wu X. Polymorphisms of STK15 (Aurora-A) gene and lung cancer risk. *Carcinogenesis* (in press), 2006.
5. Ito I, Ji L, Tanaka F, Saito Y, Gopalan B, Branch CD, Xu K, Atkinson EN, Bekele BN, Stephens LC, Minna JD, Roth JA, Ramesh R. Liposomal vector mediated delivery of the 3p FUS1 gene demonstrates potent antitumor activity against human lung cancer in vivo. *Cancer Gene Ther* 11:733-9, 2004.
6. Ito I, Began G, Mohiuddin I, Saeki T, Saito Y, Branch CD, Stephens LC, Yen N, Roth JA, Ramesh R. Increased uptake of liposomal-DNA complex by lung metastases following intravenous administration. *Mol Ther* 7:409-418, 2003.
7. Gopalan B, Ito I, Branch CD, Clifton Stephens L, Roth JA, Ramesh R. Nanoparticle-based systemic gene therapy for lung cancer: Molecular mechanisms, and strategies to suppress nanoparticle-mediated inflammatory response. *Technol. Cancer Res Treat* 3:647-657, 2004.
8. Ito I, Saeki T, Mohiuddin I, Saito Y, Vaporciyan A, Branch C, Roth JA, and Ramesh R. Persistent transgene expression following intravenous administration of a liposomal complex: role of IL-10 mediated immune suppression. *Mol Ther* 9:318-327, 2004.
9. Ji L, John D, Minna, Jack A, Roth. 3p21.3 Tumor Suppressor Cluster: Prospects for Translational Applications. (Review) *Future Oncology*, 1, 79-92, 2005.
10. Ju Z, Kapoor M, Newton K, Cheon K, Ramaswamy A, Lotan R, Strong LC, Koo JS. Global detection of molecular changes reveals concurrent alteration of several biological pathways in non-small cell lung cancer cells. *Mol Genet Genom* 274:141-54, 2005.
11. Khuri FR, Glisson BS, Kim ES, Meyers ML, Herbst RS, Thall PF, Munden RF, Statkevich YP, Bangert S, Thompson E, Cascino M, Shin DM, Papadimitrakopoulou V, Kurie JM, Kies MS, Lee JS, Fossella FV, Hong WK. Phase I study of farnesyl transferase inhibitor (FTI) SCH66336 with paclitaxel in solid tumors. *Clinical Cancer Research*, 10:2968-76, 2004.
12. Lee JJ, Bekele BN, Zhou X, Cantor SB, Komaki R, Lee JS. Decision Analysis of Prophylactic Cranial Irradiation for Patients with Small Cell Lung Cancer. *J Clin Oncol* 24:3597-603 2006.
13. Lee JJ, Feng L. Randomized phase II designs in cancer clinical trials: current status and future directions. *J Clin Oncol* 23: 4450-7, 2005.

14. Lin X, Gu J, Lu C, Spitz MR, Wu X. Expression of telomere-associated proteins as prognostic markers for overall survival in patients with non-small cell lung cancer. *Clin Cancer Res* (in press), 2006.
15. Lu C, Soria JC, Tang X, Xu XC, Wang L, Mao L, Lotan R, Kemp B, Bekele BN, Feng L, Hong WK, Khuri FR. "Prognostic Factors in Resected Stage I Non-Small Cell Lung Cancer (NSCLC): A Multivariate Analysis of Six Molecular Markers". *J Clin Oncol* 22: 4575-83, 2004.
16. Oida Y, Gopalan, B., Miyahara, R., Inoue, S., Branch, C., Mhashilkar, A.M., Roth, J.A., Chada, S., and Ramesh, R. Sulindac enhances Ad-mda7/IL-24 mediated apoptosis of human lung cancer cells. *Mol. Cancer Ther.* 4(2):291-304, 2005.
17. Orrn A, Isobe T, Itasaka A, Wu W, O'Reilly M, Hong WK, Fidler IJ, Herbst RS. Development of an Orthotopic Model to Study the Biology and Therapy of Primary Human Lung Cancer in Nude Mice. *Clin Can Res* 9:5532-9, 2003.
18. Orrn A, Isobe T, Wu W, Itasaka S, Shintani T, Shibuya K, Kenji Y, O'Reilly MS, Fidler IJ, Herbst RS. Epidermal growth factor receptor tyrosine kinase inhibitor does not improve paclitaxel effect in an orthotopic mouse model of lung cancer. *Clin Cancer Res* 10:8613-9, 2004.
19. Oridate N, Lotan R. Suppression of DNA methyltransferase 1 levels in head and neck squamous carcinoma cells using small interfering RNA results in growth inhibition and increase in Cdk inhibitor p21. *Int. J. Oncology*, 26: 757-761, 2005.
20. Sun S-Y, Zhou Z, Wang R, Khuri FR. The farnesyltransferase inhibitor Lonafarnib induces growth arrest or apoptosis of human lung cancer cells without downregulation of Akt. *Cancer Biology and Therapy*, 3:1092-8, 2004.
21. Uno F, Sasaki J, Nishizaki M, Carboni G, Xu K, Atkinson EN, Kondo M, Minna JD, Roth JA, Ji L. Myristoylation of the FUS1 protein required for tumor suppression in human lung cancer cells. *Cancer Res.* 64, 2969-2976, 2004.
22. Wei QY, Wang LE, Sturgis EM, Mao L. Expression of Nucleotide Excision Repair Proteins in Lymphocytes as a Marker of Susceptibility to Squamous Cell Carcinomas of the Head and Neck. *Cancer Epiderm Biomarkers and Prev* 14:1961-6, 2005.

Manuscripts in progress:

1. Dang W, Uno F, Minna JD, Roth JA, Ji L. Synergistic tumor suppression by coexpression of FUS1 and p53 concurrences with FUS1-mediated down regulation of MDM2, accumulation of p53, and activation of Apaf1-dependent apoptotic pathway in human NSCLC cells. (in preparation)
2. Fujimoto JY, Men T, Lee JJ, Kong M, Ayers GD, Hong WK, Lotan R. Additive and synergistic effects of 5-aza-2'-deoxycytidine and suberoylanilide hydroxamic acid (SAHA) on human lung carcinoma cells in vitro and in vivo. (in preparation)
3. Futoshi Uno, Jiichiro Sasaki, Gitanjali Jayachandran, Kai Xu, John D. Minna, Jack A. Roth, Lin Ji, Activation of apoptosis by tumor suppressor FUS1 and Apaf-1 protein interaction. *Nature*, 2006 (pending revision).
4. Gilienwater AM, Zhong M, Lotan R. Induction of apoptosis in head and neck squamous carcinoma cells by the histone deacetylase inhibitor SAHA is mediated by both mitochondrial and Fas (CD95) signaling. (ready for submission)
5. Isobe T, Orrn A, Wu W, Shintani T, Itasaka S, Shibuya K, O'Reilly MS, Herbst RS. Biology and therapy of human small cell lung cancer (SCLC) in novel orthotopic nude mouse models. (in preparation)
6. Itasaka S, Kornaki R, Shibuya K, Shintani T, Bucana CD, Herbst RS, O'Reilly MS. Targeted therapy against VEGF and EGF receptor signaling with blocks angiogenesis and improves the therapeutic efficacy of chemotherapy in a mouse model of lung cancer brain metastasis. (in preparation)
7. Kawashima H, Jayachandran G, Deng W, Xu K, Minna JD, Roth JA, Ji L. Overcoming gefitinib resistance in NSCLC via inactivation of the PI3K/AKT signaling pathway by a combination of FUS1 nanoparticles and EGFR inhibitors. (in preparation)

8. Kawashima H, Uno F, Kurie J, Minna JD, Roth JA, Ji L. Synergistic inhibition of EGFR tyrosine kinase activity and NSCLC cell growth by combination treatment with FUS1-nanoparticle and gefitinib. (in preparation)
9. Kim SW, Cheon K, Kim CH, Yoon JH, Hawke D, Kobayashi R, Lotan R, Hong WK, and Koo JS. Proteomics-Based Identification of Proteins Secreted in Apical Surface Fluid of Squamous Metaplastic Human Tracheobronchial Epithelial Cells Cultured by Three-Dimensional Organotypic Air-Liquid Interface Method. *Cancer Res* (in review), 2006.
10. Lee WS, Jimenez CA, Cheon K, Ryu SH, Wistuba II, Liu D, Lee JJ, Lotan R, Hong WK, Morice R, and Koo JS. Evaluation of Secretory Proteins as Surrogate Markers of Metaplasia/Dysplasia of Lung Mucos. (in preparation)
11. Lin X, Wu X, Katz R, Shao L, Koo P, Spitz MR. Correlations of genetic instability markers in surrogate and target tissues in lung cancer patients. (in preparation)
12. Lu C, Wistuba I, Zhou X, Bekele BN, Putnam JB, Jr., Correa A, Mao L. Prognostic role of promoter hypermethylation of death-associated protein (DAP) kinase and p 16 genes in early-stage non-small cell lung cancer. (in preparation)
13. Qiu Y, Liu X, Yue P, Lonial S, Khuri RK, Sun SY. The farnesyltransferase inhibitor R115777 upregulates DR5 expression and enhances TRAIL-induced apoptosis in human lung cancer cells. (Manuscript completed and under review by Johnson & Johnson)
14. Schabath MB, Wei Q, Greisinger AJ, Etzel CJ, Spitz MR. DNA repair capacity and prior respiratory disease jointly modify lung cancer risk. *Cancer Res* (submitted), 2006
15. Shibuya K, Ritsuko K, Shintani T, Itasaka S, Ryan A, Jürgensmeier JM, Milas L, Ang KK, Herbst RS, O'Reilly MS. Targeted therapy against VEGFR and EGFR with ZD6474 enhances the therapeutic efficacy of irradiation in an orthotopic model of human non-small cell lung cancer, *Clin Cancer Res* (submitted), 2006
16. Shintani T, Lewis VO, Komaki R, Ryan A, Herbst RS, O'Reilly MS. The anti-tumor and antiangiogenic effects of VEGFR and EGFR blockade are superior to EGFR blockade alone but are not enhanced by the addition of paclitaxel in a model of lung cancer bone metastasis. (in preparation)
17. Sun SY, Liu X, Zou W, Yue P, Zhou Z, Marcus AI, Khuri FR. Activation of the death receptor 5-mediated extrinsic apoptotic pathway contributes to farnesyltransferase inhibitor-induced apoptosis in human lung cancer cells. *Oncogene* (submitted), 2006.
18. Wu G, Deng W, Jayachandran G, Minna JD, Roth JA, Ji L. Interaction of the tumor suppressor FUS1 with PDGFR β inhibits PDGFR-mediated proliferation of human lung cancer cells. (in preparation)
19. Wu W, O'Reilly MS, Langley R, Tsan RZ, Baker CH, Bekele N, Tang XM, Onn A, Fidler IJ, Herbst RS. Expression of EGF/TGF- α by human lung cancer cells determines response to EGFR kinase inhibitors. *Cancer Res* (submitted), 2006.
20. Wu X, Isobe T, Onn A, Itasaka S, Langley RR, Shintani T, Shibuya K, Komaki R, Ryan AJ, Fidler IJ, Herbst RS, O'Reilly MS. Targeted therapy of the tumor and vascular components of orthotopic human lung cancer by combined vascular endothelial growth factor and epidermal growth factor receptor signaling blockade. *Mol Cancer Ther* (submitted), 2006.
21. Wu X, Lin J, Etzel CJ, Schabath MB, Gorlova OY, Zhang Q, Dong Q, Amos CI, Spitz MR. Interplay between mutagen sensitivity and epidemiological factors in lung cancer risk. *Am J Hum Genet* (submitted), 2006.
22. Zhong M, Gillenwater A, Lotan R. Valproic acid induces growth inhibition and apoptosis in head and neck squamous carcinoma cell lines. (in preparation)
23. Zou W, Yue P, Khuri FR, Sun SY. The farnesyltransferase inhibitor Lanafarnib induces DR5 expression through a CHOP/GADD153-dependent mechanism. (in preparation)

Meeting Abstracts:

1. Etzel CJ, Zhang Q, Schabath M, Dong Q, Wu XF, Wei QY, Spitz MR. Building a comprehensive quantitative risk assessment model for lung cancer. *Proc AACR* 46:#4051 2005.

2. Schabath MB, Wei Q, Xifeng Wu X, Spitz MR. Prior respiratory disease, DNA repair capacity, and inflammation-related genotypes modify lung cancer risk. *Proc AACR* 47:#5663, 2006.
3. Wang L, Shi Q, Guo Z, Qiao Y, Spitz MR, Wei Q. A novel assay to measure the capacity to repair N7-guanine site-specific DNA damage. *Proc AACR* 47:#5661, 2006.
4. Lu C, Wistuba I, Zhou X, Bekele BN, Putnam JB, Jr, Correa A, Mao L. Prognostic role of promoter hypermethylation of death-associated protein (DAP) kinase and p 16 genes in early-stage non-small cell lung cancer. *Proc ASCO* 24:7216, 2006.
5. Wu X, Huang M, Gu J, Amos C, Shao L, Zhang Q and Spitz M. DNA repair and cell cycle control pathways in lung cancer predisposition. *Proc AACR* 47:#5662, 2006.
6. Wu X, Lin J, Etzel C, Schabath M, Gorlova O, Zhang Q, Dong Q, Amos C and Spitz M. Interplay between mutagen sensitivity and epidemiological factors in modulating lung cancer risk. *Proc AACR* 47:#435, 2006.
7. Yang H, Spitz M, Liu J, Gu J, Lu C, Stewart D and Wu X. ATM haplotype-tagging SNPs predict non-small cell lung cancer risk. *Proc AACR* 47:#445, 2006.
8. Kim SW, Kim CH, Cheon K, Newton K, Hawke D, Kobayashi R, Koo JS. Identification of markers for squamous metaplasia of bronchial epithelial cells. *Proc AACR* 46, 2005.
9. Fujimoto JY, Hong WK, Lotan R. Antineoplastic action of 5-aza-2'-deoxycytidine and suberoylanilide hydroxamic acid (SAHA) on human lung carcinoma cells. *Proc AACR* 46: #1820, 2005.
10. Zhong M, Gillenwater A, Lotan R. Valproic acid induces growth inhibition and apoptosis in head and neck squamous carcinoma cell lines. *Proc AACR* 47:#3853, 2006.
11. Carboni GL, Shao J, Xu K, Gao B, Nishizaki M, Schmid RA, Minna JD, Roth JA, Ji L. Synergistic inhibition of tumor cell growth by CACNA2D2 and p53 via activation of DAPK pathway in lung cancer. American Association for Cancer Research (AACR), 94th Annual Meeting, Toronto, Ontario, Canada, April 5-9, 2003. *Proc. Am. Assoc. Cancer Res.*, 44:241-242, 2003.
12. Uno F, Sasaki J, Nishizaki M, Carboni G, Xu K, Minna JD, Roth JA, Ji L. Myristoylation of Fus1 protein is required for Fus1-mediated tumor suppressing activities in human lung cancer. American Association for Cancer Research (AACR), 94th Annual Meeting, Washington, District of Columbia, July 11-14, 2003. *Proc. Am. Assoc. Cancer Res.*, 44:75, 2003.
13. Jirochiro Sasaki, Futoshi Uno, John D. Minna, Jack A. Roth, Lin Ji. Enhanced Sensitivity of Tumor Cells to Chemotherapeutic Agents by Activation of FUS1 Tumor Suppressor Gene in Lung Cancer Cells. Proceedings of The 95th American Association for Cancer Research (AACR) Annual Meeting, Orlando, FL, March 27-31, 2004, Abstract #3796.
14. Futoshi Uno, Jirochiro Sasaki, Gitanjali Jayachandran, Kai Xu, John D. Minna, Jack A. Roth, Lin Ji. Activation of Apoptotic Signaling Pathway by Direct Interaction between Tumor Suppressor Fus1 and Apaf-1 proteins in Lung Cancer Cells Back to Search. Proceedings of The 95th American Association for Cancer Research (AACR) Annual Meeting, Orlando, FL, March 27-31, 2004 (AACR Scholar-in-Training Awards), Abstract #4821.
15. Hiroyuki Kawashima, Charles Lu, Jonathan Kurie, Sunil Chada, John D. Minna, Jack A. Roth, Lin Ji. Synergistic inhibition of EGFR tyrosine kinase and tumor cell growth in non-small cell lung cancer (NSCLC) by combination treatment with FUS1-nanoparticles and Gefitinib. ASCO Annual Meeting, Orlando, Florida, May 13-17, Abstract No: 7081, 2005.
16. Hiroyuki Kawashima, Futoshi Uno, Jonathan Kurie, John D. Minna, Jack A. Roth, Lin Ji. Synergistic inhibition of EGFR tyrosine kinase activity and NSCLC cell growth by combination treatment with FUS1-nanoparticle and gefitinib. American Association for Cancer Research (AACR), 96th Annual Meeting, Anaheim, CA, April 16-20, 2005. *Proc. Am. Assoc. Cancer Res.*, Vol. 46, #2707.
17. Wuguo Deng, Futoshi Uno, John D Minna, Jack A. Roth, Lin Ji. Synergistic tumor suppression by coexpression of FUS1 and p53 concurrences with FUS1-mediated down regulation of MDM2, accumulation of p53, and activation of Apaf1-dependent apoptotic pathway in human NSCLC cells. American Association for Cancer Research (AACR), 96th Annual Meeting, Anaheim, CA, April 16-20, 2005. *Proc. Am. Assoc. Cancer Res.*, Vol. 46. #3516.

18. Gopalan, B., Branch, C.D., Stephens, L.C., Roth, J.A., Ramesh, R. A novel strategy for suppressing toxicity-mediated by systemic delivery of DNA-nanoparticles. *Proc. Am. Assoc. Cancer Res.*, 46:788, abstract # 3345, 2005.
19. Hiroyuki Kawashima, Gitanjali Jayachandran, Wuguo Deng, Kai Xu, John D. Minna, Jack A. Roth, Lin Ji. Overcoming gefitinib resistance in NSCLC via inactivation of the PI3K/AKT signaling pathway by a combination of FUS1 nanoparticles and EGFR inhibitors. American Association for Cancer Research (AACR), 97th Annual Meeting, Washington DC, April 1-5, 2006. *Proc. Am. Assoc. Cancer Res.*, Vol. 47. #5426.
20. Guanglin Wu, Wuguo Deng, Gitanjali Jayachandran, John D. Minna, Jack A. Roth, Lin Ji. Interaction of the tumor suppressor FUS1 with PDGFR β inhibits PDGFR-mediated proliferation of human lung cancer cells. American Association for Cancer Research (AACR), 97th Annual Meeting, Washington DC, April 1-5, 2006. *Proc. Am. Assoc. Cancer Res.*, Vol. 47. #1460. (AACR Scholar-in-Training Awards).
21. Hittelman W N, Wang G, Koo JSP, Lu, T. The spatial distribution and etiology of genetic instability in organotypic bronchial epithelial cell cultures. *Proc. AACR* 46:3527, 2005.
22. Lu T, Hittelman WN. Assessment of subclonal evolution in human bronchial epithelial cell lines progressing toward malignancy by fluorescence inter-simple sequence repeat PCR. *Proc AACR* 44:894, 2003.
23. Lu T, Hittelman WN. Improvement and application of fluorescence inter-simple sequence repeat polymorphism chain reaction for the study of subclonal growths in lung epithelial cell populations. *Chest* 125 (Suppl. 5):110-111S, 2004.
24. Lu T, Hittelman WN. Quantitative fluorescence inter-simple sequence repeat PCR for subclonal analysis of bronchial cell populations. *Proc AACR* 45, 2004.
25. Lu T, Wistuba II, Hittelman WN. Detection of clonal and subclonal outgrowths in the upper aerodigestive tract of current and former smokers with lung cancer. *Proc AACR* 46:#2230, 2005.
26. Lu T, Wistuba II, Hittelman WN. Existence of clonal and subclonal outgrowths in the bronchial epithelium and stroma of current smokers. *Proc AACR* 47:#462, 2006.
27. Shibuya K, Komaki R, Shintani T, Wu W, Itasaka S, Isobe T, Ryan A, Herbst RS, O'Reilly, MS. Combined blockade of VEGFR and EGFR with ZD6474 enhances the anti-tumor and anti-vascular effects of radiation therapy in an orthotopic mouse model of human lung cancer. *Proceedings of AACR: #5828*, 2005.
28. Shintani T, Lewis VO, Komaki R, Wu W, Ryan A, Herbst RS, O'Reilly, MS. ZD6474 inhibits human lung cancer bone metastases in a murine model by targeting both the tumor and its vasculature. *Proceedings of AACR: # 5844*, 2005.
29. Isobe T, Onn A, Wu W, Shintani T, Itasaka S, Shibuya K, Hong WK, O'Reilly MS, Herbst RS. Biology and therapy of human small cell lung cancer (SCLC) in novel orthotopic nude mouse models. *Proceedings of AACR:#5136*, 2004.
30. Wu W, Onn A, Shintani T, Herbst RS, O'Reilly MS. ZD6474 enhances the anticancer efficacy of Paclitaxel in human Lung Cancer Models. *Angiogenesis* 7(Suppl 1):25, 2004.
31. Shibuya K, Komaki R, Wu W, Shintani T, Itasaka S, Isobe T, Ryan A, Herbst RS, O'Reilly MS. Targeted therapy against VEGFR and EGFR signaling with ZD6474 enhances the therapeutic efficacy of irradiation in an orthotopic mouse model of human non-small cell lung cancer. *Int'l J Radiation Oncol, Biology, Physics* 60(1 Suppl S):S149-50, 2004.
32. Wu W, Shintani T, O'Reilly MS, Herbst RS. Blocking VEGF and EGF receptor signaling with ZD6474 sensitizes human non-small cell lung cancer to chemotherapy with paclitaxel. *Europ J Cancer Suppl* 2(8 suppl):50, 2004.
33. Wu W, Isobe T, Itasaka S, Shintani T, Langley RR, Onn A, Hansen JC, O'Reilly MS, Herbst RS. ZD6474, a small molecule targeting VEGF and EGF receptor signaling, inhibits lung angiogenesis and metastasis and improves survival in an orthotopic model of non-small cell lung cancer. *Proceedings of AACR: # 4551*, 2004.
34. Wu W, Isobe T, Onn A, Shintani T, Itasaka S, Shibuya K, Langley RR, Hansen JC, Fidler IJ, Ryan AJ, Herbst RS, O'Reilly MS. Targeted therapy against VEGF and EGF receptor signaling with

ZD6474 blocks angiogenesis and inhibits the growth and dissemination of orthotopic human lung cancer in mice. Clin Cancer Res 9(16 Pt 2):6143s, 2003.

Project-generated grants:

1. Charlotte Geyer Foundation Fund. The grant titled "Systemic Non-Viral Gene Therapy for Lung Cancer". The preliminary data for this grant application was partly generated from studies conducted in Project 7 of **TARGET**. PI: Lin Ji, Ph.D
2. NIH U01: Mouse Models of Human Cancers Consortium 4/1/2004-3/31/2009
Projects 2 and 5: Modeling Airway Lung Cancer and the Role of Inflammation
Project leader: Lin Ji, Ph.D.
3. NCI Lung Cancer Program Project Grant (P01): "Targeting cell signaling in lung cancer to enhance therapeutic efficacy." PI: Fadlo R. Khuri. Duration: 04/01/06 -03/31/11.

Project-generated clinical trials:

Based on the preclinical findings from the **TARGET** projects, we have designed 2 clinical trials:

1. A phase II clinical trial with antiangiogenic agent ZD6474 in combination with chemotherapeutic agents in NSCLC patients (PI: Roy Herbst, M.D., Ph.D)
2. A phase II A phase II randomized trial of treatment of malignant pleural effusion with ZD6474, a novel VEGFR and EGFR tyrosine kinase inhibitor (a part of **IMPACT**). (PI: Roy Herbst, M.D., Ph.D.)

Patents (Granted and Pending):

1. Ji L, Roth JA. Detection of Expression and Posttranslational Modification of Fus1 Protein on ProteinChip Array by SELDI-TOF-MS. MDA04-107, 2004 .
2. Ji L, Roth JA, Minna JD, Lerman MI. Chromosome 3p21.3 genes as tumor suppressors. U.S. Patent, US-2004-0016006-A1; World Patent: WO 02/04511 A2. 2004.
3. Jacki Lin, Ralph B. Arlinghaus, Lin Ji, Jack A. Roth, Inhibition of Abl Kinase by FUS1 Peptide, MDA05-048, January 25, 2005.
4. Lin Ji, Jack A. Roth, A Novel Therapeutic FUS1 (FP) and FP-Nanoparticle mediated Inhibition of PTK Activities and Tumor Cell Growth, MDA05-058, March 4, 2005.
5. Gitanjali Jayachandran, Kevin Coombes, Jack Roth, Lin Ji. High throughput serum phosphopeptide profiling for early detection, molecular classification, and diagnosis of lung cancer. MDA06-040, 2006 (pending).

Project-generated resources:

Our NCI-funded Lung SPORE project builds upon this specimen and data resource. The SPORE project is evaluating telomere length in peripheral blood lymphocytes and bronchial brushings from the same patients as enrolled in our DOD project. We are also performing FISH studies on 3p and 10q in sputum as early detection markers.

CONCLUSIONS:

The **TARGET** program has proceeded as we originally proposed, with few subsequent modified aims. We have completed the approved tasks as detailed in this report. We have published 22 peer-reviewed articles with 23 additional manuscripts in-process for publication. Based on the research findings, our investigators have applied for and been awarded 3 research project grants (1 NCI Lung P01, 1 NCI U01, and 1 from a private foundation), and developed 2 clinical trials that are activated at M. D. Anderson Cancer Center. In addition, we have filed and been granted 5 patents for scientific discoveries.

Conclusions are as follows:

Project 1: Mutagen sensitivity (a measure of overall genetic instability) unmasked by *in vitro* exposure to the mutagen, benzo-a-pyrene, is a marker of constitutional genetic susceptibility and is correlated with genetic aberrations in bronchial epithelial cells and uninvolved lung tissue, but not the cancer tissue. Latent genetic instability in lymphocytes reflects generalized genetic instability in the normal, but not cancerous target tissue.

Project 2: The fluorescent inter-simple sequence repeat PCR (FISSR-PCR) studies confirm the *in situ* hybridization results and demonstrate that this technology is useful for quantifying the extent of clonal and subclonal outgrowths in the bronchial epithelium, and also demonstrated that the stroma underlying the damaged bronchial epithelium could undergo clonal change and evolution, suggesting that the stroma may play a significant role in lung tumorigenesis.

Project 3: 1) Secreted proteins (secretome) from premalignant or malignant lung cells hold promise as potential biomarkers to detect early lung cancer; 2) Expression levels of individual biomarkers identified in secretions from metaplastic squamous cells in bronchial lavage are not directly correlated with histological appearance of bronchial mucosa; 3) Primary bronchial epithelial cells isolated from bronchial mucosa of patients (64 cases) with lung cancer will be useful resources to understand the mechanisms of lung carcinogenesis, particularly molecular abnormalities in epithelial cells adjacent to tumor. In addition, they may have potential value to determine sensitivity or resistance to therapy of patients by performing treatment simulation *in vitro*.

Project 4: In this relatively large cohort of early-stage NSCLC patients, we did not detect significant statistical correlations between the promoter methylation of *p16* and *DAP kinase* and clinical outcomes. Further subset analyses stratified by gender and histology will be performed. The prognostic role of these biomarkers in NSCLC remains unclear. However, this project has produced a valuable clinical-pathological database. We have already begun a second study analyzing the prognostic role of the forkhead transcription factor FOXO3a in this patient population.

Project 5: The epigenetic modulators (demethylating agent 5-aza-CdR and histone deacetylase inhibitors SAHA and valproic acid) exert growth inhibitory and apoptosis-inducing activity in HNSCC cells and premalignant and malignant lung epithelial cells *in vitro*, and SAHA and 5-aza-CdR are also active *in vivo* especially in combination. These results strongly support that this combination should be investigated further for therapeutic use in patients with this malignancy.

Project 6: Farnesyl transferase inhibitors SCH66336 and R115777 induce apoptosis by increasing DR5 expression and TRAIL-induced apoptosis, independent of downregulating Akt and Raf/ERK pathways, and DR5, c-FLIP, and CHOP are FTI-regulated proteins. The synergistic effect of SCH66336 with taxanes required the functional HDAC6.

Project 7: The study revealed a novel molecular mechanism of FUS1-mediated tumor suppression function *in vitro* and *in vivo*. A novel DOTAP:Cholesterol:FUS1 plasmid DNA-nanoparticle for systemic treatment of lung cancer was developed and tested preclinically. Based on these preclinical efficacy and toxicity studies, a Phase I clinical trial with systemic administration of FUS1-nanoparticle was designed and approved and is open currently for advanced stage lung cancer patients at M. D. Anderson Cancer Center.

Project 8: The bcl-2 antisense oligonucleotide (ASO) effectively blocked the bcl-2 expression *in vitro*, but the limitation of the *in vivo* applicability of this antisense approach makes it less advantageous than the newly emerged siRNA strategy for future use.

Project 9: The project did not generate any positive results. The investigator discontinued the study.

Project 10: We conclude that 1) the orthotopic murine model of lung cancer is a valuable tool to test the antiangiogenic agents and their combination with cytotoxic agents; 2) The model provides a rational basis for development of anti-angiogenic therapy with conventional and emerging modalities in the treatment of lung cancer; 3) ZD6474 is a potent inhibitor of angiogenesis that is highly effective therapeutically in an orthotopic model of human lung cancer. It will be prudent to develop clinical strategies for the combination of specific protein tyrosine kinase inhibitors that block both EGFR and VEGFR signaling.

Biostatistics & Data Management Core: The Core has provided solid biostatistical support for the **TARGET** projects from the initial study design to completion of data analysis and publication. It is a valuable component of the program.

REFERENCES

1. Adjei AA, Mauer A, Bruzek L, Marks RS, Hillman S, Geyer S, Hanson LJ, Wright JJ, Erlichman C, Kaufmann SH, Vokes EE. Phase II study of the farnesyl transferase inhibitor R115777 in patients with advanced non-small-cell lung cancer. *J Clin Oncol* 21: 1760-6, 2003.
2. Baylin SB, Ohm JE. Epigenetic gene silencing in cancer - a mechanism for early oncogenic pathway addiction? *Nat Rev Cancer*. 2006;6:107-16.
3. Gore SD, Baylin S, Sugar E, Carraway H, Miller CB, Carducci M, Grever M, Galm O, Dausers T, Karp JE, Rudek MA, Zhao M, Smith BD, Manning J, Jiemjit A, Dover G, Mays A, Zwiebel J, Murgio A, Weng LJ, Herman JG. Combined DNA methyltransferase and histone deacetylase inhibition in the treatment of myeloid neoplasms. *Cancer Res*. 2006;66:6361-9.
4. Jemal A, Siegel R, Ward E, Murray T, Xu J, Smigal C, Thun MJ. Cancer Statistics, 2006. *CA Cancer J Clin*. 56:106-30, 2006.
5. Kelly WK, Marks PA. Drug insight: Histone deacetylase inhibitors--development of the new targeted anticancer agent suberoylanilide hydroxamic acid. *Nat Clin Pract Oncol* 2:150-7, 2005.
6. Nishizaki M., Sasaki, J., Fang, B., Atkinson, E.N., Minna., J.D., Roth, J., Ji, L. Synergistic tumor suppression by coexpression of FHIT-mediated MDM2 inactivation and p53 stabilization in human NSCLC cells. *Cancer Res* 64 (16), 5632-5640, 2004.
7. Templeton NS, Lasic DD, Frederik PM, Strey HH, Roberts DD, Pavlakis GN. Improved DNA: liposome complexes for increased systemic delivery and gene expression. *Nat Biotechnol* 5:647-52, 1997.
8. Templeton NS, Roberts DD, Safer B. Efficient gene targeting in mouse embryonic stem cells. *Gene Ther* 4:700-9, 1997.

List of Personnel Receiving Pay

1. Project 1 – Margaret Spitz, M.D.

- Pam Porter
- Anita Broxson
- Susan Honn
- Qiong Dong
- Reggie Salvino
- Easter Secnobia
- Yawei Qiao
- Wenhua Lang
- Yun fei Wang
- Sheri Luo
- Tanweer Zaidi
- Ricardo Fernandez
- Sherry Ritter
- Jamey Franklin
- Karen St. Julian

2. Project 2 – Walter Hittelman, Ph.D.

- Julie Izzo
- Lu Tao
- Walter Hittelman
- Bobby Brown
- Guiying Wang

3. Project 3 – Peter Koo, Ph.D.

- Fazal Haq Tabassam
- Kyounga Cheon
- Sohee Jun
- Seung Wook Kim

4. Project 4 – Charles Lu, M.D.

- Laureen Washington
- Wenhua Lang

5. Project 5 – Reuben Lotan, Ph.D.

- Numsen Hail, Jr.
- Qingguo Tao
- Claudio Schroeder
- Nitin Chakravarti
- Hyun Ho Choi

6. Project 6 – Fadlo Khuri, M.D.

- Fadlo Khuri
- Shi-Young Sun
- Heath Butler Acuff
- Xiangguo Liu
- Wei Zou
- Judie Wells

7. Project 7 – Ji Lin, Ph.D.

- Lin Ji

- Rajagopal Ramesh
- Began Gopalan
- Heping Liu
- Yiming Chen

8. Project 8 – W Roy Smythe, M.D.

- Xiaobo Cao

This project was dropped

9. Project 9 – Ara Vaporciyan, M.D.

- Chandeswar Sharma

This project was dropped.

10. Project 10 – Roy Herbst, M.D.; Michael O'Reilly, M.D.

- Jill Hansen
- Jayasri Mandal
- Kazuhisa Furutani
- Joerg Jacoby
- Erminia Massarelli
- Scott Ryan

Core A – Waun Ki Hong, M.D

- James Luca
- Brenda Coldman
- John Reyes
- Jeanne Riddle
- Tina Dellahoussaye
- Andrew Bouquard
- Debra Townley
- Anthony Perez
- Adelina Fuentes
- Johnnie Cooper
- Hong Zou

Core B – Jack Lee, Ph.D

- Jack Lee
- Diane Liu
- Xian Zhou
- Neby Bekele

APPENDIX

Appendix 1 – Project 5 Raw Data

Appendix 2 – Project 5 Figures

Appendix 3 - Manuscripts

APPENDIX I (LOTAN TARGET REPORT)

Table 2. Genes showing increased expression after treatment of HNSCC cells with SAHA (4 μ M; 24 hr)

Log2Fold Change	NAME
7.42	G antigen 1 /// G antigen 1#GAGE1
6.96	G antigen 5#GAGE5
6.45	G antigen 5#GAGE5
6.40	chemokine (C-C motif) ligand 20#CCL20
6.38	G antigen 5#GAGE5
6.27	G antigen 5#GAGE5
5.72	melanoma antigen, family A, 6#MAGEA6
5.62	melanoma antigen, family A, 3#MAGEA3
5.23	G antigen 5 /// G antigen 5#GAGE5
5.20	interferon, alpha-inducible protein 27#IFI27
5.02	decay accelerating factor for complement (CD55, Cromer blood group system)#DAF
4.84	decay accelerating factor for complement (CD55, Cromer blood group system)#DAF
4.56	deleted in azoospermia-like#DAZL
4.56	melanoma antigen, family A, 4#MAGEA4
4.15	cathepsin E#CTSE
4.13	matrix metalloproteinase 7 (matrilysin, uterine)#MMP7
4.11	melanoma antigen, family A, 12#MAGEA12
4.11	tubulin, beta polypeptide#TUBB
3.99	Homo sapiens cDNA clone IMAGE:4346793, partial cds#---
3.93	---
3.88	dehydrogenase/reductase (SDR family) member 2#DHRS2
3.85	keratin 20#KRT20
3.63	prostate differentiation factor#PLAB
3.57	melanoma antigen, family A, 5#MAGEA5
3.56	histone 2, H2aa#HIST2H2AA
3.46	interferon, alpha-inducible protein (clone IFI-6-16)#G1P3
3.46	cancer/testis antigen 1 /// cancer/testis antigen 1#CTAG1
3.44	SWI/SNF related, matrix associated, actin dependent regulator of chromatin, subfamily a, member 3#SMARCA3

3.41	synovial sarcoma, X breakpoint 1#SSX1	
3.39	interleukin 8#IL8	
3.38	melanoma antigen, family A, 1 (directs expression of antigen MZ2-E)#MAGEA1	
3.30	dehydrogenase/reductase (SDR family) member 2#DHRS2	
3.25	transmembrane 4 superfamily member 4#TM4SF4	
3.23	nerve growth factor receptor (TNFRSF16) associated protein 1#NGFRAP1	
3.22	transketolase-like 1#TKTL1	
3.07	annexin A10#ANXA10	
3.06	chondroitin sulfate proteoglycan 2 (versican)#CSPG2	
3.02	tissue inhibitor of metalloproteinase 1 (erythroid potentiating activity, collagenase inhibitor)#TIMP1	
2.99	melanoma antigen, family A, 9#MAGEA9	
2.94	cancer/testis antigen 1#CTAG1	
2.87	carcinoembryonic antigen-related cell adhesion molecule 6 (non-specific cross reacting antigen)#CEACAM6	
2.85	amphiregulin (schwannoma-derived growth factor)#AREG	
2.85	glycine amidinotransferase (L-arginine:glycine amidinotransferase)#GATM	
2.84	glycine amidinotransferase (L-arginine:glycine amidinotransferase)#GATM	
2.83	glutathione S-transferase M3 (brain)#GSTM3	
2.79	trefoil factor 1 (breast cancer, estrogen-inducible sequence expressed in)#TFF1	
2.77	histone 2, H2aa#HIST2H2AA	
2.76	cancer/testis antigen 2#CTAG2	
2.76	chondroitin sulfate proteoglycan 2 (versican)#CSPG2	
	Homo sapiens transcribed sequence with strong similarity to protein ref:NP_073729.1 (H.sapiens)	
2.74	microtubule-associated proteins 1A/1B light chain 3 [Homo sapiens]#---	
2.72	---	
2.71	aldehyde dehydrogenase 1 family, member A1#ALDH1A1	
2.71	synovial sarcoma, X breakpoint 4#SSX4	
2.70	insulin-like growth factor binding protein 1#IGFBP1	
2.70	matrix metalloproteinase 1 (interstitial collagenase)#MMP1	
2.63	G antigen, family D, 2#GAGED2	
2.62	dual specificity phosphatase 5#DUSP5	
2.61	transcobalamin I (vitamin B12 binding protein, R binder family)#TCN1	
2.59	melanoma antigen, family B, 2#MAGEB2	
2.58	histone 1, H2bk#HIST1H2BK	
2.58	interferon stimulated gene 20kDa#ISG20	
2.56	---	
2.52	tubulin, alpha 3#TUBA3	

2.51	histone 1, H1c // histone 1, H1c#HIST1H1C
2.51	---#---
2.50	clusterin (complement lysis inhibitor, SP-40.40, sulfated glycoprotein 2, testosterone-repressed
2.46	prostate message 2, apolipoprotein J)#CLU glucagon#GCG
2.45	solute carrier family 3 (cystine, dibasic and neutral amino acid transporters, activator of cystine,
2.43	dibasic and neutral amino acid transport), member 1#SLC3A1
2.42	H2B histone family, member S#H2BFS
2.41	histone 1, H2bd#HIST1H2BD
2.40	---#---
2.39	synovial sarcoma, X breakpoint 2#SSX2
2.38	---#---
2.36	POU domain, class 2, associating factor 1#POU2AF1
2.35	lipocalin 2 (oncogene 24p3)#LON2
2.35	chemokine (C-X-C motif) ligand 1 (melanoma growth stimulating activity, alpha)#CXCL1
2.31	brain expressed, X-linked 1#BEX1
2.31	S100 calcium binding protein A4 (calcium protein, calvasculin, metastasin, murine placental homolog)#S100A4
2.29	solute carrier family 16 (monocarboxylic acid transporters), member 4#SLC16A4
2.29	carcinoembryonic antigen-related cell adhesion molecule 6 (non-specific cross reacting antigen) #CEACAM6
2.29	melanoma antigen, family A, 8#MAGEA8
2.29	uroplakin 1B#UPK1B
2.27	claudin 18#CLDN18
2.25	microtubule-associated protein 1 light chain 3 beta#MAP1LC3B
2.25	hypothetical protein FLJ10097#FLJ10097
2.22	major histocompatibility complex, class I, B#HLA-B
2.21	melanoma cell adhesion molecule#MCAM
2.21	cancer/testis antigen 1#CTAG1
2.21	mucin 13, epithelial transmembrane#MUC13
2.19	glucosaminyl (N-acetyl) transferase 3, mucin type#GCNT3
2.19	H2A histone family, member B#H2AFB
2.14	major histocompatibility complex, class I, B // major histocompatibility complex, class I, B#HLA-B
2.13	DnaJ (Hsp40) homolog, subfamily D, member 1#DNAJD1
2.13	hypothetical protein DKFZp434B227#DKFZp434B227
2.13	histone 1, H2bc#HIST1H2BC

2.11	major histocompatibility complex, class I, C#HLA-C
2.10	hypothetical protein FLJ22662#FLJ22662
2.10	interferon, alpha-inducible protein (clone IFI-15K)#G1P2
2.09	thioredoxin interacting protein#TXNIP
2.08	nitric oxide synthase 3 (endothelial cell) /// nitric oxide synthase 3 (endothelial cell)#NOS3
2.05	uroplakin 1B#UPK1B
2.04	dynein, axonemal, light intermediate polypeptide 1#DNAL1
2.04	---
2.03	melanoma cell adhesion molecule#MCAM
2.02	transcriptional co-activator with PDZ-binding motif (TAZ)#TAZ
2.02	Interferon stimulated gene 20kDa#ISG20
2.01	major histocompatibility complex, class I, B#HLA-B
2.00	interferon induced transmembrane protein 1 (9-27)#IFITM1

Table 3. Genes showing decreased expression after treatment of HNSCC cells with SAHA (4 μ M; 24 hr)

Log2Fold Change	NAME
-2.00	dihydrofolate reductase#DHFR
-2.13	S-phase kinase-associated protein 2 (p45)#SKP2
	secreted phosphoprotein 1 (osteopontin, bone sialoprotein 1,
-2.14	early T-lymphocyte activation 1)#SPP1
	acetyl-Coenzyme A acyltransferase 2 (mitochondrial 3-oxoacyl-
-2.15	Coenzyme A thiolase)#ACAA2
-2.18	hypothetical protein FLJ12584#FLJ12584
-2.22	dickeopf homolog 1 (Xenopus laevis)#DKK1
-2.29	serine protease inhibitor, Kazal type, 5#SPINK5
-2.57	aldehyde dehydrogenase 3 family, member A1#ALDH3A1
-3.53	3-hydroxy-3-methylglutaryl-Coenzyme A synthase 2 (mitochondrial)#HMGCS2

Table 4. Genes showing increased expression after treatment of HNSCC cells with 5-AZA-CdR (1 μ M; 4days)

Log2Fold Change	Name of gene
5.27	tubulin, alpha 3#TUBA3
4.92	clusterin (complement lysis inhibitor, SP-40,40, sulfated glycoprotein 2, testosterone-repressed prostate message 2, apolipoprotein J)#CLU
4.47	clusterin (complement lysis inhibitor, SP-40,40, sulfated glycoprotein 2, testosterone-repressed prostate message 2, apolipoprotein J)#CLU
4.27	lectin, galactoside-binding, soluble, 1 (galectin 1)#LGALS1
4.20	annexin A1#ANXA1
3.69	carcinoembryonic antigen-related cell adhesion molecule 6 (non-specific cross reacting antigen)#CEACAM6
3.65	dehydrogenase/reductase (SDR family) member 2#DHR2
	carcinoembryonic antigen-related cell adhesion molecule 6 (non-specific cross reacting antigen) /// carcinoembryonic antigen-related cell
3.64	adhesion molecule 6 (non-specific cross reacting antigen)#CEACAM6
3.48	thioredoxin interacting protein#TXNIP
3.43	selenoprotein P, plasma, 1#SEPP1
3.42	protease, serine, 23#SPUVE
3.41	glucosaminyl (N-acetyl) transferase 3, mucin type#GCNT3
3.41	thioredoxin interacting protein#TXNIP
	aldo-keto reductase family 1, member C1 (dihydrodiol dehydrogenase 1; 20-alpha (3-alpha)-hydroxysteroid dehydrogenase) #AKR1C1
3.31	carbonic anhydrase XII#CA12
3.12	---
3.06	adaptor-related protein complex 1, gamma 1 subunit#AP1G1
3.02	thioredoxin interacting protein#TXNIP
2.96	ras homolog gene family, member E#ARHE
2.92	lectin, galactoside-binding, soluble, 3 (galectin 3)#LGALS3
2.91	aldo-keto reductase family 1, member C2 (dihydrodiol dehydrogenase 2; bile acid binding protein; 3-alpha hydroxysteroid dehydrogenase,
2.90	type III)#AKR1C2
2.83	carcinoembryonic antigen-related cell adhesion molecule 7#CEACAM7
2.75	aldo-keto reductase family 1, member C1 (dihydrodiol dehydrogenase 1; 20-alpha (3-alpha)-hydroxysteroid dehydrogenase)

2.75	hydroxyprostaglandin dehydrogenase 15-(NAD)H#IP5D
2.73	hypothetical protein FLJ20151#FLJ20151
2.72	hypothetical protein FLJ20151#FLJ20151
2.66	Kruppel-like factor 4 (gut)#KLF4
2.65	dehydrogenase/reductase (SDR family) member 2#DHRS2
2.63	carbonic anhydrase XI#CA12
2.63	serine protease inhibitor, Kazal type 1#SPINK1
2.59	keratin 20#KRT20
	aldo-keto reductase family 1, member C2 (dihydrodiol dehydrogenase 2; bile acid binding protein; 3-alpha hydroxysteroid dehydrogenase, type III) /// aldo-keto reductase family 1, member C2 (dihydrodiol dehydrogenase 2; bile acid binding protein; 3-alpha hydroxysteroid)
2.59	h#AKR1C2
2.52	interferon, alpha-inducible protein (clone IFI-6-16)#G1P3
2.52	hydroxyprostaglandin dehydrogenase 15-(NAD)#HPCD
2.51	ceroid-lipofuscinosis, neuronal 2, late infantile (Jansky-Bielschowsky disease)#CLN2
2.49	uncoupling protein 2 (mitochondrial, proton carrier) /// uncoupling protein 2 (mitochondrial, proton carrier)#UCP2
2.41	glucose-6-phosphate dehydrogenase#G6PD
2.39	metallothionein 2A#MT2A
2.39	iduronate 2-sulfatase (Hunter syndrome)#IDS
2.37	nephroblastoma overexpressed gene#NOV
2.37	keratin 19 /// keratin 19#KRT19
2.36	caveolin 1, caveolae protein, 22kDa#CAV1
2.36	basic helix-loop-helix domain containing, class B, 3#BHLHB3
2.32	decay accelerating factor for complement (CD55, Crimer blood group system)#DAF
2.30	chemokine (C-C motif) ligand 20#CCL20
2.30	metallothionein 2A#MT2A
2.29	Homo sapiens mRNA; cDNA DKFZp686L01105 (from clone DKFZp686L01105)#---
2.29	geisolin (amyloidosis, Finnish type)#GSN
2.28	keratin 8#KRT8
2.27	iduronate 2-sulfatase (Hunter syndrome)#IDS
2.25	aldo-keto reductase family 1, member B10 (aldose reductase)#AKR1B10
2.24	KIAA0152 gene product#KIAA0152
2.24	myogenic factor 3 /// myogenic factor 3#MYOD1

2.23 tumor necrosis factor receptor superfamily, member 21#TNFRSF21
 2.23 dual specificity phosphatase 5#DUSP5
 2.20 amyloid beta (A4) precursor-like protein 1#APLP1
 2.20 mucin 13, epithelial transmembrane#MUC13
 2.18 heat shock 70kDa protein 1A#HSPA1A
 2.18 aldo-keto reductase family 1, member C3 (3-alpha hydroxysteroid dehydrogenase, type I)#AKR1C3
 2.16 insulin receptor substrate 1#IRS1
 2.16 SH3 domain binding glutamic acid-rich protein like 3 /// SH3 domain binding glutamic acid-rich protein like 3#SH3BGRL3
 2.16 gelsolin (amyloidosis, Finnish type)#GSN
 2.15 tubulin, beta polypeptide#TUBB
 2.14 caveolin 2#CAV2
 2.14 serine (or cysteine) proteinase inhibitor, clade E (nexin, plasminogen activator inhibitor type 1), member 2#SERPINE2
 2.12 glucosamine (N-acetyl)-6-sulfatase (Sanfilippo disease IIID)#GNS
 2.12 pre-B-cell leukemia transcription factor interacting protein 1#PBXIP1
 2.12 hydroxyprostaglandin dehydrogenase 15-(NAD)#HPGD
 2.10 N-myc downstream regulated gene 1#NDRG1
 2.08 transcobalamin I (vitamin B12 binding protein, R binder family)#TCN1
 2.08 sialyltransferase 4A (beta-galactoside alpha-2,3-sialyltransferase)#SIAT4A
 2.07 granulin#GRN
 2.06 glucosidase, beta; acid (includes glucosylceramidase)#GBA
 2.03 hypothetical protein IMAGE3455200#IMAGE3455200
 clusterin (complement lysis inhibitor, SP-40,40, sulfated glycoprotein 2, testosterone-repressed prostate message 2, apolipoprotein J)#CLU

Table 5. Genes showing decreased expression after treatment of HNSCC cells with 5-AZA-CdR (1 μ M; 4days)

Log2Fold Change	NAME
-2.00	MCM5 minichromosome maintenance deficient 5, cell division cycle 46 (S. cerevisiae)#MCM5
-2.00	---
-2.00	thymidine kinase 1, soluble#TK1
-2.01	flap structure-specific endonuclease 1#FEN1
-2.03	cyclin G1#CCNG1
-2.03	nucleosome assembly protein 1-like 1#NAP1L1
-2.04	centromere protein A, 17kDa#CENPA
-2.06	chromosome 10 open reading frame 3#C10orf3
-2.07	Opa-interacting protein 5#OIP5
-2.08	centromere protein F, 350/400ka (mitosin)#CENPF
-2.09	nucleosome assembly protein 1-like 1#NAP1L1
-2.10	RAD51-interacting protein#PIR51
-2.10	---
-2.11	serine protease inhibitor, Kazal type, 5#SPINK5
-2.12	kinesin family member 2C#KIF2C
-2.13	uncharacterized bone marrow protein BM039#BM039
-2.13	CGI-146 protein#PNAS-4
-2.14	ornithine decarboxylase 1#ODC1
-2.14	hypothetical protein MAC30#MAC30
-2.14	eukaryotic translation elongation factor 1 beta 2#EEF1B2
-2.15	flap structure-specific endonuclease 1#FEN1
-2.15	interferon induced transmembrane protein 3 (1-8U)#FITM3
-2.16	KIAA1393#KIAA1393
-2.19	kinesin family member 20A#KIF20A
-2.21	BUB1 budding uninhibited by benzimidazoles 1 homolog beta (yeast)#BUB1B

-2.21	high-mobility group box 3#HMGB3	
-2.22	acetyl-Coenzyme A acetyltransferase 2 (acetoacetyl Coenzyme A thiolase)#ACAT2	
-2.23	SMC4 structural maintenance of chromosomes 4-like 1 (yeast)#SMC4L1	
-2.24	Homo sapiens similar to RIKEN cDNA 2610001E06 (LOC375281), mRNA#----	
-2.24	aurora kinase B#AURKB	
-2.25	ZW10 interactor#ZWINT	
-2.25	hypothetical protein MAC30#MAC30	
-2.26	hypothetical protein HSPC155#HSPC155	
-2.26	T-LAK cell-originated protein kinase#TOPK	
-2.28	dihydrofolate reductase#DHFR	
-2.28	CDC28 protein kinase regulatory subunit 1B#CKS1B	
-2.29	high-mobility group nucleosomal binding domain 2#HMGN2	
-2.29	cyclin A2#CCNA2	
-2.31	SIPL protein#SIPL	
-2.32	MCM4 minichromosome maintenance deficient 4 (S. cerevisiae)#MCM4	
-2.36	TPX2, microtubule-associated protein homolog (Xenopus laevis)#TPX2	
-2.36	emopamil binding protein (sterol isomerase)#EBP	
-2.37	serine/threonine kinase 6#STK6	
-2.38	small nuclear ribonucleoprotein polypeptide A#SNRPA	
-2.38	thyroid hormone receptor interactor 13#TRIP13	
-2.39	high-mobility group box 1#HMGB1	
-2.42	MCM7 minichromosome maintenance deficient 7 (S. cerevisiae)#MCM7	
-2.45	pituitary tumor-transforming 1#PTTG1	
-2.46	ubiquitin carrier protein#E2-EPF	
-2.49	PRO2000 protein#PRO2000	
-2.49	hyaluronan-mediated motility receptor (RHAMM)#HMMR	
-2.53	ribonucleotide reductase M1 polypeptide#RRM1	
-2.53	polymyositis/scleroderma autoantigen 1, 75kDa#PMSCL1	
-2.53	asp (abnormal spindle)-like, microcephaly associated (Drosophila)#ASPM	
-2.53	aquaporin 3#AQP3	

-2.56	interleukin-1 receptor-associated kinase 1#IRAK1	
-2.58	MAD2 mitotic arrest deficient-like 1 (yeast)#MAO2L1	
-2.62	forkhead box M1#FOXM1	
-2.67	topoisomerase (DNA) II alpha 170kDa#TOP2A	
-2.67	interferon induced transmembrane protein 2 (1-8D)#IFITM2	
-2.68	MCM7 minichromosome maintenance deficient 7 (S. cerevisiae)#MCM7	
-2.68	high-mobility group box 1#HMGB1	
-2.72	SMC4 structural maintenance of chromosomes 4-like 1 (yeast)#SMC4L1	
-2.78	cell division cycle 2, G1 to S and G2 to M#CDC2	
-2.78	baculoviral IAP repeat-containing 5 (survivin)#BIRC5	
-2.81	discs, large homolog 7 (Drosophila)#DLG7	
-2.83	secreted phosphoprotein 1 (osteopontin, bone sialoprotein I, early T-lymphocyte activation 1)#SPP1	
-2.84	macrophage migration inhibitory factor (glycosylation-inhibiting factor)#MIF	
-2.86	proliferating cell nuclear antigen#PCNA	
-2.86	cell division cycle 2, G1 to S and G2 to M#CDC2	
-2.92	serine/threonine kinase 6 /// serine/threonine kinase 6#STK6	
-2.95	H2A histone family, member X#H2AFX	
-2.97	cell division cycle 2, G1 to S and G2 to M#CDC2	
-3.08	MCM2 minichromosome maintenance deficient 2, mitotin (S. cerevisiae)#MCM2	
-3.10	high-mobility group box 1#HMGB1	
-3.14	nucleolar and spindle associated protein 1#NUSAP1	
-3.16	protein regulator of cytokinesis 1#PRC1	
-3.28	ribonucleotide reductase M2 polypeptide#RRM2	
-3.32	cyclin B1#CCNB1	
-3.39	topoisomerase (DNA) II alpha 170kDa#TOP2A	
-3.77	ubiquitin-conjugating enzyme E2C#UBE2C	
-3.82	cyclin B2#CCNB2	
-3.85	high-mobility group box 2#HMGB2	
-3.91	insulin-like growth factor binding protein 7#IGFBP7	
-4.17	ribonucleotide reductase M2 polypeptide#RRM2	

-4.26	insulin-like growth factor binding protein 7#IGFBP7
-4.45	KIAA0101 gene product#KIAA0101
-4.56	thymidylate synthetase#TYMS

Table 6. Genes showing increased expression after treatment of HNSCC cells with 5-AZA-CdR (1 μ M 4 days) and SAHA (4 μ M last 24 hr of the AZA treatment) compared to untreated control cells.

Log2Fold Change	NAME
8.22	chemokine (C-C motif) ligand 20#CCCL20
7.67	G antigen 1 /// G antigen 1#GAGE1
7.45	G antigen 5#GAGE5
7.00	G antigen 5#GAGE5
6.91	Interferon, alpha-inducible protein 27#IFI27
6.84	carcinoembryonic antigen-related cell adhesion molecule 6 (non-specific cross reacting antigen)#CEACAM6
6.65	G antigen 5#GAGE5
6.65	G antigen 5#GAGE5
6.47	dehydrogenase/reductase (SDR family) member 2#DHRS2
6.34	melanoma antigen, family A, 6#MAGEA6
6.26	lipocalin 2 (oncogene 24p3)#LCN2
6.22	melanoma antigen, family A, 3#MAGEA3
5.99	carcinoembryonic antigen-related cell adhesion molecule 6 (non-specific cross reacting antigen) /// carcinoembryonic antigen-related cell adhesion molecule 6 (non-specific cross reacting antigen)#CEACAM6
5.94	dehydrogenase/reductase (SDR family) member 2#DHRS2
5.82	decay accelerating factor for complement (CD55, Crimer blood group system)#DAF
5.68	clusterin (complement lysis inhibitor, SP-40,40, sulfated glycoprotein 2, testosterone-repressed prostate message 2, apolipoprotein J)#CLU
5.66	transcobalamin I (vitamin B12 binding protein, R binder family)#TCN1
5.65	G antigen 5 /// G antigen 5#GAGE5
5.54	transketolase-like 1#TKTL1
5.40	interleukin 8#IL8
5.35	annexin A1#ANXA1
5.30	melanoma antigen, family A, 4#MAGEA4
5.09	decay accelerating factor for complement (CD55, Crimer blood group system)#DAF
5.07	melanoma antigen, family A, 12#MAGEA12
5.01	histone 2, H2aa#HIST2H2AA
4.96	keratin 20#KRT20
4.76	clusterin (complement lysis inhibitor, SP-40,40, sulfated glycoprotein 2, testosterone-repressed prostate message 2, apolipoprotein J)#CLU

4.74	carcinoembryonic antigen-related cell adhesion molecule 7#CEACAM7	
4.62	cancer/testis antigen 1/// cancer/testis antigen 1#CTAG1	
4.58	dual specificity phosphatase 5#DUSP5	
4.55	tubulin, alpha 3#TUBA3	
4.51	histone 1, H1c/// histone 1, H1c#HIST1H1C	
4.44	melanoma antigen, family A, 1 (directs expression of antigen MZ2-E)#MAGEA1	
4.38	chemokine (C-X-C motif) ligand 1 (melanoma growth stimulating activity, alpha)#CXCL1	
4.38	melanoma antigen, family B, 2#MAGEB2	
4.35	prostate differentiation factor#PLAB	
4.30	carcinoembryonic antigen-related cell adhesion molecule 5#CEACAM5	
4.25	melanoma antigen, family A, 9#MAGEA9	
4.21	interferon, alpha-inducible protein (clone IF1-6-16)#G1P3	
4.19	tubulin, beta polypeptide#TUBB	
4.08	cancer/testis antigen 1#CTAG1	
4.08	---#---	
4.07	glucosaminyl (N-acetyl) transferase 3, mucin type#GCNT3	
	aldo-keto reductase family 1, member C1 (dihydrodiol dehydrogenase 1; 20-alpha (3-alpha)-hydroxysteroid dehydrogenase)#AKR1C1	
4.06	---#---	
4.02	---#---	
3.87	---#---	
3.84	paternally expressed 10#PEG10	
3.82	cathepsin E#CTSE	
3.82	melanoma antigen, family A, 5#MAGEA5	
3.78	cancer/testis antigen 2#CTAG2	
3.75	synovial sarcoma, X breakpoint 1#SSX1	
3.74	histone 2, H2aa#HIST2H2AA	
3.73	Homo sapiens cDNA clone IMAGE:4346793, partial cds#---	
3.65	mucin 13, epithelial transmembrane#MUC13	
3.63	deleted in azoospermia-like#DAZL	
3.60	retinoic acid induced 3#RAI3	
3.52	SWI/SNF related, matrix associated, actin dependent regulator of chromatin, subfamily a, member 3#SMARCA3	
3.47	hydroxyprostaglandin dehydrogenase 15-(NAD)#HPGD	
	aldo-keto reductase family 1, member C1 (dihydrodiol dehydrogenase 1; 20-alpha (3-alpha)-hydroxysteroid dehydrogenase)#AKR1C1	
3.44	aldehyde dehydrogenase 1 family, member A1#ALDH1A1	
3.41	matrix metalloproteinase 7 (matrilysin, uterine)#MMP7	
3.41		

3.40	paternally expressed 10#PEG10	
3.37	tissue inhibitor of metalloproteinase 1 (erythroid potentiating activity, collagenase inhibitor)#TIMP1	
	aldo-keto reductase family 1, member C2 (dihydrodiol dehydrogenase 2; bile acid binding protein, 3-alpha hydroxysteroid dehydrogenase, type III)#AKR1C2	
3.34	hydroxyprostaglandin dehydrogenase 15-(NAD)#HPGD	
3.34	cyclin-dependent kinase inhibitor 1A (p21, Cip1)#CDKN1A	
3.29	amphiregulin (schwannoma-derived growth factor)#AREG	
3.28	hypothetical protein FLJ36166#FLJ36166	
3.17	hydroxyprostaglandin dehydrogenase 15-(NAD)#HPGD	
3.12	hypothetical protein FLJ22595#FLJ22595	
3.10	matrix metalloproteinase 1 (interstitial collagenase)#MMP1	
3.07	glutathione S-transferase M3 (brain)#GSTM3	
3.05	stratfin#SFN	
3.05	synovial sarcoma, X breakpoint 4#SSX4	
3.02	tripartite motif-containing 31#TRIM31	
3.02	acetylserotonin O-methyltransferase-like#ASMTL	
3.01	extracellular matrix protein 1#ECM1	
3.00	stratfin#SFN	
2.99	---	
2.99	nerve growth factor receptor (TNFRSF16) associated protein 1#NGFRAP1	
2.99	lectin, galactoside-binding, soluble, 1 (galectin 1)#LGALS1	
2.98	laminin, alpha 3#LAMA3	
2.98	jagged 1 (Alagille syndrome)#JAG1	
2.97	ATP-binding cassette, sub-family G (WHITE), member 2#ABCG2	
	aldo-keto reductase family 1, member C2 (dihydrodiol dehydrogenase 2; bile acid binding protein; 3-alpha hydroxysteroid protein; 3-alpha h#AKR1C2	
2.97	interferon, alpha-inducible protein (clone IFI-15K)#G1P2	
2.95	---	
2.93	cancer/testis antigen 1#CTAG1	
2.93	tripartite motif-containing 31#TRIM31	
2.91	synovial sarcoma, X breakpoint 2#SSX2	
2.89	Kruppel-like factor 4 (gut)#KLF4	
2.89	GNAS complex locus#GNAS	
2.89	DnaJ (Hsp40) homolog, subfamily D, member 1#DNAJD1	

Homo sapiens transcribed sequence with strong similarity to protein ref NP_074720.1 (Hsappens) microtubule-associated
 proteins 1A/1B light chain 3 [Homo sapiens]#...
 2.87 2.84 nuclear receptor subfamily 1, group H, member 4#NR1H4
 2.82 jagged 1 (Alagille syndrome)#JAG1
 2.79 syndecan 4 (amphiglycan, ryudocan)#SDC4
 2.78 ---#---
 2.77 baculoviral IAP repeat-containing 3 /// baculoviral IAP repeat-containing 3#BIRC3
 2.76 ---#---
 2.76 glycine amidinotransferase (L-arginine:glycine amidinotransferase)#GATM
 2.76 thioredoxin reductase 1#TXNRD1
 2.74 abhydrolase domain containing 2#ABHD2
 2.73 aldo-keto reductase family 1, member B10 (aldose reductase)#AKR1B10
 2.73 iduronate 2-sulfatase (Hunter syndrome)#IDS
 2.72 acetylserotonin O-methyltransferase-like#ASMTL
 2.72 cathepsin B#CTSB
 2.72 ras homolog gene family, member E#ARHE
 2.66 amyloid beta (A4) precursor-like protein 2#APLP2
 2.66 coagulation factor II (thrombin) receptor-like 1#F2RL1
 2.65 transmembrane 4 superfamily member 4#TM4SF4
 2.63 lectin, galactose-binding, soluble, 3 (galectin 3)#LGALS3
 2.62 microtubule-associated protein 1 light chain 3 beta#MAP1LC3B
 2.61 histone 1, H2bk#HIST1H2BK
 2.60 G antigen, family D, 2#GAGED2
 2.60 glucosidase, beta; acid (includes glucosylceramidase)#GBA
 2.58 N-myc downstream regulated gene 1#NDRG1
 2.58 plasminogen activator, urokinase receptor#PLAUR
 2.58 ubiquitin carboxyl-terminal esterase L1 (ubiquitin thiolesterase)#UCHL1
 2.57 tumor necrosis factor, alpha-induced protein 2#TNFAIP2
 2.56 annexin A10#ANXA10
 2.56 serine (or cysteine) proteinase inhibitor, clade D (heparin cofactor), member 1#SERPIND1
 2.51 KIAA0415 gene product#KIAA0415
 2.51 iduronate 2-sulfatase (Hunter syndrome)#IDS
 2.50 ---#---
 2.50 glycine amidinotransferase (L-arginine:glycine amidinotransferase)#GATM
 2.50 major histocompatibility complex, class I, B#HLA-B
 2.49 glucosidase, beta; acid (includes glucosylceramidase)#GBA

2.49	S100 calcium binding protein A4 (calcium protein, calvestrasin, metastasin, murine placental homolog)#S100A4
2.48	thioredoxin interacting protein#TXNIP
2.47	histone 1, H2bd#HIST1H2BD
2.46	thioredoxin interacting protein#TXNIP
2.45	DnaJ (Hsp40) homolog, subfamily B, member 9#DNAJB9
2.44	tumor necrosis factor receptor superfamily, member 21#TNFRSF21
2.44	epithelial membrane protein 1#EMP1
2.43	protease, serine, 23#SPUVE
2.43	calbindin 2, 29kDa (calretinin)#CALB2
2.42	legumain#LGMN
2.41	tripartite motif-containing 31#TRIM31
2.41	iduronate 2-sulfatase (Hunter syndrome)#IDS
2.41	2',5'-oligoadenylate synthetase 1.40/46kDa#OAS1
2.41	serine (or cysteine) proteinase inhibitor, clade E (hexin, plasminogen activator inhibitor type 1), member 2#SERPINE2
2.41	neurofilament, heavy polypeptide 200kDa#NEFH
2.37	secretoglobulin, family 2A, member 1#SCGB2A1
2.36	major histocompatibility complex, class I, C#HLA-C
2.36	amyloid beta (A4) precursor-like protein 2#APLP2
2.36	Homo sapiens transcribed sequence with weak similarity to protein sp P05362 (H.sapiens) ICA1_HUMAN Intercellular adhesion molecule-1 precursor (ICAM-1) (Major group rhinovirus receptor) (CD54)#...
2.35	trefoil factor 1 (breast cancer, estrogen-inducible sequence expressed in)#TFF1
2.34	NACHT, leucine rich repeat and PYD containing 2#NALP2
2.33	esterase 31#FLJ21736
2.33	GABA(A) receptors associated protein like 3#GABARAPL3
2.33	solute carrier family 16 (monocarboxylic acid transporters), member 3#SLC16A3
2.32	proprotein convertase subtilisin/kexin type 5#PCSK5
2.30	GTP cyclohydrolase 1 (dopa-responsive dystonia)#GCH1
2.30	chromosome 20 open reading frame 24#C20orf24
2.30	nitric oxide synthase 3 (endothelial cell) /// nitric oxide synthase 3 (endothelial cell)#NOS3
2.30	immediate early response 3#IER3
2.29	uroplakin 1B#UPK1B
2.29	iduronate 2-sulfatase (Hunter syndrome)#IDS
2.28	acetylserotonin O-methyltransferase-like#ASMTL
2.27	MHC class I polypeptide-related sequence B#MICB
2.27	carcinoembryonic antigen-related cell adhesion molecule 7#CEACAM7

2.26	nuclear transport factor 2-like export factor 2#NXT2
2.26	aspartate beta-hydroxylase#ASPH
2.26	amyloid beta (A4) precursor-like protein 2#APLP2
2.25	tubulin beta MGC4083#MGC4083
2.25	riboflavin kinase#FLJ11149
2.25	sialidase 1 (lysosomal sialidase)#NEU1
2.25	POU domain, class 2, associating factor 1#POU2AF1
2.24	tumor necrosis factor receptor superfamily, member 21#TNFRSF21
2.24	signal transducer and activator of transcription 1, 91kDa#STAT1
2.24	laminin, beta 3#LAMB3
2.24	Niemann-Pick disease, type C1#NPC1
2.22	cathepsin B#CTSB
2.21	melanoma antigen, family A, 2#MAGEA2
2.21	selenoprotein P, plasma, 1#SEPP1
2.21	protective protein for beta-galactosidase (galactosialidosis)#PPGB
2.20	placenta-specific 8#PLAC8
2.20	chemokine (C-X-C motif) ligand 2#CXCL2
2.20	zinc finger CCH type domain containing 1#ZC3HDC1
2.20	uroplakin 1B#UPK1B
2.20	interferon gamma receptor 1 /// interferon gamma receptor 1#IFNGR1
2.19	NAD(P)H dehydrogenase, quinone 1#NQO1
2.19	FAD104#FAD104
2.19	hypothetical protein FLJ22662#FLJ22662
2.18	metallothionein 2A#MT2A
	clusterin (complement lysis inhibitor, SP-40,40, sulfated glycoprotein 2, testosterone-repressed prostate message 2,
2.18	apolipoprotein J)#CLU
2.16	carbonic anhydrase XII#CA12
2.16	major histocompatibility complex, class I, C#HLA-C
2.16	hypothetical protein FLJ10097#FLJ10097
2.15	interferon gamma receptor 1#IFNGR1
2.15	cell cycle progression 8 protein#CPR8
2.15	CD9 antigen (p24)#CD9
2.15	melanoma antigen, family A, 8#MAGEA8
2.14	hydroxysteroid (17-beta) dehydrogenase 2#HSD17B2
2.14	histone 2, H2be#HIST2H2BE
2.11	pM5 protein#PM5

2.10 thiredoxin interacting protein#TXNIP
 2.10 chromosome 21 open reading frame 4 // chromosome 21 open reading frame 4#C21orf4
 2.09 jagged 1 (Alagille syndrome)#JAG1
 2.09 v-maf musculoaponeurotic fibrosarcoma oncogene homolog F (avian)#MAFF
 2.09 cadherin 17, LI cadherin (liver-intestine)#CDH17
 2.09 interferon stimulated gene 20kDa#ISG20
 2.09 cystathionase (cystathionine gamma-lyase)#CTH
 2.08 serine (or cysteine) proteinase inhibitor, clade I (neuroserpin), member 1#SERPINI1
 2.07 histone 1, H2bc#HIST1H2BC
 2.06 nuclear factor of kappa light polypeptide gene enhancer in B-cells inhibitor, alpha#NFKBIA
 2.06 glutathione peroxidase 3 (plasma)#GPX3
 2.06 adaptor-related protein complex 1, gamma 1 subunit#AP1G1
 2.05 tubulin, beta, 2#TUBB2
 2.05 hypothetical protein LOC283820#LOC283820
 2.05 microtubule-associated protein, RP/EB family, member 2#MAPRE2
 2.05 hematopoietically expressed homeobox#HHEX
 2.05 glutathione peroxidase 2 (gastrintestinal)#GPX2
 2.04 matrix metalloproteinase 15 (membrane-inserted)#MMP15
 2.04 synovial sarcoma, X breakpoint 3#SSX3
 2.04 stratifin#SFN
 2.03 glucosamine (N-acetyl)-6-sulfatase (Sanfilippo disease IIID)#GNS
 2.03 NAD(P)H dehydrogenase, quinone 1#NQO1
 2.03 sperm specific antigen 2#SSFA2
 2.03 tubulin, beta, 4#TUBB4
 2.03 phospholipid scramblase 4#PLSCR4
 2.02 Homo sapiens cDNA: FLJ21545 fis, clone COL06195#----
 2.02 intercellular adhesion molecule 1 (CD54), human rhinovirus receptor#ICAM1
 2.02 histone 1, H4h#HIST1H4H
 2.01 prostaglandin-endoperoxide synthase 1 (prostaglandin G/H synthase and cyclooxygenase)#PTGS1
 2.01 H2B histone family, member S#H2BFS

Table 7. Genes showing decreased expression after treatment of HNSCC cells with 5-AZA-CdR (1 μ M 4 days) and SAHA (4 μ M last 24 hr of the AZA treatment).

Log2Fold Change	Name of gene
-2.02	5-hydroxytryptamine (serotonin) receptor 2B // 5-hydroxytryptamine (serotonin) receptor 2B#HTR2B
-2.02	nucleosome assembly protein 1-like 1#NAP1L1
-2.02	inorganic pyrophosphatase 2#PPA2
-2.03	solute carrier family 25 (mitochondrial carrier, adenine nucleotide translocator), member 6#SLC25A6
-2.03	SMP3 mannosyltransferase#SMP3
-2.04	eukaryotic translation initiation factor 4B#EIF4B
-2.06	LSM7 homolog, U6 small nuclear RNA associated (S. cerevisiae)#LSM7
-2.06	diclkopf homolog 1 (Xenopus laevis)#DKK1
-2.08	ribosomal protein L28#RPL28
-2.08	FK506 binding protein 11, 19 kDa#FKBP11
-2.08	Homo sapiens transcribed sequence with moderate similarity to protein sp.P05388 (H.sapiens) PLA0_HUMAN 60S acidic
-2.09	ribosomal protein P0 (L10E)#---
-2.11	ribosomal protein L14#RPL14
-2.11	basic transcription factor 3#BTTF3
-2.12	neuroepithelial cell transforming gene 1#NET1
-2.12	interferon induced transmembrane protein 2 (1-8D)#IFITM2
-2.12	histamine N-methyltransferase#HNMT
-2.14	insulin-like growth factor binding protein 4#IGFBP4
-2.15	acetyl-Coenzyme A acetyltransferase 2 (acetoacetyl Coenzyme A thiolase)#ACAT2
-2.21	general transcription factor IIIA#GTF3A
-2.21	ribosomal protein L14#RPL14
-2.23	chromosome 11 open reading frame2#C11orf2
-2.25	eukaryotic translation initiation factor 4B#EIF4B
-2.27	eukaryotic translation elongation factor 1 delta (guanine nucleotide exchange protein)#EEF1D
-2.31	nucleosome assembly protein 1-like 1#NAP1L1
-2.31	Homo sapiens similar to RIKEN cDNA 2610001E06 (LOC375281), mRNA#---
-2.32	nucleosome assembly protein 1-like 1#NAP1L1
-2.38	chromosome 6 open reading frame 48#C6orf48
-2.39	glutaminyl-tRNA synthetase#QARS
-2.40	nucleosome assembly protein 1-like 1#NAP1L1
-2.40	laminin receptor 1 (ribosomal protein SA, 67kDa)#LAMR1

-2.49	enoyl Coenzyme A hydratase 1, peroxisomal#ECH1	
-2.50	ATP synthase, H ⁺ transporting, mitochondrial F0 complex, subunit c (subunit 9), isoform 2#ATP5G2	
-2.51	high-mobility group nucleosomal binding domain 2#HMGN2	
-2.54	macrophage migration inhibitory factor (glycosylation-inhibiting factor)#MIF	
-2.54	ribosomal protein S9#RRPS9	
-2.57	KIAA1393#KIAA1393	
-2.58	ribosomal protein L22#RPL22	
-2.59	non-metastatic cells 2, protein (NM23B) expressed in#NME2	
-2.83	cyclin B2#CCNB2	
-2.83	insulin-like growth factor binding protein 7#IGFBP7	
-2.84	serine protease inhibitor, Kazal type, 5#SPINK5	
-2.85	thymidylate synthetase#TYMS	
-2.89	cyclin G1#CCNG1	
	Homo sapiens transcribed sequence with strong similarity to protein ref.NP_000974.1 (H.sapiens) ribosomal protein L22	
-2.90	proprotein; 60S ribosomal protein L22; Epstein-Barr-encoded RNA-associated protein; Epstein-Barr virus small RNA-associated protein; EBE#--	
-2.97	ribosomal protein L13a#RPL13A	
-3.01	insulin-like growth factor binding protein 7#IGFBP7	
-3.02	high-mobility group box 2#HMGGB2	
-3.30	glioma tumor suppressor candidate region gene 2#GLTSCR2	

Appendix II (Lotan Target final report)

Zhong M, Gillenwater A, Lotan R. Valproic acid induces growth inhibition and apoptosis in head and neck squamous carcinoma cell lines

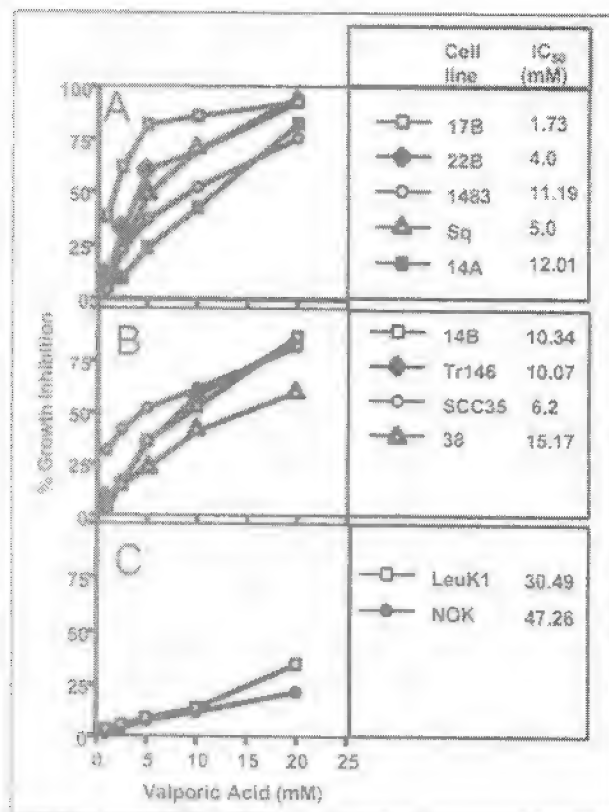


Figure 1. H&N cancer cells (A and B)) were more sensitive to VPA-induced growth inhibition than oral leukoplakia (Leuk1) and normal oral keratinocytes (NOK) isolated from gingiva (C). All cells were treated with various concentrations of VPA for 3 days before growth inhibition (GI) was measured and IC₅₀ determined by interpolation from the dose response curves.

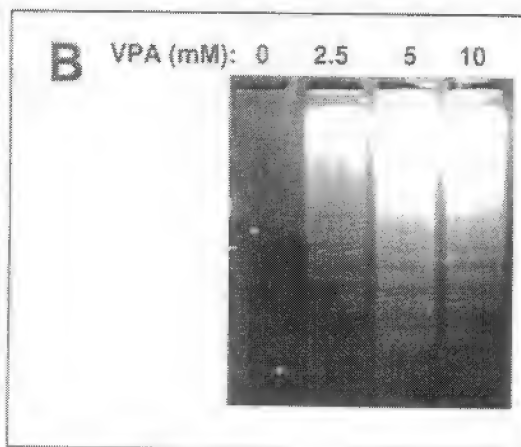
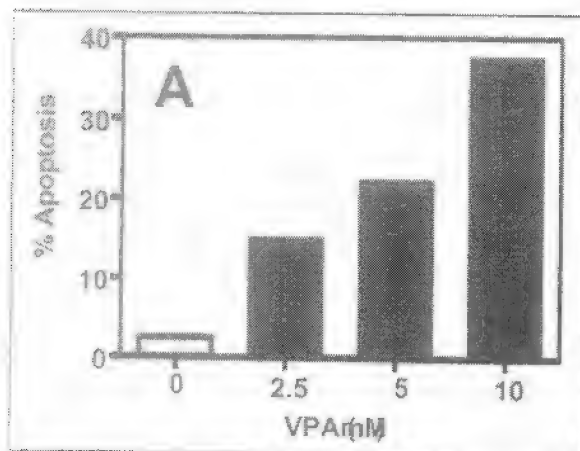


Figure 2. VPA induced apoptosis in a dose-dependent manner. 17B cells were treated with various concentrations of VPA for 16 hrs before they were harvested and used for the TUNEL (A) and DNA fragmentation (B) assays.

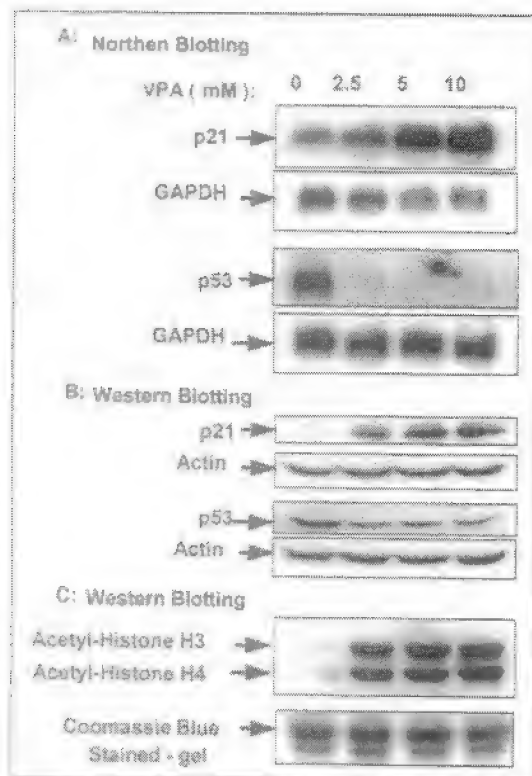


Figure 3. VPA induced p21 but not p53 mRNA and protein expression in H&N 17B cells (A), and (B) also acted as a histone H3 and H4 deacetylase inhibitor (C). 17B cells were treated with VPA for 16 hrs before cells were harvested for Northern (A), and Western blot analyses (B) and (C).

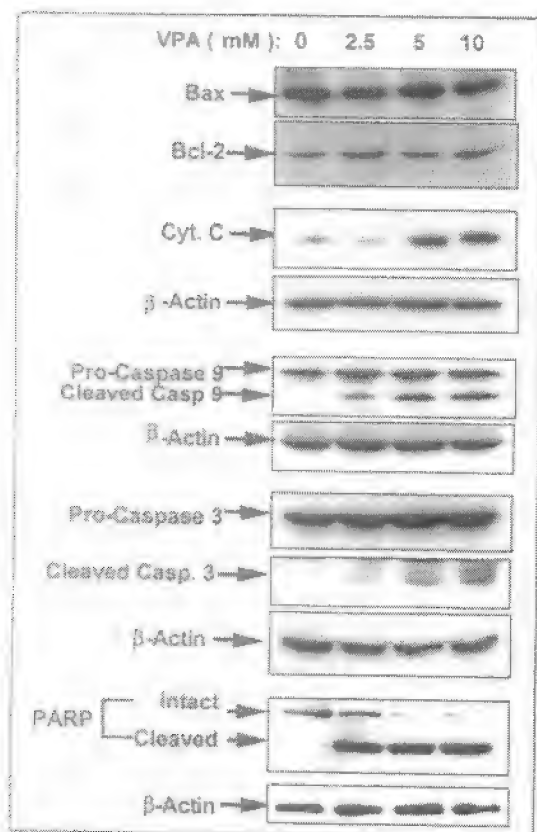


Figure 4. Effects of VPA on expression of apoptosis-related genes. 17B cells were treated with VPA for 16 hrs before cells were harvested for Western blot analysis.

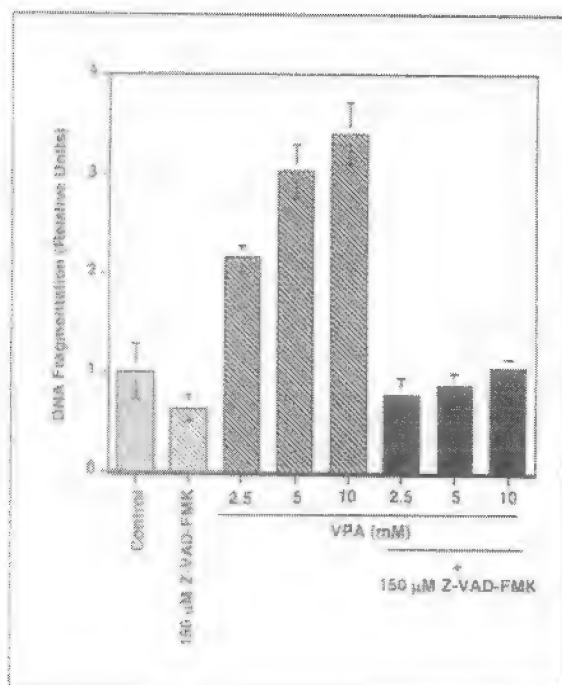


Figure 5. The caspase inhibitor Z-VAD-FMK blocked VPA-induced apoptosis in 17B cells. Cells were treated with various concentrations of VPA alone or a combination of 150 μ M Z-VAD-FMA and VPA for 16 hrs. DNA fragmentation was estimated by an ELISA assay.

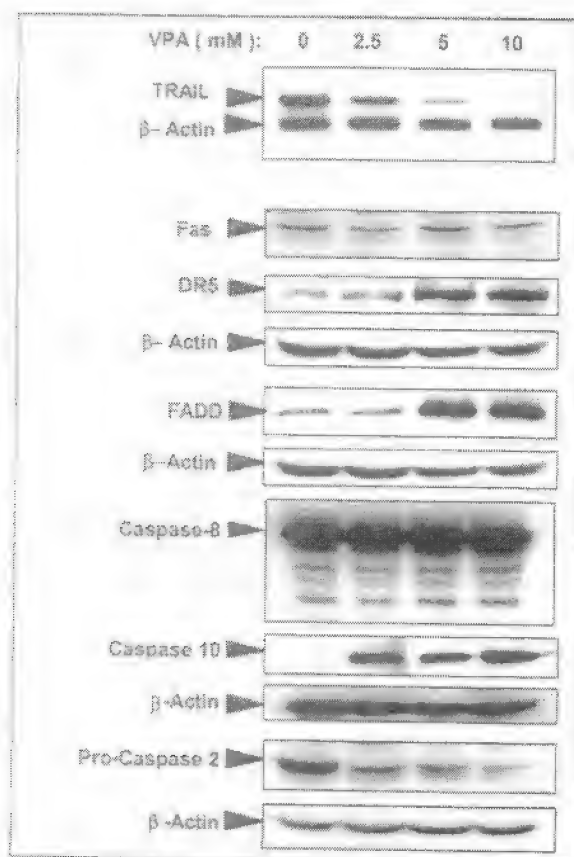


Figure 6. Effects of VPA on expression of genes involved in death receptor DR5-mediated apoptosis pathway. 17B cells were treated with VPA for 16 hrs before cells were harvested for Western blot analysis, except for TRAIL which was analyzed by RT-PCR.

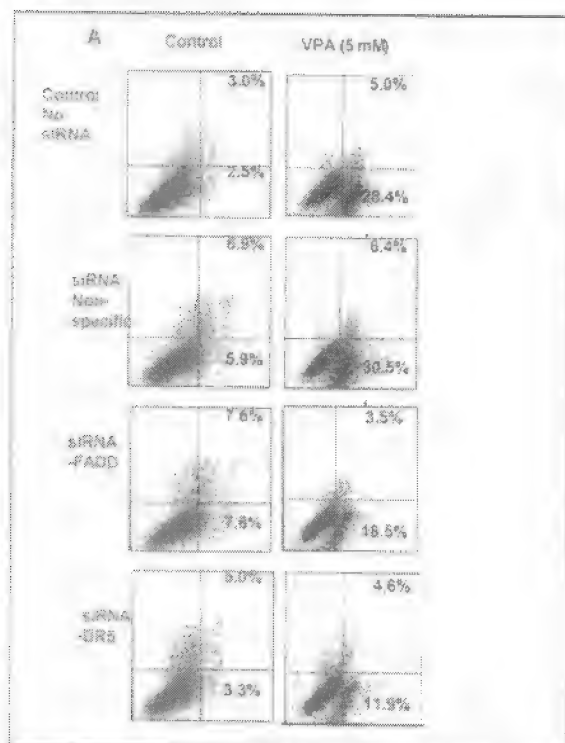


Figure 7. siRNA DR5 and siRNA FADD blocked VPA-induced apoptosis. 17B cells were transfected with siRNA for 48 hrs prior to the treatment of 5 mM of VPA for 16 hrs. Cells were subjected to Annexin V apoptosis assay (A) and Western blot analysis (B).

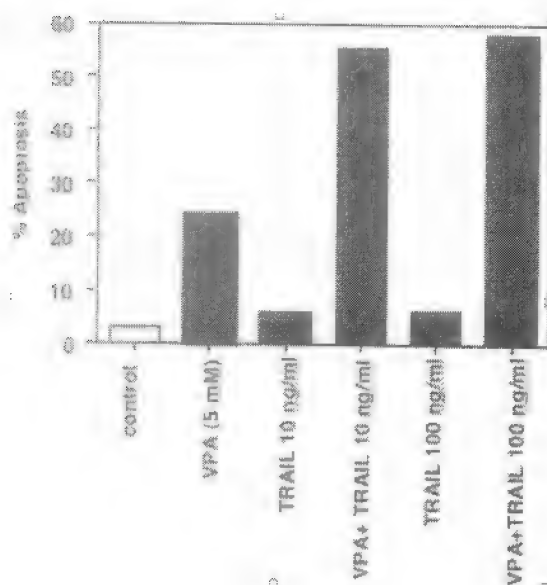
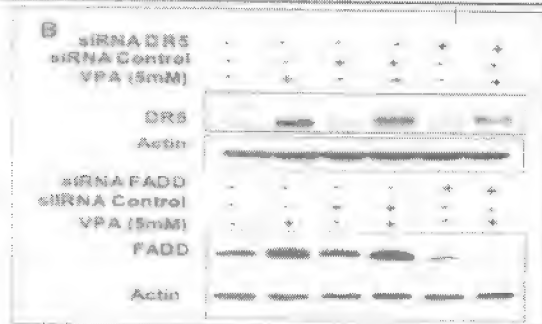


Figure 8. Synergistic effects of VPA and TRAIL on apoptosis induction. 17B cells were pretreated with TRAIL for 30 min and then co-treated with 5 mM VPA for 16 hrs. Apoptosis was examined by the Annexin V assay.

Comparison of Molecular Abnormalities in Bronchial Brushings and Tumor Touch Preparations

Potential Use of Fluorescence In Situ Hybridization to Identify Predictive Markers in Early-Stage Lung Carcinomas

Güliz A. Barkan, M.D.¹
Nancy P. Caraway, M.D.¹
Feng Jiang, M.D.¹
Tanweer M. Zaidi, M.D.¹
Ricardo Fernandez, B.S.¹
Ara Vaporciyan, M.D.²
Rodolfo Morice, M.D.³
Xian Zhou, M.S., B.S.⁴
Benjamin Nebiyu Bekele, Ph.D.⁴
Ruth L. Katz, M.D.¹

¹Department of Pathology, The University of Texas M. D. Anderson Cancer Center, Houston, Texas.

²Department of Thoracic and Cardiovascular Surgery, The University of Texas M. D. Anderson Cancer Center, Houston, Texas.

³Department of Pulmonary Medicine, The University of Texas M. D. Anderson Cancer Center, Houston, Texas.

⁴Department of Biostatistics and Applied Mathematics, The University of Texas M. D. Anderson Cancer Center, Houston, Texas.

Presented at the 92nd Annual Meeting of the United States and Canadian Academy of Pathology, Washington, D.C., March 22–28, 2003.

Supported by Grant P50CA70907 (The University of Texas at Southwestern Medical Center and M. D. Anderson Cancer Center Specialized Programs of Research Excellence in Lung Cancer), Grant T32MD110221-0766 (Transitional Approaches for the Research, Genetic Evaluation, and Treatment of Lung Cancer), and Grant R01-CA70907-02 (Workstatement 55: Identification of Predictive (Image Analysis Features in Archived Histological Sections Which Predict Recurrence of Lung Cancer or Metastatic Disease) from the National Cancer Institute, and by funding from the Division of Pathology and Laboratory Medicine

BACKGROUND. Preneoplastic lung lesions and early-stage lung carcinomas are associated with molecular abnormalities. The authors performed a pilot study to evaluate the use of DNA fluorescence in situ hybridization (FISH) probes to ascertain whether these biomarkers can predict nonsmall cell lung carcinoma (NSCLC).

METHODS. Fourteen bronchial brushings ipsilateral to the tumor (BB/Ts), tumor touch imprints, and touch imprints of the bronchus adjacent to the tumor obtained from 15 patients with early-stage NSCLC were analyzed. The LAVision multicolor probe set consisting of probes to 5p15, 6, 7p12, and 8q2 and the in-house probes 3p22.1 and 10q22 was used. Using the LAVision multicolor probe set, 25 epithelial cells were counted and considered positive if > 5 cells were abnormal. Using 3p22.1 and 10q22, \approx 100 nuclei per slide were scored. The results were tabulated as the percentage of cells with deletions compared with the centromeric probes 3 and 10. Greater than 2% of the deletions were positive for 3p22.1 and 10q22. Bronchial washings from patients without lung tumors were used as controls.

RESULTS. The BB/Ts were negative for malignant cells by cytologic evaluation and the LAVision probe set; however, the combined in-house probes for 3p22.1 and 10q22 tested on BB/Ts predicted cancer in 100% of cancer patients. FISH positivity in the lung cancers was 100% for 3p22.1 deletions, 79% for 10q22 deletions, and 57% for LAVision probes. When compared with the bronchial epithelium, tumor cells showed a 3.7-fold excess of 3p22.1 deletions, a 2-fold excess of 10q22 deletions, and a 12.6-fold excess of abnormal cells.

CONCLUSIONS. The current study indicated that detection of molecular abnormalities in bronchial epithelial cells via FISH was very useful in identifying patients at high risk for developing lung carcinoma. The molecular abnormalities identified in the BB/Ts were detected at elevated levels in the tumor specimens. *Cancer (Cancer Cytopathol)* 2005;105:35–43. © 2004 American Cancer Society.

KEYWORDS: lung, nonsmall cell, cancer, fluorescence in situ hybridization, early detection, bronchial brushing.

The University of Texas M. D. Anderson Cancer Center, for research projects by fellows.

The authors thank Aazam B. Alizadeh and Abiha Khanna for their technical assistance, Holly Turner-Jones and Raquel Vitis for their administrative assistance, and Vysis, Inc. (Downers Grove, IL) for providing a portion of the LAVision probes used in the current study.

Address for reprints: Ruth L. Katz, M.D., Department of Pathology, Unit 53, The University of Texas M. D. Anderson Cancer Center, 1515 Holcombe Boulevard, Houston, TX 77030; Fax: (713) 792-2067; E-mail: rkatz@mail.mdanderson.org

Received May 24, 2004; revision received October 8, 2004; accepted October 14, 2004.

Lung carcinoma is the leading cause of cancer deaths and accounts for 28% of all deaths in the United States annually. Furthermore, the American Cancer Society estimated that there would be 169,500 new cases of lung carcinoma in 2001.¹ The mortality rate of lung carcinoma is almost 90%, and the 5-year survival rate in patients with advanced-stage lung carcinoma is 2.5%.^{2,3} The high mortality rate is due, in part, to the lack of an effective diagnostic modality for early detection. Although chest X-rays and sputum cytology have long been used as screening modalities, these tests do not detect a sufficient number of lung carcinomas at an early enough stage to improve survival.⁴ For this reason, lung carcinoma screening is not a routine practice in the general public or even among those at increased risk for lung carcinoma, such as smokers. Thus, new methods are needed to detect early-stage lung carcinoma and its precursors in patients at high risk.

In recent years, several chromosomal and molecular abnormalities have been identified in non-small cell lung carcinomas (NSCLC), even at early stages, although early-stage carcinomas have been found to have fewer molecular alterations than advanced-stage carcinomas. Lung carcinoma development has been proposed to reflect a field cancer process in which the whole lung is exposed to a carcinogenic insult, such as tobacco smoke, increasing the risk of multistep tumor development in the respiratory tract epithelium.⁵ We hypothesized that a pattern of genetic abnormalities involving chromosomal regions 3p, 5q, 7p, 8q, and 10q in bronchial epithelial cells obtained from bronchial brushings from the tumor side (BB/Ts) is an early indicator of lung carcinoma. In the current study, we sought to determine whether a field effect exists in cytologically normal epithelium of the bronchial tree in the presence of established lung carcinoma with the use of DNA fluorescence in situ hybridization (FISH) probes. This information may be useful in identifying patients at high risk for developing lung carcinoma via endoscopic brush cytology.

MATERIALS AND METHODS

Patient and Control Population

Fifteen patients with NSCLC were entered into our prospective study. All of them had a lung mass that was operable. In addition, none of them had undergone chemotherapy or irradiation. Fifteen control subjects were selected from a group of individuals who were at high risk for developing lung carcinoma due to their smoking history but did not have a detectable lesion on a chest X-ray. Written informed consent for participation was obtained through an

institutional review board protocol. All of the patients' and control subjects' charts were reviewed for a significant medical history and smoking history. The patients' histologic lung sections were also reviewed.

Specimens

The patients underwent bronchoscopy just before surgical excision. Bronchial brushings were taken from the main stem bronchus on the tumor-bearing side. After the excision, touch imprints from the resected lung tumors (TP/Ts) and from macroscopically unremarkable bronchi adjacent to the tumors (TP/ABs) were made. Also, bronchial washings (BWs) taken from the control subjects were used as controls.

Specimen Preparation

BB/Ts were obtained from only 14 of the 15 patients. The BB/Ts were received in saline. Cytospins were prepared for cytology and FISH analysis. The cytology slides were fixed in Carnoy solution and stained with Papanicolaou stain, whereas the air-dried slides were stained with Diff-Quik (Baxter Scientific, Deerfield, IL). The cytologic features of all of the specimens (BB/Ts, TP/Ts, and TP/ABs) were assessed. Both the cytospins and touch imprints were fixed for FISH in methanol and acetic acid at a ratio of 3:1 before labeling. Cytospins were also prepared for the control subjects and stained with Papanicolaou stain. As in the study cases, FISH was performed for three probe sets.

DNA Probe Sets

Three probe sets were used. One was the commercially available multicolor probe set LAVision (Vysis, Downers Grove, IL). This set included four probes: a centromeric probe to chromosome 6 generated from a repetitive probe sequence and three unique sequence probes to 5p15 (LSI 5p15), 7p12 (LSI EGFR), and 8q24 (LSI MYC). The probes were labeled with Spectrum Aqua, Spectrum Green, Spectrum Red, and Spectrum Gold, respectively. The second probe set included centromeric 3 (CEP3; Vysis) and the locus-specific probe 3p22.1, which was developed in-house. The third probe set consisted of centromeric 10 (CEP10; Vysis) and the locus-specific probe 10q22, which was also developed in-house. These probes were mixed with blocking DNA, enriched in repetitive sequences, and hybridized to the specimens.

DNA for 3p22.1 and 10q22 was labeled by using a nick translation kit (Roche Diagnostics Corporation, Indianapolis, IN). DNA and the labeling enzyme were placed in a 15 °C water bath for 1 hour. Next, the probe was transferred to ice. A gel was run to determine the length of the DNA fragments, which had to be 500–2000 base pairs. The probe was then placed in a 65 °C water

TABLE 1
Univariate Analysis of Distribution of Covariates by Cancer Status

Cancer	No.	Mean	SD	Minimum	Median	Maximum	P-value
Age							0.004
No	12	56.9	11.1	42	57	83	
Yes	15	59.0	7.5	57	71	84	
Pack-years							0.33
No	15	37.3	25.0	0	30	97	
Yes	15	48.8	33.2	0	50	120	
3pCEP3-DEL							< 0.0001
No	15	1.2	0.9	0	1	2	
Yes	15	7.1	3.8	1	7	14	
10qCEP10-DEL							< 0.001
No	15	1.2	0.9	0	1	2	
Yes	15	23.9	13.2	9	22	50	
3pCEP3-TPVAB							< 0.001
No	15	1.3	0.9	0	1	2	
Yes	15	7	1.6	2	6	16	
10qCEP10-DEL							0.0002
No	14	0.8	0.8	0	1	2	
Yes	15	4	2.1	2	4	9	
10qCEP10-TPV1							< 0.001
No	14	0.8	0.8	0	1	2	
Yes	15	13.1	7.0	5	10	27	
10qCEP10-TPVAB							< 0.001
No	14	0.8	0.8	0	1	2	
Yes	13	6	3.3	1	5	14	
LAV-TPV1							0.25
No	15	0.3	0.5	0	0	1	
Yes	14	1.1	1.7	0	0	5	
LAV-TPVAB							< 0.001
No	15	0.3	0.5	0	0	1	
Yes	14	8.6	0.1	0	6	23	
LAV-3pAB							0.28
No	15	0.3	0.5	0	0	1	
Yes	12	0.8	1.2	0	0	3	

DEL, bichromal loss; TPV, touch preparation; LAV, LAVision; 3pCEP3, ratio of 3p deletions to CEP3; 10qCEP10, ratio of 10q deletions to CEP10; TPV1, touch preparation of tumor; TPVAB, touch preparation of adjacent bronchus; SD, standard deviation.

bath for 15 minutes and stored in a 20 °C freezer. The detailed methodology for this in-house probe preparation was described previously by Jiang and Katz.⁶

Fluorescence In Situ Hybridization Procedure

Slides were immersed in 2 × standard sodium citrate (SSC) for 3 minutes at 77 °C and then in a protease solution (50 ml of 1 × phosphate-buffered saline [PBS], pH < 2.0, and 25 mg of protease). Protease digestion was then performed (5–6 minutes for cytopins and 7–8 minutes for touch preparations). Slides were then washed in 1 × PBS for 5 minutes and subsequently fixed in a 1% formaldehyde solution for 5 minutes. Afterward, the slides were again washed with 1 × PBS for 5 minutes and dehydrated in sequential 70%, 85%, and 100% ethanol solutions. After a brief period of drying, the probe mixture was applied to the

target areas on each slide, covered with a coverslip, and sealed with rubber cement. The slides were then kept in a hybrid machine (Vysis) for ≥ 20 hours at 37 °C. After the rubber cement and coverslips were removed, the slides were washed in a 50% formamide solution (pH 7.45) in 3 separate jars for 10 minutes each at 45 °C. Next, the slides were washed in 2 × SSC for 10 minutes at 45 °C and then in 2 × SSC/0.1% ethoxylated octyl phenol (NP-40) for 10 minutes. The slides were then dried. Slides were counterstained with 4' 6-Diamidino-2-phenylindole dihydrochloride (DAPI; 10 µL per slide), coverslipped, and viewed under a fluorescent microscope (Leica DWRXA or Leica DMLB; Leica Microsystems, Inc., Buffalo, NY) with the appropriate filters for the probes.

Using the LAVision multicolor probe, 25 nonoverlapping cells with distinct signals were counted per

sample, and the chromosomal abnormalities were scored. A cell was abnormal if it had aneuploidy of two or more chromosomes. If more than five cells were abnormal, the sample was positive as per the recommendation of the probe manufacturer based on studies performed with another multicolor probe (UroVysion; Vysis). For 3p22.1 and 10q22, the hybridized slides were counted with the use of appropriate filter sets for visualizing Spectrum Green or Spectrum Orange as well as DAPI counterstain. In addition, ≥ 100 nuclei from each slide were scored with a triple filter. The nuclei of individual cells that did not overlap were chosen for analysis. Slides were analyzed only if 80% of the cells were interpretable in the field of view and the brightness of the signals was $\geq 2+$ on a scale of 0–3+. Each cell was scored individually for the number of green (3p22.1 or 10q22) and orange signals (CEP3 or CEP10, respectively) that were used as internal controls. Cells with fewer green signals than orange signals were positive, reflecting deletion. The ratio of green to orange signals was interpreted as the percentage of deleted cells. To avoid misinterpretation due to insufficient hybridization, cells were counted only if at least one bright orange and one bright green signal were present. Split signals were counted as one if the space between them was less than the diameter of a single signal. A control specimen was used for each batch. Based on a leave-one-out analysis, $> 2\%$ of the deletions were positive for 3p22.1 and 10q22.

Data Analysis

Univariate data were summarized using standard descriptive statistics in Table 1. The purpose of our study was to assess the predictive ability of various genetic deletions with respect to cancer status. Instead of concentrating exclusively on the significance of *P* values, we focused on the prediction rate of each marker. When prediction is the primary goal of analysis, the gold standard in assessment of the predictor is a test and validation set. Usually, such a set is used when the sample size is adequately large. Our sample was small, so we implemented a leave-one-out validation scheme to assess the predictive ability of the genetic markers using univariate logistic regression. With this scheme, we modeled the relation between the response variable and predictor for all but one data point. Once a model was fit, the response was then predicted for the data point that was left out. This process was repeated for all data points. The sensitivity and specificity values were then calculated based on the leave-one-out validation results and are presented in Tables 2–4. With small samples, this procedure is more robust in modeling overfitting and results in more realistic predictions when compared with na-

TABLE 2
Leave-One-Out Table for 3p:CEP3-BB/T Using a Deletion Rate of $> 2\%$ to Predict Cancer Status

Predicted cancer	Cancer (%)	
	Yes	No
Yes	15 (100.0)	0 (0.0)
No	0 (0.0)	15 (100.0)

3p:CEP3: ratio of 3p deletions to CEP3; BB/T: bronchial brushing on tumor side.

TABLE 3
Leave-One-Out Table for 10q:CEP10-BB/T Using a Deletion Rate of $> 2\%$ to Predict Cancer Status

Predicted cancer	Cancer (%)	
	Yes	No
Yes	15 (100.0%)	3 (21.4%)
No	0 (0.0%)	11 (78.6%)

10q:CEP10: ratio of 10q deletions to CEP10; BB/T: bronchial brushing on tumor side.

TABLE 4
Leave-One-Out Table for Combined 3p:CEP3-BB/T and 10q:CEP10-BB/T Using a Deletion Rate of $> 2\%$ to Predict Cancer Status

Predicted cancer	Cancer (%)	
	Yes	No
Yes	15 (100.0)	0 (0)
No	0 (0.0)	14 (100.0)

3p:CEP3: ratio of 3p deletions to CEP3; 10q:CEP10: ratio of 10q deletions to CEP10; BB/T: bronchial brushing on tumor side.

ive methods.⁷ In addition, associations between categorical variables were assessed via crosstabulation and the Fisher exact test.⁸ All of the computations were carried out with the use of the SAS software program (SAS Institute Inc., Cary, NC) on a Dell personal computer (Dell, Round Rock, TX) equipped with the Windows NT operating system (Microsoft, Redmond, WA) via standard procedures.⁹

RESULTS

Patients

The study included 12 men and 3 women with a mean age of 69.8 years (range, 57–84 years). One of the patients was a nonsmoker, and all of the others had a smoking history ranging from 9.5 to 120.0 pack-years. The control specimens were from 15 patients who did not have a history of lung carcinoma. The control

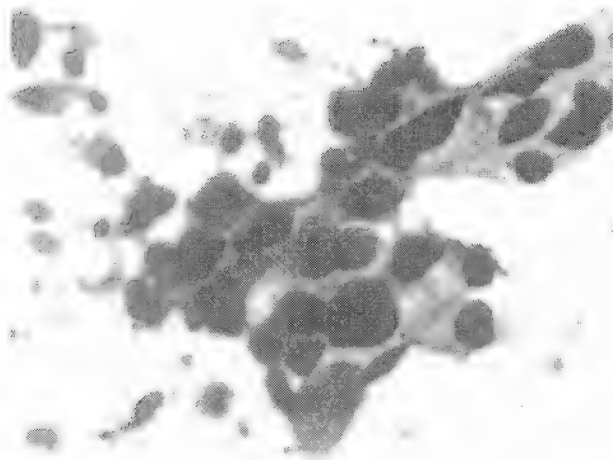


FIGURE 1. Tumor touch imprints showing an adenocarcinoma (Papanicolaou stain, original magnification $\times 200$.)

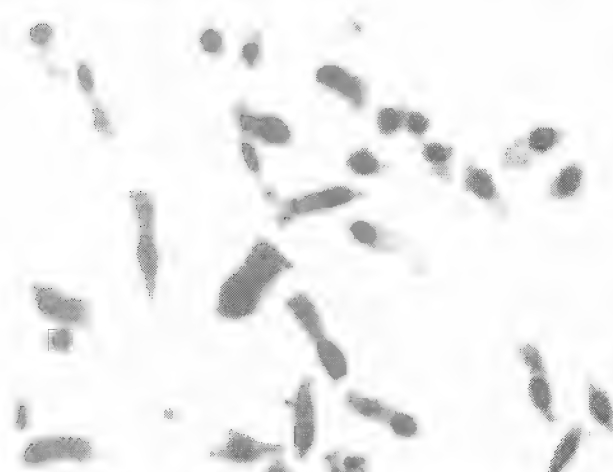


FIGURE 2. Bronchial brush specimen showing unremarkable bronchial epithelium on cytoprep preparations. (Papanicolaou stain, original magnification $\times 600$.)

subjects were 6 men and 7 women with a mean age of 56.9 years (range, 42–83 years). Fourteen of the control subjects had a smoking history ranging from 15 to 75 pack-years.

Cytology/Histology

Histologic examination of the excised tumor specimens showed that there were six adenocarcinomas (Fig. 1), seven squamous cell carcinomas, and two NSCLCs with sarcomatoid change. Touch imprint preparations were made from all of the tumors.

On cytologic evaluation, the BB/Ts were negative for malignant cells (Fig. 2). However, basal cell hyperplasia, squamous metaplasia, goblet cell metaplasia, and rare dysplastic cells were detected in four, five,



FIGURE 3. Interphase fluorescence in situ hybridization (FISH) analysis on bronchial brushings showing a normal diploid population comprising two aqua, two green, two red, and two gold signals using a multicolor FISH analysis probe set (aqua, 6 centromeric; green, 7p12; red, 8p15; and gold, 8q24). (FISH, original magnification $\times 600$.)

three, and three specimens, respectively. TP/ABs, which were available from 12 patients, showed carcinoma in 1 specimen, dysplasia in 1 specimen, and bronchial hyperplasia/reactive bronchial epithelium in three specimens. Cytologic evaluation of the BWs demonstrated basal cell hyperplasia in five patients and squamous metaplasia in four patients.

Fluorescence In Situ Hybridization Analysis

LAVysion multicolor FISH analysis showed that all 14 BB/Ts were negative for malignant cells (Fig. 3). However, five BB/Ts showed single chromosomal abnormalities, predominantly polysomy of 7p12. Also, 11 of the 14 specimens showed deletions of both 3p22.1 (Fig. 4) and 10q22 (Fig. 5). In the carcinomas, the incidence values of positivity were 57% (8 of 14) for the LAVysion probe set (Fig. 6), 100% (14 of 14) for 3p22.1 deletions (Fig. 7), and 79% (11 of 14) for 10q22 deletions (Fig. 8). LAVysion multicolor FISH analysis failed to demonstrate abnormal cells in TP/ABs, although 8 of 12 (67%) and 11 of 12 (92%) of these touch imprints were positive for 3p22.1 and 10q22, respectively. When compared with the adjacent bronchial epithelium, tumor cells showed a 3.7-fold excess of 3p deletions, a 2-fold excess of 10q deletions, and a 12.6-fold excess of abnormal cells by the LAVysion test. Table 1 shows the distribution of the age, pack-years of smoking, and FISH results of the patients and control subjects according to cancer status. The sensitivity and specificity values of the LAVysion multicolor probe set in detecting molecular abnormalities in the BB/Ts were 40% and 73%, respectively. The sensitivity and specificity

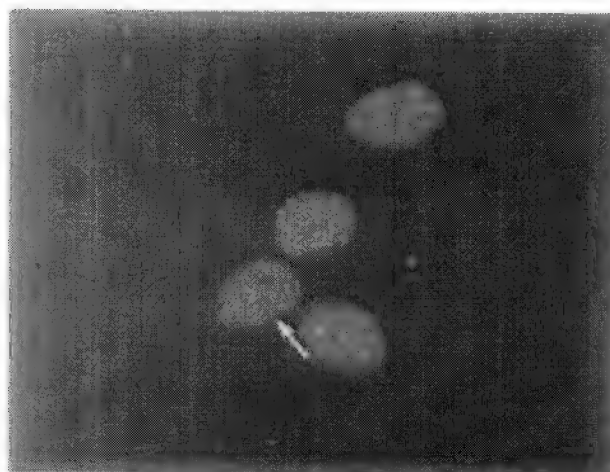


FIGURE 4. Interphase fluorescence in situ hybridization (FISH) analysis on a bronchial brush specimen from the tumor side showing a nucleus with a deletion (arrow) of 3p22.1 (one green signal, 3p22.1, relative to two red signals, CEP3). (FISH, original magnification $\times 600$.)

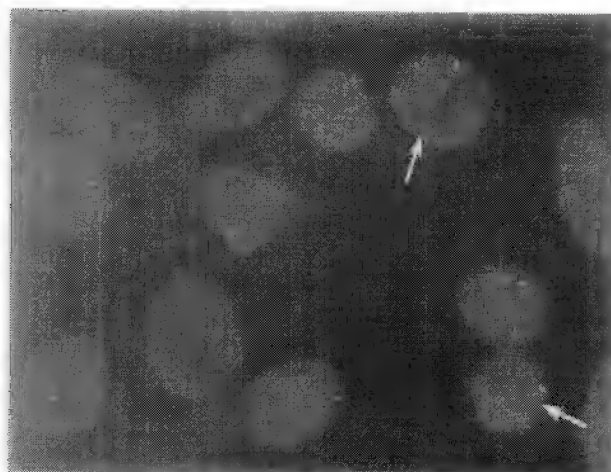


FIGURE 5. Interphase fluorescence in situ hybridization (FISH) analysis on a bronchial brush specimen from the tumor side showing deletions (arrows) of the 10q22 locus-specific probe (loss of green signals, 10q22, relative to red signals, CEP10). (FISH, original magnification $\times 600$.)

values of 3p deletions $> 2\%$ in the BB/T to predict tumor were both 100% (Table 2). The sensitivity and specificity values of 10q deletions from BB/T were 100% and 78.6%, respectively (Table 3). The leave-one-out method showed that a 2% cutoff for both 3p and 10q deletions resulted in 100% sensitivity and specificity for the presence of cancer (Table 4). There was not a significant difference in the molecular abnormalities observed in the BB/Ts, TP/ABs, and TP/Ts of the patients with squamous cell carcinoma and those with adenocarcinoma (Table 5). Finally, the effect of smoking could not be determined with the current data, as there was not a

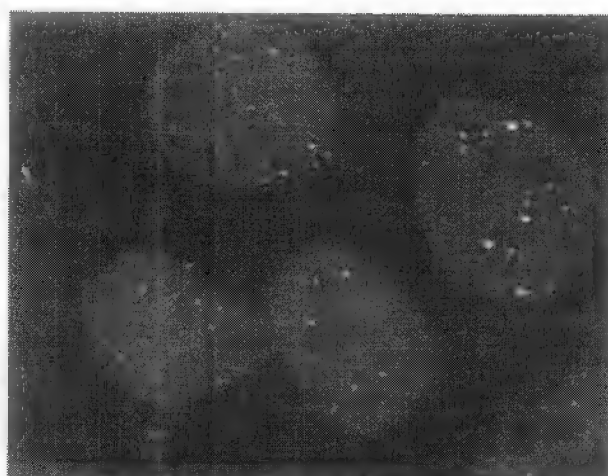


FIGURE 6. Interphase fluorescence in situ hybridization (FISH) analysis on tumor touch imprints showing enlarged aberrant nuclei with polysomies of CEP 7p12, 5p15, and 8q24 indicated by extra red, green, gold, and aqua signals using the multicolor FISH probe set. (FISH, original magnification $\times 600$.)



FIGURE 7. Interphase fluorescence in situ hybridization (FISH) analysis on tumor touch imprints showing deletions (arrow) of the 3p22.1 locus-specific probe (loss of green signals, 3p22.1, relative to red signals, CEP3). (FISH, original magnification $\times 600$.)

sufficient number of patients or control subjects who were nonsmokers.

DISCUSSION

Currently, there are no efficient or accurate screening methods for early detection of lung carcinomas.⁸ The lack of standard screening procedures often leads to diagnosis of these tumors at an advanced stage, which is associated with a poor prognosis and a high mortality rate. The standard of practice in the evaluation of patients for a possible lung carcinoma is a chest



FIGURE 8. Interphase fluorescence in situ hybridization (FISH) analysis on tumor touch imprints showing tumor nuclei with deletions (arrow) of the 10q22 locus-specific probe (loss of green signals, 10q22, relative to the red signals, CEP-12). (FISH, original magnification $\times 800$.)

X-ray and pulmonary function tests followed by a computed tomography scan. Sputum cytology is usually not submitted due to its low sensitivity in detecting neoplastic cells. In patients with a suspected central mass, bronchoscopy is performed and bronchial washes, bronchial brushes, and transbronchial biopsy specimens are obtained. If the mass is peripheral, then the first approach is usually via a percutaneous fine-needle aspiration biopsy. In the current study, we focused on bronchial brush specimens from the side of the suspected tumor as a less invasive method to diagnose the presence of early lung carcinoma. We demonstrated that although most BB/Ts do not contain frankly malignant cells according to cytologic analysis, the majority of them displayed obvious molecular abnormalities of 3p22.1 and 10q22 according to FISH.

In recent years, multiple chromosomal and molecular alterations have been demonstrated in early-stage lung carcinomas^{10–15} using comparative genomic hybridization,^{16–18} microsatellite instability analysis,^{19,20} and FISH.^{21–25} Of these techniques, FISH has been used successfully for the targeted analysis of numeric chromosomal abnormalities in interphase nuclei in various types of solid tumors.^{26–29} Interphase FISH is a relatively easy technique that can detect rare events such as a deletion or addition of a specific gene in a single cell nucleus derived from normal-appearing or cancer cells.

3p is presumed to be the site of multiple tumor suppressor genes, including FHIT (3p14) and RASSF1A (3p21.3). Recent molecular studies showed deletions

in the 3p region in morphologically normal areas of bronchial epithelium in patients with lung carcinoma.³⁰ Deletions in this region are believed to be early and frequent events in lung carcinoma tumorigenesis.^{31,32}

The 10q22 probe used in our study encompasses the gene encoding the surfactant-associated protein (SP-A). SP-A is a hydrophilic protein that facilitates the surface-tension-lowering properties of surfactant phospholipids in alveoli, regulates surfactant phospholipid synthesis, and counteracts the inhibitory effects of plasma proteins released during lung injury.³¹ We postulate that low levels of SP-A, such as those resulting from genetic deletions, may increase host susceptibility to infections and the effects of carcinogenic agents. Loss of 10q22 also has been identified in NSCLC, especially squamous cell carcinoma.^{32,33} In a large retrospective study of patients with Stage I cancer, we demonstrated that deletion of 10q22 in bronchial tissue adjacent to NSCLC is strongly associated with early recurrence of lung carcinoma (unpublished data).

The LAVysion four-color probe set comprises a cocktail of 5p, 7p, 8q, and centromeric 6 nucleic acid probes and has been designed to enhance the detection of malignant cells of NSCLC in sputum samples. Gene amplification in the 5p region is one of the most consistent alterations in NSCLCs and is strongly associated with tumor development, progression, and metastasis. The epidermal growth factor receptor (EGFR) gene, which is located on chromosome 7p, is overexpressed in BWs from smokers as well as in NSCLCs.³⁴ Although EGFR overexpression by immunohistochemistry is increased in patients at high risk for developing lung carcinoma, especially smokers,³⁵ EGFR as an independent prognostic factor appears to be controversial.³⁶ *C-myc* is a nuclear phosphoprotein that participates in cell growth and tumor development by activating transcription of growth-stimulating genes. *C-myc* is located on chromosome 8q and is amplified in both small cell and non-small cell lung carcinomas.

In a retrospective study of BWs from 46 patients with histologically proven lung carcinoma, Sokolova et al.²² found that the sensitivity for the detection of carcinoma cells was 82% for FISH with the LAVysion multicolor probe. In comparison, others found the sensitivity of cytology to be 54%.²³ In a similar multicolor FISH study by Romeo et al.¹⁴ comparing tumor touch imprints of nonsmall cell carcinomas and sputa, the authors noted high frequencies of abnormal cells in all 20 imprints. However, none of the cytologically normal sputa demonstrated any abnormalities in FISH with the multicolor probe.

TABLE 5
Examination of Differences in Molecular Abnormalities by Site Versus Histology

Histology	No.	Mean	SD	Minimum	Median	Maximum	P value
3pCPS-BB/T							0.70
Adenocarcinoma	6	7.67	3.14	3.14	3	7.5	
Squamous Ca	8	7.13	3.99	3.68	3	6	
3pCPS-TP/AB							0.94
Adenocarcinoma	5	6.80	3.27	3.27	2	6	
Squamous Ca	7	7.71	4.55	4.27	3	6	
3pCPS-TP/T							0.95
Adenocarcinoma	6	22.67	9.47	5.45	13	23.5	
Squamous Ca	8	26.63	15.94	16.90	9	32	
10qCPS-BB/T							0.56
Adenocarcinoma	6	4.17	2.04	2.04	2	4	
Squamous Ca	8	3.88	2.65	2.47	2	6	
10qCPS-TP/AB							0.35
Adenocarcinoma	5	6.40	1.67	1.67	5	6	
Squamous Ca	7	6.14	4.59	4.22	3	4	
10qCPS-TP/T							0.85
Adenocarcinoma	6	13.17	7.99	7.99	8	12	
Squamous Ca	8	13.25	7.06	6.67	5	10	
LAV-BB/T							0.14
Adenocarcinoma	5	2.40	2.50	0.00	0	3	
Squamous Ca	8	0.25	0.48	0.00	0	0	
LAV-TP/T							1.00
Adenocarcinoma	5	8.80	8.87	3.87	0	6	
Squamous Ca	8	8.75	8.83	8.68	0	5.5	
LAV-TP/AB							0.54
Adenocarcinoma	5	0.60	1.34	1.34	0	8	
Squamous Ca	6	1.00	1.26	0	.5	3	

Note: * denotes loss of heterozygosity; LAVy: LAVision; 3pCPS: ratio of 3p deletions; 10qCPS: ratio of 10q deletions; CPS10: TP/T: touch preparation; TP/AB: touch preparation of adjacent bronchus; Ca: carcinoma; SD: standard deviation.

In the current study, evaluation of molecular abnormalities in bronchial epithelial cells via FISH was very useful in identifying patients who were at high risk for developing lung carcinoma. Deletions of 3p22.1 and 10q22 were detected at least two to four times more often in BB/Ts than abnormal cells by LAVysion probe set, which were detected only infrequently in BB/Ts when compared with TP/Ts. These results may reflect the finding that the tumor suppressor genes on 3p22.1 and 10q22 are deleted earlier in the genetic instability events involved in carcinogenesis than the oncogenes located on 5p15, 7p12, and 8q24. Therefore, 3p22.1 and 10q22 appear to be far more sensitive markers than the multicolor probe set in detecting a field effect in early-stage lung carcinomas. It is noteworthy that there was no significant difference in the molecular abnormalities of 3p22.1 and 10q22 for the different histologies of NSCLC regardless of anatomic site, suggesting that these abnormalities occur in the tumor stem cells before histologic differentiation takes place.

Our findings are compelling and may lead to the use

of FISH as a valuable adjunct to cytology of bronchial brush specimens in high-risk patients with radiographically detected lung lesions, the majority of which are benign. A larger prospective trial must be performed to validate the current study in establishing the use of FISH analysis of bronchoscopy specimens and eventually sputa, as an adjunct to cytology in the early detection of lung carcinoma.

REFERENCES

1. American Cancer Society. Cancer facts and figures. Atlanta: American Cancer Society, 2002.
2. Mulshine JL, Linnoila RI, Jensen SM, et al. National targets for the early detection of lung cancer. *J Natl Cancer Inst Monogr*. 1992;13:183-190.
3. American Lung Association. Best practices and program services: trends in lung cancer morbidity and mortality. New York: American Lung Association, 2001.
4. Fossella FV, Komaki R, Putman JB, editors. Lung cancer. New York: Springer-Verlag, 2003.
5. Braakhuis BJ, Tabor MP, Kummer JA, Leemans CR, Brakenhoff RH. A genetic explanation of Slaughter's concept of field cancerization: evidence and clinical implications. *Cancer Res*. 2003;63:1727-1730.

8. Bana J, Katz RL. Use of interphase fluorescence in situ hybridization as a powerful diagnostic tool in cytology. *Diagn Mol Pathol*. 2002;11:47-57.
9. Efron B, Tibshirani RJ. An introduction to the bootstrap. New York: Chapman & Hall; 1993.
10. Freedman DW, Cochran WG. Statistical methods. 7th ed. Ames: Iowa State University Press; 1980.
11. SAS Institute. SAS/STAT user's guide. Version 8. Cary, NC: SAS Institute, Inc.; 1999.
12. Michaliniak S, Gaziari S, Brambilla E, Robert-Nicoud M. Detection of chromosomal imbalances in neuroendocrine and non-small-cell lung carcinomas. *Cancer Genet Cytogenet*. 1999;114:22-30.
13. Feder M, Siegfried JM, Balshem A, et al. Clinical relevance of chromosome abnormalities in non-small cell lung cancer. *Cancer Genet Cytogenet*. 1998;102:25-31.
14. Deguchi T, Zhou F, Feder M, Lin W, Klein-Szanto AJ, Testa JR. Detection of aneuploidy in interphase nuclei from non-small cell lung carcinomas by fluorescence in situ hybridization using chromosome-specific repetitive DNA probes. *Cancer Genet Cytogenet*. 1998;89:120-125.
15. Kubokura H, Tenjin T, Akiyama H, et al. Relations of the c-myc gene and chromosome 8 in non-small cell lung cancer: analysis by fluorescence in situ hybridization. *Ann Thorac Cardiovasc Surg*. 2001;7:197-203.
16. Roman MS, Sokolova IA, Morrison LE, et al. Chromosomal abnormalities in non-small cell lung carcinomas and in bronchial epithelia of high-risk smokers detected by multiplex interphase fluorescence in situ hybridization. *J Mol Diagn*. 2003;5:103-112.
17. Testa JR, Siegfried JM. Chromosomal abnormalities in human non-small cell cancer. *Cancer Res*. 1992;52(9 Suppl.):2705-2706s.
18. Reed T, Petersen I, Holtgreve-Grez H, et al. Mapping of multiple DNA gains and losses in primary small cell lung carcinomas by comparative genomic hybridization. *Cancer Res*. 1994;54:1801-1806.
19. Taubold A, Liehr T, Ries J, Grotz S, Hassfurter E, Gebhart E. CGH detected DNA sequence copy number amplifications can be confirmed by interphase-FISH: new possibilities for prognostic approaches in oral squamous carcinomas. *Int J Mol Med*. 1998;2:555-560.
20. Taguchi T, Cheng GZ, Bell DW, et al. Combined chromosome microdissection and comparative genomic hybridization detect multiple sites of amplification DNA in a human lung carcinoma cell line. *Genes Chromosomes Cancer*. 1997;26:239-247.
21. Gazdar AF, Minna JD. Molecular detection of early lung cancer. *J Natl Cancer Inst*. 1999;91:299-301.
22. Liliogra T, Mahoney P, Xinaras G, et al. Cancer-specific genomic instability in bronchial lavage: a molecular tool for lung cancer detection. *Cancer Res*. 2001;61:1309-1313.
23. Sanchez-Cespedes M, Ahrentz SA, Piantadosi S, et al. Chromosomal alteration in lung adenocarcinoma from smokers and nonsmokers. *Cancer Res*. 2001;61:1309-1313.
24. Sokolova IA, Bubendorf L, O'Hare A, et al. A fluorescence in situ hybridization-based assay for improved detection of lung cancer cells in bronchial washing specimens. *Cancer*. 2002;96:306-315.
25. McCarthy PM, Jelsing NC. An advocacy perspective on screening and early diagnosis of lung cancer. *Cancer*. 2000;89:2510-2514.
26. Tockman MS. Advances in sputum analysis for screening and early detection of lung cancer. *Cancer Control*. 2000;7:19-24.
27. Schenk T, Ackermann J, Brunner C, et al. Detection of chromosomal aneuploidy by interphase in situ hybridization in bronchoscopically gained cells from lung cancer patients. *Chest*. 1997;111:1691-1696.
28. Stamouli MI, Ferri AD, Panani AD, et al. Application of multiplex fluorescence in situ hybridization in the cytogenetic analysis of primary gastric carcinoma. *Cancer Genet Cytogenet*. 2002;135:23-27.
29. Fuller CE, Perry A. Fluorescence in situ hybridization (FISH) in diagnostic and investigative neuropathology. *Brain Pathol*. 2002;12:67-86.
30. Dalquen P, Kleiber B, Grilli B, Herzog M, Bubendorf L, Oberholzer M. DNA image cytometry and fluorescence in situ hybridization for noninvasive detection of urothelial tumors in voided urine. *Cancer*. 2002;96:374-379.
31. Engel H, Friedrich J, Kleespies C, et al. Detection of chromosomal aberrations in tumor cells and tumor infiltrating lymphocytes by molecular cytogenetics in patients with gynecological cancer. *Cancer Genet Cytogenet*. 1998;106:159-165.
32. Zabarovsky ER, Lerman MI, Minna JD. Tumor suppressor genes on chromosome 3p involved in the pathogenesis of lung and other cancers. *Oncogene*. 2002;21:6915-6935.
33. Khubchandani KR, Snyder JM. Surfactant protein a (SP-A): the alveolus and beyond. *FASEB J*. 2001;15:59-69.
34. Petersen S, Aninat-Meyer M, Schluns K, Gellert K, Dietel M, Petersen I. Chromosomal alterations in the clonal evolution to the metastatic stage of squamous cell carcinomas of the lung. *Br J Cancer*. 2000;82:65-73.
35. Petersen S, Wolf G, Bockmuhl U, Gellert K, Dietel M, Petersen I. Allelic loss on chromosome 10q in human lung cancer: association with tumor progression and metastatic phenotype. *Br J Cancer*. 1998;77:270-276.
36. Piyathilake CJ, Frost AR, Manne U, et al. Differential expression of growth factors in squamous cell carcinoma and precancerous lesions of the lung. *Clin Cancer Res*. 2002;8:734-744.
37. Barsky SH, Roth MD, Kleerup EC, Simmons M, Tashkin DP. Histopathologic and molecular alterations in bronchial epithelium in habitual smokers of marijuana, cocaine, and/or tobacco. *J Natl Cancer Inst*. 1998;90:1198-1205.
38. Brabender J, Danenberg KD, Metzger R, et al. Epidermal growth factor receptor and HER2-neu mRNA expression in non-small cell lung cancer is correlated with survival. *Clin Cancer Res*. 2001;7:1850-1855.

Cytokinesis-Blocked Micronucleus Assay as a Novel Biomarker for Lung Cancer Risk

Randa A. El-Zein, Matthew B. Schabath, Carol J. Etzel, Mirtha S. Lopez, Jamey D. Franklin, and Margaret R. Spitz

Departments of Epidemiology, The University of Texas M.D. Anderson Cancer Center, Houston, Texas

Abstract

In this case-control study, we modified the cytokinesis-block micronucleus (CBMN) assay, an established biomarker for genomic instability, to evaluate susceptibility to the nicotine-derived nitrosamine 4-(methylnitrosamino)-1-(3-pyridyl)-1-butanone (NNK) by measuring the frequency of NNK-induced chromosomal damage endpoints (micronuclei, nucleoplasmic bridges, and nuclear buds) per 1,000 binucleated lymphocytes. Spontaneous and NNK-induced chromosomal damage were significantly higher in lung cancer patients compared with controls. Forty-seven percent of cases (versus 12% of controls) had ≥ 4 spontaneous micronuclei, 66% of cases (and no controls) had ≥ 4 spontaneous nucleoplasmic bridges, and 25% of cases (versus 5% of controls) had ≥ 1 spontaneous nuclear bud ($P < 0.001$). Similarly, 40% of cases (versus 6% of the controls) had ≥ 5 NNK-induced micronuclei, 89% of cases (and no controls) had ≥ 6 induced nucleoplasmic bridges, and 23% of cases (versus 2% of controls) had ≥ 2 induced nuclear buds ($P < 0.001$). When analyzed on a continuous scale, spontaneous micronuclei, nucleoplasmic bridges, and nuclear buds were associated with 2-, 29-, and 6-fold increases in cancer risk, respectively. Similarly, NNK-induced risks were 2.3-, 45.5-, and 10-fold, respectively. We evaluated the use of CBMN assay to predict cancer risk based on the numbers of micronuclei, nucleoplasmic bridges, and nuclear buds defined by percentile cut points in controls. Probabilities of being a cancer patient were 96%, 98%, and 100% when using the 95th percentiles of spontaneous and NNK-induced micronuclei, nucleoplasmic bridges, and nuclear buds, respectively. Our study indicates that the CBMN assay is extremely sensitive to NNK-induced genetic damage and may serve as a strong predictor of lung cancer risk. (Cancer Res 2006; 66(12): 6449-56)

Introduction

Lung cancer is the leading cause of cancer mortality in the United States, and there is an urgent need to improve outcome by identifying and validating markers to predict risk and allow early diagnosis (1). A crucial early event in carcinogenesis is the induction of the genomic instability phenotype, which enables an initiated cell to evolve into a cancer cell by achieving a greater proliferative capacity (2). It is well known that cancer results from an accumulation of multiple genetic changes that can be

mediated through chromosomal changes and that have the potential to be cytogenetically detectable (3). It has been hypothesized that the level of genetic damage in peripheral blood lymphocytes reflects the amount of damage in the precursor cells that lead to the carcinogenic process in target tissues (4). Evidence that cytogenetic biomarkers are positively correlated with cancer risk has been strongly validated in recent results from both cohort and nested case-control studies showing that chromosome aberrations are a marker of cancer risk (5-9), reflecting both the genotoxic effects of carcinogens and individual cancer susceptibility.

The cytokinesis-block micronucleus (CBMN) assay in human lymphocytes is one of the most commonly used methods for measuring DNA damage because it is relatively easier to score micronuclei than chromosome aberrations (2). Micronuclei originate from chromosome fragments or whole chromosomes that fail to engage with the mitotic spindle and therefore lag behind when the cell divides. Compared with other cytogenetic assays, quantification of micronuclei confers several advantages, including speed and ease of analysis, no requirement for metaphase cells, and reliable identification of cells that have completed only one nuclear division. This prevents confounding effects caused by differences in cell division kinetics because expression of micronuclei, nucleoplasmic bridges, or nuclear buds is dependent on completion of nuclear division (10). Because cells are blocked in the binucleated stage, it is also possible to measure nucleoplasmic bridges originating from asymmetrical chromosome rearrangements and/or telomere end fusions (11, 12). Nucleoplasmic bridges occur when the centromeres of dicentric chromosomes or chromatids are pulled to the opposite poles of the cell at anaphase. In the CBMN assay, binucleated cells with nucleoplasmic bridges are easily observed because cytokinesis is inhibited, preventing breakage of the anaphase bridges from which nucleoplasmic bridges are derived; thus, the nuclear membrane forms around the nucleoplasmic bridge. Both micronuclei and nucleoplasmic bridges occur in cells exposed to DNA-breaking agents (13, 14). In addition to micronuclei and nucleoplasmic bridges, the CBMN assay allows for the detection of nuclear buds, which represent a mechanism by which cells remove amplified DNA and are therefore considered a marker of possible gene amplification [reviewed by Fenech (14)]. The CBMN test is gradually replacing the analysis of chromosome aberrations in lymphocytes because micronuclei, nucleoplasmic bridges, and nuclear buds are easy to recognize and score and the results can be obtained in a shorter time (15).

More than 80% of lung cancers are attributed to tobacco exposure. However, because only a fraction of long-term smokers (~15%) will develop lung cancer in their lifetime (16), it is proposed that genetic factors play a role in individual susceptibility. An individual's DNA repair capacity may play a significant role in modifying risk for cancer. The tobacco-specific nitrosamine

Requests for reprints: Randa A. El-Zein, Department of Epidemiology, The University of Texas M.D. Anderson Cancer Center, Unit 1346, P.O. Box 301439, Houston, TX 77030-1439. Phone: 713-745-2536; Fax: 713-792-9566; E-mail: relzein@mdanderson.org.

©2006 American Association for Cancer Research.
0732-183X/06/6612-6449/\$20.00

4-(methylnitrosamino)-1-(3-pyridyl)-1-butanone (NNK) is a strong pulmonary carcinogen and a potent inducer of lung adenocarcinoma, now the leading lung cancer subtype in the United States (17). Studies on the metabolism of NNK have shown that it induces cross links in DNA; interacts with DNA, forming different types of adducts; and increases the frequency of chromosome aberrations (18, 19). Harris (20) reported that DNA adducts derived from NNK are present at a higher level in lung tissues from lung cancer patients than controls, and metabolites of NNK are found in the urine of people who use tobacco products or are exposed to environmental tobacco smoke. The repair kinetics for NNK-induced genetic damage has not been clearly elucidated but may involve several DNA repair pathways, including base excision and nucleotide excision repair pathways (21). In the current study, we used the CBMN assay to measure NNK-induced micronuclei, nucleoplasmic bridge, and nuclear bud frequencies and conducted a pilot proof-of-principle case-control study to evaluate whether NNK-induced damage was associated with lung cancer risk.

Materials and Methods

Study population. Cases and controls for this analysis were accrued from a ongoing molecular epidemiologic study on susceptibility markers for lung cancer. Cases ($n = 139$) were consecutive patients with newly diagnosed, previously untreated, histologically confirmed lung cancer patients. All cases were recruited from The University of Texas M.D. Anderson Cancer Center with no age, gender, ethnicity, tumor histology, or disease stage restrictions. Healthy controls ($n = 130$) were recruited from the Kelsey-Seybold Clinics, Houston's largest private multispecialty medical group. Controls were matched to the cases on age (± 5 years), gender, ethnicity, and smoking status (current and former). Data related to the subjects' medical history, family history of cancer, smoking habits, and occupational history were obtained through an interviewer-administered self-care questionnaire and by review of an institutional electronic medical history database. The institutional review boards at both The University of Texas M. D. Anderson Cancer Center and Kelsey-Seybold Clinics approved this study. After giving informed consent, all study participants donated a 10-ml blood sample, which was drawn into coded heparinized tubes.

Peripheral blood lymphocyte cultures for CBMN test. The CBMN test was done using the cytochalasin B technique described by Fenech and Murray (22) and following recommendations from the International Chromosome Project on Micronucleus Frequency in Human Populations (HUMN Project) to measure micronuclei, nucleoplasmic bridges, and nuclear buds in untreated cells and NNK-treated cells. Duplicate lymphocyte cultures were prepared for each study subject. Each culture contained 2.0×10^6 cells in 5 ml RPMI 1640 supplemented with 100 units/ml penicillin, 100 μ g/ml streptomycin, 10% fetal bovine serum, and 2 mmol/L L-glutamine (Life Technologies/Invitrogen, Carlsbad, CA) and 18-phoscoeraguaran (Remel, Lenexa, KS). For the cultures treated with NNK, 24 hours after initiation, the peripheral blood lymphocytes were trypsinized and the supernatant growth medium was removed and reserved. The peripheral blood lymphocytes were resuspended in 5 ml serum-free RPMI 1640 supplemented with 0.24 mmol/L NNK (a dose previously used by us and others; refs. 23-26; CAS no. 64091-91-4, National Cancer Institute, Midwest Carcinogen Repository, Kansas City, MO; purity, >98%) and incubated at 37°C in the presence of 5% CO₂ for 1 hour. Next, the peripheral blood lymphocytes were washed twice with serum-free RPMI 1640, transferred to clean tubes, and reincubated for 6 hours in the reserved supernatant. At 48 hours after initiation, cells were blocked in cytokinesis by adding cytochalasin B (Sigma, St. Louis, MO; final concentration, 4 μ g/ml). Similarly, cultures for the determination of spontaneous damage (untreated cells) were handled in the same manner, with the exception of treatment with NNK. The total incubation time for all cultures was 72 hours. After incubation, the cells were fixed in 3:1 methanol/

glacial acetic acid, dropped onto clean microscopic slides, air-dried, and stained with Giemsa stain. For each sample, 1,000 binucleated cells were scored blindly using a Nikon (Lewisville, TX) E-400 light optical microscope following the scoring criteria outlined by HUMN Project (2, 22, 27); the numbers of micronuclei, nucleoplasmic bridges, and nuclear buds per 1,000 binucleated cells were recorded. For quality control, 20% of the slides were randomly selected and blindly rescored and the results were compared with the original scoring.

Statistical analysis. All analyses were done using the Intercooled Stata 8.0 statistical software package (Stata Corp., College Station, TX). Pearson's χ^2 test was used to test for differences between cases and controls in terms of gender, alcohol consumption, and family history of cancer. Student's t test was used to test differences in mean age and average number of cigarettes smoked per day. We used the nonparametric Wilcoxon's rank-sum test (continuous) and the Pearson's χ^2 test (categorical) to compare the distribution of spontaneous and NNK-induced micronuclei, nucleoplasmic bridges, and nuclear buds between cases and controls. We also constructed dot charts using S-Plus (version 6.2, Insightful Corp., Seattle, WA, 2003) to compare the distribution of spontaneous and NNK-induced micronuclei, nucleoplasmic bridges, and nuclear buds between cases and controls. Odds ratios (OR) and 95% confidence intervals (95% CI) were calculated to provide an estimate of the risk of lung cancer associated with the number of spontaneous and NNK-treated micronuclei, nucleoplasmic bridges, and nuclear buds per 1,000 cells. Unconditional multivariable logistic regression analysis was used to control for confounding by age, gender, alcohol consumption, smoking status, and years smoked.

Results

Demographics and the study population. The demographic characteristics of the 139 cases and 130 controls are summarized in Table 1. Cases and controls did not differ significantly in terms of gender. However, on average, the cases were 2.5 years younger (mean age \pm SE, 58.4 \pm 0.41) than the controls (mean age \pm SE,

Table 1. Distribution of selected host characteristics by case-control status

Variable	Case patients ($n = 139$)	Control subjects ($n = 130$)	P^*
Age (yr), mean \pm SE	58.4 \pm 0.41	60.9 \pm 0.32	<0.001
Gender, n (%)			
Men	97 (69.8)	93 (71.5)	0.752
Women	42 (30.2)	37 (28.5)	
Family history of cancer, n (%)			
No	106 (76.3)	101 (77.7)	0.760
Yes	33 (23.7)	29 (22.3)	
History of alcohol use, n (%)			
Yes	91 (65.5)	65 (50.0)	0.003
No	47 (33.5)	59 (45.4)	
Cigarette smoking, mean \pm SE			
No, years smoked [†]	42.1 \pm 0.50	37.7 \pm 0.84	<0.001
No, cigarettes smoked per day [‡]	20.0 \pm 1.38	29.2 \pm 1.21	0.651

NOTE: All study subjects are self-reported Caucasians and current smokers.

* P s were derived from the χ^2 test for categorical variables and Student's t test for continuous variables. All P s are two sided.

[†] Data were missing for 1 case and 6 controls.

[‡] Data were missing for 1 case.

[§] Data were missing for 6 cases and 2 controls.

Table 2. Overall spontaneous and NNK-induced frequencies of micronuclei, nucleoplasmic bridges, and nuclear buds per 1,000 binucleated cells by age, gender, and years smoked in lung cancer cases and controls

	Case mean \pm SE (median)	Control mean \pm SE (median)
Spontaneous		
Overall		
Micronuclei	1.41 \pm 0.13 (3.0)	1.98 \pm 0.12 (2.0)
Nucleoplasmic bridges	1.14 \pm 0.10 (4.0)	0.57 \pm 0.07 (0.0)
Nuclear buds	0.28 \pm 0.04 (0.0)	0.05 \pm 0.02 (0.0)
Males		
Micronuclei	3.47 \pm 0.17 (3.0)	1.95 \pm 0.13 (2.0)
Nucleoplasmic bridges	4.13 \pm 0.12 (4.0)	0.57 \pm 0.08 (0.0)
Nuclear buds	0.29 \pm 0.05 (0.0)	0.06 \pm 0.03 (0.0)
Females		
Micronuclei	3.26 \pm 0.25 (3.0)	2.05 \pm 0.18 (2.0)
Nucleoplasmic bridges	4.17 \pm 0.16 (4.5)	0.57 \pm 0.13 (0.0)
Nuclear buds	0.26 \pm 0.07 (0.0)	0.0 \pm 0.0 (0.0)
Age ≤ 62 y		
Micronuclei	3.44 \pm 0.15 (3.0)	1.97 \pm 0.14 (2.0)
Nucleoplasmic bridges	4.02 \pm 0.12 (4.0)	0.56 \pm 0.09 (0.0)
Nuclear buds	0.25 \pm 0.04 (0.0)	0.05 \pm 0.02 (0.0)
Age > 62 y		
Micronuclei	3.54 \pm 0.27 (3.0)	1.98 \pm 0.18 (2.0)
Nucleoplasmic bridges	4.44 \pm 0.16 (5.0)	0.60 \pm 0.11 (0.0)
Nuclear buds	0.39 \pm 0.10 (0.0)	0.05 \pm 0.03 (0.0)
Years smoked ≤ 37		
Micronuclei	4.50 \pm 0.42 (3.5)	1.88 \pm 0.21 (2.0)
Nucleoplasmic bridges	3.50 \pm 0.38 (3.0)	0.42 \pm 0.12 (0.0)
Nuclear buds	0.13 \pm 0.03 (0.0)	0.0 \pm 0.0 (0.0)
Years smoked > 37		
Micronuclei	3.43 \pm 0.14 (3.0)	2.00 \pm 0.13 (2.0)
Nucleoplasmic bridges	4.13 \pm 0.10 (4.0)	0.61 \pm 0.09 (0.0)
Nuclear buds	0.29 \pm 0.04 (0.0)	0.06 \pm 0.03 (0.0)
History of alcohol use: yes		
Micronuclei	3.07 \pm 0.16 (3.00)	2.00 \pm 0.15 (2.00)
Nucleoplasmic bridges	4.19 \pm 0.13 (4.00)	0.58 \pm 0.11 (0.00)
Nuclear buds	0.29 \pm 0.05 (0.00)	0.07 \pm 0.03 (0.00)
History of alcohol use: no		
Micronuclei	3.32 \pm 0.23 (3.00)	1.88 \pm 0.16 (2.00)
Nucleoplasmic bridges	4.02 \pm 0.16 (4.00)	0.55 \pm 0.10 (0.00)
Nuclear buds	0.27 \pm 0.07 (0.00)	0.03 \pm 0.02 (0.00)
NNK-induced		
Overall		
Micronuclei	4.32 \pm 0.10 (4.0)	2.62 \pm 0.10 (3.0)
Nucleoplasmic bridges	8.12 \pm 0.19 (8.0)	2.36 \pm 0.09 (2.0)
Nuclear buds	1.07 \pm 0.09 (1.0)	0.12 \pm 0.03 (0.0)
Males		
Micronuclei	4.37 \pm 0.13 (4.0)	2.63 \pm 0.11 (3.0)
Nucleoplasmic bridges	8.07 \pm 0.23 (8.0)	2.27 \pm 0.10 (2.0)
Nuclear buds	1.07 \pm 0.11 (1.0)	0.12 \pm 0.03 (0.0)
Females		
Micronuclei	4.16 \pm 0.17 (4.0)	2.51 \pm 0.23 (2.0)
Nucleoplasmic bridges	8.29 \pm 0.32 (8.0)	2.68 \pm 0.19 (2.0)
Nuclear buds	1.07 \pm 0.12 (1.0)	0.11 \pm 0.05 (1.0)
Age ≤ 62 y		
Micronuclei	4.22 \pm 0.11 (4.0)	2.58 \pm 0.14 (2.0)
Nucleoplasmic bridges	8.11 \pm 0.23 (8.0)	2.41 \pm 0.11 (2.0)
Nuclear buds	1.12 \pm 0.11 (1.0)	0.13 \pm 0.04 (0.0)

Table 2. Overall spontaneous and NNK-induced frequencies of micronuclei, nucleoplasmic bridges, and nuclear buds per 1,000 binucleated cells by age, gender, and years smoked in lung cancer cases and controls (Cont'd)

	Case mean \pm SE (median)	Control mean \pm SE (median)
Age > 62 y		
Micronuclei	4.54 \pm 0.22 (4.0)	2.75 \pm 0.15 (3.0)
Nucleoplasmic bridges	8.15 \pm 0.33 (8.0)	2.35 \pm 0.14 (2.0)
Nuclear buds	0.90 \pm 0.17 (1.0)	0.10 \pm 0.05 (0.0)
Years smoked ≤ 37		
Micronuclei	3.63 \pm 0.32 (4.0)	2.33 \pm 1.02 (2.0)
Nucleoplasmic bridges	9.25 \pm 0.96 (8.3)	2.36 \pm 0.19 (2.0)
Nuclear buds	1.13 \pm 0.41 (1.0)	0.06 \pm 0.04 (0.0)
Years smoked > 37		
Micronuclei	4.33 \pm 0.10 (4.0)	2.69 \pm 0.12 (3.0)
Nucleoplasmic bridges	8.07 \pm 0.19 (8.0)	2.39 \pm 0.09 (2.0)
Nuclear buds	1.08 \pm 0.01 (1.0)	0.13 \pm 0.04 (0.0)
History of alcohol use: yes		
Micronuclei	4.37 \pm 0.14 (4.00)	2.61 \pm 0.15 (2.00)
Nucleoplasmic bridges	8.14 \pm 0.24 (8.00)	2.32 \pm 0.12 (2.00)
Nuclear buds	1.04 \pm 0.11 (1.00)	0.11 \pm 0.04 (0.00)
History of alcohol use: no		
Micronuclei	4.26 \pm 0.14 (4.00)	2.54 \pm 0.15 (3.00)
Nucleoplasmic bridges	8.04 \pm 0.32 (8.00)	2.40 \pm 0.13 (2.00)
Nuclear buds	1.09 \pm 0.18 (1.00)	0.14 \pm 0.04 (0.00)

60.9 \pm 0.32; $P < 0.001$). Twenty-four percent of the patients self-reported a family history of cancer in first-degree relatives compared with 22% of the controls ($P = 0.780$). Cases had, on average, smoked cigarettes for 42.1 years compared with 37.7 years for controls ($P < 0.001$), but both groups smoked about the same number of cigarettes per day (mean number of cigarettes per day \pm SE, 30.2 \pm 1.38 for cases and 29.2 \pm 1.21 for controls; $P = 0.651$).

Frequencies of cytogenetic endpoints by case-control status. Overall, the lung cancer cases exhibited significantly higher values of all cytogenetic end points than the controls (Table 2). The P s for all Wilcoxon's rank-sum tests were < 0.001 .

Frequencies of spontaneous cytogenetic endpoints. Data on spontaneous micronucleus, nucleoplasmic bridge, and nuclear bud frequencies by age, gender, and years of smoking are summarized in Table 2. Table 3 shows that ~47% of the cases had ≥ 4 micronuclei per 1,000 binucleated cells compared with 12% of control subjects and that 40% of the control subjects had 0 or 1 micronucleus compared with only 9% of the cases ($P < 0.001$). The mean number of spontaneous micronuclei \pm SE was significantly higher in the cases (3.41 \pm 0.13) than in the control subjects (1.98 \pm 0.12; $P < 0.001$). Similarly, ~66% of the cases had ≥ 4 nucleoplasmic bridges compared with none of the control subjects, whereas 86% of the controls had 0 or 1 nucleoplasmic bridge compared with none of the cases ($P < 0.001$). Furthermore, the number of spontaneous nucleoplasmic bridges was significantly higher in the cases (mean \pm SE, 4.14 \pm 0.10) than in the controls (mean \pm SE, 0.57 \pm 0.07; $P < 0.001$). With regard to frequency of nuclear bud distribution, ~95% of the controls exhibited no spontaneous buds compared with 73% of cases. Only 5% of the controls had 1 spontaneous bud compared with 25% of the cases ($P < 0.001$). Overall, the average number of spontaneous buds was

Table 3. Distributions and risk estimates of lung cancer for spontaneous and NNK-induced micronuclei, nucleoplasmic bridges, and nuclear buds

Variable	Case patients, n (%)	Control subjects, n (%)	OR (95% CI)* or P†
Micronuclei			
Pearson's χ^2 test			
Spontaneous			
0 or 1	43 (9.4)	52 (40.0)	
2 or 3	61 (43.9)	63 (48.3)	
≥4	60 (46.8)	15 (11.5)	<0.001
NNK induced			
1 or 2	5 (3.0)	69 (49.2)	
3 or 4	79 (56.1)	58 (44.6)	
≥5	86 (40.3)	8 (6.2)	<0.001
Multivariate logistic regression analysis			
Spontaneous	139	130	2.06 (1.60-2.65)
NNK induced	139	130	2.32 (2.32-4.80)
Nucleoplasmic bridges			
Pearson's χ^2 test			
Spontaneous			
0 or 1	0 (0.0)	112 (86.2)	
2 or 3	48 (34.5)	18 (13.9)	
≥4	91 (65.5)	0 (0.0)	<0.001
NNK induced			
0 or 2	0 (0.0)	89 (64.6)	
3 or 5	15 (10.8)	46 (35.4)	
≥6	124 (89.2)	0 (0.0)	<0.001
Multivariate logistic regression analysis			
Spontaneous	139	130	29.05 (7.48-112.80)
NNK induced	139	130	45.52 (4.48-422.17)
Nuclear buds			
Pearson's χ^2 test			
Spontaneous			
0	102 (73.4)	122 (95.3)	
1	35 (25.3)	6 (4.7)	
≥2	2 (1.4)	0 (0.0)	<0.001
NNK induced			
0	48 (34.5)	113 (86.9)	
1	59 (42.5)	15 (11.5)	
≥2	32 (23.0)	2 (1.5)	0.001
Multivariate logistic regression analysis			
Spontaneous	139	130	6.53 (2.37-18.91)
NNK induced	139	130	10.10 (4.67-21.87)

*Adjusted by age, gender, history of alcohol use, number of years smoked, and number of cigarettes smoked per day.

†P's are derived from the Pearson's χ^2 test and are two sided.

significantly higher in the cases than in the controls (mean \pm SE, 0.28 ± 0.04 and 0.05 ± 0.02 , respectively; $P < 0.001$). No substantial differences were detected when the frequencies of micronuclei, nucleoplasmic bridges, and nuclear buds were stratified by gender, age, family history of cancer, number of years smoked, number of cigarettes per day, tumor histology, or disease stage. When the spontaneous micronuclei data were analyzed as a continuous variable, using multivariate logistic regression, there was a 2.06-fold

increase in lung cancer risk (95% CI, 1.60-2.65) for each 1-unit increase in micronucleus frequency. Similarly, when spontaneous nucleoplasmic bridges were analyzed as a continuous variable, there was a 29.05-fold increase in lung cancer risk (95% CI, 7.48-112.80) for each 1-unit increase in nucleoplasmic bridges. For the nuclear buds, there was a 6.5-fold increase in lung cancer risk (95% CI, 2.37-18.91) for each 1-unit increase in spontaneous bud frequency (Table 3).

Frequencies of NNK-induced cytogenetic endpoints. Data on NNK-induced micronuclei, nucleoplasmic bridge, and nuclear bud frequencies by age, gender, and smoking status are also summarized in Table 2. Table 3 shows that substantially more cases had ≥ 5 NNK-induced micronuclei per 1,000 binucleated cells than controls (40% versus 6%); conversely, far fewer cases than controls had only 1 or 2 NNK-induced micronuclei (4% versus 49%; $P < 0.001$; Fig. 1A). The differences were even more pronounced for spontaneous and NNK-induced nucleoplasmic bridges. The mean number of NNK-induced micronuclei \pm SE was significantly higher in cases (4.32 ± 0.10) than in controls (2.62 ± 0.10 ; $P < 0.001$). As reported in Table 3, ~89% of the case patients had ≥ 6 NNK-induced nucleoplasmic bridges compared with none of the control subjects. Conversely, 65% of the control subjects had 0 to 2 NNK-induced nucleoplasmic bridges compared with none of the case patients ($P < 0.001$; Fig. 1B). The number of NNK-induced nucleoplasmic bridges was also significantly higher in cases (mean \pm SE, 8.12 ± 0.19) than in controls (mean \pm SE, 2.38 ± 0.09 ; $P < 0.001$).

There were no substantial differences when the frequencies of NNK-induced micronuclei and nucleoplasmic bridges were stratified by gender, age, family history of cancer, number of years smoked, number of cigarettes per day, tumor histology, or disease stage. When the NNK-induced micronuclei data were analyzed as a continuous variable, there was a 2.32-fold increase in lung cancer risk (95% CI, 2.32-4.80) for each 1-unit increase in NNK-induced micronuclei. Similarly, NNK-induced nucleoplasmic bridges showed a 45.52-fold increase in lung cancer risk (95% CI, 4.48-422.17) for each 1-unit increase in frequency. With regard to bud distribution, 23% of the cases had ≥ 2 NNK-induced buds compared with ~2% of controls: 87% of the controls had no NNK-induced buds compared with 35% of the case patients ($P < 0.001$; Fig. 1C). The number of NNK-induced buds was significantly higher in cases than in controls (mean \pm SE, 1.07 ± 0.09 and 0.12 ± 0.03 , respectively; $P < 0.001$). When the nuclear bud frequency was analyzed as a continuous variable, there was a 10.1-fold increase in lung cancer risk (95% CI, 4.67-21.87) for each 1-unit increase in NNK-induced buds. Similar patterns of difference between cases and controls were observed for micronuclei, nucleoplasmic bridges, and nuclear buds within subgroups of subjects stratified by gender, age, family history of cancer, number of years smoked, number of cigarettes per day, tumor histology, and disease stage (Table 3).

To ensure quality control, 20% of the slides were randomly selected for blind rescoring. Agreement between the original data and the rescored data was measured using the Cohen's κ statistical test. A statistically significant value of $P < 0.001$ was obtained for both spontaneous and NNK-induced variables, indicating that the agreement between the original and the rescored data was not attributable to random chance.

CBMN assay results as a predictor of case-control status. Using the 75 percentile of the controls as a cutoff, the sensitivity of the CBMN assay was 96.4%, 100%, and 100% for the micronuclei,

nucleoplasmic bridges, and nuclear buds, respectively. The specificity of the assay was 93.0%, 100%, and 100% for the micronuclei, nucleoplasmic bridges, and nuclear buds, respectively. The probabilities that a study subject was a case based on various cut points for the numbers of micronuclei, nucleoplasmic bridges, and nuclear buds were calculated (Table 4). The numbers of micronuclei, nucleoplasmic bridges, and nuclear buds were defined by percentile cut points in the control data. The probability of being a case increased as the percentile cut points increased for high numbers of micronuclei, nucleoplasmic bridges, or nuclear buds. The numbers of spontaneous and NNK-induced micronuclei showed no difference in terms of predictive capacity at the 90th percentile. The numbers of spontaneous and NNK-induced nucleoplasmic bridges showed a slight difference in terms of predictive capacity at the 90th percentile, with the number of induced nucleoplasmic bridges having a better predictive capacity than that of spontaneous nucleoplasmic bridges. The number of NNK-induced nuclear buds showed the highest predictive capacity of the three end points at and above the 85th percentile. On combining all three end points and by using the 75 percentile of the controls as a cutoff, the CBMN assay sensitivity for detecting NNK-induced damage was 96.4%, with 80.8% specificity and 84.3% positive predictive value.

Discussion

In the current study, we tested the sensitivity of the study subjects' lymphocytes to the tobacco-specific nitrosamine NNK, because it represents an important class of carcinogens known to be associated with the development of lung cancer, particularly adenocarcinoma, which is now the leading lung cancer histologic subtype in the United States, having surpassed squamous cell carcinoma (17). Our results show that cases and controls had differential sensitivity to the genotoxic effects of NNK. The lymphocytes from patients with lung cancer were significantly more sensitive to NNK, with 1.6-, 3.4-, and 8.9-fold increases in micronucleus, nucleoplasmic bridge, and nuclear bud frequencies, respectively, over controls. The results of this analysis also show that NNK-induced cytogenetic damage (expressed in terms of micronucleus, nucleoplasmic bridge, and nuclear bud frequencies) seems to be a highly sensitive predictor of lung cancer status.

Tobacco smoke contains an array of potent carcinogens, including polycyclic aromatic hydrocarbons, aromatic amines, and *N*-nitrosamines. Among the polycyclic aromatic hydrocarbons, benzo[*a*]pyrene has been the most extensively studied, and our research to date has focused largely on this carcinogen. Benzo[*a*]pyrene is an effective pulmonary carcinogen, inducing

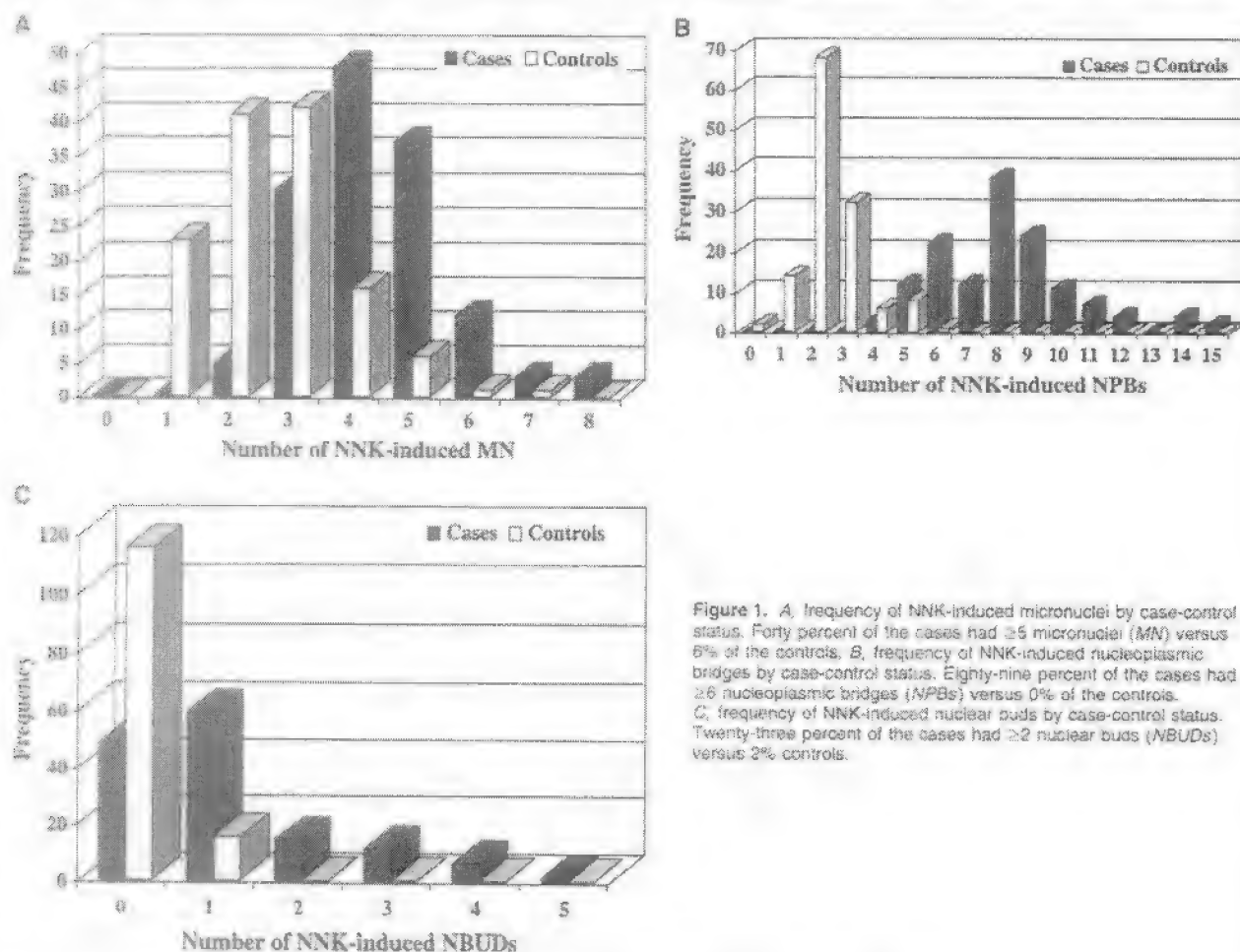


Figure 1. A, frequency of NNK-induced micronuclei by case-control status. Forty percent of the cases had ≥ 5 micronuclei (MN) versus 6% of the controls. B, frequency of NNK-induced nucleoplasmic bridges by case-control status. Eighty-nine percent of the cases had ≥ 6 nucleoplasmic bridges (NPBs) versus 0% of the controls. C, frequency of NNK-induced nuclear buds by case-control status. Twenty-three percent of the cases had ≥ 2 nuclear buds (NBUDs) versus 2% controls.

Table 4. Probability of being a case based on various percentile cut points for the numbers of micronuclei, nucleoplasmic bridges, and nuclear buds in the controls

Percentile of controls	Spontaneous			NNK induced			Spontaneous and NNK induced		
	Micronuclei	Nucleoplasmic bridges	Nuclear buds	Micronuclei	Nucleoplasmic bridges	Nuclear buds	Micronuclei	Nucleoplasmic bridges	Nuclear buds
25	70.1	72.8	86.0	67.0	75.1	85.8	85.6	84.3	82.4
50	70.1	72.8	86.0	67.0	75.1	85.8	85.6	84.3	82.4
75	79.1	72.8	86.0	81.3	75.1	100.0	85.6	89.7	100.0
90	81.3	88.5	86.0	81.3	90.8	100.0	95.6	96.3	100.0
95	81.3	88.5	86.0	87.5	94.4	100.0	95.6	98.2	100.0

predominantly squamous cell carcinoma on intratracheal instillation into rats and hamsters. Tobacco-specific nitrosamines are found in high concentrations in mainstream smoke (28). The most potent carcinogenic member of this group, as shown in experimental animals, is NNK (29). NNK induces lung adenocarcinoma independent of route of administration and in both susceptible and resistant strains of mice (30). The estimated NNK dose of lifetime smokers (2 packs daily for 40 years) is 1.6 mg NNK/kg body weight (31), close to the lowest dose shown to induce lung tumors in rats (1.8 mg/kg ref. 32). The total level of NNK in mainstream smoke is 3 to 15 times that of benzo[a]pyrene (33). Gender differences and DNA repair allelic variants have been reported to modulate the effect of NNK-induced genotoxic damage using the conventional chromosome aberration assay (24, 25) or fluorescence *in situ* hybridization assay using chromosome-specific probes in healthy smokers and nonsmoker controls (26). In addition, NNK was shown to be a potent mutagen using both the Ames *Salmonella* assay and the micronucleus test in Swiss mice (34).

The CBMN assay is a genotoxicity assay that provides simultaneous information on a variety of chromosomal damage endpoints that reflect chromosomal breakage, chromosome rearrangements, and gene amplification. In the current study, the frequencies of micronuclei, nucleoplasmic bridges, and nuclear buds were significantly higher in the lung cancer patients than in controls. Cheng et al. reported similar results after evaluating the micronucleus frequency in 32 patients with lung cancer and 55 controls (35). The significantly higher spontaneous micronuclei levels observed in the cases suggest a higher background level of genetic instability in the cancer patients. The effect of smoking on micronucleus frequency in peripheral blood lymphocytes has not been consistent across studies, which generally have been small and not properly designed to detect the effect of smoking as the main outcome measure (36–38). However, a pooled reanalysis of 14 databases (5,710 subjects, of which 1,409 were current smokers) from the IHMN Project revealed that micronucleus frequency was not influenced by the number of cigarettes smoked per day among subjects occupationally exposed to genotoxic agents, whereas a U-shaped curve was observed for nonexposed smokers, with a significant increase of micronucleus frequency in individuals smoking ≥30 cigarettes per day (frequency ratio, 1.59; 95% CI, 1.35–1.88; ref. 39). Our results showed no significant association between micronucleus frequency and age, gender, or smoking status, which is in agreement with the results reported by Cheng et al. (35). The current study is, to our knowledge, the first to report a significantly higher frequency of spontaneous nucleoplasmic

bridges and nuclear buds in a lung cancer case-control study, thus supporting the hypothesis of breakage-fusion-bridge cycle mechanism of hypermutation during carcinogenesis (reviewed in refs. 2, 13). Gisselsson et al. (40) reported that abnormal nuclear morphology (associated with nucleoplasmic bridges, micronuclei, and nuclear buds) is indicative of significant genomic instability within cells and is a common feature of a wide variety of cancers. An increase in the frequency of these chromosomal damage end points in a surrogate tissue, such as peripheral blood lymphocytes, would imply constitutional sensitivity to genetic damage.

Several epidemiologic studies employing a variety of measures of DNA repair capacity have been done to compare cancer patients and healthy control subjects and thereby assess the role of repair capacity in cancer risk (19). Using a variety of *in vitro* assays, we have shown previously (41–45) that sensitivity to mutagens varies widely between subjects with and without cancer and that this variation translates into interindividual variability in susceptibility to *in vitro* carcinogenic challenge. The mutagen sensitivity assay measures indirectly an individual's DNA repair capacity from cellular damage remaining after an *in vitro* mutagenic exposure and subsequent recovery. This assay, developed by Hsu et al. (46), reflects general and nonspecific impairment of the DNA repair machinery and host genomic stability.

Our current study is, to our knowledge, the first to validate the use of the CBMN assay, with NNK as the challenge mutagen, in a case-control study by testing the sensitivity of this genomic instability biomarker as a predictor of lung cancer risk. Table 4 shows the predictive probabilities for being a case based on various cutpoints for the numbers of spontaneous and induced micronuclei, nucleoplasmic bridges, and nuclear buds, alone and in combination, as defined by the frequency distribution in control subjects. The probability of being a case increased as the percentile cutpoints increased for all cytogenetic end points and the highest probabilities were observed when spontaneous and NNK-induced cytogenetic events were combined. The case-control differences were so striking that we considered, but rejected, alternative explanations. All the cases were enrolled at diagnosis and before initiating treatment; the assays were done blindly and in batches. We rescored randomly selected samples and obtained high levels of reliability. Further, the values did not differ according to smoking duration or intensity and especially not disease stage (lessening the likelihood that this is a tumor marker rather than a marker of risk).

This assay has been used to study susceptibility to other mutagenic agents. Scott et al. (47) showed that individuals who developed breast cancer and their relatives were more sensitive than controls to the DNA-damaging effect of ionizing radiation as

than by micronucleus frequency. This sensitivity was observed in 10 of 11 cases of BRCA1 mutation carriers and was indicative of a defect in double-strand break repair (48), thus suggesting that this assay is useful not only as a marker of DNA damage but also as a means of measuring the DNA repair phenotype. Umegaki and Fenech (11) recently validated the use of nucleoplasmic bridges as a biomarker of DNA damage in a human B lymphoblastoid cell line (WIL2-NS). Nucleoplasmic bridge frequency in binucleated cells increased up to 20-fold in the WIL2-NS cells relative to control cells in response to agents known to induce DNA strand breaks; the effects were found to be dose dependent. Crott et al. (49) recently reported that the frequency of nucleoplasmic bridges and nuclear buds correlated significantly and negatively with folic acid concentrations, suggesting that these chromosomal end points may be induced by folic acid deficiency. In addition, Kimura et al. (50) showed a significant effect of methylenetetrahydrofolate reductase C677T polymorphism and folic acid concentration on micronuclei, nucleoplasmic bridges, and nuclear buds in human lymphocytes. Recently, our group reported that polymorphisms in genes involved in folate metabolism were associated with lung cancer risk, an effect that may be modulated by dietary nutrient intake (51). We plan on genotyping all of the study subjects in our current study to determine the effect of genetic polymorphisms in the folate pathway on modulating the frequency of the measured

endpoints. In addition, one of the advantages of the CBMN assay is the capability of comprehensively assessing DNA damage through measuring the frequency of apoptosis, necrosis, and number of micronuclei in mononucleated cells. Such variables are available for all the study subjects included in our study and we plan to report our findings as soon as the data analysis is complete.

In summary, our study shows differential sensitivity of peripheral blood lymphocytes from lung cancer patients and healthy controls to NNK-induced genetic damage. The data provide convincing evidence that the CBMN assay is a robust test for detection of this sensitivity and yields results that are a good predictor of lung cancer risk. The simplicity, rapidity, and sensitivity of the CBMN test make it a valuable tool for screening and possibly for prioritizing potential cases for early detection of the disease. This assay seems to give results that yield more accurate predictions than other phenotypic assays also undergoing assessment in this population of lung cancer cases and controls.

Acknowledgments

Received 1/26/2006; revised 3/30/2006; accepted 4/18/2006.

Grant support: National Cancer Institute grants CA55769, CA98549, CA70607, DMD17-02-10706, FAMR, and NIGMS ES07784.

The costs of publication of this article were defrayed in part by the payment of page charges. This article must therefore be hereby marked advertisement in accordance with 18 U.S.C. Section 1734 solely to indicate this fact.

References

1. Hirsch FR, Viscusi JR, Nolinski J, Zachariae M, Miller S. Cancer developments in the treatment of lung cancer. *Drug Ther Bull* 2002;39:581-5.
2. Fenech M. Chromosomal biomarkers of genomic instability relevant to cancer. *Drug Discov Today* 2002;7:1129-37.
3. Salmon I, Bureau J, Gaddard AB. Chromosome aberrations and cancer. *Cancer* 1991;284:153-60.
4. Hagmar L, Bonassi S, Stromberg U, et al. Chromosomal aberrations in lymphocytes predict human cancer: a report from the European Study Group on Chromosomal Biomarkers and Health (ESCH). *Cancer Res* 2002;62:417-21.
5. Liu SH, Ling JC, Chen YH, et al. Increased chromosome-type chromosome aberration frequencies as biomarkers of cancer risk: a blackfoot endemic area. *Cancer Res* 1999;59:4941-4.
6. Bonassi S, Hagmar L, Stromberg U, et al. Chromosomal aberrations in lymphocytes predict human cancer independently in response to carcinogens. European Study Group on Chromosomal Biomarkers and Health. *Cancer Res* 2004;64:19-23.
7. Bonassi S, Zujewski A, Norppa H, Hagmar L. Chromosomal aberrations and risk of cancer in humans: an epidemiologic perspective. *Cytogenet Genome Res* 2004;134:89-93.
8. Armstrong J, Lavin K, Rossner P, et al. Risk of cancer in an occupationally exposed cohort with increased level of chromosomal aberrations. *Environ Health Perspect* 1991;93:1-5.
9. Tucker JT, Poppe M. Chromosome aberrations, micronuclei, aneuploidy, sister chromatid exchanges, and cancer risk assessment. *Mutat Res* 1996;365:177-90.
10. Fenech M. The *in vitro* micronucleus technique. *Mutat Res* 2002;513:87-95.
11. Umegaki K, Fenech M. Cytokinesis-block micronucleus assay in WIL2-NS cells: a sensitive system to detect chromosomal damage induced by reactive oxygen species and activated human neutrophils. *Mutagenesis* 1999;14:281-5.
12. Stewenius Y, Gorunova L, Jonson T, et al. Structural and numerical chromosome changes in colon cancer develop through telomere-mediated anaphase bridges, not through mitotic multipolarity. *Proc Natl Acad Sci U S A* 2005;102:5541-5.
13. Fenech M, Crott JW. Micronuclei, nucleoplasmic bridges and nuclear buds induced in folic acid deficient human lymphocytes—evidence for breakage-fusion-bridge cycles in the cytokinesis-block micronucleus assay. *Mutat Res* 2002;504:131-6.
14. Fenech M. Biomarkers of genetic damage for cancer epidemiology. *Toxicology* 2002;181:2411-6.
15. Serrano-Garcia I, Montero-Montoya R. Micronuclei and chromatin buds are the result of related genotoxic events. *Environ Mol Mutagen* 2001;28:38-45.
16. Spitz MR, Wei Q, Dong Q, Amos CI, Wu X. Genetic susceptibility to lung cancer: the role of DNA damage and repair. *Cancer Epidemiol Biomarkers Prev* 2003;12:689-98.
17. Tinnin MJ, Lally CA, Flannery JT, Jr. Cigarette smoking and changes in the histopathology of lung cancer. *J Natl Cancer Inst* 1997;89:1380-6.
18. Wertheim AB, Corvase E. Oxygen radicals potentiate the genetic toxicity of tobacco-specific nitrosamines. *Clin Genet* 1992;44:88-91.
19. Berwick M, Vines P. Markers of DNA repair and susceptibility to cancer in humans: an epidemiologic review. *J Natl Cancer Inst* 2000;92:874-97.
20. Hecht SJ. Human urinary carcinogen metabolites: biomarkers for investigating tobacco and cancer. *Carcinogenesis* 2002;23:907-22.
21. Cloutier JF, Drouin R, Weinfeld M, O'Connor TR, Costantini A. Characterization and mapping of DNA damage induced by reactive metabolites of 4-(methylnitrosamino)-1-(3-pyridyl)-1-butanone (NNK) at nucleotide resolution in human genomic DNA. *J Mol Biol* 2001;313:339-57.
22. Fenech M, Morley AA. Measurement of micronuclei in lymphocytes. *Mutat Res* 1985;147:29-36.
23. Abdel-Rahman SZ, El Zein RA. The ²⁹⁹Gln polymorphism in the DNA repair gene XRCC1 modulates the genotoxic response induced in human lymphocytes by the tobacco-specific nitrosamine NNK. *Cancer Lett* 2000;159:63-71.
24. Hib CE, Affatato AA, Wolfe KJ, et al. Gender differences in genetic damage induced by the tobacco-specific nitrosamine NNK and the influence on the ²⁹⁹Gln polymorphism in the XRCC1 gene. *Environ Mol Mutagen* 2005;42:1-9.
25. Affatato AA, Wolfe KJ, Lopez MS, Hallberg C, Amannhusser MM, Abdel-Rahman SZ. Effect of XPD/ERCC2 polymorphisms on chromosome aberration frequencies in smokers and on sensitivity to the mutagenic tobacco-specific nitrosamine NNK. *Environ Mol Mutagen* 2004;44:65-73.
26. Abdel-Rahman SZ, Salama SA, Au WW, Hamada FA. Role of polymorphic CYP2E1 and CYP2D6 genes in NNK-induced chromosome aberrations in cultured human lymphocytes. *Pharmacogenetics* 2000;10:239-49.
27. Fenech M, Chang WP, Kirsch-Volders M, Holland N, Bonassi S, Zeiger E. HUMN Project: detailed description of the scoring criteria for the cytokinesis-block micronucleus assay using isolated human lymphocyte cultures. *Mutat Res* 2003;534:65-75.
28. Brunnemann KD. Determination of nicotine and minor tobacco alkaloids in indoor air by absorption and gas chromatography. *IARC Sci Publ* 1993;109:175-80.
29. Spiegelhalder B, Bartsch H. Tobacco-specific nitrosamines. *Eur J Cancer Prev* 1996;5:33-8.
30. Hecht SJ, Hoffmann D. The relevance of tobacco-specific nitrosamines to human cancer. *Cancer Surv* 1989;27:3-94.
31. Hecht SJ, Hoffmann D. Tobacco-specific nitrosamines, and important group of carcinogens in tobacco and tobacco smoke. *Carcinogenesis* 1988;9:875-84.
32. Adams JD, O'Mara-Adams KJ, Hoffmann D. Toxic and carcinogenic agents in unadulterated mainstream smoke and sidestream smoke of different types of cigarettes. *Carcinogenesis* 1987;8:729-31.
33. Hecht SJ. Tobacco smoke carcinogens and lung cancer. *J Natl Cancer Inst* 1998;191:1194-210.
34. Padma PR, Antonkar AJ, Blide SV. Mutagenic and cytogenetic studies of *N*-nitrosanornicotine and 4-(methylnitrosamino)-1-(3-pyridyl)-1-butanone. *Cancer Lett* 1989;46:173-80.
35. Cheng TJ, Christiani DC, Xu X, Wain JC, Wiencke JH, Kelsey KT. Increased micronucleus frequency in lymphocytes from smokers with lung cancer. *Mutat Res* 1996;349:43-50.

40. Fenech M, Lippman D, Kirch-Nielsen M, Stromberg U, Cornfield S, Tucker JD. Human population studies with cytogenetic biomarkers: review of the literature and future perspectives. *Environ Mol Mutagen* 2005;35:232-40.
41. Fenech M. The cytokinesis-block micronucleus technique and its application to genotoxicity studies in human populations. *Environ Health Perspect* 1993;101:363-71.
42. de Lorenzo U, Lee-Mae MB, Lager M, Garraud H, Botta A, Fenech M. The micronucleus assay in human lymphocytes: screening for inter-individual variability and application to bio-monitoring. *Carcinogenesis* 1994;15:117-21.
43. Fenech M, Sord M, Lippman D, et al. Effect of smoking status on the frequency of micronuclei in human lymphocytes: results from the Human MicroNucleus project. *Mutat Res* 2003;543:153-65.
44. Cornfield S, Lippman D, Haggard M, et al. Abnormal nuclear shape in solid tumors reflects mitotic instability. *Lab Invest* 2003;83:199-206.
45. El Zet R, Bondy ML, Wang LE, et al. Risk assessment for developing gliomas: a comparison of two cytogenetic approaches. *Mutat Res* 2001;490:35-44.
46. Wei Q, Gu J, Cheng L, et al. Benzo(a)pyrene diol-epoxide-induced chromosomal aberrations and risk of lung cancer. *Cancer Res* 1996;56:3975-9.
47. Spitz MR, Wei Q, Li G, Wu X. Genetic susceptibility to tobacco carcinogenesis. *Cancer Invest* 1999;17:645-59.
48. Wu X, Lippman SM, Lee JJ. Chromosome instability in lymphocytes: a potential indicator of predisposition to oral premalignant lesions. *Cancer Res* 2002;62:2812-8.
49. Schanath MB, Spitz MR, Grossman HB, et al. Genetic instability in bladder cancer assessed by the comet assay. *J Natl Cancer Inst* 2003;95:540-7.
50. Hsu TC, Johnston DA, Cherry LM, et al. Sensitivity to genotoxic effects of bleomycin in humans: possible relationship to environmental carcinogenesis. *Int J Cancer* 1985;33:403-9.
51. Neom D, Barber JB, Levine RL, Burrill W, Roberts SA. Radiation-induced micronucleus induction in lymphocytes identifies a high frequency of radio-sensitive cases among breast cancer patients: a test for predisposition? *Br J Cancer* 1998;77:614-20.
52. Rothfuss A, Schatz P, Bochum S, et al. Induced micronucleus frequencies in peripheral lymphocytes as a screening test for carriers of a BRCA1 mutation in breast cancer families. *Cancer Res* 2000;60:390-4.
53. Crott JW, Mashima ST, Ames BN, Fenech M. The effect of folic acid deficiency and MTHFR C677T polymorphism on chromosome damage in human lymphocytes *in vitro*. *Cancer Epidemiol Biomarkers Prev* 2001;10:1089-96.
54. Kimura M, Umegaki K, Higuchi M, Thomas P, Fenech M. Methylenetetrahydrofolate reductase C677T polymorphism, folic acid and riboflavin are important determinants of genome stability in cultured human lymphocytes. *J Nutr* 2004;134:48-56.
55. Shi Q, Zhang Z, Li G, et al. Polymorphisms of methionine synthase and methionine synthase reductase and risk of lung cancer: a case-control analysis. *Pharmacogenomics* 2005;15:547-55.

Liposomal vector mediated delivery of the 3p *FUS1* gene demonstrates potent antitumor activity against human lung cancer *in vivo*

Isao Ito,¹ Lin Ji,¹ Fumihiko Tanaka,¹ Yuji Saito,¹ Began Gopalan,¹ Cynthia D Branch,¹ Kai Xu,¹ E Neely Atkinson,² Benjamin N Bekele,² L Clifton Stephens,³ John D Minna,⁴ Jack A Roth,¹ and Rajagopal Ramesh¹

¹Section of Thoracic Molecular Oncology, Department of Thoracic and Cardiovascular Surgery, The University of Texas MD Anderson Cancer Center, Houston, Texas 77030, USA; ²Department of Biostatistics, The University of Texas MD Anderson Cancer Center, Houston, Texas 77030, USA; ³Department of Veterinary Medicine and Surgery, The University of Texas MD Anderson Cancer Center, Houston, Texas 77030, USA, and ⁴Department of Internal Medicine and Pharmacology, Hamon Center for Therapeutic Oncology Research, The University of Texas Southwestern Medical Center, Dallas, Texas 75390, USA.

Lung cancer is one of the leading causes of death in the world. The underlying cause for lung cancer has been attributed to various factors that include alteration and mutation in the tumor suppressor genes. Restoration of normal function of the tumor suppressor gene is a potential therapeutic strategy. Recent studies have identified a group of candidate tumor suppressor genes on human chromosome 3p21.3 that are frequently deleted in human lung and breast cancers. Among the various genes identified in the 3p21.3 region, we tested the antitumor activity of the *FUS1* gene in two human non-small-cell lung cancer (NSCLC) xenografts *in vivo*. Intratumoral administration of *FUS1* gene complexed to DOTAP:cholesterol (DOTAP:Chol) liposome into subcutaneous H1299 and A549 lung tumor xenograft resulted in significant ($P=.02$) inhibition of tumor growth. Furthermore, intravenous injections of DOTAP:Chol-*FUS1* complex into mice bearing experimental A549 lung metastasis demonstrated significant ($P=.001$) decrease in the number of metastatic tumor nodules. Finally, lung tumor-bearing animals when treated with DOTAP:Chol-*FUS1* complex demonstrate prolonged survival (median survival time: 80 days, $P=.01$) compared to control animals. This result demonstrates the potent tumor suppressive activity of the *FUS1* gene and is a promising therapeutic agent for treatment of primary and disseminated human lung cancer.

Cancer Gene Therapy (2004) 11, 733–739. doi:10.1038/sj.cgt.7700756

Published online 15 October 2004

Keywords: *FUS1*; lung cancer; liposome; tumor suppressor

Lung cancer is the most common malignancy and leading cause of death in the Western world.¹ Current treatment strategies include surgery, chemotherapy, radiation, or a combination of therapies.^{2–5} Despite significant advances made during the past several decades in the treatment of lung cancer, the overall 5-year survival rate is poor. Therefore, identification of new therapeutic targets and treatment strategies are essential for successful control of the development and progress of lung cancer. Although many genes that are frequently altered in lung cancer have been identified in the past, most of these changes occur at later stages of cancer

progression. Thus, identification of gene(s) that are altered in the early preneoplastic stages and restoration of these gene functions may prevent tumor progression. Therefore, exhaustive searches for the identification of genes that are altered early in the lung carcinogenesis pathway are underway by several investigators. Recent studies have demonstrated allelic loss of the 3p chromosome, in particular 3p21.3 in lung and breast cancers.^{6–10} Several genes identified in the 3p region have been well characterized with a few of them demonstrating tumor suppressive activities. More recently, frequent deletion of a 630-kb region on chromosome 3p21.3 have been demonstrated in lung cancers.¹¹ Subsequent studies narrowed a defined 120-kb subregion that is lost in 80% of primary lung cancers.¹² Furthermore, this region has been identified to be lost in the early preneoplastic lesions suggesting a potential role for regulating cell homeostasis. Located on this 120-kb region are nine putative tumor suppressor genes that include the *FUS1* gene.¹¹ Although

Received February 17, 2004

Address correspondence and reprint requests to: Dr Rajagopal Ramesh, MD, Section of Thoracic Molecular Oncology, Department of Thoracic and Cardiovascular Surgery, The University of Texas MD Anderson Cancer Center, 1515 Holcombe, Unit 445, Houston, TX 77030, USA. E-mail: rramesh@mdanderson.org

the exact function of the *FUS1* gene is not known, recent studies have reported *FUS1* to be a tumor suppressor gene.^{11,14} More recently, myristoylation of the *FUS1* protein was shown as a requirement for the tumor-suppressor function.¹⁵ Based on these reports, we tested the tumor suppressor activity of the *FUS1* gene in human non-small-cell lung cancers using a nonviral gene therapeutic approach.

Gene delivery vector utilized in the present study was a cationic DOTAP:cholesterol (DOTAP:Chol) liposome that has been shown to deliver genes effectively to the lungs when administered intravenously.¹⁶ Using DOTAP:Chol liposome, we have previously demonstrated effective gene delivery of tumor suppressor genes to subcutaneous and disseminated lung metastasis resulted in a therapeutic efficacy.^{17,18} In addition, systemic injection of DOTAP:Chol-DNA complex demonstrated no significant organ-related toxicity. These results demonstrated DOTAP:Chol liposome to be an ideal vector for systemic delivery of therapeutic genes.

In the present study, we demonstrate intratumoral delivery of *FUS1* plasmid DNA complexed to DOTAP:Chol liposome resulted in suppression of tumor growth. Furthermore, systemic delivery of the liposome-DNA complex resulted in inhibition of experimental lung metastasis and prolonged animal survival. This study demonstrates the potent tumor suppressor activity of the *FUS1* and indicates it to be a therapeutic gene for the treatment of primary and disseminated lung cancer.

Material and methods

Materials

DOTAP and cholesterol were purchased from Avanti Polar Lipids (Albaster, AL). RPMI-1640 medium, Ham's F12 medium and fetal bovine serum (FBS) were purchased from GIBCO-BRL-Life Technologies (New York, NY). Rabbit anti-FUS1 polyclonal antibody was developed against a synthetic oligopeptide (gasgskarglw-p-fusaa) derived from the N-terminal amino-acid sequence of the FUS1 protein (Bethyl Laboratories, Montgomery, TX) and used for immunohistochemical analysis and Western blotting.¹⁵

Cell lines and animals

Human non-small-cell lung carcinoma (NSCLC) cell line H1299 was a gift from Drs Adi Gazdar and John D Minna (UT Southwestern Medical Center, Dallas, TX). A549 cells were purchased from American Type Culture Collection (Manassas, VA). H1299 and A549 cells were maintained in RPMI-1640 and Ham's F12 medium, respectively, that were supplemented with 10% FBS, 1% glutamine and antibiotics. Cells were regularly passaged and tested for presence of mycoplasma. Female BALB/c nude (nu/nu) mice (Charles River Laboratories, Wilmington, MA), 4–6 weeks old, used in the study were maintained in a pathogen-free environment and handled

according to the institutional guidelines established for animal care and use.

Cloning and purification of plasmids

FUS1 cDNA and CAT cDNA was subcloned into the multiple cloning site of pVAX plasmid DNA vector containing kanamycin resistance marker (Invitrogen Inc, Carlsbad, CA). Additional vector developed in the laboratory included the pLJ143/KGB2/FUS1 plasmid vector that consisted of a CMV minimum promoter with an E1 enhancer at the 3' end, a BGH-poly A signal sequence at the 5' end, kanamycin-resistance gene, and a minimum pMB1 origin of replication (ori) sequence. The presence of the appropriate inserts was confirmed by DNA sequence analysis and by restriction enzyme analysis. The plasmids were subsequently transformed into *Escherichia coli* DH5- α strain (Stratagene, Carlsbad, CA) and were purified as described previously.^{16,17}

Synthesis of liposomes and preparation of DNA:liposome complex

An amount of 20 mM DOTAP:Chol liposome was synthesized and extruded through Whatman Filters (Kent, UK) of decreasing size (1.0, 0.45, 0.2, and 0.1 μ m) as described previously.^{17,18} For preparation of DNA:liposome complexes DOTAP:Chol (20 mM) stock solution and DNA solution diluted in 5% dextrose in water (D5W) were mixed in equal volumes and mixed to give a final concentration of 4 mM DOTAP:Chol–150 μ g DNA in 300 μ l final volume (ratio 1:2.6) as described previously.¹⁷ The DNA:liposome mixture thus prepared was used in all the experiments described in the present study.

Measurement of particle size analysis

Freshly prepared DNA:liposome complexes were analyzed for mean particle size using the N4 particle size analyzer (Coulter, Miami, FL). The average particle size of the DNA:liposome complexes ranged between 375 and 400 nm.

In vitro transfection and transgene expression

Human NSCLC cells (H1299, and A549) were seeded in six-well plates at 5×10^5 cells/well for Western blot analysis and 10^5 cells/well in two-well chamber slides for immunocytochemical analysis. The following day, cells were transfected with DOTAP:Chol-FUS1 complex (2.5 μ g DNA) in serum-free medium for 3 hours. Following transfection, cells were replenished with complete medium and incubated at 37°C. For Western blot analysis, cells were harvested at 24 and 48 hours post transfection and analyzed for FUS1 protein expression. For immunocytochemical analysis, cells were fixed in 1% glutaraldehyde and stained as described previously.¹⁹ FUS1 expression was detected using a polyclonal rabbit anti-human FUS1 polyclonal antibody.

Effect of DOTAP:Chol-FUS1 complex on subcutaneous lung tumor xenograft

Prior to the start of the experiment mice were irradiated (3.5 Gy) using a cesium source to enhance tumor uptake. Briefly, female nu/nu mice were injected with 5×10^6 H1299 cell and A549 cells into the lower right flank. Tumor formation in mice was observed twice or three times weekly. Treatment was initiated when the tumors were 50–100 mm³ in size (day 0). Animals were divided into groups ($n=10$ /group) and treated with FUS1 plasmid DNA, treated with DOTAP:Chol-CAT complex, and treated with DOTAP:Chol-FUS1 complex. Animals were treated daily by intratumoral injections for a total of six doses (50 μ g DNA/dose). Tumors were measured every 2 or 3 days by using calipers. The tumor volume was calculated as described previously.¹⁷ Animals were euthanized by CO₂ inhalation when the tumor had reached 1.5 cm³ in size or was necrotic.

Effect of DOTAP:Chol-FUS1 complex on experimental lung metastasis

To establish lung metastasis, female nu/nu mice were injected intravenously via tail vein with 1×10^6 A549 tumor cells suspended in 200 μ l of sterile PBS. After 6 days, mice were divided into groups ($n=10$ /group) and treated as follows: treated with PBS, treated with plasmid DNA alone, treated with liposome alone, treated with

DOTAP:Chol-CAT complex, and treated with DOTAP:Chol-FUS1 complex. Mice were treated with 10 μ g DNA:liposome complex intravenously (i.v.) via tail vein using a 27-gauge needle daily for a total of six doses. Animals were euthanized by CO₂ inhalation 3-weeks following the last dose. Lungs from each of the mice from the five groups were injected intratracheally with India ink and fixed in Feketes solution. The therapeutic effect of each groups were determined by counting the number of metastatic tumor nodules in each lung under a dissecting microscope without knowledge of the treatment groups. The data were analyzed and interpreted as statistically significant if the *P*-value was <.05 by the Mann-Whitney rank-sum test.

Animal survival experiments

To determine the therapeutic effect of DOTAP:Chol-FUS1 complex on animal survival female nu/nu mice were injected intravenously via tail vein with 1×10^6 A549 tumor cells suspended in 200 μ l of sterile PBS. After 6 days, mice were divided into groups ($n=5$ /group) and treated as follows: treated with PBS, treated with plasmid DNA alone, treated with liposome alone, treated with DOTAP:Chol-CAT complex, and treated with DOTAP:Chol-FUS1 complex. Mice were treated daily by i.v. injections of the liposome:DNA complex (10 μ g DNA) via the tail vein using a 27-gauge needle. Animals received a total of six doses (10 μ g DNA/dose). Animals were

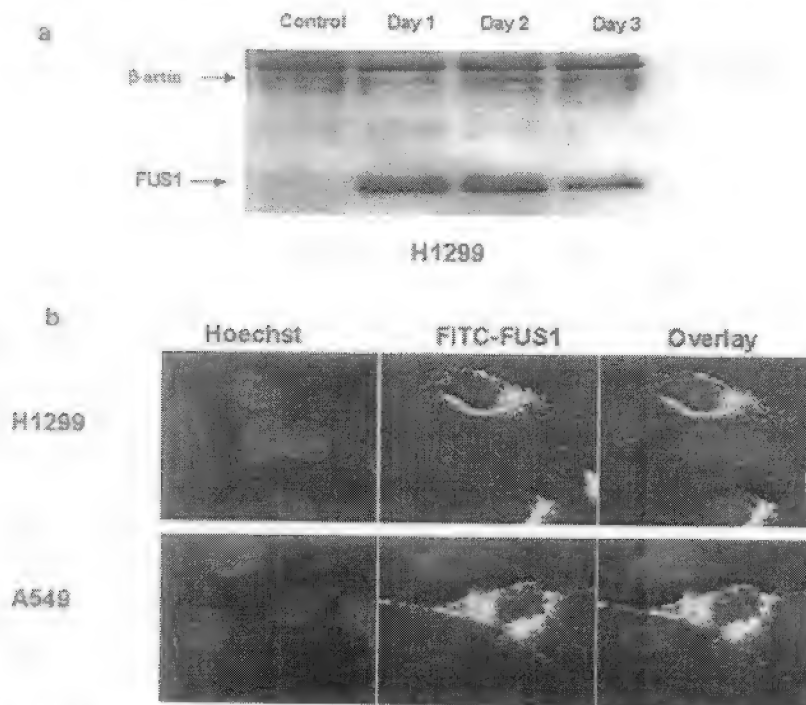


Figure 1 Expression of FUS-1 in lung cancer cells. Human non-small-cell lung cancer cells (H1299) were transfected with DOTAP:Chol-FUS1 complex (2.5 μ g DNA) and analyzed for FUS1 expression using an anti-FUS1 monoclonal antibody. (a) Western blot analysis demonstrated FUS1 expression on days 1, 2 and 3 after transfection. (b) Immunohistochemical analysis revealed cell membrane, cytoplasm, and perinuclear staining for FUS1. Hoechst staining indicates the nucleus of the cell.

monitored daily for morbidity and mortality. Animals that were moribund were euthanized by CO₂ inhalation. The therapeutic effects of the treatments were determined by statistical analysis using the Kaplan-Meier survival estimation and Wilcoxon signed-rank sum tests.

Terminal deoxynucleotidyl transferase (TdT)-mediated dUTP uridine triphosphate nick-end labeling (TUNEL) assay for DNA fragmentation

To determine the fate of tumor cell following treatments, subcutaneous tumor tissues harvested from animals that received various treatments were subjected to TUNEL staining as described previously.¹⁹ Slides were counterstained with 0.4% methyl green. In all the staining procedures, appropriate negative controls were included. Stained tissue sections was observed under microscopy and the number of TUNEL positive cells, an indicator of apoptotic cells, were determined by semiquantitative analysis as described elsewhere.¹⁹

Statistical analysis

The statistical significance of the experimental results was calculated using the Whitney rank-sum test for tumor measurements and lung metastases, and the Wilcoxon log-rank test and Kaplan-Meier survival test for animal survival.

Results

In vitro expression of FUS1 protein

Prior to testing the therapeutic effect of *FUS1* gene *in vivo*, transgene expression of the *FUS1* plasmid DNA complexed to DOTAP:Chol liposome was tested *in vitro*. Transfection of lung tumor cells, H1299 and A549 resulted in detection of FUS1 protein at 24 h and 48 h (Fig 1a). Furthermore, FUS1 protein was localized in the cytoplasm and perinucleus of the tumor cells as demonstrated by immunohistochemical analysis (Fig 1b).

Intratumoral injection of DOTAP:Chol-FUS1 complex suppresses tumor growth

We tested the tumor suppressor function of *FUS1* gene *in vivo* by direct intratumoral injection of DOTAP:Chol-FUS1 complex. Treatment of subcutaneous lung tumor xenograft (H1299, and A549) for a total of six doses with DOTAP:Chol-FUS1 complex resulted in a significant suppression of tumor growth ($P = .005$ for H1299, and $P = .01$ for A549) compared to control animals that were treated with *FUS1* plasmid DNA, and treated with DOTAP:Chol-CAT complex (Fig 2).

The fact that the tumor inhibition was due to *FUS1* protein expression was demonstrated by immunohistochemical analysis. FUS1 protein expression was detected in the subcutaneous tumor tissues primarily localized to the cytoplasm as observed *in vitro* (data not shown). Expression was primarily observed in the tumor cells.

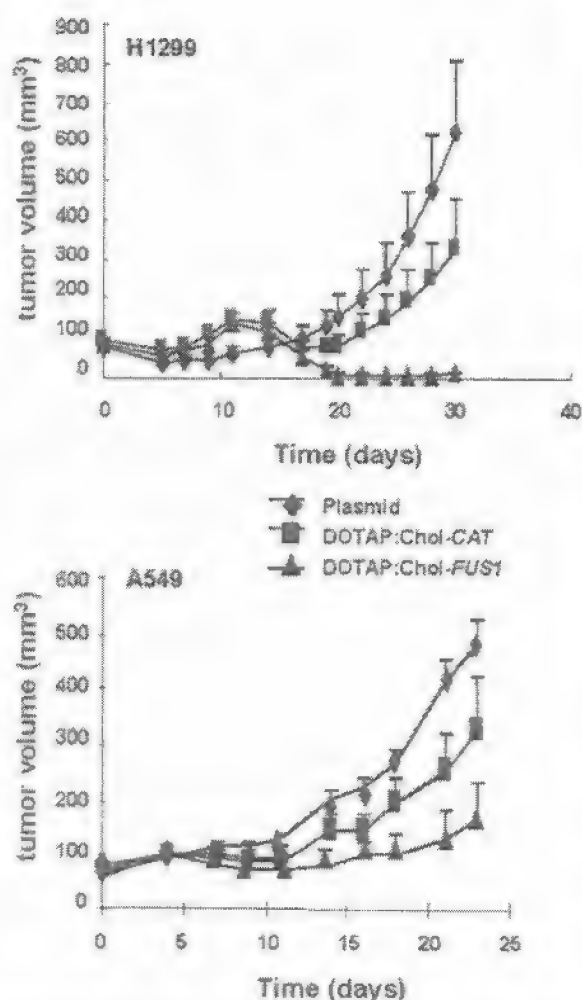


Figure 2 Inhibition of subcutaneous lung tumor xenografts by FUS1. Subcutaneous lung tumor xenografts were established by injecting H1299 and A549 tumor cells (5×10^5) in nude mice. Animals were randomly divided into groups ($n = 10$ /group) and treated with *FUS1* plasmid, treated with DOTAP:Chol-CAT complex, and treated with DOTAP:Chol-FUS1 complex. Animals were treated when tumors were 50–100 mm³ (day 0) daily for a total of six doses (50 µg DNA/dose) and tumor growth monitored. A significant inhibition of tumor growth was observed in both, H1299 ($P = .005$) and A549 ($P = .01$) tumor-bearing mice treated with DOTAP:Chol-FUS1 complex. In contrast, no significant growth inhibition was observed in control animals that were treated with PBS and treated with DOTAP:Chol-CAT complex. Error bars denote standard error.

However, expression in other cells intermixed with tumor cells were also observed. The subtype of cells staining positive for FUS1 in the tumor was not determined. Furthermore, tumors treated with DOTAP:Chol-FUS1 complex underwent significant apoptotic cell death as evidenced by TUNEL staining compared to tumors from those animals that were treated with plasmid DNA or DOTAP:Chol-CAT complex (Fig 3). Induction of apoptotic cell death was observed in both H1299 and A549 tumors.

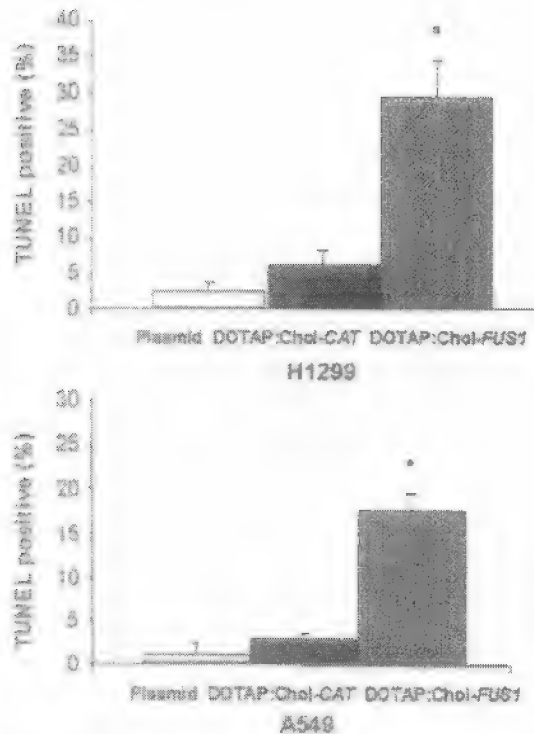


Figure 3 Induction of apoptosis in subcutaneous tumors treated with DOTAP:Chol-FUS1. Subcutaneous lung tumor (H1299 and A549) xenografts that were treated with FUS1 plasmid, treated with DOTAP:Chol-CAT complex, and treated with DOTAP:Chol-FUS1 complex were harvested and subjected to TUNEL staining. Animals were treated DOTAP:Chol-FUS1 complex demonstrated 15–35% TUNEL-positive staining of tumor tissues (33% for H1299 and 18% for A549; $P = .001$). In contrast, no significant growth inhibition was observed in control animals that were treated with PBS and treated with DOTAP:Chol-CAT complex. Error bars denote standard error.

Intravenous injection of DOTAP:Chol-FUS1 complex inhibits experimental lung metastasis

To test the tumor suppressor activity of FUS1 on experimental lung metastases, lung tumors were established by injecting A549 tumor cells via tail vein. Intravenous treatments of these lung tumor bearing animals with DOTAP:Chol-FUS1 complex resulted in a significant inhibition ($P = .001$) of lung metastases compared to control animals that were treated with PBS, treated with FUS1 plasmid DNA, treated with liposome alone, and treated with DOTAP:Chol-CAT complex (Fig 4). Animals treated with DOTAP:Chol-CAT complex demonstrated some tumor inhibition. The ability of DOTAP:Chol-CAT complex treatments to demonstrate some antitumor activity is not surprising and is attributed to nonspecific antitumor activity. However, tumor inhibition was not significant compared to animals treated with PBS, treated with FUS1 plasmid DNA and treated with liposome. These results show that the therapeutic effect observed in lung tumor-bearing animals when treated with DOTAP:Chol-wtFUS1 is specific to wtFUS1.

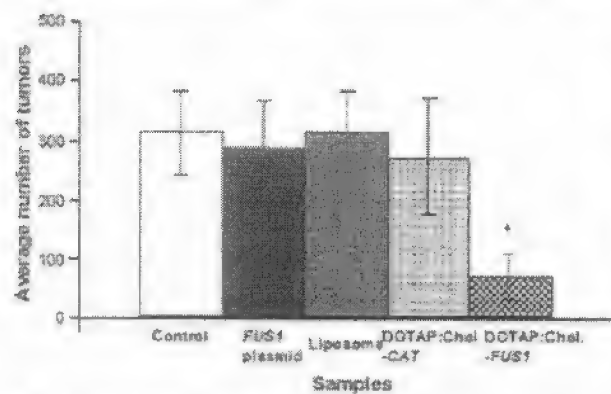


Figure 4 DOTAP:Chol-FUS1 complex inhibits experimental lung metastasis. Experimental lung metastasis was established in nude mice by injecting A549 tumor cells (10^6) via tail vein. After 6 days, animals were divided randomly into groups ($n = 10/\text{group}$) and treated with PBS, treated with plasmid DNA alone ($10 \mu\text{g}$), treated with liposome alone, treated with DOTAP:Chol-CAT complex, and treated with DOTAP:Chol-FUS1 complex. Animals were treated daily for a total of six doses ($10 \mu\text{g}$ DNA/dose) via tail vein. Animals were euthanized 3-weeks after the last treatment; lungs were injected with India ink solution and harvested. Lungs were examined under a stereomicroscope and the number of tumor nodules counted. A significant ($P = .001$) reduction in the number of tumor nodules was observed in animals treated with DOTAP:Chol-FUS1 complex compared to control animals. Error bars denote standard error.

Intravenous treatment of lung tumor-bearing animals with DOTAP:Chol-FUS1 complex prolongs animal survival

We next evaluated the effect of DOTAP:Chol-FUS1 treatments on animal survival. Treatment of experimental A549 lung tumor-bearing animals with DOTAP:Chol-FUS1 complex resulted in a significant ($P = .01$) and prolonged survival (mean survival time = 80 days) (Fig 5). In contrast, no significant survival of animals was observed that were treated with PBS (mean = 47.8), treated with FUS1 plasmid (mean = 51.6), treated with liposome (mean = 47.2), and treated with DOTAP:Chol-CAT complex (mean = 47.8). Furthermore, histopathological analysis of various organs demonstrated no significant treatment-related toxicity.

Discussion

We have previously demonstrated DOTAP:Chol liposome effectively deliver tumor suppressor genes, *p53* and *Fhit*, to lungs and inhibited lung tumor growth.¹⁷ However, recent studies indicate that alterations in the *p53* and *Fhit* gene occur in the later stages of lung cancer development.⁷ Thus, restoration of a gene that is altered early in tumor progression may be a better therapeutic for lung cancer treatment. Recently, identification of nine genes in a narrow 120-kb region on chromosome 3p21.3 has been reported.¹² FUS1 is one among the nine genes located in this region. However, the tumor suppressor

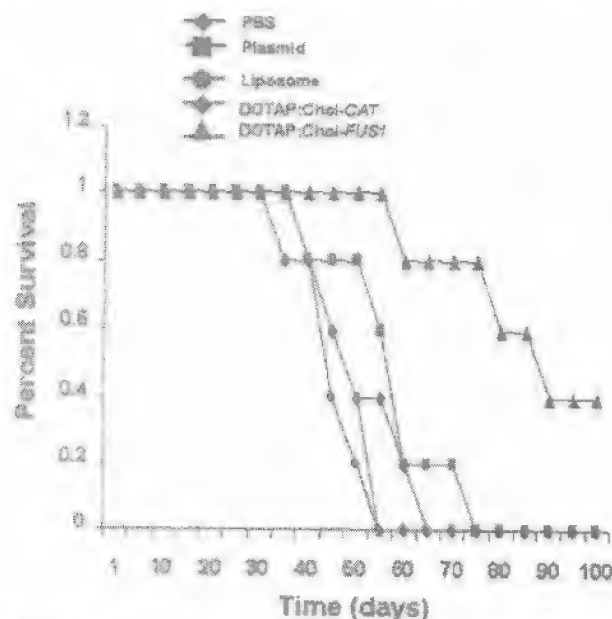


Figure 5 Treatment with DOTAP:Chol-FUS1 complex increases animal survival. Experimental lung metastasis was established in nude mice by injecting A549 tumor cells (10^6) via tail vein. After 6 days, animals were divided randomly into groups ($n = 5/\text{group}$) and treated with PBS, treated with plasmid DNA alone (10 μg), treated with liposome alone, treated with DOTAP:Chol-CAT complex, and treated with DOTAP:Chol-FUS1 complex. Animals were treated daily for a total of six doses (10 μg DNA/dose) via tail vein. Following the last treatment, animals were monitored daily for morbidity and mortality. Survival was estimated by using the Kaplan-Meier and Wilcoxon signed-rank tests. Survival was significantly longer in animals treated with DOTAP:Chol-FUS1 complex (mean survival time: 80 days; $P = 0.01$) compared to animals that were treated with PBS (mean survival time: 47.8 days), treated with plasmid DNA alone (mean survival time: 51.8 days), treated with liposome alone (mean survival time: 47.2 days), and treated with DOTAP:Chol-CAT complex (mean survival time: 47.8 days).

functions of each of the nine genes have not been well studied. In the present study, we therefore tested the tumor suppressor activity of *FUS1* gene in human lung cancer cells.

Treatment of subcutaneous and experimental lung metastasis with *FUS1* gene resulted in significant suppression of tumor growth with induction of apoptosis. The ability of *FUS1* to induce apoptosis and inhibit tumor growth is similar to findings reported by Ji et al.¹⁴ That the observed tumor suppression was due to *FUS1* expression was demonstrated by immunohistochemistry. Although the exact function(s) of *FUS1* gene is not known, localization of the *FUS1* protein to the cell membrane, cytoplasm and perinucleus suggest that it may have role in signal transduction. More recently, myristoylation of *FUS1* protein as a requirement for tumor-suppressive activity was demonstrated.¹⁵ However, further characterization of this gene is essential to elucidate its function.

To further evaluate the effects of systemic delivery of *FUS1* on experimental lung metastasis, lung tumor-

bearing animals were treated with liposome-*FUS1* complex. A significant inhibition of lung metastatic tumor nodules was observed in animals treated with liposome-*FUS1* DNA complex. The tumor inhibitory effect by *FUS1* was comparable to that observed when treated with p53.¹⁷ However, unlike our previous study, we used lower concentrations of plasmid DNA in the present study and still achieved the same therapeutic effect. These results suggest two possibilities, one that *FUS1* may be more potent than p53 and two, use of lower concentrations of plasmid DNA will result in achieving the same therapeutic effect. Preliminary results indicate that *FUS1* is more potent than p53 (data not shown). Supporting this observation is the study by Ji et al.^{14,15} In their study, treatment with Ad-*FUS1* inhibited tumor metastases more effectively than Ad-p53. Use of lower concentrations of plasmid DNA also will minimize the DNA associated inflammatory response resulting in reduced toxicity and therefore be of advantage when used in clinical trials. However, further detailed comparative studies are warranted to justify these observations. The nonspecific antitumor activity observed with the *CAT* DNA is not surprising and is in agreement with previous reports where nonspecific antitumor activity was demonstrated when treated with control plasmid DNA's complexed to liposomal vectors.^{17,20-23} The induction of an inflammatory response following injection of liposome-DNA complex has been shown to mediate the nonspecific activity antitumor activity.^{20,21} However, the antitumor activity observed in animals treated with *wt-FUS1* was significantly higher than in animals treated with *CAT* demonstrating the specificity.

The effect of *FUS1* treatments on animal survival was next evaluated. Treatment with DOTAP:Chol-*FUS1* complex significantly prolonged survival of A549 lung tumor-bearing animals. At the time of writing this report, 40% of the tumor-bearing mice treated with DOTAP:Chol-*FUS1* complex were still alive (125 days) indicating that tumors were either eliminated or their growth delayed. Whatever the reason may be, it is clear that *FUS1* can suppress tumor growth and prolong survival.

Although we have demonstrated *FUS1* has potent tumor suppressive activity, the functions of some of the other genes located in the 120-kb region have not been studied. Ji et al.¹⁴ recently demonstrated antitumor activity for three of the nine genes. Thus, treatment of lung cancer with a combination of these genes may result in a more potent therapeutic effect than that observed with individual genes. Additionally, combination of DOTAP:Chol-*FUS1* treatment with other treatment strategies such as chemotherapy may result in a more effective tumor suppression and is of clinical relevance. These possibilities are currently under investigation in our laboratory.

In conclusion, we have demonstrated the tumor suppressive activity of *FUS1* gene and that intratumoral and systemic delivery of *FUS1* gene is a potential therapeutic strategy for the treatment of early preneoplastic lesions as well as in the treatment of localized and disseminated lung tumors.

Acknowledgments

We thank Nora Rios for assistance in preparation of the manuscript. This work was supported in part by Public Health Service Grant P01 CA78778-01A1 (JAR), by the Specialized Program of Research Excellence (SPORE) in Lung Cancer 2P50-CA70970-04 (JDM and JAR); by a Career Development Award P50-CA70907-5 (RR); by gifts to the Division of Surgery, from Tenneco and Exxon for the Core Laboratory Facility; by the UT MD Anderson Cancer Center Support Core Grant CA 16672; by the Texas Tobacco Settlement Fund as appropriated by the Texas State Legislature (Project 8), by the MD Anderson WM Keck Center for Cancer Gene Therapy (JR, RR); by Texas Higher Education Coordinating Board ATP/ARP Grant 003657-0078-2001 (RR); by ELSCT Lung Cancer Program grant DAMD17-01-1-0689 (LJ, RR); by TARGET Lung Cancer Grant DAMD17-02-1-0706 (LJ, RR); by Cancer Center Support (CORE) Grant CA 16672; and by a sponsored research agreement with Introgen Therapeutics, Inc.

References

1. Carbone DA, Minna JD. *In vivo* gene therapy of human lung cancer using wild-type p53 delivered by retrovirus. *J Natl Cancer Inst*. 1994;86:1437-1438.
2. Hansen HH, Ruch M. Lung cancer. *Cancer Chemother Biol Response Mod*. 1999;18:336-356.
3. Hoffman PC, Mauer AM, Vokes EE. Lung cancer. *Lancet*. 2000;355:478-485.
4. Park BJ, Leake D, Altorki N. Staging and the surgical management of lung cancer. *Radiol Clin North Am*. 2000;34:545-561.
5. Brann PA, Soriano A, Johnson G, Hensley L. New therapeutic strategies for lung cancer: biology and molecular biology come of age. *Chest*. 2000;117:163S-168S.
6. Zechbauer-Muller S, Gazdar AF, Minna JD. Molecular pathogenesis of lung cancer. *Ann Rev Physiol*. 2002;64:681-708.
7. Gazdar A, Roth JA, Minna JD. Focus on lung cancer. *Cancer Cell*. 2002;1:49-52.
8. Wistuba II, Behrens C, Virmani AK, et al. High resolution chromosome 3p allelotyping of human lung cancer and preneoplastic premalignant bronchial epithelium reveals multiple, discontinuous sites of 3p allele loss and three regions of frequent breakpoints. *Cancer Res*. 2000;60:1949-1960.
9. Girard L, Zechbauer-Muller S, Virmani AK, Gazdar AF, Minna JD. Genome-wide allelotyping of lung cancer identifies new regions of allelic loss, differences between small cell lung cancer and non-small cell lung cancer, and loss clustering. *Cancer Res*. 2000;60:4894-4906.
10. Maitra A, Wistuba II, Washington C, et al. High-resolution chromosome 3p allelotyping of breast carcinomas and precursor lesions demonstrates frequent loss of heterozygosity and a discontinuous pattern of allele loss. *Am J Pathol*. 2001;159:119-130.
11. Lerman MI, Minna JD. The 630-kb lung cancer homozygous deletion region on human chromosome 3p21.3: identification and evaluation of the resident candidate tumor suppressor genes. *Cancer Res*. 2000;60:6116-6133.
12. Sekido Y, Ahmadian M, Wistuba II, et al. Cloning of a breast cancer homozygous deletion junction narrows the region of search for a 3p21.3 tumor suppressor gene. *Oncogene*. 1998;16:3151-3157.
13. Kondo M, Ji L, Kanibayashi C, Tomizawa Y, et al. Overexpression of candidate tumor suppressor gene FUS1 isolated from the 3p21.3 homozygous deletion region leads to G1 arrest and growth inhibition of lung cancer cells. *Oncogene*. 2001;20:6258-6262.
14. Ji L, Nishizaki M, Gao B, et al. Expression of several genes in the human chromosome 3p21.3 homozygous deletion region by an adenovirus vector results in tumor suppressor activities *in vitro* and *in vivo*. *Cancer Res*. 2002;62:2715-2720.
15. Uno F, Sasaki I, Nishizaki M, et al. Myristoylation of Fus1 protein is required for tumor suppression in human lung cancer cells. *Cancer Res*. 2004;64:2969-2976.
16. Templeton NS, Lasic DD, Frederik PM, et al. Improved DNA:liposome complexes for increased systemic delivery and gene expression. *Nat Biotechnol*. 1997;15:647-652.
17. Ramesh R, Saeki T, Templeton NS, et al. Successful treatment of primary and disseminated lung cancers by systemic delivery of tumor suppressor genes using an improved liposome vector. *Mol Ther*. 2001;3:337-350.
18. Ito I, Began G, Mohiuddin I, et al. Increased uptake of liposomal-DNA complexes by lung metastases following intravenous administration. *Mol Ther*. 2003;7:409-418.
19. Saeki T, Mhashilkar A, Swanson X, et al. Inhibition of lung cancer growth following adenovirus-mediated mda-7 gene expression *in vivo*. *Oncogene*. 2002;21:4558-4566.
20. Li S, Rizzo MA, Bhattacharya S, Huang L. Characterization of cationic lipid-protamine-DNA (LPD) complexes for intravenous gene delivery. *Gene Therapy*. 1998;5:930-997.
21. Tan Y, Li S, Pitt BR, Huang L. The inhibitory role of CpG immunostimulatory motifs in cationic lipid vector mediated transgene expression *in vivo*. *Hum Gene Ther*. 1999;10:2153-2161.
22. Dow SW, Fradkin LG, Liggitt DH, et al. Lipid-DNA complexes induce potent activation of innate immune responses and antitumor activity when administered intravenously. *J Immunol*. 1999;163:1552-1561.
23. Ito I, Saeki T, Mohiuddin I, et al. Persistent transgene expression following intravenous administration of a liposomal complex: role of IL-10 mediated immune suppression. *Mol Ther*. 2004;9:318-327.

Increased Uptake of Liposomal-DNA Complexes by Lung Metastases Following Intravenous Administration

Isao Ito,¹ Gopalan Began,¹ Imran Mohiuddin,¹ Tomoyuki Saeki,¹ Yuji Saito,¹
Cynthia D. Branch,¹ Ara Vaporciyan,¹ L. Clifton Stephens,² Nancy Yen,¹
Jack A. Roth,¹ and Rajagopal Ramesh^{1,*}

¹Department of Thoracic and Cardiovascular Surgery and ²Department of Veterinary Medicine and Surgery,
The University of Texas M. D. Anderson Cancer Center, Houston, Texas 77030

* To whom correspondence and reprint requests should be addressed at the Department of Thoracic and Cardiovascular Surgery, The University of Texas M. D. Anderson Cancer Center, P.O. Box 445, 1515 Holcombe Boulevard, Houston, TX 77030. Fax: (713) 794-4901. E-mail: ramesh@mdanderson.org

We have investigated the effects of an improved liposomal formulation (extruded DOTAP:cholesterol (DOTAP:Chol)-DNA complex) on transgene expression in tumor cells and normal cells of murine and human origin both *in vitro* and *in vivo*. *In vitro*, transgene expression was significantly increased ($P = 0.01$) in human tumor cells compared to normal human cells. The increased transgene expression was due to increased uptake of the liposome-DNA complex by tumor cell phagocytosis. Furthermore, immunohistochemical analysis demonstrated a greater transgene expression in lung tumors than in surrounding normal tissues. Increased transgene expression due to enhanced uptake of the liposome-DNA complexes by tumor cells *in vivo* was also demonstrated using fluorescently labeled DOTAP:Chol liposomes. Finally, evaluation of lung tissue explants obtained from patients undergoing pulmonary resection demonstrated significantly higher ($P = 0.001$) transgene expression in tumor cells than in normal cells. Thus, we demonstrated that intravenous injection of DOTAP:Chol-DNA complex results in increased transgene expression in tumor and is due to increased phagocytosis of the complexes by tumor cells.

Key Words: liposome, gene therapy, phagocytosis, cancer, metastasis

INTRODUCTION

Progression of cancer is a multistep process in which the disease eventually becomes disseminated. Current treatments for disseminated tumors have had limited success because of treatment-related toxicity. A new alternative treatment strategy for cancer is gene therapy, which has shown promise in clinical trials [1-6]. This approach has, however, been limited to the treatment of locoregional disease because of the lack of a vector that can efficiently and selectively deliver genes systemically.

An alternative to adenoviral vectors is nonviral liposomal delivery systems that can be administered intravenously with limited vector-associated toxicity, resulting in higher transgene expression, especially in the lungs [7]. The development of efficient nonviral vectors that, when injected systemically, can selectively deliver therapeutic genes to tumors will provide novel therapeutic options for the treatment of cancer. Tumor targeting using tumor-specific promoters, attachment of ligands to the liposome surface, and pegylation of liposomes has been tested previously [8-16]. Although some degree of tumor targeting

has been demonstrated using these targeted delivery systems, the level of transgene expression is often decreased. Recent studies have demonstrated that liposome-DNA complexes elicit an inflammatory response when injected systemically, resulting in suppression of transgene expression [17-22]. Furthermore, failure to achieve increased or sustained gene expression following repeated injections has been another major obstacle in the development of therapeutic applications of liposomes [18,23].

We recently showed that extruded cationic liposome (DOTAP:cholesterol, or DOTAP:Chol)-DNA complexes can achieve effective levels of transgene expression in tumor-bearing lungs and, when injected intravenously, can cure immunocompetent mice with disseminated experimental metastases, with minimal toxicity [24]. In the same study, we also showed that repeated daily injections resulted in a dose-dependent increase in transgene expression in tumor-bearing lungs. The unexpected curative potential of these complexes for disseminated disease and the apparent high levels of their expression in tumors raised an important question: were these effects due to

increased expression of the transgene in tumor cells or due to increased uptake of the liposomes by tumor cells compared to surrounding normal cells?

In the study presented here, we demonstrate that intravenous injection of DOTAP:Chol liposome-DNA complexes *in vivo* results in significantly higher transgene expression in lung tumor cells than in normal cells and that this increased expression is due to increased uptake of these liposome-DNA complexes by tumor cells. Furthermore, transgene expression is demonstrated to be significantly higher in primary human lung tumor explants than in normal cells. Thus, utilizing the inherent property of tumor cells for increased liposomal-DNA complex uptake, effective delivery of therapeutic genes to the tumor can be achieved following systemic delivery.

RESULTS

Cell Viability and Luciferase (*luc*) Gene Expression in Liposome-DNA Complex-Transfected Normal and Tumor Cells

We transfected normal human lung fibroblasts (WI38, MRC9), normal human bronchial epithelial cells (NHBE), human lung tumor cells (A549, H1299, H358, H322, and H460), murine fibroblasts (NIH/3T3, 10T1/2), and murine fibrosarcoma cells (UV2237m, K1735) all with DOTAP:Chol-*luc* DNA complex (Fig. 1). Determination of cell viability at 24 and 48 h after transfection demonstrated no significant toxicity in any of the cell lines tested (Fig. 1A). To determine whether differences existed in transgene expression between normal and tumor cells, we assayed transfected cells for *luc* activity. *luc* expression was 2 to 4 logs greater ($P = 0.01$) in human tumor cells compared to normal cells of human origin (Fig. 1B). However, *luc* expression in murine tumor cells was only 2- to 2½-fold greater compared to normal cells ($P = 0.04$; Fig. 1B).

In Vitro Uptake of Liposome-DNA Complex

Analysis of the liposome-DNA complex uptake in human tumor cells relative to normal human cells by fluorescence microscopy and flow cytometry revealed increased uptake in tumor cells compared to normal cells (Fig. 2). However, increased uptake of liposome-DNA complex was also observed in endothelial cells (HUVEC). The difference in the uptake of the liposome complex by these cells correlated with luciferase expression (Fig. 2).

Role of Phagocytic and Pinocytic Activity in the Uptake of Liposome-DNA Complex by Tumor Cells

We transfected tumor cells (H1299) with fluorescently labeled DOTAP:Chol-*luc* DNA complex (Figs. 3B and 3C) and positively charged 2- μ m fluorescent latex microspheres (Fig. 3A) with or without cytochalasin B, an in-

hibitor of phagocytosis and pinocytosis, and observed them under a fluorescence microscope using a fluorescein or a rhodamine filter. Tumor cells transfected in the absence of cytochalasin B showed greater punctate fluorescence in the cytoplasm, indicating greater uptake of the liposome-DNA complex (Fig. 3B). In contrast, liposome-DNA complex uptake was blocked in cells transfected in the presence of the drug. Hoechst staining revealed presence of intact nucleus in the cells that were untreated or treated with cytochalasin B.

Uptake of Liposome-DNA Complex by Tumor Cells *In Vivo*

We injected UV2237m lung-tumor-bearing C3H/Ncr mice with fluorescently labeled DOTAP:Chol-*luc* DNA complex (50 μ g DNA) via a tail vein. Animals receiving no treatment served as controls. We euthanized the animals at 24 h after injection, harvested their lungs, and prepared cryosections. Examination of tissue sections under fluorescence microscopy revealed intense fluorescence by tumor cells compared to surrounding normal cells (Fig. 4D). Minimal fluorescence was observed in controls (Fig. 4B). Further confirmation that the observed intense fluorescence was indeed from tumor cells was obtained by examining a hematoxylin-stained serial tissue section under bright-field microscopy (Figs. 4A and 4C).

To confirm further that the increased uptake of the liposome-DNA complex by tumor cells also resulted in increased transgene expression, we stained tissue sections for luciferase protein by immunohistochemical technique. Protein expression was greater in tumor cells (Fig. 4E) than in surrounding normal cells (Fig. 4H), indicating that tumor cells were the primary source of the observed *luc* expression. Furthermore, we observed *luc* expression to be higher in tumor-bearing lung tissue (Fig. 4E) than in the non-tumor-bearing lung tissue (Fig. 4G). A lung tissue section from a tumor-bearing animal receiving no treatment served as negative control (Fig. 4F). Additional controls included tissues stained with secondary antibody alone (Fig. 4I). Semiquantitative analysis demonstrated a significant ($P = 0.01$) increase in luciferase protein expression as indicated by the brown staining in the tumor tissue area compared to surrounding normal tissue area (Fig. 4J).

To confirm further that the observed result is not unique to UV2237m lung tumors, we performed similar experiments in nude mice bearing human A549 lung tumors. We injected the animals with DOTAP:Chol-*luc* DNA complex 2 or 3 weeks after tumor cell injection. The tumor load at 2 weeks is less and the tumors are small compared to tumor load and size at 3 weeks (data not shown). Immunohistochemical analysis of lung tissues 24 h after injection of liposome-DNA complex demonstrated increased luciferase expression ($P = 0.01$) in tu-

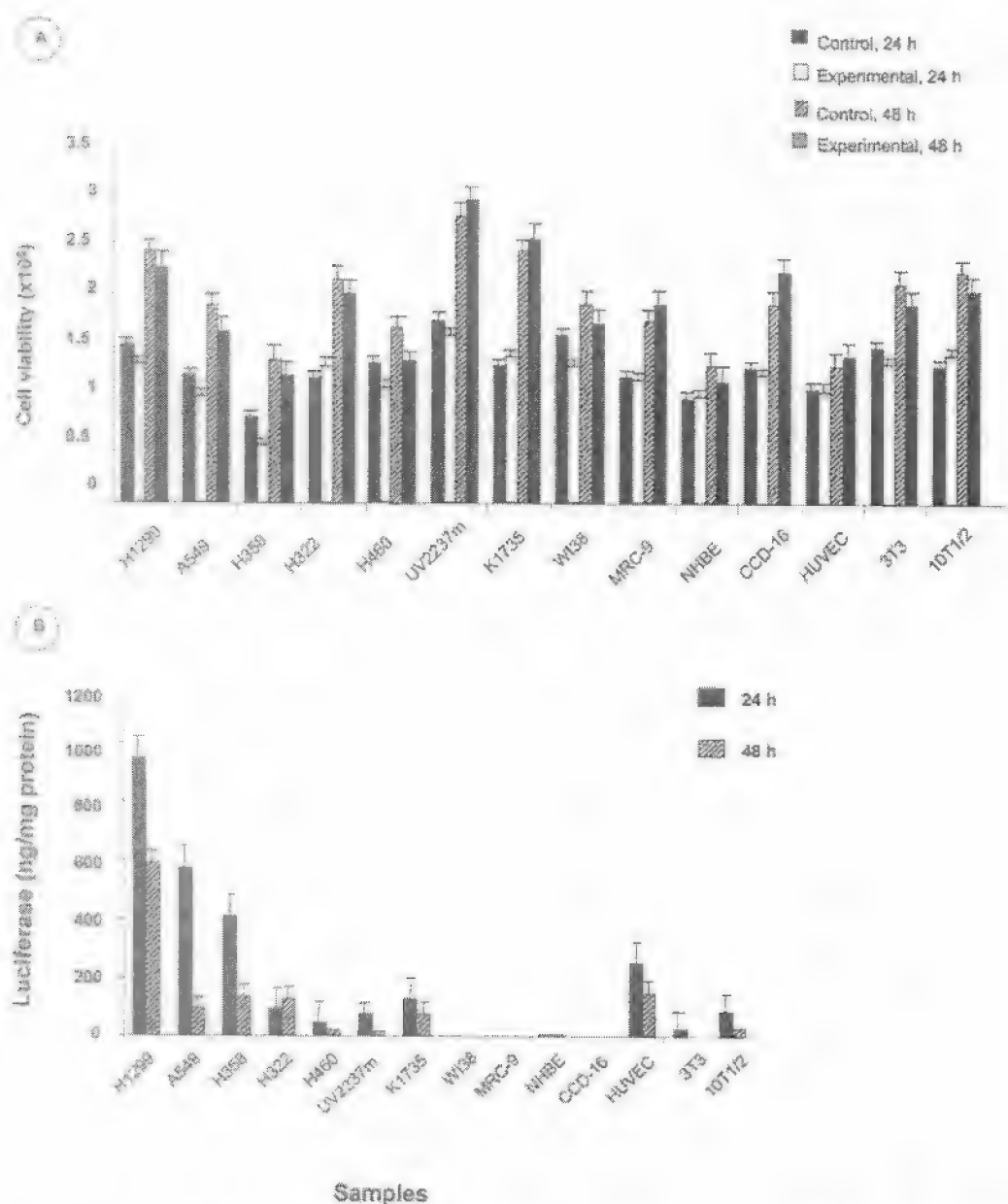


FIG. 1. Effect of liposome-DNA complex transfection on cell viability and luc expression in tumor cells and normal cells. Cells analyzed were human lung tumor cells (H1299, H358, H460, A549), normal lung fibroblast cells (W138, CCD-16, MRC-9), normal bronchial epithelial cells (NHBE), human umbilical vein endothelial cells (HUVEC), murine fibroblasts (3T3, 10T1/2), and murine fibrosarcoma (UV2237m, K1735) cells. Cells (5×10^5) were either not transfected (control) or transfected with DOX-luc-DNA complex and harvested at 24 and 48 h after transfection and analyzed for cell viability by trypan exclusion assay (A) and for luc activity using a luciferase assay kit (B). No significant toxicity was observed in transfected tumor and normal cells of both human and murine origin compared to untransfected control cells (A). luc expression was higher in both human tumor cells ($P = 0.01$) and murine tumor cells ($P = 0.04$) compared to normal cells (B). luc activity was expressed as nanograms per milligram of total protein. Each time point represents the mean of triplicate wells. Error bars represent standard errors.

norm compared to surrounding normal tissues (Figs. 5A and 5B). Furthermore, we observed increased luciferase expression in the tumor tissue in lungs that had small

tumors and in lungs that had large tumors. These results indicate that increased uptake of liposome-DNA complex by tumor cells is not dependent on the tumor size or load.

Comparison of *luc* Expression in Alveolar Macrophages, Tumor-Bearing Lungs, and Non-Tumor-Bearing Lungs

We transfected alveolar macrophages isolated from UV2237m lung-tumor-bearing mice and non-tumor-bearing animals with DOTAP:Chol-*luc* complex and compared them in UV2237m tumor cells, which served as positive control. We determined *luc* expression 24 h after transfection. *luc* expression was significantly lower ($P = 0.0001$) in alveolar macrophages isolated from tumor-bearing animals than in alveolar macrophages from non-tumor-bearing animals (Fig. 6A). To eliminate the possibility that the difference in luciferase expression was due to cytotoxicity, cell viability assay was performed after transfection with DOTAP:Chol-*luc* DNA complex. No significant difference in cytotoxicity was observed between macrophages isolated from tumor-bearing animals and those isolated from non-tumor-bearing animals (Fig. 6B). Furthermore, analysis for luciferase expression in tumor-bearing and non-tumor-bearing lungs from which the alveolar macrophages were isolated demonstrated no significant difference in the expression levels (Fig. 6C). These results indicate that alveolar macrophages from lung-tumor-bearing animals are less transfectable than those from non-tumor-bearing animals.

In Vitro Comparison of *luc* Expression of Tumor Cells and Normal Cells Isolated from Primary Human Lung Tumor Explants

To determine whether differences in transgene expression also occurred in primary human lung tumor cells and normal cells, we obtained lung tissue explants from patients undergoing pulmonary resection for primary non-small-cell lung cancer. Tissue explants were confirmed as tumor or normal by histopathological analysis. Tumors were classified as poorly to moderately differentiated adenocarcinoma while normal pulmonary tissue comprised primarily fibroblasts. Cells isolated from normal and tumor tissue explants were transfected with DOTAP:Chol-*luc* DNA complex, and *luc* expression was determined 24 h after transfection. We observed significantly higher *luc* expression ($P = 0.001$) in tumor cells (2 ± 0.1 ng/mg protein) than in normal cells (0.06 ± 0.02 ng/mg protein), a finding consistent with those in established cultures of tumor and normal cells reported above.

DISCUSSION

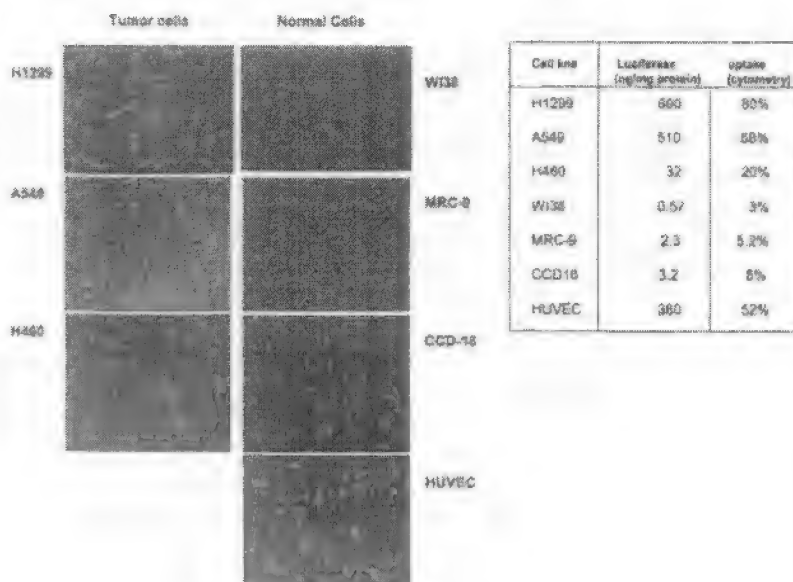
We recently demonstrated that very high levels of transgene expression can be achieved in tumor-bearing lungs when an extruded DOTAP:cholesterol-DNA complex is injected intravenously into both immunodeficient and immunocompetent animals and that this treatment has minimal toxicity [24]. In that study, repeated daily tail vein injections resulted in dose-dependent increases in

transgene expression in lung-tumor-bearing animals and successfully cured one-third of mice with disseminated experimental metastases in a human xenograft model. The curative potential for disseminated disease and the apparent high levels of transgene expression in tumors were unexpected. One possibility for this observed therapeutic effect is that the uptake of liposome-DNA complexes by tumor cells and normal cells is the same, but tumor cells express the transgene more efficiently than normal cells. The second possibility is that the uptake of the complexes is increased in tumor cells over normal cells, which leads to higher expression levels of the transgene in the tumors. In the study presented here, we investigated the effects of the extruded DOTAP:Chol liposome-DNA complex on transgene expression in lung tumors and their surrounding normal tissues as well as the underlying mechanism both *in vitro* and *in vivo*.

Preliminary *in vitro* studies using tumor cells, normal fibroblasts, and endothelial cells of both murine and human origin demonstrated the DOTAP:Chol-*luc* DNA complex to be nontoxic to these cells. Analysis of these cells for transgene expression demonstrated increased *luc* expression in tumor cells over normal cells except endothelial cells. It is possible that the observed difference in transgene expression is due to differences in cellular proliferation rates between tumor and normal cells [30]. However, the differences observed in the present study cannot be attributed to cellular proliferation since the rate of proliferation of the different cell types used in the present study were similar except for NHBE and HUVEC (data not shown). The observed difference in transgene expression between tumor cells and normal cells might be due to any of several other known mechanisms, including differences in cell surface charge, phagocytic activity, endocytic activity, endosomal release, nuclear uptake, and transcriptional activity [31–36].

On the basis of these known differences, we studied the uptake of liposome-DNA complexes by normal and tumor cells using fluorescently labeled DOTAP:Chol liposome. Tumor cells had increased uptake of the liposome-DNA complexes over normal cells that correlated with increased luciferase activity. Surprisingly, endothelial cells also demonstrated increased uptake and expression. Since similar levels of luciferase activity were observed in tumor cells transfected with unlabeled DOTAP:Chol- and fluorescently labeled DOTAP:Chol-DNA complex, increased uptake cannot be attributed to the use of fluorescent lipid (data not shown). To identify the processes that mediate increased uptake of liposome-DNA complex by tumor cells, we examined surface charge using cationized ferritin, which attaches to the cell surface as a function of surface charge [37,38]. No significant difference was observed in the percentage binding of cationized ferritin to both tumor cells and NHBE and it did not correlate with the luciferase activity (data not shown). However, the increased uptake of liposome-DNA complex was observed

FIG. 2. Increased uptake of liposome-DNA complex by tumor cells. Tumor cells (H1299, A549, H460), normal cells (MRC-9, CCD-16), and endothelial cells (HUVEC) were transfected with fluorescently labeled DOTAP:Chol-DNA complex. Cells were analyzed for liposome-DNA complex uptake by fluorescence microscopy and flow cytometry and for luciferase expression by luminometer. Increased uptake was observed in tumor cells and in endothelial cells compared to normal cells. Increased uptake by tumor cells and HUVEC correlated with increased luciferase expression. Luciferase expression is expressed as nanograms per milligram of protein.



to be due to the phagocytic activity of the tumor cells since uptake was inhibited in the presence of cytochalasin B, an inhibitor of phagocytosis and pinocytosis. The ability of tumor cells to exhibit phagocytic activity is not surprising and is well documented [39]. However, greater phagocytic activity by tumor cells than by normal phagocytic and nonphagocytic cells treated with this liposome-DNA formulation has not been previously reported.

To explore further whether a similar phenomenon occurred *in vivo*, murine syngeneic lung-tumor-bearing animals were injected with the fluorescent liposome-DNA complex. They revealed increased uptake in the tumor cells compared to the surrounding normal cells. Furthermore, the increased uptake by tumors *in vivo* correlated with increased luciferase expression as demonstrated by immunohistochemical studies. Increased uptake of cationic liposome-DNA complexes by tumor cells *in vivo* following systemic delivery has been reported previously, consistent with the present report [40–43]. However, previous studies have attributed increased uptake of liposome-DNA complexes to leaky vasculature in the tumors. On the basis of our results, we believe that in addition to the presence of leaky vasculature in the tumors, increased phagocytic activity of the tumor cells is responsible for the observed increased uptake of DOTAP:Chol-DNA complex by tumor cells *in vivo*. Transgene expression in various other organs examined was very low (data not shown). Furthermore, real-time PCR analysis demonstrated low copy numbers of plasmid DNA in the liver, spleen, and ovaries compared to the lung (data not shown), suggesting that lung is the primary target for the intravenously injected DOTAP:Chol-DNA complex. This observation is in agreement with previously published reports [7,24]. However, in the presence of tumors in the

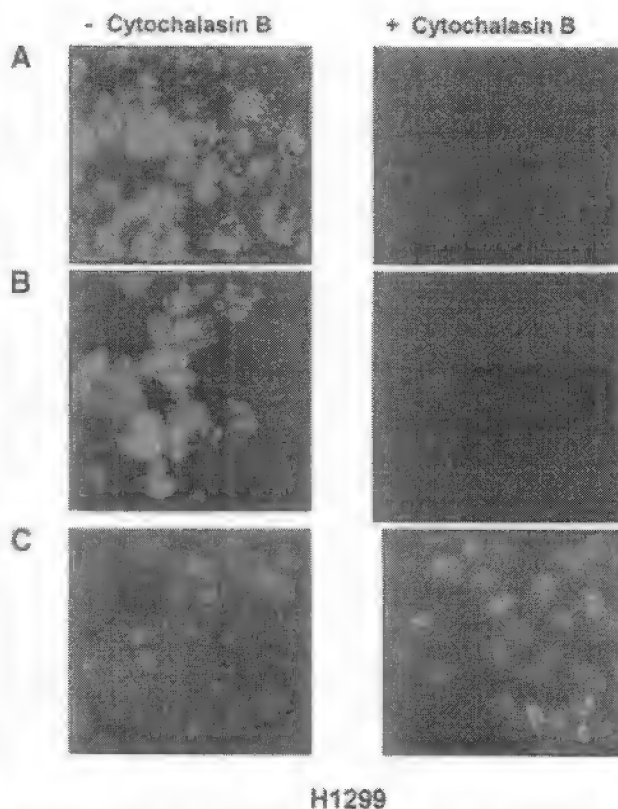


FIG. 3. Increased uptake of liposome-DNA complex by tumor cells is due to phagocytosis. Tumor cells (H1299) were transfected with 2 µm fluorescent microspheres (A) or fluorescently labeled DOTAP:Chol-DNA complex (B) in the presence or absence of cytochalasin B. Cytochalasin B, an inhibitor of phagocytosis, inhibited uptake of fluorescently labeled DOTAP:Chol-DNA complex by tumor cells (original magnification $\times 200$). Hoechst staining of cells indicates intact nucleus (C).

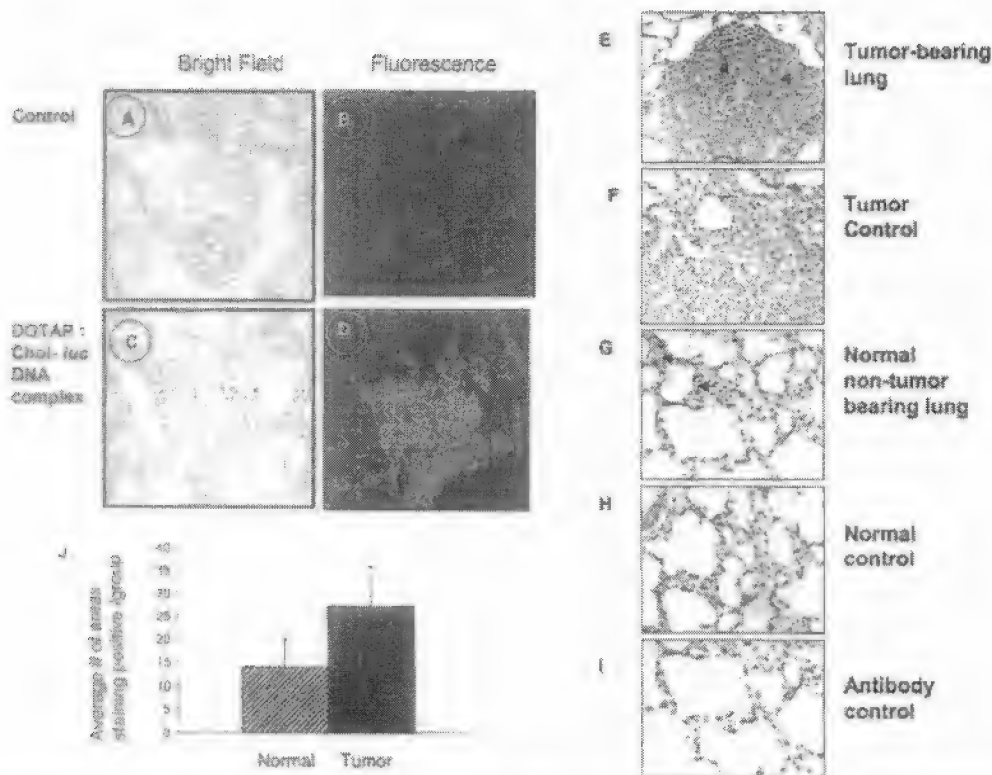


FIG. 4. Increased luciferase expression by lung tumors *in vivo* is due to increased uptake of liposome-DNA complex. UV2237m lung-tumor-bearing mice were injected with fluorescently labeled DOTAP:Chol-luc DNA complex via tail vein (C, D). Animals receiving no treatment served as controls (A, B). The animals were euthanized by CO₂ inhalation at 24 h after injection, and their lungs were isolated. Bright-field microscopy of hematoxylin-stained lung tissue sections revealed the presence of tumors in the lungs (A, C). Fluorescence microscopy of an unstained lung tissue section demonstrated greater fluorescence by tumor cells than by surrounding normal cells (D). Minimal fluorescence was observed in control tissue sections (B). Immunohistochemical analysis of lung tumor sections for luciferase protein demonstrated increased luciferase expression by tumors as indicated by the brown staining (E) compared to their surrounding normal tissue (H) and non-tumor-bearing lung tissue (G). Tumor-bearing lungs receiving no treatment (F) and tissue sections stained with no secondary antibody (I) served as controls (original magnification $\times 200$). Arrows indicate cells staining positive for luciferase protein. Semiquantitative analysis of the areas staining positive indicated tumors staining more positively than surrounding normal tissues ($P = 0.01$) (J).

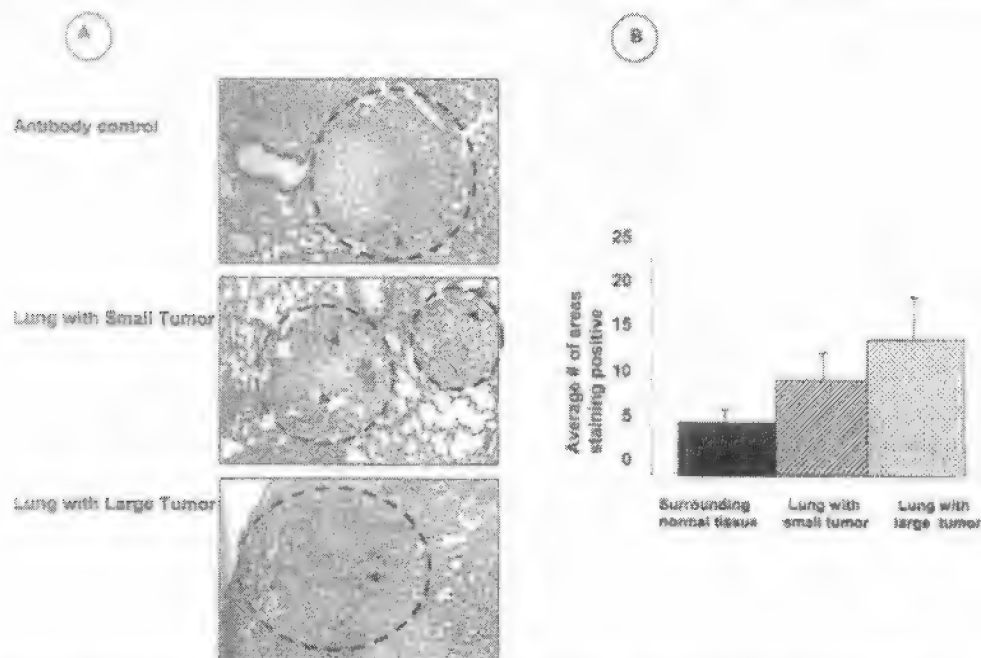


FIG. 5. Increased uptake of liposome-DNA complex by A549 lung tumors *in vivo*. Nude mice were injected with A549 lung tumor cells via tail vein. Animals were injected with DOTAP:Chol-luc DNA complex 2 weeks (small tumors) and 3 weeks (large tumors) after tumor cell inoculation. Tumor-bearing animals receiving no treatment served as controls. Immunohistochemical analysis of lungs harvested 24 h after treatment demonstrated higher luc expression ($P = 0.01$) in the tumors compared to surrounding normal tissues as indicated by the brown staining (A, B). Increased luciferase expression was observed in tumors that were small and in tumors that were large. Arrows indicate positive staining.

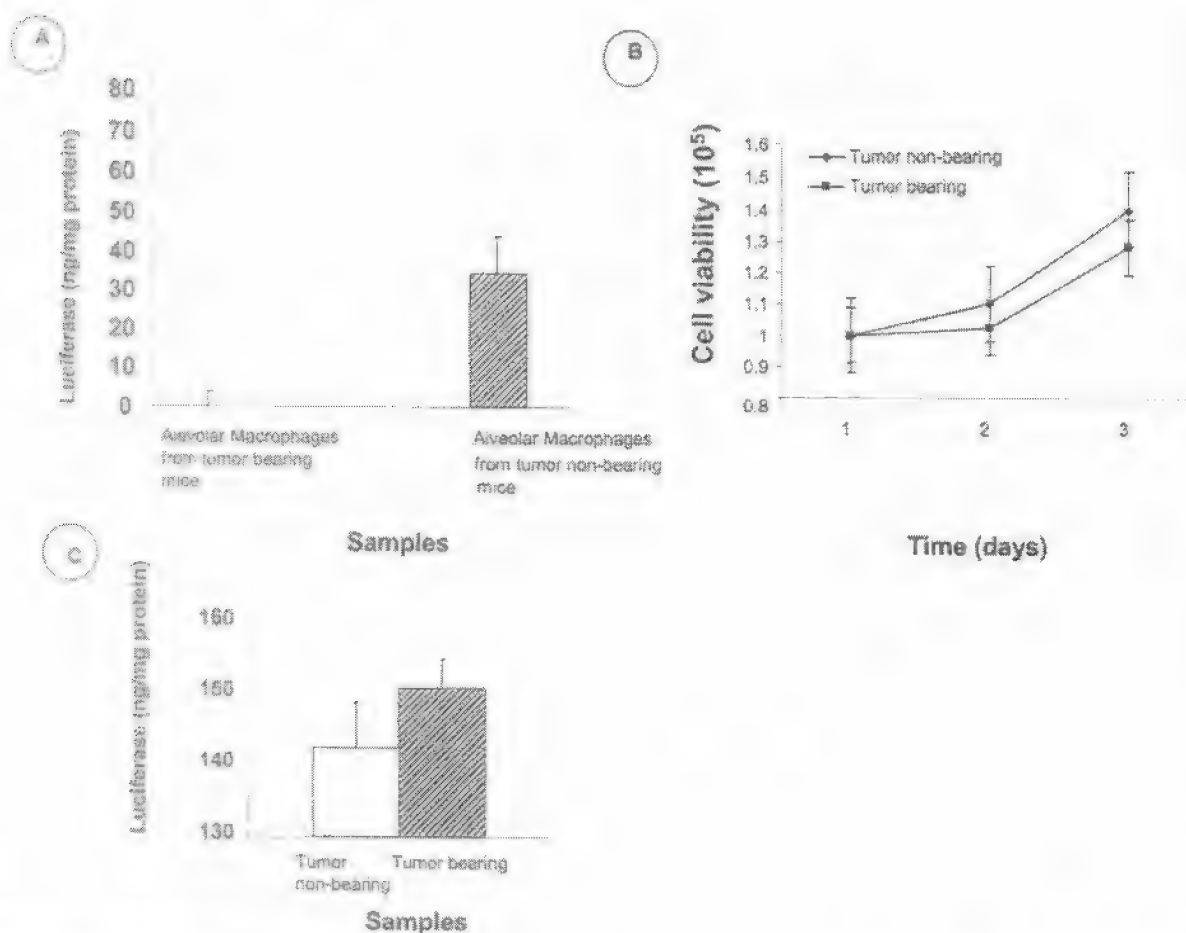


FIG. 6. Comparison of luc expression in alveolar macrophages isolated from tumor-bearing and non-tumor-bearing animals. Alveolar macrophages isolated from C57BL/6 lung-tumor-bearing and non-tumor-bearing animals were transfected with DOTAP:Chol-luc DNA complex and analyzed for luc expression 24 h after transfection. luc expression was significantly ($P = 0.001$) higher in macrophages isolated from non-tumor-bearing animals compared to those from tumor-bearing animals (A). Cell viability assay indicated no significant difference in proliferation between macrophages isolated from tumor-bearing animals and those isolated from non-tumor-bearing animals (B). Analysis of lungs for luc expression demonstrated no significant difference between tumor-bearing and non-tumor-bearing animals (C). luc activity was expressed as nanograms per milligram of total protein. Experiments were done in triplicate and bars denote standard errors.

lungs, increased uptake occurs in the tumors compared to the surrounding normal lung tissue. We next evaluated whether increased uptake of liposome-DNA complex is unique to murine tumors or is a generalized phenomenon that can be observed with other tumors. Increased expression in human A549 lung tumors was observed compared to surrounding normal cells. Furthermore, the increased uptake of liposome-DNA complex was observed in lungs that had small tumors as well as in lungs that had large tumors, indicating that tumor size and number of tumors were not factors.

Additional evidence for increased uptake of the liposome-DNA complex by tumor cells was obtained from transmission electron microscope studies (data not shown). One argument that can be made from our *in vivo*

results is that alveolar macrophages, which are also phagocytic, must phagocytose the injected complexes as efficiently as the tumor cells. Transfection of alveolar macrophages isolated from lung-tumor-bearing animals with DOTAP:Chol-luc DNA complex *in vitro* yielded significantly lower luc expression than transfection of macrophages from non-tumor-bearing animals. The findings presented in the present study contrast with previous reports demonstrating liposome-DNA complex to be a major target for macrophages and the reticuloendothelial system [44,45]. However, one major difference between our study and others is that we performed our experiments in tumor-bearing animals, while previously reported studies were based on experiments conducted in animals without tumors [44,45].

To test whether the pathophysiological state of the animal was important for normal functions of the macrophage, we conducted a separate but parallel set of experiments in which alveolar macrophages isolated from animals without tumors were transfected with DOTAP:Chol-*luc* DNA complex. *luc* expression was extremely significantly higher in macrophages from non-tumor-bearing compared to macrophages from tumor-bearing animals. One possibility for this difference is that the alveolar macrophages present in the tumor microenvironment are less phagocytic or are inactivated by factors produced by the tumor cells. Inactivation of macrophages in the tumor microenvironment has been previously demonstrated [46–48]. In fact alveolar macrophages from tumor-bearing animals were observed to be functionally inactive as indicated by stimulation assays (unpublished data).

Finally, increased uptake of liposome-DNA complex was demonstrated by transfecting primary tumor cells of poorly to moderately differentiated adenocarcinoma type and normal cells. Increased *luc* expression was observed in tumor cells compared to normal cells. The observation that tumor cells of poorly differentiated origin expressed *luc* at greater levels fits well with the findings of Matsui et al. [28], who showed that poorly differentiated airway epithelial cells phagocytose liposome-DNA complex more effectively, resulting in higher levels of transgene expression than in well-differentiated cells. Thus, transfection of primary tumor cells from tissue explants using DOTAP:Chol-DNA complex has been shown for the first time and supports our findings in established tumor cell lines.

Although the present study demonstrates that increased uptake of liposome-DNA complexes by tumor cells over surrounding normal cells is due to increased phagocytosis, it is also possible that other factors such as endosomal release, nuclear uptake, and increased transcription, may play a role. Further examination of these individual phenomena may help give a better understanding of the underlying differences between tumor and normal cells and in the development of an effective gene delivery vector. However, a note of caution is that the experimental metastases model used in the present study, although performed in such a way that the lung metastases are established, has limitations. It does not recapitulate the full sequence of events (from premalignancy to invasion and metastases) that primary tumors undergo. These cancer cells may undergo additional changes. Thus it may not be predictive of the responses of these tumors to a systemically delivered gene therapy agent. Therefore, the results of the present study, though relevant for lung cancer therapy, represent only an intermediate step on the path toward the development of a systemic gene transfer agent with broad utility.

METHODS

Materials. All lipids (DOTAP, cholesterol) were purchased from Avanti Polar Lipids (Alabaster, AL). Fluorescent cholesterol analog 22-(N-(7-nitrobenz-2-oxa-1,3-diazol-4-yl)amino)-23,24-bisnor-5-cholesterol (fluorescein) was purchased from Molecular Probes (Eugene, OR). RPMI 1640 medium, modified Eagle's medium (MEM), and fetal bovine serum (FBS) were purchased from GIBCO BRL Life Technologies (New York, NY). Polyclonal goat anti-human luciferase antibody was purchased from Promega Laboratories (Madison, WI).

Cell lines and animals. Human non-small-cell lung carcinoma (NSCLC) cell lines (A549, H1299, H460, H322, and H358) and normal human lung fibroblast cell lines (WI38, CCD16, and MRC-9) were obtained from American Type Culture Collection (ATCC; Rockville, MD) and maintained as per the supplier's recommendations. Human normal bronchial epithelial cells (NHBE) were obtained from Clonetics (Walkersville, MD) and maintained as recommended by the supplier. Murine fibrosarcoma cells (UV2237 and K1735) obtained from Dr. Isaiah Fidler, M. D. Anderson Cancer Center, and murine fibroblasts (NIH/3T3 and 10T1/2) purchased from ATCC were maintained in RPMI 1640 medium. Four- to six-week-old female C3H/Nei mice (National Cancer Institute, Frederick, MD) and nude mice (Charles River Laboratory, Wilmington, DE) used in the study were maintained in a pathogen-free environment and handled according to institutional guidelines established for animal care and use.

Primary human lung cancer cells and normal epithelial cells were obtained from patients undergoing pulmonary resection. Tumor specimens were excised from surrounding normal epithelium and both normal parts and tumor parts were cut into smaller pieces. A pathologist used cytopathological and histopathological analysis to classify tissue specimens as tumor or normal. A total of five specimens from five individual patients were obtained. Tumor tissues from all five patients were histopathologically classified as poorly to moderately differentiated adenocarcinoma. Single-cell suspensions from tissues were prepared as previously described [25].

Purification of plasmids. The plasmid carrying the luciferase (*luc*) gene, under the control of the CMV40 promoter, was grown under ampicillin selection in the *Escherichia coli* host strain DH5 α and purified by using an alkaline lysis method [7,26]. Endotoxin levels of purified plasmids were determined by using the chromogenic limulus amoebocyte lysate kinetic assay kit (Kinetic-QCL; BioWhittaker, Walkersville, MD). The concentration and purity of the purified plasmid DNA were determined by OD_{260/280} ratios.

Synthesis of liposomes and preparation of liposome-DNA complexes. Liposome (20 mM DOTAP:Chol) was synthesized and extruded through Whatman filters (Kent, UK) of decreasing sizes (1.0, 0.45, 0.2, and 0.1 μ m) as previously described [7]. Fluorescently labeled DOTAP:Chol liposomes were synthesized using the same procedure except that cholesterol was replaced with a fluorescent cholesterol analog (fluorescein) [27] and stored in the dark.

Particle size analysis. Freshly prepared liposome-DNA complexes were analyzed for mean particle size by using the N4 particle size analyzer (Coulter, Miami, FL). The mean particle sizes of the liposome-DNA complexes ranged between 300 and 325 nm.

In vitro transfection, cell viability, and *luc* gene expression. Human NSCLC cells, normal lung fibroblasts, NHBE cells, murine tumor cells (UV2237, K1735), and murine fibroblasts (NIH/3T3, 10T1/2), were seeded in six-well plates at 5×10^5 cells/well. The following day, cells were transfected with DOTAP:Chol-*luc* DNA complex (2.5 μ g DNA) in serum-free medium for 3 h. Following transfection, cells were replenished with appropriate medium for each cell line containing 10% FBS, and incubation was continued. Cells were harvested at 24 and 48 h after transfection. Cell viability was determined by trypan blue exclusion assay and *luc* expression by using the luciferase assay kit (Promega) as previously described [24]. Luciferase expression was expressed as nanograms per milligram protein by comparing with recombinant luciferase protein. Cells that were not transfected served as controls.

in vitro uptake of liposome-DNA complex. Tumor cells and normal lung fibroblast cells were seeded in six-well plates at 5×10^5 cells/well. The following day, cells were transfected with fluorescently labeled DOTAP:Chol-luc DNA complex (2.5 μ g DNA) in serum-free medium and analyzed after 3 h by fluorescence microscopy. Cells were analyzed for luciferase expression 24 h later, expressed as described above.

Fluorescent activity. C127 tumor cells were seeded in six-well plates at 5×10^5 cells/well. The following day, cells were transfected with fluorescently labeled DOTAP:Chol-luc DNA complex (2.5 μ g DNA) or positively charged 3- μ m fluorescent microspheres (0.006%) (Molecular Probes, Eugene, Oregon) in serum-free medium in the absence or presence of 5 μ g/ml cytochrome c (Sigma Chemicals, St. Louis, MO) as previously described [28]. Three hours after transfection cells were stained with Hoechst 33348 and analyzed under fluorescence microscopy using a rhodamine, fluorescein, and UV filter.

Uptake and expression of DOTAP:Chol-luc DNA complex in vivo. C127 lung tumors were established in C3H mice by injecting 1×10^6 cells iv. Three weeks after tumor cell injection, uptake and expression of the liposome-DNA complex were determined using fluorescently labeled liposome-DNA complex. Animals were injected with fluorescent liposome-luc DNA complex (50 μ g DNA) via a tail vein. At 24 h after treatment animals were euthanized, and their lungs were harvested and embedded in OCT medium for cryosectioning. Tissue sections (4 μ m) were analyzed directly under fluorescence microscopy. Sections from non-tumor-bearing animals and untreated tumor-bearing animals served as controls.

In a separate set of experiments, A549 lung tumors were established in nude mice as previously described [24]. Briefly, A549 tumor cells (1×10^6) were injected into nude mice via the tail vein. Animals were injected with DOTAP:Chol-luc DNA complex at 2 weeks after tumor cell inoculation (low tumor load) or at 3 weeks (high tumor load) after inoculation. Animals were euthanized 24 h later and tumor-bearing lungs examined for luciferase protein expression by immunohistochemistry as described below.

Immunohistochemical analysis. Luciferase protein expression in the tissue sections was detected by immunohistochemical analysis as previously described [24] using a goat polyclonal luciferase antibody. Luc proteins were detected by reaction with DAB by enhancement using the avidin-biotin-peroxidase ABC kit (Vector Laboratories, Burlingame, CA). The slides were then counterstained with hematoxylin and mounted with Aquamount (Fisher Laboratories, Pittsburgh, PA). Controls included tissues with no primary antibody and only secondary antibody. The luciferase protein expression level in the tumor and the surrounding normal tissue was semiquantitatively determined by analysis image analysis using Opcom 8 software. Briefly, for each tissue section the total area staining positive as indicated by brown staining and the number of tumor areas staining positive was determined. The ratio of tumor area to total area of the tissue staining positive was then represented as percentage positive for tumor. A total of three samples comprising 15 sections for each group were analyzed in a blind fashion and represented as an average number for each sample.

Luc expression in alveolar macrophages, normal lungs, and tumor-bearing lungs. JY2237 lung-tumor-bearing and non-tumor-bearing mice ($n = 15$) were injected with DOTAP:Chol-luc DNA complex (50 μ g DNA) iv. Twenty-four hours later, animals were euthanized and alveolar macrophages from the lungs isolated as previously described [29]. Briefly, macrophages from bronchoalveolar lavage were collected and separated. More than 85% of the cell population was confirmed to be macrophages by a cytopathologist. The harvested macrophages were counted and plated into 6-well plates for luciferase expression (10^6 cells/well) and into 12-well plates for cell viability (1×10^5 cells/well). Plates were incubated overnight at 37°C in a 5% CO₂ incubator. Twenty-four hours later, macrophages were transfected either with naked luc plasmid DNA or with DOTAP:Chol-luc DNA complex (2.5 μ g DNA). Twenty-four hours later cells were harvested and analyzed for viability by trypan blue exclusion assay or assayed for luc expression. Luc expression was expressed as nanograms per milligram of protein. Experiments were performed in duplicate. Untransfected

cells served as controls. In addition, the lungs harvested from tumor-bearing and non-tumor-bearing animals for isolating macrophages were analyzed for luc expression as described above.

Luc expression in tumor cell explants. Primary cells isolated from normal and tumor tissue explants were plated at a density of 5×10^5 cells/well in six-well plates and transfected with DOTAP:Chol-luc DNA complex (2.5 μ g DNA). Transfection and analysis for luc expression were performed as described above. Cells receiving no treatment served as controls.

Statistical analysis. The statistical significance of the experimental results was calculated using Student's *t* test and the Mann-Whitney test.

ACKNOWLEDGMENTS

The authors thank C. Rahj Robinson, Debra Cameron, and Joyce M. Foud, Department of Pathology, for help in obtaining tissue specimens, and Peggy James for preparation of the manuscript. This work was supported in part by Public Health Service Grant P01CA78778-01A1 (J.A.R.), by the Specialized Program of Research Excellence (SPOR) in Lung Cancer (P50-CA70907) (J.A.R.), by the Texas Tobacco Settlement Fund, by the M. D. Anderson Cancer Center W. M. Keck Center for Cancer Gene Therapy, by Cancer Center Support (CORE) Grant CA 16672, by Career Development Award P50-CA70907-5 (R.R.), by a University of Texas M. D. Anderson Cancer Center Institutional Research Grant (R.R.), by a grant from the W. M. Keck Foundation Fund for Human Cancer Gene Prevention and Therapy (R.R.), by BECT Lung Cancer Program Grant DAMD17-01-1-0689, by TARGET Lung Cancer Grant DAMD17-02-0706, by Texas Higher Education Coordinating Board ATP/ARP Grant 003657-0078-2001 (R.R.), and by a sponsored research agreement with Inogen Therapeutics, Inc.

RECEIVED FOR PUBLICATION JUNE 7, 2001; ACCEPTED JANUARY 2, 2003.

REFERENCES

- Swisher, S. G., et al. (1999). Adenoviral mediated p53 gene transfer in advanced non-small cell lung cancer. *J. Natl. Cancer Inst.* 91: 763-771.
- Roth, J. A., et al. (1996). Retrovirus-mediated wild-type p53 gene transfer to tumors of patients with lung cancer. *Nat. Med.* 2: 985-991.
- Clayman, C. L., et al. (1998). Adenovirus-mediated p53 gene transfer in patients with advanced recurrent head and neck squamous cell carcinoma. *J. Clin. Oncol.* 16: 2221-2232.
- Nabel, C. J., et al. (1993). Direct gene transfer with DNA-liposome complexes in melanoma: expression, biologic activity, and lack of toxicity in humans. *Proc. Natl. Acad. Sci. USA* 90: 11302-11311.
- Hung, M. C., Wang, S. C., and Homobaghi, G. (1999). Targeted HER-2/neu-overexpressing cancer cells with transcriptional repressor genes delivered by cationic liposome. In *Non Viral Vectors for Gene Therapy* (L. Huang, M. C. Hung, and E. Wagner, Eds.), pp. 352-372. Academic Press, San Diego.
- Nemunaitis, J., et al. (2000). Adenovirus-mediated p53 gene transfer in sequence with cisplatin to tumors of patients with non-small-cell lung cancer. *J. Clin. Oncol.* 18: 609-622.
- Templeton, N. S., et al. (1997). Improved DNA: liposome complexes for increased systemic delivery and gene expression. *Nat. Biotechnol.* 15: 647-652.
- Kurane, S., et al. (1998). Targeted gene transfer of adenocarcinoma using a combination of tumor-specific antibody and tissue-specific promoter. *Jpn. J. Cancer Res.* 89: 1213-1219.
- Kumtori, M., et al. (2000). Selective inhibition of hepatoma cells using diphtheria toxin A under the control of the promoter/enhancer region of the human alpha-fetoprotein gene. *Jpn. J. Cancer Res.* 91: 343-350.
- Chen, L., et al. (1998). Targeted in vivo delivery of therapeutic gene into experimental squamous cell carcinomas using anti-epidermal growth factor receptor antibody: immunogenic approach. *Hum. Gene Ther.* 9: 2673-2681.
- Park, J. W., et al. (1995). Development of anti-p185HER2 immuno-liposomes for cancer therapy. *Proc. Natl. Acad. Sci. USA* 92: 1327-1331.
- Hara, T., et al. (1995). Receptor-mediated transfer of pSV2CAT DNA to mouse liver cells using asialofetuin-labeled liposome. *Gene Ther.* 2: 784-788.
- Lee, R. J., and Huang, L. (1996). Folate-targeted, anionic liposome-entrapped polylysine-condensed DNA for tumor cell-specific gene transfer. *J. Biol. Chem.* 271: 8481-8487.
- Xu, L., Prohlo, K. E., and Chang, L. H. (1997). Transferrin-liposome-mediated p53 sensitization of squamous cell carcinoma of the head and neck to radiation in vitro. *Hum. Gene Ther.* 8: 467-475.
- Woodie, M. C., et al. (1992). Versatility of lipid compositions showing prolonged circulation with sterically stabilized liposomes. *Biochim. Biophys. Acta* 1105: 193-200.

16. Marmigliani, K. L., et al. (2001). Effective targeting of solid tumors in patients with locally advanced cancers by radiolabeled pegylated liposomes. *Clin. Cancer Res.* 7: 243-254.
17. Li, S., et al. (1998). Characterization of cationic lipid-protamine-DNA (LPD) complexes for intravenous gene delivery. *Gene Ther.* 5: 930-937.
18. Li, S., et al. (1999). Effect of immune response on gene transfer to the lung via systemic administration of cationic liposome vectors. *Am. J. Physiol.* 276: L796-L804.
19. Ferreira, R. U., et al. (1996). Cationic lipids enhance cytokine and cell influx levels in the lung following administration of plasmid-cationic lipid complexes. *J. Immunol.* 156: 4580-4586.
20. Yan, Y., et al. (1996). The inhibitory role of CpG immunostimulatory motifs in cationic lipid vector-mediated transgene expression *in vivo*. *Hum. Gene Ther.* 10: 2153-2161.
21. Olson, S. W., et al. (1999). Lipid-DNA complexes induce potent activation of innate immune responses and antitumor activity when administered intravenously. *J. Immunol.* 163: 1332-1341.
22. Qin, L., et al. (1999). Promoter attenuation in gene therapy: interferon-gamma and tumor necrosis factor alpha inhibit transgene expression. *Hum. Gene Ther.* 8: 2019-2029.
23. Yang, Y., et al. (1997). Characterization of cationic liposome-mediated gene transfer *in vivo* by intravenous administration. *Hum. Gene Ther.* 8: 1565-1594.
24. Nakagami, T., et al. (2001). Successful treatment of primary and disseminated human lung cancers by systemic delivery of tumor suppressor genes using an improved cationic vector. *Mol. Ther.* 3: 332-350, doi:10.1006/mthe.2001.0266.
25. Muehle, J. C., et al. (1991). Characterization of cells obtained by mechanical and enzymatic means from human melanoma, sarcoma and lung tumors. *Cancer Res.* 51: 1618-1624.
26. Caenazzo, K. M. L., et al. (1999). Fetal gene transfer by transabdominal injection of cationic liposome-DNA complexes. *Nat. Biotechnol.* 17: 1188-1192.
27. Sporn, C. B., et al. (1998). A fluorescent cholesterol analog traces cholesterol absorption: A pathway and is essential *in vivo* and *in vitro*. *J. Lipid Res.* 39: 1747-1757.
28. Kram, H., Johnson, L. C., Randall, S. H., and Boucher, R. C. (1997). Loss of binding and entry of liposome-DNA complexes decreases transfection efficiency in differentiated alveolar epithelial cells. *J. Biol. Chem.* 272: 11110-11126.
29. Masary, M. A., Hard, T. J., and Corbett, J. A. (2000). Adoptive transfer of acute lung injury. *Am. J. Physiol Lung Cell Mol Physiol* 279: R85-R91.
30. Lachy, S., et al. (1994). Increased gene expression after liposome-mediated arterial gene transfer associated with intimal smooth muscle cell proliferation: *in vitro* and *in vivo* findings in a rabbit model of vascular injury. *J. Clin. Invest.* 93: 652-661.
31. Schramova, J., et al. (1997). Electron microscopic demonstration of the interaction of liposomes and cells *in vitro*. *Biol. Mem.* 43: 761-767.
32. Moller, S. B., et al. (2000). Controlled release of doxorubicin from polyacrylate-co-glycolize microspheres significantly enhances cytotoxicity against cultured AIDS-related Kaposi's sarcoma cells. *Anticancer Res.* 20: 2817-2825.
33. Friend, D. S., Papahadjopoulos, D., and Dees, R. J. (1986). Endocytosis and intracellular processing accompanying transfection mediated by cationic liposome. *Biochem. Biophys. Acta* 1278: 41-50.
34. Chu, Q., et al. (1999). Binding and uptake of cationic lipid: DNA complexes by polarized airway epithelial cells. *Hum. Gene Ther.* 10: 25-36.
35. Barry, M. E., et al. (1999). Role of endogenous endonucleases and tissue site in transfection and CpG-mediated immune activation after naked DNA injection. *Hum. Gene Ther.* 10: 2461-2480.
36. Zabner, J., et al. (1993). Cellular and molecular barriers to gene transfer by a cationic lipid. *J. Biol. Chem.* 268: 18997-19007.
37. King, C. A., and Preston, T. M. (1977). Fluoresceinated cationized ferritin as a membrane probe for anionic sites at the cell surface. *FEBS Lett.* 73: 59-63.
38. Williams, M. C. (1984). Endocytosis in alveolar type II cells: effect of charge and size of tracers. *Proc. Natl. Acad. Sci. USA* 81: 6054-6058.
39. Ryser, H., Caulfield, J. B., and Aub, J. C. (1982). Studies on protein uptake by isolated tumor cells. *J. Cell Biol.* 14: 255-268.
40. Amis, R., et al. (2000). Cationic lipid-based delivery system for systemic cancer gene therapy. *Cancer Gene Ther.* 7: 1156-1164.
41. Thurston, G., et al. (1998). Cationic liposomes target angiogenic endothelial cells in tumors and chronic inflammation in mice. *J. Clin. Invest.* 101: 1401-1413.
42. Binslie, R., Thamm, D., MacIver, C., and Dow, S. (2001). Inhibition of tumor angiogenesis by systemic gene delivery in dogs with soft tissue sarcomas. *Proc. Am. Assoc. Cancer Res.* 42: 204 [Abstract].
43. Liu, Y., et al. (1999). Systemic gene delivery expands the repertoire of effective anti-angiogenic agents. *J. Biol. Chem.* 274: 13338-13344.
44. McLean, I. W., Thurston, G., and McDonald, D. M. (1999). Sites of uptake and expression of cationic liposome/DNA complexes injected intravenously. In *Non Viral Vectors for Gene Therapy* (L. Huang, M. C. Hung, and E. Wagner, Eds.), pp. 119-135. Academic Press, San Diego.
45. Liu, Y., et al. (1997). Factors influencing the efficiency of cationic liposome-mediated intravenous gene delivery. *Nat. Biotechnol.* 15: 167-173.
46. Satomayor, E. M., et al. (1991). Role of tumor-derived cytokines on the immune system of mice bearing a mammary adenocarcinoma. *J. Immunol.* 147: 2816-2823.
47. Lopez, D. M., et al. (1996). Cytokine production by lymphoreticular cells from mammary tumor bearing mice: the role of tumor derived factors. *Anticancer Res.* 16: 3923-3930.
48. Satomayor, E. M., et al. (1993). Impaired activation of tumoricidal function in macrophages from mammary tumor bearers: the role of IFN- γ . *Int. J. Oncol.* 3: 719-727.

Nanoparticle Based Systemic Gene Therapy for Lung Cancer: Molecular Mechanisms and Strategies to Suppress Nanoparticle-Mediated Inflammatory Response

www.tcrn.org

Began Gopalan, Ph.D.¹
Isao Ito, M.D.¹
Cynthia D. Branch, B.S.¹
Clifton Stephens, D.V.M.²
Jack A. Roth, M.D.¹
Rajagopal Ramesh, Ph.D.^{1*}

Cancer gene therapy for the treatment of lung cancer has shown promise in the laboratory and in Phase I/II clinical trials. However, it is currently limited to treating localized tumors due to host-immunity against the gene delivery vector and the transgene. Therefore, there is a tremendous effort to develop and test alternate gene delivery vectors that are efficient, non-immunogenic, and applicable for systemic therapy. One such gene delivery vehicle is the non-viral vector DOTAP-cholesterol (DOTAP:Chol) nanoparticle. Preclinical studies from our laboratory has shown that DOTAP:Chol nanoparticles are effective systemic gene delivery vectors that efficiently deliver tumor-suppressor genes to disseminated lung tumors. Based on our findings we have recently initiated a Phase-I trial for systemic treatment of lung cancer using a novel tumor suppressor gene, *FUS1*. Although DOTAP:Chol nanoparticles complexed to DNA (DNA-nanoparticles) are efficient vectors for systemic therapy induction of an inflammatory response in a dose-dependent fashion has also been observed thereby limiting its use. A better understanding of the underlying mechanism for DNA-nanoparticles-mediated inflammatory response will allow us to develop strategies to suppress inflammation and expand the therapeutic window in treating human cancer.

In the present study we conducted experiments examining the mechanism of nanoparticle-mediated inflammatory response *in vitro* and *in vivo*. We demonstrate that systemic administration of DNA-nanoparticles induced multiple signaling molecules both *in vitro* and *in vivo* that are associated with inflammation. Use of small molecule inhibitors against the signaling molecules resulted in their suppression and thereby reduced inflammation without affecting transgene expression. Our results provide a rationale to use small molecule inhibitors to suppress nanoparticle-mediated inflammation when administered systemically. Further development and testing will allow us to incorporate this strategy into future clinical trials that is based on systemic non-viral vector gene therapy.

Key words: Gene therapy, Systemic, Nanoparticle, Inflammation, Naproxen, Cytokines.

Introduction

Lung cancer is one of the leading causes of death in the world (1). Despite recent advances in treatment strategies, drug resistance, loco-regional and dis-

¹Department of Thoracic and Cardiovascular Surgery

²Department of Veterinary Medicine and Surgery

The University of Texas

M. D. Anderson Cancer Center

1515 Holcombe Blvd., Box 445

Houston, TX 77030 USA

* Corresponding Author:
Rajagopal Ramesh, Ph.D.
Email: ramesh@mdanderson.org

Abbreviations: DOTAP, Diethyl oleyl-1,2-bis (oleoyloxy)-3-(trimethyl ammonio) propane; Chol, Cholesterol; PG- E_2 , Prostaglandin E_2 ; COX-2, Cyclooxygenase; MAPK, Mitogen activated protein kinase; TNF, Tumor necrosis factor; IL, Interleukin; NF κ B, Nuclear factor kappa-B; AP-1, Activator protein 1.

can failure and poor response to therapy contribute to a low overall 5-year survival rate for common epithelial cancers, including lung cancer (1). Therefore, novel forms of therapy are urgently needed. Gene transfer strategies with the tumor suppressor gene *p53* have shown clinical promise in Phase I/II trials for non-small cell lung cancer and head and neck squamous cell carcinoma (2-6). However, this strategy has been limited to loco-regional treatment because of adenovirus-mediated toxicity and immune responses associated with systemic delivery (7, 8). An alternate to adenoviral vector system is to use non-viral gene delivery systems, which have been shown to be effective in delivering therapeutic genes to cancer sites when administered systemically (10-17). The advantage of using non-viral vector systems is that they are easy to manufacture and less immunogenic (18). Furthermore, it is feasible to develop non-viral vectors that target the tumor or tumor vasculature specifically. The best strategy one could envision for lung cancer treatment is a vehicle that systemically delivers a therapeutic agent to the primary tumor site and to distant metastatic sites without undue toxicity.

A non-viral vector that has been shown to efficiently deliver genes to the lungs when administered intravenously is the cationic DOTAP:cholesterol (DOTAP:Chol) nanoparticle (10, 11). Based on these reports we have tested DOTAP:Chol nanoparticles as a gene-delivery vehicle for treatment of lung cancer. Preclinical efficacy studies from our laboratory demonstrated intravenous injection of DOTAP:Chol nanoparticles containing therapeutic genes (*p53* or *mda-7*-nanoparticles) in mice bearing experimental lung metastasis resulted in effective transgene expression in the tumors leading to a significant therapeutic effect (12, 19). Furthermore, intravenous administration of plasmid DNA containing nanoparticles resulted in increased transgene expression in the lung tumors compared to the surrounding normal lung tissue that resulted in an increased therapeutic effect (20). Increased transgene expression in the tumors was due to increased and selective uptake of the nanoparticles by the tumors in the lungs compared to the surrounding normal tissue (20). In a more recent study we have demonstrated the tumor suppressive effect of a novel 3p gene, *FUS1*, on disseminated lung tumors when injected intravenously (21, 22). These results suggest systemic delivery of therapeutic genes (*p53*, *Flk1*, *FUS1*, *mda-7*) to disseminated tumors is feasible using DOTAP:Chol nanoparticles. Based on our results, we have recently initiated a Phase-I clinical trial for systemic treatment of lung cancer using the *FUS1* tumor suppressor gene complexed with DOTAP:Chol nanoparticles.

Although DOTAP:Chol nanoparticles have been shown to be an effective systemic gene delivery vehicle, induction of an inflammatory response in a dose-dependent fashion has also been observed resulting in toxicity (Ramesh *et al.*,

unpublished data). Induction of inflammatory response following systemic administration of DOTAP:Chol-DNA nanoparticles is not surprising. Induction of an inflammatory response has previously been reported using other non-viral vectors (23-29). Thus, the therapeutic window for DOTAP:Chol nanoparticle based systemic gene therapy for cancer will be limited. Therefore, a better understanding of the mechanism of DNA-nanoparticle-mediated inflammatory response will enable us to develop strategies to overcome this limitation and thereby increase the therapeutic window to deliver higher doses of the therapeutic gene.

Recent studies have demonstrated immunostimulatory CpG motifs present in the plasmid DNA to play a major role in lipoplex-mediated inflammation. Reducing the number of CpG sequences in the plasmid DNA has been shown to reduce the inflammatory response and increase transgene expression (30, 31). Additional strategies tested to overcome the inflammatory response include the use of PCR-amplified DNA fragments instead of full-length pDNA (32) and the use of immunosuppressant (33). All of these strategies have shown improvements in reducing inflammation. However, they have not been able to completely suppress or eliminate the inflammatory response. Furthermore, some of the strategies have not been feasible in a clinical setting. Therefore, additional strategies are warranted. A better understanding of the underlying mechanism for DNA-nanoparticles-mediated inflammatory response will allow us to develop effective strategies to suppress inflammation and expand the therapeutic window in treating human cancer.

In the present study we conducted experiments examining the mechanism of nanoparticles-mediated inflammatory response *in vitro* and *in vivo*. We demonstrate that systemic administration of DNA-nanoparticles induced multiple signaling molecules both *in vitro* and *in vivo* that are associated with inflammation. Furthermore, use of small molecule inhibitors targeted against the signaling molecules resulted in their suppression and thereby reduced inflammation without affecting transgene expression. Our results provide a rationale to use small molecule inhibitors to suppress DNA-nanoparticles-mediated inflammation when administered systemically. Further development and testing will allow us to incorporate this strategy into future clinical trials that are based on systemic non-viral gene therapy.

Materials and Methods

Materials

All lipids (DOTAP, Cholesterol) were purchased from Avanti Polar Lipids (Alabaster, AL). Naproxen for tissue culture experiments was purchased from Sigma Chemicals (St. Louis, MO). Clinical grade Naproxen for *in vivo* stud-

was purchased from Pharmacy at M. D. Anderson Cancer Center (Houston, TX). U0126 and SB203580 were purchased from Calbiochem (San Diego, CA). Antibodies against phosphorylated p38MAPK, pJNK, p44/42MAPK, pATF2, and p-c-Jun were purchased from Cell Signaling (Cambridge, MA). Anti-COX-2 antibody was purchased from Cayman Chemicals (Ann Arbor, MI).

Cells and Culture Methods

Human fibroblast (MRC-9) cell line was purchased from American Tissue Culture Collection (Rockville, MD). Cells were maintained in the appropriate medium as recommended by the supplier. Cells were regularly passaged and maintained at 37 °C in humidified atmosphere with 5% CO₂.

Animals

Four to six-week-old female C3H/NCr mice (National Cancer Institute, Frederick, MD) used in the study were maintained in a pathogen-free environment and handled according to institutional guidelines established for animal care and use.

Preparation of DNA-nanoparticles

Synthesis and preparation of DOTAP:Chol. nanoparticles carrying the *FUS1* gene (*FUS1*-nanoparticles) was carried out as previously described (12). Freshly prepared *FUS1*-nanoparticles were used in each experiment described in the present study. Particle size analysis showed the *FUS1*-nanoparticles were 300–350 nm in size.

In Vitro Experiments

To determine the effect of *FUS1*-nanoparticles on the activation of signaling molecules associated with inflammation, MRC-9 fibroblast cells were seeded in six-well plates (5×10^5 cells/well) and incubated overnight at 37 °C and 5% CO₂. The following day, tissue culture medium was replaced with fresh medium and cells were either not treated or treated with various concentrations of SB203580 (p38MAPK inhibitor; 10, and 30 μ M), U0126 (p44/42 MAPK inhibitor; 10, 30 μ M), or with Naproxen (COX-2 inhibitor; 0.5mM). Two-three hours after treatment, cells were transfected with *FUS1*-nanoparticles (2.5 μ g DNA) in 0.2% serum medium. Cells were harvested at different time-points (2h, 4h, 15h) after transfection, washed, and cell lysates prepared as previously described (12). Untransfected cells treated with PBS served as control in these experiments. Cell lysates were subjected to western blotting analysis and probed with various antibodies as previously described (19, 20). In all the experiments, β -actin was detected using anti- β -actin antibody (Sigma Chemicals, St. Louis, MO) as a measure of internal loading control.

To determine the effect of inhibitors on transgene expression, cells were transfected with a marker gene, luciferase (*luc*), complexed with DOTAP:Chol. nanoparticles (*luc*-nanoparticles). All other experimental conditions were the same as described above. Luciferase expression was determined using the luciferase assay kit (Promega, Madison, WI) as previously described (19). Luciferase expression was expressed as relative light units per mg of protein (RLU/mg). Assays were performed in triplicates. Experiments were performed two times and the results represented as the average of two separate experiments.

Electrophoretic Mobility Shift Assay (EMSA)

MRC-9 cells were seeded in six well plates at 1.3×10^6 cells/well for EMSA. The following day cells were replaced with 0.2% serum medium and then preincubated for 3 h in the absence or presence of naproxen before the cells were transfected with *FUS1*-nanoparticles (2.5 μ g DNA). Cells were harvested at 2, 4 and 15h after transfection and nuclear extracts prepared. To the nuclear extracts (10 μ g), DNA binding reaction mixture containing [γ -³²P]-ATP radiolabeled AP-1 oligonucleotide and 0.5 μ g poly (dI-dC) were added and incubated at 25 °C for 30 min in 5X gel shift binding buffer [20% glycerol, 5mM MgCl₂, 2.5mM EDTA, 2.5 mM DTT, 250mM NaCl, 50mM Tris-HCl (pH 7.5)]. The complexes were subsequently resolved on 5% nondenaturing polyacrylamide gels in 0.5 \times Tris-borate EDTA buffer for 1h 30 min at 300 V. The bands were visualized by autoradiography.

PGE₂ Production Assay

Cells were seeded in 6-well plates ($1-3 \times 10^6$ cells/well) and incubated at 37 °C. Twenty-four hours later, the culture medium was replaced and replenished with fresh medium supplemented with 0.2% serum. Cells were then either not treated or treated with naproxen (0.5mM). At 3.5 h after treatment cells were transfected with *FUS1*-nanoparticles (2.5 μ g DNA). The amount of PGE₂ secreted into the culture supernatant at various time (2h, 4h, and 15h) points was determined using the PGE₂ enzyme immunoassay (Cayman Chemicals, Ann Arbor, MI). Assay was performed according to manufacturer's protocol.

In Vivo Experiments

To determine the effect of intravenous administration of *FUS1*-nanoparticles on inflammation and the potential use of inhibitors, *in vivo* experiments were conducted in immunocompetent female C3H mice. Mice were divided into three groups (n=5/group). Group 1 did not receive any treatment. Group 2 received a single dose of naproxen (15 mg/Kg) orally 3h prior to intravenous injection of *FUS1*-nanoparticles. Group 3 received intravenous injection of

FUS1-nanoparticles only. The amount of plasmid DNA injected was 100 μ g. The rationale for selecting this dose was based on our previous results which showed that 100 μ g of *FUS1* plasmid DNA produced acute inflammation that was lethal resulting in 100% mortality (Gopalan *et al.*, unpublished data). The procedure for intravenous injections of DNA containing nanoparticles has previously been reported (12, 19, 20). At 2h, 4h, 6h and 15h after treatment with *FUS1*-nanoparticles, animals were euthanized and blood and organs (lung, liver, spleen) collected. Blood samples were analyzed for mouse TNF- α by ELISA (R&D Systems, MI). Tissue samples were analyzed for expression of inflammation-associated signaling molecules by western blotting (20).

Results

FUS1 nanoparticles Induces Inflammation-associated Signaling Molecules In Vitro

To test whether *FUS1*-nanoparticles can induce inflammation-associated signaling molecules and whose expression small molecule inhibitors, can suppress, we first conducted *in vitro* experiments. Transfection of MRC-9 cells with *FUS1*-nanoparticles resulted in a significant increase in the expression of p38MAPK, pJNK, p44/42MAPK, and its downstream substrates pATF-2, pc-Jun, and COX-2 compared to untreated control cells (Fig. 1). The activation of various inflammation-associated signaling molecules indicate the ability of *FUS1*-nanoparticles to induce an inflammatory response.

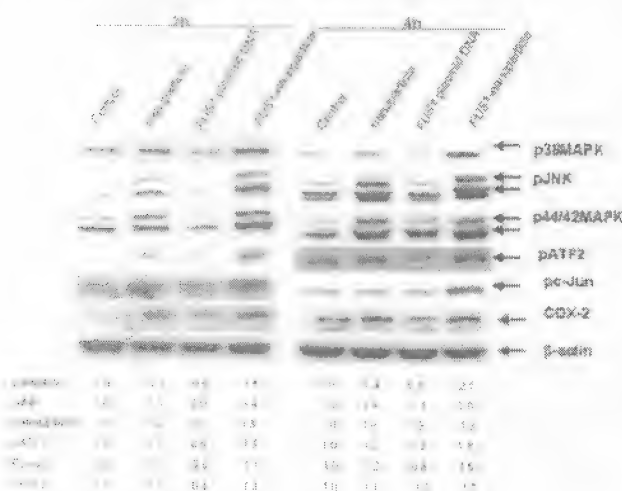


Figure 1. *FUS1*-nanoparticle-mediated induction of inflammation-associated signaling molecules. MRC-9 cells were transfected with empty nanoparticles, naked plasmid DNA or *FUS1*-nanoparticles and analyzed for inflammation-associated signaling molecules by western blotting at 2h and 4h after transfection. Cells that did not receive any treatment served as negative control. β -actin was detected as internal loading controls. The expression levels were determined by densitometry and the values determined with β -actin value set to 1.

Small Molecule Inhibitors Suppress Inflammation-associated Signaling Molecules Induced by *FUS1*-nanoparticles

The ability of *FUS1*-nanoparticles to induce inflammation-associated signaling molecules *in vitro* suggested its potential limitation *in vivo*. Therefore we tested the ability of small molecule inhibitors to inhibit inflammation-associated signaling molecules induced by *FUS1*-nanoparticles. For this purpose we tested inhibitors specifically targeted towards p38MAPK (SB 203580), p44/42 MAPK (U0126) or COX-2 inhibitor (Naproxen). Treatment of cells with various doses of SB 203580 prior to transfection with *FUS1*-nanoparticles resulted in a marked suppression of p38 MAPK expression and its downstream substrates, pATF-2, pc-Jun, and COX-2 compared to cells that were only transfected with *FUS1*-nanoparticles (Fig. 2A). The inhibitory effect was observed to be time-dependent and not dose-dependent. Baseline p38MAPK expression was observed in untreated control cells. Similarly, treatment of cells with U0126 resulted in a significant inhibition in p44/42 MAPK expression and its downstream substrates compared to cells that did not receive any treatment and cells that were transfected with *FUS1*-nanoparticles only (Fig. 2B). The inhibitory activity exerted by U0126 was neither time-nor dose-dependent. p44/42MAPK expression levels were decreased more than the baseline expression seen in untreated control cells. These results suggest that p38MAPK and p44/42MAPK can be effectively inhibited using inhibitors targeted towards these molecules.

The effect of naproxen, a non-steroidal anti-inflammatory small molecule targeted to COX-2 was next investigated. Treatment of cells with naproxen prior to transfection with *FUS1*-nanoparticles resulted in a significant inhibition of various MAPK that included p38MAPK, pJNK, and p44/42MAPK compared to cells that were transfected with *FUS1*-nanoparticles only (Fig. 2C). The inhibitory effect on various MAPK correlated with decreased expression of their downstream substrates, pATF-2, pc-Jun and COX-2. Additionally the inhibitory effect on MAPK expression appeared to increase over time. Baseline expression of p38MAPK, pJNK, and p44/42MAPK was observed in untreated control cells. These results demonstrate that naproxen in addition to inhibiting COX-2 also inhibited all three kinases that are associated with inflammation. Thus naproxen appears to function as a broad-spectrum inhibitor inhibiting multiple signaling molecules. Furthermore, based on its ability to function as a broad-spectrum inhibitor we speculated that naproxen would be more effective than SB 203580 and U0126 *in vivo*. Hence, in all subsequent experiments we tested naproxen.

FUS1-nanoparticle-mediated Activation of AP-1 is Inhibited by Naproxen

Recent studies have demonstrated activation of p38MAPK by CpG containing DNA leads to the activation of transcription

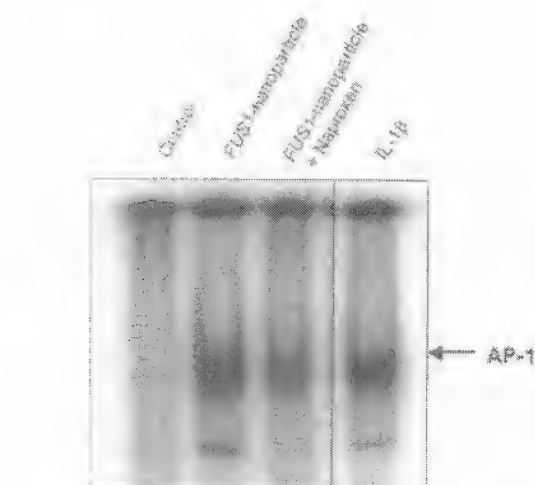
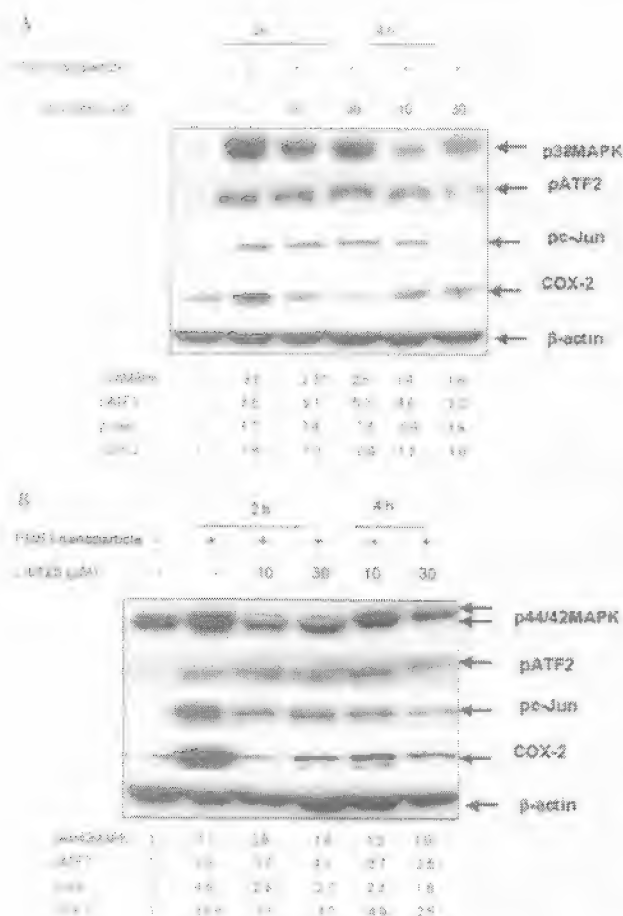


Figure 3: *FUS1*-nanoparticle-mediated activation of AP-1 is inhibited by naproxen. MRC-9 fibroblast cells were not treated or treated with naproxen (0.5 nM), prior to transfection with *FUS1*-nanoparticles. Cells not receiving any treatment served as control. At 2h after transfection cells were harvested, nuclear extracts prepared, and AP-1 binding activity using consensus oligonucleotide probe was determined by EMSA. Untreated cells served as control in these experiments.

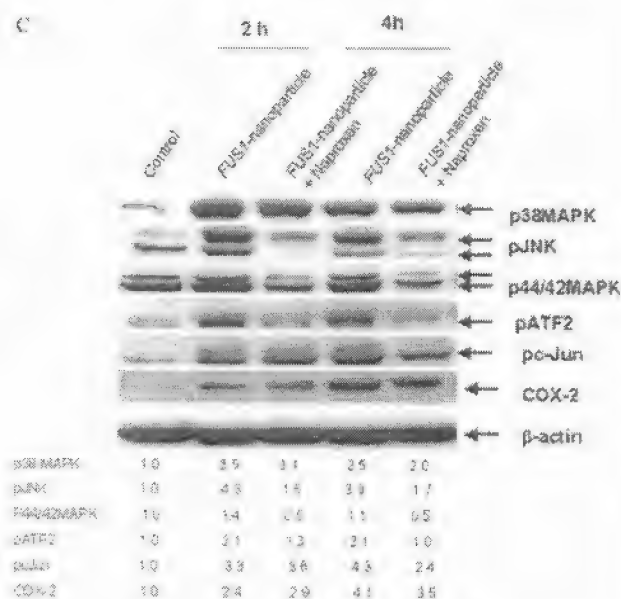


Figure 2: Suppression of *FUS1*-nanoparticle induced inflammation-associated signaling molecules by small molecule inhibitors. Cells pretreated with various concentrations of A. p38MAPK inhibitor, SB 303580; B. p44/42MAPK inhibitor, U0126; and C. COX-2 inhibitor, naproxen were transfected with *FUS1*-nanoparticles. At 2h and 4h after transfection cells were harvested and analyzed for signaling molecules by western blot analysis. β -actin was detected as internal loading controls. The expression levels were determined by densitometry and the values determined with control value set to 1.

factor CREB/AP-1, that is an important mediator of inflammation (34). Presence of consensus AP-1 DNA binding site in the promoter region of several genes including COX-2 has been reported (34). Based on these reports and ability of *FUS1*-nanoparticles to induce COX-2 expression we speculated activation of AP-1 and that pretreatment with naproxen will result in reduced AP-1 DNA binding activity. Therefore to test this possibility, cells treated with *FUS1*-nanoparticles in the presence or absence of naproxen were analyzed for AP-1 DNA binding activity by electro-mobility shift assay (EMSA). Untreated cells served as control in these experiments. Increased AP-1 activity was observed in *FUS1*-nanoparticles transfected cells compared to untreated control cells (Fig. 3). In contrast, treatment with naproxen resulted in inhibition of AP-1 activity. Our data shows *FUS1*-nanoparticle treatment results in activation of AP-1 that is inhibited by naproxen. Furthermore, AP-1 activation correlated with the activation of MAPK molecules that are upstream to these transcriptional factors. Correlation was also observed with the activation of COX-2 that is downstream of AP-1.

FUS1-nanoparticle Induced PGE₂ Production is Inhibited by Naproxen

PGE₂ is a substrate for COX-2. Activation of COX-2 results in breakdown of PGE₂ into its metabolites that are potent

inducers of inflammation (35, 36). Since naproxen inhibited lipoplex-induced COX-2 expression, we tested whether PGE₂ production is also inhibited. To test this possibility secreted PGE₂ levels were measured in the tissue culture medium growing cells that were transfected with *FUS1*-nanoparticles in the presence or absence of naproxen. PGE₂ expression levels were determined by ELISA. As shown in Figure 4, treatment of cells with *FUS1*-nanoparticles resulted in a time-dependent increase in the secreted PGE₂ levels (2000-4000 pg/ml) compared to the basal level in untreated control cells (10 pg/ml). However, pretreatment of cells with naproxen prior to transfection with *FUS1*-nanoparticles resulted in a significant inhibition of PGE₂ (33-120 pg/ml; $P = <0.001$). In fact the inhibition was almost complete starting from 2h after transfection. Similar results were also obtained from murine macrophage cell line (RAW 264.7; data not shown). These results demonstrate the ability to naproxen to effectively inhibit both COX-2 expression and its substrate PGE₂ that are important mediators of inflammation.

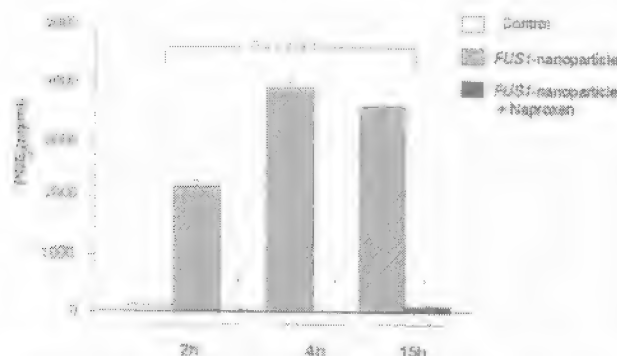


Figure 4: Inhibition of *FUS1*-nanoparticles induced PGE₂ production by naproxen. Cells were either not treated or treated with naproxen (0.5 mM) prior to transfection with *FUS1*-nanoparticles (2.5µg DNA). Tissue culture supernatant was collected at various time points and analyzed for PGE₂ concentration using a PGE₂ enzyme immunoassay kit. A significantly inhibition in PGE₂ levels were observed in naproxen treated cells compared to cells that were not treated with naproxen. Naproxen inhibited PGE₂ levels at all time points tested. Data is represented as the average of triplicate wells. Bars denote standard error.

Nanoparticle-mediated Transgene Expression Is Not Affected by Naproxen

Although suppression of nanoparticle-mediated signaling molecules was demonstrated, one question that remains unanswered are the effects of the inhibitors on transgene expression. The possibility that the inhibitors can also suppress transgene expression existed. Furthermore, previous studies have shown that inflammatory cytokines inhibit transgene expression (37). Therefore we investigated the effect of naproxen treatment on transgene expression using luciferase as a marker gene. Luciferase expression was observed at 15h in both cells that were transfected with *luc*-nanoparticles containing naproxen and in cells that were transfected with

luc-nanoparticles and not treated with naproxen (Fig. 5; $P = <0.001$). Furthermore, luciferase expression was greatly increased in naproxen treated cells compared to cells that were not treated with naproxen. No luciferase expression was observed in cells that were untreated (control) or treated with empty nanoparticles. Enhanced transgene expression was also observed in lung tumor cells that were transfected with *luc*-nanoparticles in the presence of naproxen (data not shown). Thus, naproxen treatment results in selective inhibition of signaling molecules associated with inflammation without affecting transgene expression.

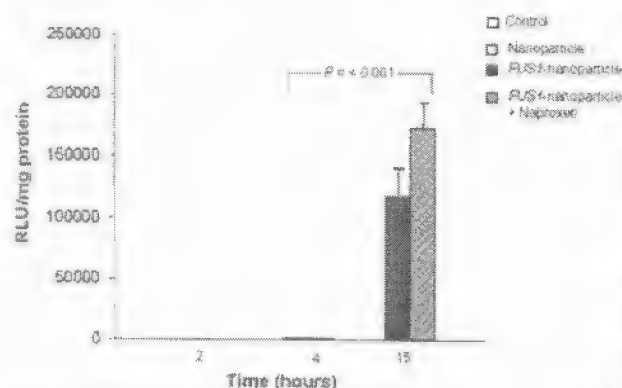


Figure 5: Naproxen does not affect transgene expression. Cells were either not treated or treated with naproxen prior to transfection with *luc*-nanoparticles. At 2h, 4h, and 15h after transfection cell lysates were prepared and assayed for luciferase activity. Luciferase activity was observed in both naproxen treated and untreated cells. However, a slight increase in luciferase activity was observed in naproxen treated cells. Luciferase activity was expressed as relative light units per milligram of protein (RLU/mg protein). Results are represented as the average of triplicates. Error bar denotes standard error.

FUS1-nanoparticles-induced Inflammatory Response Is Suppressed by Naproxen In Vivo

Preliminary studies from our laboratory demonstrated showed that intravenous injection of *FUS1*-nanoparticles resulted in the induction of an inflammatory response that was dose-dependent. Injection of 100µg of *FUS1* plasmid DNA complexed to DOTAP:Chol. nanoparticles resulted in acute inflammatory response resulting in 100% mortality (Gopalan et al., unpublished data). Based these observations we tested whether pretreatment of animals with naproxen prior to intravenous injection of a lethal dose of *FUS1*-nanoparticles would suppress the acute inflammatory response. Suppression of inflammation by naproxen was determined by measuring TNF-α, a key mediator of inflammation (38), and by analyzing the lung tissues for the inflammation-associated signaling molecules at various (2h, 4h, 15h) time points after treatment.

Analysis for TNF-α in the blood of animals that were injected with *FUS1*-nanoparticles showed maximum TNF-α

expression levels at 2h (873 pg/ml) and decreased over time (Fig. 6A; $P = <0.04$). In contrast, the TNF- α expression levels was reduced by half at 2h (411 pg/ml) in animals that were pretreated with naproxen prior to injection of *FUS1*-nanoparticles. Reduced TNF- α in naproxen treated animals was also observed at all time points tested. These results showed that naproxen suppressed *FUS1*-nanoparticles induced TNF- α .

We next tested for the expression of inflammation-associated signaling molecules in the lung tissues of mice that were either treated with naproxen or not treated with naproxen. As observed in our *in vitro* experiments, a marked activation of p38MAPK, pJNK, p44/42MAPK and their downstream substrates pATF2, pc-JUN, and COX-2 was observed in the lung of mice that were intravenously injected with *FUS1*-nanoparticles compared to the lungs of control mice that did not receive any treatment (Fig. 6B). Activation of the signaling molecules was observed at all time points tested with maximum activation occurring at 2h that correlated with TNF- α production. However, activation of the various signaling molecules was markedly suppressed in the lungs of mice that were treated with naproxen prior to receiving *FUS1*-nanoparticles. Suppression of activation of signaling molecules by naproxen was observed as early as 2h after *FUS1*-nanoparticles treatment. The inhibitory activity of naproxen on the activation of signaling molecules correlated with its inhibitory activity on TNF- α . Our results show that naproxen inhibits TNF- α production by inhibiting various signaling molecules that are associated with its induction.

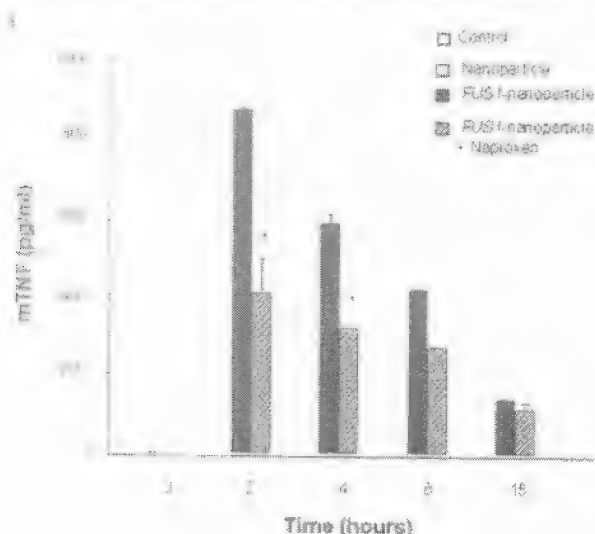
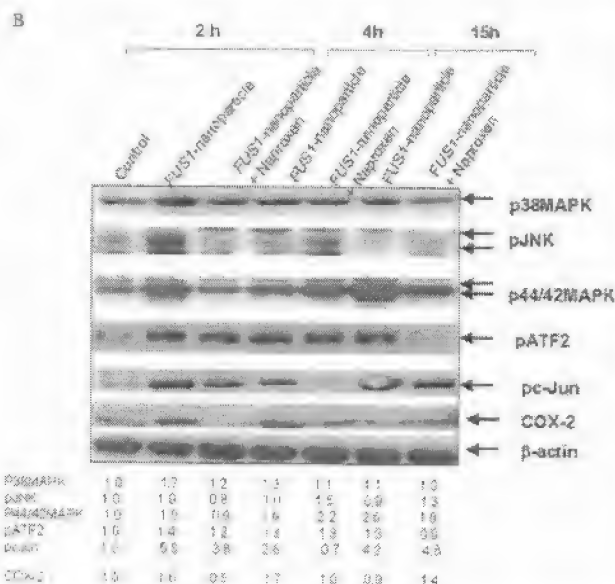


Figure 6: *FUS1*-nanoparticles induced inflammatory response is inhibited by naproxen *in vivo*. Mice were divided into three groups and treated as follows: Group 1 received no treatment and served as control; Group 2 received an intravenous injection of *FUS1*-nanoparticles; Group 3 received an oral dose of naproxen (15mg/Kg) 3h prior to receiving an intravenous injection of *FUS1*-nanoparticles. Animals were euthanized at various time points and analyzed for TNF- α in the blood and signaling molecules in lung tissues. **A.** *FUS1*-nanoparticle-mediated TNF- α expression was

Discussion

We have previously demonstrated DOTAP:Chol. nanoparticles to be an efficient systemic gene delivery vehicle that effectively delivers therapeutic genes (*p53*, *Fhit*, *FUS1*, *mda-7*) to primary and disseminated lung tumors in mice resulting in a therapeutic effect (12, 19, 20). Furthermore, we have recently shown that tumors in the lung selectively uptake DOTAP:Chol-DNA nanoparticles compared to surrounding normal tissues resulting in increased transgene expression in the tumors (20). Based on the unique properties of DOTAP:Chol. nanoparticles and the results obtained in our preclinical studies, we have recently initiated a Phase-I clinical trial for systemic treatment of lung cancer with the *FUS1* tumor suppressor gene. However preclinical toxicity studies from our laboratory revealed dose-limiting toxicity for *FUS1*-nanoparticles (Ramesh *et al.*, unpublished data). Toxicity was associated with the induction of an acute inflammatory response. Induction of an inflammatory response following intravenous administration of DNA containing nanoparticles is not surprising and is in agreement with previous reports from other laboratories (25-30). However, our results also suggested the potential limitation of DOTAP:Chol-DNA nanoparticles for systemic therapy. Furthermore, it was also realized that the therapeutic window to observe a response in a clinical setting would be narrow. Thus if the doses required to achieve a therapeutic



markedly suppressed in Group 3 mice compared to TNF- α expression in Group 2 mice. Baseline TNF- α levels were observed in Group 1 mice. Bars denote standard error. **B.** inhibition of various inflammation-associated signaling molecules was observed in the lungs of Group 3 mice compared to the lungs from Group 2 mice. Baseline expression levels of the signaling molecules were observed in the lungs of Group 1 mice. The expression levels were determined by densitometry and the values determined with control value set to 1.

response were close or higher than the maximum tolerated dose (MTD) than it would not be possible to successfully treat patients and achieve a therapeutic response. We therefore explored strategies to overcome the existing limitation—induction of inflammatory response, thereby making DOTAP-Chol nanoparticles based systemic therapy feasible as well increasing the therapeutic window.

In order to overcome the existing limitation, we had to have a better understanding of the underlying mechanism responsible for nanoparticles-mediated inflammatory response. A role for p38MAPK, p44/42MAPK, and JNK in inflammation has previously been demonstrated (39-41). Based on these reports we first examined for these inflammation-associated signaling molecules after *FUS1*-nanoparticles treatment. *In vitro* experiments showed *FUS1*-nanoparticles activated MAPK's (p38, p44/42), JNK, and their substrates that included pATF and pc-Jun suggesting that these molecules may be participate in nanoparticle-mediated inflammation.

Although activation of MAPK's and their substrates was observed, they alone do not directly contribute to inflammation. One molecule that is frequently activated by these kinases is COX-2 resulting in PGE₂ production. Activation of COX-2 by MAPK's and JNK has been shown to depend on the cell type, stimuli, and species. Furthermore, each MAPK has a different regulatory role in COX-2 gene transcription. In macrophages activated by human herpesvirus 6, JNK has been shown to play a critical regulatory role in human COX-2 gene transcription (42). Similarly, a role for JNK in murine MC3T3-E1 osteogenic cells stimulated with TNF- α plus IL-1 β has been reported (43). Requirement of both ERK and JNK for COX-2 promoter activity induced by IgE receptor aggregation has been shown in mast cells (44) while a role for ERK1/2 and p38MAPK in regulating HSP60-induced COX-2 expression has been shown in macrophages and endothelial cells (45). Increased levels of COX-2 lead to production of PGE-2, a breakdown product of arachidonic acid. Elevated levels of COX-2, and PGE₂ have been reported in inflammation and its associated disease process (46, 47). Similarly, the presence of CpG motifs in the plasmid DNA has been shown to induce COX-2 expression and prostaglandin production contributing to the development of airway inflammation (48). In the present study we showed activation of both COX-2 and PGE₂ production after *FUS1*-nanoparticle treatment suggesting that they may play a role in nanoparticle-mediated inflammation. However, the kinase (p38MAPK, p44/42MAPK, and JNK) activating COX-2 and PGE₂ production is not clear since all three kinases were activated. We are currently investigating the role of individual kinase in the *FUS1*-nanoparticle-mediated inflammatory response.

Activation of COX-2 by MAPK's including ERK, JNK and p38MAPK have been shown to be mediated by AP-1 (49).

AP-1 is a potent transcriptional activation factor that can bind to the promoter region of several genes and activate their transcription. We therefore analyzed for AP-1 activation by EMSA. A significant activation of AP-1 was observed in *FUS1*-nanoparticle treated cells. Activation of AP-1 was observed as early as 2h that correlated with the activation of MAPK's and COX-2. Our results demonstrate that the molecular signaling pathway for *FUS1*-nanoparticle-mediated inflammatory response involves all three MAPKs (p38MAPK pJNK and ERK) leading to COX-2 and PGE-2 production via AP-1 activation. The possibility of NF κ B involvement, another transcriptional factor, was also examined. However, activation of NF κ B was not observed in lipoplex treated cells (data not shown). To our knowledge this is the first report detailing the pathways for nanoparticle-mediated inflammatory response.

Now that we have identified the signaling molecules associated with inflammation, we next investigated the potential use of small molecule inhibitors targeted towards p38MAPK (SB 203580), p44/42MAPK (U0126), and COX-2 (naproxen) thereby suppressing inflammation. *In vitro* experiments demonstrated that each of these inhibitors was able to significantly and selectively suppress activation of the target molecule when cells were pretreated prior to treatment with *FUS1*-nanoparticles. Furthermore, inhibition of activation of the target molecules resulted in the suppression of COX-2 expression. Additionally, treatment with the inhibitors did not affect the transgene expression. These exciting results raise the possibility of their potential use in suppressing nanoparticle-mediated inflammation via inhibition of COX-2, a downstream target common to the MAPK's. However, their use is limited to *in vitro* situations unless they are proven to be effective *in vivo*.

We next investigated whether *FUS1*-nanoparticle-mediated activation of signaling molecules observed *in vitro* is also activated *in vivo* and can be inhibited by small molecule inhibitors. For this purpose mice that were either not treated or treated with an oral dose of naproxen were subsequently injected with a lethal dose of *FUS1*-nanoparticles and analyzed for suppression of inflammation at various levels. Analysis for TNF- α , a proinflammatory cytokine produced following systemic administration of *FUS1*-nanoparticles was significantly suppressed in naproxen treated animals compared to animals that did not receive naproxen treatment. Molecular analysis of lung tissues for activation of signaling molecules that were identified in our *in vitro* experiments demonstrated activation of all of the markers (p38MAPK, p44/42MAPK, JNK, COX-2) in *FUS1*-nanoparticles treated animals. However, activation of these molecules was significantly inhibited by naproxen akin to our *in vitro* results. The suppression of activation of these various inflammation-associated signaling molecules by naproxen resulted in 100%

survival of animals receiving a lethal dose of *FUS1*-nanoparticles (Gopalan *et al.*, unpublished data). Furthermore, naproxen treatment did not inhibit *FUS1* protein expression *in vivo* but rather slightly enhanced the expression suggesting the possibility for enhanced therapeutic effect (data not shown). The ability of naproxen to inhibit COX-2 expression is expected and not surprising (50, 51). However, inhibition of MAPK's by naproxen observed in the present study was unexpected and surprising. Based on our results we speculate that naproxen in addition to its direct inhibitory activity on COX-2 also inhibits additional molecules such as MAPK's as shown in Figure 7. It will be interesting to test whether combination of naproxen with nanoparticles carrying a tumor suppressor gene such as *FUS1* will enhance the therapeutic effect. We are currently examining the mechanism by which naproxen inhibits MAPK's. Whatever the underlying mechanism of action by naproxen may be, our results clearly demonstrated that pretreatment of animals with naproxen prior to systemic administration of *FUS1*-nanoparticles results in suppression of nanoparticle-mediated inflammation leading to animal survival.

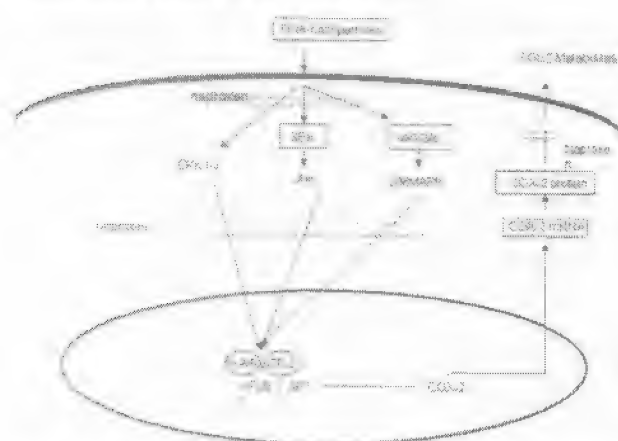


Figure 7. Schematic representation of the inflammation-associated signaling pathways induced by DNA-nanoparticle and potential targets for naproxen. Intravenous injection of plasmid DNA containing nanoparticles results in activation of the various signaling molecules leading to the activation of COX-2 that breaks down arachidonic acid into PGE₂ metabolites. Production of PGE₂ metabolites leads to inflammation. However, naproxen inhibits PGE₂ production by inhibiting COX-2. Additional potential inhibitory targets for naproxen include the MAPK's, NFκB and AP-1.

In conclusion we have demonstrated the signaling mechanism and strategies to suppress nanoparticle-mediated inflammatory response. Thus, use of small molecule inhibitors such as naproxen alone or in combination with other small molecule inhibitors prior to nanoparticle based systemic therapy will be of clinical significance both in terms of suppressing toxicity as well increasing the therapeutic window. However, additional preclinical studies related to toxicity, dosing, and therapeutic efficacy are warranted prior to incorporation of this strategy in future Phase I/II clinical trials.

Acknowledgments

The authors thank Dr. Lin Ji (M. D. Anderson Cancer Center) for providing the *FUS1* expressing plasmid vector; and Alma Vega for preparation of the manuscript. This work was supported in part by the Texas Higher Education Coordinating Board ATP/ARP Grant 003657-0078-2001 (R. R.), by a Career Development Award from The University of Texas M. D. Anderson Cancer Center SPORE in Lung Cancer P50-CA70907-5 (R. R.), by Public Health Service Grant P01CA78778-01A1 (J. A. R.), by the Texas Tobacco Settlement Fund, by the BESCT Lung Cancer Program Grant DAMD17-01-1-0689 (Project # 3), by the TARGET Lung Cancer Grant DAMD17-02-1-0706 (Project # 7), by the Institutional Research Grant (R. R.), by a Grant from the W. M. Keck Foundation (R. R.), by Cancer Center Support (CORE) Grant CA16672, grant, and by a sponsored research agreement with Introgen Therapeutics, Inc.

References

- Greenlee, R. T., Murray, T., Bolden, S., and Wingo, P. A. Cancer Statistics, 2000. *CA Cancer J. Clin.* 50, 7-26 (2000).
- Roth, J. A., Nguyen, D., Lawrence, D. D., Kemp, B. L., Carrasco, C. H., Person, D. Z., Hong, W. K., Komaki, R., Lee, J. J., Nesbitt, J. C., Pisters, K. M. W., Putnam, J. B., Jr., Schea, R., Shin, D. M., Walsh, G. L., Dolomente, M. M., Han, C. I., Martin, F. D., Yen, N., Xu, K., Stephens, L. C., McDonnell, T. J., Mukhopadhyay, T., and Cai, D. Retrovirus-mediated Wild-type p53 Gene Transfer to Tumors of Patients With Lung Cancer. *Nat. Med.* 2, 985-991 (1996).
- Swisher, S. G., Roth, J. A., Nemunaitis, J., Lawrence, D. D., Kemp, B. L., Carrasco, C. H., Connors, D. G., el Naggat, A. K., Fossella, F., Glisson, B. S., Hong, W. K., Khuri, F. R., Kurie, J. M., Lee, J. J., Lee, J. S., Mack, M., Merritt, J. A., Nguyen, D. M., Nesbitt, J. C., Perez-Soler, R., Pisters, K. M. W., Putnam, J. B., Jr., Richi, W. R., Sayin, M., Schump, D. S., Shin, D. M., Shufkin, A., Walsh, G. L., Wait, J., Weill, D., and Waugh, M. K. A. Adenovirus-mediated p53 Gene Transfer in Advanced Non-small Cell Lung Cancer. *J. Natl. Cancer Inst.* 91, 763-771 (1999).
- Nemunaitis, J., Swisher, S. G., Timmons, T., Connors, D., Mack, M., Doerksen, L., Weill, D., Wait, J., Lawrence, D. D., Kemp, B. L., Fossella, F., Glisson, B. S., Hong, W. K., Khuri, F. R., Kurie, J. M., Lee, J. J., Lee, J. S., Nguyen, D. M., Nesbitt, J. C., Perez-Soler, R., Pisters, K. M. W., Putnam, J. B., Richi, W. R., Shin, D. M., Walsh, G. L., Merritt, J., and Roth, J. A. Adenovirus-mediated p53 Gene Transfer in Sequence with Cisplatin to Tumors of Patients with Non-small Cell Lung Cancer. *J. Clin. Oncol.* 18, 609-622 (2000).
- Clayman, G. L., El-Naggat, A. K., Lippman, S. M., Henderson, Y. C., Frederick, M., Merritt, J. A., Zumstein, L. A., Timmons, T. M., Liu, T.-J., Ginsberg, L., Roth, J. A., Hong, W. K., Bruso, P., and Goepfert, H. Adenovirus-mediated p53 Gene Transfer in Patients with Advanced Recurrent Head and Neck Squamous Cell Carcinoma. *J. Clin. Oncol.* 16, 2221-2232 (1998).
- Swisher, S. G., Roth, J. A., Komaki, R., Gu, J., Lee, J. J., Hicks, M., Ro, J., Hong, W. K., Merritt, J. A., Ahrar, K., Atkinson, N., Correa, A. M., Dolomente, M., Dreiling, L., El-Naggat, A. K., Fossella, F., Francisco, R., Glisson, B., Grammer, S., Herbst, R., Huaranga, A., Kemp, B., Khuri, F. R., Kurie, J. M., Lian, Z., McDonnell, T. J., Morice, R., Morello, F., Mosheim, M., Munden, R., Papadimitrakopoulou, V., Pisters, K. M. W., Putnam, J. B., Jr., Sarabia, A. J., Shelton, T., Stevens, C., Shin, D. M., Smythe, W. R.,

- Wanieryan, A., Walsh, G. L., Yin, M. Induction of p53 Regulated Genes and Tumor Regression in Lung Cancer Following Intratumoral Delivery of Adenoviral p53 (RPR/INGN 201) and Radiation Therapy. *Clin. Cancer Res.* 9, 93-101 (2003).
7. Marshall, E. Gene Therapy Death Prompts Review of Adenovirus Vector. *Science* 286, 2244-2245 (1999).
8. Kato, T., Morgan, D., Krahl, T., Sarvetnick, N., Sherman, L., and Verma, I. Cellular Immune Response to Adenoviral Vector Infected Cells Does Not Require *De Novo* Viral Gene Expression: Implications for Gene Therapy. *Proc. Natl. Acad. Sci. USA* 95, 11777-11782 (1998).
9. Liu, Y., Munkes, L. C., Liggitt, D. H., Brown, C. S., Solodin, I., Wata, T. M., and Debs, R. J. Factors Influencing the Efficiency of Cationic Liposome-mediated Intravenous Gene Delivery. *Nat. Biotechnol.* 15, 167-173 (1997).
10. Templeton, N. S., Lasic, D. D., Frederik, P. M., Strey, H. H., Roberts, D. D., and Pavlakis, G. N. Improved DNA: Liposome Complexes for Increased Systemic Delivery and Gene Expression. *Nat. Biotechnol.* 15, 647-652 (1997).
11. Gaensler, K. M. L., Tu, G. H., Bruch, S., Liggitt, D., Lipshutz, G. S., Methas, A., Harrison, M., Heath, T. D., and Debs, R. J. Fetal Gene Transfer by Transvenous Injection of Cationic Liposome-DNA Complexes. *Nat. Biotechnol.* 17, 1188-1192 (1999).
12. Ramesh, R., Saeki, T., Templeton, N. S., Ji, L., Stephens, L. C., Ito, J., Wilson, C. R., Wu, Z., Branch, C. D., Minna, J. D., and Roth, J. A Successful Treatment of Primary and Disseminated Human Lung Cancers by Systemic Delivery of Tumor Suppressor Genes Using an Improved Liposome Vector. *Mol. Ther.* 3, 337-350 (2001).
13. Cristiano, R. J. and Roth, J. A. Epidermal Growth Factor Mediated DNA Delivery into Lung Cancer Cells Via the Epidermal Growth Factor Receptor. *Cancer Gene Ther.* 3, 4-10 (1996).
14. Cristiano, R. J. and Roth, J. A. Molecular Conjugates: A Targeted Gene Delivery Vector for Molecular Medicine. *J. Mol. Med.* 73, 479-486 (1995).
15. Lemosmore, C. L., Olson, F. M., Xu, B., Kinsey, B. M., Waldrep, J. C., Hua, P., Bhogal, B., and Knight, V. Aerosol Delivery of Robust Polyethyleneimine-DNA Complexes for Gene Therapy and Genetic Immunization. *Mol. Ther.* 1, 180-188 (2000).
16. Lu, H., Zhang, Y., Roberts, D. D., Osborne, C. K., and Templeton, N. S. Enhanced Gene Expression in Breast Cancer Cells *In Vitro* and Tumors *In Vivo*. *Mol. Ther.* 6, 783-792 (2002).
17. Shu, H. Y., Liang, R., Templeton, N. S., and Zhang, M. Inhibition of Human Tumor Progression by Systemic Delivery of the Maspin Gene in a Syngeneic Tumor Model. *Mol. Ther.* 5, 755-761 (2002).
18. Nudome, T. and Huang, L. Gene Therapy Progress and Prospects: Nonviral vectors. *Gene Ther.* 9, 1647-1652 (2002).
19. Ramesh, R., Bo, L., Saito, Y., Wu, Z., Mhashikar, A. M., Wilson, D. R., Branch, C. D., Chada, S., and Roth, J. A. Local and Systemic Inhibition of Lung Tumor Growth After Nanoparticle Mediated maspin/IL-24 Gene Delivery. *DNA and Cell Biol.* (in press).
20. Liu, C., Began, G., Mohiuddin, I., Saeki, T., Saito, Y., Branch, C. D., Stephens, L. C., Yen, N., Roth, J. A., and Ramesh, R. Increased Uptake of Liposome-DNA Complex by Lung Metastases Following Intravenous Administration. *Mol. Ther.* 7, 409-418 (2003).
21. Liu, C., Ji, L., Tomka, F., Began, G., Cynthia, D. B., Kai, X., Atkinson, E. N., Bekke, B. N., Stephens, C., Minna, J. D., Roth, J. A., and Ramesh, R. Liposomal Vector Mediated Delivery of the 3p FUS1 Gene Demonstrates Potent Antitumor Activity Against Human Lung Cancer *In Vivo*. *Cancer Gene Ther.* (in press).
22. Uno, F., Sasaki, J., Nishizaki, M., Carboni, G., Xu, K., Atkinson, E. N., Rando, M., Minna, J. D., Roth, J. A., and Ji, L. Myristoylation of the Fes1 Protein Is Required for Tumor Suppression in Human Lung Cancer Cells. *Cancer Res.* 64, 2969-2976 (2004).
23. Whitmore, M., Li, S., and Huang, L. LPD Lipopolyplex Initiates a Potent Cytokine Response and Inhibits Tumor Growth. *Gene Ther.* 6, 1867-1875 (1999).
24. Huang, L. and Li, S. Liposomal Gene Delivery - A Complex Package. *Nat. Biotechnol.* 15, 620-621 (1997).
25. Li, S., Wu, S. P., Whitmore, M., Loeffert, E. J., Wang, L., Watkins, S. C., Pitt, B. R., and Huang, L. Effect of Immune Response on Gene Transfer to the Lung Via Systemic Administration of Cationic Lipidic Vectors. *Am. J. Physiol.* 276, L796-L804 (1999).
26. Freemark, B. D., Blezinger, H. P., Florack, V. J., Nordstrom, J. L., Long, S. D., Deshpande, D. S., Nochumson, S., and Petrak, K. L. Cationic Lipids Enhance Cytokine and Cell Influx Levels in the Lung Following Administration of Plasmid-cationic Lipid Complexes. *J. Immunol.* 160, 4580-4586 (1998).
27. Tousignant, J. D., Zhao, H., Yew, N. S., Cheng, S. H., Eastman, S. J., and Scheule, R. K. DNA Sequences in Cationic Lipid: pDNA-mediated Systemic Toxicities. *Hum. Gene Ther.* 14, 203-214 (2003).
28. Dow, S. W., Fradkin, L. G., Liggitt, D. H., Willson, A. P., Heath, T. D., and Potter, T. A. Lipid-DNA Complexes Induce Potent Activation of Innate Immune Responses and Antitumor Activity When Administered Intravenously. *J. Immunol.* 163, 1552-1561 (1999).
29. Scheule, R. K., St George, J. A., Bagley, R. G., Marshall, J., Kaplan, J. M., Akita, G. Y., Wang, K. X., Lee, E. R., Harris, D. J., Jiang, C., Yew, N. S., Smith, A. E., and Cheng, S. H. Basis of Pulmonary Toxicity Associated with Cationic Lipid-mediated Gene Transfer to the Mammalian Lung. *Hum. Gene Ther.* 8, 689-707 (1997).
30. Yew, N. S., Zhao, H., Wu, I. H., Song, A., Tousignant, J. D., Przybylska, M., and Cheng, S. H. Reduced Inflammatory Response to Plasmid DNA Vectors by Elimination and Inhibition of Immunostimulatory CpG Motifs. *Mol. Ther.* 1, 255-262 (2000).
31. Yew, N. S., Zhao, H., Wu, I. H., Song, A., Tousignant, J. D., Przybylska, M., and Cheng, S. H. CpG-depleted Plasmid DNA Vectors with Enhanced Safety and Long-term Gene Expression *In Vivo*. *Mol. Ther.* 5, 731-738 (2000).
32. Hoffman, C. R., Dileo, J. P., Li, Z., Li, S., and Huang, L. Efficient *In Vivo* Gene Transfer by PCR Fragment with Reduced Inflammatory Activity. *Gene Ther.* 8, 71-74 (2001).
33. Tan, Y., Li, S., Pitt, B. R., and Huang, L. The Inhibitory Role of CpG Immunostimulatory Motifs in Cationic Lipid Vector-Mediated Transgene Expression *In Vivo*. *Hum. Gene Ther.* 10, 2153-2161 (1999).
34. Yeo, S. J., Gravis, D., Yoon, J. G., and Yi, A. K. Myeloid Differentiation Factor 88-dependent Transcriptional Regulation of Cyclooxygenase-2 Expression by CpG DNA: Role of NF κ B and p38. *J. Biol. Chem.* 278, 22563-22573 (2003).
35. DeWitt, D. L. Prostaglandin Endoperoxidase Synthase: Regulation of Enzyme Expression. *Biochem. Biophys. Acta* 1083, 121-134 (1991).
36. Ghosh, D. K., Misukonis, M. A., Reich, C., Pisetsky, D. S., and Weinberg, J. B. Host Response to Infection: The Role of CpG DNA in Induction of Cyclooxygenase 2 and Nitric Oxide Synthase 2 in Murine Macrophages. *Infect. Immun.* 69, 7703-7710 (2001).
37. Baurz, J. E., Zou, Y., and Korfhagen, T. R. Inhibitory Effects of Tumor Necrosis Factor- α on Cationic Lipid-Mediated Gene Delivery to Airway Cells *In Vitro*. *Biochim. Biophys. Acta* 1535, 100-109 (2001).
38. Palladino, M. A., Bahja, F. R., Theodorakis, E. A., and Moldawer, L. L. Anti-TNF- α Therapies: The Next Generation. *Nat. Rev. Drug Dis.* 2, 736-746 (2003).
39. Kumar, S., Boehm, J., and Lee, J. C. p38 MAPKs: Key Signalling Molecules as Therapeutic Targets for Inflammatory Diseases. *Nat. Rev. Drug Dis.* 2, 717-726 (2003).
40. Manning, A. M. and Davis, R. J. Targeting JNK for Therapeutic Benefit: From Junk to Gold. *Nat. Rev. Drug Dis.* 2, 554-565 (2003).

41. Lu, W. C., Zhou, M., Shankavaram, U., Peng, G., and Wahl, L. M. Differential Regulation of Lipopolysaccharide-induced Monocyte Matrix Metalloproteinase (MMP)-1 and MMP-9 by p38 and Extracellular Signal-regulated Kinase 1/2 Mitogen-activated Protein Kinases. *J. Immunol.* 170, 6244-6249 (2003).
42. Jurdik, M.-E., Gravel, A., Gosselin, J., Tremblay, M. J., and Plamand, L. Activation of Monocyte Cyclooxygenase-2 Gene Expression by Human Herpesvirus 6: Role for Cyclic AMP-response Element-binding Protein and Activator Protein-1. *J. Biol. Chem.* 277, 30665-30674 (2002).
43. Wadleigh, D. I., and Herschman, H. R. Transcriptional Regulation of the Cyclooxygenase-2 Gene by Diverse Ligands in Murine Macrophages. *Biochem. Biophys. Res. Comm.* 264, 865-870 (2000).
44. Reddy, S. T., Wadleigh, D. I., and Herschman, H. R. Transcriptional Regulation of the Cyclooxygenase-2 Gene in Activated Mast Cells. *J. Biol. Chem.* 275, 3107-3113 (2000).
45. Smarak, B., Heck, D. E., Mariano, T. M., Gartner, C. R., Sur, R., Laskin, D. L., and Laskin, J. D. Induction of Cyclooxygenase-2 by Heat Shock Protein 90 in Macrophages and Endothelial Cells. *Am. J. Physiol.* 283, C1267-C1277 (2002).
46. Turini, M. E. and DuBois, R. N. Cyclooxygenase-2: A Therapeutic Target. *Annual Review of Medicine* 53, 35-57 (2002).
47. FitzGerald, G. A. COX-2 and Beyond: Approaches to Prostaglandin Inhibition in Human Disease. *Nature Reviews Drug Discovery* 2, 879-890 (2003).
48. Chen, Y., Zhang, J., Moore, S. A., Ballas, Z. K., Portanova, J. P., Krieg, A. M., and Berg, D. J. CpG DNA Induces Cyclooxygenase-2 Expression and Prostaglandin Production. *Int. Immunol.* 13, 1015-1020 (2001).
49. Kang, G., Kong, P. J., Yuh, Y. J., Lim, S. Y., Yim, S. V., Chun, W., and Kim, S. S. Curcumin Suppresses Lipopolysaccharide-induced Cyclooxygenase-2 Expression by Inhibiting Activator Protein 1 and Nuclear Factor KappaB Bindings in BV2 Microglial Cells. *J. Pharmacol. Sci.* 94, 325-328 (2004).
50. Barrios-Rodiles, M., Keller, K., Belley, A., and Chadee, K. Nonsteroidal Antiinflammatory Drugs Inhibit Cyclooxygenase-2 Enzyme Activity but not mRNA Expression in Human Macrophages. *Biochim. Biophys. Res. Comm.* 225, 896-900 (1996).
51. Zyglewska, T., Sanduja, R., Ohashi, K., Loose-Mitchell, D. S., Sanduja, S. K., and Wu, K. K. Inhibition of Endothelial Cell Prostaglandin H Synthase Gene Expression by Naproxen. *Biochim. Biophys. Acta* 1131, 78-82 (1992).

Date Received: August 2, 2004

Persistent Transgene Expression Following Intravenous Administration of a Liposomal Complex: Role of Interleukin-10-Mediated Immune Suppression

Isao Ito,* Tomoyuki Saeki,[†] Imran Mohiuddin, Yuji Saito,[†]
Cynthia D. Branch, Ara Vaporciyan, Jack A. Roth, and Rajagopal Ramesh[‡]

Department of Thoracic and Cardiovascular Surgery, The University of Texas M. D. Anderson Cancer Center, Houston, TX 77030, USA

**Current address: Department of Surgery, Tokai University School of Medicine, Oiso Hospital, Kanagawa, Japan.*

[†]Current address: Department of Surgery, Jikei University School of Medicine, Tokyo, Japan.

To whom correspondence and reprint requests should be addressed at the Department of Thoracic and Cardiovascular Surgery, The University of Texas M. D. Anderson Cancer Center, 1515 Holcombe Boulevard, Box 445, Houston, TX 77030, USA. Fax: (713) 794-4901. E-mail: ramesh@mdanderson.org.

Studies conducted in non-tumor-bearing, immunocompetent mice have shown that intravenous administration of liposome-DNA complex elicits an inflammatory response that results in a failure to sustain adequate transgene expression. In the present study, however, we investigated the effects of a cationic liposomal DOTAP:cholesterol (DOTAP:Chol)-DNA complex on cytokine production and transgene expression in both experimental lung tumor-bearing (TB) mice and non-tumor-bearing (NTB) syngeneic mice and nude mice. Intravenous injection of DOTAP:Chol-luciferase (*luc*) DNA complex resulted in tumor necrosis factor- α levels that were 50% lower and interleukin-10 levels that were 50–60% higher in TB mice than in NTB mice. Furthermore, a significant increase in *luc* expression ($P = 0.001$) that persisted for 7 days was observed in TB mice. In contrast, *luc* expression decreased significantly from day 1 to day 2 in NTB mice. Also, *luc* expression was two- to threefold higher in TB mice that were given multiple injections of DOTAP:Chol-*luc* complex than in mice who received a single injection. In contrast, *luc* expression was significantly suppressed following multiple injections in NTB mice ($P = 0.01$). Further analysis revealed IL-10 protein expression by the tumor cells in TB mice. Injection of anti-IL-10 antibody in TB mice resulted in a significant decrease in *luc* expression ($P = 0.01$) compared with that in mice injected with a control antibody. Based on these findings, we conclude that transgene expression persists in TB mice and is partly mediated by IL-10. Additionally, multiple injections of liposome-DNA complex can increase transgene expression in TB mice. These findings have clinical applications in the treatment of cancer.

Key Words: gene therapy, liposome, IL-10, cancer, cytokines, inflammation, lung, gene expression

INTRODUCTION

The development of efficient nonviral vectors that can deliver therapeutic genes when injected systemically will provide novel therapeutic options for the treatment of disseminated cancers. However, recent studies have demonstrated that liposomal vectors elicit an inflammatory response when injected systemically resulting in toxicity [1–7]. Induction of inflammatory responses due to the presence of immunostimulatory CpG sequences in plasmid DNA has been reported previously [8–12].

Associated with the inflammatory response is the production of proinflammatory cytokines (tumor necrosis factor- (TNF- α), interleukin-1 (IL-1), IL-6), which in turn have been shown to inhibit transgene expression [9,13]. Failure to achieve sustained transgene expression following repeated injections has also been attributed to the production of these proinflammatory cytokines [13]. Furthermore, a 3- to 4-day interval between injections was shown to be necessary to achieve sustained gene expression [14]. This need for injections at intervals has

been attributed to the cells' "refractory" state [14]. Thus, the inability to increase transgene expression following repeated injections has been a major obstacle in the development of therapeutic applications of liposomes. Likewise, reducing the number of CpG sequences in the plasmid DNA has been shown to reduce the inflammatory response and increase transgene expression [15]. These results, however, were obtained from studies of non-tumor-bearing (NTB), immunocompetent animals.

In contrast to these reports, we recently demonstrated effective gene transfer to experimental lung tumors in mice following intravenous injections of extruded DOTAP:cholesterol (DOTAP:Chol)-DNA:liposome complex [16]. In that study, although animals were treated with repeated injections, the relative effectiveness of multiple treatments was not studied. However, the major difference between the results of our study and those of others is that we conducted experiments in tumor-bearing (TB) animals, while others studied NTB animals. It is therefore possible that the pathophysiological condition of the animal may influence transgene expression following intravenous administration of the liposome:DNA complex.

Several preclinical and clinical studies have demonstrated functional alterations of immune cells (macrophages, neutrophils, and T cells) resulting in immune suppression in lung cancer [17–21]. These alterations have been attributed to several factors, including the production of immunosuppressive factors by tumor cells [22–25] and alterations in the immune cell receptors [26]. On the basis of these reports, we speculated that TB and NTB animals might respond differently to liposome:DNA complexes administered intravenously.

In the present study, we investigated the effects of intravenous administration of DOTAP:Chol-DNA complex on the cytokine profile and transgene expression of lung TB and NTB immunocompetent mice and nude mice.

RESULTS

Cytokine Expression Following Intravenous Injection of DOTAP:Chol-luciferase (*luc*) DNA Complex

Prior to the start of the experiment, we established lung tumors by injecting 1×10^6 UV2237m or A549 cells intravenously via the tail vein into female C3H and nude mice, respectively. Ten to fifteen days after injection of tumor cells, we treated the animals with DOTAP:Chol-*luc* complex. Note that at this time the tumors are well established in the lungs and can be detected histologically (data not shown). Animals receiving no treatment served as controls. In a separate but parallel set of experiments, NTB animals were also untreated or treated with DOTAP:Chol-*luc* complex.

We analyzed serum samples from NTB and lung TB C3H mice injected with DOTAP:Chol-*luc* DNA complex

for cytokine levels at regular time intervals. TNF- α , IL-1 α , interferon- γ (IFN- γ), and IL-10 were produced by TB and NTB mice, with maximum peak levels observed in both groups at 2 h for TNF- α and at 6 h for IFN- γ (Fig. 1A). We observed maximum levels of IL-10 expression at 12 and 24 h in both groups. However, TNF- α levels were 50% lower in TB mice than in NTB mice. In contrast, IL-10 levels were 50–60% higher in TB mice (Fig. 1A). The expression of cytokines was time dependent over the 24-h postinjection period. IL-1 α levels did not differ significantly in animals from the two groups. Cytokine levels except those of IL-1 α were not detected in control animals that were not treated, were treated with naked plasmid DNA, or were treated with an empty liposome (data not shown).

To examine whether a similar phenomenon occurred in other tumor models we also determined serum cytokine levels in A549 lung TB nude mice and compared them to NTB nude mice (Fig. 1B). Both TB and NTB nude mice produced TNF- α , IL-1 α , IFN- γ , and IL-10. The time courses for production of these cytokines were identical to those observed in C3H mice described above, with maximum production occurring at 2 h for TNF- α and at 6 h for IFN- γ . Similarly, we observed maximum levels of IL-10 expression at 12 and 24 h in TB and NTB mice. However, the levels of the cytokine produced in nude mice differed from the levels produced in C3H mice (Figs. 1A and 1B). Furthermore, TNF- α levels were moderately reduced in TB nude mice compared to NTB mice. The difference in the reduction of TNF- α levels in TB C3H mice and TB nude mice can be attributed to strain difference. However, other possibilities may exist and need additional investigation. In TB C3H mice we observed a significant increase in IL-1 α at 12 h compared to NTB mice. This increase in IL-1 α levels is not clear and needs additional investigation. These results demonstrate that increased IL-10 is produced in TB mice compared to NTB mice following injection of DOTAP:Chol-DNA complex.

Transgene Expression Persists in Tumor-Bearing Mice Following a Single Intravenous Injection of DOTAP:Chol-*luc* DNA Complex

To determine transgene expression *in vivo*, we injected lung TB and NTB C3H mice intravenously via the tail vein with DOTAP:Chol-*luc* DNA complex and removed their lungs at different times and analyzed them for luc activity. We observed luc expression in both TB and NTB mice, with maximal gene expression occurring 24 h after treatment in both groups (Fig. 2A). However, luc expression in NTB mice had decreased by 48 h after treatment and reached baseline levels by 72 h; luc expression remained at baseline through day 7. In contrast, levels of luc activity remained significantly higher than baseline ($P = 0.01$) in TB animals through

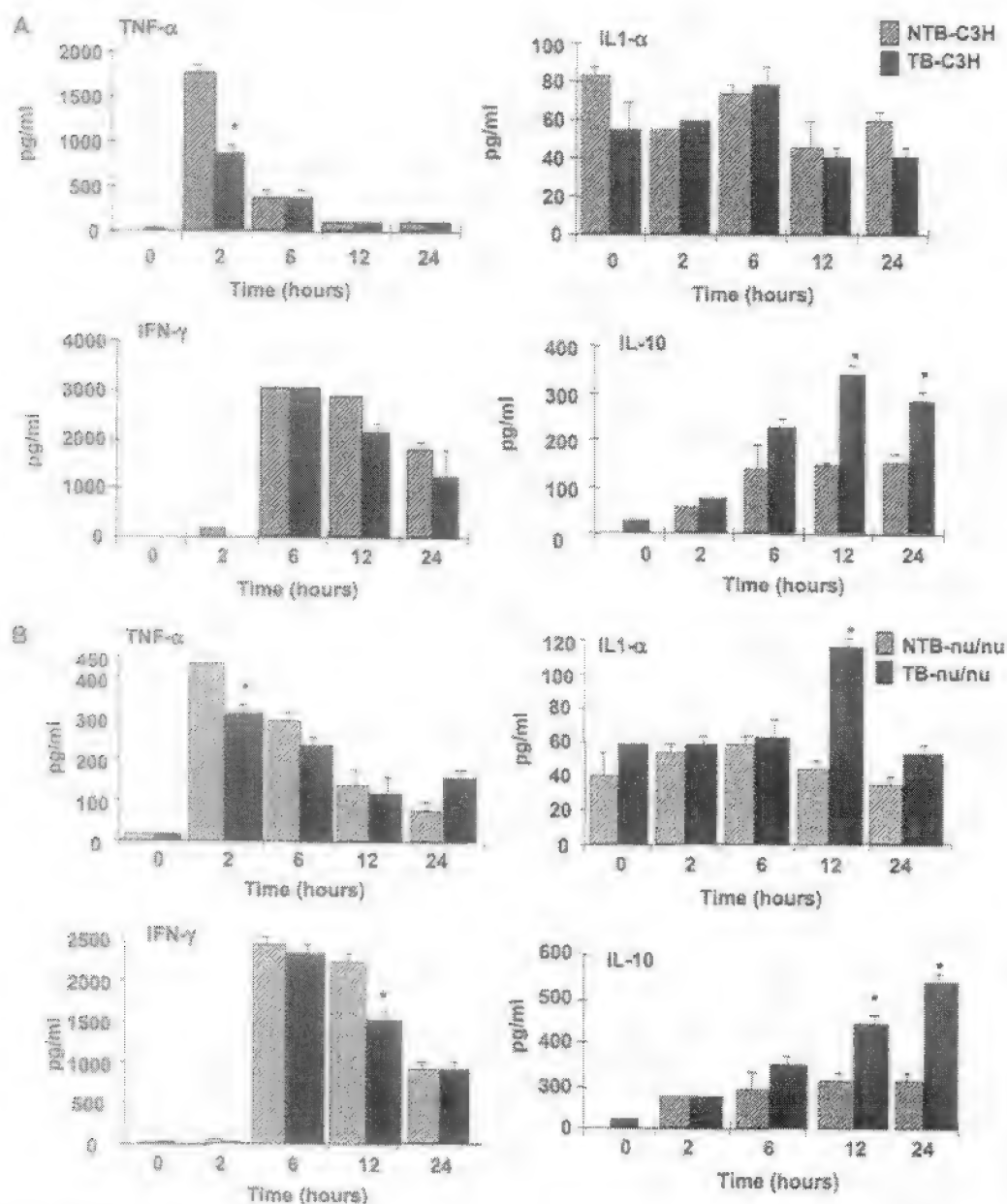


FIG. 1. Cytokine profile following systemic injection of DOTAP:Chol-luc DNA complex. Serum was collected from lung TB and NTB mice at 0, 2, 6, 12, and 24 h after injection of DOTAP:Chol-luc DNA complex (50 μ g) and was assayed for cytokines (TNF- α , IL-1 α , IFN- γ , IL-10) using ELISA. Untreated TB and NTB animals served as controls from each group. (A) Cytokine profile in UV2337m TB and NTB mice. (B) Cytokine profile in AS49 lung TB and NTB mice. Data represent the average cytokine levels in four animals per group per time point.

day 7. However, a trend in decline (50%) of luc expression was observed on day 7 compared to day 1 in TB animals.

We performed an analysis of transgene expression in AS49 lung TB and NTB nude mice. We observed increased luc expression at 24 h in both groups after

treatment (Fig. 2B). However, significant levels of luc expression persisted in TB mice until day 7 compared to NTB mice. Although luc expression in NTB mice did not reach baseline levels as observed in C3H mice, luc expression was significantly reduced by day 3 compared to day 1. These results demonstrate that persistent trans-

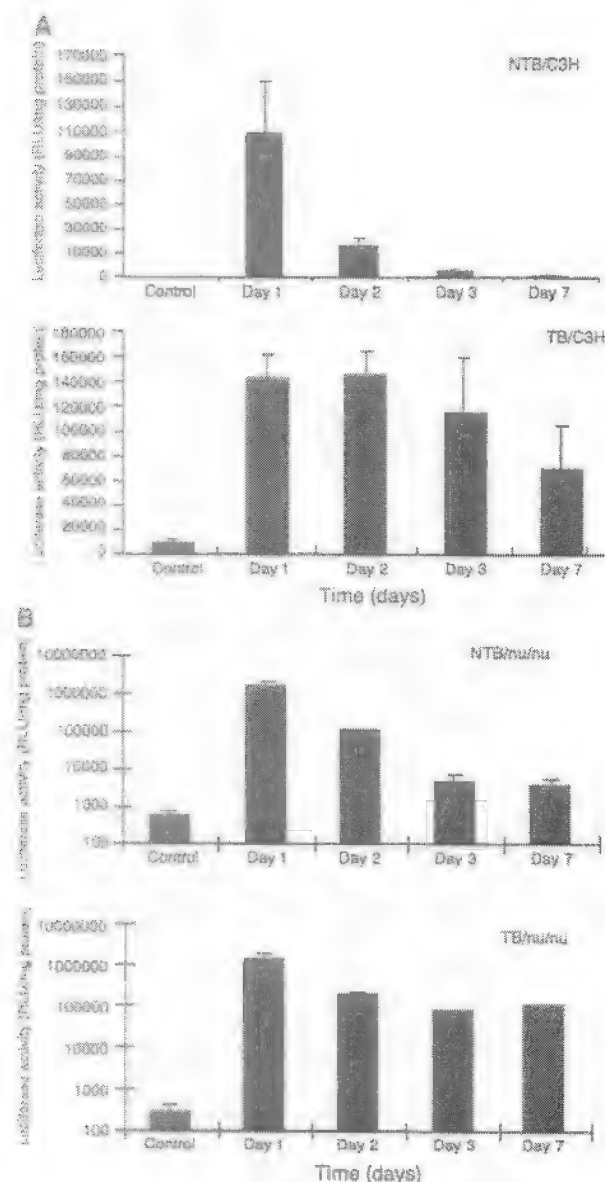


FIG. 3. Persistent transgene expression occurs in TB animals. (A) UV2237M TB and NTB C3H mice and (B) A549 TB and NTB nude mice were injected with DOTAP:Chol-luc DNA complex via the tail vein. Their lungs were resected on days 1, 2, 3, and 7 after treatment and analyzed for luc expression. Luc activity is expressed as relative light units (RLU) per milligram of total protein. Each time point represents the average luc activity in four animals. Bars represent standard deviation.

gene expression occurs in TB mice compared to NTB mice.

Repeated Injections of DOTAP:Chol-luc DNA Complex Result in Increased Transgene Expression

We next evaluated the effects of repeated injections on transgene expression in both lung TB and NTB C3H mice

and nude mice. We injected the animals via the tail vein with the DOTAP:Chol-luc DNA complex either one time or daily for 3 consecutive days. We analyzed lungs for luc activity 48 h after injection. In C3H mice luc expression was observed in both TB and NTB mice. In TB C3H mice, however, luc expression was twofold greater ($P = 0.001$) in mice treated three times than in mice treated once (Fig. 3A). In contrast, NTB mice treated three times expressed significantly lower levels of luc than did those treated only once ($P = 0.01$). Similarly, analysis of luc expression in TB nude mice and NTB nude mice demonstrated expression of luc expression (Fig. 3B). TB nude mice that received three treatments demonstrated threefold increase in luc expression compared to mice treated once ($P = 0.001$). In contrast, NTB mice that received three treatments showed decreased luc expression compared to mice receiving a single treatment. Thus, expression of luc in TB mice receiving multiple treatments was higher than in TB mice receiving a single treatment. Furthermore, luc expression in TB mice receiving multiple treatments was higher than in NTB mice that received multiple treatments. These results demonstrate that repeated injections of DOTAP:Chol-DNA complex in TB mice results in increased transgene expression and are in agreement with our previous results [16].

Lung Tumor Cells Express IL-10

To determine whether tumor cells contributed to the production of IL-10, we stained lungs from UV2237m TB and NTB mice for murine IL-10. TB lungs, especially tumor cells, stained intensely for IL-10 (Fig. 4). We also observed staining of infiltrating lymphocytes in the lung tumor sections. In contrast, NTB lung cells showed very little IL-10 expression. We also observed IL-10 protein expression in human lung tumor cell lines and in clinical specimens from patients diagnosed with lung cancer (data not shown). To determine further the levels of IL-10 produced by UV2237m tumor cells, we analyzed cell culture supernatants for IL-10 production by ELISA. The level of IL-10 produced by murine tumor cells was approximately 30 pg/ml (data not shown). These results demonstrate that tumor cells in addition to lymphocytes produce IL-10.

Alveolar Macrophages from Lung TB Mice Are Less Responsive to Stimulation

Since we had observed IL-10 production by lung TB mice, we examined the suppressive effects of IL-10 on alveolar macrophages by macrophage activation assay. We plated alveolar macrophages isolated from lung TB and NTB C3H mice in 96-well plates and stimulated them with phorbol myristic acetate (PMA). We measured stimulation of macrophages by addition of 2',7'-dichlorofluorescein diacetate. Macrophages from NTB mice showed significantly more activation ($P = 0.001$) than those from TB mice (Fig. 5A). Furthermore, a significant reduction

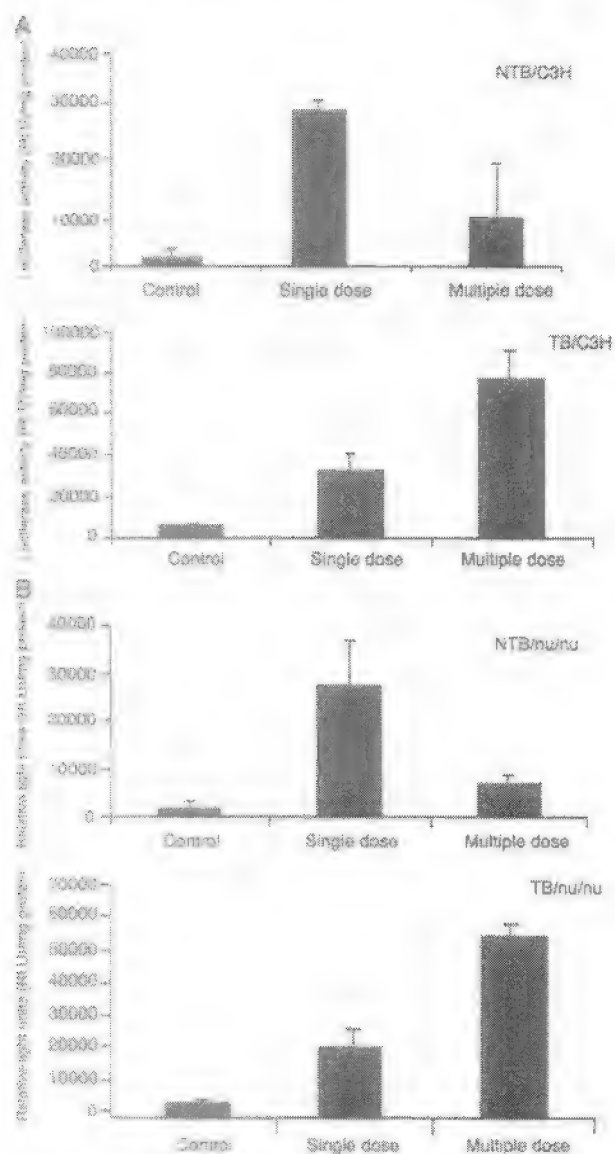


FIG. 3. 24 hr multiple treatments resulted in increased transgene expression. TB and NTB C3H or nude mice injected either once or three times with DOTAP:Chol-luc DNA complexes (50 μ g DNA/dose) via a tail vein were assayed for luc activity. (A) A twofold increase in luc activity was observed in TB C3H mice receiving three treatments compared with those receiving one treatment. In contrast, luc activity in NTB C3H mice receiving three treatments was significantly lower than in those receiving one treatment. (B) Luc activity in TB nude mice receiving three treatments showed two- to threefold increase in luc activity compared with those receiving one treatment. In contrast, luc activity in NTB nude mice receiving three treatments was significantly lower than in those receiving one treatment. Luc activity is expressed as RLU per microgram of total protein. Bars represent standard deviation.

($P = 0.01$) in TNF- α production by alveolar macrophages from TB mice was observed when the macrophages were treated with LPS (Fig. 5B). In contrast, macrophages from

NTB animals produced higher levels of TNF- α when treated with LPS.

Neutralization of IL-10 in TB Animals Results in Decreased Transgene Expression

To determine the effects of IL-10 on transgene expression *in vivo*, we injected TB animals with a mouse IL-10 neutralizing antibody 24 h prior to injection of DOTAP:Chol-luc DNA complex. Analysis of the lungs 48 h after liposome-DNA complex injection showed a significant reduction in luc expression ($P \leq 0.01$) compared with that in TB animals that were not treated with the neutralizing IL-10 antibody (DOTAP:Chol-luc complex

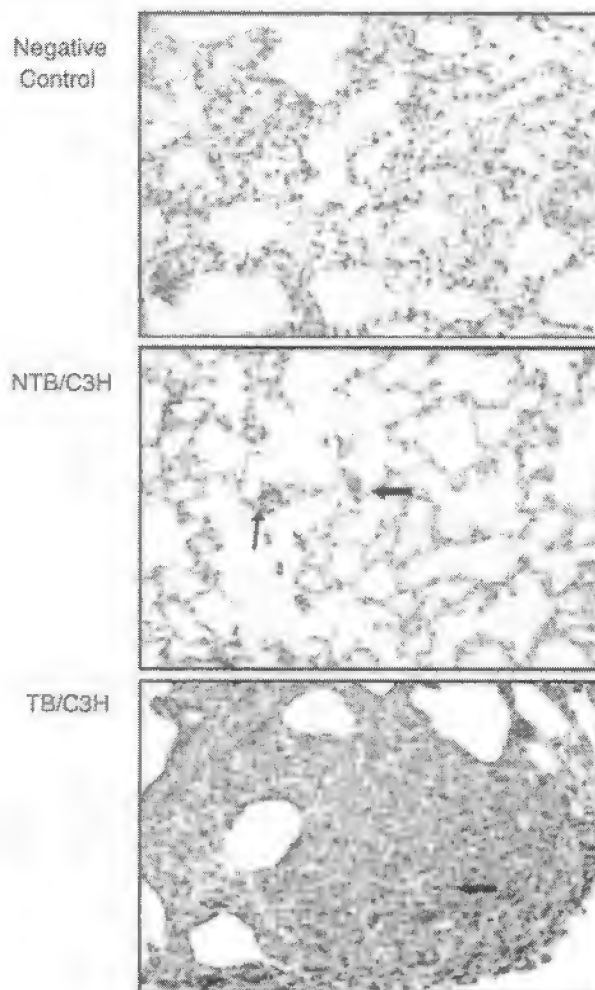


FIG. 4. UV2237M tumor cells produce IL-10. UV2237M TB and NTB lung tissue sections were immunohistochemically stained for mouse IL-10. IL-10 was detected in lung tissue sections as indicated by the intense brown cytoplasmic staining. Staining for IL-10 in NTB lung tissue sections was weak. Tissue sections stained only with secondary antibody served as negative controls. Arrows indicate cells staining positive for IL-10.

only) and in animals that were treated with a control isotypic antibody (Fig. 6). Luc expression was also significantly lower in animals that received the control IgG antibody than in animals that did not receive any

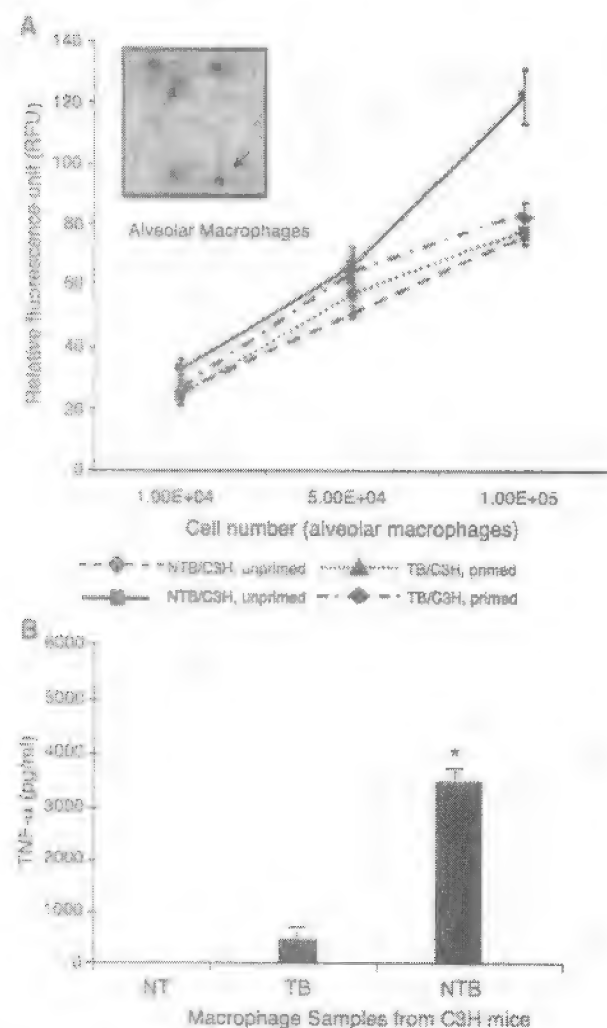


FIG. 5. Alveolar macrophages (AM) from TB mice are less responsive to PMA stimulation. (A) Alveolar macrophages from TB and NTB C5H mice were plated in 96-well plates at various cell densities and incubated overnight at 37°C. Cells were exposed to PMA (1 µg/ml) for 1 h. After 1 h, 2',7'-dichlorofluorescein diacetate was added and incubated for 30 min. Macrophage stimulation was detected by measuring the fluorescence intensity at 520 nm in a spectrofluorometer. AM from TB animals responded to PMA stimulation significantly compared to those from NTB animals. AM not exposed to PMA served as controls. Values shown are the means of quadruplicate wells. Bars represent standard error. (B) Alveolar macrophages from TB and NTB C5H mice were treated with LPS (1 µg/ml) for 24 h and the culture medium was assayed for mature TNF-α. A significant amount of TNF-α protein was detectable in the medium from AM harvested from NTB mice compared to that from TB mice. AM not exposed to LPS served as negative control (NT). Positive control included was provided in the kit. Data are represented as the means of quadruplicate wells. Bars represent standard error.

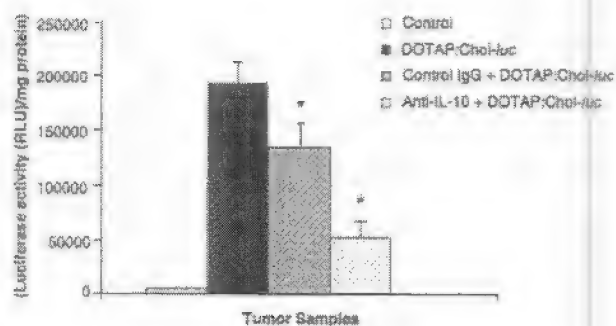


FIG. 6. Neutralization of IL-10 in TB mice results in decreased transgene expression. Lung tumors were established in C5H mice by injecting UV2237m cells (1×10^6 cells/well) via the tail vein. Three weeks later, animals were divided into three groups and treated as follows: group 1 received no treatment, group 2 received an intraperitoneal (ip) injection of isotypic control IgG antibody (20 µg), and group 3 received an ip injection of neutralizing anti-IL-10 antibody (20 µg). Twenty-four hours later, animals from all three groups were treated with DOTAP:Chol-luc DNA complex via the tail vein. Animals that did not receive any treatment served as negative controls. Animals were euthanized 48 h after injection, and their lungs were removed and analyzed for luc activity. Luc expression was significantly less in animals from group 3 than in those from groups 1 and 2. A significant reduction in luc activity was also observed in group 2 compared with group 1, indicating nonspecific inhibition. Luc activity is expressed as RLU per milligram of total protein. Bars represent standard error.

antibody treatment, indicating nonspecific inhibition of gene expression.

DISCUSSION

The present study demonstrated for the first time that transgene expression persists in TB animals but not in NTB animals. Although persistent transgene expression was demonstrated in TB animals *in vivo*, the cell types that primarily express the transgene were not investigated in the present study. However, we have recently demonstrated that tumor cells primarily express the transgene at higher levels compared to surrounding normal tissues, both *in vitro* and *in vivo* [27]. Based on our previous observation we can speculate that persistent transgene expression primarily occurs in tumor cells. However, expression can also persist in other cell types that are present within the tumor microenvironment.

The underlying mechanism for the prolonged transgene expression was next examined. It is possible that inflammatory cytokines (TNF-α, IL-1α), which have been previously shown to inhibit transgene expression, may be altered in TB animals or that the immune cells (macrophages, neutrophils, T cells) that produce the inflammatory cytokines are functionally altered in TB animals [17–25]. To understand the mechanism involved, we measured cytokine expression levels in TB and NTB animals after intravenous administration of a liposome-DNA complex. TNF-α, IL-1α, IFN-γ, and IL-10 expression was observed in both TB animals and NTB animals.

However, TNF- α levels were 50% lower in TB animals. The role of TNF- α as a proinflammatory cytokine and its primary source, alveolar macrophages, are well known [20,28]. It appears that the alveolar macrophages may be functionally suppressed by soluble factors released by the *in situ* tumor [29,30]. As a result, production of TNF- α and other cytokines triggered by TNF- α may also be reduced, thereby allowing persistent transgene expression. The observation that IL-10 levels were higher in TB animals supports this hypothesis. The inhibitory effects of IL-10 on macrophages and TNF- α production are well documented [29–34]. Similarly, IL-10 expression by tumor cells has been previously demonstrated [35–39]. Based on these reports we next determined the source of IL-10. Immunohistochemical analysis of TB lung tissue sections demonstrated intense cytoplasmic staining for IL-10 in UV1237m tumor cells. Additionally, *in vitro* assay demonstrated IL-10 production by tumor cells albeit at low levels. The difference in *in vitro* and *in vivo* IL-10 levels can be due to several reasons that include difference in tumor cell number, cell type (tumor cells, epithelial cells, mononuclear cells, etc.), and *in situ* tumor conditions. In support of this are the findings that IL-10 staining was also observed in infiltrating lymphocytes. Additionally, IL-10 expression was also observed in the surrounding normal tissues that comprised fibroblast and epithelial cells. In contrast, IL-10 expression was observed to be minimal in NTB lung tissue sections.

IL-10 is a Th₂-type cytokine that acts as an immunosuppressor under a variety of conditions and is primarily produced by macrophages and T cells [36,37]. Production of IL-10 and its effects on immune cells have been shown in a variety of human cancers [39–43]. In fact, it has been shown that IL-10 production by tumor cells suppresses the immune functions of macrophages and T cells, thereby promoting tumor growth [44–49]. Furthermore, when present in the tumor microenvironment, macrophages can produce IL-10 in an autocrine fashion, resulting in functional inactivation [36,37]. Based on these findings, we examined the effect of exogenous IL-10 on transgene expression in alveolar macrophages from TB and NTB animals, as well as the effect of PMA on macrophage stimulation as a measure of function. Transgene expression was significantly higher in alveolar macrophages from NTB animals compared with those from TB animals. However, in the presence of IL-10, transgene expression was significantly suppressed in macrophages from NTB animals (data not shown). This observation suggests two possibilities: the transgene expression was transcriptionally suppressed or the macrophages were functionally inactivated, resulting in a decreased inflammatory response. We believe that functional inactivation is a more likely mechanism since alveolar macrophages from TB animals, when exposed to PMA, were not stimulated. In contrast, macrophages from NTB animals, when exposed to

PMA, were observed to undergo significant stimulation. Furthermore, a reduction in TNF- α production was observed in alveolar macrophages from TB animals compared with those from NTB animals.

The difference in the alveolar macrophage function may partly explain the observed increase in transgene expression in TB mice receiving repeated treatments compared to NTB mice. Although persistent and increased transgene expression has been demonstrated in TB mice it is not clear whether this is a local effect or a systemic effect. Preliminary studies from our laboratory indicate that this is primarily a local effect that is influenced by the tumor microenvironment. Analysis of transgene expression in mice bearing subcutaneous tumors demonstrated an increase in transgene expression over time when the mice were injected with a single dose of DOTAP:Chol-luc DNA complex. However, analysis of the normal tumor-free lungs from these subcutaneous tumor-bearing mice demonstrated a decrease in transgene expression over time (data not shown). We are currently conducting additional studies in the laboratory to delineate the local versus systemic effect.

Finally, the effect of IL-10 on transgene expression was demonstrated by *in vivo* neutralization experiments conducted in TB animals. Treating animals with a neutralizing anti-IL-10 antibody prior to injection of the liposome-DNA complex resulted in an approximately 50% reduction in luc expression compared with animals that did not receive the neutralizing antibody and animals that received an isotypic control antibody. These results indicate that blocking IL-10 activity might restore the inflammatory response, thereby resulting in decreased transgene expression levels. Based on these results, we would like to propose the following hypothesis: Tumor cells in addition to infiltrating inflammatory cells produce IL-10, which acts in an autocrine fashion to promote its growth and produce more IL-10 and in paracrine fashion to suppress the functions of immune cells (macrophages, monocytes, T cells) present in the tumor microenvironment or stimulate them to produce more IL-10 (Fig. 7). Intravenous injection of liposome-DNA complex in TB animals thus results in a diminished inflammatory response, resulting in persistent and enhanced transgene expression following repeated multiple treatments and in therapeutic effect. A note of caution in that apart from IL-10 other immunosuppressive factors produced by the tumor cells may also play a role in the observed persistent transgene expression. We are currently investigating these possibilities in the laboratory.

In conclusion, this study demonstrates for the first time that a diminished inflammatory response, partly mediated by IL-10, leads to persistent gene expression in lung TB animals. This phenomenon allows multiple treatments, resulting in enhanced transgene expression and therapeutic efficacy. Thus, repeated delivery of ther-

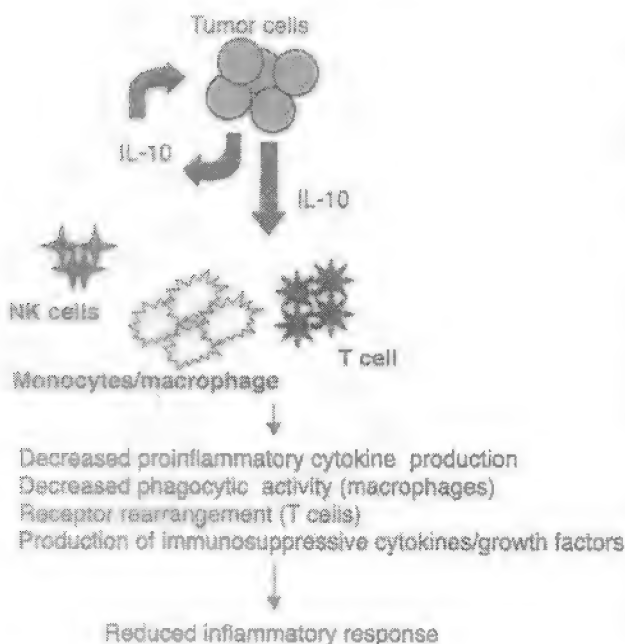


FIG. 7. Schematic representation of IL-10 production by tumor cells and its effects on immune cells and inflammatory response. Tumor cells produce IL-10, which acts in an autocrine fashion to promote growth and production of more IL-10 and in a paracrine fashion to suppress the functions of immune cells (macrophages, T cells) present in the tumor milieu by decreasing phagocytic activity and proinflammatory cytokine production (IL-1, TNF- α , IL-6) and rearranging receptors. Intravenous injection of liposome-DNA complexes in TB animals thus results in a diminished inflammatory response, resulting in persistent and enhanced transgene expression after repeated treatments and in a therapeutic effect.

apeutic genes encapsulated in a liposome is feasible for lung cancer treatment.

MATERIALS AND METHODS

Materials. All lipids (DOTAP, cholesterol) were purchased from Avanti Polar Lipids (Alabaster, AL, USA). RPMI 1640 medium and fetal bovine serum were purchased from Invitrogen (New York, NY, USA). Polyclonal anti-human IL-10 antibody and anti-mouse IL-10 monoclonal antibody were obtained from Pharmingen (San Diego, CA, USA). Anti-IL-10 neutralizing antibody was purchased from Biosource International (Camarillo, CA, USA) and isotypic IgG antibody was purchased from Wako Chemicals (St. Louis, MO, USA).

Cell lines and animals. Murine fibrosarcoma cells (UV2237) obtained from Dr. Ismail Fidler, M.D. Anderson Cancer Center, were maintained in RPMI 1640 medium. Human A549 lung cancer cells were obtained from American Tissue Culture Collection (Rockville, MD, USA) and maintained in Ham's F12 medium. Cells were regularly passaged and tested for the presence of mycoplasma. Four- to six-week-old female C3H/NeJ mice (National Cancer Institute, Frederick, MD, USA) and athymic nude mice (Charles River Laboratories, Wilmington, DE, USA) used in the study were maintained in a pathogen-free environment and handled according to institutional guidelines established for animal care and use.

Purification of plasmids. Growth and purification of plasmids used in the study have been described previously [16].

Synthesis, preparation, and particle size analysis of liposome:DNA complexes. The synthesis of 20 mM DOTAP:Chol, the preparation of liposome:DNA complexes, and the determination of mean particle sizes in freshly prepared liposome:DNA complexes have been described previously [16,50].

Cytokine profiles in TB and NTB mice. Experimental lung tumors were established by injecting 1×10^6 UV2237m and A549 tumor cells into C3H/NeJ mice and nude mice, respectively. Tumor cells were injected via the tail vein. Ten to fifteen days after tumor cell injection animals were given a single intravenous injection of DOTAP:Chol-luc DNA complex (50 μ g DNA) via the tail vein. Cytokine profiles were determined in these lung TB mice and compared with those in NTB mice after treatment. Serum samples were collected from the animals at 0, 2, 6, 12, and 24 h after injection; the samples were stored at -80°C and analyzed for cytokines using murine cytokine ELISA kits (R&D Systems, Inc., Minneapolis, MN, USA). Assays were performed in quadruplicate according to the manufacturer's guidelines.

Luciferase expression in TB and NTB animals. Lung TB and NTB C3H mice and nude mice were injected with a single dose of DOTAP:Chol-luc DNA:liposome complex (50 μ g DNA) via the tail vein. On days 1, 2, 3, and 7 after injection, the animals were euthanized using CO_2 inhalation, and their lungs were resected. The lungs were snap-frozen in liquid nitrogen and analyzed for luc expression as described previously [50]. Luc was expressed as relative light units (RLU) per milligram of protein. Four animals were analyzed at each of the time points. The experiments were performed twice, and the results reported were the average means of the two experiments.

In vivo luc expression following single and multiple treatments with DOTAP:Chol-luc DNA complex. UV2237m lung TB ($n = 15$) and NTB ($n = 15$) C3H mice and A549 lung TB ($n = 15$) and NTB ($n = 15$) nude mice were divided into three groups each. Five TB and five NTB mice were treated with intravenous injections of DOTAP:Chol-luc DNA complex once, and five more from each group were treated daily for 3 days. Five TB mice and five NTB mice did not receive any treatment and served as controls. The mice were euthanized by CO_2 inhalation 48 h after treatment, and their lungs were resected. Total protein was extracted from the lung tissues by homogenizing the tissue in lysis buffer and assaying for luc activity as described above (RLU/mg of protein). Each experiment was performed at least three times and the results reported were the means of the three experiments.

Immunohistochemical analysis. UV2237m lung tumors removed from C3H/NeJ mice were fixed in 10% buffered formalin before being embedded in paraffin and cut into 4- μ m sections. Sections were stained for murine IL-10 expression as previously described [16]. Briefly, tissue sections were treated with 0.3% H_2O_2 in methanol for 30 min to block endogenous peroxidase activity and subsequently incubated with normal goat serum for 30 min at room temperature. Following incubation, slides were treated with goat polyclonal anti-IL-10 antibody for 60 min. After 30 min more of incubation with an appropriate secondary antibody (provided with the ABC kit; Vector Laboratories, Burlingame, CA, USA), IL-10 protein was detected in tissues using diaminobenzidine enhanced with the avidin-biotin reaction ABC kit. The slides were then counterstained with hematoxylin and mounted with Aqua-Mount (Lerner Laboratories, Pittsburgh, PA, USA).

Alveolar macrophage activation assay. Alveolar macrophages from TB and NTB C3H mice were acquired as previously described [27,51]. Briefly, the mice were euthanized using CO_2 inhalation, and an incision was made in the region of the trachea. Once the trachea was exposed, a 21-gauge needle was inserted, and 10 ml of sterile Hanks' balanced salt solution (HBSS) was infused into the lungs with a 10-ml syringe. After the lungs were flushed with HBSS, the remaining liquid was aspirated into a sterile Falcon centrifuge tube placed on ice. The procedure was repeated three to four times. Cells were centrifuged at 1000 rpm for 10 min, washed

cells and seeded in six-well plates. An aliquot of the cell preparation was subjected to cytopathological analysis, and more than 90% of the cells were identified as macrophages. Alveolar macrophages thus isolated were used for activation assay. Briefly, alveolar macrophages from TB and NTB C3H mice were plated in 96-well plates at varying cell densities (1×10^4 , 5×10^4 , and 1×10^5 cells/well) and incubated overnight at 37°C. The next day, PMA was added (1 μ g/ml) to the wells and incubated. One hour after incubation with PMA, 2',7'-dichlorofluorescein diacetate (DCFH-DA; Sigma Chemicals) was added to the wells. DCFH-DA is a substrate that is converted into a fluorescent 2',7'-dichlorofluorescein product by cellular peroxidase produced by alveolar macrophages [32]. The amount of fluorescence produced is directly proportional to the macrophage response (activation) to PMA. This test is routinely used to measure alveolar macrophage response to various stress inducers [53,54]. Plates were incubated in the dark for 60 min, after which the plates were read in a spectrophluorometer at 485 nm excitation and 520 nm emissions. Values were obtained, and the results reported were the average of quadruplicate for each sample.

In a separate but parallel set of experiments, alveolar macrophages from TB and NTB C3H mice were plated in 96-well plates and incubated overnight. The next day, cells were treated with LPS (1 μ g/ml; Sigma Chemicals) and culture supernatants assayed for TNF- α production using a murine TNF- α ELISA kit (R&D Systems). Untreated cells served as negative controls. Positive control was provided in the kit.

In vivo neutralization experiments with anti-IL-10 antibody. UV2237 (inbred TB C3H mice ($n = 15$)) were divided into three groups and treated as follows: group 1 ($n = 5$) received no treatment; group 2 ($n = 5$) received a single intraperitoneal injection of control isotypic IgG antibody (20 μ g); and group 3 ($n = 5$) received a single intraperitoneal injection of murine anti-IL-10 neutralizing antibody (20 μ g). Twenty-four hours later, mice from all three groups were injected with DOTAP:Chol:Luc DNA complex (50 μ g DNA) via the tail vein. An additional group of animals ($n = 5$) that did not receive any treatment served as negative control for these experiments. The mice were euthanized 48 h after treatment with DOTAP:Chol:Luc, and their lungs were resected and analyzed for luc activity as described above. Experiments were performed twice and results reported were the averages of two separate experiments.

Statistical analysis. The statistical significance of the experimental results was calculated using ANOVA. A P value <0.05 was considered significant.

ACKNOWLEDGMENTS

The authors thank Dawn Chialore for editorial assistance and Anna Vega for preparation of the manuscript. This work was supported in part by the Texas Cancer Research Coordinating Board, ATP&RP Grant 003657-0028-2001 (J.R.), by a Career Development Award from The University of Texas M. D. Anderson Cancer Center, SPURC in Lung Cancer P50-CA70907-5 (R.R.), by Public Health Service Grant P01CA78728-01A1 (J.A.R.) by the Texas Tobacco Settlement Fund by the RESCT Lung Cancer Program, Grant DAMD17-01-1-0089 (Project 3c; by TARGET Lung Cancer Grant DAMD17-01-1-0086 (Project 7); by an Institutional Research Grant (R.R.); by a Grant from the W. M. Keck Foundation (R.R.); by Cancer Center Support (CORE) Grant CA44492 and by a sponsored research agreement with Introgen Therapeutics, Inc.

RECEIVED FOR PUBLICATION MAY 26, 2003; ACCEPTED JANUARY 9, 2004

REFERENCES

1. Whitmore, M., et al. (1999). LPS lipopolyplex initiates a potent cytokine response and inhibits tumor growth. *Gene Ther.* 6: 1867–1875.
2. Huang, L., and Li, J. (1997). Liposomal gene delivery—a complex package. *Nat Biotechnol.* 15: 425–431.
3. Li, S., et al. (1999). Effect of immune response on gene transfer to the lung via systemic administration of cationic lipid-pDNA complexes. *Am J Physiol.* 276: L796–L804.
4. Whitmore, M., et al. (1998). Cationic lipids enhance cytokine and cell influx levels in

- the lung following administration of plasmid-cationic lipid complexes. *J. Immunol.* 160: 4580–4586.
5. Whitmore, M., et al. (1999). LPS lipopolyplex initiates a potent cytokine response and inhibits tumor growth. *Gene Ther.* 6: 1867–1875.
6. Ose, S. W., et al. (1999). Lipid-DNA complexes induce potent activation of innate immune responses and antitumor activity when administered intravenously. *J. Immunol.* 163: 1552–1561.
7. Sebeule, R. K. J., et al. (1997). Basis of pulmonary toxicity associated with cationic lipid-mediated gene transfer to the mammalian lung. *Hum. Gene Ther.* 8: 689–707.
8. Tussignat, J. D., et al. (2003). DNA sequences in cationic lipid-pDNA-mediated systemic toxicities. *Hum. Gene Ther.* 14: 203–214.
9. Fan, Y., et al. (1999). The inhibitory role of CpG immunostimulatory motifs in cationic lipid vector mediated transgene expression in vivo. *Hum. Gene Ther.* 10: 2153–2161.
10. Yew, N. S., et al. (2000). Reduced inflammatory response to plasmid DNA vectors by elimination and inhibition of immunostimulatory CpG motifs. *Mol. Ther.* 1: 255–262.
11. Schwartz, D. A., et al. (1997). CpG motifs in bacterial DNA cause inflammation in the lower respiratory tract. *J. Clin. Invest.* 100: 68–73.
12. McLachlan, C., et al. (2000). Bacterial DNA is implicated in the inflammatory response to delivery of DNA/DOTAP to mouse lungs. *Gene Ther.* 7: 384–392.
13. Qin, L., et al. (1997). Promoter attenuation in gene therapy: interferon-gamma and tumor necrosis factor alpha inhibit transgene expression. *Hum. Gene Ther.* 8: 2019–2029.
14. Li, S., et al. (1998). Characterization of cationic lipid-protamine-DNA (LPD) complexes for intravenous gene delivery. *Gene Ther.* 5: 930–937.
15. Yew, N. S., et al. (2002). CpG-depleted plasmid DNA vectors with enhanced safety and long-term gene expression in vivo. *Mol. Ther.* 5: 731–738.
16. Ramani, R., et al. (2001). Successful treatment of primary and disseminated human lung cancers by systemic delivery of tumor suppressor genes using an improved liposome vector. *Mol. Ther.* 3: 337–350.
17. Kudo, T., Yasumoto, K., Yano, T., Nakashashi, H., Sugimachi, K., and Nomoto, K. (1987). Role of antitumor activity of alveolar macrophages in lung cancer patients. *Cancer Res.* 47: 2199–2202.
18. Sotomayor, E. M., et al. (1991). Impaired activation of tumoricidal function in macrophages from mammary tumor-bearing mice: the role of IFN- γ . *Int. J. Oncol.* 3: 719–727.
19. Sotomayor, E. M., et al. (1995). Decreased macrophage mediated cytotoxicity in mammary tumor-bearing mice is related to alterations in nitric oxide production and/or release. *Int. J. Cancer* 60: 660–667.
20. Mazzocchi, G., et al. (1999). Lymphocyte subpopulations anomalies in lung cancer patients and relationship to the stage of disease. *In Vivo* 13: 203–209.
21. Koutami, M. K., Gargavall, V. C., Kastirakis, N. G., Asimakopoulou, P. J., and Kittas, C. (2002). Prognostic factors in non-small cell lung carcinoma. *Anticancer Res.* 22: 347–374.
22. Sotomayor, E. M., et al. (1991). Role of tumor-derived cytokines on the immune system of mice bearing a mammary adenocarcinoma. *J. Immunol.* 147: 2816–2823.
23. Lopez, D. M., et al. (1996). Cytokine production by lymphoreticular cells from mammary tumor-bearing mice: the role of tumor-derived factors. *Anticancer Res.* 16: 3923–3930.
24. Lopez, D. M., et al. (1991). Modulation of the immune system by mammary tumor derived factors. *Cancer Invest.* 9: 643–653.
25. Ghosh, P., et al. (1995). Gradual loss of T-helper 1 populations in spleen of mice during progressive tumor growth. *J. Natl. Cancer Inst.* 87: 1478–1483.
26. Beutler, L., and Cerami, A. (1989). The biology of cachectin/TNF- α as primary mediator of host response. *Annu. Rev. Immunol.* 7: 625.
27. Ito, T., et al. (2003). Increased uptake of liposomal-DNA complexes by lung metastases following intravenous administration. *Mol. Ther.* 7: 409–418.
28. Vassalli, P. (1992). The pathophysiology of tumor necrosis factor. *Annu. Rev. Immunol.* 10: 411.
29. Fiorentino, D. F., Zlotnik, A., Mossmann, T., Howard, M., and O'Garra, A. (1991). IL-10 inhibits cytokine production by activated macrophages. *J. Immunol.* 147: 3815.
30. Aleva, D. G., Burget, C. J., and Elger, K. D. (1994). Tumor-induced regulation of suppressor macrophage nitric oxide and TNF- α production: role of tumor-derived IL-10, TGF- β , and prostaglandin E $_2$. *J. Immunol.* 153: 1674.
31. Karnovsky, T., Alexander, H. R., Fong, M., and Strassman, G. (1995). Potential involvement of IL-10 in suppressing tumor-associated macrophages. *J. Immunol.* 154: 3583–3590.
32. Bogdan, C. Y., Vodovotz, Y., and Nathan, C. (1991). Macrophage deactivation by interleukin-10. *J. Exp. Med.* 174: 1349.
33. de Waal Malefyt, R., Abrams, J., Bennett, B., Figdor, C., and deVries, J. E. (1991). Interleukin-10 inhibits cytokine synthesis by human monocytes: an autoregulatory role for IL-10 production by monocytes. *J. Exp. Med.* 174: 1209.
34. Strassman, G., Koota, V., Finkelman, F., Fong, M., and Kambayashi, T. (1994). Evidence for the involvement of interleukin 10 in the differential deactivation of murine peritoneal macrophages by prostaglandin E $_2$. *J. Exp. Med.* 180: 2365.
35. Casti, C. A., et al. (1993). Interleukin 10 production by human carcinoma cell lines and its relation to interleukin 6 expression. *Int. J. Cancer* 55: 96.
36. Howard, M., and O'Garra, A. (1992). Biological properties of interleukin 10. *Immunol. Today* 13: 198.

37. Mosse, B. W., et al. (1992). Interleukin-10. *Annu. Rev. Immunol.* 11: 165-190.
38. Boercher, A. E., et al. (1999). Identification of an IL-10 producing HLA DR negative monocyte subset in the malignant ascites of patients with ovarian carcinoma that inhibits cytokine protein expression and proliferation of autologous T cells. *J. Immunol.* 163: 6251-6260.
39. Gaudin, W. H., et al. (1992). Presence of interleukin-10 (IL-10) in the ascites of patients with ovarian and other intra-abdominal cancers. *Cytokine* 4: 385-390.
40. de Waal Malefyt, R., et al. (1991). IL-10 and viral IL-10 strongly reduce antigen-specific human T cell proliferation by diminishing the antigen-presenting capacity of monocytes via downregulation of class II MHC expression. *J. Exp. Med.* 174: 911-924.
41. Fiorentino, D. F., et al. (1991). IL-10 acts on the antigen-presenting cells to inhibit cytokine production by Th1 cells. *J. Immunol.* 146: 3444-3451.
42. Ding, L., and Librecht, S. M. (1992). IL-10 inhibits mitogen-induced T cell proliferation by selectively inhibiting macrophage costimulatory function. *J. Immunol.* 148: 3133-3139.
43. Rogiers, C., Vercruysen, Y., and Nathan, C. (1991). Macrophage deactivation by interleukin-10. *J. Exp. Med.* 174: 1549-1555.
44. Armstrong, L., India, R., and Adler, A. (1996). Interleukin-10 (IL-10) regulation of human monocyte tumor alpha (TNF-alpha) from human alveolar macrophages and peripheral blood monocytes. *Immunol.* 51: 143-149.
45. Kage, P., et al. (1992). IL-10, T lymphocyte inhibitor of human blood cell production of IL-1 and tumor necrosis factor. *J. Immunol.* 148: 808-814.
46. de Waal Malefyt, R., Yssel, H., and de Vries, J. E. (1993). Direct effects of IL-10 on subsets of human CD4⁺ T cell clones and resting T cells. *J. Immunol.* 150: 4754-4765.
47. Yue, F. Y., et al. (1997). Interleukin-10 is a growth factor for human melanoma cells and downregulates HLA class-I, HLA class-II and ICAM-1 molecules. *Int. J. Cancer* 71: 630-637.
48. Lu, Z. Y., et al. (1995). Interleukin-10 is a proliferation factor but not differentiation factor for human myeloma cells. *Blood* 85: 2521-2527.
49. Masboud, R., et al. (1995). Interleukin-10 is an autocrine growth factor for acquired immunodeficiency syndrome-related B-cell lymphoma. *Blood* 85: 3423-3430.
50. Templeton, N. S., et al. (1997). Improved DNA:liposome complexes for increased systemic delivery and gene expression. *Nat. Biotechnol.* 15: 647-652.
51. Moxley, M. A., Baird, T. L., and Corbett, J. A. (2000). Adoptive transfer of acute lung injury. *Am. J. Physiol. Lung Cell Mol. Physiol.* 279: 983-993.
52. Wan, X. S., Zhou, Z., and Kennedy, A. R. (2003). Adaptation of the dichlorofluorescein assay for detection of radiation-induced oxidative stress in cultured cells. *Radiat. Res.* 160: 622-630.
53. Goldsmith, C. A., Imrich, A., Danare, H., Ning, Y. Y., and Kobzik, L. (1998). Analysis of air pollution particulate-mediated oxidant stress in alveolar macrophages. *J. Toxicol. Environ. Health A* 54: 529-545.
54. Tsai, I. J., Kao, M. H., and Han, S. H. (1999). The respiratory burst activity of activated eosinophils in atopic asthmatics. *Int. Arch. Allergy Immunol.* 119: 38-44.

3p21.3 tumor suppressor cluster: prospects for translational applications

Lin Ji¹, John D Minna,
Jack A Roth

Author for correspondence:
Assistant Professor,
Department of Thoracic &
Cardiovascular Surgery Unit
447, The University of Texas
M.D. Anderson Cancer
Center, P.O. Box 301402,
Houston, Texas
77230-1402, USA
Tel.: +1 713 565 9193
Fax: +1 713 796 4592
jiminna@mdanderson.org

Chromosomal abnormalities at the 3p21.3 region, including homozygous deletions and loss of heterozygosity and expressional deficiencies in 3p21.3 genes including transcriptional silences by promoter hypermethylation, altered mRNA splicing and aberrant transcripts, and lost or defect protein translation and post-translational modifications, are frequently found in most human cancers. Inactivation of 3p21.3 genes in primary tumors affects a wide spectrum of key biological processes such as cell proliferation, cell cycle kinetics, signaling transduction, ion exchange and transportation, apoptosis and cell death, and demonstrates the molecular signatures of carcinogenesis. Restoration of defective 3p21.3 genes with several wild-type 3p21.3 genes suppresses tumor cell growth both *in vitro* and *in vivo*. These findings suggest several 3p21.3 genes as potential tumor suppressors and implicates these 3p21.3 genes for future development as biomarkers for the early detection and diagnosis of cancer, and as prognostic and therapeutic tools for cancer prevention and molecular cancer therapy.

Human cancer development is a dynamic, complex, progressive and multistep process, involving many genes and gene products that systematically, quantitatively and accumulatively affect a biological network of cellular signaling and functional pathways [1–3]. Advances in human genomic, molecular and biomedical technologies have facilitated the rapid and effective identification of cancer-associated homozygous deletions and loss of heterozygosity (LOH) in critical chromosomal regions and mutations as well as transcriptional and translational defects of genes and gene products that carry cancer hallmarks [4–7]. The localization and identification of potential tumor suppressor genes (TSGs) and oncogenes on the short arm of human chromosome 3, especially the 3p21.3 region, in various tumors and in early carcinogenesis represent some of the most exciting progresses in recent cancer genomic, cytogenetic, and molecular biological research [8–10]. This article provides an overview of the most current progress in molecular genetic research and functional characterization of these novel 3p21.3 genes in human cancers. The major intentions of this article are to present a perspective on 3p21.3 genes as potential tumor suppressor cluster in carcinogenesis and as novel therapeutic agents and rational targets for molecular cancer prevention and therapy, and to briefly describe the clinical progress in using these 3p21.3 genes as biomarkers or surrogates for predicting prognosis or therapeutic response based on their genetic or expressional status in somatic

lesions and as therapeutics based on their tumor suppressing activities for human cancers.

Genetic abnormalities of chromosome 3p & 3p21 region in primary cancers

Tumor suppressor genes play a major role in the pathogenesis of human lung cancers. Genomic and cytogenetic studies of allelotyping, LOH and somatic mutations of human cancers have provided valuable insights into the chromosomes targeted for genetic inactivation during tumorigenesis and act as useful tools in identifying putative TSGs [9–13]. Homozygous deletion and LOH of critical chromosomal regions and TSGs have been frequently observed in various chromosomal locations in human cancers [9–13]. Known TSGs, such as *Rb*, *p53*, *FHIT* and putative TSGs have been found at chromosome regions 3p, 5q, 6p, 8p, 9p and 11p, as well as other sites [9,10,12]. Cytogenetic and allelotyping studies of fresh tumors and tumor cell lines have shown that allele loss from several distinct regions on chromosome 3p, including 3p25, 3p21–22, 3p14 and 3p12–13, are the most frequent and earliest genomic abnormalities involved in a wide spectrum of human cancers including lung [8–10,12,14,15], breast [11,16,17], head and neck [18–20], ovarian [21,22], cervical/uterus [23–27], colorectal [28,29], pancreatic [30,31], esophageal [32–36], bladder [37,38] and many more [39–46] (Table 1). These results strongly suggest the potential for genomic instability and genetic aberrations in the 3p region leading to a predisposition for lung and other human cancer pathogenesis.

Keywords: 3p21.3 region,
tumor suppressor cluster,
cancer therapy, tumor
suppressor genes

future
medicine

Table 1. Genomic abnormalities of chromosome 3p and 3p21 region in human cancers.

Primary tumor site	% genomic abnormality	Refs
Lung	65-95	[8,10,12,14]
Breast	30-87	[11,16,17]
Head & neck	30-69	[18-20]
Ovarian	>50	[21,22]
Cervical/uterus	40-90	[23-27]
Colorectal	14-33	[28,29]
Pancreatic	35-45	[30,31]
Esophageal	13-55	[32-36]
Renal cell	45-87	[44,130]
Bladder	25-60	[37,38]
Nasopharyngeal	79-90	[41,42,131]
Follicular and papillary thyroid	17-67	[43]
Liver	35-46	[39]
Skin	>15	[40]
Gall bladder	35-65	[45,46]

Candidate tumor suppressor genes in the 3p21.3 region

Multiple overlapping homozygous deletions have been found in the 3p21.3 chromosomal region in small cell lung cancer (SCLC) cell lines H740, H1450 and GLC20, and in the breast cancer cell line HCC1500. These discoveries have narrowed the search for putative TSGs to a critical region of approximately 120 kb [47,48]. The putative 3p21.3 tumor suppressor region was identified by allelotyping designed to define areas of LOH in matched tumor and normal tissue pairs and by examining uncommon examples of homozygous deletions. Nine genes (*CACNA2D2*, *PLG*, *101P6*, *FUS1*, *BLU*, *RASSF1*, *NPRL2*, *HYAL2* and *HYAL1*), as illustrated in Figure 1, were either disrupted by or immediately flanked the nested lung and breast cancer homozygous deletions found in the 3p21.3 region [9,10,13]. The cDNAs of these genes were isolated and cloned and mutations in these genes were identified in various tumors and tumor cell lines by single-strand conformation polymorphism and DNA sequencing analysis [8-10,13]. A number of the cDNA clones demonstrated approximately 50% amino acid homology to known genes. For example, the predicted amino acid sequence of *CACNA2D2* and functional analysis showed that *CACNA2D2* is the α -2- δ regulatory subunit of a voltage-gated

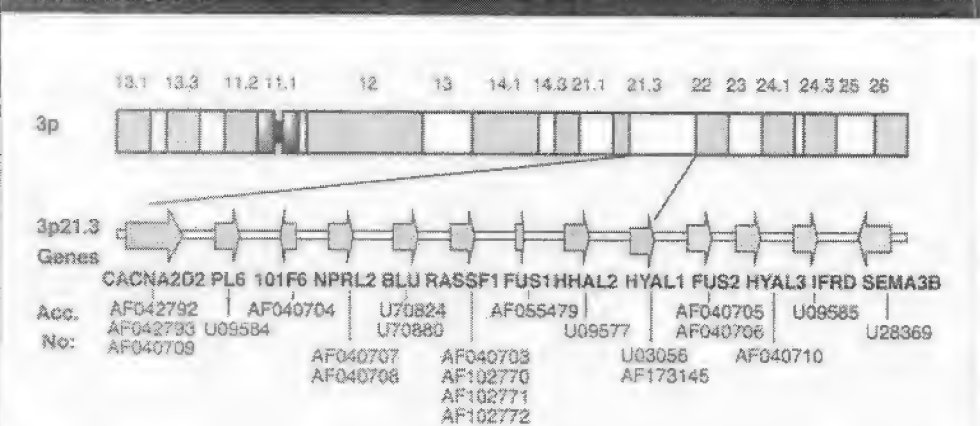
Ca^{2+} channel gene [49,50]; *NPRL2* is homologous to a nitrogen permease regulator; *RASSF1* is a homolog of a mouse Ras-binding protein, Maxp1/Nore1; *HYAL2* and *HYAL1* are hyaluronidases [8]; *101P6* is recently identified to be a member of the di-heme cytochrome (cyt)- b_{558} protein family [51], as demonstrated by a more than 90% alignment of consensus amino acid sequences in the ferric reductase transmembrane domain of the cyt- b_{558} ; *BLU* and *FUS-1* have no homology to known genes [8].

Genomic changes in the 3p21.3 region can be found in smoke-damaged respiratory epithelium and preneoplastic lesions and may be involved in inactivation of several potential TSGs such as the 3p21.3 genes and the 3p14.2 gene *FHIT*, and in the activation of oncogenes in the region [52]. Furthermore, studies of lung preneoplasia indicate that 3p21.3 allele loss is the earliest lung-cancer-associated genetic abnormality detected thus far. Since the allele loss occurs in preneoplastic lesions, this suggests that one or more 3p21.3 recessive oncogenes function as 'gate-keepers' in the molecular pathogenesis of lung and many other human cancers [52,53]. An integrated study of the molecular mechanisms and anticancer efficacy of these novel 3p21.3 TSGs, complemented with advanced technologies and systematic methodologies, may provide insight into the role of 3p21.3 TSGs in human cancer pathogenesis. Findings from these studies may have substantial implications for the future development and use of these 3p21.3 TSGs as cytogenetic biomarkers for early detection, prevention, diagnosis and molecular staging of human cancers and as therapeutic tools for human cancer gene therapy.

Inactivation of potential 3p21.3 TSGs in human primary cancers

It is widely accepted that most cancers arise as a consequence of the stepwise accumulation of genetic changes and somatic mutations in cancer susceptibility genes such as oncogenes and TSGs. These genes directly regulate cell proliferation and differentiation, or indirectly promote tumorigenesis by maintaining the genomic integrity of the cell, controlling cell death and apoptosis, and providing a stromal microenvironment for cellular neoplastic transformation [3,54,55]. Subsequent mutations and functional modulations such as gain or loss of function of these genes and gene products, further drives tumor progression towards to malignancy, invasion and metastases. However, growing

Figure 1. Scheme of human chromosome 3 and 3p21.3 candidate tumor suppressor genes.



The ideogram of the banding pattern of the chromosome 3p short arm is shown on the top and the genes in the 3p21.3 overlapping homozygous deletion region are showed on the bottom. The 3p21.3 genes are represented by green filled arrows with indications of the transcriptional orientations. The positions and sizes of genes on the chromosome are schematic and the GenBank accession numbers for each gene are given under the lines. Four genes immediately adjacent to 3p21.3 genes are represented by blue filled arrows.

evidence indicates that development of human cancers in general and carcinomas in particular, may be mechanically more complex than the original belief that manifestation of a cancer phenotype required a high mutation rate [56]. Recently, Wand and colleagues directly measured mutations in sporadic colon carcinoma and found that the total number of mutations was considerably lower than predicted, and suggested that increased gene mutation rate alone may not be the key to tumorigenesis [57,58]. Moreover, intragenic mutations that occur during the development of most sporadic human carcinoma are restricted to a small subset of genes such as *ras*, *p53*, *Rb*, *Akt* and *Wnt* [58,59,60]. Mutations in 3p21.3 genes are rare and only a few mutations that alter or truncate amino acid sequences have been found in a number of 3p21.3 genes including, *NPRL2*, *BLU*, *FUS1*, and *HYAL1*, and only two missense mutations were detected in *RASSF1A* in more than 200 human primary cancer samples [61,62]. However, none of the genes have been shown to be frequently and somatically mutated in human cancers including lung cancers and cancer cell lines [8,61,62]. Therefore, some other mechanisms such as chromosome instability, dramatic gains and losses of genetic materials (aneuploidy), promoter methylation, haploinsufficiency, altered RNA splicing, as well as defects in transcriptional, translational and post-translational processes that are frequently found in the 3p

region and in 3p21.3 genes, may play an important role in the ultimate inactivation of 3p21.3 TSGs in primary tumors.

Aberrant epigenetic methylation in the promoter region of growth regulatory genes is now recognized as a common alternative mechanism for gene inactivation in human cancers [63,64]. In fact, there are as many, if not more, TSGs inactivated by epigenetic promoter hypermethylation as they are by somatic mutations in coding regions [63-65]. *RASSF1A* is one of the 3p21.3 genes that has been extensively analyzed for its methylation pattern of the CpG island in the promoter and for expression in a variety of primary human cancer and cancer cell lines as summarized in a recent review by Damann and colleagues [65]. For example, *RASSF1A* is methylated in more than 90% of SCLCs and in more than 50% of non-small cell lung cancers (NSCLC) for which its expression is lost with such methylation. In contrast, *RASSF1A* was not methylated in a large number of normal lung samples obtained during lung tumor resection and was unmethylated and expressed in epithelial cell cultures [8,12,14,66]. Loss of expression correlated with promoter hypermethylation of *RASSF1A* gene [62,65,67,68]. In a preliminary immunohistochemical (IHC) study of human lung tumors and uninvolved normal tissues, the expression of *RASSF1A* was also detected in normal bronchial epithelial samples but not in the paired tumor samples [Unpublished Data].

Furthermore, reversion of epigenetic methylation by treatment with the DNA methylation inhibitor, 5-aza-2'-deoxycytidine (AZA) [32,61,62,63,67,69-70] or by RNA interference-mediated breakdown of DNA methyltransferase 1 [77] leads to re-expression of the silenced gene *RASSF1A* in various cancer cell lines. Promoter hypermethylation has also been detected in several other 3p21.3 genes including *BLU* [67,78,79], *CACNA2D2* [10], *HYAL1* [80] and *SEMA3B* [77,81], which correlates with the loss of these 3p21.3 genes in various human cancers. These results suggest that epigenetic silencing of 3p21.3 TSGs plays a critical role in their inactivation in primary cancers and in tumorigenesis.

The *FUS1* gene is another potential 3p21.3 TSG that has been found to be inactivated in primary tumors by alternative mechanisms, such as influence from the stochastic effects of 3p21.3 allele haploinsufficiency and the defect translation and post-translational modifications of the gene products, other than by the classic two-hit model that requires mutation in one allele and silencing or loss on another, or by epigenetic silencing with promoter methylation [82,83]. The cloned cDNA of *FUS1* is 333 bp and encodes a protein of 110 amino acid residues. Only a few mutations, including miss-sense mutations and C-terminal deletion mutation in the *FUS1* gene, have been identified in primary lung cancer samples. The expression of *FUS1* mRNA was successfully detected but no evidence of promoter methylation could be demonstrated in lung cancers [10,82,84]. Based on this observation, it has been hypothesized that given the lung cancer growth suppressing properties of *FUS1* both *in vitro* and in animal models, it would have to act as a TSG in a haploinsufficient manner, since most lung cancers experienced allele loss in this 3p21.3 region [84]. Although *FUS1* mRNA transcription could be detected on northern blots of RNA prepared from lung cancer cell lines, however no any endogenous *FUS1* protein could be detected in these lung cancer cells on western blots using the affinity purified, anti-*FUS1* peptide antibodies [10,82,83]. IHC analysis of *FUS1* expression on the conventional tissue sections of paired lung cancer and noninvolved normal samples, or microtissue arrays (Unpublished Data) with lung cancer samples at various pathological stages demonstrated that normal lung epithelial cells expressed *FUS1*, but most (> 50%) lung cancers did not [83]. Uno and colleagues [83] recently used a surface-enhanced laser-desorption/ionization-time-of-

flight mass spectrometry (SELDI-TOF-MS) on an anti-*FUS1* antibody capture ProteinChip array, to analyze the status of expression and post-translational modifications of *FUS1* protein in primary lung cancer and cancer cell lines [83]. Wild-type *FUS1* was indentified as an *N*-myristoylated protein and significant loss of expression or a myristoylation defect of the *FUS1* protein in those primary lung cancer and cancer cell lines was found [83]. These results suggest a novel alternative mechanism for the inactivation of tumor suppressors in human cancer and a role for deficient post-translational modification in TSG-mediated carcinogenesis and warrant further study of alternative inactivation mechanisms of 3p21.3 TSGs in the pathogenesis of lung and other human cancers.

Tumor suppression activities of 3p21.3 genes

Activities of 3p21.3 genes affect and regulate many biological processes such as cell differentiation, proliferation, cell cycle kinetics, signalling transduction, ion exchange and transportation, apoptosis and cell death. These biological activities directly or indirectly associate with the observed tumor suppression activities of several 3p21.3 genes when they are reactivated in 3p-deficient tumor cells, although the molecular mechanisms involved remain largely unknown.

One of the criteria for defining the role of 3p genes as TSGs is to demonstrate that the tumor phenotype marked by inactivation of the 3p21.3 genes can be rescued by replacing the mutated or deleted genes with the wild-type alleles. If frequent LOH, homozygous deletions, or, in some cases, abnormal transcripts and mutations of 3p21.3 genes, are the targets of carcinogens, and the loss of 3p21.3 gene function leads to human cancers, one might predict that replacement of the deleted 3p21.3 genes with the wild-type genes would result in tumor suppression similar to that observed with the classic *Rb* or *p53* TSGs. Ji and colleagues used recombinant adenoviruses to introduce wild-type 3p21.3 genes into NSCLC tumors or cell lines in which 3p21.3 genes were either heterozygously or homozygously deleted to characterize the genes' potential tumor suppressing functions *in vitro* and *in vivo* [85]. It was demonstrated that introducing wild-type *FUS1*, *101F6*, *NPRL2* and *RASSF1A* by recombinant adenoviral vector-mediated transfer into lung cancer cells with abnormal 3p21.3 genes inhibited tumor cell growth and induced apoptosis. Moreover,

intratumoral injection of recombinant adenoviral vectors containing these wild-type 3p21.3 genes significantly suppressed the growth of human NSCLC xenografts and systemic administration of protamine-complexed adenoviral vectors carrying the genes efficiently inhibited experimental metastases of lung cancer cells in xenograft murine models. Their results strongly suggested that *FUS1*, *RASSF1A*, *101P6* and *NPR2* genes in the 3p21.3 chromosomal region function individually as TSGs or collectively as a tumor suppressor region *in vitro* and *in vivo*.

Tumor suppressing activities of 3p21.3 TSGs are hallmarked typically by their capabilities in inhibition of tumor cell growth, induction of apoptosis and alteration of cell cycle kinetics *in vitro* and *in vivo*. However, the molecular mechanism and signaling pathway involved in these 3p21.3 TSG-mediated biological processes and their roles in pathogenesis of human cancer remain to be elucidated. For example, reactivation of wild-type *FUS1* in *FUS1*-expression-deficient NSCLC cells resulted in cell cycle arrest at the G1 phase and accumulation at the S phase and led to induction of apoptosis [8,82,83]. In an attempt to identify the potential cellular targets of the FUS1 protein to gain insight into the mechanism of its function, the authors used a ProteinChip array based analysis of protein-protein interaction and peptide mapping with SELDI-TOF-MS, and recently discovered that the FUS1 protein directly interacts with the apoptotic protease activation factor (Apaf) 1 protein [86]. Using an immunofluorescence imaging analysis with FUS1 and Apaf1 antibodies, the co-localization of the Apaf1 was also detected with wild-type FUS1 in a distinct mitochondrial and endoplasmic reticulum membrane location that is characterized by a typical FUS1 protein subcellular pattern in living tumor cells [86]. These findings suggest that the FUS1 protein may function as a key mediator in the Apaf1-mediated mitochondrial apoptosis pathway by recruiting and directing cytoplasmic Apaf1 protein to a critical cellular location and activating it *in situ*, and by upregulating the activity of other proapoptotic effectors such as p53. More detailed studies of the interactions of FUS1 proteins with its cellular targets and molecular actions are now in progress.

The RASSF1A protein has been reported to play an important role in regulation of the cell cycle process. The transient expression of *RASSF1A* in NSCLC cells induced G1 cell cycle arrest [87] and S phase inhibition [88,89], inhibited

accumulation of cyclin D1 protein engaging the Rb-family cell cycle checkpoint [90], and increased sensitivity to staurosporine, a potent apoptosis inducer and phospholipid/ Ca^{2+} -dependent protein kinase inhibitor, induced apoptosis [87]. Song and colleagues recently demonstrated that RASSF1A protein spatiotemporally regulated the stability of mitotic cyclins and the timing of mitotic progression by interacting with cdc-20, which leads to inactivation of anaphase-promoting complex (APC) and prevents degradation of cyclin A and B until the spindle checkpoint becomes fully operational [89,91]. Conversely, the siRNA-mediated depletion of *RASSF1A* accelerated mitotic cyclin degradation and mitotic progression as the result of premature APC activation [89]. Overexpression of the *RASSF1A* gene has also been shown to suppress cell growth and anchorage-independent colony formation on soft agar in renal carcinoma cells [92]. It has also been shown to retard cell proliferation in *RASSF1A*-deficient nasopharyngeal carcinoma (NC) cells *in vitro* and reduce the tumorigenic potential of NC cells transfected with wild-type *RASSF1A* in nude mice [93]. These findings strongly suggest that *RASSF1A* is an important tumor suppressor, responsible for inhibiting cell proliferation and regulating multiple levels of the cell cycle process, especially in mitotic progression.

CACNA2D2 is characterized structurally as a new α_1 282 auxiliary subunit of the voltage-activated calcium channel (VACC) protein complex [8,49,94]. The CACNA2D2 protein is highly expressed in normal lung tissue, but either absent or underexpressed in more than 50% of lung cancers [49]. Early loss of CACNA2D2 expression was also observed in the pathogenesis of lung cancer [95]. Ectopic expression of *CACNA2D2* by adenoviral-vector mediated wild-type *CACNA2D2* gene transfer in various 3p21.3-deficient NSCLC cell lines showed a profound effect on mitochondria homeostasis, cell proliferation, apoptosis and intracellular Ca^{2+} levels [49,94]. CACNA2D2-induced apoptosis has been shown to be mediated through a cellular process involved in the regulation of intracellular Ca^{2+} -levels, the disruption of mitochondria membrane integrity, the release of cytochrome c and the activation of downstream caspases [94].

Wild-type SEMA3B and SEMA3F proteins, members of the secreted and membrane-associated semaphorin/collapsing protein family involved in nerve growth cone migration [10],

induce apoptosis and inhibit tumor-cell-induced colony formation on soft agar and tumor cell growth when reintroduced into lung cancer cells, while the cancer-acquired missense mutants have lost their activities [99,100]. Similarly, SEMA3B and SEMA3F-mediated tumor suppressing activities are also observed in human ovarian adenocarcinoma tumor xenograft in nude mice [97]. SEMA3B may also involve inhibition of tumor-cell-induced angiogenesis and invasion by interfering with VEGF function through competitively binding to neuropilin (NP)-1 and -2, the coreceptors of several vascular endothelial growth factor (VEGF) isoforms and SEMA3 family proteins [96-98]. Transcription of *SEMA3B* mRNA is induced by exogenous expression of wild-type *p53* in *p53*-deficient glioblastoma cells and in response to genotoxic stresses caused by treatment with adriamycin or ultraviolet (UV) irradiation in a *p53*-dependent manner, suggesting that *SEMA3B* might play a role in regulating cell proliferation by mediating *p53* tumor-suppressing activities [99]. It has recently been found that SEMA3F located at the interface of adjacent interacting cells inhibited cell attachment and spreading in human mammary tumor cells, suggesting that SEMA3F may play a role in cell motility and cell adhesion. Loss of *SEMA3F* expression enhances metastatic potential [10,100]. These results consistently suggest the tumor-suppressing function of SEMA3B and SEMA3F in human cancers.

The *HYAL1* and -2 proteins are members of a large family of hyaluronidases that are required for breakdown of hyaluronan (HA), an abundant component of the extracellular matrix [103,104]. Modulations in HA may alter the interaction between infiltrating inflammatory renal cortex cells and resident cells [102]. The activity of *HYAL1* and -2 in periodontal ligament fibroblasts is essential for extracellular HA metabolism under physiological and inflammatory conditions [103]. Levels of HA in surrounding tumor cells often correlate with the potential of tumor progression. In addition, overproduction of HA enhances anchorage-independent tumor cell growth [10,80]. Loss of *HYAL* activities may permit HA accumulation that may be one of prerequisites for carcinogenesis [10,95,104]. Hypoxia stress significantly reduces both *HYAL1* mRNA transcription and protein activity in glioma cells, suggesting the involvement of *HYAL* proteins in tumor-cell-induced angiogenesis and invasion [105]. Loss of expression and activity of *HYAL1* protein was observed in number of cancer cell lines, correlating with loss

of gene expression from the promoter hypermethylation [80]. Forced expression of *HYAL1* in *HYAL*-dysfunctional cell lines resulted in cell cycle arrest and induction of apoptosis *in vitro*, and rendered tumorigenicity of surviving tumor cell clones in nude mice [10]. Together, based on the evidence that multiple *3p21.3* genes exhibit various degrees of tumor suppression activity, we strongly suggest that genes in *3p21.3* may function together as an integrated tumor suppressor region through their diverse biological activities.

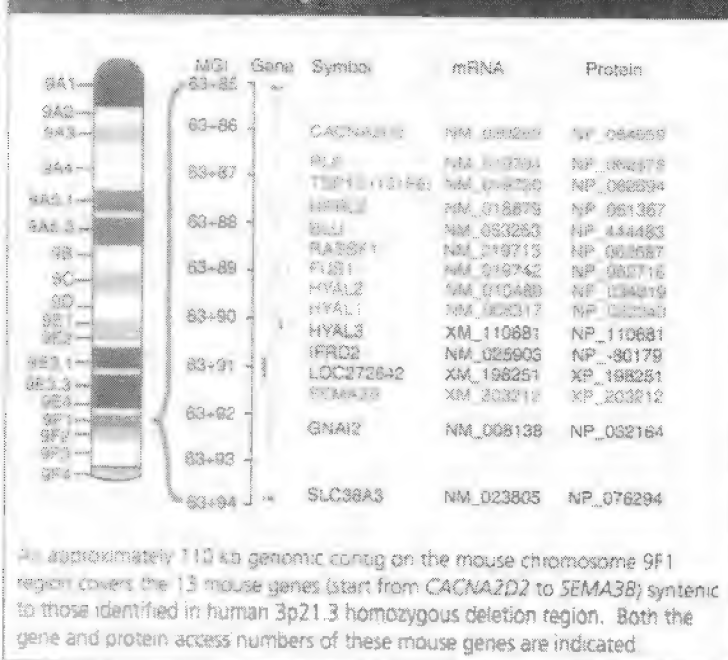
3p21.3-targeted mouse model for human cancers

Comparison of molecular abnormalities in mouse cancer models with those occurring in humans has revealed that mouse lung tumors are histologically most similar to human adenocarcinomas and genetic abnormalities such as *K-ras*-activating mutations (seen in 80-90% of mouse tumors), LOH at mouse chromosome 4 and inactivating TSG mutations of murine *p53* at mouse chromosome 11 and *Rb*, *FHIT* genes at chromosome 14 could also be found in humans at the equivalent chromosome locus and in human gene and protein counterparts [106-108]. Thus, while there are some differences, in general, it would be expected that the mouse lung tumor models would also share similarities with human lung cancer in terms of *3p21.3* allele loss, particularly given the first results with the *FHIT* gene [106]. Because of the importance of *3p21.3* allele loss in the pathogenesis of human lung cancers, it would be extraordinarily valuable to have a mouse model that mimics human lung cancer by undergoing allele loss or cancer-related genetic changes in attempts to use genes in this human *3p21.3* region for development of early detection and therapeutic treatments of lung cancer. The mouse autologs of *3p21.3* TSGs have recently been identified in the mouse genome and their loci have been mapped to the mouse chromosome 9F1-2 region [8,109] (Figure 2). These mouse genes, like their human counterparts, are surprisingly clustered in a region approximately 200 kb region of the mouse chromosome 9 with an extremely high density.

The mouse ducky mutant is a novel recessive phenotype characterized by spike wave seizures and cerebellar ataxia and a model for absence epilepsy [110]. The underlying mutations have been mapped to the *CACNA2D2* gene in mouse chromosome 9F, in which either the introduction of premature stop codon causes

the predicted protein truncation [110,111], or a 38 kb duplication comprising the 117 nucleotides of exon 3 results in the expression of a full length protein with predicted duplication of 39 amino acid at the N-terminus [112]. All of these mutations resulted in the abnormal function of the *CACNA2D2* protein in regulation of Ca^{2+} channel activities in mice, and led to the ducky phenotype. Loss of *RASSF1* in *RASSF1*^{-/-} mouse embryonic fibroblasts renders the cells more sensitive to the antimicrotubule agent nocodazole-induced depolymerization of microtubules and alters microtubule stability, which in turn, may affect spindle assembly and chromosome attachment involved in mechanisms of protecting cells from genomic instability and transformation in response to the carcinogenic stimulus [113]. A larger homozygous deletion, approximately 370 kb, in the mouse syntenic chromosome contig of the human 3p21.3 region, has recently been reported by Smith and colleagues to be embryonic lethal in mice [114]. At the beginning of their work, no detailed information on the mouse sequence was available. Therefore the 370 kb deletion was far too large for a critical chromosome region corresponding to the overlapping homozygous deletion region at the 3p21.3 region found in human lung and breast cancers.

Figure 2. Genetic and physical characterization of the mouse 9F1 chromosome contig homologous to the human 3p21.3 homozygous deletion region.



Chromosome engineering technology in the mouse has demonstrated the potential to permit recapitulation of human chromosomal abnormalities, even in situations where the affected gene is unknown [115]. The chromosomal abnormalities are created in embryonic stem (ES) cells by gene targeting and *Cre-loxP* recombination, which can be transmitted through the germ line. This strategy could be used to engineer chromosomes somatically, that is, in a tissue- or cell-type-specific manner without the strong positive selection schemes that are used in cell culture. Tissue-specific deletions also enable recessive genetics to be employed somatically, for instance, to induce LOH to model genetic changes in human cancers or to conduct screens for novel tumor suppressor genes in combination with mutagenesis strategies. Somatic induced deletions may avoid the developmental problems associated with larger germline deletions and consequently, a larger chromosomal region can be studied in a single animal [114-116]. These chromosome engineering technologies are best used in strategies for studying the role of novel 3p21.3 TSGs that are profoundly affected by the chromosome instability in cancer pathogenesis. We are now using a rapid strategy with combined technologies of the *LoxP*-3p21.3 chromosome engineering and tissue-specific *Cre* expression system to conditionally knock out a smaller (approximately 110 kb) genomic DNA contig at mouse chromosome 9F1 region, which mapped at chromosome 9 flanking a genomic sequence contig commencing from about 138360 k at the *CACNA2D2* locus and ending at 108470 k at the *SEMA3B* locus to confirm the role of the 3p21.3-encoded proteins as a tumor suppressor region. The mouse chromosome region of approximately 110 kb covers 13 mouse orthologues of human 3p21.3 genes, including the reported potential 3p21.3 TSGs *CACNA2D2*, *101F6*, *RASSF1*, *FUS1*, *HYAL1*, and *SEMA3B* (Figure 2). Similarly, murine models with conditional ablation of individual 3p21.3 TSGs are also now under development. The development of these murine models of human cancer-carrying chromosomal and genetic abnormalities of 3p21.3 TSGs would provide insight into the molecular mechanisms of 3p21.3 TSGs as a complex genetic trait and thus identify the multiple genetic variant alleles involved in the development of human cancers as well as offer valuable tools for evaluating novel cancer preventing and therapeutic agents and strategies.

Current translational applications with 3p21.3 TSGs

The rapid progress in detecting acquired abnormalities of gene-specific epigenetic promoter methylation has made it possible to use these detection technologies and 3p21.3 genes as biomarkers for the early prediction and diagnosis of human lung cancer, especially in conjunction with analysis of smoking history [117,118]. The hypermethylation of *RASSF1A* promoter is one of the most frequent epigenetic alterations and significantly correlates the loss of expression and pathogenesis in many forms of human cancers [16,123,125]. Unique profiles of aberrant *RASSF1A* methylation have been detected in various types of lung tumors at different pathological stages [119,120] and the methylation-mediated silencing of *RASSF1A* has been reported to significantly correlate with impaired lung cancer patient survival [61,121], poor prognosis and advanced tumor stage [61,122], and with earlier recurrence in Stage I and II NSCLC patients [123]. Hypermethylation of the *RASSF1A* promoter has been found to be significantly associated with the starting age of smoking, although no relationship has been found between *RASSF1A* methylation and other smoking variables, suggesting that *RASSF1A* promoter methylation may be an independent prognostic factor in NSCLC and a useful predictor of lung cancer risk among smokers starting at an early age [78]. In addition, *RASSF1A* methylation in combination with *K-ras* mutation has been shown to have an adverse synergistic effect on patient's survival in NSCLCs [71,72]. Muller and colleagues have recently used a high-throughput DNA methylation assay to systematically analyze aberrant methylation of several independent markers in the serum of breast cancer patients to evaluate their prognostic significance [124]. They found that methylated *RASSF1A* and APC were independently associated with poor outcome and had the worst prognosis with a relative risk of death of 5.7. Due to the frequent occurrence of tumor-acquired promoter methylation of 3p21.3 TSGs, these results underscore the importance of using detailed analysis of 3p21.3 TSG methylation patterns for early detection, molecular staging and prognosis of human cancers.

Multiple 3p21.3 genes show different degrees of tumor-suppressing activities in various human cancers both *in vitro* and in preclinical animal models. To translate these findings to clinic applications for molecular cancer therapy, the

authors recently developed a systemic treatment strategy by using a novel *FUS1*-expressing plasmid vector complexed with dioleoyltrimethylammonium propanecarboxylate (DOTAP:Chol) liposome, termed *FUS1*-nanoparticle, for treating lung cancer and lung metastases [83,125]. In a pre-clinical trial, it has been shown that intratumoral administration of *FUS1*-nanoparticles to subcutaneous NSCLC H1299 and A549 tumor xenograft resulted in significant inhibition of tumor growth. Intravenous injections of *FUS1*-nanoparticles into mice bearing experimental A549 lung metastasis demonstrated a significant decrease in the number of metastatic tumor nodules. Lung tumor-bearing animals, when treated with *FUS1*-nanoparticles, demonstrate prolonged survival, median survival time of 80 days, compared with control animals. These results demonstrate the potent tumor suppressive activity of the *FUS1* gene and the *FUS1*-nanoparticle as a promising therapeutic agent for the treatment of primary and disseminated human lung cancer [83,125]. Based on these studies, a Phase I clinical trial with *FUS1*-mediated molecular therapy by systemic administration of *FUS1*-nanoparticles is now underway in Stage IV lung cancer patients, at the University of Texas MD Anderson Cancer Center in Houston, USA.

Conclusions

The most frequent and early chromosomal and genomic losses and genetic aberrations in the 3p region and 3p21.3 genes are widely found in many types of human cancer. These putative 3p21.3 TSGs are shown to be inactivated in primary tumors more frequently by alternative mechanisms such as epigenetic promoter methylation, aberrant gene splicing and truncation, deficient translation and post-translational modifications of gene products, rather than by somatic mutations observed in classic TSGs such as *p53* and *Rb*. 3p21.3 genes engaged in diverse biological activities governing many key cellular signalling and regulatory processes associated with cell differentiation, proliferation and death. Many 3p21.3 genes demonstrate tumor-suppressing activities in many human cancers *in vitro* and *in vivo*, suggesting that 3p21.3 genes function together as part of a tumor suppressor region in which they interact either to promote tumorigenesis by haploinsufficiency, loss of expression, or rarely, mutations, or to suppress tumor growth through their functional activation of tumor-suppressing pathways. These findings of 3p21.3 TSGs warrant further studies of the

molecular mechanisms involving inactivation and activation of 3p21.3 TSGs in human tumorigenesis and stimulate translational applications using them as anticancer molecular therapeutic agents and targets.

Future perspective

Recent progress in evaluating correlations of the inactivation of 3p21.3 TSGs with pathogenesis of various primary human cancers, in characterizing biological functions and exploring molecular mechanisms of these novel 3p21.3 TSG involved in tumor suppressing and other important biological processes provide us with a framework to form strategies for future translation of these exciting findings into cancer prediction, diagnosis, prognosis, prevention and therapy.

Frequent tumor-acquired promoter hypermethylation in 3p21.3 genes offers a new alternative and important mechanism for inactivating TSGs. In addition, multiple growth-related genes such as *RAR β* , *p16* and *PHIT* are also methylated in individual cancers [126]. The extent and patterns of methylation appears to increase with age [127-129] and vary with smoking history [119,120,128]. As such, it will be interesting to test if these 3p21.3 gene methylations occur as part of the aging process in order to systematically investigate 3p21.3 TSGs and other methylation marker genes in smoking damaged epithelium. This will aid in determining the nature of the tumor-acquired methylation in carcinogenesis and in evaluating the use of the promoter methylation as an intermediate marker of early cancer diagnosis, risk assessment, and response to chemoprevention. The reversal of tumor-acquired epigenetic silencing of 3p21.3 TSGs by demethylation agents, such as AZA, may offer a rational treatment strategy for cancers. The silencing of genes by epigenetic mechanisms involve both DNA and histone modifications and are almost universally associated with histone deacetylation, which is catalyzed by histone deacetylases (HDACs) [127]. An increased density of *RASSF1A* promoter methylation has been shown to be associated with altered chromatin, marked by a depletion of acetylated histones and methylated histone lysine residues [9]. Therefore, a combination treatment with DNA methyltransferase and HDAC inhibitors or interference RNAs may offer a potential epigenetic therapy strategy.

Since the genomic and genetic abnormalities in the 3p region occur in the earliest stage of cancer development, this provides an

opportunity to use 3p21.3 genes as biomarkers for early cancer detection, screening and chemoprevention. For example, the 3p21.3 101F6 has been recently identified as a member of the *cyt-b₅₆₁* protein family, which is involved in the regeneration and maintenance of vitamin C, a well known antioxidant. Restoration of the defect 101F6 gene by wt-101F6 transfer or supplement of functional 101F6 protein or peptides in high-risk patients with potential 3p21.3 deficiency may offer a useful molecular cancer prevention strategy.

The potent tumor suppressing activities, multifunctional characteristics, and direct protein-protein interactions with many important cellular targets demonstrated in 3p21.3 genes, offer great opportunities to develop these 3p21.3 TSGs as gene replacement therapeutics by applying them individually or together and by combining them with other TSGs such as p53, or with chemotherapeutics such as protein kinase inhibitors, microtubule-interfering agents, DNA-damaging agents, apoptosis modulators and inhibitors of angiogenesis and telomerase, to systematically suppress tumor growth and reverse the carcinogenic effects of 3p21.3 TSG defects. Over the next decade it is likely that more efficient and less toxic gene delivery systems will emerge and that 3p21 TSGs will be prime candidates for the development of gene therapeutics given their frequent inactivation in many cancers early in the process of carcinogenesis. The information of 3p21.3 TSGs will be applied in the areas of early detection, risk assessment and evaluating chemoprevention efforts, particularly through detecting methylated promoter sequences and loss of gene expression and in the therapeutic areas, either systemic gene therapy or through the systemic administration of small molecules that mimic the effect of the tumor-suppressor gene products. One could also speculate that increasing knowledge of biological pathways and networks of the 3p21.3 TSGs and functional domains of the gene products may lead to the development of pathways, key regulatory elements, and molecular structure-targeted 'smart drugs' with highly selective anticancer activity.

Acknowledgements

This article is supported by the National Cancer Institute, the National Institutes of Health (SPORE P50CA70907; CA71618); Department of Defense BESCT (DAMD17-01-1-0689) and TARGET (DAMD17-02-1-0706) Lung Cancer Programs.

Executive summary

Genetic abnormalities of 3p & 3p21.3 region in primary cancers

- Allele loss and genetic alteration in chromosome 3p, particularly in 3p21.3 region, are the most frequent and the earliest genomic abnormalities found in a wide spectrum of human cancers. For instance, loss of heterozygosity (LOH) in 3p21.3 region occurs in more than 65% of NSCLC and 95% of SCLC and in 30–87% of breast cancers.

Candidate tumor suppressor genes in the 3p21.3 region

- Nine candidate tumor suppressor genes (TSGs) have been identified in an approximately 120 kb 3p21.3 overlapping homozygous deletion region found in lung and breast cancers.
- Genomic aberrations can be found in smoke damaged respiratory epithelium and occurs in preneoplastic lesions, suggesting one or more 3p21.3 genes function as 'gate-keepers' in pathogenesis of human cancers.

Inactivation of 3p21.3 TSGs in human cancers

- 3p21.3 TSGs are rarely inactivated in human primary cancers by somatic mutations but frequently silenced by alternative mechanisms such as epigenetic promoter methylation of genes and inactivated by loss of expression of gene and gene products or deficiency of post-translational modifications.

Tumor suppression activities of 3p21.3 genes

- Activities of 3p21.3 genes affect and regulate many important biological processes such as cell differentiation, proliferation, cell cycle kinetics, signaling transduction, ion exchange and transportation, apoptosis and cell death.
- Multiple 3p21.3 genes exhibit various degrees of tumor suppression activity *in vitro* and *in vivo* by inhibition of tumor cell growth, induction of apoptosis and alteration of cell cycle kinetics, suggesting that 3p21.3 genes may function as an integrated tumor suppressor region through their diverse biological activities.

3p21.3-targeted mouse model for human cancer

- The mouse autologs of 3p21.3 TSGs have been identified and located at mouse chromosome 9F1-2 region. These mouse genes, like their human counterparts, are clustered in an approximately 200 kb region in 9F with an extremely high density.
- Several mouse mutants of 3p21.3 gene deficiency have been shown to lead to pathogenesis of severe disease and to embryonic lethality. The underline mutations for the mouse ducky mutant, a model for absence epilepsy, have been mapped to the 3p21.3 *CAICHA2D2* gene in mouse chromosome 9F; loss of *RASSF1A* in *RASSF1A*^{-/-} embryonic fibroblasts renders these cells more sensitive to the carcinogen-induced mouse genomic instability and transformation; and the deletion of a 370 kb syntenic chromosome contig of the human 3p21.3 region in mouse chromosome 9 is embryonic lethal.
- Mouse models with conditional ablation of syntenic 3p21.3 region or individual 3p21.3 genes in a specific tissue or organ site would offer valuable tools for elucidating molecular mechanisms of 3p21.3 TSGs in the development of human cancers and for evaluating novel cancer preventing and therapeutic agents and strategies.

Current translational applications with 3p21.3 TSGs

- The hypermethylation of *RASSF1A* promoter is one of the most frequent epigenetic alterations and significantly correlates carcinogenesis in many forms of human cancers. Systematical analysis of *RASSF1A* promoter methylation patterns has been applied for molecular staging and prognosis of human cancers.
- A Phase I clinical trial with the novel FUS1-mediated molecular therapy by a systemic administration of FUS1-expressing plasmid vector complexed with DOTAP/cholesterol nanoparticles is now underway in Stage IV lung cancer patients at MD Anderson Cancer Center, Houston, Texas, USA.

Bibliography

Topics of special note have been highlighted as follows: (*) of interest; (**) of considerable interest; (**) to readers.

1. Hatakeyama T, Weinberg RA: The hallmarks of cancer. *Cell* 110(1), 57–70 (2000).
2. Kimino H: Cancer as a robust system: implications for anticancer therapy. *Nature Rev Cancer* 4(12), 213–235 (2004).
3. Michor F, Iwasa Y, Nowak MA: Dynamics of cancer progression. *Nature Rev Cancer* 4(12), 197–208 (2004).
4. Futreal PA, Coin L, Marshall M *et al*: A census of human cancer genes. *Nature Rev Cancer* 4(12), 177–183 (2004).
5. Claessens T, Bekiranov S: Making the most of microarray data. *Nature Genet* 24(3), 204–206 (2000).
6. Galitski T, Saldanha AJ, Styles CA, Lander ES, Fink GR: Ploidy regulation of gene expression. *Science* 285(5423), 251–254 (1999).
7. Stratton MR, Futreal PA: Cancer: understanding the target. *Nature* 430(6995), 30 (2004).
8. Lerman MI, Minna JD: The 630-kb lung cancer homozygous deletion region on human chromosome 3p21.3: identification and evaluation of the resident candidate tumor suppressor genes. The International Lung Cancer Chromosome 3p21.3 Tumor Suppressor Gene Consortium. *Cancer Res* 60(21), 6116–6133 (2000).
9. Sekido Y, Fong KM, Minna JD: Molecular genetics of lung cancer. *Annu. Rev. Med.* 54:73–5487 (2003).
10. Zabarovsky ER, Lerman MI, Minna JD: Tumor suppressor genes on chromosome 3p involved in the pathogenesis of lung and other cancers. *Oncogene* 21(45), 6915–6935 (2002).
11. Miller BJ, Wang D, Kratz R, Wright EA: Pooled analysis of loss of heterozygosity in breast cancer: a genome scan provides comparative evidence for multiple tumor suppressors and identifies novel candidate regions. *Am. J. Hum. Genet.* 73(4), 748–767 (2003).
12. Minna JD, Fong K, Zochbauer-Muller S, Gazdar AF: Molecular pathogenesis of lung

- cancer and potential translational applications. *Cancer J* 8(Suppl. 1): S41-S46 (2002).
- ▶ 13. Thilagalingam S, Foy KL, Cheng KH *et al*: Loss of heterozygosity as a predictor to map tumor suppressor genes in cancer: molecular basis of its occurrence. *Curr Opin Oncol* 14(1): 65-72 (2002).
 - ▶ 14. Wistuba II, Gazdar AF, Minna JD: Molecular genetics of small cell lung carcinoma. *Semin Oncol* 28(Suppl. 4): 3-13 (2001).
 - ▶ 15. Yan PS, Shi H, Rahmarpanah F *et al*: Differential distribution of DNA methylation within the RASSF1A CpG island in breast cancer. *Cancer Res* 63(19): 6178-6180 (2003).
 - ▶ 16. Maitra A, Wistuba II, Washington C *et al*: High-resolution chromosome 3p allelotyping of breast carcinomas and precancerous lesions demonstrates frequent loss of heterozygosity and a discontinuous pattern of allelic loss. *Am J Pathol* 159(1): 119-130 (2001).
 - ▶ 17. Yang Q, Yoshimura G, Mori I, Sakurai T, Sakurai K: Chromosome 3p and breast cancer. *J Hum Genet* 47(9): 453-454 (2002).
 - ▶ 18. Chakraborty SB, Dasgupta S, Roy A *et al*: Differential deletions in 3p are associated with the development of head and neck squamous cell carcinoma in Indian patients. *Cancer Genet Cytogenet* 146(2): 150-158 (2004).
 - ▶ 19. Glavin D, Volavsek M, Potocnik U, Ravnik Glavic M, Gale N: Low microsatellite instability and high loss of heterozygosity rates indicate dominant role of the suppressor pathway in squamous cell carcinomas of head and neck and loss of heterozygosity of 11q14.3 correlates with tumor grade. *Cancer Genet Cytogenet* 140(1): 27-32 (2003).
 - ▶ 20. Rammund SH, Wellenbosky HJ, Bernauer HS, Jacob B, Mann WJ: Investigations for fine mapping of amplifications in chromosome 3p26.3-28 frequently occurring in squamous cell carcinomas of the head and neck. *Oncology* 62(4): 383-392 (2002).
 - ▶ 21. Moudenan EN, Premeau N, Provencher D, Mac-Meson AM, Tonn PN: Comparative analysis of loss of heterozygosity of specific chromosomes 3, 13, 17, and X loss and TP53 mutations in human epithelial ovarian cancer. *Mol Cytogenet* 34(2): 78-89 (2002).
 - ▶ 22. Simsi A, Palacios D, Linhan WM, Merino MJ, Abari A: Detection of loss of heterozygosity at chromosome 3p25-26 in primary and metastatic ovarian clear-cell carcinoma: utilization of microdissection and polymerase chain reaction in archival tissues. *Diag Cytopathol* 24(5): 328-332 (2001).
 - ▶ 23. Avevedo CM, Henriquez M, Emmert-Buck MR, Chuquai RF: Loss of heterozygosity on chromosome arms 3p and 6q in microdissected adenocarcinomas of the uterine cervix and adenocarcinoma *in situ*. *Cancer* 94(3): 799-802 (2002).
 - ▶ 24. Delias A, Thorhorst J, Jiang F *et al*: Prognostic value of genomic alterations in invasive cervical squamous cell carcinoma of clinical stage IB detected by comparative genomic hybridization. *Cancer Res* 59(14): 3473-3479 (1999).
 - ▶ 25. Herceg CB, Crist KA, Sabourin CL *et al*: Chromosome 3p tumor-suppressor gene alterations in cervical carcinomas. *Mol Carcin* 30(3): 159-168 (2001).
 - ▶ 26. Senchenko V, Liu J, Braga E *et al*: Deletion mapping using quantitative real-time PCR identifies two distinct 3p21.3 regions affected in most cervical carcinomas. *Oncogene* 22(19): 2984-2992 (2003).
 - ▶ 27. Tsai TS, Chen HH, Chan SH *et al*: Clinical significance of allelotyping profiling for urothelial carcinoma. *Urology* 62(2): 378-384 (2003).
 - ▶ 28. Goel A, Arnold CN, Niedzwiecki D *et al*: Characterization of sporadic colon cancer by patterns of genomic instability. *Cancer Res* 63(7): 1608-1614 (2003).
 - ▶ 29. Yashiro M, Carethers JM, Laghi L *et al*: Genetic pathways in the evolution of morphologically distinct colorectal neoplasms. *Cancer Res* 61(6): 2676-2683 (2001).
 - ▶ 30. Hesson CJ, Lindberg D, Einarsson A *et al*: Genetic alterations on 3p, 11q13, and 18q in nonfamilial and MEN 1-associated pancreatic endocrine tumors. *Genet Chrom Cancer* 26(3): 258-264 (1999).
 - ▶ 31. Iacobuzio-Donahue CA, van der Heijden MS, Baumgartner MR *et al*: Large-scale allelotyping of pancreaticobiliary carcinoma provides quantitative estimates of genome-wide allelic loss. *Cancer Res* 64(3): 871-875 (2004).
 - ▶ 32. Hu N, Roth MJ, Polymenopoulos M *et al*: Identification of novel regions of allelic loss from a genome-wide scan of esophageal squamous-cell carcinoma in a high-risk Chinese population. *Genet Chrom Cancer* 27(3): 217-228 (2000).
 - ▶ 33. Kuroki T, Trapasso E, Yendamuri S *et al*: Allele loss and promoter hypermethylation of VHL, RAR- β , RASSF1A, and FHIT tumor suppressor genes on chromosome 3p in esophageal squamous cell carcinoma. *Cancer Res* 63(13): 3724-3728 (2003).
 - ▶ 34. Mueller J, Werner M, Siewert JR: Malignant progression in Barrett's esophagus: pathology and molecular biology. *Recent Results Cancer Res* 15529-15541 (2000).
 - ▶ 35. Shimada Y, Sato F, Watanabe G *et al*: Loss of fragile histidine triad gene expression is associated with progression of esophageal squamous cell carcinoma, but not with the patient's prognosis and smoking history. *Cancer* 89(1): 5-11 (2000).
 - ▶ 36. Wei F, Ni J, Wu SS *et al*: Cytogenetic studies of esophageal squamous cell carcinomas in the northern Chinese population by comparative genomic hybridization. *Cancer Genet Cytogenet* 138(1): 38-43 (2002).
 - ▶ 37. Li M, Zhang ZH, Reuter VE, Cordon-Cardo C: Chromosome 3 allelic losses and microsatellite alterations in transitional cell carcinoma of the urinary bladder. *Am J Pathol* 149(1): 229-235 (1996).
 - ▶ 38. Reznikoff CA, Belair CD, Yeager TR *et al*: A molecular genetic model of human bladder cancer pathogenesis. *Semin Oncol* 23(5): 571-584 (1996).
 - ▶ 39. Finkelsztain SD, Marsh WJ, Demetris AJ *et al*: Microdissection-based allelotyping discriminates *de novo* tumor from intrahepatic spread in hepatocellular carcinoma. *Hepatology* 37(4): 871-879 (2003).
 - ▶ 40. Hussein MR, Sun M, Roggero E *et al*: Loss of heterozygosity, microsatellite instability, and mismatch repair protein alterations in the radial growth phase of cutaneous malignant melanomas. *Mol Carcinog* 34(1): 35-44 (2002).
 - ▶ 41. Liu XQ, Chen HK, Zhang XS *et al*: Alterations of BLU, a candidate tumor suppressor gene on chromosome 3p21.3, in human nasopharyngeal carcinoma. *Int J Cancer* 106(1): 60-25 (2003).
 - ▶ 42. Lo KW, Huang DP: Genetic and epigenetic changes in nasopharyngeal carcinoma. *Semin Cancer Biol* 12(6): 451-462 (2002).
 - ▶ 43. Rodriguez-Serra A, Catarino A, Soares J: Loss of heterozygosity in follicular and papillary thyroid carcinomas. *Cancer Genet Cytogenet* 141(1): 26-31 (2003).
 - ▶ 44. Velickovic M, Delahunt B, Storkel S, Graben SK: VHL and FHIT locus loss of heterozygosity is common in all renal cancer morphotypes but differs in pattern and prognostic significance. *Cancer Res* 61(12): 4815-4819 (2001).
 - ▶ 45. Wistuba II, Tang M, Maitra A *et al*: Genome-wide allelotyping analysis reveals multiple sites of allelic loss in gallbladder carcinoma. *Cancer Res* 61(9): 3795-3800 (2001).

- 46. Wistuba II, Ashfaq R, Maitra A *et al.*: Fragile histidine-triad gene abnormalities in the pathogenesis of gallbladder carcinoma. *Ann. J. Pathol.* 160(6), 2075-2079 (2002).
- 47. Wistuba II, Behrens C, Virmani AK *et al.*: High resolution chromosome 3p allelotyping of human lung cancer and preneoplastic/preinvasive bronchial epithelium reveals multiple, discontinuous sites of 3p allele loss and three regions of frequent breakpoints. *Cancer Res.* 60(7), 1949-1960 (2000).
- 48. Daly MC, Xiang RH, Buchlagen D *et al.*: A homozygous deletion on chromosome 3 in a small cell lung cancer cell line correlates with a region of tumor suppressor activity. *Oncogene* 8(7), 1721-1729 (1993).
- 49. Guo BY, Schabo Y, Maximov A *et al.*: Functional properties of a new voltage-dependent calcium channel $\alpha 2\delta 2$ auxiliary subunit gene (CACNA2D2). *J. Biol. Chem.* 275(16), 12237-12242 (2000).
- 50. Wistuba II, Behrens C, Virmani AK *et al.*: High resolution chromosome 3p allelotyping of human lung cancer and preneoplastic/preinvasive bronchial epithelium reveals multiple, discontinuous sites of 3p allele loss and three regions of frequent breakpoints. *Cancer Res.* 60(7), 1949-1960 (2000).
- 51. Verelst W, Asard H: A phylogenetic study of cytochrome b561 proteins. *Genome Biol.* 4(6), R43 (2003).
- 52. Zochbauer-Müller S, Gazdar AF, Minna JD: Molecular pathogenesis of lung cancer. *Ann. Rev. Physiol.* 64:631-64708 (2002).
- 53. Wistuba II, Behrens C, Virmani AK *et al.*: High resolution chromosome 3p allelotyping of human lung cancer and preneoplastic/preinvasive bronchial epithelium reveals multiple, discontinuous sites of 3p allele loss and three regions of frequent breakpoints. *Cancer Res.* 60(7), 1949-1960 (2000).
- 54. Michler J, Frank SA, May RM, Iwasa Y, Nowak MA: Somatic selection for and against cancer. *J. Theor. Biol.* 225(3), 477-482 (2003).
- 55. Suter CM, Heimann K, Tomlinson IP: Genomic instability - the engine of tumorigenesis? *Nature Rev. Cancer Biol.* 7(1), 701-708 (2003).
- 56. Pihan GD: Mutations and aneuploidy: co-occurrences in cancer? *Cancer Cell* 4(2), 100-104 (2003).
- 57. Wang L, Cammings JM, Shen D *et al.*: Three classes of genes mutated in colorectal cancers with chromosomal instability. *Cancer Res.* 64(9), 2998-3001 (2004).
- 58. Wang TL, Rago C, Silliman N *et al.*: Prevalence of somatic alterations in the colorectal cancer cell genome. *Proc. Natl. Acad. Sci. USA.* 99(5), 3076-3080 (2002).
- 59. Sherr CJ, McCormick P: The RB and p53 pathways in cancer. *Cancer Cell* 2(2), 103-112 (2002).
- 60. Sherr CJ: Principles of tumor suppression. *Cell* 116(2), 235-246 (2004).
- 61. Burber DG, Forgas E, Zochbauer-Müller S *et al.*: Epigenetic inactivation of RASSF1A in lung and breast cancers and malignant phenotype suppression. *J. Natl. Cancer Inst.* 93(9), 691-699 (2001).
- 62. Dammann R, Schagdarsurengin U, Liu L *et al.*: Frequent RASSF1A promoter hypermethylation and K-ras mutations in pancreatic carcinoma. *Oncogene* 22(24), 3806-3812 (2003).
- 63. Haiech CL, Jones PA: Meddling with methylation. *Nature Cell Biol.* 5(6), 502-504 (2003).
- 64. Jones PA, Baylin SB: The fundamental role of epigenetic events in cancer. *Nature Rev. Genetics* 3(6), 415-428 (2002).
- 65. Dammann R, Schagdarsurengin U, Sammakia M *et al.*: Epigenetic inactivation of the Ras-association domain family 1 (RASSF1A) gene and its function in human carcinogenesis. *Histol. Histopathol.* 18(2), 665-677 (2003).
- 66. Zabarovsky ER, Lerman MI, Minna JD: Tumor suppressor genes on chromosome 3p involved in the pathogenesis of lung and other cancers. *Oncogene* 21(45), 6915-6935 (2002).
- 67. Agathangelou A, Dallol A, Zochbauer-Müller S *et al.*: Epigenetic inactivation of the candidate 3p21.3 suppressor gene BLU in human cancers. *Oncogene* 22(10), 1580-1588 (2003).
- 68. Dammann R, Yang G, Pfeifer GP: Hypermethylation of the CpG island of Ras association domain family 1A (RASSF1A), a putative tumor suppressor gene from the 3p21.3 locus, occurs in a large percentage of human breast cancers. *Cancer Res.* 61(7), 3105-3109 (2001).
- 69. Astuti D, Agathangelou A, Honorio S *et al.*: RASSF1A promoter region CpG island hypermethylation in pheochromocytomas and neuroblastomas tumours. *Oncogene* 20(51), 7573-7577 (2001).
- 70. Byun DS, Lee MG, Chae KS, Ryu BG, Chu SC: Frequent epigenetic inactivation of RASSF1A by aberrant promoter hypermethylation in human gastric adenocarcinoma. *Cancer Res.* 61(19), 7034-7038 (2001).
- 71. Kim DH, Kim JS, Park JH *et al.*: Relationship of Ras association domain family 1 methylation and K-ras mutation in primary non-small cell lung cancer. *Cancer Res.* 63(19), 6206-6211 (2003).
- 72. Kim DH, Kim JS, Ji YI *et al.*: Hypermethylation of RASSF1A promoter is associated with the age at starting smoking and a poor prognosis in primary non-small cell lung cancer. *Cancer Res.* 63(13), 3743-3746 (2003).
- 73. Murray PG, Qiu GH, Fu L *et al.*: Frequent epigenetic inactivation of the RASSF1A tumor suppressor gene in Hodgkin's lymphoma. *Oncogene* 23(6), 1326-1331 (2004).
- 74. Reifenberger J, Knobbe CB, Sterzinger AA *et al.*: Frequent alterations of Ras signaling pathway genes in sporadic malignant melanomas. *Int. J. Cancer* 109(3), 377-384 (2004).
- 75. Toyooka S, Carbone M, Toyooka KO *et al.*: Progressive aberrant methylation of the RASSF1A gene in simian virus 40 infected human mesothelial cells. *Oncogene* 21(27), 4340-4344 (2002).
- 76. Spugnardi M, Tommasi S, Dammann R, Pfeifer GP, Hoon DS: Epigenetic inactivation of RAS association domain family protein 1 (RASSF1A) in malignant cutaneous melanoma. *Cancer Res.* 63(7), 1639-1643 (2003).
- 77. Suzuki M, Sunaga N, Shames DS *et al.*: RNA interference-mediated knockdown of DNA methyltransferase 1 leads to promoter demethylation and gene re-expression in human lung and breast cancer cells. *Cancer Res.* 64(9), 3137-3143 (2004).
- 78. Hesson L, Bieche I, Krex D *et al.*: Frequent epigenetic inactivation of RASSF1A and BLU genes located within the critical 3p21.3 region in gliomas. *Oncogene* 23(13), 2408-2419 (2004).
- 79. Qiu GH, Tan LK, Loh KS *et al.*: The candidate tumor suppressor gene BLU, located at the commonly deleted region 3p21.3, is an E2F-regulated, stress-responsive gene and inactivated by both epigenetic and genetic mechanisms in nasopharyngeal carcinoma. *Oncogene* 23(27), 4793-4806 (2004).
- 80. Csoka AB, Frost GI, Stern R: The six hyaluronidase-like genes in the human and mouse genomes. *Matrix Biol.* 20(8), 499-508 (2001).
- 81. Kuroki T, Trapasso F, Yendamuri S *et al.*: Allelic loss on chromosome 3p21.3 and promoter hypermethylation of semaphorin 3B in non-small cell lung cancer. *Cancer Res.* 63(12), 3352-3355 (2003).

- 92. Kondo M, Li L, Kamabayashi C *et al*: Overexpression of candidate tumor suppressor gene FICD isolated from the 3p21.3 homozygous deletion region leads to G1 arrest and growth inhibition of lung cancer cells. *Oncogene* 20(43), 6258-6262 (2001).
- 93. Liao F, Suzuki J, Nishizaki M *et al*: Myristoylation of the hsa1 protein is required for tumor suppression in human lung cancer cells. *Cancer Res* 64(9), 2969-2974 (2004).
- 94. Li L, Nishizaki M, Guo B *et al*: Expression of several genes in the human chromosome 3p21.3 homozygous deletion region by an adenoviral vector results in tumor suppressor activities *in vitro* and *in vivo*. *Cancer Res* 62(19), 2715-2720 (2002).
- 95. Li L, Nishizaki M, Guo B *et al*: Impression of several genes in the human chromosome 3p21.3 homozygous deletion region by an adenoviral vector results in tumor suppressor activities *in vitro* and *in vivo*. *Cancer Res* 62(9), 2715-2720 (2002).
96. Uno F, Suzuki J, Jayachandran G *et al*: Activation of apoptotic signaling pathway by direct interaction between tumor suppressor hsa1 and Apaf-1 proteins in lung cancer cells. *Proc Am Assoc Cancer Res* 45 (2004).
- 97. Agarwal-Gupta A, Brodie L, Ahmed Choudhury I *et al*: Identification of novel gene expression targets for the Ras association domain family 1 (RASSF1A) tumor suppressor gene in non-small cell lung cancer and neuroblastoma. *Cancer Res* 63(17), 5344-5351 (2003).
- 98. Venoni SL, Dello A, Agarwal-Gupta A *et al*: Identification of the E1A-regulated transcription factor p120 E4F as an interacting partner of the RASSF1A candidate tumor suppressor gene. *Cancer Res* 64(1), 102-107 (2004).
- 99. Song MS, Song S, Anad NG *et al*: The tumor suppressor RASSF1A regulates mitosis by inhibiting the APC/Cdc20 complex. *Nature Cell Biol* 6(2), 129-137 (2004).
- 100. Stiverhum L, Minna J, Sakamaki T, Postell R, White MA: The RASSF1A tumor suppressor blocks cell cycle progression and inhibits cyclin D1 accumulation. *Mol Cell Biol* 22(12), 4307-4318 (2002).
- 101. Mahe E: RASSF1A, the new guardian of mitosis. *Nature Genet* 46(2), 117-118 (2004).
- 102. Drajcinski K, Briga E, Kulmin I *et al*: The candidate tumor suppressor gene, RASSF1A, from human chromosome 3p21.3 is involved in kidney tumorigenesis. *Proc Natl Acad Sci USA* 98(13), 7504-7509 (2001).
- 103. Chow LS, Lo KW, Kwong J *et al*: RASSF1A is a target tumor suppressor from 3p21.3 in nasopharyngeal carcinoma. *Int J Cancer* 109(6), 839-847 (2004).
- 104. Carboni GL, Gao B, Nishizaki M *et al*: CACNA2D2-mediated apoptosis in NSCLC cells is associated with alterations of the intracellular calcium signaling and disruption of mitochondria membrane integrity. *Oncogene* 22(4), 615-626 (2003).
- 105. Angeloni D, Wei MH, Duh FM, Johnson BE, Lerman MI: A G-to-A single nucleotide polymorphism in the human $\alpha 2\delta 2$ calcium channel subunit gene that maps at chromosome 3p21.3. *Mol Cell Probes* 14(1), 53-54 (2000).
96. Tomizawa Y, Sekido Y, Kondo M *et al*: Inhibition of lung cancer cell growth and induction of apoptosis after co-expression of 3p21.3 candidate tumor suppressor gene SEMA3B. *Proc Natl Acad Sci USA* 98(24), 13934-13939 (2001).
97. Tso C, Xiang RH, Bracht T, Naylor SL: Human Semaphorin 3B (SEMA3B) located at chromosome 3p21.3 suppresses tumor formation in an adenocarcinoma cell line. *Cancer Res* 62(2), 542-546 (2002).
- 98. Ara J, Bannerman D, Hahn A, Ramirez S, Pleasure D: Modulation of sciatic nerve expression of class 3 semaphorins by nerve injury. *Neurochem Res* 29(6), 1153-1159 (2004).
99. Ochi K, Mori T, Toyama Y, Nakamura Y, Arakawa H: Identification of semaphorin3B as a direct target of p53. *Neoplasia (NY)* 4(1), 82-87 (2002).
- 100. Brambilla E, Constanin B, Drabkin H, Roche J: Semaphorin SEMA3F localization in malignant human lung and cell lines: A suggested role in cell adhesion and cell migration. *Am J Pathol* 156(3), 939-950 (2000).
- 101. Shurdehorst TL, Wilson MD, Wicklow BA, Wilkins JA, Triggs-Raine BL: Characterization of the murine hyaluronidase gene region reveals complex organization and cotranscription of *Hyal1* with downstream genes, *Fus2* and *Hyal3*. *J Biol Chem* 277(25), 23008-23018 (2002).
- 102. Selbi W, de la MC, Hascall V, Phillips A: BMP-7 modulates hyaluronan-mediated proximal tubular cell-monocyte interaction. *J Am Soc Nephrol* 15(5), 1199-1211 (2004).
- 103. Ohno S, Iqin C, Doi T, Yoneno K, Tanne K: Expression and activity of hyaluronidase in human periodontal ligament fibroblasts. *J Periodontol* 73(11), 2331-2337 (2002).
- 104. Csoka AB, Scherer SW, Stern R: Expression analysis of six paralogous human hyaluronidase genes clustered on chromosomes 3p21 and 7q51. *Genomics* 60(3), 356-361 (1999).
- 105. Junker N, Latini S, Petersen LN, Kristjansen PE: Expression and regulation patterns of hyaluronidases in small cell lung cancer and glioma lines. *Oncol Rep* 10(3), 609-616 (2003).
- 106. Tuveson DA, Jacks T: Modeling human lung cancer in mice: similarities and shortcomings. *Oncogene* 18(38), 5318-5324 (1999).
- 107. Balmain A: Cancer as a complex genetic trait: tumor susceptibility in humans and mouse models. *Cell* 108(2), 145-152 (2002).
108. Balmain A, Gray J, Ponder B: The genetics and genomics of cancer. *Nature Genet* (33 Suppl) 238-244 (2003).
- 109. Shibata K, Itoh M, Aizawa K *et al*: RIKEN Integrated Sequence Analysis (RISA) System-384-Format Sequencing Pipeline with 384 Multiplexed Sequencer. *Genome Res* 10(11), 1757-1771 (2000).
- 110. Brodbeck J, Davies A, Courtney JM *et al*: The ducky mutation in *Cacna2d2* results in altered Purkinje cell morphology and is associated with the expression of a truncated $\alpha 2\delta 2$ protein with abnormal function. *J Biol Chem* 277(10), 7684-7693 (2002).
- 111. Barclay J, Balaguero N, Mione M *et al*: Ducky mouse phenotype of epilepsy and ataxia is associated with mutations in the *Cacna2d2* gene and decreased calcium channel current in cerebellar Purkinje cells. *J Neurosci* 21(16), 6095-6104 (2001).
- 112. Brill J, Klocke R, Paul D *et al*: *entla*, a novel epileptic and ataxic *Cacna2d2* mutant of the mouse. *J Biol Chem* 279(8), 7322-7330 (2004).
- 113. Liu L, Tommasi S, Lee DH, Dammann R, Pfeifer GP: Control of microtubule stability by the RASSF1A tumor suppressor. *Oncogene* 22(50), 8125-8136 (2003).
- 114. Smith AJ, Xian J, Richardson M, Johnstone KA, Rabbitts PH: Cre-loxP chromosome engineering of a targeted deletion in the mouse corresponding to the 3p21.3 region of homozygous loss in human tumours. *Oncogene* 21(29), 4521-4529 (2002).
- 115. Zheng B, Sage M, Sheppard EA, Jurecic V, Bradley A: Engineering mouse chromosomes with Cre-loxP: range, efficiency, and somatic applications. *Mol Cell Biol* 20(2), 648-655 (2000).
- 116. Johnson L, Mercer K, Greenbaum D *et al*: Somatic activation of the K-ras oncogene causes early onset lung cancer in mice. *Nature* 410(6832), 1111-1116 (2001).
- 117. Zochbauer-Muller S, Gazdar AE, Minna JD: Molecular pathogenesis of lung cancer. *Annu Rev Physiol* 64(681-697) (2002).

- 118. Zochbauer-Muller S, Lam S, Toyooka S *et al*: Aberrant methylation of multiple genes in the upper aerodigestive tract epithelium of heavy smokers. *Int J Cancer* 107(4): 612-616 (2003).
- 119. Toyooka S, Toyooka KO, Maruyama R *et al*: CpG methylation profiles of lung tumors. *Mol Cancer Ther* 1(1): 61-67 (2001).
- 120. Toyooka S, Maruyama R, Toyooka KO *et al*: Smoke exposure, histologic type and geography related differences in the methylation profiles of non-small cell lung cancer. *Int J Cancer* 103(2): 155-160 (2003).
- 121. Tanizawa Y, Kishino T, Konda H *et al*: Clinical pathological significance of epigenetic silencing of RASSF1A at 3p21.3 in stage I lung adenocarcinoma. *Clin Cancer Res* 8(7): 3482-3488 (2002).
- 122. Agathangelou A, Honorio S, Macartney DP *et al*: Methylation associated inactivation of RASSF1A from region 3p21.3 in lung, breast and ovarian tumours. *Oncogene* 20(12): 1800-1810 (2001).
- 123. Endoh H, Yatabe Y, Shimizu S *et al*: RASSF1A gene inactivation in non-small cell lung cancer and its clinical implication. *Int J Cancer* 100(1): 43-51 (2003).
- 124. Muller HM, Widschwendter A, Fiegl H *et al*: DNA methylation in serum of breast cancer patients: an independent prognostic marker. *Cancer Res* 63(22): 7641-7645 (2003).
- 125. Ito S, Ji L, Tanaka F *et al*: Liposomal vector mediated delivery of the 3p FUS1 gene demonstrates potent antitumor activity against human lung cancer *in vivo*. *Cancer Gene Ther* 11(11): 733-739 (2004).
- 126. Zochbauer-Muller S, Fong KM, Virmani AK *et al*: Aberrant promoter methylation of multiple genes in non-small cell lung cancers. *Cancer Res* 61(1): 249-255 (2001).
- 127. Egger G, Liang G, Aparicio A, Jones PA: Epigenetics in human disease and prospects for epigenetic therapy. *Nature* 429(6990): 457-463 (2004).
- 128. Issa JP: Methylation and prognosis: of molecular clocks and hypermethylator phenotypes. [comment]. *Clin Cancer Res* 9(8): 2879-2881 (2003).
- 129. Issa JP: Age-related epigenetic changes and the immune system. *Clin Immunol* 109(1): 103-108 (2003).
- 130. Chino K, Esumi M, Ishida H, Okada K: Characteristic loss of heterozygosity in chromosome 8p and low frequency of replication errors in sporadic renal cell carcinoma. *J Urol* 162(2): 614-618 (1999).
- 131. Lo KW, Teo PM, Hui AB *et al*: High resolution allelotype of microdissected primary nasopharyngeal carcinoma. *Cancer Res* 60(13): 3348-3353 (2000).

Affiliations

- **Liu Ji, PhD**
Department of Thoracic & Cardiovascular Surgery,
The University of Texas MD Anderson Cancer
Center, Holcombe Blvd., Unit 445, Houston, Texas
77030, USA
Tel: +1 713 563 9143
Fax: +1 713 794 4901
lj@mdanderson.org
- **John D Minna, MD**
Maroon Center for Therapeutic Oncology Research,
The University of Texas Southwestern Medical
Center, Dallas, Texas 75390, USA
Tel: +1 214 648 4900
Fax: +1 214 648 4940
john.minna@utsouthwestern.edu
- **Jack A Roth, MD**
Department of Thoracic & Cardiovascular Surgery,
The University of Texas MD Anderson Cancer
Center, Holcombe Blvd., Unit 445, Houston, Texas
77030, USA
Tel: +1 713 792 7664
Fax: +1 713 794 4901
jroth@mdanderson.org

Z. Ju · M. Kapoor · K. Newton · K. Cheon
A. Ramaswamy · R. Lotan · L. C. Strong · J. S. Koo

Global detection of molecular changes reveals concurrent alteration of several biological pathways in nonsmall cell lung cancer cells

Received: 23 September 2004 / Accepted: 6 May 2005 / Published online: 28 July 2005
© Springer-Verlag 2005

Abstract To identify the molecular changes that occur in non-small cell lung carcinoma (NSCLC), we compared the gene expression profile of the NCI-H292 (H292) NSCLC cell line with that of normal human tracheobronchial epithelial (NHTBE) cells. The NHTBE cells were grown in a three-dimensional organotypic culture system that permits maintenance of the normal pseudostratified mucociliary phenotype characteristic of bronchial epithelium *in vivo*. Microarray analysis using the Affymetrix oligonucleotide chip U95Av2 revealed that 1,857 genes showed a > 1.5-fold change in expression in the H292 cell line relative to the NHTBE cells. Specifically, 418 genes were downregulated and 1,265 were up-regulated in the H292 cells. The expression data for selected genes were validated in several different NSCLC cell lines using quantitative real-time PCR and Western analysis. Further analysis of the differentially expressed genes indicated that WNT responses, apoptosis, cell cycle regulation and cell proliferation were significantly altered in the H292 cells. Functional analysis using fluorescence-activated cell sorting confirmed concurrent changes in the activity of these pathways in the H292 line. These findings show that (1) NSCLC cells display deregulation of the

WNT, apoptosis, proliferation and cell cycle pathways, as has been found in many other types of cancer cells, and (2) that organotypically cultured NHTBE cells can be used as a reference to identify genes and pathways that are differentially expressed in tumor cells derived from bronchogenic epithelium.

Keywords Microarray analysis · Gene expression profile · Biological pathways · Normal human tracheobronchial epithelium (NHTBE) · Nonsmall cell lung cancer (NSCLC)

Introduction

Lung cancer remains a leading cause of cancer death, with an overall 10-year survival rate as low as 8–10% (Fry et al. 1999). It was estimated that more than 170,000 new cases of lung cancer would appear in the United States in 2003 and that about 150,000 individuals would die of the disease (Jemal et al. 2003). Lung cancer occurs in two major subtypes—nonsmall cell lung carcinoma (NSCLC) and small cell lung carcinoma. NSCLC accounts for approximately 80% of all cases, and is further classified as adenocarcinoma, squamous cell carcinoma or large cell carcinoma, based on cell morphology. It is widely accepted that the progenitor cell of adenocarcinoma and squamous cell carcinoma is the epithelial cell of the lung. Squamous cell carcinoma originates mainly from genetically altered surface epithelial cells in the conducting airways, while adenocarcinoma arises from alveolar type II epithelial cells in the lung itself. A better understanding of the etiology and pathogenesis of epithelial cancers should facilitate the identification of novel and better targets for the treatment and prevention of NSCLC.

The recent development of cDNA and oligonucleotide microarray analysis enables us to comprehensively analyze gene expression profiles in NSCLC cells and classify lung cancers at the molecular level (for recent reviews, see Petty et al. 2004; Whitsett et al. 2004 and

Communicated by G. Georgiev.

Z. Ju · M. Kapoor · A. Ramaswamy
Section of Cancer Genetics and Microarray Core Facility,
The University of Texas M. D. Anderson Cancer Center,
Houston, TX, 77030, USA

L. C. Strong
Department of Molecular Genetics, The University of Texas M. D.
Anderson Cancer Center, Houston, TX, 77030, USA

K. Newton · K. Cheon · R. Lotan · J. S. Koo (✉)
Department of Thoracic/Head and Neck Medical Oncology,
The University of Texas M. D. Anderson Cancer Center,
Houston, TX, 77030, USA
E-mail: kskoo@mdanderson.org
Fax: +1-713-7945997

Z. Ju
Molecular Biosciences Research Group, Department of Chemistry
and Biochemistry, Texas State University, San Marcos,
TX, 78666, USA

references therein). However, the use of epithelial tissue from sites adjacent to tumors as the normal control in such studies has drawn criticism (Braakhuis et al. 2004), as this tissue often includes histologically normal but genetically abnormal cells (Braakhuis et al. 2003). In the present study we have used primary organotypically cultured normal human tracheobronchial epithelial (NHTBE) cells as our control. We previously demonstrated that primary TBE cells adopt the mucociliary epithelial organization found *in vivo* when grown and maintained in a retinoid-sufficient bronchial epithelial cell growth medium (BEGM) using a three-dimensional organotypic air-liquid interface (ALI) culture method. We have already demonstrated the utility of this system for studying the physiology of airway epithelium (Koo et al. 1999a, b). Given that lung cancers originate from epithelial cells and that NSCLC cell lines represent mixed histotypes, we chose the human mucoepidermoid pulmonary carcinoma line NCI-H292 (H292) as the counterpart of normal bronchial epithelial cells to identify differentially expressed genes. The H292 cells retain epithelial morphology in culture, and are defined as a mucin-producing NSCLC cell line because they stain positive for mucicarmine (mucous differentiation). They also stain positively for keratin and vimentin, which are indicative of squamous differentiation. The cells have been widely used as surrogate epithelial cells for studying the regulation of *MUC5AC*, a marker for mucin gene expression in the mucous goblet cell of the bronchial surface epithelium (Takeyama et al. 1999; Koo et al. 2002; Lemjabbar and Basbaum 2002).

We used RNAs isolated from fully differentiated NHTBE cells and from the H292 NSCLC cell line to identify expressed genes by oligonucleotide microarray analysis on Affymetrix chips. The results revealed that 1,683 genes were differentially expressed (i.e., showed a ≥ 1.5 -fold change in transcription level). Analysis of the differentially expressed genes revealed concurrent alterations in several biological pathways, including WNT and apoptosis pathways, cell cycle regulation and cell proliferation, in the H292 cell line. The differential expression of selected genes was further verified by real-time PCR and Western analysis in several other NSCLC cell lines. The NHTBE cells promise to be a useful control for the study of lung epithelial carcinogenesis. This study describes alterations in biological networks associated with NSCLC carcinogenesis, and provides a valuable resource for the identification and characterization of diagnostic markers and targets for lung cancer prevention and therapeutics.

Materials and methods

Three-dimensional organotypic ALI culture of NHTBE cells

Passage 1 NHTBE cells (Clonetics, San Diego, CA, USA) were subcultured once and then stored in liquid

nitrogen. The stored cells were used for further cultures as described previously (Koo et al. 1999a, b). Briefly, 1×10^5 passage-2 NHTBE cells were seeded onto 24-mm permeable membranes (Transwell-Clear culture inserts; Corning, Acton, MA, USA) in a 1:1 mixture of BEGM (Clonetics) and Dulbecco's Modified Eagle's Medium (DMEM) supplemented with insulin (5 $\mu\text{g}/\text{ml}$), hydrocortisone (0.072 $\mu\text{g}/\text{ml}$), epidermal growth factor (0.5 ng/ml), T_3 (10^{-8} M), transferrin (10 $\mu\text{g}/\text{ml}$), epinephrine (0.6 $\mu\text{g}/\text{ml}$), bovine pituitary extract (0.8%), BSA (0.5 mg/ml), gentamicin (50 $\mu\text{g}/\text{ml}$) and retinoic acid (5×10^{-6} M). The cultures were kept submerged for the first 7 days, and the medium was removed from the apical compartment to provide the air-liquid interface (ALI) on day 7 or 8 when the cultures were confluent. Culture was continued under these conditions for a further 21 days (changing the medium daily) to generate fully differentiated mucociliary bronchial epithelial cells.

Culture of NSCLC cell lines

The NSCLC cell lines NCI-H226 (H226), H292, NCI-H520 (H520), NCI-H1563 (H1536), NCI-H1703 (H1703), NCI-H1734 (H1734), NCI-H1975 (H1975), NCI-H2228 (H2228), NCI-H2170 (H2170), and A549 were purchased from the American Type Culture Collection (Manassas, VA, USA). All of the cell lines were maintained in RPMI 1640 medium (Gibco BRL, Life Technologies, Grand Island, NY, USA) supplemented with 10% fetal bovine serum (Hyclone, Logan, Utah), penicillin (100 U/ml), and streptomycin (100 mg/ml) on treated, nonpyrogenic, polystyrene tissue culture dishes at 37°C and a pH of 7.0–7.2 in a humidified atmosphere (95% air/5% CO_2). Total RNA for microarray analysis and real-time PCR, and whole-cell lysates for Western analysis, were prepared from the cultured cells 3 days after the monolayers had become confluent.

Histology

For histological analysis, NHTBE and H292 cells were grown on porous membrane inserts (Transwell-Clear plates) in their optimal media (BEGM:DMEM mixture and RPMI with 10% FBS, respectively; see above) for 28 and 10 days, respectively. The detailed method was described previously (Gray et al. 1996; Koo et al. 1999b). The cultures were fixed in 10% neutral buffered formalin, embedded in paraffin, sectioned, and stained with hematoxylin-eosin (HE). The sections were then examined under the microscope and photographed.

RNA and oligonucleotide microarray preparation

Total RNA was extracted from cells using the RNeasy Kit (Qiagen, Valencia, CA, USA) according to the manufacturer's protocol. The Affymetrix (Santa Clara,

MA, USA) GeneChip U95Av2 was employed for microarray hybridizations. This GeneChip carries 12,626 human genes. Each gene is represented by 11–20 different 25mers referred to as perfect match (PM) oligonucleotides, and each PM oligonucleotide is paired with a mismatch (MM) oligonucleotide having a 1-base mismatch at the thirteenth base. Each of the 11–20 PM-MM pairs representing a gene is termed a 'probe set'. Thus, the U95Av2 chip contains 12,626 probe sets. The oligonucleotides are directly synthesized on a silicon chip using a combination of photolithography and combinatorial chemistry.

For microarray hybridization, we followed the protocol described in the Affymetrix manual to synthesize double-stranded cDNA from mRNA and then used this cDNA to synthesize complementary RNA (cRNA). The cRNA was labeled and used for hybridization with the GeneChips. Briefly, 5 µg of total RNA was converted into first-strand cDNA by reverse transcription (RT) in a 20-µl reaction containing 200 U of SuperScript II (Invitrogen, Carlsbad, CA, USA) and 100 pmol of T7-(dT)₂₄ primer [5'-GGCCAGTGAATTGTAA-TACGACTCACTATAGGGAGGCGG-(dT)₂₄-3'] (GeneSet, San Diego, CA, USA). The reaction was incubated at 42°C for 1 h. The second strand of the cDNA was synthesized at 16°C for 2 h in the presence of DNA polymerase I (40 U), DNA ligase (10 U), RNase H (2 U), and 1x second strand buffer (Invitrogen). The double-stranded cDNA was then blunt-ended using 10 U of T4 DNA polymerase, purified by extraction with phenol/chloroform, and transcribed into cRNA in the presence of biotin-labeled ribonucleotides using the BioArray HighYield RNA Transcript Labeling Kit (Affymetrix) as described by the manufacturer. This biotin-labeled cRNA was purified using the Qiagen RNeasy Kit, quantified, and fragmented by incubation at 94°C for 35 min in the presence of 1 (fragmentation buffer [40 mM TRIS-acetate (pH 8.0), 100 mM potassium acetate, and 30 mM magnesium acetate]). The fragmented cRNA was then used for hybridization to the U95Av2 chip at 42°C for 16 h. The chips were washed and stained using Affymetrix GeneChip Fluidic, and scanned and visualized using a GeneArray Scanner (Hewlett-Packard, Palo Alto, CA, USA).

To maintain experimental consistency, approximately equal numbers of cells were collected at similar stages, and the same group of researchers performed the RNA isolation and microarray hybridization in a repeat experiment.

Data collection and bioinformatic analysis

The microarray hybridization data were collected using the Affymetrix Microarray Suite 5.0 software (MAS 5.0). After collection, the data were exported to the Affymetrix MicroDB for further analysis using the Affymetrix Data Mining Tool 3.0 (DMT). The signal-intensity data extracted with the DMT were statistically

analyzed using S-plus 2000 software (Mathsoft, Cambridge, MA, USA) to obtain correlation coefficients and scatter plots for evaluation of the reproducibility and quality of the array analysis. The qualified data sets were then analyzed using DNA-Chip Analyzer software (dChip) (Li and Wong 2001). Briefly, the array data sets were first normalized using a default baseline array; the PM-MM model was then employed to calculate the expression values. To identify the differentially expressed genes using dChip, we set 100 as the average signal-intensity difference to avoid the effects of unreliable low intensity, and used the lower confidence bound of fold change (LBFC; 90%) as the conservative relative change (1.5×). The differentially expressed genes were then subjected to clustering, categorical, and pathway analysis using dChip and public databases such as PubMed (<http://www.ncbi.nlm.nih.gov/entrez/query.fcgi?db=PubMed>), EASEonline (<http://david.niaid.nih.gov/david/upload1.asp>) and the Kyoto Encyclopedia of Genes and Genomes (KEGG, <http://www.genome.ad.jp/kegg/>). Details of the genes (and gene products) specifically considered in this present work are listed in the Tables.

Quantitative real-time PCR (qRT-PCR)

We used qRT-PCR to validate 15 of the differentially expressed genes identified via microarray analysis. The primer pairs used are listed in Table 1. PCR was performed in 25-µl volumes in an iCycler (Bio-Rad, Hercules, CA, USA) using SYBR Green PCR Core Reagents (Applied Biosystems). The reaction contained 0.2-mM primers (Invitrogen), 3-mM MgCl₂, and 3 µl of the RT mix. The housekeeping gene glyceraldehyde-3-phosphate dehydrogenase (GAPDH) was chosen as the reference. Each sample was duplicated in each run, and the experiment was repeated four times. The reactions for tested genes and GAPDH were set up in separate wells of the same 96-well plate, and a prerun using a well factor solution (Bio-Rad) to subtract the background was carried out, followed by an initial denaturation step at 95°C for 10 min. PCR was performed for 40 cycles of denaturation at 95°C for 20 s, and elongation at 60°C for 60 s. Because GAPDH was consistently expressed at a moderate level in the microarray experiment, each PCR result was normalized against the value for GAPDH.

Western analysis

Western analysis used to confirm that differential gene expression was reflected at the translation level. Antibodies raised against beta-catenin (E-5, 1:500), CDK1 (B-6, 1:1000), CCNB1 (GNS-1, 1:1000), GAS6 (D-18, 1:1000), AKT (C-20, 1:1000), API (IAP-1, 1:1000), and BCL2 (C-2, 1:1000) were purchased from Santa Cruz Biotechnology (Santa Cruz, CA, USA). An anti-β-actin

Table 1 Primer pairs used for qRT-PCR

Target gene	Sequence (5'-3')
AATF	TCAGCCTGTCCAGAGAGTT and CGAAGGAGCTGGTGGTAAAA (AATF)
AKT	CACACCACCTGACCAAGATG and CTGGCCGAGTAGGAGAACTG-3'
API5	ACAGGCCGACCTAGAACAGA and AGGGAGAACCTGCTCACAGA
AXL	GACGGGTCTGTGTCCAATCT and ACGAGAAGGCAGGAGTTGAA
BCLX	GGAGCTGGTGGTTGACTTTC and CTCCGATTCAAGTCCCTTCTG
CDK1	CTTTCCATGGGGATTGAGA and AGGCTTCTCGTTTCCATTT
CYCS	TGGGGAAATTGCTTCACTGT and CTTCAACCCTTGCCTTTAAGA
GAS6	GGACCTCGTGCAGCCTATAA and CCTGGATGGTGGTGTCTTCT
IGFBP4	GACCATCGTCTTCTCTCA and GTCTGGACCTCGTGACCATT
KRT6E	CATTGGAGGTGGCTTCAGTT and GAGGAGGAGGTGGTGGTGTGA
LOH1ICR2A	AACCCAAGCCTGATGTCAAC and ACTTGCTGGAGTCTCCCTGA
MYC	GGCAAAAGGTCAGAGTCTGG and GTGCATTTTCGGTTGTTGC
SFRP1	GCTCCAGTTTGCAATTTGGAT and ACCTGAGCCTCTGCATCTA
TF	CCTGATCCATGGGCTAAGAA and CCTCCACAGGTTTCTCGGTA
TP53	TTGGGTCTTTGAACCCTTG and CCACAACAAAACACCAGTGC

antibody (AC-15, 1:5,000) was purchased from Sigma (St. Louis, MO, USA) and used as an internal control. Whole-cell extracts were obtained by lysing cells with 1 ml of lysis buffer [(20% glycerol, 4% SDS, and 0.3% dichlorodiphenyltrichloroethane in 20 mM TRIS-HCl, (pH 6.8)] per well. The cell lysate was quantified, and a total of 30 μ l of the lysate was electrophoresed on SDS-polyacrylamide gels (10%) and transferred to nitrocellulose membranes. Membranes were blocked, incubated with primary antibodies, and subsequently incubated with diluted (1:2,000) horseradish peroxidase-conjugated goat antirabbit IgG or goat antimouse IgG (Bio-Rad). Labeled bands were detected using the SuperSignal West Pico Chemiluminescent Substrate (Pierce, Rockford, Ill.) and exposed to Hyper MP autoradiography film (Amersham, Little Chalfont, Bucks., UK) or Kodak Scientific Image Film (Eastman Kodak, Rochester, NY, USA). β -Actin was used as an internal control.

Fluorescence-activated cell sorting (FACS)

FACS was used to monitor the cell cycle, apoptosis, cell proliferation, and the mitochondrial membrane potential. For cell cycle analysis, cells were seeded in 2 ml of medium at a density of 1×10^5 cells/well in 6-well plates. After the cells had reached confluence, the attached cells were flushed twice with $1 \times$ phosphate-buffered saline (PBS), trypsinized, washed, and resuspended in $1 \times$ PBS.

For cell cycle analysis, a 2-ml aliquot of cell suspension (approximately 10^6 cells) was added to 5 ml of 95% ethanol under gentle vortexing, and then fixed for at least 30 min at room temperature. The fixed cells were then pelleted by centrifugation, resuspended in 1 ml of 50 μ g/ml propidium iodide (PI; Sigma) and 100 μ l of 1 mg/ml RNase (Roche, Indianapolis, Ind.), and incubated at 37°C for 30 min before being loaded onto a FACScan (BD Biosciences, Franklin Lakes, NJ, USA).

For apoptosis analysis, the cell pellet ($\sim 10^6$ cells) obtained after trypsinization and washing was resuspended and stained using the Annexin-V-FLUOS staining kit (Roche) as described in the manufacturer's

instructions. Cells that had not been stained with annexin were used as the controls.

For cell proliferation analysis, cells were seeded into 6-well culture plates at a density of 1×10^5 cells/well. After the cells reached the exponential growth stage, bromodeoxyuridine (BrdU) was added directly to the medium at a final concentration of 10 μ M. The cells were incubated at 37°C for 60 min and stained using the Anti-BrdU-FITC Kit (BD Biosciences) following the manufacturer's instructions. Cells that had not been exposed to anti-BrdU-FITC were used as controls. The absorbance of the FITC at 488 nm was measured using a FACScan (BD Biosciences).

For mitochondrial membrane potential analysis, the mitochondrial membrane potential was normalized and measured using two-color staining with MitoTracker Green (MTGreen) and CMXRosamine (CMXRos) dyes (Molecular Probes, Eugene, OR, USA). Confluent cells were harvested and resuspended at a concentration of 10^6 cells/ml in prewarmed cell culture medium. A 1-ml aliquot was removed to a 15-ml Falcon tube and incubated in a 37°C water bath for at least 5 min. Next, 1 μ l each of the dye stock solutions (200 μ M MTGreen and 200 μ M CMXRos) was added to the cell suspension and mixed well. The cell suspension was incubated at 37°C for 60 min in the dark. The cells were then washed three times using 1 ml of $1 \times$ PBS, and the cell pellet was resuspended in 500 μ l of medium. Immediately after staining, flow cytometry was performed with a FACScan (BD Biosciences) using an excitation wavelength of 488 nm. We measured the emissions with a 530-nm bandpass filter for MTGreen and a 630-nm long-pass filter for CMXRos.

Statistical analysis

The qRT-PCR and FACS data were subjected to statistical analysis. The qRT-PCR experiment was repeated two to four times with duplicates of each sample. In each qRT-PCR, a GAPDH standard curve was generated using the log-starting quantity of a serial dilution of the RT mix. The serial dilution factor was $1/2^n$ ($n = 5$); each

dilution was measured in duplicate. Data acquisition and standard curve generation were performed using an iCycler 3.0 (Bio-Rad). Transcript levels were calculated from the slope of the standard curve using the formula $x(y-b)/a$, where x is the \log_{10} value of the transcript-starting amount, y is the C_t value, a is the slope, and b is the y interception. The relative change was obtained using the ratio of inverse \log_{10} values of x between the tumor and normal cells. Standard errors (SE) were obtained for the fold change based on the repeated QRT-PCR experiments using statistical functions in the Excel software program (Microsoft, Redmond, WA, USA).

The FACS analysis was repeated at least three times. FACS data were collected using a FACScan (BD Biosciences) and analyzed using the WinMDI software (version 2.8) (<http://facs.scripps.edu/software.html>) and Excel statistical functions.

Results

Histological analysis of NHTBE and H292 cells grown in ALI culture

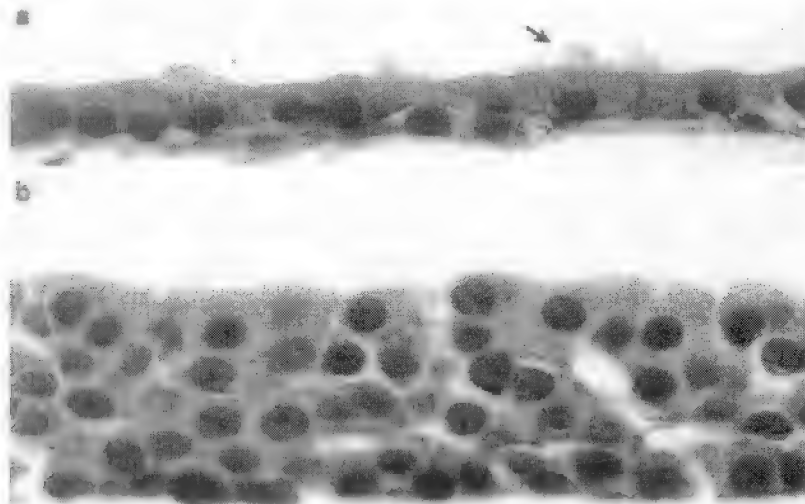
Primary or early passage NHTBE cells were cultured under organotypic ALI conditions in defined serum-free medium supplemented with growth factors and hormones as described previously (Koo et al. 1999a, b). The morphological pattern of differentiation mimicked that of

pseudostratified mucociliary bronchial epithelium *in vivo*, as shown in Fig. 1. Basal cells attached to the basement membrane and a significant number of ciliated cells were clearly visible in the polarized columnar epithelium that formed in the culture system. Under these conditions, the ability of these cells to differentiate into mucous and ciliated cells was maintained. The use of ALI cultures for the study of bronchial epithelial cell biology was demonstrated previously (Gray et al. 1996; Kolodziejewski et al. 2002; Koo et al. 1999b; Singer et al. 2004). In sharp contrast, H292 NSCLC cell lines cultured under similar conditions generated multiple layers of cells that did not display any obvious basal-apical polarity.

Oligonucleotide microarray analysis

To elucidate the molecular events involved in lung epithelial carcinogenesis, we examined global gene expression in NHTBE cells and the H292 cell line using the Affymetrix oligonucleotide chip U95Av2 as described in Materials and methods. The experiment was performed in duplicate. To check the quality of the experiment, we generated scatter plots and calculated correlation coefficients between replicates. We found a strong correlation between replicates within the same samples. The correlation coefficient was 0.97 for NHTBE replicates (Fig. 2a) and 0.99 for H292 replicates (Fig. 2b), and the linear relationship in the x - y plane was close to diagonal (Fig. 2a, b), indicating that the replicates within the samples were highly reproducible and consistent. In contrast, the relationship between replicates of different samples (Fig. 2c-f) was marked by a high degree of scatter and was not linear. Accordingly, the correlation coefficients (0.79, 0.79, 0.85, and 0.85, respectively) were much lower than those for within-sample comparisons, indicating that the nature of the samples had a greater effect on data variation than handling error. Therefore, we concluded that these microarray hybridizations were

Fig. 1 a, b Histological analysis of NHTBE and H292 cells grown in ALI culture. a NHTBE cells were grown under ALI conditions in the presence of retinoic acid (5×10^{-8} M) for 28 days, then fixed in 10% neutral buffered formalin, embedded in paraffin, sectioned, and stained with hematoxylin and eosin. For the detection of mucous goblet cells, the section was also stained with Alcian Blue-Periodic Acid Schiff's (arrows). b Histological section of H292 cells grown in RPMI1640 supplemented with 10% fetal bovine serum for 10 days in ALI culture were prepared and stained with hematoxylin and eosin as described above for NHTBE cells



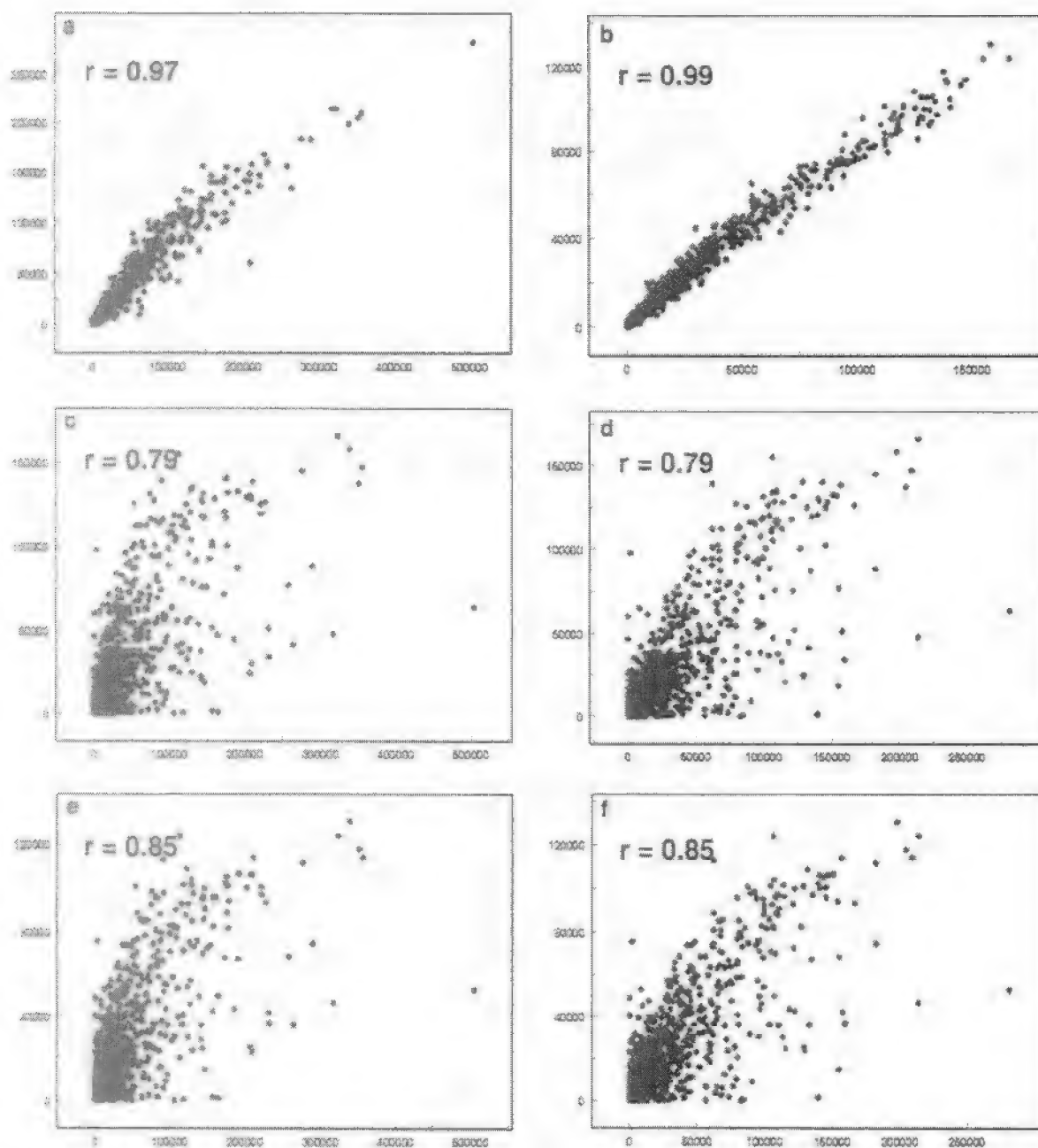


Fig. 2 a-f. Scatter plots of microarray signal intensity data. a Replicate 1 of NHTBE plotted against each other. b Replicates of H292. c Replicate 1 of NHTBE versus replicate 1 of H292. d Replicate 1 of NHTBE versus replicate 2 of H292. e Replicate 2 of NHTBE versus replicate 1 of H292. f Replicate 2 of NHTBE versus replicate 2 of H292. r is the correlation coefficient.

successful and likely to provide reliable data for further analysis.

Differentially expressed genes and the gene expression profile

After qualification and quantification of the microarray experiment, gene expression in the two cell lines was

analyzed, and differentially expressed genes were identified using dChip. Out of 12,625 genes analyzed, 418 were downregulated, and 1,265 were upregulated by at least 1.5-fold in H292 cells relative to the NHTBE cells. The downregulated genes included genes related to the cytoskeleton structure, immunoglobulins, inflammatory stress, the basement membrane, small cytokines, stress responses, and tumor suppressors. The upregulated genes were related mainly to antiapoptosis, the cell cycle, cell growth, extracellular proteins, heat shock proteins, nucleic acid-binding proteins, transcription, and translation. These differentially expressed genes provided the pool for further genomic analysis on biological pathways, biomarkers therapeutic targets (data not shown).

Elucidation of biological pathways

To elucidate the biological pathways affected in the H292 cells, we first used the 'Classify Genes' option in JChip to separate the 1,683 differentially expressed genes into ontology groups. Based on molecular functions, we obtained 1,158 gene ontology groups (approximately 1.5 unique genes per group). Disregarding the more general group categories (such as cell, receptor, kinase, inhibitor, and enzyme), we focused on identification of the groups associated with particular functions and pathways. After data mining, we found that the expression of genes in 30 ontology groups closely related to apoptosis, cell cycle, cell proliferation, and WNT responses (Table 2) were substantially altered in the H292 cell line when compared with NHTBE cells. These groups contained 594 genes representing 146 unique genes (approximately 5.1 unique genes per group), which were subsequently assigned to the four pathways. The overlapping genes were arbitrarily assigned to one or other of these pathways using published information from PubMed, EASEonline, and KEGG. In summary, 18, 56, 48, and 10 unique genes were assigned to the apoptosis, cell cycle, proliferation, and WNT pathways, respectively (data not shown). Differentially expressed genes that showed a more than three-fold change or are directly related to the WNT, cell cycle, proliferation, and apoptosis pathways are listed in Table 3.

Table 2 Gene ontology (GO) classification of differentially expressed genes related to the apoptosis, cell cycle, and proliferation pathways, identified via microarray analysis

GO group	Number of genes
Apoptosis	35
Apoptosis inhibition	7
Apoptosis regulator	7
Cell cycle	77
Cell cycle arrest	8
Cell cycle checkpoint	8
Cell cycle control	50
Cell cycle regulatory	8
Cell death	38
Cell proliferation	75
Control of mitosis	4
DNA replication and chromosome cycle	21
G1/S transition in mitotic cell cycle	8
G2/M transition in mitotic cell cycle	6
Ligand-regulated transcription regulator	11
M phase	13
M phase of mitotic cell cycle	13
Mitosis	15
Mitotic cell cycle	37
Positive control of cell proliferation	21
Negative control of cell proliferation	14
Regulation of CDK activity	6
S phase of mitotic cell cycle	16
Transcription	99
Transcription factor	20
Transcription regulator	48
Translation elongation factor	1
Translation factor	20
Translation initiation factor	5
WNT signaling	10

Validation of the differentially expressed genes

A subset of the differentially expressed genes was chosen for validation by qRT-PCR and Western analysis (Table 3). Fifteen genes, SFRP1, CDK1, MYC, AXL, GAS6, IGFBP4, AATF, AKT, API5, BCLX, CYCS, LOH11CR2A, TP53, KRT6E, and TF, were selected for qRT-PCR validation. SFRP1, which is related to the WNT pathway, was upregulated 12.8-fold in H292 cells compared to NHTBE cells. The cell cycle genes CDK1 and MYC were upregulated 8.0- and 6.2-fold, respectively; the proliferation genes AXL, GAS6, and IGFBP4 were upregulated 2.9-, 18.6-, and 2.6-fold, respectively. The antiapoptosis genes AATF, AKT, API5, and BCLX were upregulated by 43.5-, 23.0-, 38.4-, and 17.7-fold, respectively; the proapoptosis gene LOH11CR2A was downregulated by 33.9-fold, and the proapoptosis genes CYCS and TP53 were upregulated by 27.8- and 23.3-fold, respectively.

Seven genes, Beta-catenin, CDK1, CCNB1, GAS6, AKT, API5, and BCL2, were selected to validate gene expression at the translation level in the NSCLC cell lines H292, H1975, H226, H2170, H520, H1734, H1703, A549, H1536, and H2228 using Western analysis. The transcription levels of these genes in H292 cells were determined by microarray analysis or qRT-PCR. Western analysis revealed that the levels of their products were also elevated in H292 cells compared with those in NHTBE cells (Fig. 3). The expression levels of the proteins Beta-catenin, GAS6, AKT, API5, and BCL2 varied among the different lung cancer cell lines tested. Strikingly, CDK1 and CCNB1 were highly expressed in almost all of the lung cancer cell lines but not in NHTBE cells. The gene expression levels detected by qRT-PCR and Western analysis were in good agreement with those detected by microarray analysis (Table 3).

Validation by FACS analysis of changes in apoptosis, cell cycle kinetics, and cell proliferation

As the expression of genes related to the apoptosis, cell cycle, and proliferation pathways was greatly altered in H292 cells relative to the NHTBE cells, we used FACS analysis to verify that the processes they are expected to mediate or control were altered in a similar manner. Cell cycle analysis using propidium iodide staining indicated that there were significant differences in the numbers of cells in the M4 (apoptotic or necrotic cells), G1/G0, S, and G2 phases between H292 and NHTBE cells (Fig. 4a-c). A significantly lower percentage of H292 cells was found to be in the M4, G1/G0, and G2 phases compared with NHTBE cells, but a significantly higher percentage was in S phase (Fig. 4c). These findings indicate that in H292 cells both the G1/S and G2/M transitions are altered. To confirm these findings and this interpretation, we used more specific methods to analyze apoptosis and cell proliferation in NHTBE and H292 cells (see Materials and methods). To analyze

Table 3 Differentially expressed genes related to WNT pathways, apoptosis, or cell proliferation-identified via microarray analysis

Gene symbol ^a	Gene (product) description	LBFC ^b	Relative change based on qRT-PCR	Western analysis
WNT pathway related				
CDH1	Catenin (cadherin-associated protein), beta 1 (88 kDa)	1.9	NA	Confirmed
CREB	CREB-binding protein	2.3	NA	
CK1	Casein kinase 1	1.7	NA	
CK2	Casein kinase 2	3.8	NA	
DISC	Human Dishevelled protein	2.1	NA	
GAS1	Growth arrest-specific 6	2.4	18.6 ± 2.0	Confirmed
MYC	v-myc myelocytomatosis viral oncogene homolog	3.3	6.2 ± 2.3	
SPRP	Secreted Frizzled-related protein 1	24.3	12.8 ± 5.4	
TCF	T-cell factor	2.1	NA	
Cell cycle related				
CCNB1	Cyclin B1	3.0	NA	Confirmed
CDK1	Cyclin-dependent kinase 1	1.4	8.0 ± 1.4	Confirmed
CITED2	Chp/p300-interacting transactivator	5.2	NA	
E2F	E2F transcription factor 3	3.2	NA	
FEN1	Flap structure-specific endonuclease 1	4.7	NA	
MAD1L1	MAD1 [mitotic arrest deficient-like 1 (yeast)]	3.9	NA	
PDGFA	Platelet-derived growth factor alpha polypeptide	6.6	NA	
SMC1L1	SMC1 [structural maintenance of chromosomes 1-like 1 (yeast)]	3.6	NA	
SMC4L1	SMC4 [structural maintenance of chromosomes 4-like 1 (yeast)]	3.9	NA	
TP53	Tumor protein p53 (Li-Fraumeni syndrome)	3.0	23.3 ± 11.4	
Apoptosis related				
AATF	Apoptosis-antagonizing transcription factor	2.4	43.5 ± 2.7	
AKT	v-akt murine thymoma viral oncogene	1.2	23.0 ± 2.5	Confirmed
API5	Apoptosis inhibitor 5	1.5	38.4 ± 2.3	Confirmed
BCL2	B-cell lymphoma/leukemia-2	2.3	NA	
BCLX	BCL2-like 1	1.2	17.7 ± 2.1	
CYCS	Cytochrome c	2.9	27.8 ± 1.7	
FANCG	Fanconi's anemia, complementation group G	-9.0	NA	
LOH11CK2A	Loss of heterozygosity, 11. chromosomal region 2, gene A	-6.2	-33.9 ± 17.5	
Cell proliferation				
AKR1C3	Aldo-keto reductase family 1, member C3	-3.6	NA	
ANL	ANL receptor tyrosine kinase	24.7	2.9 ± 1.4	
CSU1	CSE1 [chromosome segregation 1-like (yeast)]	3.9	NA	
EGFR	Epidermal growth factor receptor (v-erb-b oncogene)	3.4	NA	
FSCN1	Singed-like (<i>Drosophila</i>) (fascin homolog, sea urchin)	5.5	NA	
GPNMB	Glycoprotein (transmembrane) Nmb	-4.5	NA	
IGFBP4	Insulin-like growth factor-binding protein 4	6.6	2.6 ± 0.7	
MATK	Megakaryocyte-associated tyrosine kinase	3.6	NA	
RARRES3	Retinoic acid receptor responder (tazarotene induced) 3	-9.6	NA	
SERPINF1	Serine (or cysteine) proteinase inhibitor	-3.5	NA	
TGFBI	Transforming growth factor beta-induced	3.5	NA	
Others				
KRT6L	Keratin 6	-5.4	-64.0 ± 29.7	
TF	Transferrin	-22.5	-18.5 ± 6.6	

^a NA, not available.^b Gene symbols obtained from EASEonline.

The data shown indicate the relative changes in expression (LBFC, lower confidence bound of fold change) obtained from microarray analysis. Positive and negative numbers represent upregulation and downregulation, respectively, in H292 cells.

^c The data shown indicate the relative changes in expression (± SE) obtained from QRT-PCR analysis. The values are averages of two to four QRT-PCR experiments.

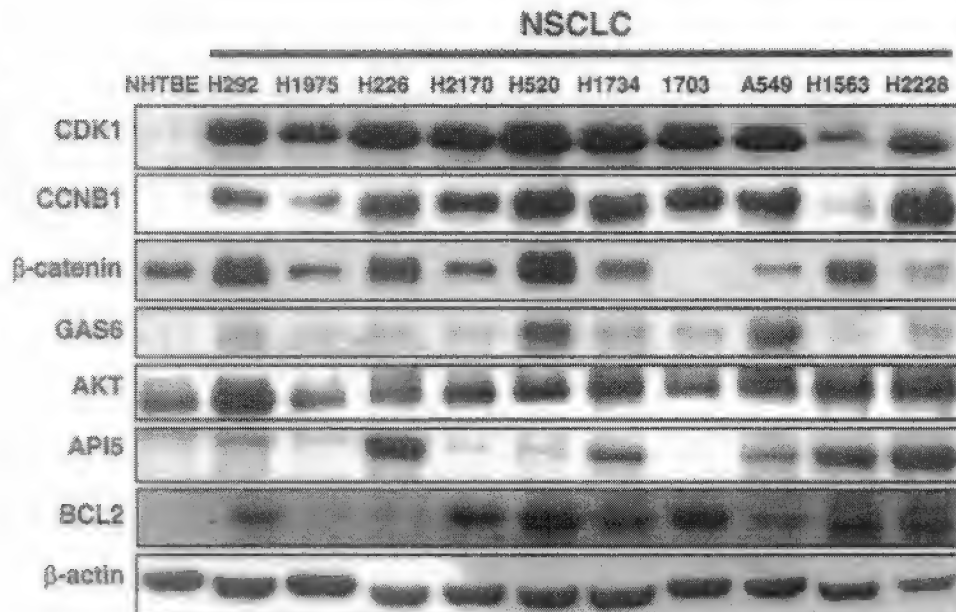
^d Western analysis was used to confirm expression of some of the gene products.

apoptosis, we used Annexin-V-FLUOS in combination with PI to distinguish apoptotic and necrotic cells from viable cells by characterizing the loss of plasma membrane asymmetry, and we performed mitochondrial membrane potential analysis with MTGreen and CMXRos to further elucidate the interaction between BCL2 and CYCS in the H292 cells. The Annexin-V-FLUOS experiment showed that 27.04% of the NHTBE cells underwent programmed cell death, but only 2.05% of the H292 cells did so (Fig. 4d). Analysis of the mitochondrial membrane potential also showed a

statistically significant difference between NHTBE and H292 cells (Fig. 5). Specifically, H292 cells showed significantly less loss of membrane potential than NHTBE cells did. This may be due mainly to BCL2-dependent inhibition of the release of CYCS from the mitochondria in the H292 cells.

In addition, to measure cell proliferation, we calculated the ratio of BrdU-stained nuclei to the total number of nuclei. Immunohistochemical staining using an anti-BrdU-FITC antibody indicated that 19.75% of the H292 cells but only 5.16% of the NHTBE cells were

Fig. 3 Western analysis of selected gene products in various cell lines to validate that the differential expression of genes detected in H292 cells is reflected at the translation level. All of the tested proteins were evaluated in H292 cells and in NHTBE cells (β -actin was used as an internal control)



in the S phase (Fig. 4d). Thus, the H292 cells show a significantly higher rate of cell cycle progression and cell proliferation and a lower level of apoptosis than the NHTBE cells.

Discussion

It is generally accepted that NSCLC, adenocarcinoma and squamous cell carcinoma in the lung generally arise from airway and alveolar epithelial cells. Numerous previous microarray analyses of NSCLC tissues and cell lines focused on survival prediction, molecular characteristics, tumor classification, target identification, and tumor and cell line integration (Petty et al. 2004; Whitsett et al. 2004). However, the use of morphologically normal tissue taken from sites adjacent to tumor tissue as the normal control has provoked concern. In addition, it has been well documented that bronchial epithelial cells do not retain the normal mucociliary phenotype if they are grown and maintained submerged in culture medium on a two-dimensional plastic culture plate (Wu et al. 1990; Ostrowski and Nettiessheim 1995). In this study we used organotypically cultured, fully differentiated, normal primary bronchial epithelial cells, which recapitulate the *in vivo* differentiation of bronchial epithelia as our normal control. The H292 NSCLC cell line was used as the tumor counterpart for microarray analysis and several NSCLC cell lines maintained under their optimal culture conditions were used to verify differential expression of selected genes.

In order to evaluate the usefulness of our model for the study of lung carcinogenesis, we compared our results with gene expression-profiling studies recently done by others using lung specimens and cell lines (Nacht et al. 2001; Amatschek et al. 2004; Kettunen et al. 2004). One should note that it is difficult to

compare studies that use different array platforms or methods (cDNA array; cDNA subtraction; serial analysis of gene expression, SAGE), different types of specimens (tumor tissue vs. normal tissue; tumor tissue vs. tumor cell lines), and different analytical and statistical algorithms, as already pointed out by Kettunen et al. (2004). These differences could contribute to a certain degree of disagreement among studies. We found that our set of differentially expressed genes showed 86.7%, 68.4%, and 62.5% agreement with those presented by Kettunen et al. (2004), Amatschek et al. (2004) and Nacht et al. (2001), respectively (Table 4). Of the upregulated genes identified by Kettunen et al. (2004) in a comparison of tumor tissue with normal tissue, 15 genes overlapped with our set, and 13 (86.7%) of these, including the genes for integrin beta 4 (ITGB4), retinoic acid receptor gamma (RAR γ), insulin-like growth factor-binding protein 5 (IGFBP5), and integrin alpha 6 (ITGA6)—those most highly upregulated in lung specimens—agreed with the expression changes detected in this study. These results indicate that the organotypically cultured primary bronchial epithelial cells could be a useful model for normal controls in the study of lung epithelial carcinogenesis.

We also assigned the differentially expressed genes to biological pathways, and found that genes related to the WNT, apoptosis and cell cycle pathways, and to cell proliferation, were concurrently deregulated in the NSCLC cells. A scheme depicting the biological network consisting of three pathways [WNT, cell cycle and apoptosis, which include the mitochondrially and tumor necrosis factor (TNF)-regulated pathways], and the proliferation phenotype, that are deregulated in H292 cells was constructed based on our findings and data mining using public database PubMed and the KEGG (Fig. 6).

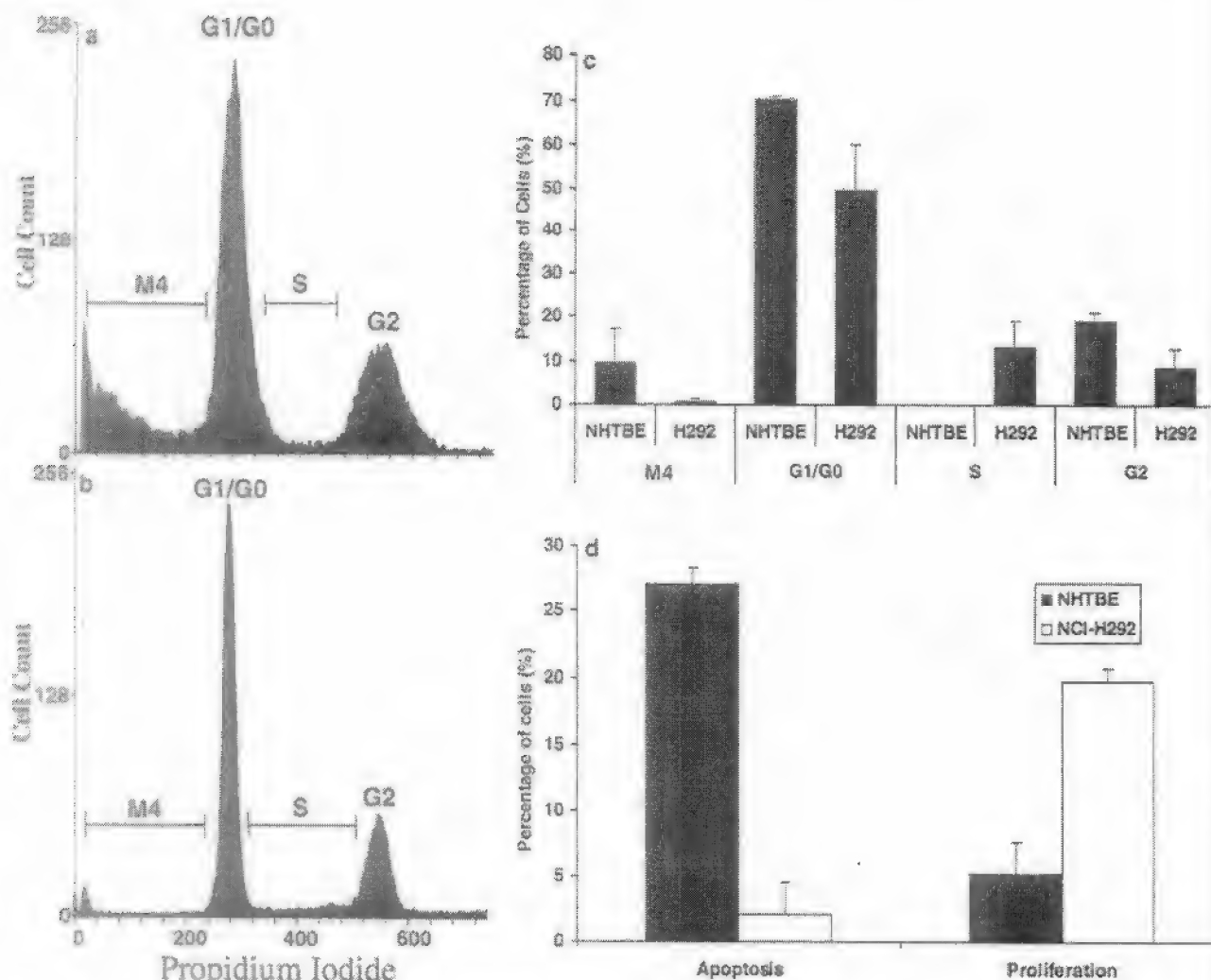


Fig. 4 a-d FACS analysis of the cell cycle, apoptosis, and proliferation in NHTBE and H292 cells. Panels a and b show the results of repeated experiments, which indicate that there were significant differences between the two cell lines. a NHTBE cells. A significantly higher percentage of the NHTBE cells is in the M4 (apoptosis or necrosis) or G2 phase. b H292 cells. A significantly higher percentage of H292 cells is in S phase. c Summary of the statistical analysis. d Comparisons of rates of apoptosis and cell proliferation between the NHTBE and H292 cells indicate that the H292 cells are more active in proliferation and less active in apoptosis. Thus, about 19.75% of the H292 cells progressed from the G1 checkpoint to S phase, but only about 5.16% of the NHTBE cells were in S phase. Moreover, only 2.05% of the H292 cells, compared with 27.04% of the NHTBE cells, were found to be apoptotic.

The WNT pathway has been shown to be involved in approximately 90% of colorectal cancers (Giles et al. 2003). Although differential regulation of components of the the WNT pathway such as β -catenin and Disheveled (Dvl) was previously reported in lung cancer (Smythe et al. 1999), the role of the WNT pathway in lung epithelial carcinogenesis is much less clear. In the current study, we found that 10 WNT pathway-related genes (SFRP, SFRP1, CK1, CK2, Dvl, GAS6, β -catenin, PP2A, CBP, and TCF) were upregulated in H292 cells. For-

mation of WNT-SFP complexes triggers activation of the WNT pathway by activating Dvl, which is also activated through phosphorylation by casein kinase (CK) (Willert et al. 1997). The activated Dvl inhibits formation of a complex comprising Beta-catenin, APC, Axin, and GSK. GAS6, a growth factor, inhibits GSK activity and induces upregulation of cytosolic Beta-catenin (Goruppi et al. 2001). The tumor suppressor genes coding for APC, Axin, and GSK did not show changes in expression in H292 cells, but those for CBP and TCF, which form a transcriptional regulatory complex with β -catenin, were significantly upregulated in H292 cells. Activation of the WNT pathway can account for the overexpression of MYC (which is one of the pathway's critical targets) and an oncogene that has been demonstrated to be overexpressed in NSCLC (Broers et al. 1993).

Surprisingly, SFRP1 was also overexpressed in H292 cells. SFRPs have been reported to sequester WNTs by direct binding (Uren et al. 2000), thus inactivating the WNT pathway. WNTs are secreted growth-factor-like proteins that include at least 19 different isoforms. However, not every isoform induces the release of

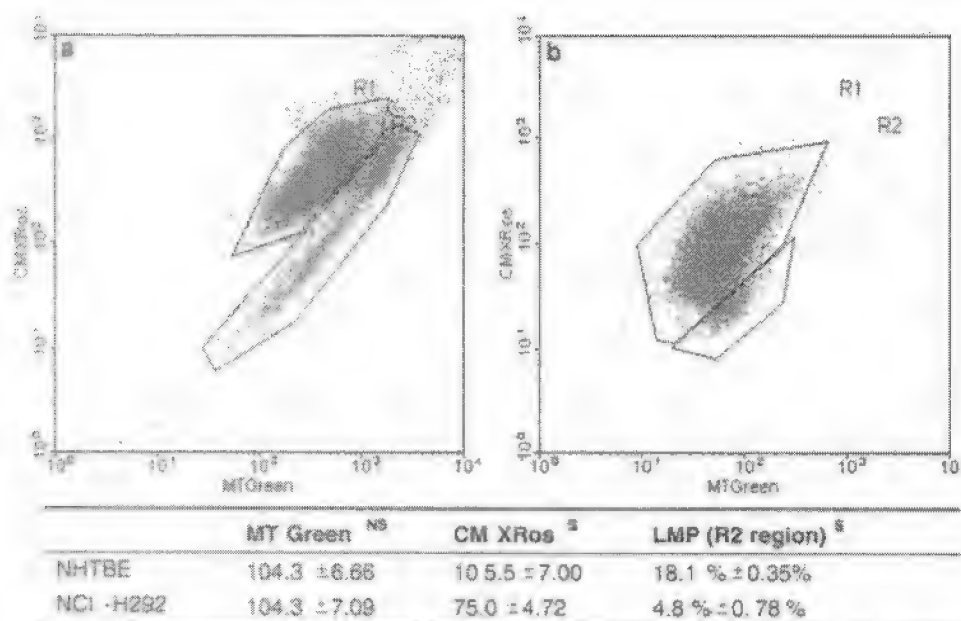


Fig. 5 a, b Measurement of apoptosis based on the loss of mitochondrial membrane potential. Cells were treated with MTGreen (which stains all mitochondria) and CMXRos (which enters mitochondria that show a loss of membrane potential). Panels a and b show combination dot plots for total NHTBE (a) and H292 (b) cells stained with both agents. Areas marked R2 encompass the apoptotic cells, which show a loss of mitochondrial membrane potential. The Table below the graphs summarizes the data obtained from the membrane potential analysis. The values in the MTGreen and CMXRos columns represent the total events (numbers of cells) detected in the MTGreen and CMXRos channels. The MTGreen value is a measure of the number of mitochondria per cell, the CMXRos value is a measure of the induction of apoptosis, as indicated by a drop in mitochondrial membrane potential. The values in the LMP column indicate the percentages of apoptotic cells (those located in the R2 region) in the two dot plots. NS and S represent nonsignificant and significant differences between the NHTBE and H292 cells.

β -catenin and enhances expression of targets of the WNT pathway. Recent discoveries have demonstrated that WNT5a inhibits B cell proliferation and suppresses hematopoietic malignancies (Liang et al. 2003), and promotes degradation of β -catenin (Topol et al. 2003). WNT7a was also reported to be absent, or present in reduced amounts, in lung cancer cells and primary tumors (Calvo et al. 2000). WNT5a and WNT7a have both been implicated as potential tumor suppressor genes (Ohiro et al. 2003; Topol et al. 2003). Thus, further studies will be needed to clarify whether SFRP1 sequesters tumor-suppressing WNTs and prevents tumor-suppressing signals from reaching the WNT pathway. Taken together, our results strongly suggest that the WNT pathways play an important role in lung epithelial cell carcinogenesis.

Genes involved in cell cycle regulation and cell proliferation were also upregulated in H292. Cell cycle genes—specifically CCNB1 and CDK1, the key regulators of the G2/M transition—were ubiquitously overexpressed in all of the NSCLC cell lines tested, but

their expression levels were significantly lower in the NHTBE cells (Fig. 3). CCNB1 and CDK1 form a complex that promotes the G2/M cell cycle transition (Pines 1999; Wasner et al. 2003). It has been reported that patients whose tumors expressed CCNB1 at a high level had a significantly shorter survival time than did patients whose tumors expressed CCNB1 at a low level (Soria et al. 2000), but the roles of the CCNB1-CDK1 complex in lung carcinogenesis is unclear. Further studies of these two genes in NSCLC may contribute to the identification of biomarkers or therapeutic targets. Expression of many cell-proliferation-related genes was substantially altered (at least threefold) in H292 cells. Specifically, the antiproliferation genes RARRES3, GPNMB, AKR1C3, and SERPINF1 were downregulated, and the pro-proliferation genes EGFR, TGFBI, MATK, CSE1, FSCN1, and IGFBP4 were upregulated in H292 cells. In addition, AXL is known to be involved in the neoplastic transformation of fibroblast and leukemia cells (O'Bryan et al. 1991; Neubauer et al. 1997) and GAS6 induces expression of AXL. Both GAS6 and AXL were substantially upregulated in H292 cells. Further characterization of these genes and their functions in normal epithelial cells and lung cancer cells may be helpful in understanding cell cycle regulation and cell proliferation in NSCLC.

Apoptosis was blocked in H292 cells. Apoptosis is regulated by two pathways involving mitochondrial components and TNF, respectively (Budihardjo et al. 1999; Datta et al. 1999). In H292 cells, BCL2, BAG1, AKT, and heat shock proteins may block the mitochondrial pathway that induces apoptosis. BCL2, which has been previously reported to be abnormally expressed in NSCLC (Han et al. 2002), blocks the release of CYCS by blocking the mitochondria voltage-dependent anion channel (Shimizu et al. 1999). HSP70 and HSP90 have been reported to be antiapoptotic proteins (Beere et al.

Table 4 Comparison of differentially expressed genes identified in the present study with data from previous studies

Gene product (name)	LBFC	Compatible with previous findings
A kinase (PRKA) anchor protein (gravin) 12 (AKAP12)	26.5	No ^a
Arachidonate 5-lipoxygenase (ALOX5)	-18.3	Yes ^a
BENE	-3.1	Yes ^a
Bone morphology protein 5 (BMP5)	-2.2	Yes ^a
Caveolin 1 (CAV1)	1.8	No ^a
Cyclin B1 (CCNB1)	3.0	Yes ^{a, b}
Collagen 4, alpha 2 (COL4A2)	3.5	Yes ^a
Desmoplakin 1 (DPI)	6.4	Yes ^{a, c}
High-mobility group protein (HMG1)	2.2	Yes ^a
Insulin-like growth factor-binding protein 5 (IGFBP5)	2.5	Yes ^a
Integrin beta 4 (ITGB4)	1.9	Yes ^a
Integrin group	2.8	Yes ^a
Integrin, alpha 6 (ITGA6)	3.0	Yes ^a
Retinoic acid receptor, gamma (RARG)	2.3	Yes ^a
STAT inducer STAT inhibitor 3 (SOCS3)	-2.1	Yes ^a
Aldehyde reductase family 1, member C3 (AKR1C3)	-5.3	No ^b
Balloon pempigoid antigen 1 (230/240kD) (BPAG1)	7.3	Yes ^b
Calannin (CALU)	2.6	Yes ^b
Cytochrome P450, subfamily 1 (CYP1B1)	2.2	Yes ^b
Glycosylated (transmembrane) nmh (GPNMB)	-7.9	No ^b
Glyoxalase 1 (GLO1)	1.9	Yes ^b
Keratin 6A (KRT6A)	-7.0	No ^b
Laminin, gamma 2 (LAMC2)	-2.8	No ^b
Ornithine decarboxylase 1 (ODC1)	4.5	Yes ^b
Parathyroid hormone-like hormone (PTHrP)	2.1	Yes ^b
Phosphoglycerate kinase 1 (PGK1)	1.9	Yes ^b
Prostaglandin-endoperoxide synthase 2 (PGES2)	5.4	Yes ^b
RAN, member RAS oncogene family (RAN)	2.8	Yes ^b
Reticulocalbin 1, EF-hand calcium-binding domain (RCN1)	2.9	Yes ^b
Transmembrane 4 super family member 1 (TM4SF1)	-2.7	No ^b
TGF-beta factor 3 (mesenchymal) (TGF3)	-2.7	No ^b
Tripartite motif-containing 29 (TRIM29)	2.9	Yes ^b
Aldehyde reductase family 1, member B10 (AKR1B10)	-2.4	No ^c
Keratin 18 (KRT18)	-2.3	Yes ^c
Keratin 17 (KRT17)	5.2	No ^c
Keratin 19 (KRT19)	-3.8	Yes ^c
Keratin 6A (KRT6A)	-7.0	Yes ^c
Myosin I (MYO1)	-6.3	No ^c
Small proline-rich protein 1B (Cornifin)	-5.5	Yes ^c
Tubulin, beta polypeptide (TubulinB)	2.5	Yes ^c

^a Kettunen et al. (2004)^b Amatschek et al. (2004)^c Naeini et al. (2001)

2000; Pandey et al. 2000). HSP70 is localized in both the cytoplasm and the nucleus in 90% of NSCLC cells (Malusecka et al. 2001). HSP70 binds to APAF1 and prevents the recruitment of caspases to the apoptosome complex (Beere et al. 2000), while HSP90 inhibits CYCS-mediated oligomerization of APAF1 and subsequent activation of procaspase 9 (Pandey et al. 2000). The TNF pathway may contribute to the inhibition of apoptosis in H292 cells, as genes for key members of the TNF pathway (TNF, TNF receptor, nuclear factor- κ B, and API) were all substantially upregulated in H292 cells.

Although we maintained primary NHTBE, H292, and other NSCLC cells under conditions that are optimal for culture of the respective lines, as shown by us and others (Rose et al. 2001; Koo et al. 2002), and performed experiments when cultures had reached a stable plateau phase in order to minimize the effect of exponential cell growth on the expression profiles, a caveat to the inter-

pretation of our current results is that the gene expression profiles were compared between NHTBE cells and pulmonary mucocypidermoid NCI-H292 cell line, and thus some of the profiles may only represent subsets of genes unique to the in vitro culture system. Further verification of the differentially expressed genes using clinical tumor samples is required. However, it is noteworthy that the organotypic bronchial epithelial cells in culture, which mimic in vivo airway epithelium, can provide a useful model system for understanding the progression of normal bronchial epithelial cells to premalignant and malignant transformation.

In summary, by comparing the gene expression profile of H292 NSCLC cells with that of NHTBE cells cultured in a three-dimensional organotypic culture system, we were able to identify genes (CCNB1 and CDK1, etc.) which could be potential biomarkers and therapeutic targets. Our results suggest that the abnormal growth

- Karttunen L, Anttila S, Seppanen JK, Karjalainen A, Edgren H, Lindstrom L, Salovaara R, Nissen AM, Salo J, Mattson K, Haefliger I, Knuutila S, Wikman H (2004) Differentially expressed genes in non-small cell lung cancer: expression profiling of cancer-related genes in squamous cell lung cancer. *Cancer Genet Cytogenet* 149:98-106
- Kobayashi PJ, Musial A, Kuo JS, Eissa NT (2002) Ubiquitination of inducible nitric oxide synthase is required for its degradation. *Proc Natl Acad Sci USA* 99:12315-12320
- Kuo JS, Jetten AM, Belloni P, Yoon JH, Kim YD, Nettesheim P (1999a) Role of retinoid receptors in the regulation of mucin gene expression by retinoic acid in human tracheobronchial epithelial cells. *Biochem J* 338:351-357
- Kuo JS, Yoon JH, Gray T, Norford D, Jetten AM, Nettesheim P (1999b) Restoration of the mucous phenotype by retinoic acid in retinoid-deficient human bronchial cell cultures: changes in mucin gene expression. *Am J Respir Cell Mol Biol* 10:61-62
- Kuo JS, Kim YD, Jetten AM, Belloni P, Nettesheim P (2002) Overexpression of mucin genes induced by interleukin-1 beta, tumor necrosis factor-alpha, lipopolysaccharide, and neutrophil elastase is inhibited by a retinoic acid receptor alpha antagonist. *Exp Lung Res* 28:315-332
- Lemjabbar H, Basbaum C (2002) Platelet-activating factor receptor and ADAM10 mediate responses to *Staphylococcus aureus* in epithelial cells. *Nat Med* 8:41-46
- Li C, Wong WH (2001) Model-based analysis of oligonucleotide arrays: expression index computation and outlier detection. *Proc Natl Acad Sci USA* 98:31-36
- Liang H, Chen Q, Coles AH, Anderson SJ, Pihan G, Bradley A, Gorman R, Jurcic R, Jones SN (2003) Wnt5a inhibits B cell proliferation and functions as a tumor suppressor in hematopoietic tissue. *Cancer Cell* 4:349-360
- Matuszewska E, Zborek A, Krzyzowska-Gruba S, Krawczyk Z (2001) Expression of heat shock proteins HSP70 and HSP27 in primary non-small cell lung carcinomas. An immunohistochemical study. *Anticancer Res* 21:1015-1021
- Nade M et al (2001) Molecular characteristics of non-small cell lung cancer. *Proc Natl Acad Sci USA* 98:15203-15208
- Neubauer A, Burchett A, Marwald C, Gruss HJ, Serke S, Huhn D, Wang B, Liu E (1997) Recent progress on the role of Axl, a receptor tyrosine kinase, in malignant transformation of myeloid leukemias. *Leuk Lymphoma* 25:91-96
- O'Bryan JP, Frye RA, Cagwell PC, Neubauer A, Kitch B, Prokop C, Espinosa R III, Le Beau MM, Earp HS, Liu ET (1991) *axl*, a transforming gene isolated from primary human myeloid leukemia cells, encodes a novel receptor tyrosine kinase. *Mol Cell Biol* 11:5016-5031
- Ohira T et al (2003) WNT7a induces E-cadherin in lung cancer cells. *Proc Natl Acad Sci USA* 100:10429-10434
- Ostrowski LE, Nettesheim P (1995) Inhibition of ciliated cell differentiation by fluid submersion. *Exp Lung Res* 21:957-970
- Pantley P, Saleh A, Nakazawa A, Kumar S, Srinivasula SM, Kumar V, Weichselbaum R, Nalin C, Alnemri ES, Kufe D, Choudhury S (2000) Negative regulation of cytochrome c-mediated oligomerization of Apaf-1 and activation of procaspase-9 by heat shock protein 90. *EMBO J* 19:4310-4322
- Petty RD, Nicolson MC, Kerr KM, Collie-Duguid E, Murray GI (2004) Gene expression profiling in non-small cell lung cancer: from molecular mechanisms to clinical application. *Clin Cancer Res* 10:3237-3248
- Pines J (1999) Four-dimensional control of the cell cycle. *Nat Cell Biol* 1:E73-E79
- Rose MC, Nickola TJ, Voynow JA (2001) Airway mucus obstruction: mucin glycoproteins. *MUC* gene regulation and goblet cell hyperplasia. *Am J Respir Cell Mol Biol* 25:533-537
- Shimizu S, Narita M, Tsujimoto Y (1999) Bcl-2 family proteins regulate the release of apoptogenic cytochrome c by the mitochondrial channel VDAC. *Nature* 399:483-487
- Singer M, Martin LD, Vargafig BB, Park J, Gruber AD, Li Y, Adler KB (2004) A MARCKS-related peptide blocks mucus hypersecretion in a mouse model of asthma. *Nat Med* 10:193-196
- Smythe WR, Williams JP, Wheelock MJ, Johnson KR, Kaiser LR, Albelda SM (1999) Cadherin and catenin expression in normal human bronchial epithelium and non-small cell lung cancer. *Lung Cancer* 24:157-168
- Soria JC, Jang SJ, Khuri FR, Hassan K, Liu D, Hong WK, Mao L (2000) Overexpression of cyclin B1 in early-stage non-small cell lung cancer and its clinical implication. *Cancer Res* 60:4000-4004
- Takeyama K, Dabbagh K, Lee HM, Agusti C, Lausier JA, Ueki IF, Grattan KM, Nadel JA (1999) Epidermal growth factor system regulates mucin production in airways. *Proc Natl Acad Sci USA* 96:3081-3086
- Topol L, Jiang X, Choi H, Garrett-Beal L, Carolan PJ, Yang Y (2003) Wnt-5a inhibits the canonical Wnt pathway by promoting GSK-3-independent beta-catenin degradation. *J Cell Biol* 162:899-908
- Uren A, Reichsman F, Anesi V, Taylor WG, Muraiso K, Bottaro DP, Cumberledge S, Rubin JS (2000) Secreted Frizzled-related protein-1 binds directly to Wntless and is a biphasic modulator of Wnt signaling. *J Biol Chem* 275:4374-4382
- Wasner M, Tschop K, Spiesbach K, Haugwitz U, John C, Mossner J, Mantovani R, Engeland K (2003) Cyclin B1 transcription is enhanced by the p300 coactivator and regulated during the cell cycle by a CHR-dependent repression mechanism. *FEBS Lett* 536:66-70
- Whitsett JA et al (2004) Functional genomics of lung disease. *Am J Respir Cell Mol Biol* 31:S1-S81
- Willert K, Brink M, Wodarz A, Varmus H, Nusse R (1997) Casein kinase 2 associates with and phosphorylates dishevelled. *EMBO J* 16:3089-3096
- Wu R, Martin WR, Robinson CB, St George JA, Plopper CG, Kurland G, Last JA, Cross CE, McDonald RJ, Boucher R (1990) Expression of mucin synthesis and secretion in human tracheobronchial epithelial cells grown in culture. *Am J Respir Cell Mol Biol* 3:467-478

Phase I Study of the Farnesyltransferase Inhibitor Lonafarnib with Paclitaxel in Solid Tumors

Fadilo R. Khuri,¹ Bonnie S. Glisson,² Edward S. Kim,² Paul Statkevich,³ Peter F. Thall,² Michael L. Meyers,³ Roy S. Herbst,² Reginald F. Munden,² Craig Tendler,⁴ Yali Zhu,³ Sandra Bangert,² Elizabeth Thompson,² Charles Lu,² Xue-Mei Wang,² Dong M. Shin,² Merrill S. Kies,² Vili Papadimitrakopoulou,² Frank V. Fossella,² Paul Kirschmeier,³ W. Robert Bishop,³ and Waim Ki Hong²

¹Winship Cancer Institute, Emory University, Atlanta, Georgia; ²The University of Texas M. D. Anderson Cancer Center, Houston, Texas; and ³Schering-Plough Research Institute, Kenilworth, New Jersey

ABSTRACT

Purpose: To establish the maximum tolerated dose of lonafarnib, a novel farnesyltransferase inhibitor, in combination with paclitaxel in patients with solid tumors and to characterize the safety, tolerability, dose-limiting toxicity, and pharmacokinetics of this combination regimen.

Experimental Design: In a Phase I trial, lonafarnib was administered p.o., twice daily (b.i.d.) on continuously scheduled doses of 100 mg, 125 mg, and 150 mg in combination with i.v. paclitaxel at doses of 135 mg/m² or 175 mg/m² administered over 3 h on day 8 of every 21-day cycle. Plasma paclitaxel and lonafarnib concentrations were collected at selected time points from each patient.

Results: Twenty-four patients were enrolled; 21 patients were evaluable. The principal grade 3/4 toxicity was diarrhea (5 of 21 patients), which was most likely due to lonafarnib. Dose-limiting toxicities included grade 3 hyperbilirubinemia at dose level 3 (100 mg b.i.d. lonafarnib and 175 mg/m² paclitaxel); grade 4 diarrhea and grade 3 peripheral neuropathy at dose level 3A (125 mg b.i.d. lonafarnib and 175 mg/m² paclitaxel); and grade 4 neutropenia with fever and grade 4 diarrhea at level 4 (150 mg b.i.d. lonafarnib and 175 mg/m² paclitaxel). The maximum tolerated dose established by the continual reassessment method was

lonafarnib 100 mg b.i.d. and paclitaxel 175 mg/m². Paclitaxel appeared to have no effect on the pharmacokinetics of lonafarnib. The median duration of therapy was eight cycles, including seven cycles with paclitaxel. Six of 15 previously treated patients had a durable partial response, including 3 patients who had previous taxane therapy. Notably, two of five patients with taxane-resistant metastatic non-small cell lung cancer had partial responses.

Conclusions: When combined with paclitaxel, the recommended dose of lonafarnib for Phase II trials is 100 mg p.o. twice daily with 175 mg/m² of paclitaxel i.v. every 3 weeks. Additional studies of lonafarnib in combination regimens appear warranted, particularly in patients with non-small cell lung cancer.

INTRODUCTION

Mutations of the *ras* family of oncogenes that result in unregulated cell proliferation are common in human cancers (1). The *ras* mutations have been implicated in the development of colorectal cancer and have been associated with shortened survival in several tumor types, including non-small cell lung cancer (NSCLC; Refs. 2-6). *Ras* genes encode a protein, p21, that is located on the inner surface of the plasma membrane (1, 7). The p21 protein has GTPase activity and participates in signal transduction. Activation of the *ras* oncoprotein requires prenylation, a process that is catalyzed by farnesyltransferase (8-12).

Farnesyltransferase inhibitors (FTIs) are a novel class of compounds that block this critical enzymatic step in the formation of active *ras* proteins (8-13). Lonafarnib (Sarasar; Schering-Plough Corporation, Kenilworth, NJ) is a tricyclic nonpeptidomimetic compound (Fig. 1) that is active against a variety of tumors *in vitro* and in animal models of cancer (14). The antitumor activity of lonafarnib and other FTIs is related to the inhibition of farnesylation, although controversy currently surrounds the exact farnesylated proteins that are the key targets of FTIs (15, 16). For example, Ashar *et al.* (17) and Crespo *et al.* (18) have shown that FTIs have important effects on cell cycle arrest. The data of Crespo *et al.* suggest a direct effect on spindle formation with resultant prometaphase accumulation of mitotic lung cancer cells. Ashar *et al.* also showed that CENP-E and CENP-F, two centromeric proteins preferentially expressed in mitotic cells, are direct substrates for FTIs, and that their prenylation is completely inhibited by lonafarnib (19).

Compelling data reported by Moasser *et al.* supplied the scientific underpinning for our present study (20). They showed that, in several cell lines initially resistant to paclitaxel, the addition of a FTI enhanced the sensitivity of those cell lines to paclitaxel. Subsequent preclinical studies have demonstrated synergistic effects with lonafarnib plus paclitaxel on a number of human cell lines *in vitro* (21, 22) and enhanced activity *in vivo* (22). In the NCI-H460 lung cancer xenograft model, inhi-

Received 10/15/03; revised 12/16/03; accepted 1/9/04.

Grant support: F. Khuri was supported by Schering-Plough Research Institute and DAMD 17-02-1-0706.

The costs of publication of this article were defrayed in part by the payment of page charges. This article must therefore be hereby marked advertisement in accordance with 18 U.S.C. Section 1734 solely to indicate this fact.

Requests for reprints: Fadilo R. Khuri, Winship Cancer Institute, Emory University, 1365 Clifton Road NE, Building C-3094, Atlanta, GA 30322. Phone: (404) 778-4250; fax: (404) 778-5520; E-mail: fkhuri@emory.edu.

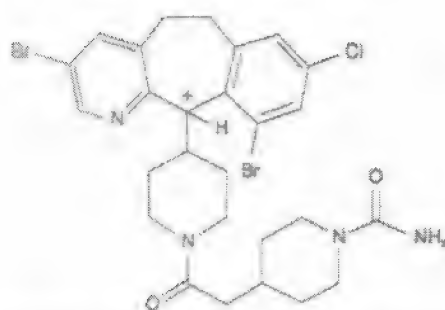


Fig. 1. Structure of lonafarnib [1-(1R)-4-[2-[4-(3,10-dibromo-8-chloro-6,11-digerm-5,6-benzop[5,6]cyclohepta[1,2b]pyridin-1-yl)-1-piperazin-2-yl]-2-oxoethyl]-1-piperidinecarboxamide].

tion of tumor growth was significantly greater with oral lonafarnib plus i.p. paclitaxel than with either agent alone (86% versus 52% and 61%, respectively; $P < 0.05$). Tumor growth inhibition on days 7 and 14 were 56 and 65% greater, respectively, with the combination than with paclitaxel alone. In line *tv-wp-mcf* transgenic male mice, which develop paclitaxel-resistant mammary tumors at 6–9 weeks of age, oral lonafarnib significantly inhibited tumor growth ($P = 0.05$) and also sensitized the tumors to paclitaxel treatment, so that the combination of lonafarnib plus paclitaxel was more effective than lonafarnib alone ($P = 0.06$ for days 7 to 21; Refs. 22, 23). One proposed explanation for the synergistic activity is that treatment with FTI causes cells to accumulate in the G_2 -M phase of the cell cycle in which paclitaxel is most effective (21, 24).

The main objectives of this trial were to establish the maximum tolerated dose (MTD) of lonafarnib, a novel FTI, in combination with paclitaxel in patients with solid tumors and to characterize the safety, tolerability, and dose-limiting toxic effects of this combination in patients with advanced solid malignancies. Furthermore, we particularly wanted to see whether durable responses could be achieved in a variety of taxane-sensitive tumors in patients previously treated with taxanes. Finally, we sought to characterize the pharmacokinetics of multiple-dose lonafarnib after its daily oral administration and of paclitaxel coadministered with daily lonafarnib.

PATIENTS AND METHODS

We sought to establish the MTD and the dose-limiting toxicity (DLT) of the lonafarnib/paclitaxel combination in adult patients with solid tumors. Previously treated patients and untreated patients were allowed to participate in the study. Eligibility criteria included a Karnofsky performance status of at least 70%, a histologically confirmed malignancy for which no curative treatment was available, measurable disease, and adequate hematological parameters [including a WBC count $\geq 3,000/\text{mm}^3$, an absolute neutrophil count of $1,500/\mu\text{l}$ ($\geq 1.5 \times 10^9/\text{liter}$), a platelet count $\geq 100 \times 10^9/\text{liter}$, and a hemoglobin level ≥ 10 g/dl]. Furthermore, patients were required to have adequate renal function, with a serum creatinine level ≤ 1.5 times the upper limit of normal or a measured 12-h creatinine clearance time of ≥ 50 ml/min/1.73 m^2 . Also mandatory were normal hepatic function [baseline transaminase levels

≤ 3 times the upper limit of normal, bilirubin ≤ 2.0 mg/dl, and albumin ≥ 3.0 g/dl] and no manifestations of a malabsorption syndrome. All patients had to sign a written informed consent approved by the Institutional Review Board at the University of Texas M. D. Anderson Cancer Center. Patients taking agents that might alter the metabolism of lonafarnib via the CYP3A4 hepatic enzymatic system (such as azoles, macrolides, cyclosporin, systemic corticosteroids, estrogens, antiepileptic drugs, rifampin, or isoniazid), or who had metastases to the brain were excluded from the study.

Patients received lonafarnib capsules p.o. twice daily (b.i.d.) with food as 50-mg, 75-mg, and 100-mg formulations in combination with paclitaxel administered i.v. every 3 weeks at 135 mg/m^2 or 175 mg/m^2 over 3 h (Fig. 2). Premedication consisted of 20 mg i.v. dexamethasone and 8 mg of i.v. ondansetron.

Statistical Methods. The dose-finding portion of the trial was conducted in a group of patients with a variety of different head and neck and lung cancers. The principal scientific goal was to determine a MTD, defined as the dose level at which the toxicity rate was closest to 20% and less than 33% with at least 33% of patients experiencing dose-limiting toxicities (DLT) at the next higher level. DLT was defined as the following: absolute neutrophil count $< 500/\mu\text{l}$ for longer than 5 days or with fever $\geq 38.3^\circ\text{C}$; grade 4 thrombocytopenia (platelets $< 25,000/\mu\text{l}$) or anemia (Hb < 6.5 g/dl); grade 3–4 nausea/vomiting or grade 3 diarrhea despite optimal antiemetic or antidiarrheal treatment; or any other grade 3 treatment-related nonhematological toxicity; and treatment delay for toxicity lasting > 2 weeks.

Associations between pairs of variables were assessed using the Fisher exact test, Kruskal-Wallis test, and Jonkheere-

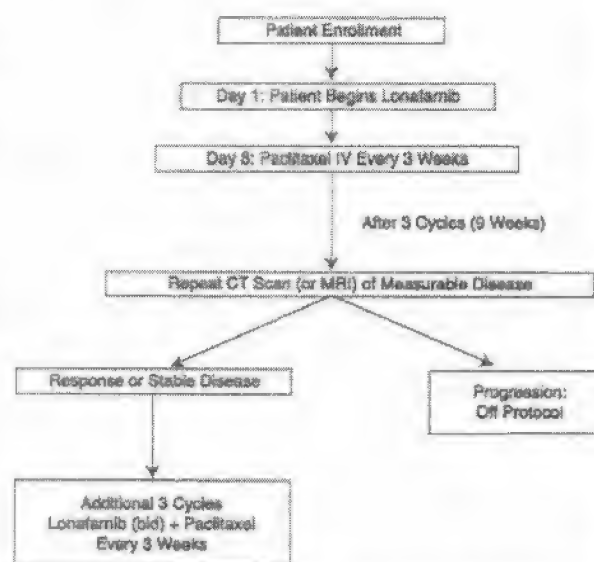


Fig. 2. Study design. Patients begin lonafarnib 1 week before receiving paclitaxel. Reevaluation occurs after every three cycles of treatment. If patients have responsive or stable disease, they proceed on study. If patients have progressive disease, they go off the study protocol. CT, computed tomography; MRI, magnetic resonance imaging.

Table 1. Number of patients and cycles by dose level of paclitaxel and lonafarnib in Phase I trial

Dose level	Paclitaxel (mg/m ²)	Lonafarnib (mg b.i.d.)	Cycles	No. of patients
1	135	50	0	0
2	135	100	1-9	3
			10-15	2
			16-32	1
3	175	100	1-3	9
			4-6	6
			7	5
			8	4
			9	2
			10-11	1
4A	175	125	1	5
			2-5	6
			4-6	5
			7-8	4
			9-10	3
			11-17	2
			18-24	1
4	175	150	1-2	4
			3-7	3
			8	2
			9-27	1

Terpstra test (25). Regression models of toxicity on the doses of paclitaxel and lonafarnib, and the indicator of prior chemotherapy, were fit using exact logistic regression (26, 27). Confidence intervals for probabilities of toxicity at particular dose and prior chemotherapy combinations were computed by repeating the exact logistic regression on 1000 bootstrap samples of the data. All of the computations were carried out using StatXact and SAS Proc Logistic.

Pharmacokinetic Methods. Plasma lonafarnib and paclitaxel concentrations were determined using validated liquid chromatography with tandem mass spectrometric detection and the high-performance liquid chromatography method, respectively. The lower limits of quantitation were 5.00 and 10.0 ng/ml plasma for lonafarnib and paclitaxel, respectively, and the linear ranges were 5.00-2500 ng/ml and 10.0-2500 ng/ml, respectively. The assay precision (% coefficient of variation) and accuracy (% bias) were <11% and <10%, respectively, for lonafarnib, and <7% and <6%, respectively, for paclitaxel. Noninterference from the respective coadministered drug was demonstrated for both of the lonafarnib and paclitaxel methods.

Blood samples (1-3 ml) for determination of plasma lonafarnib and paclitaxel concentrations were collected on day 1 of Cycle 1. Plasma was separated by centrifugation (4°C, ~3000 rpm for 15 min), then divided into two aliquots, and was stored frozen at -70°C until shipped to the analytical facility.

Individual plasma lonafarnib and paclitaxel concentrations were used for pharmacokinetic analysis using model-independent methods. The maximum plasma concentration (C_{max}) and time of maximum plasma concentration (T_{max}) were the observed values. The terminal phase rate constant (λ) was calculated as the negative of the slope of the log-linear terminal portion of the plasma concentration-versus-time curve using

linear regression. The terminal phase half-life, $t_{1/2}$, was calculated as $0.693/\lambda$. The area under the plasma concentration-versus-time curve from time 0 to the time of final quantifiable sample ($AUC_{(0-t)}$) and from time 0 to 12 h ($AUC_{(0-12\text{ h})}$) was calculated using the linear trapezoidal method. For paclitaxel, the $AUC_{(0-t)}$ was extrapolated to infinity when appropriate as follows: $AUC_{(0-\infty)} = AUC_{(0-t)} + C_{(t)}/\lambda$, where $C_{(t)}$ is the estimated concentration determined from linear regression at time t . Total body clearance, CL/F (lonafarnib) or CL (paclitaxel), was calculated by the following equation: $CL/F = \text{Dose}/AUC$. The apparent volume of distribution, Vd/F (lonafarnib) or Vd (paclitaxel), was calculated as: $Vd/F = (\text{Dose}/AUC)/\lambda$.

For paclitaxel, the volume of distribution at steady state, Vd_{ss} , was estimated as total body clearance multiplied by mean residence time (MRT).

RESULTS

Twenty-four patients with a mean age of 58.3 years were enrolled on this Phase I study at the University of Texas M. D. Anderson Cancer Center, with the enrollment of new patients beginning on June 16, 1999, and continuing through March 30, 2000. Twenty-one patients actually received both paclitaxel and lonafarnib (Table 1). Patients were predominantly male (67%) and Caucasian (92%), with Karnofsky performance status of 90 to 100 (71%; Table 2). Slightly more than one-half of the patients had a primary diagnosis of NSCLC.

Toxicities. Among all of the dose levels, 92% of patients reported at least one toxicity at any grade and 54% of patients reported at least one grade 3/4 treatment-emergent nonhematological adverse event judged to be related to the study drugs. The most common treatment-related treatment-emergent nonhematological adverse events (including all grades) reported were gastrointestinal effects in 92% of patients (diarrhea 92%, nausea 79%, vomiting 50%, constipation 46%, stomatitis 38%, abdominal pain 29%); fatigue (88%), alopecia (83%), peripheral neuropathy (79%), arthralgia (71%), infections and infestations in 50% of patients (folliculitis 38%, oral candidiasis 13%, pneu-

Table 2. Patient demographics and disease characteristics

Subjects (n)	24
Age (yr)	
Median	59.5
Range	41-75
Sex	
Men	16 (67%)
Women	8 (33%)
Karnofsky performance status:	
Missing	1 (4%)
70-85	6 (25%)
90-100	17 (71%)
Histology	
NSCLC*	14 (58%)
Salivary	6 (25%)
HNSCC	4 (17%)
Prior chemotherapy (n = 21)	13
Prior taxane (n = 21)	9

* NSCLC, non-small cell lung cancer; HNSCC, head and neck squamous cell carcinoma.

Table 3 Number of patients with severe (grade 3) or life-threatening (grade 4) nonhematologic toxicities

Toxic effect	Dose level 2 (n = 3)		Dose level 3 (n = 9)		Dose level 3A (n = 5)		Dose level 4 (n = 4)	
	Grade 3	Grade 4	Grade 3	Grade 4	Grade 3	Grade 4	Grade 3	Grade 4
Headache	0	0	0	0	1	0	0	0
Cardiac arrest	0	0	0	0	0	0	0	1
Chest wall pain	0	0	1	0	0	0	0	0
Diarrhea	0	0	2	0	1	1	2	0
Dysphagia	0	0	1	0	0	0	0	0
Dyspnea	0	0	0	0	1	0	0	0
Fatigue/weakness	0	0	0	0	0	0	2	0
Hypoglycemia	0	0	0	0	0	0	1	0
Neutropenic peritonitis	0	0	0	0	1	0	0	0
Fever	0	0	1	0	0	0	0	0
Infection (pneumonia)	0	0	0	0	1	0	0	0
Necrosis, benign and malignant	0	0	1	0	0	0	0	0
Hyperbilirubinemia	0	0	1	0	0	0	0	0

Table 4 Number of patients with hematological toxicities by dose level during the treatment period

Toxic effect	Dose level 2			Dose level 3			Dose level 3A			Dose level 4		
	All	Gd 3	Gd 4	All	Gd 3	Gd 4	All	Gd 3	Gd 4	All	Gd 3	Gd 4
Neutropenia	0	0	0	2	0	1	2	1	1	0	0	0
Leukopenia	1	0	0	4	1	1	3	1	0	1	1	0
Thrombocytopenia	1	0	0	2	1	0	3	0	0	2	0	0

Gd, grade.

mania (4%), respiratory system disorders (63%), anorexia (54%), rash (46%), weight decrease (29%); dizziness (25%); fever, blurred vision, liver and biliary system disorders, dehydration, myalgia, dry skin (21% each). All other adverse events occurred in fewer than 10% of patients. Grade 3 and grade 4 nonhematological toxicities by dose level are listed in Table 3.

Hematological toxicities occurred in 54% (13 of 24) of patients overall. Seven patients (29%) had grade 3/4 hematological toxicities. Table 4 shows that any grade and grade 3/4 anemia occurred in 34% (8 of 24) and 4% (1 of 24) of patients, respectively; any and grade 3/4 leukopenia occurred in 38% (9 of 24) and 21% (5 of 24) patients, respectively; and any and grade 3/4 neutropenia occurred in 17% (4 of 24) and 13% (3 of 24) of patients, respectively. Thrombocytopenia at any level was not observed in this study.

Both hematological and nonhematological toxic effects were generally mild and were neither more common nor more severe than those expected with paclitaxel. Patients had a median of one prior treatment with 13 of 22 evaluable patients having had prior chemotherapy including 9 who had a

prior taxane (Table 2). Seven of the 9 patients previously treated with a taxane had disease progression on or within 3 months of taxane-based therapy, and 10 of 13 pretreated patients overall had progression of disease on or within 3 months of therapy.

Protocol-Defined DLTs. Overall, seven patients had DLTs as defined by protocol. No DLTs were seen at dose level 2. One patient at dose level 3 had grade 3 bilirubinemia. When the dose was escalated to level 4 (150 mg b.i.d. lonafarnib and 175 mg/m² paclitaxel) two of four patients had dose-limiting toxic effects in the first cycle (one grade 4 neutropenic fever, one grade 4 diarrhea). We then introduced dose level 3A (125 mg b.i.d. of lonafarnib, 175 mg/m² of paclitaxel) to determine whether an intermediate dose level would be tolerated. At this dose, two patients had grade 4 diarrhea in the first cycle. All of the DLTs were reversible on modification or cessation of treatment. On the basis of analysis of all available safety data, it has been determined that lonafarnib 100 mg b.i.d. and paclitaxel 175 mg/m² is appropriate for further evaluation in patients with NSCLC.

Table 5 Mean (percentage coefficient of variation) pharmacokinetic parameters of lonafarnib

Parameter	Dose level 2	Dose level 3	Dose level 3A	Dose level 4
C_{max} (ng/mL)	760 (25)	960 (40)	1394 (35)	1267 (35)
Median T_{max} (h); range	5; 3-8	3; 0-10	8; 4-12	5; 3-6
AUC_{0-12h} (ng·h/mL)	5550 (51)	8789 (32)	12803 (36)	15443 (NA)
CL/F (mL/min)	364 (54)	207 (33)	181 (36)	165 (NA)
C_{min} (ng/mL)	286 (84)	524 (51)	883 (35)	1010 (47)

C_{max} , maximum plasma concentration; T_{max} , time of maximum plasma concentration; AUC_{0-12h} , the area under the plasma concentration-time curve from time 0 to 12 h; CL/F, total body clearance (lonafarnib); C_{min} , minimum plasma clearance.

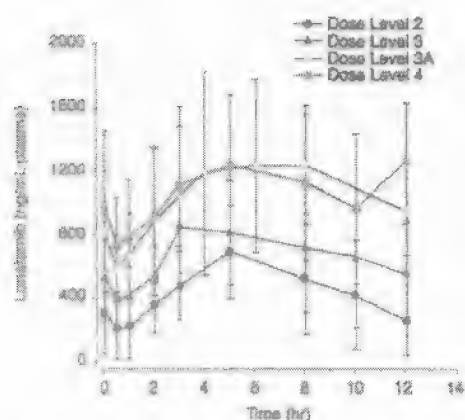


Fig. 3. Mean (± 1 SD) plasma lonafarnib concentrations after multiple-dose oral administration of lonafarnib in combination with single-dose 3-h i.v. infusion of paclitaxel to patients with solid tumors.

Pharmacokinetics of Lonafarnib. Nineteen patients had samples collected for pharmacokinetic evaluations. Lonafarnib was slowly absorbed after oral administration with food. Median T_{max} ranged from 3 to 8 h (Table 5; Fig. 3). Half-life ($t_{1/2}$) could not be estimated in this study because of the lack of a definitive terminal phase in the plasma concentration-*versus*-time profiles after b.i.d. oral administration of lonafarnib with food (see Fig. 3). Mean plasma lonafarnib concentrations at 12 h after the dose were ~34–59% of the corresponding mean C_{max} values. The mean total body clearance ranged from 165 to 364 mL/min. The increases in lonafarnib AUC values were dose-related after oral administration of 100 mg, 125 mg, and 150 mg in combination with paclitaxel 175 mg/m². After administration of lonafarnib 100 mg with paclitaxel 175 mg/m², the mean lonafarnib C_{max} and AUC values were higher than those with paclitaxel 135 mg/m². However, given the variability of the data and sample size, the distribution of individual C_{max} and AUC values encompassed the same range, regardless of paclitaxel dose (Fig. 4). The C_{max} and AUC values obtained in this trial with lonafarnib 100 mg in combination with paclitaxel were similar to those obtained in previous Phase I trials in which lonafarnib 100 mg was administered alone (Table 6; Refs. 25–30). Thus, these observations suggest that a single dose of either 135 mg/m² or 175 mg/m² of paclitaxel did not affect the pharmacokinetics of lonafarnib.

Pharmacokinetics of Paclitaxel. Plasma paclitaxel concentrations (C_{max} and AUC) were similar among the dose groups for paclitaxel 175 mg/m² with lonafarnib 100 mg, 125 mg, and 150 mg (Table 7; Figs. 5 and 6). There appear to be no effects on paclitaxel pharmacokinetics at a dose of 175 mg/m² paclitaxel when the lonafarnib dose is increased from 100 mg to 150 mg. The relationships between dose and paclitaxel C_{max} or AUC values were disproportionate after the administration of paclitaxel 135 mg/m² and 175 mg/m² in combination with lonafarnib 100 mg: a 30% increase in paclitaxel dose resulted in an increase of ~74% in C_{max} and ~87% in AUC . This finding provided additional evidence for the nonlinear disposition for paclitaxel, as noted previously (31).

Plasma paclitaxel concentrations decreased rapidly im-

mediately after cessation of the 3-h infusion, which was followed by a prolonged terminal phase (see Fig. 5). The mean terminal elimination $t_{1/2}$ of paclitaxel ranged from 12 to 19 h when blood samples were collected up to 48 h postdose for the first 17 patients. The mean $t_{1/2}$ was ~6 h when blood samples were collected up to 24 h postdose for patients 18–24 (see Table 7). The 6-h half-life was similar to that reported in the literature (31). The C_{max} and AUC values obtained in this study were similar to those previously reported when paclitaxel was given alone as a 3-h i.v. infusion (Table 8; Ref. 31).

Clinical Activity. The median number of treatment cycles on trial was eight, with a median of seven cycles containing paclitaxel. Activity was seen at the four dose levels studied (2, 3, 3A, and 4). Nine responses were durable, which we defined as a response detected at three or six cycles and confirmed at six or eight cycles, with median response duration of 6 months (range, 4–14 months). Most provocatively, we saw meaningful responses in three patients who had received prior taxane-based therapy, including two of five NSCLC patients who met the standard definition of taxane resistance (progression on or within 3 months

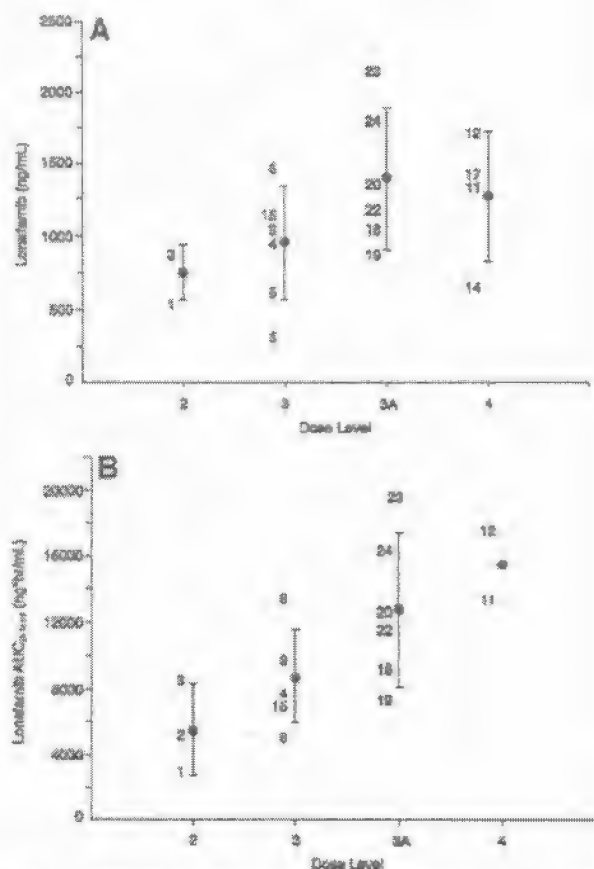


Fig. 4. Individual and mean (± 1 SD) C_{max} (A) and $AUC_{0-12 h}$ values (B) of lonafarnib after multiple-dose oral administration of lonafarnib in combination with single-dose 3-h i.v. infusion of paclitaxel to patients with solid tumors.

Table 5 Mean (coefficient of variation) pharmacokinetic parameters of ionafarnib after multiple-dose administration of ionafarnib 100 mg alone (previous Phase I studies) or in combination with paclitaxel (this study)

Study	Dose	n	C_{max}^a (ng/ml)	AUC_{0-12}^b (ng/h/ml)
This study	100 + 135 ^b	3	760 (25)	5550 (51)
This study	100 + 175 ^b	8	960 (40)	8789 ^c (32)
Conner <i>et al</i> . ²	100 ^c	3	942 (58)	7299 (75)
Ahrei <i>et al</i> . ³	100	1	1680 (NA)	18295 (NA)
Florsvitz <i>et al</i> . ⁴	100	2	784 (NA)	6221 (NA)

^a C_{max} , maximum plasma concentration; AUC_{0-12}^b , the area under the plasma concentration - versus - time curve from time 0 to 12 h; NA, not appropriate (sample size < 3).

^bIonafarnib dose (mg) + paclitaxel dose (mg/m²).

^c $n = 6$.

Ref. 34.

Ionafarnib alone dose (mg).

Ref. 37.

Ref. 33.

Table 7 Mean (percentage coefficient of variation) pharmacokinetic parameters of paclitaxel

Parameter	Dose level 2	Dose level 3	Dose level 3A	Dose level 4
C_{max}^a (ng/ml)	1937 (19)	3368 (53)	4258 (43)	3515 (38)
AUC_{0-12}^a (ng/h/ml)	9926 (7)	18563 (40)	17526 (38)	17634 (23)
$t_{1/2}$ (h)	18.6 (12)	13.3 (9)	5.62 (15)	12.1 (24)
CL (ml/min/m ²)	227 (8)	182 (43)	183 (33)	171 (19)
Vd (liter/m ²)	365 (7)	211 (47)	88.1 (35)	174 (9)
$Vdss$ (liter/m ²)	130 (16)	90.6 (54)	40.2 (47)	66.9 (12)

^a C_{max} , maximum plasma concentration; AUC_{0-12}^a , area under the plasma concentration - versus - time curve from time 0 to the final quantifiable sample extrapolated to infinity; $t_{1/2}$, terminal phase half-life; CL , total body clearance; Vd , volume of distributions; $Vdss$, the volume of distribution at steady state.

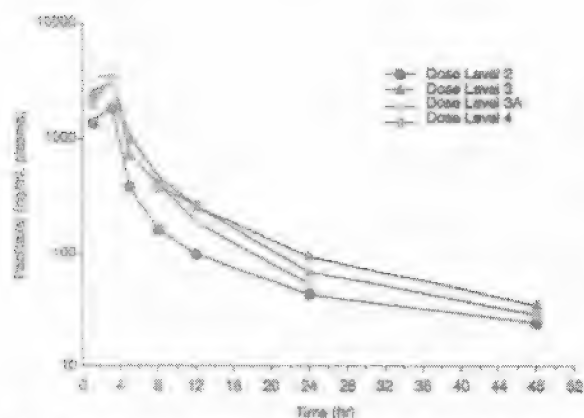


Fig. 5 Mean plasma paclitaxel concentrations after single-dose 3-h i.v. infusion of paclitaxel in combination with multiple-dose oral administration of ionafarnib to patients with solid tumors.

of taxane therapy). Only 4 of 21 patients had progressive disease by cycle 3, although all 21 patients had manifested disease progression within 3 months of study enrollment.

At the cycle-3 assessment interval, 7 patients demonstrated a partial response, 10 had minor responses or stable disease, and 1 had progressive disease (Table 9). Six of 7 responses were confirmed after six cycles. When total responses achieved on study were examined, 6 (50%) of the 12 patients with NSCLC achieved a partial response. In the setting of head and neck

squamous cell carcinoma, two of the three patients had a partial response, and the one patient with a salivary gland tumor had prolonged disease stabilization and was treated for 30 cycles before disease progression. No significant associations were noted between response after three cycles or after six cycles and the dose of either ionafarnib ($P = 0.81$, $P = 0.70$, respectively) or paclitaxel ($P = 0.19$, $P = 0.32$, respectively).

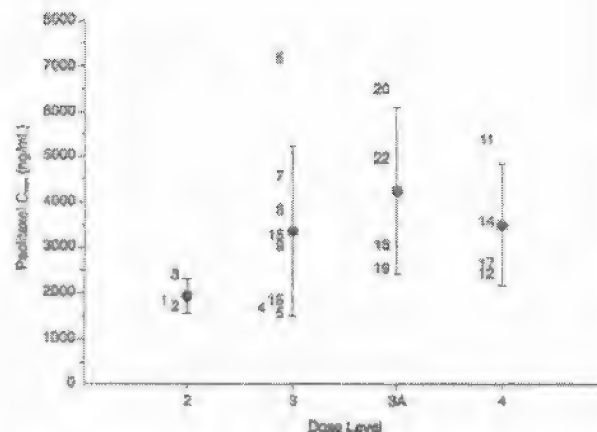


Fig. 6 Individual and mean (± 1 SD) C_{max} values of paclitaxel after single-dose 3-h i.v. infusion of paclitaxel in combination with multiple-dose oral administration of ionafarnib to patients with solid tumors.

Table 8. Mean (coefficient of variation) pharmacokinetic parameters of paclitaxel after 3-h i.v. infusion of paclitaxel 135 mg/m² or 175 mg/m² in combination with multiple-dose lonafarnib 100 mg b.i.d., 125 mg b.i.d., or 150 mg b.i.d. (this study) or alone (previously reported study)

Dose	Study	n	C _{max} (ng/ml)	AUC _{0-∞} (ng·h/ml)	CL (ml/min/m ²)
135	This study	3	1937 (19)	9936 (7)	227 (8)
	Gianni <i>et al</i> . ^a	4	2818 (12)	9308 (10)	247 (9)
175	This study	16	3627 (46)	18309 ^b (34)	179 ^c (34)
	Gianni <i>et al</i> . ^a	3	5038 (15)	15797 (16)	190 (16)

C_{max}, maximum plasma concentration; AUC_{0-∞}, area under the plasma concentration - versus - time curve from time 0 to the final quantifiable sample extrapolated to infinity; CL, total body clearance.

^a Data from ref. 25.

^b n = 15.

DISCUSSION

Other than the occasionally dose-limiting side effect of diarrhea, lonafarnib did not seem to contribute any significant side effects to those caused by paclitaxel. Patients with previous chemotherapy had a higher risk of toxicity. The substantial overlap of the eight 90% confidence intervals is due in large part to the small sample size ($n = 21$ evaluable patients). The only discernable trend with dose is an increase in the upper confidence limit with increasing total combined dose. Seven of the eight confidence intervals contain the targeted 30% toxicity rate. More precise estimates of the probability of toxicity would necessitate a larger sample size. The MTDs of lonafarnib and paclitaxel in this trial were lower than the doses recommended for either agent alone. The MTD of lonafarnib alone was determined to be 200 mg b.i.d. DLTs in studies of lonafarnib alone were generally similar to those seen in this trial and included reversible renal insufficiency (elevated creatinine levels), gastrointestinal symptoms (diarrhea, nausea, vomiting, anorexia), and hematological toxicities. Phase I studies of paclitaxel have demonstrated an MTD of 200 mg/m² for a single continuous infusion 14 regimen. Myelosuppression and neurotoxicity are

the primary DLTs of paclitaxel. Severe allergic reactions and skin rash associated with the vehicle (cremaphor EL) necessitate pretreatment with dexamethasone, diphenhydramine, and cimetidine or ranitidine.

No pharmacokinetic evidence was observed that either paclitaxel or lonafarnib enhanced the metabolism of the other agent. The pharmacokinetic values suggest that areas under the curve of both drugs were achieved in the active range. The target exposure for lonafarnib in clinical studies was to maintain a predose concentration in the range of 1–1.5 μ M based on the concentration required to inhibit anchorage-independent growth of a series of human tumor cell lines.

We saw encouraging clinical activity in this Phase I study of combined paclitaxel and lonafarnib, confirming the preclinical activity previously reported for this combination (14, 20, 22, 32–34). Several Phase I studies of farnesyltransferase inhibitors have now been published (28–30, 35–39). Before this study, a total of two responses have been documented (one each with tipifarnib and lonafarnib) in previously treated patients with NSCLC (29, 36). The activity manifested with this protocol using fairly moderate doses of lonafarnib and paclitaxel is more

Table 9. Clinical activity of lonafarnib in combination with paclitaxel

After 3 Cycles	
Partial response	7 patients (3 previously treated with taxanes)
Minor response	3 patients
Stable disease	7 (4 previously treated with taxanes)
Progressive disease	4 (2 previously treated with taxanes)
Not assessed	3 (1 did not tolerate lonafarnib at 125 mg b.i.d.)
Median no. of total cycles on study	8 (range, 2–30)
Median no. of paclitaxel courses on study	7 (range, 2–30)
After 6 to 9 Cycles	
Partial response	8 patients (3 previously treated with taxanes)
Minor response	2 patients
Stable disease	6 (4 previously treated with taxanes)
Progressive disease	2 (2 previously treated with taxanes)
Not assessed	3
Median no. of total cycles on study	8 (range, 2–30)
Median no. of paclitaxel courses on study	7 (range, 2–30)
Any response by histology	
NSCLC ^a	12 patients (6 PR, 3 MR or StD, 3 PD) ^b
HNSCC	3 patients (2 PR, 1 StD)
Salivary	6 patients (1 PR, 4 StD, 1 PD)

^a NSCLC, non-small cell lung cancer; PR, partial response; MR, minor response; StD, stable disease; PD, progressive disease; HNSCC, head and neck squamous cell carcinoma.

^b Five patients (all NSCLC) were considered taxane-refractory/resistant. PRs were seen in 2 of 5 taxane-refractory/resistant NSCLC patients.

substantial. It is particularly heartening because little if any evidence exists to support the efficacy of paclitaxel as a second-line agent when administered as a 3-h infusion on a 3-week cycle (40–44).

The extent of disease stabilization that our trial revealed with this regimen was dramatic in an extensively pretreated heterogeneous patient population with progressive disease at the time of study enrollment. Recent evidence suggests that the stabilization of NSCLC may lead to clinically meaningful survival benefits.

In conclusion, this is the first reported clinical study of the combination of a taxane with a farnesyltransferase inhibitor in human solid tumors. Phase II trials of the combination as first-line and second-line therapy of stage III and IV NSCLC are ongoing to confirm or refute our data-driven hypothesis, namely, that lonafarnib may enhance taxane sensitivity and possibly overcome clinical taxane resistance in solid tumors.

ACKNOWLEDGMENTS

We thank Judie Wells for transcription and editing of the manuscript, Julie Starr for her expert editorial assistance, and Delores Curtis and Stephen Maxwell for biostatistical support.

REFERENCES

- Bos JL. ras oncogenes in human cancer: a review. *Cancer Res* 1979;39:4682–9.
- Jeranian M. *Cancer Res* 1990;50:1352.
- Seftas RJ, Kibbehar RE, Delrosio O, et al. K-ras oncogene activation as a prognostic marker in adenocarcinoma of the lung. *N Engl J Med* 1990;323:561–5.
- Rosell R, Li S, Skolov Z, et al. Prognostic impact of mutated K-ras in surgically resected non-small cell lung cancer patients. *Oncogene* 1997;8:2407–12.
- Macats N, Porta M, Carominas JM, et al. Ki-ras mutations in exocrine pancreatic cancer: association with clinico-pathological characteristics and with tobacco and alcohol consumption. PANK-ras I Project Investigators. *Int J Cancer* 1997;70:661–7.
- Sigala K, Molberg K, Albores-Saavedra J, et al. K-ras mutations and their role at 3q and 18q in the development of human pancreatic tumors. *Int J Cancer* 1997;71:205–17.
- Rao CJ, Yan YX, Graeme-Cook F, et al. Ki-ras and p53 mutations in pancreatic ductal adenocarcinoma. *Pancreas* 1996;12:10–7.
- Hodgson U, McCormick F. Regulators and effectors of ras proteins. *Annu Rev Cell Dev Biol* 1991;7:601–32.
- Grider JB. Lipid modifications of proteins in the ras superfamily. In: Greenbaum L, Hokey B, editors. *GTPases in biology*. New York: Springer-Verlag; 1993. p. 335–44.
- Hancock JF, Magee AI, Childs JE, Marshall CJ. All ras proteins are palmitoylated but only some are prenylated. *Cell* 1989;57:1167–77.
- Hancock JF, Paterson H, Marshall CJ. A polybasic domain or palmitoylation is required in addition to the CAAX motif to localize GTPases to the plasma membrane. *Cell* 1990;63:133–9.
- Jackson JH, Cochran CG, Bourne JR, et al. Farnesol modification of K-ras exon 4B protein is essential for transformation. *Proc Natl Acad Sci USA* 1990;87:3042–6.
- Kato K, Cox AD, Hsaka MM, et al. Isoprenoid addition of Ras protein is the critical modification for its membrane association and transforming activity. *Proc Natl Acad Sci USA* 1992;89:6403–7.
- Bommarit E, Windle JJ, Von Hoff DD. Ras protein farnesyltransferase: a strategic target for anticancer therapeutic development. *J Clin Oncol* 1999;17:3631–52.
- Liu M, Bryani MS, Chen J, et al. Antitumor activity of SCH 66336, an orally bioavailable tricyclic inhibitor of farnesyl protein transferase, in human tumor xenograft models and wap-ras transgenic mice. *Cancer Res* 1998;58:4947–56.
- Cox AD, Der CJ. Farnesyltransferase inhibitors and cancer treatment: targeting simply ras? *Biochim Biophys Acta* 1997;1333:F51–71.
- Du W, Prendergast GC. Activation of the PI3K-AKT pathway masks the proapoptotic effects of farnesyltransferase inhibitors. *Cancer Res* 1999;59:4208–12.
- Ashar HR, James L, Gray K, et al. The farnesyl transferase inhibitor SCH 66336 induces a G(2) → M or G(1) pause in sensitive human tumor cell lines. *Exp Cell Res* 2001;262:17–27.
- Crespo NC, Ohkanda J, Yen TJ, Hamilton AD, Sefti SM. The farnesyltransferase inhibitor, FTI-2153, blocks bipolar spindle formation and chromosome alignment and causes prometaphase accumulation during mitosis of human lung cancer cells. *J Biol Chem* 2001;276:16161–7.
- Ashar HR, James L, Gray K, et al. Farnesyl transferase inhibitors block the farnesylation of CENP-E and CENP-F and alter the association of CENP-E with the microtubules. *J Biol Chem* 2000;275:30451–7.
- Moasser MM, Sepp-Lorenzino L, Kohl NE, et al. Farnesyl transferase inhibitors cause enhanced mitotic sensitivity to Taxol and epothilones. *Proc Natl Acad Sci USA* 1998;95:1369–74.
- Nielsen LL, Shi B, Hajian G, et al. Combination therapy with the farnesyl protein transferase inhibitor SCH66336 and SCH58500 (p53 adenovirus) in preclinical cancer models. *Cancer Res* 1999;59:5896–901.
- Shi B, Yaremko B, Hajian G, et al. The farnesyl protein transferase inhibitor SCH66336 synergizes with taxanes in vitro and enhances their antitumor activity in vivo. *Cancer Chemother Pharmacol* 2000;46:387–93.
- Porter GM, Armstrong L, Nielsen LL. Strategy for developing transgenic assays for screening antineoplastic drugs that affect tubulin polymerization. *Lab Anim Sci* 1995;45:145–50.
- Donaldson KL, Goolsby GL, Wahl AF. Cytotoxicity of the anticancer agents cisplatin and Taxol during cell proliferation and the cell cycle. *Int J Cancer* 1994;57:847–55.
- Hirji KF. Exact distributions for polytomous data. *J Am Stat Assoc* 1992;87:487–92.
- Mehra CR, Patel NR, Jajoo B. Exact logistic regression: theory, methods and software. Technical report. Cambridge, MA: Cytel Software Corporation; 1993.
- Mehra CR, Patel NR, Senchaudhuri P. Efficient Monte Carlo methods for conditional logistic regression. *J Am Stat Assoc* 2000;95:99–108.
- Adjei AA, Erlichman C, Davis JN, et al. A Phase I trial of the farnesyl transferase inhibitor SCH66336: evidence for biological and clinical activity. *Cancer Res* 2000;60:1871–7.
- Harwitz HI, Colvin OM, Petros WP, et al. Phase I and pharmacokinetic study of SCH66336, a novel Farnesyl transferase inhibitor [abstract]. *Proc Am Soc Clin Oncol* 1999;18:599.
- Eskens F, Awada A, Cutler D, et al. Phase I and pharmacokinetic study of the oral farnesyl transferase inhibitor SCH 66336 given twice daily to patients with advanced solid tumors. *J Clin Oncol* 2001;19:1167–75.
- Gianni L, Kearns CM, Gian A, et al. Nonlinear pharmacokinetics and metabolism of paclitaxel and its pharmacokinetic/pharmacodynamic relationships in humans. *J Clin Oncol* 1995;13:180–90.
- Kohl NE, Omer CA, Conner MW, et al. Inhibition of farnesyltransferase induces regression of mammary and salivary carcinomas in ras transgenic mice. *Nat Med* 1995;1:792–97.
- Sun J, Qian Y, Hamilton AD, Sefti SM. Ras CAAX peptidomimetic FTI276 selectively blocks tumor growth in nude mice of a human lung carcinoma with K-Ras mutation and p53 deletion. *Cancer Res* 1995;55:4243–7.
- Prendergast GC, Davide JP, deSolms SJ, et al. Farnesyltransferase inhibition causes morphological reversion of ras-transformed cells by a complex mechanism that involves regulation of the actin cytoskeleton. *Mol Cell Biol* 1994;14:4193–202.

33. Zajewski J, Horak ID, Bol CJ, et al. Phase I and pharmacokinetic study of farnesyl protein transferase inhibitor R115777 in advanced cancer. *J Clin Oncol* 2000;18:927-41.
34. Schellens JHM, de Klerk G, Swart M, et al. Phase I and pharmacologic study with the novel farnesyltransferase inhibitor (FTI) R115777 [abstract]. *Proc Am Assoc Cancer Res* 1999;40:4780.
35. Sognes S, Yao S-L, Britten C, et al. Pharmacokinetics and pharmacodynamics of the farnesyl protein transferase inhibitor (L-718, 123) in solid tumors [abstract]. *Proc Am Assoc Cancer Res* 1999;40:3413.
36. Brown CD, Rowinsky E, Yao S-L, et al. The farnesyl protein transferase (FPTase) inhibitor L-718,123 in patients with solid cancers [abstract]. *Proc Am Soc Clin Oncol* 1999;18:597.
37. Hudes GR, Schol J, Baab J, et al. Phase I clinical and pharmacokinetic trial of the farnesyltransferase inhibitor R115777 on a 21-day dosing schedule [abstract]. *Proc Am Soc Clin Oncol* 1999;18:601.
38. Huisman C, Smit EF, Giaccone G, Postmus PE. Second-line chemotherapy in relapsing or refractory non-small cell lung cancer: a review. *J Clin Oncol* 2000;18:3722-30.
39. Fossella FV, Lee JS, Shin DM, et al. Phase II study of docetaxel for advanced or metastatic platinum-refractory non-small cell lung cancer. *J Clin Oncol* 1995;13:645-51.
40. Gatzemeier U, von Pawel J, Gottfried M, et al. Phase III comparative study of high-dose cisplatin versus a combination of paclitaxel and cisplatin in patients with advanced non-small cell lung cancer. *J Clin Oncol* 2000;18:3590-9.
41. Socinski MA, Steagall A, Gillenwater H. Second-line chemotherapy with 96-hour infusional paclitaxel in refractory non-small cell lung cancer: report of a Phase II trial. *Cancer Investig* 1999;17:181-8.
42. Stewart DJ, Tomiak EM, Goss G, et al. Paclitaxel plus hydroxyurea as second-line therapy for non-small cell lung cancer. *Lung Cancer* 1996;15:115-23.

Decision Analysis for Prophylactic Cranial Irradiation for Patients With Small-Cell Lung Cancer

J. Jack Lee, B. Nebiyu Bekele, Xian Zhou, Scott B. Cantor, Ritsuko Komaki, and Jin Soo Lee

From the Department of Biostatistics & Applied Mathematics, and Department of Radiation Oncology, The University of Texas M.D. Anderson Cancer Center, Houston, TX; and Research Institute and Hospital, National Cancer Center Korea, Gyeonggi-do, Republic of Korea.

Submitted February 10, 2006; accepted April 17, 2006.

Supported in part by the National Cancer Institute Grants No. CA15672 and CA91844, and the Department of Defense Grants No. DAMD17-01-1-0689, DAMD17-02-1-0706, and W81XWH-04-1-0142.

J.J.L. and B.N.B. contributed equally to the work.

Authors' disclosures of potential conflicts of interest and author contributions are found at the end of this article.

Address reprint requests to J. Jack Lee, PhD, Department of Biostatistics & Applied Mathematics, The University of Texas M.D. Anderson Cancer Center, 1515 Holcombe Blvd, Unit 447, Houston, TX 77030-4009; e-mail: jll@mdanderson.org.

© 2006 by American Society of Clinical Oncology

0732-183X/06/2422-3597/\$20.00

DOI: 10.1200/JCO.2006.08.0632

ABSTRACT

Purpose

Prophylactic cranial irradiation (PCI) has been shown to provide survival benefit in patients with limited disease small-cell lung cancer (LD-SCLC) who have achieved complete response. However, PCI may also produce long-term neurotoxicity (NT). The benefits and risks of PCI in LD-SCLC are evaluated.

Methods

We developed a decision-analytic model to compare quality-adjusted life expectancy (QALE) in a cohort of SCLC patients who do or do not receive PCI by varying survival rates and the frequency and severity of PCI-related NT. Sensitivity analyses were applied to examine the robustness of the optimal decision.

Results

At current published survival rates (26% 5-year survival rate with PCI and 22% without PCI) and a low NT rate, PCI offered a benefit over no PCI (QALE = 4.31 and 3.70 for mild NT severity; QALE = 4.09 and 3.70 for substantial NT severity, respectively). With a moderate NT rate, PCI was still preferred. If the PCI survival rate increased to 40%, PCI outperformed no PCI with a mild NT severity. However, no PCI was preferred over PCI (QALE = 5.72 v 5.47) with substantial NT severity. Two-way sensitivity analyses showed that PCI was preferred for low NT rates, mild NT severity, and low long-term survival rates. Otherwise, no PCI was preferred.

Conclusion

The current data suggest PCI offers better QALE than no PCI in LD-SCLC patients who have achieved complete response. As the survival rate for SCLC patients continues to improve, NT rate and NT severity must be controlled to maintain a favorable benefit-risk ratio for recommending PCI.

J Clin Oncol 24:3597-3603. © 2006 by American Society of Clinical Oncology

INTRODUCTION

The brain is recognized as a frequent site of metastasis in small-cell lung cancer (SCLC) patients. Approximately 14% to 24% of SCLC patients have demonstrable CNS metastases at initial presentation, usually in combination with other extrathoracic sites.^{1,2} Even after initial response to chemotherapy, the incidence of clinically detectable brain metastases increased with increased length of survival and reaches 50% at 2 years.^{3,4} With autopsy cases included, CNS metastases can be as high as 80% at 2 years.⁵ Moreover, treatment of brain metastases is unsatisfactory—only about half of patients achieve a useful palliation after whole-brain irradiation, and median survival is less than 3 months after metastasis to the brain.⁶ In considering the poor outcome of patients who developed brain metastases, Hansen⁷ proposed prophylactic brain irradiation, later re-

named prophylactic cranial irradiation (PCI), for all patients with SCLC.

During the last three decades, there has been much debate on whether and how PCI should be used in the management of SCLC. The point of contention centers on the determination of the risks of short-term and long-term toxicity and benefits of reduction in brain metastasis and prolonging overall survival by PCI. Because of the intense research⁸⁻³¹ and two recent meta-analyses,^{32,33} a general consensus has been reached in the following areas: PCI is recommended for patients with limited disease (LD) SCLC who have achieved complete response (CR); the commonly accepted dose of PCI ranges from 24 to 36 Gy, with once-daily or twice-daily fractions equal to 2 to 3 Gy/d; PCI and concomitant chemotherapy can increase toxicity and should be avoided; PCI significantly reduces the risk of brain metastasis by approximately 50% (hazard ratio, 0.46³² and

0.48³³); PCI prolongs survival (hazard ratio for mortality, 0.84³² and 0.82³³); and acute radiation-induced toxicities are typically mild and resolved within a few months.

Despite the above-described advancements, only limited data on long-term PCI toxicities are available.²³⁻²⁹ To date, there are no reliable data to estimate the frequency and severity of the long-term toxicities induced by PCI. PCI is now routinely recommended for those patients who achieved CR to chemotherapy. These patients may be at increased risk of chronic neurotoxicity (NT) because they have a greater potential for long-term survival. Moreover, as more effective chemotherapy and combined chemoradiation improves the overall outcome and long-term survival of SCLC patients, the potential risk of chronic NT will be greater and the quality of life (QOL) becomes a more important consideration among the long-term survivors.

The purpose of this study was to explore the benefits and risks of PCI in LD-SCLC patients who have achieved CR. We examine the benefit-risk ratio of PCI by varying the cure fraction, NT rate, and the severity of NT. We postulate that in those subpopulations with higher cure fractions (we use 5-year survival as a surrogate for cure fraction), there will be increased risk and severity of NT, thus making the optimal decision uncertain. We use a decision-analysis framework to model the trade-off between survival and NT. The benefit of PCI is assessed by varying the long-term survival rate and the rate and severity of NT using a simulation. Given that PCI has become a standard treatment for LD-SCLC patients who have achieved CR, it is no longer ethical to conduct randomized controlled trials including an arm with no PCI. The decision-theoretic framework, then, is established to provide an analytic assessment of the overall value of PCI. The implications and future directions are also discussed.

METHODS

We examined the quality-adjusted life expectancy (QALE) for patients receiving PCI and compared their QALE with patients not receiving PCI after considering the impact of NT on QOL.³⁴ A decision-analytic model was used to compare QALE in the groups treated with PCI and no PCI using a large cohort ($N = 100,000$) of simulated patients. To incorporate the impact of chronic NT on the QOL of PCI-treated patients, QALE was calculated based on the following assumptions.

Survival Functions

Results from reported meta-analyses^{32,33} were used to determine the benefit of PCI therapy relative to no PCI. The relative failure rate (RFR) of PCI to no PCI at 5 years was estimated at 94.2% (81% and 86% for PCI and no PCI, respectively). Because heterogeneous patient populations were included in the meta-analyses, 5-year survival rates for PCI patients with LD were obtained from a recently reported Intergroup SCLC study.³⁵ Specifically, the 5-year survival rate for the PCI group was 26% and, with the RFR of 94.2%, we calculated the updated no PCI 5-year survival rate to be 22%. Survival times in our simulation were modeled using a truncated log-normal distribution in the first 15 years. After 15 years, the survival distribution of long-term lung cancer survivors³⁶ was assumed. The 5-year relative benefit of PCI to no PCI was held constant in our study. The log-normal assumption fit well with the survival data for the LD-SCLC patients who have achieved CR.³⁷

Assumptions for the Onset and Frequency of NT

It is a challenge to provide an accurate estimate of the onset and frequency of NT induced by PCI. Fifteen percent to more than 90% of the SCLC patients show cognitive dysfunction and impairment of neuropsychological assessment before PCI.^{27,38} Chemotherapy, aging, paraneoplastic syndromes, micrometastases, and so on can complicate the issue further. Significant NTs were reported when PCI was used in the past. For example, one study showed

that 63% of the patients receiving PCI had NT occurring as late as 54 months after irradiation.^{39,41} Most severe toxicities were associated with high PCI dose of more than 40 Gy and/or concomitant chemotherapy. Since then, the PCI regimen has been modified. Recent literature showed that PCI-induced NT is much reduced. In fact, two randomized trials showed that there was no noticeable NT within the first 2 years of PCI. There were, however, no sufficient data to estimate the long-term toxicity.^{26,29} A recent report indicating that among the nine patients who survived for more than 5 years after PCI, two had impairment of memory and two had dizziness. One of eight patients underwent computed tomography or magnetic resonance imaging showed a mild cortical atrophy in the brain.⁴²

We explored various possibilities of NT rates and, among them, two cases were studied in depth: the low NT rate model and the moderate NT rate model, corresponding to 30% and 50% latent NT rates, respectively. Given that most patients do not survive long enough to experience NT, when the 5-year survival rate for PCI group was 26%, a 30% latent NT rate resulted in 7.8% of the observed NT and a 50% latent NT rate resulted in a 13% of the observed NT. These assumptions are consistent with the results showing a 5-year NT of 10%.²⁴ The functional form of NT rate is listed in Appendix 1.

Assumption for the Effect of NT on QOL

Because NT is degenerative in nature, we constructed a decreasing QOL utility function, with a utility of 1 corresponding to a fully functional life without NT after patients were treated for their SCLC and achieved CR, and a utility of 0 corresponding to death. Patients who developed NT after PCI will have a utility between 0 and 1 depending on the severity of NT. We study two different settings depicting a case in which utility decreases only mildly and another case in which utility decreases substantially over time using mixtures of exponential functions (Appendix 2). The minimum utility for the mildly and substantially decreasing cases were set at 0.7 and 0.4, respectively. The average QOL utility functions during years after PCI treatment are plotted in Figure 1. For the low NT rate (Fig 1A), scenarios 1 and 2 showed that average QOL utility decreased to 0.91 and 0.82 by year 15 with mild and substantial NT, respectively. Similarly, for the moderate NT rate (Fig 1B), scenarios 3 and 4 illustrated that the average QOL utility decreased to 0.85 for the mild NT case and 0.70 for the substantial NT case by 15 years. Consistent with clinical observation, the average utility decline in the first 2 years was minimal in all scenarios.

QALE

The relationship between QOL and survival is summarized by the QALE. In our simulation, let N_{PCI} be the total number of patients receiving PCI and let S_i be the observed survival time (in days) for the i th patient. To estimate the QALE we first need to estimate the quality-adjusted life years for the i th patient (QALY _{i}) receiving PCI, which is defined as

$$\text{QALY}_i = \frac{\sum_{j=1}^{S_i} U_{ij}}{365.25}$$

where U_{ij} is the utility for the i th patient on the j th day for $i=1, \dots, N_{\text{PCI}}$ and $j=1, \dots, S_i$.

We obtain the QALE by taking the average of the QALY values for all patients receiving PCI

$$\text{QALE} = \frac{\sum_{i=1}^{N_{\text{PCI}}} \text{QALY}_i}{N_{\text{PCI}}}$$

Sensitivity Analysis

Sensitivity analysis was conducted by varying the parameters of simulation studies to provide a comprehensive assessment of the benefit-risk ratio of PCI. The values and ranges of parameters evaluated were 5-year survival rates in the no-PCI groups (22% or 36%, and in a more general case, ranging from 10% to 70%); latent NT rate (30% and 50% corresponding to low and moderate observed NT, respectively, and in a more general case, ranging from 10%

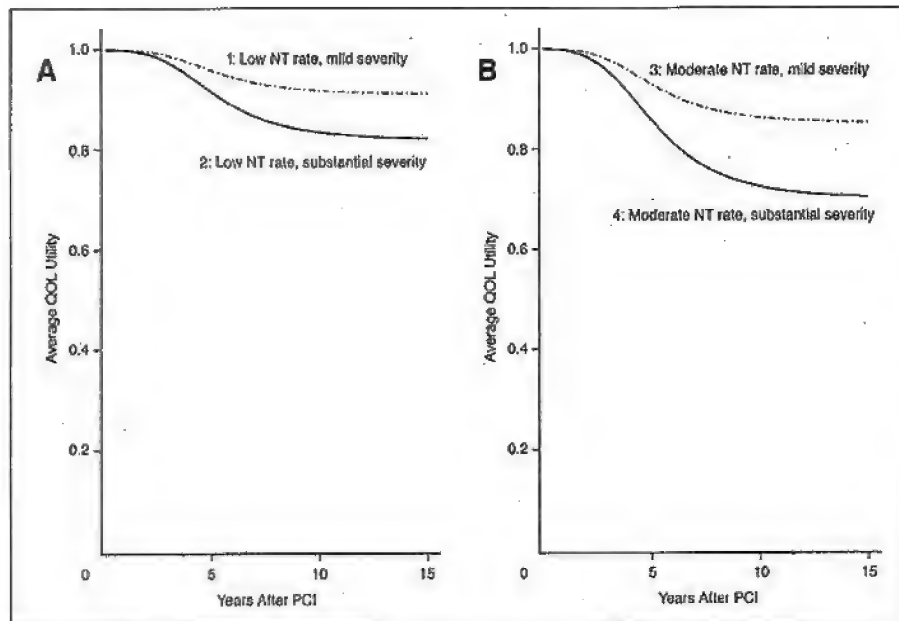


Fig 1. Utility functions reflecting average quality of life (QOL) over time for four scenarios with low and moderate neurotoxicity (NT) rates and mild and substantial severity of NT. The average QOL utility decreases by 15 years after prophylactic cranial irradiation (PCI) for scenarios 1, 2, 3, and 4 are 91%, 82%, 85%, and 70%, respectively.

to 70%); and decrease of utility function (mildly or substantially decreasing utility cases, as described). Multiple scenarios were generated by varying the cure rate, latent NT rate, and NT severity level. By varying the 5-year survival rate in the no-PCI group and the latent NT rate, two-way sensitivity analysis was performed to evaluate the benefit-risk of PCI and no PCI using QALE as the outcome measure. A wide range of parameters were evaluated; thus, the findings from each scenario could be viewed as results obtained from specific subpopulations or from future SCLC patients with better survival outcome.

RESULTS

Quality-Adjusted Survival and QALE

Quality-adjusted survival curves for various NT rates and 5-year survival rates are shown in Figures 2 and 3 for the low and moderate NT rate, respectively. Estimated survival curves for PCI without NT were included for reference purposes. Figure 2A shows that for

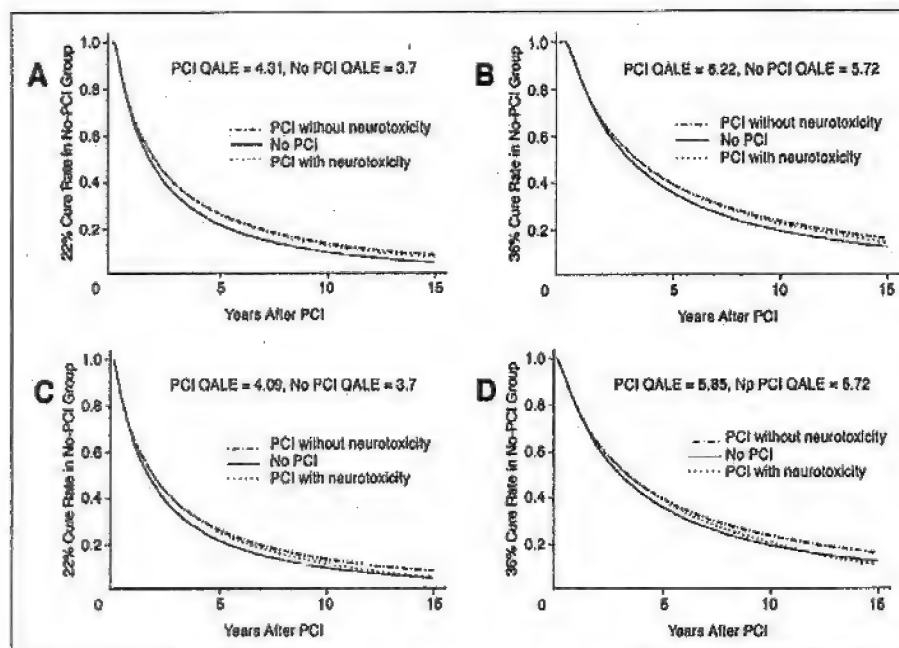


Fig 2. Quality-adjusted survival curves for prophylactic cranial irradiation (PCI) and no-PCI groups with a latent 30% neurotoxicity (NT) rate. Mildly decreasing utility assuming (A) 22% cure rate and (B) 36% cure rate in the no-PCI group. Substantially decreasing utility assuming (C) 22% cure rate and (D) 36% cure rate in the no-PCI group.

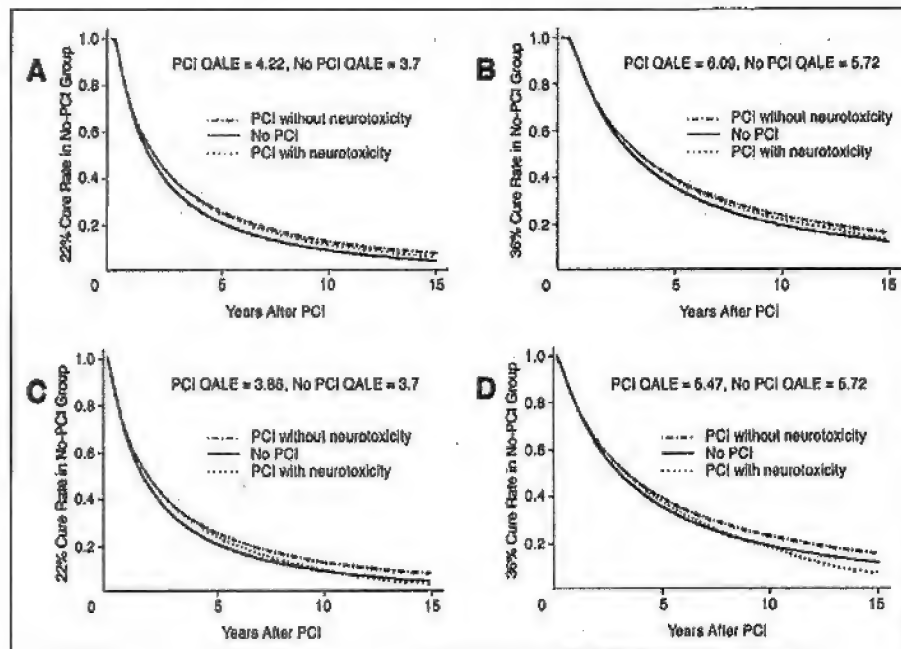


Fig 3. Quality-adjusted survival curves for prophylactic cranial irradiation (PCI) and no PCI groups with a latent 50% neurotoxicity (NT) rate. Mildly decreasing utility assuming (A) 22% cure rate and (B) 36% cure rate in the no PCI group. Substantially decreasing utility assuming (C) 22% cure rate and (D) 36% cure rate in the no PCI group. QALE, quality-adjusted life expectancy.

scenario 1, with low NT rate and mild NT severity, PCI is always better than no PCI when the 5-year survival rate is 22% in the no-PCI group (26% in the PCI group) even after adjusting for NT. The QALE (in QALYs) of the PCI group is 16% better than that in the no-PCI group (4.31 for PCI v 3.70 for no PCI). Figure 2B showed that the QALE of the PCI group is 9% better than that of the no-PCI group (6.22 for PCI v 5.72 for no PCI) when the cure rate in the no-PCI group increased to 36%. With substantial NT deficit, benefit in QALE of PCI was 11% compared with that of no PCI (4.09 for PCI v 3.70 for no PCI) with 22% cure rate (Fig 2C). The loss in benefit of the PCI, however, can be seen in Figure 2D when the cure rate in the no-PCI group increased to 36% with substantial NT. QALE for the PCI group was only 2% better than that of the no-PCI group (5.85 for PCI v 5.72 for no PCI). Note that the quality-adjusted survival curves of PCI and no PCI crossed after 11 years, indicating the loss of benefit of PCI in long-term survivors. In summary, with a low NT rate, PCI is better than no PCI in all scenarios depicted in Figure 2 except for long-term survivors after 11 years (Fig 2D). As the 5-year survival rate increases or the severity of NT increases, the benefit of PCI over no PCI becomes less evident.

In Figure 3, the adjusted survival plots were calculated assuming the moderate NT rate. QALE is still better for PCI group in mild NT (Fig 3A: QALE, 4.22 for PCI v 3.70 for no PCI, 14% better in PCI group; Fig 3B: QALE, 6.09 for PCI v 5.72 for no PCI, 6% better in PCI group) assuming 22% and 36% of cure rates in the no-PCI group, respectively. The QALE is still 4% better in the PCI group compared with the no-PCI group in Figure 3C when the cure rate in the no-PCI group is 22% with moderate NT and substantial NT severity, although the curves crossed after 10 years of follow-up. The pronounced effect of NT becomes apparent between years 10 and 15 (Fig 3D) when the cure rate in the no-PCI group reaches 36% with moderate NT rate and substantial NT severity. As a result, the QALE is 4% lower in PCI group compared with the no-PCI group (QALE, 5.47 for PCI v 5.72 for no PCI). All panels show that PCI is better than no PCI for the first

8 years. As patients continue to survive, it can be seen that quality-adjusted survival is more affected during later years when the cumulative effects of NT and its severity are experienced fully.

Two-Way Sensitivity Analysis

Figure 4A gives a contour plot showing the regions in which no PCI is preferred (gray-shaded area) or PCI is preferred (open area without shading) when utility is assumed to decrease mildly during 15 years. In this case, at current 5-year survival rates of 22% for the no-PCI group, it is clear that PCI is overwhelmingly preferred versus no PCI except in extreme cases when the latent NT rate and the survival rate are extremely high (for example, when both of them are > 60%). In all cases when the latent NT rate is less than 54% or 5-year survival rate is less than 46%, PCI is preferred.

Similarly, Figure 4B shows the regions in which no PCI is preferred or PCI is preferred when utility is assumed to decrease substantially during 15 years. At current 5-year survival rates of 22% for the no-PCI group, PCI is preferred except when the latent NT rate is higher than 53%. When the survival rate for the no-PCI group increased to 36%, PCI is preferred when latent NT rate is less than 37%. At a 30% latent NT rate, the 5-year survival rate for the no-PCI group must be at least 43% (PCI survival rate of 46%) before no PCI is preferred versus PCI. At a latent NT rate of 50%, no PCI is preferred when the 5-year survival rate for the no-PCI group is 26% (PCI survival rate of 30%) or higher.

DISCUSSION

The current study has addressed key points relevant to the issues that physicians should consider before recommending PCI therapy to SCLC patients who have achieved CR. Under various scenarios we showed that the benefit of PCI relative to no PCI depends on the rate

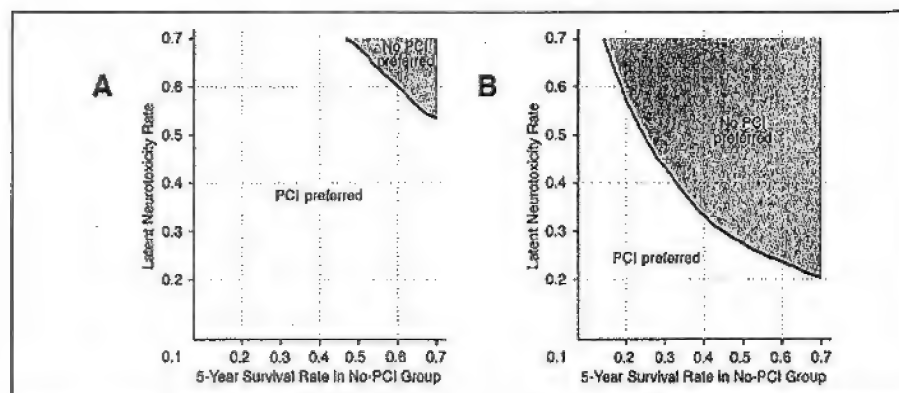


Fig 4. Two-way sensitivity analysis by varying 5-year survival rate in no PCI group and latent neurotoxicity rate with (A) mildly decreasing utility, and (B) substantially decreasing utility, respectively. The white, open area indicates the region where PCI is preferred; the gray, shaded area indicates where no PCI is preferred.

and severity of NT and the cure fraction. Our analysis supports the current standard practice of giving PCI to LD-SCLC patients who have achieved CR, assuming that the NT rate is low and the toxicity is mild. As the 5-year survival rates increase due to improved therapies, PCI may have inferior QALE relative to no PCI. Furthermore, there may be subsets of patients, who because of their baseline characteristics (such as younger patients and females), having higher cure potential than the average patients. A better understanding of the extent and severity of long-term NT would permit us to better delineate the most appropriate treatment options for those patients.

As reported in the literature, increase in the total dose and higher dose fractionation reduces the CNS relapse rate. However, because higher dose fractions potentially are associated with increased risk of NT, a total dose of 24 to 36 Gy given during 2 to 3 weeks has become more widely recommended.^{46,53} How the modification of total dose and dose fraction schedule will affect efficacy and the rates of NT is unclear, but perhaps the ongoing Radiation Therapy Oncology Group study (RTOG 0212) will help clarify the issue. The latent NT rate and the severity of toxicity are also critical in determining the relative benefit of administering PCI. Our analysis suggests that, with the current survival rate, if we have mildly decreasing utility, PCI is always preferred. But with substantially decreased utility, no PCI can yield higher QALE if the latent NT rate is 53% or higher.

PCI is a cost-effective treatment, which improves the QOL-adjusted survival for LD-SCLC patients who achieved CR and is considered a standard treatment for this patient population.⁴³⁻⁵³ Our decision analysis conforms to the prevailing view that the benefit of PCI outweighs the risk and offers better QALE based on the current data. As the systematic therapy continues to improve, however, it is possible that PCI may result in inferior QALE when the cure fractions are substantially higher than the current level (eg, when 5-year survival

of the no-PCI group is greater than 43% with substantial NT at a 30% latent NT rate).

The validity of our decision analysis depends on the assumptions of the models and their parameters. The assumption that RFR of the PCI group is 94.2% of the no-PCI group could vary. Because of the inherent nature of PCI (ie, because its therapeutic effect is localized to the irradiated brain without any conceivable effects on the systemic disease), one may consider the PCI effect as a constant rather than a fixed proportion in long-term survivors. As the cure rate increases, the fixed-proportion assumption on RFR could err on the side of favoring PCI. Conversely, one may argue that the effect of PCI should be more pronounced, particularly in LD-SCLC patients, because a higher proportion of treatment failure occurs in the brain compared with that in patients with more extensive diseases. In addition, assumptions on the long-term toxicity of PCI, including the frequency and severity of toxicity and the QOL measures in patients, may vary as well. The long-term toxicity data should be documented prospectively and systematically to provide more specific information in evaluating the risk and benefit of PCI.

In summary, the role of PCI in SCLC patients needs to be reviewed critically as survival rates increase, especially for those patients who have achieved CR, and therefore have a greater potential for long-term survival. Additional efforts are needed to increase the effectiveness of tumor control while reducing the long-term toxicity to make PCI as safe and effective as possible. In addition, with the increasing understanding of the molecular profile and its association with the likelihood of developing brain metastasis and/or the susceptibility to PCI-induced NT in patients with SCLC, tailored treatment regimens can be developed to maximize the efficacy while minimizing the potential toxicity.^{54,55}

REFERENCES

- Argiris A, Murren JR: Staging and clinical prognostic factors for small-cell lung cancer. *Cancer J* 7:437-447, 2001
- Hochstenbag MMH, Twijnstra A, Wilmink JT, et al: Asymptomatic brain metastases (BM) in small cell lung cancer: MR-imaging is useful at initial diagnosis. *J Neurooncol* 48:243-246, 2000
- Bunn PA, Nugent JL, Matthews MJ: Central nervous system metastases in small cell lung carcinoma. *Semin Oncol* 5:314-322, 1978
- Komaki R, Cox JD, Whitson W: Risk of brain metastases from small carcinoma of the lung related to length of survival and prophylactic irradiation. *Cancer Treat Rep* 65:811-814, 1981
- Nugent JL, Bunn PA, Matthews MJ, et al: CNS metastases in small cell bronchogenic carcinoma: Increasing the frequency and changing pattern with lengthening of survival. *Cancer* 44:1885-1893, 1979
- Carmichael J, Crane JM, Bunn PA, et al: Results of therapeutic cranial irradiation in small cell lung cancer. *Int J Radiat Oncol Biol Phys* 14:455-459, 1988
- Hansen HH: Should initial treatment of small cell carcinoma include systemic chemotherapy and brain irradiation? *Cancer Chemother Rep* 34:239-241, 1973
- Jackson DV Jr, Richards FII, Copper MR, et al: Prophylactic cranial irradiation in small cell carcinoma of the lung: A randomized study. *JAMA* 237:2730-2733, 1977
- Cox JD, Petrovich Z, Paig C, et al: Prophylactic cranial irradiation in patients with inoperable carcinoma of the lung: Preliminary report of a cooperative trial. *Cancer* 42:1135-1140, 1978

10. Boileau DD, Kane RC, Bernath AM, et al: Low dose elective brain irradiation in small cell carcinoma of the lung. *Int J Radiat Oncol Biol Phys* 5:941-945, 1979
11. Hansen HH, Dornbrowsky P, Hirsch FR, et al: Prophylactic irradiation in bronchogenic small cell carcinoma: A comparative trial of localized versus extensive radiotherapy including prophylactic cranial irradiation in patients receiving combination chemotherapy. *Cancer* 46:279-284, 1980
12. Maurer LH, Tullch M, Weiss RB, et al: A randomized combination modality trial in small cell carcinoma of the lung: Comparison of combination chemotherapy-radiation therapy versus cyclophosphamide-radiation therapy effects of maintenance chemotherapy and prophylactic whole brain irradiation. *Cancer* 45:30-39, 1980
13. Eagan RT, Frytak S, Lee RE, et al: A case for preplanned thoracic and prophylactic whole brain radiation therapy in limited small cell lung cancer. *Cancer Clin Trials* 4:261-266, 1981
14. Catane R, Schwade JG, Yarr I, et al: Follow-up neurological evaluation in patients with small cell lung carcinoma treated with prophylactic cranial irradiation and chemotherapy. *Int J Radiat Oncol Biol Phys* 7:105-109, 1981
15. Katsenis AT, Karpasitis N, Giannakakis D, et al: Elective brain irradiation in patients with small-cell carcinoma of the lung: Preliminary report, in Protilix G (ed): *Lung Cancer: Etiology, Epidemiology, Prevention, Early Diagnosis, Treatment*. Amsterdam, The Netherlands, Excerpta Medica, 1982, pp 277-284
16. Moutain CF, Vincent R, Wilson HE, et al: Intensive chemotherapy and radiotherapy of small cell carcinoma of the lung-regional disease. Abstracts of the Third World Conference on Lung Cancer, Tokyo, Japan, pp 153, May 17-20, 1982 (abstr)
17. Aroney RS, Aisner J, Wesley MN, et al: Value of prophylactic cranial irradiation given at complete remission in small cell lung carcinoma. *Cancer Treat Rep* 67:575-582, 1983
18. Seydel HG, Creech R, Pagano M, et al: Prophylactic versus no brain irradiation in regional small cell lung carcinoma. *Am J Clin Oncol* 8:218-223, 1985
19. Johnson BE, Becker B, Goff WB II, et al: Neurologic, neuropsychologic, and computed cranial tomography scan abnormalities in 2- to 10-year survivors of small-cell lung cancer. *J Clin Oncol* 3:1659-1667, 1985
20. Lee JS, Umsewasdi T, Lee YY, et al: Neurotoxicity in long-term survivors of small cell lung cancer. *Int J Radiat Oncol Biol Phys* 12:313-321, 1986
21. Laukkanen E, Klonoff H, Allan B, et al: The role of prophylactic brain irradiation in limited stage small cell lung cancer: Clinical, neuropsychologic, and CT sequelae. *Int J Radiat Oncol Biol Phys* 14:1109-1117, 1988
22. Niiranen A, Holsti P, Salmo M: Treatment of small cell lung cancer: Two-drug versus four-drug chemotherapy and loco-regional irradiation with or without prophylactic cranial irradiation. *Acta Oncol* 28:501-505, 1989
23. Ohonoshi T, Ueoka H, Kawahara S, et al: Comparative study of prophylactic cranial irradiation in patients with small cell lung cancer achieving a complete response: A long-term follow-up result. *Lung Cancer* 10:47-54, 1993
24. Shaw EG, Su JQ, Eagan RT, et al: Prophylactic cranial irradiation in complete responders with small-cell lung cancer: Analysis of the Mayo Clinic and North Central Cancer Treatment Group data bases. *J Clin Oncol* 12:3227-3232, 1994
25. Cull A, Gregor A, Hopwood P, et al: Neurological and cognitive impairment in long-term survivors of small cell lung cancer. *Eur J Cancer* 30:1067-1074, 1994
26. Arriagada R, Le Chevalier T, Borie F, et al: Prophylactic cranial irradiation for patients with small-cell lung cancer in complete remission. *J Natl Cancer Inst* 87:183-190, 1995
27. Komaki R, Meyers CA, Shin DM, et al: Evaluation of cognitive function in patients with limited small cell lung cancer prior to and shortly following prophylactic cranial irradiation. *Int J Radiat Oncol Biol Phys* 33:179-182, 1995
28. Wagner H, Kim K, Turrisi A: A randomized phase III study of prophylactic cranial irradiation versus observation in patients with small cell lung cancer achieving a complete response: Final report of an incomplete trial by the Eastern Cooperative Oncology Group and Radiation Therapy Oncology Group (E3589/R92-01). *Proc Am Soc Clin Oncol* 15:376, 1996
29. Gregor A, Cull A, Stephens RJ, et al: Prophylactic cranial irradiation is indicated following complete response to induction therapy in small cell lung cancer: Results of a multicenter randomized trial. *Eur J Cancer* 33:1752-1758, 1997
30. Laplanche A, Monnet I, Santos-Miranda S, et al: Controlled clinical trial of prophylactic cranial irradiation for patients with small cell lung cancer in complete remission. *Lung Cancer* 21:193-201, 1998
31. Fonseca R, O'Neill BP, Foote RL, et al: Cerebral toxicity in patients treated for small cell carcinoma of the lung. *Mayo Clin Proc* 74:461-465, 1999
32. Auperin A, Arriagada R, Pignon JP, et al: Prophylactic cranial irradiation for patients with small-cell lung cancer in complete remission. *N Engl J Med* 341:476-484, 1999
33. Meert AP, Paesmans M, Berghmans T, et al: Prophylactic cranial irradiation in small cell lung cancer: A systematic review of the literature with meta-analysis. *BMC Cancer* 1:5-13, 2001
34. Billingham LJ, Abrams KR: Simultaneous analysis of quality of life and survival data. *Stat Methods Med Res* 11:25-48, 2002
35. Turrisi AT, Kim K, Blum R, et al: Twice-daily compared with once-daily thoracic radiotherapy in limited small-cell lung cancer treated concurrently with cisplatin and etoposide. *N Engl J Med* 340:265-271, 1999
36. National Center for Health Statistics: Vital statistics of the United States, 1995, preprint of Vol II, Mortality, Part A, Sec 6, life tables. Hyattsville, MD, National Center for Health Statistics, 1998
37. Tai P, Tonita J, Yu E, et al: Twenty-year follow-up study of long-term survival of limited-stage small-cell lung cancer and overview of prognostic and treatment factors. *Int J Radiat Oncol Biol Phys* 56:626-633, 2003
38. Kanard A, Frytak S, Jatol A: Cognitive dysfunction in patients with small-cell lung cancer: Incidence, causes, and suggestions on management. *J Support Oncol* 2:127-132, 2004
39. Minna JD, Higgins GA, Glatstein EJ: Cancer of the lung, in DeVita VT, Hellman SJ, Rosenberg SA (eds): *Cancer: Principles & Practice of Oncology* (ed 2). Philadelphia, PA, J.B. Lippincott, 1985, pp 507-597
40. Fleck JF, Einhorn LH, Lauer RC, et al: Is prophylactic cranial irradiation indicated in small-cell lung cancer? *J Clin Oncol* 8:209-214, 1990
41. Kurup A, Hanna NH: Treatment of small cell lung cancer. *Crit Rev Oncol Hematol* 62:117-126, 2004
42. Cao K-J, Huang H-Y, Tu M-C, et al: Long-term results of prophylactic cranial irradiation for limited-stage small-cell lung cancer in complete remission. *Chin Med J* 118:1258-1262, 2005
43. Tai THP, Yu E, Dickof P, et al: Prophylactic cranial irradiation revisited: Cost-effectiveness and quality of life in small-cell lung cancer. *Int J Radiat Oncol Biol Phys* 52:68-74, 2002
44. Vines EF, Le Pechoux C, Arriagada R: Prophylactic cranial irradiation in small cell lung cancer. *Semin Oncol* 30:38-46, 2003
45. Le Pechoux C, Arriagada R: Prophylactic cranial irradiation in small cell lung cancer. *Hematol Oncol Clin North Am* 18:355-372, 2004
46. Pottgen C, Eberhardt W, Stuschke M: Prophylactic cranial irradiation in lung cancer. *Curr Treat Options Oncol* 5:43-50, 2004
47. Arriagada R, Le Chevalier T, Riviere A, et al: Patterns of failure after prophylactic cranial irradiation in small-cell lung cancer: Analysis of 505 randomized patients. *Ann Oncol* 13:748-754, 2002
48. Chua YJ, Steer C, Yip D: Recent advances in management of small-cell lung cancer. *Cancer Treat Rev* 30:521-543, 2004
49. Sorensen JB: The role of prophylactic brain irradiation in small cell lung cancer treatment. *Monaldi Arch Chest Dis* 59:128-133, 2003
50. Kotalik J, Yu E, Markman BR, et al: Practice guideline on prophylactic cranial irradiation in small-cell lung cancer. *Int J Radiat Oncol Biol Phys* 50:309-316, 2001
51. Turrisi AT III: Limited stage small cell lung cancer: Treatment and therapy. *Curr Treat Options Oncol* 4:61-64, 2003
52. Simon M, Argiris A, Murren JR: Progress in the therapy of small cell lung cancer. *Crit Rev Oncol Hematol* 49:119-133, 2004
53. Jackman DM, Johnson BE: Small-cell lung cancer. *Lancet* 366:1385-1396, 2005
54. Bubb RS, Komaki R, Hachiya T, et al: Association of Ki-67, p53, and bcl-2 expression of the primary non-small-cell lung cancer lesion with brain metastatic lesion. *Int J Radiat Oncol Biol Phys* 53:1216-1224, 2002
55. Milas J, Komaki R, Hachiya T, et al: EGFR, COX-2 and BAX expression in the primary non-small cell lung cancer and brain metastases. *Clin Cancer Res* 9:1070-1076, 2003
56. Wimo A, Mattson B, Krakau I: Cost-utility analysis of group living in dementia Care. *Int J Technol Assess Health Care* 11:49-65, 1995

Acknowledgment

We thank Craig Stevens, MD, PhD, and Bonnie S. Glisson, MD, for their helpful comments.

Acknowledgment

The Acknowledgment is included in the full-text version of this article, available online at www.jco.org. It is not included in the PDF version (via Adobe® Reader®).

Authors' Disclosures of Potential Conflicts of Interest

The authors indicated no potential conflicts of interest.

Author Contributions

Conception and design: J. Jack Lee, B. Nebiyu Bekele, Scott B. Cantor, Jin Soo Lee
Data analysis and interpretation: J. Jack Lee, B. Nebiyu Bekele, Xian Zhou, Scott B. Cantor, Ritsuko Komaki, Jin Soo Lee
Manuscript writing: J. Jack Lee, B. Nebiyu Bekele, Xian Zhou, Scott B. Cantor, Jin Soo Lee
Final approval of manuscript: J. Jack Lee, B. Nebiyu Bekele, Xian Zhou, Scott B. Cantor, Ritsuko Komaki, Jin Soo Lee

Randomized Phase II Designs in Cancer Clinical Trials: Current Status and Future Directions

J. Jack Lee and Lei Feng

From the Department of Biostatistics & Applied Mathematics, The University of Texas M.D. Anderson Cancer Center, Houston, TX.

Submitted March 28, 2004; accepted March 2, 2005.

Supported by grants from the National Cancer Institute CA16672 and CA97007, and Department of Defense DAMD17-02-1-0706.

Authors' disclosures of potential conflicts of interest and author contributions are found at the end of this article.

Address reprint requests to J. Jack Lee, PhD, Department of Biostatistics & Applied Mathematics, 1515 Holcombe Boulevard, Unit 447 Houston, TX 77030-4009; e-mail: jilee@mdanderson.org.

© 2005 by American Society of Clinical Oncology

0732-183X/05/2319-4450/\$20.00

DOI: 10.1200/JCO.2005.03.197

ABSTRACT

Purpose

Randomized phase II (RPh2) designs are popular in cancer clinical trials because of the smaller sample size requirements when multiple treatments are being evaluated. We reviewed the use of RPh2 designs and give comments on future directions.

Design

The trial design, statistical properties, conduct, data analysis, results, and reporting were examined in RPh2 trials reported from 1986 to 2002.

Results

A statistical design was reported in only 46% of the 266 cancer trials, and approximately half of those provided inadequate information. Most studies applied randomization to achieve patient comparability, while embedding a one-sample phase II design within each treatment arm. Seventy-five percent of the trials' accruals were within $\pm 10\%$ of their targets. The average accrual rate was 3.3 patients per month. Planned interim analyses were reported in 27% of the trials, and 56% of the trials were stopped early; 69%, 13%, 13%, and 4% of the trial discontinuations were because of lack of efficacy, efficacy, toxicity, and slow accrual, respectively. Thirty-nine trials (14%) recommended or started phase III evaluations, with four positive reports in six phase III studies identified.

Conclusion

There is a trend of increasing use of RPh2 designs in cancer research. Continued improvement in study design, conduct, analysis, and reporting is required to enhance the quality of RPh2 designs. The accrual rate and success rate of the trials remain low, and therefore, futility stopping rules to terminate ineffective treatment arm(s) should be implemented more frequently. More innovative, flexible RPh2 designs are needed to facilitate the development of effective cancer treatments.

J Clin Oncol 23:4450-4457. © 2005 by American Society of Clinical Oncology

INTRODUCTION

Phase II trials play a pivotal role in anticancer drug development. After the determination of a drug's safety profile and appropriate dosage levels in phase I studies, phase II trials are conducted to provide initial assessments of treatment efficacy (phase IIA) and to identify promising agents to send to phase III for additional evaluation (phase IIB).^{1,2} The use of high-throughput technology in screening natural and synthetic compounds and the development of molecular target

agents has resulted in a dramatic increase in the number of potential anticancer drugs under study. It has been estimated that more than 400 new compounds are now available for testing.³ Despite the large number of potential drugs to be tested, the percentage of patients enrolled onto clinical trials remains at a dismal rate of 3% to 5% among the potentially eligible patient population.⁴ Von Hoff⁵ reported that only 29 of the 280 new agents (10%) brought into phase I trials from 1975 to 1994 were eventually approved for clinical use. These findings of limited patient

resources, low success rates, and large numbers of potential agents indicate that phase II trials should be designed and conducted to effectively eliminate the inefficacious agents and efficiently use the scarce resources.

Many phase II designs have been proposed to address these needs. For phase IIA trials, Gehan's design,⁶ Simon's two-stage designs,⁷ and Fleming's two-stage design⁸ are among the most commonly used methodologies for testing the efficacy of a single treatment regimen (ie, one-arm design). In addition, three-stage designs^{9,10} and several variations of the Bayesian design¹¹⁻¹³ have also been proposed. The primary end point is typically the rate of short-term tumor response. These methods are based on statistical hypothesis testing that compares the response rate with a preselected fixed target. By controlling both type I and type II error rates, inefficacious regimens can be screened out (subject to a small type I error rate), whereas promising regimens can be recommended for additional evaluation (ensured by sufficiently high power or a small type II error rate).

For phase IIB trials, two or more regimens demonstrating initial efficacy are compared. Formal hypothesis testing comparing the response rates between different regimens may require a prohibitively large sample size. Alternatively, the Simon, Wittes, and Ellenberg (SWE) design¹⁴ compares the response rates in multiple treatment arms through a ranking and selection procedure. On the surface, this "play-the-winner" method may appear to be efficient compared with the hypothesis testing method. For example, 146 patients per arm are required for testing response rates of 10% v 25% with 90% power and two-sided 5% type I error rate. Conversely, SWE design only required 21 patients per arm. However, the type I error rate for SWE design is not controlled. In fact, the false-positive rate can range from 20% to more than 40% in simulation studies.¹⁵

In this review, we evaluate the use of randomized phase II (RPh2) trials in studying multiple treatment regimens. We are interested in identifying the types of RPh2 designs and how they are used in cancer clinical trials. We are particularly interested in the design properties, as well as the conduct and results of each study. We characterize the practice pattern and identify deficiencies. We also discuss alternative approaches, such as adaptive randomization under a Bayesian framework, and indicate future needs for multiarm RPh2 trial designs in oncology.

PATIENTS AND METHODS

Identification and Selection of Studies

We conducted a computerized literature search for studies published between 1986 and 2002. We used both PubMed and Science Citation Index to search for the terms "randomized" + either "phase II" or "phase 2" in all text including the title, keywords, and abstract, and selected only articles published in English. After the preliminary selection, we went through each of the

abstracts and eliminated the studies that were not randomized phase II trials. When multiple articles reported the results from the same trial, we included collective information, but counted only the latest publication in our review. We also excluded articles reporting only interim results. It is likely that our search did not identify all legitimate RPh2 studies because PubMed, Science Citation Index, and our searching criteria are in no way exhaustive. However, this searching mechanism should cover most of the RPh2 trials reported in the English literature.

We identified a total of 470 trials, with 266 (57%) reporting RPh2 studies in cancer trials. These are the focus of our study. Reports not considered here represented trials in the areas of cardiovascular disease ($n = 38$), HIV/AIDS ($n = 29$), infectious disease ($n = 17$), neurology/psychology ($n = 17$), hematologic/immunologic disease ($n = 16$), genitourinary disease ($n = 15$), injury/surgery ($n = 13$), gastroenterology ($n = 12$), neurology ($n = 11$), respiratory disease ($n = 10$), and trials involving other diseases ($n = 26$).

Data Presentation and Analysis

We extracted the following information from each article: year of publication; journal name; name and type of agents under study; disease site; study duration; whether the statistical design was mentioned; type of design; design properties, such as number of treatment arms and randomization scheme; whether a placebo, standard therapy, or no treatment control was used; type of end point used; proposed sample size; actual sample size; accrual period; type I and type II error rates; interim analysis; whether a trial was stopped early; whether hypothesis testing was conducted at the end of the trial; study result; if promising agents were sent to phase III for additional evaluation; and the outcome of phase III studies.

Type of agents is classified as chemotherapeutic (cytotoxic), biologic (biologically derived agents such as interferon, interleukin, colony-stimulating factor, monoclonal antibody, angiogenesis inhibitor, other small molecules with specific molecular targets, and so on), antitoxicity (to ameliorate toxicity), hormonal, preventive (used with cancer prevention end points), and others.

Specific randomization schema, such as simple randomization, stratified or permuted block, and dynamic allocation randomization, was recorded if reported in the article. Otherwise, we assume simple randomization was used if no randomization scheme was mentioned. We considered that a trial was stopped early if one or more arms were stopped. Available information was extracted and recorded to a data collection form and entered into an Access database. Given the large number of trials, complexity, and time frame of publication of the trials reviewed, we decided not to contact individual authors for the missing information.

We used descriptive statistics, frequency tabulations, and histograms to summarize the data. We applied a χ^2 test to examine the association between two categorical variables, and used the Cochran-Armitage trend test to compare the change of proportion over time. All of the tests were two sided with a 5% significance level.

RESULTS

General Trial Design Properties

Figure 1 shows that the number of publications describing RPh2 trial designs has increased over time, reflecting the increasing popularity of this type of design in cancer

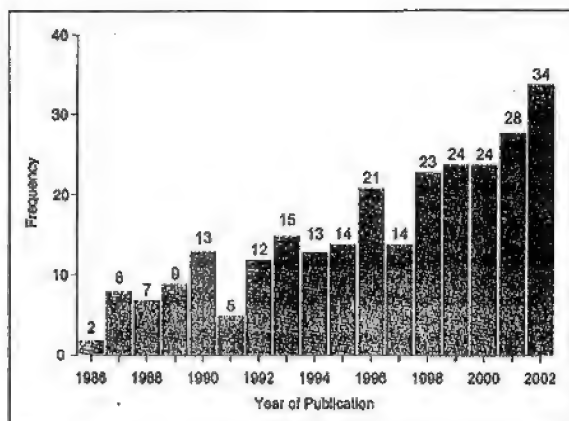


Fig 1. Histogram of number of randomized phase II cancer studies published from 1986 to 2002.

clinical trials. There were 28 and 34 RPh2 studies published in 2001 and 2002, respectively. Table 1 shows that the *Journal of Clinical Oncology* published the most articles describing RPh2 cancer trials, followed by *Cancer* and the *Annals of Oncology*.

Table 2 lists the general design properties of RPh2 trials. With respect to the treatment modality, 211 trials investigated a single modality and 55 trials studied combinations of different modalities. The most common single-agent treatment was still chemotherapeutic agents, which were involved in 131 of the trials (49%), followed by biologic agents. Trials reporting the use of combined modalities included 26 trials studying the combination of chemotherapeutic and biologic agents, and 12 trials evaluating the chemotherapy plus radiation combination. Biologic agents were combined with other modalities such as surgery or radiation in six trials. The study of biologic

Table 1. Number of Publications by Journal

Journal	No.	%
<i>Journal of Clinical Oncology</i>	38	13.5
<i>Cancer</i>	27	10.2
<i>Annals of Oncology</i>	22	8.3
<i>British Journal of Cancer</i>	12	4.5
<i>American Journal of Clinical Oncology</i>	11	4.1
<i>Lung Cancer</i>	9	3.4
<i>European Journal of Cancer</i>	7	2.6
<i>Clinical Cancer Research</i>	8	3.0
<i>Seminars in Oncology</i>	6	2.3
<i>Oncology</i>	6	2.3
<i>Gynecology Oncology</i>	8	2.3
<i>Investigational New Drugs</i>	6	2.3
<i>Leukemia</i>	6	2.3
Others (n < 5)	104	39.1
Total	266	100.0

Table 2. General Design Properties of Randomized Phase II Designs

Type of Agent	No.	%
Treatment modality		
Single treatment modality (N = 211)		
Chemotherapeutic	131	49.2
Biologic	36	13.5
Antitoxicity	16	8.0
Hormonal	11	4.1
Preventive	10	3.8
Other single modality	7	2.6
Combined treatment modality (N = 55)		
Chemotherapeutic + biologic	26	9.8
Chemotherapeutic + radiation therapy	12	4.5
Chemotherapeutic + others	6	2.3
Biologic + others	6	2.3
Other combination treatment	5	1.9
Primary end point		
Clinical response rate	194	72.9
Toxicity	18	6.0
Time to event	13	4.9
Event/incidence rate	10	3.8
Biomarker response	9	3.4
Pharmacological	6	2.3
Others	18	6.8
No. of study groups		
2	221	83.1
3	33	12.4
≥ 4	12	4.5
Was placebo used?		
No	254	95.5
Yes	12	4.5
Blinding of the trial		
Open (unblinded)	244	91.7
Double blinded	20	7.5
Single blinded	2	0.8
Randomization scheme		
Simple	159	59.8
Stratified	83	31.2
Permuted block	18	6.8
Dynamic allocation	6	2.3
Total sample size per design (N = 122)		
≤ 30	8	6.6
31-100	85	69.7
101-200	24	19.7
201-400	6	4.1
Total	266	100.0

agents showed an increase over time, increasing from 18% in 1986 to 1994, to 30% in 1995 to 2002 ($P = .03$, χ^2 test). Overall, biologic agents either as a single agent or in combination were studied in 70 of the trials (26%). Of 266 trials, 194 trials (73%) used clinical response rate as the primary end point of the study. Other types of end points reported include toxicity, time-to-event end points, event/incidence rate, biomarkers, and pharmacologic end points. (Table 2)

Most of the RPh2 trials (221; 83%) involved two study groups. Only 12 of the RPh2 trials (5%) used a placebo, whereas 254 of the trials (95%) did not. Open or unblinded

trial designs were used in 244 of the RPh2 trials (92%), whereas only 20 (7%) were double-blinded trials, and two (1%) were single-blinded trials. All 12 placebo-controlled trials were double-blinded trials using noncytotoxic agents. In terms of randomization, 60% of the trials used simple randomization, whereas 31% used stratified randomization. Permuted block randomization, with or without stratification, was applied in 7% of the trials, whereas only 2% of the trials used a dynamic allocation scheme (eg, minimization algorithm) to balance the potential prognostic factors. The vast majority of the trials (96%) randomly assigned participants with equal probability into the treatment arms. A randomization ratio of 2:1 was used in 4% of the trials, and only one trial used a 4:1 ratio. The planned sample size was reported in 122 articles (46%). Total sample sizes ranged from 28 to 390 (mean, 88; median, 80) and a standard deviation (SD) of 53. The mean average sample size per group was 39 (median, 37); the first and third quartiles were 25 and 50, respectively.

Statistical Design Properties

One hundred twenty-three articles (46%) reported the statistical design. The percentages of articles mentioning statistical design were 15%, 36%, 47%, and 62% for the publication years of 1986 to 1989, 1990 to 1994, 1995 to 1999, and 2000 to 2002, respectively. The increasing trend of reporting the trial design was statistically significant ($P < .0001$, Cochran-Armitage trend test). Among the articles that reported the statistical design, 49% provided sufficient information for characterizing the design. Therefore, only 60 (23%) of the 266 articles provided adequate information on the trial's statistical design.

The SWE design was used in 13 of the trials (11%; Table 3). The remaining trials were designed by one-stage (39%), two-stage (45%), or three-stage (3%) hypothesis testing or estimation methods. Two-stage designs were most commonly used in RPh2 trials ($n = 55$). Bayesian designs were used in two trials and a group sequential design was reported in one article. The majority of the trials (83%) were designed based on a binomial distribution because binary outcomes, such as the response rate, are the most commonly chosen primary end points in RPh2 trials. This result indicates that most of the RPh2 trials are based on a single-arm trial design embedded in a randomized, multiarm setting.

More detailed information on trial design was listed as follows. There were 73 articles that reported designs based on a one-sided test, and 31 were based on a two-sided test. Only 70 articles reported an alpha value (type I error), and 95 reported the study power. Among them, most of the trials ($n = 55$) were designed based on a 5% type I error rate. Type I error rates between 5% and 10% were also common ($n = 11$). Study power between 80% and 89% characterized 40 of the trials, whereas 53 trials had at least 90% power. For trials applying clinical response rate as the primary end point, the null re-

Table 3. Type of Statistical Design Used in Randomized Phase II Trials Among the Studies With Reported Statistical Designs ($N = 123$)

Statistical Design	No.	%
Design categories		
SWE randomized phase II	13	10.6
1-stage design	48	39.0
1-sample binomial	14	
2-sample binomial	15	
2-sample continuous	12	
2-sample survival	7	
2-stage design	55	44.7
Gehan's	14	
Simon's optimal	14	
Simon's minimax	11	
Ad-hoc binomial	10	
Fleming's	3	
Multinomial	2	
Logistic	1	
3-stage design	4	3.3
EORTC binomial	3	
Ensign's binomial	1	
Others	3	2.4
Bayesian binomial	2	
Group sequential binomial	1	
Design by type of primary end points		
Binomial	102	82.9
Continuous	12	9.8
Survival	7	5.7
Multinomial	2	1.6
Total	123	100.0

Abbreviations: SWE, Simon, Wittes, Ellenberg; EORTC, European Organization for the Research and Treatment of Cancer.

sponse rate typically ranges from 0% (Gehan's design) to 30%, with the target improvement rate of 10% to 20%.

Trial Conduct

The means (medians) of the total accrual, eligible participants, and assessable participants were 85.0 (72), 81.6 (67), and 77.6 (64), respectively. When enrolled participants were combined across all trials, only 4% of patients enrolled were ineligible, and more than 91% of the enrolled patients were assessable. At the trial level, the percentage of ineligible patients ranged from 0% to 31% of all patients enrolled (median, 0%; mean, 3%). Among eligible patients, the percentage of inassessable patients ranged from 0% to 43% (median, 1%; mean, 5%). The proportion of assessable patients among the total enrolled patients ranged from 57% to 100% (median, 95%; mean, 92%), which indicated that most trials were well conducted in general. Wide ranges in the total accruals, between 14 and 369, were reported. The SD was 53.2, indicative of a large variation in sample size in RPh2 studies. In addition, 168 trials reported the accrual duration. The mean accrual duration was 2.3 years (median, 1.9 years) with an SD of 1.4 years, and ranged from 0.2 to 10 years. The average accrual rate was 3.3 patients per month. Additional analysis showed that 75% of the trials

completed accrual within 3 years. The remaining 20% of the trials completed accrual in 3 to 5 years. More than 5 years were required to complete accrual in 5% of the trials.

Fifteen trials recruited exactly the same number of patients as planned without early stopping. Thirty trials were stopped early per design and, therefore, the target sample size is considered the same as the actual sample size. Compared with the target sample size, 23, 10, and four trials were below the planned accrual, and 24, nine, and three trials were above the planned accrual by less than 10%, 10% to 25%, and 25% to 50%, respectively. The remaining four trials had accruals that were more or less than 50% of the target accrual. Seventy-five percent of the trials had accrual within $\pm 10\%$ of the target accrual.

Statistical Analysis

Statistical analysis with respect to hypothesis testing and estimation is summarized by the type of end points. A trial may have one or more end points. For the response rate, 128 trials performed estimation only; 97 performed hypothesis testing. For the survival end points, 66 trials performed estimation only, whereas 125 trials tested the survival end points between treatment arms. For a toxicity end point, 137 trials reported estimation only and the remaining 111 trials reported hypothesis testing. Scattered reports that analyzed pharmacology, biomarker, and other end points were also found, with 16 trials reporting estimation and 43 trials reporting hypothesis testing. Although most of the trials were not designed to have enough statistical power for between-treatment comparison, the percentages of positive test results were 27% for binomial end point, 29% for survival end point, 57% for toxicity end point, and 67% for other end points, respectively. High percentages of significant findings are likely due to reporting bias (significant results are more likely to be reported).

Study Conclusions

Interim analyses were planned in 72 (27% of 266) trials (Table 4). Among them, 40 stopped early and 32 did not. Five trials did not have planned interim analyses but were stopped early. Therefore, 45 of 266 (17%) trials were terminated early. The reasons for early termination included the following: futility or lack of efficacy (69%), efficacy (13%), toxicity (13%), and slow accrual (4%).

At the conclusion of the RPh2 studies, 21% of the trials recommended no additional study, either due to toxicity or lack of efficacy, or both. No recommendation was made in 34% of the trials. Reports that the treatment regimen(s) merited additional study were made in 26% of the trials. In addition, additional studies (non-phase III) had been initiated in 5% of the trials. The remaining 14% either recommended a phase III study ($n = 18$) or indicated that a phase III study was already underway ($n = 21$).

Table 4. Interim Analysis and Early Stopping of the Trial

	Was Trial Stopped Early?		Total
	No	Yes	
Was interim analysis planned?			
No	189	5	194
Yes	32	40	72
Total	221	45	266
Reason for Early Stopping			
	No.	%	
Lack of efficacy/futility	31	68.9	
Efficacy	6	13.3	
Toxicity	6	13.3	
Slow accrual	2	4.4	
Total	45	100.0	

Results in Phase III Trials

We also performed a literature search for subsequent phase III trial reports on the 39 trials mentioned above that either recommended phase III studies or had phase III studies already underway. Of the six follow-up studies we found, four reported positive phase III results. These included the following studies: radiotherapy plus amifostine in head and neck cancer patients¹⁶; vorozole with megestrol acetate in postmenopausal advanced breast cancer patients¹⁷; combined cisplatin and carboplatin in addition to mitomycin and ifosfamide in patients with stage IV non-small-cell lung cancer¹⁸; and cisplatin plus gemcitabine plus vinorelbine in advanced non-small-cell lung cancer.¹⁹ The other two phase III trials reported negative results, which included the study of sequential high-dose methotrexate, fluorouracil, and doxorubicin in advanced gastric cancer,²⁰ and gemcitabine plus cisplatin in advanced non-small-cell lung cancer.²¹

DISCUSSION

With emerging technologies in screening active compounds and advancements in targeted therapy, promising treatment regimens have been identified at an increasingly fast pace. The high cost of drug development and limited patient resources, however, prohibit sending every promising treatment to a full-scale phase III evaluation. Therefore, phase II trials play a pivotal role in screening out inefficacious regimens and sending the most promising ones for additional evaluation. Early phase II studies are typically single-arm trials to examine whether the regimen yields the desired treatment efficacy. After screening out unpromising agents, a more challenging task is to identify the most promising ones among a large number of potentially active agents for additional development. RPh2 studies arise to meet such needs. Our review shows that the use of RPh2 studies in cancer research has increased in recent years. It is expected that this trend will continue.

An initial motivation for this review was to examine the frequency and usage of the SWE trial design for RPh2 studies in cancer research. To our surprise, only 13 of the reported 266 trials applied the SWE design, indicating that the ranking and selection methodology was not widely used in this setting. This could be attributed to several limitations of the design. SWE design works best when there is only one true successful treatment, with the other contenders falling below par. When there are several comparable, active regimens, the SWE method cannot accurately differentiate the best one from the better ones because it always selects the arm with the best observed outcome as the most successful treatment, regardless of whether none of the regimens work, some of them work, or all of them work well. Without the protection of controlling type I error rate, the SWE design also has a limited scope for making comparisons among treatment arms.¹⁵ In addition, the SWE RPh2 design does not provide early stopping rules to terminate inefficacious arm(s) early based on interim results. To remedy the problem, Steinberg and Venzon²² developed methods for selecting a promising agent early based on a two-stage ranking and selection procedure.

The vast majority of the RPh2 designs were based on methodology geared toward single-arm phase II studies. These trials were not designed to provide head-to-head comparisons across treatment arms. However, randomization was used as a tool for allocating patients evenly into multiple treatment arms to balance the known and unknown prognostic factors; hence, patient comparability is enhanced.²³ The majority of the trials (60%) applied simple randomization, which does not guarantee balance in number of patients assigned to each treatment or balance in prognostic factors within each treatment. With a small number of prognostic factors, stratified randomization and/or permuted block design can be used to increase the effectiveness of randomization.^{24,25} In the presence of a large number of prognostic factors, dynamic allocation should be considered to enhance randomization balance for a heterogeneous sample of moderate size.²⁶

Depending on type of agents, end points and trial designs should be chosen such that the efficacy of the regimens can be evaluated properly. Although response rate is a reasonable choice for cytotoxic drugs, it may not be appropriate for biologic agents, which may exert a cytostatic effect. Target-based primary end points such as molecular imaging or receptor modulation need to be selected carefully to best measure the pertinent treatment effects. In addition, efficacy assessment should be blinded to the treatment assignment to reduce the evaluation bias.

When several agents in a trial aim at a common target, randomized design can be applied among eligible patients presenting the target. For agents with different targets, parallel design can be considered to enroll patients with relevant targets onto corresponding treatment arms. Using a biomarker response is appealing, but validation is required to link the marker response to clinical significance. Because

targeted, biologic agents may not work for everyone, patient selection is essential for the success of the trial. Because of the low response rate in the general population, a target-enriched study population has been proposed recently to enhance the efficiency of the trials.²⁷⁻²⁹ Simon and Maitournam³⁰ described a method to compute the relative efficiency of targeted designs versus the design without selection and showed that targeted clinical trials can dramatically reduce the number of patients required for study in cases where the mechanism of action of the drug is understood and an accurate assay for responsiveness is available.

Many trials were designed with at least 90% power, reflecting the importance of controlling the type II error in RPh2 studies. In phase II settings, controlling the type II error can be more important than controlling the type I error because a false-negative result could essentially terminate the development of a promising agent, whereas a false-positive result can be identified in future phase II or III studies. Formal hypothesis testing comparing end points among treatment arms was commonly reported. With the limited sample size, RPh2 trials typically do not have sufficient statistical power for such comparisons and such practice should be discouraged. Point and CI estimations should be performed, instead.

In all 266 trials, only 72 trials (27%) had planned interim analyses. It is interesting to note that 56% of the trials with planned interim analyses stopped early. In addition, among the trials stopped early, 69% of them were due to lack of efficacy, indicating that the majority of the studied regimens did not meet expectations. Without considering the false-negative rate, an additional 28% ($73\% \times 56\% \times 69\%$) of the RPh2 trials could have been stopped early by identifying inefficacious agents had early stopping rules been implemented. This calculation assumes that all trials need interim analyses and that the probability of stopping and the percentage of ineffective agents were similar between the trials with and without interim analyses. Although these assumptions may not always hold, the calculation provides us with a rough estimate on the magnitude of additional resources that could be saved by incorporating interim analysis in the study design.

Continuing to find improved cancer treatment is an uphill battle. Although enthusiasm is a driving force for discovery, the reality is that most new regimens probably will not be much improved over the existing ones. Early stopping due to futility or lack of efficacy is critically important for RPh2 studies, not only to save resources and gain trial efficiency, but also to limit the number of patients receiving sub-par treatments as soon as they are identified. A general overview of various design considerations is described in Lee et al.³¹

Only a small fraction of the trials were conducted exactly as planned. It is more a rule than an exception that the actual conduct of clinical trials may deviate from the protocol. Although investigators have the responsibility to follow the protocol as much as possible, statisticians are called to develop more flexible designs to meet the practical needs of clinical

trials. To date, most clinical trial designs are based on the so-called frequentist's approach, which involves computing the probability of the observed events given the design parameters. When the study conduct deviates from the design, all of the design properties (such as controlling type I and type II error rates) may no longer hold. For example, Simon's optimal two-stage design will neither be optimal nor have the desired operating characteristics if the sample size at each stage is different from the sample size specified by the design, or when the actual response rates differ from the target responses rates.

One alternative is a flexible design applying the Bayesian approach, which computes the probability of the parameters given the observed events. The Bayesian approach is consistent with the likelihood principle in the sense that the inference is based on the observed outcome and not on some hypothetical sampling or design parameters. Frequentist's designs are more rigid and less robust to the design change. In contrast, the Bayesian design is intrinsically adaptive and data-driven, which allows the inference to be less dependent on the study design. Advancements in computing algorithms (such as the Monte-Carlo Markov chain) and in computing power have made the implementation of Bayesian methodology quite feasible. The Bayesian clinical trial method is an active area of research, with several developments reported in the recent literature, such as a predictive probability approach,³² response-adaptive randomization,³³ hierarchical Bayes model,³⁴ seamless phase II/III trials,³⁵ a decision-theoretic approach for designs with multiple end points,³⁶ and so on.

There were also reports of a flexible design based on the frequentist's approaches. For example, Karrison et al³⁷ developed a group-sequential, response-adaptive design to allow random assignment of more patients into the better-performing arms, which can be adapted to the randomized phase II setting. Scher and Heller³⁸ proposed an integrative phase II/III design to evaluate multiple experimental treatments with a survival end point. In the last two decades, a plethora of statistical designs for phase II studies have been published in the statistical literature, but few of these have actually been used. Increasing the implementation of new statistical designs in actual clinical trials will require better communication between statisticians and the clinicians conducting trials, as well as the development of practical designs with good statistical properties and easily accessible computing tools with friendly user interface.

Several authors have shown that the reporting quality of phase II studies in the literature is generally poor. The percentages of trials with identifiable statistical designs were reported to be 12% by Kramar et al,³⁹ 20% by Mariani and Marubini,⁴⁰ and 35% by Perrone et al.⁴¹ We also found a similar result, with only 23% of the reported RPh2 trials having adequate descriptions of their statistical designs. Encouragingly, the percent of the trial reports including design information has increased over time from 15% in the late 1980s to 62% in 2000 to 2002. The statistically significant trend of an increasing report of statistical design is likely the result of a combination of factors. These include the increasing awareness of the importance of study design, increasing understanding and appreciation of biostatistics in clinical trials, tighter control in the clinical trials approval process (institutional review boards, funding agencies, industry, and regulatory bodies), voices from many advocates stressing the need to improve clinical trial reporting, and a favorable response from journal editors.⁴² Continuing effort is still much needed to enhance the design, conduct, and reporting of RPh2 studies.

In summary, current RPh2 trials are primarily designed based on existing one-sample methods with add-on randomization to improve patient comparability. Innovative designs are much needed to allow researchers and clinicians to address important issues such as study population enrichment, selection and validation of most appropriate target-based end points, dynamic and adaptive randomization, flexible study accrual, conduct, and monitoring, early stopping rule for futility, and so on. For the establishment of initial efficacy of a single-arm phase IIA trial, an RPh2 trial provides additional assessment of treatment efficacy by studying multiple treatment regimens of interest concurrently; hence, it generates valuable information for designing phase III trials. Thus, efficient and well-conducted RPh2 trials can be instrumental toward the successful development of effective cancer treatments.

Acknowledgment

The authors thank two reviewers and Donald A. Berry, PhD, for constructive comments, and LeeAnn Chastain and Jennifer Dupre for editorial assistance.

Authors' Disclosures of Potential Conflicts of Interest

The authors indicated no potential conflicts of interest.

REFERENCES

- Mariani L, Marubini E: Design and analysis of phase II cancer trials: A review of statistical methods and guidelines for medical researchers. *Int Stat Rev* 64:61-88, 1996
- Thall PF, Simon RM: Recent developments in the design of phase II clinical trials, in Thall PF (ed): *Recent Advances in Clinical Trial Design and Analysis*. Boston, MA, Kluwer Academic Publishers, 1995, pp 49-71
- Cornis RL, Miller JD, Aldige CR, et al: Public attitudes toward participation in cancer clinical trials. *J Clin Oncol* 21:830-835, 2003
- Cassileth BR: Clinical trials: Time for action. *J Clin Oncol* 21:765-766, 2003
- Von Hoff DD: There are no bad anticancer agents, only bad clinical trial designs: Twenty-first Richard and Hinda Rosenthal Foundation Award Lecture. *Clin Cancer Res* 4:1079-1086, 1998
- Gehan EA: The determination of the number of patients required in a preliminary and a follow-up trial of a new chemotherapeutic agent. *J Chronic Dis* 13:346-353, 1961
- Simon R: Optimal two-stage designs for phase II clinical trials. *Control Clin Trials* 10:1-10, 1989

8. Fleming TR: One sample multiple testing procedure for phase II clinical trials. *Biometrics* 38:143-151, 1982
9. Ensign LG, Gehan EA, Kamen DS, et al: An optimal three-stage design for phase II clinical trials. *Stat Med* 13:1727-1736, 1994
10. Chen TT: Optimal three-stage designs for phase II cancer clinical trials. *Stat Med* 16:2701-2711, 1997
11. Thall PF, Simon R: Practical Bayesian guidelines for phase II clinical trials. *Biometrics* 50:337-349, 1994
12. Thall PF, Simon R: A Bayesian approach to establishing sample size and monitoring criteria for phase II clinical trials. *Control Clin Trials* 15:463-481, 1994
13. Leung S, Heng-Yan D, Wang Y-G: A Bayesian decision approach for sample size determination in phase II trials. *Biometrics* 57:309-312, 2001
14. Simon R, Wittes RE, Ellenberg SS: Randomized phase II clinical trials. *Cancer Treat Rep* 69:1375-1381, 1985
15. Liu FY, LeBlanc M, Desai M: False positive rates of randomized phase II designs. *Control Clin Trials* 20:343-352, 1999
16. Brizel DM, Wasserman TH, Henke M, et al: Phase III randomized trial of amifostine as a radioprotector in head and neck cancer. *J Clin Oncol* 18:3339-3345, 2000
17. Goss PE, Winer EP, Tannock IF, et al: Randomized phase III trial comparing the new potent and selective third-generation aromatase inhibitor vorozole with megestrol acetate in postmenopausal advanced breast cancer patients. *J Clin Oncol* 17:52-63, 1999
18. Sculier JP, Lafitte JJ, Paesmans M, et al: Phase III randomized trial comparing moderate-dose cisplatin to combined cisplatin and carboplatin in addition to mitomycin and ifosfamide in patients with stage IV non-small-cell lung cancer. *Br J Cancer* 83:1128-1135, 2000
19. Comella P, Frasci G, Panza N, et al: Randomized trial comparing cisplatin, gemcitabine, and vinorelbine with either cisplatin and gemcitabine or cisplatin and vinorelbine in advanced non-small-cell lung cancer: Interim analysis of a phase III trial of the southern Italy Cooperative Oncology Group. *J Clin Oncol* 18:1451-1457, 2000
20. Vanhoefler U, Rougier P, Wilke H, et al: Final results of a randomized phase III trial of sequential high-dose methotrexate, fluorouracil, and doxorubicin versus etoposide, leucovorin, and fluorouracil versus infusional fluorouracil and cisplatin in advanced gastric cancer: A trial of the European Organization for Research and Treatment of Cancer Gastrointestinal Tract Cancer Cooperative Group. *J Clin Oncol* 18:2648-2657, 2000
21. Scagliotti GV, De Marinis F, Rinaldi M, et al: Phase III randomized trial comparing three platinum-based doublets in advanced non-small-cell lung cancer. *J Clin Oncol* 20:4285-4291, 2002
22. Steinberg SM, Venzon DJ: Early selection in a randomized phase II clinical trial. *Stat Med* 21:1711-1726, 2002
23. Friedman LM, Furberg CD, DeMets DL: *Fundamentals of Clinical Trials*, 3rd ed. New York, NY, Springer, 1998, pp 61-81
24. Kernan WN, Viscoli CM, Makuch RW, et al: Stratified randomization for clinical trials. *J Clin Epidemiol* 52:1289-1290, 1999
25. Pocock SJ, Simon R: Sequential treatment assignment with balancing for prognostic factors in the controlled clinical trial. *Biometrics* 31:103-115, 1975
26. Scott NW, McPherson GC, Ramsay CR, et al: The method of minimization for allocation to clinical trials: A review. *Control Clin Trials* 23:662-674, 2002
27. Roberts TG Jr, Lynch TJ Jr, Chabner BA: The phase III trial in the era of targeted therapy: Unraveling the "go or no go" decision. *J Clin Oncol* 21:3683-3695, 2003
28. Blakey DC: Anti-cancer drug discovery and development summit. *Expert Opin Investig Drugs* 12:1577-1582, 2003
29. Rosner GL, Stadler W, Ratain MJ: Randomized discontinuation design: Application to cytostatic antineoplastic agents. *J Clin Oncol* 20:4478-4484, 2002
30. Simon R, Maitournam A: Evaluating the efficiency of targeted designs for randomized clinical trials. *Clin Cancer Res* 10:6759-6763, 2004
31. Lee JJ, Lieberman R, Sloan JA, et al: Design considerations for efficient prostate cancer chemoprevention trials. *Urology* 57:206-212, 2001 (4 Suppl 1)
32. Johns D, Andersen JS: Use of predictive probabilities in phase II and phase III clinical trials. *J Biopharm Stat* 9:67-69, 1999
33. Berry DA, Eick SG: Adaptive assignment versus balanced randomization in clinical trials: A decision analysis. *Stat Med* 14:231-246, 1995
34. Thall PF, Wathen JK, Bekele BN, et al: Hierarchical Bayesian approaches to phase II trials in diseases with multiple subtypes. *Stat Med* 22:763-780, 2003
35. Inoue LY, Thall PF, Berry DA: Seamlessly expanding a randomized phase II trial to phase III. *Biometrics* 58:823-831, 2002
36. Stallard N, Thall PF, Whitehead J: Decision theoretic designs for phase II clinical trials with multiple outcomes. *Biometrics* 55:971-977, 1999
37. Karrison TG, Huo D, Chappell R: A group sequential, response adaptive design for randomized clinical trials. *Control Clin Trials* 24:508-522, 2003
38. Scher HI, Heller G: Picking the winners in a sea of plenty. *Clin Cancer Res* 8:400-404, 2002
39. Kramar A, Potvin D, Hill C: Multistage designs for phase II clinical trials: Statistical issues in cancer research. *Br J Cancer* 74:1317-1320, 1996
40. Mariani L, Marubini E: Content and quality of currently published phase II cancer trials. *J Clin Oncol* 18:429-436, 2000
41. Perrone F, Di Maio M, De Maio E, et al: Statistical design in phase II clinical trials and its application in breast cancer. *Lancet Oncol* 4:305-311, 2003
42. Altman DG: Poor-quality medical research: What can journals do? *JAMA* 287:2765-2767, 2002

Prognostic Factors in Resected Stage I Non-Small-Cell Lung Cancer: A Multivariate Analysis of Six Molecular Markers

Charles Lu, Jean-Charles Soria, Ximing Tang, Xiao-Chun Xu, Luo Wang, Li Mao, Reuben Lotan, Bonnie Kemp, B. Nebiyu Bekele, Lei Feng, Waun K. Hong, and Paolo R. Khuri

From the Departments of Thoracic/Head and Neck Medical Oncology, Clinical Cancer Prevention, Pathology, and Biostatistics, The University of Texas M.D. Anderson Cancer Center, Houston, TX; Institut Gustave Roussy, Villejuif, France; and Winship Cancer Institute, Emory University, Atlanta, GA.

Submitted January 13, 2004; accepted August 26, 2004.

Supported in part by National Cancer Institute grant No. K12 CA088094 and the Department of Defense, Biology, Education, Screening, Chemoprevention, and Treatment of Lung Cancer grant No. DAMD17-01-1-0689 and Translational Approaches for the Reversal, Genetic, Evaluation and Treatment of Lung Cancer grant No. DAMD17-02-1-0706.

Presented in part at the 93rd Annual Meeting of the American Association for Cancer Research, San Francisco, CA, April 6-10, 2002.

Authors' disclosures of potential conflicts of interest and author contributions are found at the end of this article.

Address reprint requests to Charles Lu, MD, SM, The University of Texas M.D. Anderson Cancer Center, 1515 Holcombe Boulevard, Box 432, Houston, TX 77030-4009; e-mail: cliu@mdanderson.org.

© 2004 by American Society of Clinical Oncology

0732-183X/04/2222-4575/\$20.00

DOI: 10.1200/JCO.2004.01.091

ABSTRACT

Purpose

To analyze the prognostic significance of six molecular biomarkers (death-associated protein kinase [DAPK] promoter methylation, interleukin-10 [IL-10] protein expression, cyclooxygenase-2 [COX-2] mRNA expression, human telomerase reverse transcriptase catalytic subunit [hTERT] mRNA expression, retinoic acid receptor-beta [RAR-β] mRNA expression, and K-ras mutational status) in stage I non-small-cell lung cancer (NSCLC) patients.

Patients and Methods

Biomarker analyses were performed on tumors from 94 patients with stage I NSCLC who underwent surgical resection at our institution. A minimum follow-up period of 5 years was required. DAPK methylation was assessed by methylation-specific polymerase chain reaction (PCR). RAR-β, COX-2, and hTERT mRNA levels were determined by in situ hybridization with digoxigenin-labeled antisense riboprobes. K-ras mutation status was determined by the PCR-primer introduced restriction with enrichment for mutant alleles method. IL-10 protein expression was analyzed by immunohistochemistry using a polyclonal antihuman IL-10 antibody. Cancer-specific survival was analyzed with a Cox proportional hazards model. To identify independent prognostic factors, a stepwise selection method was used.

Results

DAPK methylation, IL-10 lack of expression, COX-2 expression, hTERT expression, RAR-β expression, and K-ras mutations were observed in 46.8%, 29.8%, 59.6%, 34.0%, 23.4%, and 34.0% of patients, respectively. In the final model, DAPK methylation and IL-10 lack of expression were significant negative prognostic factors for cancer-specific survival, whereas COX-2 expression was of borderline significance.

Conclusion

In this cohort of resected stage I NSCLC patients, molecular markers that independently predict cancer-specific survival have been identified. The prognostic roles of DAPK methylation, IL-10, and other biomarkers in NSCLC merit further investigation.

J Clin Oncol 22:4575-4583. © 2004 by American Society of Clinical Oncology

INTRODUCTION

Lung cancer remains a worldwide public health issue of immense proportions. In the year 2003, cancers of the lung and bronchus are expected to continue to account for the most cancer deaths in the United States (157,200 deaths or 28.2%), more than the estimated total number of deaths

as a result of cancers of the breast, prostate, colon, and rectum combined.¹ Approximately 80% of lung cancers will have non-small-cell carcinoma histology.²

Approximately 25% of patients present with early-stage disease.³ The standard treatment is surgical resection with appropriate lymph node sampling or dissection. Although early-stage non-small-cell lung

cancer (NSCLC) patients have a relatively favorable prognosis, the risk of disease recurrence and death remains substantial. Five-year survival rates for pathologic stages I and II disease are 57% to 67% and 38% to 55%, respectively.⁴ Identification of reliable prognostic factors for disease recurrence and death could have significant clinical import. Patients in a high-risk group, for example, would be appropriate candidates for novel adjuvant or chemoprevention strategies.

Both our group⁵⁻¹² and others¹³⁻¹⁶ have focused on identifying molecular prognostic factors in early-stage NSCLC. We have established a retrospective cohort of stage I NSCLC patients who underwent surgical resection at our institution. Over the past few years, investigators in our group have analyzed a number of tumor biomarkers within this valuable clinical research database.

Given the roles that retinoids play in the regulation of cell growth, differentiation, and apoptosis, Khuri et al⁸ investigated the prognostic significance of retinoic acid receptor-beta (RAR- β) mRNA expression in 156 patients. Because RAR- β expression seems to be suppressed during carcinogenesis, these investigators hypothesized that lower RAR- β levels would predict a poor clinical outcome. Surprisingly, overall survival was significantly worse in patients with strongly positive RAR- β expression. Because one RAR- β isoform, RAR- β 4, may promote hyperplasia and neoplasia,¹⁷ the authors hypothesized that differential expression of RAR- β isoforms may be a possible explanation for their unexpected findings.

Khuri et al⁹ subsequently evaluated cyclooxygenase-2 (COX-2) mRNA expression and correlated it with the expression of RAR- β in this cohort of stage I NSCLC patients. COX-2 overexpression had previously been demonstrated in lung, head and neck, and other tumors,¹⁸⁻²⁰ and cell line data indicated that retinoic acid could suppress COX-2.²¹ These investigators found that COX-2 expression was associated with worse overall and disease-free survival and that COX-2 and RAR- β mRNA levels were correlated. These findings were in conflict with the prior cell line data, which would have predicted that RAR- β upregulation should downregulate COX-2.

Telomerase is a ribonucleoprotein that lengthens and maintains the ends of chromosomes that are shortened with successive cell divisions.²² Telomerase is expressed in up to 85% of NSCLC tumors and plays a critical role in sustaining cellular immortality and carcinogenesis.^{23,24} Wang et al¹¹ examined mRNA expression of the human telomerase reverse transcriptase catalytic subunit (hTERT) in 153 patients from our database. Positive hTERT expression was significantly associated with worse overall and disease-specific survival.

Tang et al⁷ examined hypermethylation of the death-associated protein kinase (*DAPK*) promoter in 135 patients from this cohort. Epigenetic inactivation of tumor suppressor

genes by promoter hypermethylation frequently occurs in NSCLC.^{25,26} *DAPK* is a putative tumor-suppressor gene that encodes for a calmodulin-dependent kinase that possesses a death domain at its C terminus.²⁷ *DAPK* is required for interferon-gamma-induced apoptosis and seems to suppress the metastatic ability of lung cancer cells.²⁸ In the study by Tang et al,⁷ *DAPK* hypermethylation was significantly associated with poorer overall and disease-specific survival.

Soria et al¹² examined the role of interleukin-10 (IL-10) protein expression among 135 patients. The immunomodulatory effects of IL-10 have demonstrated conflicting results in various tumor systems. Some reports support the role of IL-10 in helping tumors evade immunosurveillance because IL-10 can inhibit macrophage, T-cell, and antigen-presenting cell functions.^{29,30} Others have demonstrated that IL-10 may function as a potent inhibitor of tumor growth and metastasis.^{31,32} In this study, IL-10 lack of expression was significantly associated with poorer overall and disease-specific survival.

The aforementioned hypothesis-driven studies each focused on one or a few biomarkers. To simultaneously examine multiple potential molecular prognostic factors in this clinical research database, we identified 94 patients who had complete information for a panel of six biomarkers (RAR- β , COX-2, hTERT, *DAPK* promoter methylation, IL-10, and *K-ras*). Multivariate Cox regression analysis was used to identify independent predictors of cancer-specific survival in this population of resected stage I NSCLC patients.

PATIENTS AND METHODS

Study Population

Five hundred ninety-five consecutive patients with stage I NSCLC underwent definitive surgical resection, defined as a lobectomy or a pneumonectomy, from 1975 to 1990 at The University of Texas M.D. Anderson Cancer Center (Houston, TX). Patients did not receive preoperative or postoperative chemotherapy or radiotherapy. We retrospectively identified 185 patients for whom both tissue samples and a median follow-up period of more than 5 years were available. All available tissue blocks were reviewed by a thoracic pathologist (B.K.), and 163 cases had adequate tumor present in the surgical specimen. The patient population was identified through a search of the Tumor Registry database maintained by the Department of Medical Informatics at The University of M.D. Anderson Cancer Center. Survival status was verified and updated from Tumor Registry records as of December 1, 2000. This study was reviewed and approved by the institutional review board and conducted in accordance with its policies.

Five published studies^{7-9,11,12} had previously examined different molecular prognostic factors among the 163 patients with sufficient tumor specimens and more than 5 years of follow-up data. The sample sizes ranged from 135 to 160 patients. A total of

94 patients had complete information for a panel of six biomarkers, and these patients were included in our analysis.

Methylation-Specific Polymerase Chain Reaction (PCR)

These methods have been previously described.⁷ Briefly, 8- μ m sections from paraffin-embedded tissue blocks were obtained, and regions with tumor cells were dissected under a stereomicroscope. In the initial chemical modification step, 200 ng of DNA from each tumor was denatured by NaOH and treated with sodium bisulfite (Sigma Chemical Co, St Louis, MO). DNA was recovered in water and was ready to add to a PCR with the use of specific primers for either the methylated or the unmethylated DAPK promoter, as described previously.³³ DNA was amplified for 35 cycles, and PCR products were separated on 2% agarose gels and visualized. For each DNA sample, primer sets for methylated DNA and unmethylated DNA were used for analysis. The hypermethylation status was determined by visualizing a 98-base pair (bp) PCR product with the methylation-specific primer set. All PCRs were repeated twice, and the results were reproducible.

Immunohistochemical Staining for IL-10 Protein

Paraffin-embedded, 4- μ m-thick tissue sections were stained for IL-10 protein using a primary goat polyclonal antihuman IL-10 antibody (AF-217-NA; R&D Systems, Minneapolis, MN) as previously described.¹² Routinely processed tissue sections of normal lymph nodes and tonsils were used as positive staining controls and were also stained with the primary antibody omitted to confirm staining specificity. Normal bronchial epithelial cells that constitutively produce IL-10 were also used as internal positive controls.³⁴

The IL-10 labeling index was defined as the percentage of tumor cells displaying cytoplasmic immunoreactivity and was calculated by counting IL-10-stained tumor cells among at least 1,000 tumor cells for each section as previously described.¹² On the basis of previous reports, if 10% or more of the tumor cells were positive for IL-10, the case was considered to be IL-10 positive.³⁵ All slides were scored concomitantly by a pathologist (X.T.) and another investigator (J.-C.S.) in a blinded manner.

hTERT In Situ Hybridization (ISH)

These methods have been previously described.¹¹ The riboprobes were a 430-bp EcoRV-BamHI fragment of the hTERT cDNA that has been used in other studies^{36,37} as well as part of exon 1 from the heterogeneous nuclear ribonucleoprotein A1 as a control to verify sample quality. The single-strand-specific, digoxigenin-labeled riboprobes were generated by *in vitro* transcription. ISH was performed as previously described.³⁷ Slides displaying a diffuse but clear cytoplasmic signal were considered to be positive, as reported by Falchetti et al.³⁸ More specifically, our slides were rated as positive if a definite and clear signal was present in more than two large areas on the slide. Slides with faint signal, the absence of signal, or only focal positivity were considered to be negative. We did not grade the intensity of the hybridization signals.

COX-2 and RAR- β ISH

COX-2 and RAR- β mRNA were detected in 4- μ m-thick sections from paraffin-embedded tissue using nonradioactive ISH with digoxigenin-labeled antisense riboprobes as previously described.^{8,9,39} Retinoid X receptor- α (RXR- α), which is present in greater than 90% of NSCLCs,⁴⁰ was used as a control to detect RNA degradation. The rationale for using RXR- α as a control for

intact RNA was the observation that all 70 cases of NSCLC and normal lung tissue expressed RXR- α mRNA in a previous study.⁴⁰ Stained sections were reviewed by three independent researchers, including two pathologists, in a blinded fashion. Only cytoplasmic staining was considered positive. Because normal bronchial epithelium expresses RAR- β , positive and aberrant RAR- β expression was defined as $\geq 10\%$ and less than 10% intratumoral staining, respectively.⁸ The RAR- β probe that was used identified all RAR- β isoforms. COX-2 expression was defined as either positive (present) or negative (absent).⁹

K-ras Mutation Analysis With PCR-Primer Introduced Restriction With Enrichment for Mutation Alleles (PCR-PIREMA)

A modified PCR-PIREMA method was used to detect K-ras codon 12 mutations.⁴¹ Briefly, 8- μ m sections from paraffin-embedded tissue blocks were obtained, and regions with tumor cells were dissected under a stereomicroscope. Dissected tissues were digested in 200 μ L of digestion buffer containing 50 mmol/L Tris-HCl (pH 8.0), 1% sodium dodecyl sulfate, and proteinase K (0.5 mg/mL) at 42°C for 36 hours. The digested products were purified by extracting with phenol-chloroform twice. DNA was then precipitated by the ethanol precipitation method in the presence of glycogen (Roche Biochemicals, Indianapolis, IN), recovered in distilled water, and then stored at -20°C until used for PCR.

Briefly, PCR around K-ras codon 12 was performed using a mismatched primer (forward primer: 5'-TGAATATAAACTGTGGTAGTTGGACCT-3'; reverse primer: 5'-CTGTATCAAAGAATGGTCC TGCACC-3') that introduced an *Mva*I restriction site into the PCR products derived from normal alleles. *Mva*I digestion of the PCR products left only the PCR products derived from mutant alleles intact, after which further PCR selectively amplified the mutant PCR products. The first PCR reaction was performed with mixtures containing 0.5 μ L of DNA recovery solution, 10 ng of each nucleotide, and the mismatched primer to introduce an *Mva*I restriction site flanking the K-ras exon 1, with 15 cycles at an annealing temperature of 55°C. The first PCR products were digested with *Mva*I and diluted 1:100. One microliter of the diluted product was amplified by 20 cycles of PCR with the same primers at an annealing temperature of 40°C, and the products were digested with *Mva*I a second time. The second PCR products were diluted 1:100, amplified by 35 cycles with the previous forward primer and a new reverse primer (5'-CTCTATTGTTGGATCATATTCGTCCAC-3') at an annealing temperature of 65°C, and digested with *Mva*I a third time. The final digested products were then electrophoresed on 2.5% agarose gels and stained with ethidium bromide. A digestion-resistant 106-bp band indicated the presence of a K-ras codon 12 mutation. Extensive measures were taken to prevent cross-contamination of samples. A normal control sample and a known mutation sample were included in all of the experiments.

Statistical Analyses

Overall survival, disease-specific survival, and disease-free survival were analyzed in this study. Survival curves were estimated by the Kaplan-Meier method. The log-rank test was used to compare survival time between groups. Fisher's exact test was used to analyze the association between categorical variables. Using a stepwise selection method, a Cox proportional hazards model was created to identify independent predictors of survival, with adjustment for relevant clinical covariates (tumor stage, histology,

smoking status, and sex). All statistical tests were two-sided, and $P < .05$ was considered statistically significant.

All survival curves were calculated from the date of surgery. Overall survival took all deaths (cancer related or not) into account. Disease-specific survival time was calculated from the date of surgery to death from cancer-related causes. Disease-free survival time was calculated from the date of surgery to relapse or death from cancer-related causes.

RESULTS

Data for a panel of six molecular markers (RAR- β , COX-2, hTERT, *DAPK* promoter methylation, IL-10, and *K-ras*) were available for 94 patients in our retrospective cohort. These patients were the study population for our analysis. Patient characteristics are listed in Table 1. Median follow-up time for alive patients and those lost to follow-up was 10.9 years. Sixty-nine patients have died. Twenty-nine deaths were cancer related.

The frequency of each molecular marker, displayed as a negative prognostic factor, is listed in Table 2. Univariate analyses of each molecular marker and its association with disease-specific survival and overall survival were performed (Table 3). Similar univariate survival analyses of clinical variables (age, sex, and smoking status) were performed. A highly significant association was demonstrated between age (< 60 years $v \geq 60$ years) and overall survival ($P = .003$). Sex and smoking status were not associated with overall or disease-specific survival. Age ≥ 60 years was associated with a significant increased risk of noncancer-

Table 2. Frequency of Molecular Markers in Stage I NSCLC

Molecular Marker	Frequency (%)
COX-2 expression	60
<i>DAPK</i> methylation	47
<i>K-ras</i> mutation	34
hTERT expression	34
IL-10 lack of expression	30
RAR- β expression	23

Abbreviations: NSCLC, non-small-cell lung cancer; COX-2, cyclooxygenase-2; *DAPK*, death-associated protein kinase; hTERT, human telomerase reverse transcriptase catalytic subunit; IL-10, interleukin-10; RAR- β , retinoic acid receptor-beta.

related death ($P < .001$) and was not associated with disease-specific survival ($P = .577$). This phenomenon is likely explained by the relatively long follow-up of these subjects and by the fact that the majority of deaths (40 of 69 deaths) were unrelated to cancer. In light of these findings, we reasoned that disease-specific survival would serve as a more clinically relevant end point for this cohort, although we continued to include overall survival in our analyses. Disease-specific survival stratified by each molecular marker is shown in Figure 1.

A multivariate Cox proportional hazards model was created to identify predictors of disease-specific survival (Table 4). *DAPK* promoter methylation and IL-10 lack of expression were significant negative prognostic factors for disease-specific survival, whereas COX-2 expression was of borderline significance. The same variables were selected when tumor stage, histology, smoking status, and sex were included in the model. The poorer disease-specific and overall survival of patients with both *DAPK* methylation and IL-10 lack of expression are illustrated in Figure 2. We defined these patients as a high-risk group, and the remaining patients were defined as a low-risk group. A log-rank test assessing the difference in survival between these groups was statistically significant for both disease-specific survival ($P < .0001$) and overall survival ($P < .0001$). We note that the definitions of the high- and low-risk groups are data dependent. That is, the definition of high risk was not determined a priori. A similar model for overall survival yielded three significant negative prognostic factors (age ≥ 60 years, $P = .0017$; COX-2 expression, $P = .021$; and *DAPK* methylation, $P = .044$), whereas IL-10 lack of expression was of borderline significance ($P = .069$).

Exploratory analyses of the relationships between the various molecular markers were performed. Significant associations were found between hTERT and COX-2 expression (odds ratio [OR], 6.14; 95% CI, 2.09 to 18.04; $P = .0004$) and *K-ras* mutations and *DAPK* methylation (OR, 2.64; 95% CI, 1.10 to 6.36; $P = .032$). Associations between IL-10 lack of expression and hTERT expression (OR, 2.63; 95% CI, 1.06 to 6.67; $P = .056$), IL-10 lack of

Table 1. Patient Characteristics

Characteristic	No. of Patients	%
Age, years		
Median	63.5	
Range	41-82	
Sex		
Male	72	77
Female	22	23
Race		
White	83	88
Other	11	12
Smoker		
Yes	82	87
No	5	6
Unknown	7	7
Histology		
Adenocarcinoma	39	41
Squamous cell carcinoma	39	41
Other	16	17
TNM stage		
T1N0M0	44	47
T2N0M0	50	53

Abbreviation: TNM, tumor-node-metastasis.

Table 3. Univariate Analysis of Molecular Markers With Disease-Specific and Overall Survival

Molecular Marker	Disease-Specific Survival			Overall Survival		
	Hazard Ratio	95% CI	P	Hazard Ratio	95% CI	P
IL-10 lack of expression	3.17	1.53 to 6.62	.002	1.98	1.21 to 3.25	.007
DAPK methylation	3.00	1.39 to 6.47	.005	1.69	1.05 to 2.72	.030
hTERT expression	2.39	1.15 to 4.97	.020	1.48	0.91 to 2.42	.116
COX-2 expression	2.44	1.08 to 5.54	.032	1.80	1.09 to 2.96	.022
RAR- β expression	1.47	0.66 to 3.25	.345	1.23	0.72 to 2.09	.446
K-ras mutation	1.00	0.45 to 2.20	.998	1.18	0.71 to 1.95	.517

Abbreviations: IL-10, interleukin-10; DAPK, death-associated protein kinase; hTERT, human telomerase reverse transcriptase catalytic subunit; COX-2, cyclooxygenase-2; RAR- β , retinoic acid receptor-beta.

expression and COX-2 expression (OR, 2.63; 95% CI, 0.99 to 7.14; $P = .066$), and COX-2 expression and RAR- β expression (OR, 2.88; 95% CI, 0.96 to 8.64; $P = .08$) were of borderline significance.

We also investigated other models by performing all two-variable, three-variable, and four-variable multivariate models. On the basis of these analyses, only DAPK methylation and IL-10 lack of expression were statistically significant ($P < .05$) for all models. Furthermore, the three-

variable model, including DAPK methylation, IL-10 lack of expression, and COX-2 expression, had the lowest Akaike Information Criterion (AIC) value of 224.029 (although the two-variable model that excluded COX-2 expression had an AIC of similar value). We noted that there was some evidence of association between IL-10 lack of expression and hTERT expression (OR, 2.63; $P = .056$) and IL-10 lack of expression and COX-2 expression (OR, 2.63; $P = .066$). Moreover, hTERT and COX-2 expression were highly

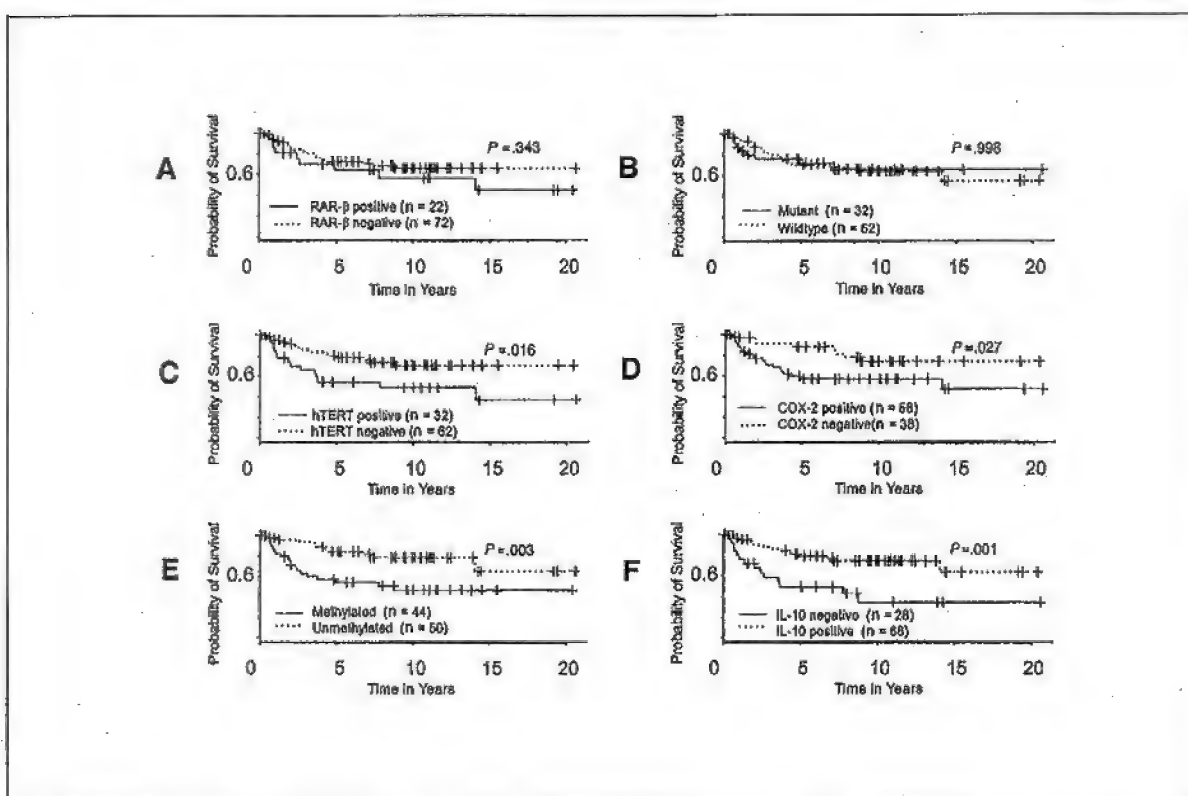


Fig 1. Disease-specific survival stratified by (A) retinoic acid receptor-beta (RAR- β) mRNA expression, (B) K-ras mutation status, (C) human telomerase reverse transcriptase catalytic subunit (hTERT) mRNA expression, (D) cyclooxygenase-2 (COX-2) mRNA expression, (E) death-associated protein kinase (DAPK) methylation, and (F) interleukin-10 (IL-10) protein expression.

Table 4. Multivariate Cox Regression Model for Disease-Specific Survival

Molecular Marker	Hazard Ratio	95% CI	P
DAPK methylation	3.11	1.42 to 6.79	.004
IL-10 lack of expression	2.62	1.24 to 5.56	.012
COX-2 expression	2.13	0.92 to 4.95	.077

Abbreviations: DAPK, death-associated protein kinase; IL-10, interleukin-10; COX-2, cyclooxygenase-2.

associated (OR, 6.14; $P = .0004$). We ensured that the effect of these variables was not masked by collinearity by modeling them separately. Specifically, we modeled COX-2 expression with DAPK methylation (AIC = 228.135) and hTERT expression with DAPK methylation (AIC = 228.654). Neither of these models provided better fit than the model chosen.

DISCUSSION

Our findings further characterize and extend our group's previous research efforts to identify novel molecular prog-

nostic factors in patients with early-stage NSCLC. We identified 94 patients with complete information for a panel of six molecular markers. Each biomarker had been previously studied as a prognostic factor based on its role in carcinogenesis. When analyzed individually, five of these biomarkers (RAR- β , COX-2, hTERT, DAPK promoter methylation, and IL-10) were demonstrated in prior studies^{7-9,11,12} by our group to be significant predictors of survival. One available marker (K-ras) was included in the current analysis based on published data demonstrating that it had prognostic significance in early-stage NSCLC,^{14,42} even though it did not have prognostic significance in univariate analysis in our patients. Our multivariable analysis indicates that two biomarkers (DA PK promoter methylation and IL-10) function as independent predictors of disease-specific survival, and a third biomarker (COX-2) is of borderline significance in this cohort. These findings should be confirmed in other NSCLC patient populations.

Our results further support the importance of epigenetic gene regulation in lung carcinogenesis. Others have demonstrated that aberrant promoter methylation of DAPK and other genes frequently occurs in NSCLC tumors,^{25,26} suggesting that methylation may be a common mechanism of inactivation of cancer-related genes. DAPK promoter methylation was the most statistically significant predictor of survival in our study. Kim et al⁴³ investigated the role of DAPK methylation in 185 NSCLC patients who underwent surgical resection, including 102 patients with stage I disease. DAPK methylation was significantly correlated with advanced stage, suggesting that DAPK may be important in the progression of NSCLC. Stage I patients with DAPK methylation had worse overall survival, although this association was not statistically significant. The authors noted that patient follow-up data was limited, and this factor may have contributed to their findings. Harden et al⁴⁴ examined promoter methylation of a panel of five genes in tumors and lymph nodes of 90 stage I NSCLC patients. Interestingly, patients with both DAPK and *adenomatous polyposis coli* gene methylation had poorer overall survival that did not reach statistical significance, although the methylation of either gene alone was not a predictor of survival. Possible explanations for these results include the relatively low frequency of DAPK methylation (17%) compared with our findings (47%). The smaller number of patients with DAPK methylation ($n = 15$) would result in the study having less power to detect significant associations with survival.

The role of IL-10 in carcinogenesis remains controversial. Our findings indicate that loss of IL-10 expression predicts poor disease-specific survival in early-stage NSCLC. Human bronchial epithelial cells constitutively produce IL-10, which may regulate the local immune response in normal lungs.³⁴ IL-10 also seems to have

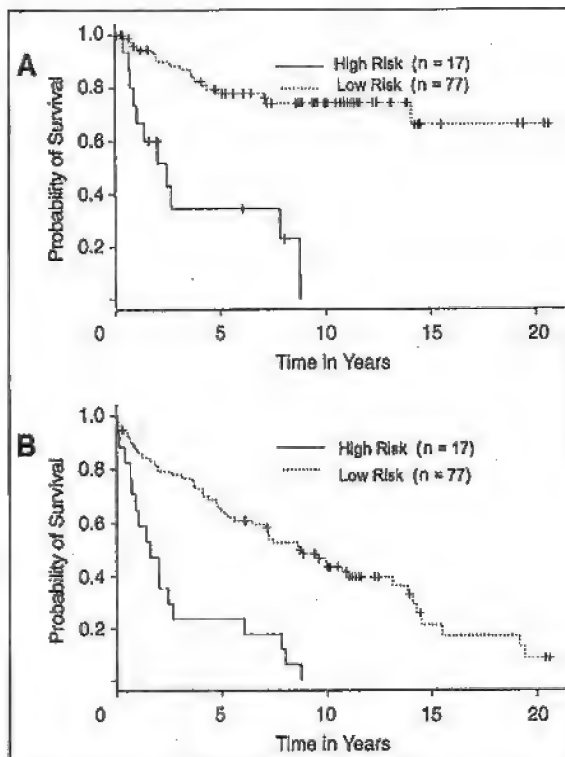


Fig 2. Disease-specific survival (A) and overall survival (B) of patients with both death-associated protein kinase methylation and interleukin-10 lack of expression (high risk) versus other patients (low risk).

significant inhibitory effects on tumor growth and metastasis in multiple animal models and tumor types, including melanoma, breast cancer, prostate cancer, and Burkitt's lymphoma.^{31,32,45-47} Evidence suggests that IL-10 exerts its antitumor and antimetastatic activity by inhibiting angiogenesis, and this activity is, in part, mediated by the downregulation of angiogenic molecules, such as vascular endothelial growth factor, IL-1 β , tumor necrosis factor- α , IL-6, and matrix metalloproteinase-9 (MMP-9), in tumor-associated macrophages.⁵¹ In addition, IL-10 may also directly affect the secretion of angiogenic molecules from the tumor. Stearns et al⁴⁶ demonstrated that IL-10 induces tissue inhibitor of metalloproteinase-1 production and inhibits MMP-2 and MMP-9 secretion by human prostate cancer cell lines orthotopically implanted into mice, resulting in decreased tumor microvessel formation and increased mice survival. In a murine mammary tumor model, the antitumor and antimetastatic effects of IL-10 gene transfection were associated with elevated nitric oxide levels in tumors.⁴⁸ Others have shown that IL-10 can directly inhibit the proliferation of endothelial cells stimulated with vascular endothelial growth factor or fibroblast growth factor-2 in vitro.⁴⁷ An intriguing molecular epidemiologic case-control study demonstrated that IL-10 promoter polymorphisms that resulted in lower IL-10 expression were associated with an increased risk of developing melanoma.⁴⁹ Furthermore, some authors have suggested that lung cancer cells can modulate IL-10 expression by stromal components. In the present study, only nine of 94 samples displayed tumor-infiltrating lymphocytes or tumor-associated macrophages, therefore hindering any relevant analysis of IL-10 production by infiltrating immune cells.

The data supporting the antitumor and antimetastatic activity of IL-10 are compelling, but most preclinical models using IL-10 to mediate such effects do so at concentrations that far exceed the levels demonstrated in lung cancer patients. Other authors have demonstrated that IL-10 is a potent immunosuppressive molecule that may promote lung cancer growth by suppressing T-cell and macrophage function and enabling tumors to escape immune detection.⁵⁰⁻⁵² Elevated baseline serum IL-10 levels were found to be independent predictors of poorer survival in 60 advanced-stage NSCLC patients receiving platinum-based chemotherapy.⁵³ Hatanaka et al⁵⁴ measured IL-10 mRNA levels by reverse transcriptase PCR in the tumors of 82 NSCLC patients who underwent surgical resection. Their assay demonstrated IL-10 expression in 83% of the surgical specimens. In contrast to our results, IL-10 expression was significantly associated with worse survival. The reasons for these discrepant findings remain unclear. These investigators included patients with stages I to IIIB disease in their study and used a different IL-10 assay (mRNA v protein) than the assay we used in our study. These factors may have contributed to these divergent results.

Our exploratory analyses demonstrate a highly significant association between hTERT expression and COX-2 expression ($P = .0004$). A precise explanation for this correlation is lacking, although various COX-2 inhibitors have been reported to inhibit both tumor growth and telomerase activity in mice.^{55,56} We also observed a significant association between *K-ras* mutations and *DAPK* methylation ($P = .032$). Reports suggesting that DNA methylation may be regulated by the *ras* signaling pathway^{57,58} are consistent with these findings. However, others have not found correlations between *ras* mutations and promoter hypermethylation in NSCLC tumors.^{43,59} Clearly, a better understanding of the significance of these associations will require future studies. Our analyses also demonstrate a borderline significant association between IL-10 lack of expression and COX-2 expression ($P = .066$).^{60,61} This finding is consistent with data suggesting that IL-10 has the capacity to potentially downregulate COX-2. Therefore, in the absence of IL-10, COX-2 and its derived products would be more abundant and could further promote tumor progression.

This study is limited by its retrospective nature and the inclusion only of patients with complete information for all six biomarkers. It is difficult to speculate on potential biases affecting our results. It is possible, for example, that small tumors with limited tissue availability were underrepresented in this cohort. These results should be validated in a separate population of NSCLC patients.

In conclusion, our analysis of six molecular markers in patients with resected stage I NSCLC yielded two independent predictors of poorer disease-specific survival: *DAPK* methylation and IL-10 lack of expression. Future studies are warranted to further define their roles in tumor proliferation and metastasis. However, these and other potential molecular prognostic factors have yet to be validated, and thus, the integration of molecular marker assessments into the routine clinical management of NSCLC has remained an elusive goal. As the number of potential molecular markers increases, it has become more difficult to assess which prognostic factors are likely to be clinically relevant. A comprehensive multivariable analysis is not feasible because the majority of studies analyze only a single or a few biomarkers at a time. In this regard, the development of high-throughput technologies to determine gene-expression profiles and proteomic patterns of tissue specimens represents a significant methodologic advance. Several recent reports have demonstrated that mRNA and protein patterns of NSCLC tumors may be predictive of survival.^{62,63} Hopefully, these technologies will eventually provide the clinician with a reliable, validated molecular staging system that will improve therapeutic strategies for NSCLC.

Authors' Disclosures of Potential Conflicts of Interest

The authors indicated no potential conflicts of interest.

REFERENCES

- Jemal A, Murray T, Samuels A, et al: Cancer statistics, 2003. *CA Cancer J Clin* 53:5-26, 2003
- Travis W, Travis LB, Devesa SS: Lung cancer incidence and survival by histologic type. *Cancer* 75:191-202, 1995 (suppl 1)
- Fry W, Phillips JL, Menck HR: Ten-year survey of lung cancer treatment and survival in hospitals in the United States. *Cancer* 86:1867-1876, 1999
- Mountain CF: Revisions in the International System for Staging Lung Cancer. *Chest* 111:1710-1717, 1997
- Tseng JE, Kemp BL, Khuri FR, et al: Loss of Fhit is frequent in stage I non-small cell lung cancer and in the lungs of chronic smokers. *Cancer Res* 59:4798-4803, 1999
- Herbst RS, Yano S, Kuniyasu H, et al: Differential expression of E-cadherin and type IV collagenase genes predicts outcome in patients with stage I non-small cell lung carcinoma. *Clin Cancer Res* 6:790-797, 2000
- Tang X, Khuri FR, Lee JJ, et al: Hypermethylation of the death-associated protein (DAP) kinase promoter and aggressiveness in stage I non-small-cell lung cancer. *J Natl Cancer Inst* 92:1511-1516, 2000
- Khuri FR, Lotan R, Kemp BL, et al: Retinoic acid receptor-beta as a prognostic indicator in stage I non-small-cell lung cancer. *J Clin Oncol* 18:2798-2804, 2000
- Khuri FR, Wu H, Lee JJ, et al: Cyclooxygenase-2 overexpression is a marker of poor prognosis in stage I non-small cell lung cancer. *Clin Cancer Res* 7:861-867, 2001
- Zhou X, Kemp BL, Khuri FR, et al: Prognostic implication of microsatellite alteration profiles in early-stage non-small cell lung cancer. *Clin Cancer Res* 6:559-565, 2000
- Wang L, Soria JC, Kemp BL, et al: hTERT expression is a prognostic factor of survival in patients with stage I non-small cell lung cancer. *Clin Cancer Res* 8:2883-2889, 2002
- Soria JC, Moon C, Kemp BL, et al: Lack of interleukin-10 expression could predict poor outcome in patients with stage I non-small cell lung cancer. *Clin Cancer Res* 9:1785-1791, 2003
- Pastorino U, Andreola S, Tagliabue E, et al: Immunocytochemical markers in stage I lung cancer: Relevance to prognosis. *J Clin Oncol* 15:2858-2865, 1997
- Kwiatkowski DJ, Harpole DH Jr, Godleski J, et al: Molecular pathologic subtyping in 244 stage I non-small-cell lung cancer patients: Clinical implications. *J Clin Oncol* 16:2468-2477, 1998
- D'Amico TA, Massey M, Herndon JE II, et al: A biologic risk model for stage I lung cancer: Immunohistochemical analysis of 408 patients with the use of ten molecular markers. *J Thorac Cardiovasc Surg* 117:736-743, 1999
- Ahrendt SA, Hu Y, Buta M, et al: p53 mutations and survival in stage I non-small-cell lung cancer: Results of a prospective study. *J Natl Cancer Inst* 95:961-970, 2003
- Berard J, Gaboury L, Landers M, et al: Hyperplasia and tumours in lung, breast and other tissues in mice carrying a RAR beta 4-like transgene. *EMBO J* 13:5570-5580, 1994
- Taketo MM: Cyclooxygenase-2 inhibitors in tumorigenesis (Part II). *J Natl Cancer Inst* 90:1609-1620, 1998
- Hida T, Yatabe Y, Achiwa H, et al: Increased expression of cyclooxygenase 2 occurs frequently in human lung cancers, specifically in adenocarcinomas. *Cancer Res* 58:3761-3764, 1998
- Wolff H, Saukkonen K, Anttila S, et al: Expression of cyclooxygenase-2 in human lung carcinoma. *Cancer Res* 58:4997-5001, 1998
- Li M, Song S, Lippman SM, et al: Induction of retinoic acid receptor-beta suppresses cyclooxygenase-2 expression in esophageal cancer cells. *Oncogene* 21:411-418, 2002
- Hahn WC: Role of telomeres and telomerase in the pathogenesis of human cancer. *J Clin Oncol* 21:2034-2043, 2003
- Hiyama K, Hiyama E, Ishioka S, et al: Telomerase activity in small-cell and non-small-cell lung cancers. *J Natl Cancer Inst* 87:895-902, 1995
- Kim NW, Platyszek MA, Prowse KR, et al: Specific association of human telomerase activity with immortal cells and cancer. *Science* 266:2011-2015, 1994
- Zochbauer-Muller S, Fong KM, Maitra A, et al: 5' CpG island methylation of the Fhit gene is correlated with loss of gene expression in lung and breast cancer. *Cancer Res* 61:3581-3585, 2001
- Esteller M, Corn PG, Baylin SB, et al: A gene hypermethylation profile of human cancer. *Cancer Res* 61:3225-3229, 2001
- Deiss LP, Feinstein E, Berissi H, et al: Identification of a novel serine/threonine kinase and a novel 15-kD protein as potential mediators of the gamma interferon-induced cell death. *Genes Dev* 9:15-30, 1995
- Inbal B, Cohen O, Polak-Charcon S, et al: DAP kinase links the control of apoptosis to metastasis. *Nature* 390:180-184, 1997
- Beissert S, Hosoi J, Grabbe S, et al: IL-10 inhibits tumor antigen presentation by epidermal antigen-presenting cells. *J Immunol* 154:1280-1286, 1995
- Rohrer JW, Coggins JH Jr: CD8 T cell clones inhibit antitumor T cell function by secreting IL-10. *J Immunol* 155:5719-5727, 1995
- Huang S, Ullrich SE, Bar-Eli M: Regulation of tumor growth and metastasis by interleukin-10: the melanoma experience. *J Interferon Cytokine Res* 18:697-703, 1999
- Kundu N, Beatty TL, Jackson MJ, et al: Antimetastatic and antitumor activities of interleukin 10 in a murine model of breast cancer. *J Natl Cancer Inst* 88:536-541, 1996
- Esteller M, Sanchez-Cespedes M, Rosell R, et al: Detection of aberrant promoter hypermethylation of tumor suppressor genes in serum DNA from non-small cell lung cancer patients. *Cancer Res* 59:67-70, 1999
- Bonfield TL, Konstan MW, Burfeind P, et al: Normal bronchial epithelial cells constitutively produce the anti-inflammatory cytokine interleukin-10, which is downregulated in cystic fibrosis. *Am J Respir Cell Mol Biol* 13:257-261, 1995
- Fujieda S, Lee K, Sunaga H, et al: Staining of interleukin-10 predicts clinical outcome in patients with nasopharyngeal carcinoma. *Cancer* 85:1439-1445, 1999
- Kolquist KA, Ellisen LW, Counter CM, et al: Expression of TERT in early premalignant lesions and a subset of cells in normal tissues. *Nat Genet* 19:182-186, 1998
- Soria JC, Moon C, Wang L, et al: Effects of N-(4-hydroxyphenyl)retinamide on hTERT expression in the bronchial epithelium of cigarette smokers. *J Natl Cancer Inst* 93:1257-1263, 2001
- Falchetti ML, Pallini R, D'Ambrosio E, et al: In situ detection of telomerase catalytic subunit mRNA in glioblastoma multiforme. *Int J Cancer* 88:895-901, 2000
- Xu XC, Ro JY, Lee JS, et al: Differential expression of nuclear retinoid receptors in normal, premalignant, and malignant head and neck tissues. *Cancer Res* 54:3580-3587, 1994
- Xu XC, Sozzi G, Lee JS, et al: Suppression of retinoic acid receptor beta in non-small-cell lung cancer in vivo: Implications for lung cancer development. *J Natl Cancer Inst* 89:624-629, 1997
- Jacobson DR, Mills NE: A highly sensitive assay for mutant ras genes and its application to the study of presentation and relapse genotypes in acute leukemia. *Oncogene* 9:553-563, 1994
- Slebos RJ, Kibbelaar RE, Dalesio O, et al: K-ras oncogene activation as a prognostic marker in adenocarcinoma of the lung. *N Engl J Med* 323:561-565, 1990
- Kim DH, Nelson HH, Wiencke JK, et al: Promoter methylation of DAP-kinase: Association with advanced stage in non-small cell lung cancer. *Oncogene* 20:1765-1770, 2001
- Harden SV, Tokumaru Y, Westra WH, et al: Gene promoter hypermethylation in tumors and lymph nodes of stage I lung cancer patients. *Clin Cancer Res* 9:1370-1375, 2003
- Gerard CM, Bruyns C, Delvaux A, et al: Loss of tumorigenicity and increased immunogenicity induced by interleukin-10 gene transfer in B16 melanoma cells. *Hum Gene Ther* 7:23-31, 1996
- Stearns ME, Garcia FU, Fudge K, et al: Role of interleukin 10 and transforming growth factor beta1 in the angiogenesis and metastasis of human prostate primary tumor lines from orthotopic implants in severe combined immunodeficiency mice. *Clin Cancer Res* 5:711-720, 1999
- Cervenak L, Morbidelli L, Donati D, et al: Abolished angiogenicity and tumorigenicity of Burkitt lymphoma by interleukin-10. *Blood* 98:2568-2573, 2000
- Kundu N, Dorsey R, Jackson MJ, et al: Interleukin-10 gene transfer inhibits murine mammary tumors and elevates nitric oxide. *Int J Cancer* 76:713-719, 1998
- Howell WM, Turner SJ, Bateman AC, et al: IL-10 promoter polymorphisms influence tumour development in cutaneous malignant melanoma. *Genes Immun* 2:25-31, 2001
- Sherma S, Stolins M, Lin Y, et al: T cell-derived IL-10 promotes lung cancer growth by suppressing both T cell and APC function. *J Immunol* 163:5020-5028, 1999
- Spagnoli GC, Juretic A, Schultz-Thater E, et al: On the relative roles of interleukin-2 and interleukin-10 in the generation of lymphokine-

activated killer cell activity. *Cell Immunol* 146: 391-405, 1993

52. Huang M, Sharma S, Mao JT, et al: Non-small cell lung cancer-derived soluble mediators and prostaglandin E2 enhance peripheral blood lymphocyte IL-10 transcription and protein production. *J Immunol* 167:5512-5520, 1996

53. De Vita F, Orditura M, Galizia G, et al: Serum interleukin-10 levels as a prognostic factor in advanced non-small cell lung cancer patients. *Chest* 117:365-373, 2000

54. Hatanaka H, Abe Y, Kamiya T, et al: Clinical implications of interleukin (IL)-10 induced by non-small-cell lung cancer. *Ann Oncol* 11:815-819, 2000

55. Nishimura G, Yanoma S, Mizuno H, et al: A selective cyclooxygenase-2 inhibitor suppresses tumor growth in nude mouse xenografted with

human head and neck squamous carcinoma cells. *Jpn J Cancer Res* 90:1152-1162, 1999

56. Lonnroth C, Andersson M, Lundholm K: Indomethacin and telomerase activity in tumor growth retardation. *Int J Oncol* 18:929-937, 2001

57. Rouleau J, MacLeod AR, Szyf M: Regulation of the DNA methyltransferase by the Ras-AP-1 signaling pathway. *J Biol Chem* 270: 1595-1601, 1995

58. Bigey P, Ramchandani S, Theberge J, et al: Transcriptional regulation of the human DNA methyltransferase (dnmt1) gene. *Gene* 242:407-418, 2000

59. Pulling LC, Divine KK, Klinge DM, et al: Promoter hypermethylation of the O6-methylguanine-DNA methyltransferase gene: More common in lung adenocarcinomas from never-smokers than smokers and associated

with tumor progression. *Cancer Res* 63:4842-4848, 2003

60. Moore KW, de Waal Malefyt R, Coffman RL, et al: Interleukin-10 and the interleukin-10 receptor. *Annu Rev Immunol* 19:683-765, 2001

61. Molina-Holgado E, Arevalo-Martin A, Ortiz S, et al: Theiler's virus infection induces the expression of cyclooxygenase-2 in murine astrocytes: Inhibition by the anti-inflammatory cytokines interleukin-4 and interleukin-10. *Neurosci Lett* 324:237-241, 2002

62. Beer DG, Kardia SL, Huang CC, et al: Gene-expression profiles predict survival of patients with lung adenocarcinoma. *Nat Med* 8:816-824, 2002

63. Yanagisawa K, Shyr Y, Xu BJ, et al: Proteomic patterns of tumour subsets in non-small-cell lung cancer. *Lancet* 362:433-439, 2003

Attention Authors: You Asked For It - You Got It!

Online Manuscript System Launched November 1st

On November 1st, JCO formally introduced its online Manuscript Processing System that will improve all aspects of the submission and peer-review process. Authors should notice a quicker turnaround time from submission to decision through this new system.

Based on the well known Bench>Press system by HighWire Press, the JCO Manuscript Processing System promises to further JCO's reputation of providing excellent author service, which includes an already fast turnaround time of 7 weeks from submission to decision, no submission fees, no page charges, and allowing authors to freely use their work that has appeared in the journal.

JCO's Manuscript Processing System will benefit authors by

- eliminating the time and expense of copying and sending papers through the mail
- allowing authors to complete required submission forms quickly and easily online
- receiving nearly immediate acknowledgement of receipt of manuscripts
- tracking the status of manuscripts at any time online and
- accessing all reviews and decisions online.

Authors are encouraged to register at <http://submit.jco.org>.

For more details on JCO's new online Manuscript Processing System, go online to <http://www.jco.org/nlsc/announcements.shtml>. Also, watch upcoming issues of JCO for updates like this one.

Sulindac enhances adenoviral vector expressing *mda-7/IL-24*-mediated apoptosis in human lung cancer

Yasuhisa Oida,¹ Began Gopalan,¹ Ryo Miyahara,¹ Satoshi Inoue,¹ Cynthia D. Branch,¹ Abner M. Mhashilkar,⁴ E. Lin,² B. Nebiyu Bekele,² Jack A. Roth,¹ Sunil Chada,^{3,4} and Rajagopal Ramesh¹

Departments of ¹Thoracic and Cardiovascular Surgery, ²Biostatistics, and ³Experimental Therapeutics, University of Texas M.D. Anderson Cancer Center, and ⁴Introgen Therapeutics, Inc., Houston, Texas

Abstract

Several studies have shown antitumor activities of the melanoma differentiation-associated gene 7 (*mda-7*) and the nonsteroidal anti-inflammatory drug sulindac when used as a monotherapies against a wide variety of human cancers. However, the combined effects of *mda-7* and sulindac have not previously been tested. Therefore, we tested the antitumor activity of an adenoviral vector expressing *mda-7* (Ad-*mda-7*) in combination with sulindac against non-small cell lung cancer cells *in vitro* and *in vivo*. When treated with Ad-*mda-7* in combination with sulindac, human lung cancer cells (A549 and H1299) underwent growth suppression resulting in apoptosis. The growth inhibition induced by Ad-*mda-7* in combination with sulindac was significantly greater than that observed with Ad-*mda-7* or sulindac alone. Furthermore, the degree of growth inhibition induced using this combination was dose-dependent for sulindac. Treatment with Ad-*mda-7* in combination with sulindac had no growth inhibitory effects on human normal lung (CCD-16) fibroblasts. We then investigated the mechanism by which sulindac enhances Ad-*mda-7*-mediated apoptosis. Sulindac increased expression of ectopic MDA-7 protein in tumor cells, thereby increasing the expression of downstream

effectors RNA-dependent protein kinase, p38MAPK, caspase-9, and caspase-3 and enhancing apoptosis of non-small cell lung cancer cells. Pulse-chase experiments showed that the increased expression of MDA-7 protein in sulindac-treated cells was due to increased half-life of the MDA-7 protein. Finally, treatment of human lung tumor xenografts in nude mice with Ad-*mda-7* plus sulindac significantly suppressed growth ($P = 0.001$) compared with Ad-*mda-7* or sulindac alone. Our results show for the first time that combined treatment with Ad-*mda-7* plus sulindac enhances growth inhibition and apoptosis of human lung cancer cells. The increased antitumor activity observed with the combination treatment is a result of increased half-life of MDA-7 protein. Regulation of protein turnover is a heretofore-unrecognized mechanism of this nonsteroidal anti-inflammatory drug. [Mol Cancer Ther 2005;4(2):291-304]

Introduction

The novel gene *mda-7*, also known as *IL-24*, belongs to the interleukin (IL)-10 cytokine family (1, 2). We and others have previously shown that *mda-7/IL-24*, when expressed ectopically, exhibits potent tumor suppressive activity against a variety of human cancer cells with minimal or no toxic effects to normal cells (3-12). Additionally, an adenoviral vector expressing *mda-7* (Ad-*mda-7*) administered intratumorally to human lung tumor xenografts has shown antitumor and antiangiogenic activities (13). The mechanism by which *mda-7* exerts its cytotoxic effects varies and is cell-type dependent. A number of molecular effectors have been shown to play a role in *mda-7*-mediated apoptosis including activation of the caspase cascade (5, 6), activation of RNA-dependent protein kinase (PKR; ref. 14), activation of c-Jun-NH₂-kinase (JNK; ref. 15), inhibition of phosphoinositide-3 kinase (16), activation of the stress response known as the unfolded protein response (17), activation of p38MAPK (18), and activation of Fas-FasL.⁵ However, although the upstream initiator effectors differ among the tumor cell types tested, the downstream pathways seem to converge at the level of mitochondrial disruption and activation of the caspase cascade and culminating in apoptosis. In addition to its antitumor activity, we recently showed antimetastatic activity of MDA-7 against human lung tumor cells both *in vitro* and *in vivo* (19). The results of these studies strongly indicate that *mda-7/IL-24* is a potent tumor suppressor gene. Additional evidence in support of this hypothesis is the

Received 10/26/04; revised 12/1/04; accepted 12/30/04.

Grant support: NIH/National Cancer Institute grants R01-CA102716 and PO1 CA06294 (R. Ramesh), and CA89778, CA88421, CA097598 (S. Chada); Cancer Center support grant CA16672; Texas Higher Education Coordinating Board ATP/ARP grant 003657-0078-2001; institutional research grant from University of Texas M.D. Anderson Cancer Center; and sponsored research agreement with Introgen Therapeutics, Inc.

The costs of publication of this article were defrayed in part by the payment of page charges. This article must therefore be hereby marked advertisement in accordance with 18 U.S.C. Section 1734 solely to indicate this fact.

Requests for reprints: Rajagopal Ramesh, Department of Thoracic and Cardiovascular Surgery, University of Texas M.D. Anderson Cancer Center, Unit 445, 1515 Holcombe Boulevard, Houston, TX 77030. Phone: 713-563-9144; Fax: 713-794-4901. E-mail: rramesh@mdanderson.org
Copyright © 2005 American Association for Cancer Research.

⁵B. Gopalan, S. Sharma, A. Litvak, S. Chada, and R. Ramesh, unpublished data.

finding of Ellerhorst et al. (20) who showed an inverse correlation between MDA-7 expression and melanoma progression. In recent studies, we showed that the MDA-7 protein is secreted and that the secreted protein, sMDA-7, has potent antiangiogenic activity (21). Caudell et al. (22) further showed that sMDA-7 functions as a Th1 cytokine. Collectively, these studies show that the *mda-7* gene encodes multiple functions and holds considerable promise for cancer therapy. On the basis of its unique properties, a phase I trial of an adenoviral vector expressing *mda-7* (Ad-mda7/INGN-241) for treatment of patients with solid tumors has been completed. In this study, Ad-mda7/INGN-241 was administered intratumorally to 22 patients. Preliminary results indicated that Ad-mda7 was well tolerated with no unusual toxicities and induced high levels of apoptosis in tumors (23, 24). Although Ad-mda7 is being tested as a monotherapy, combination of Ad-mda7 with conventional therapies, such as radiotherapy and chemotherapy, and other novel therapies, such as steroids, antisense, oligonucleotides, and nonsteroidal anti-inflammatory drugs (NSAID), will likely prove even more effective. Treatment of lung cancer cells and gliomas with Ad-mda7 in combination with radiotherapy enhanced growth suppression both *in vitro* and *in vivo* (15, 25, 26). In addition, Ad-mda7 combined with antisense oligonucleotides against *ras* inhibited the growth of pancreatic cancer cells (27). Ad-mda7 combination with Herceptin exhibited enhanced activity against Her-2/neu-positive breast cancer cell *in vitro* and *in vivo* (28). Sulindac, a NSAID family member, is well known for its anti-inflammatory activity, which derives from its ability to inhibit the cyclooxygenase (COX) enzymes (29). Recent studies have revealed a link between COX-2 expression and carcinogenesis, suggesting that inhibiting COX-2 can prevent cancer growth or progression (30). In fact, NSAID treatment of patients with adenomatous polyposis coli resulted in regression of colonic adenoma thereby reducing the risk of colon cancer (31–33). Based on the findings of the above studies, the beneficial effects of NSAIDs have also been tested in the prevention of lung, esophageal, prostate, pancreatic, and gastric cancers, in which COX-2 is constitutively expressed (30, 33–37). The results of these studies have clearly shown that the antitumor activity of sulindac or other NSAID occurs by inhibiting COX-2. However, sulindac sulfone, a metabolite of sulindac lacking the inhibitory effects on COX-2, reduced the incidence of tumors in animal models of breast and colon cancer (35, 38). Subsequent studies have shown that sulindac and its metabolites induce apoptosis of various cultured tumor cell lines including a lung cancer cell line through COX-independent pathways (34, 39). The mechanism by which sulindac sulfone exert its antiproliferative and antineoplastic activity is by inhibition of cyclic guanosine 3',5'-monophosphate phosphodiesterase, activation of protein kinase G, and phosphorylation of selective substrates, such as β -catenin and JNK (40). From these studies, it is now evident that sulindac and its metabolites exert potent antitumor activity against a broad spectrum of human

cancer cells by inhibiting various signaling pathways. Recent *in vitro* and *in vivo* studies have shown that anticancer drugs, such as cisplatin, paclitaxel, or docetaxel, in combination with sulindac metabolites, had synergistic inhibitory effects in lung cancer cells (31, 42). Similarly, combined treatment of sulindac plus epidermal growth factor receptor inhibitor or sulindac plus lactacystin enhanced antitumor activity against colorectal cancer cells (43). The mechanism by which sulindac and its metabolites increased antitumor activity of lactacystin was by affecting the proteasome activity. Previous studies using chemotherapy treatment strategies have shown that combination with sulindac and its metabolites enhances the drug's potency (41–44). Studies have also shown that combining gene therapy with various drugs enhanced transduction efficiency resulting in enhanced tumor cell killing (45). However, the combination of gene therapy with sulindac has not been previously reported. We therefore examined the effect of sulindac in combination with Ad-mda7 against human lung cancer cells. Our results show, for the first time, that treatment of human lung cancer cells with sulindac in combination with Ad-mda7 leads to enhanced additive to synergistic growth inhibition and cell killing. Furthermore, we show that enhanced killing is due to increased half-life of MDA-7 protein and not due to increased transduction efficiency. Additionally, the enhanced killing is selective for tumor cells with minimal effect on normal cells. The findings of the present study provide a basis for combining Ad-mda7 with sulindac for lung cancer treatment.

Materials and Methods

Cell Lines and Cell Culture

Human non-small cell lung cancer cell lines A549 (adenocarcinoma, wild type for p53) and H1299 (large cell carcinoma, null type for p53) were obtained from Drs. A. Gazdar and J.D. Minna (University of Texas Southwestern Medical Center, Dallas, TX). The normal lung fibroblast cell line CCD-16 was obtained from American Type Culture Collection (Rockville, MD). A549 and H1299 cells were maintained in appropriate medium as previously described (5). CCD-16 cells were cultured in α media supplemented with 10% fetal bovine serum (Life Technologies, Grand Island, NY) and maintained at 37°C in a humidified 5% CO₂ plus 95% air atmosphere.

Agents

Sulindac, sulindac sulfone, MG132 (a proteasome inhibitor), and cycloheximide (a protein synthesis inhibitor) were obtained from Sigma Chemical Co. (St. Louis, MO). Sulindac was dissolved in 1 mol/L Tris-HCl (pH 8.0), to make 100 mmol/L stock solution. MG132 was dissolved in DMSO to make 10 mmol/L stock solution. These stock solutions were stored frozen at –20°C.

Recombinant Adenoviral Vector

Ad-mda7 and Ad-luc vectors were constructed and purified as previously reported (5, 6). The transduction efficiencies for the cell lines were determined with an

adenoviral vector carrying green fluorescent protein (Ad-GFP). Transduction efficiency was >80% when infected with 3,000 viral particles per cell (vp/cell; data not shown). On the basis of these results, cells were treated with 3,000 vp/cell in all subsequent experiments. To determine the effect of sulindac on adenovirus transduction, tumor and normal cells were infected with Ad-GFP at 100 vp/cell and analyzed for GFP expression at 24 hours by fluorescence-activated cell sorting (FACS; Table 1).

Cell Proliferation Assay

All three cell lines (A549, H1299, and CCD-16) were seeded in 60-mm-diameter tissue culture dishes at a density of 1×10^5 cells/dish in triplicate. The next day, cells were treated with PBS (control), Ad-luc (3,000 vp/cell; control), Ad-mda7 (3,000 vp/cell; control), sulindac, or a combination of PBS plus sulindac, Ad-luc plus sulindac, or Ad-mda7 plus sulindac. The concentrations of sulindac tested were 0.125, 0.25, and 0.5 mmol/L. At 72 hours after the start of treatment, the cells were harvested by trypsinization, washed, and subjected to trypan blue exclusion assay as previously described (5). Cell growth was determined by calculating the mean of the cell counts for each treatment group and expressed as a percentage of the total number of cells treated with PBS, Ad-luc, or Ad-mda7 treatment alone (set to 100%).

Cell Cycle Distribution and Apoptosis

Cells (5×10^5) were seeded in a 10-cm-diameter tissue culture dish and treated with PBS, Ad-luc (3,000 vp/cell), Ad-mda7 (3,000 vp/cell), sulindac, or a combination of PBS plus sulindac, Ad-luc plus sulindac, or Ad-mda7 plus sulindac. Each treatment group was tested in triplicate. The concentrations of sulindac used were the same as those for the cell proliferation assay. At 72 hours after the start of the treatment, cells were harvested, washed, and analyzed for cell cycle phases and apoptotic fraction as previously described (5). The cell cycle phases and DNA contents were analyzed using FACScan (EPICS XL-MCL, Beckman Coulter, Fullerton, CA). In a separate set of experiment, cells were treated with Ad-p53 (50 vp/cell) or a combination of Ad-p53 and sulindac. All other experimental conditions were the same as described above.

Table 1. Transduction efficiency in lung cancer (A549 and H1299) and normal (CCD-16) cells treated with Ad-GFP and sulindac

Cell line	Sulindac (mmol/L)			
	0	0.125	0.25	0.5
A549	48.8 \pm 6.5	52.4 \pm 0.6	51.5 \pm 1.3	65.0 \pm 1.5*
H1299	79.5 \pm 2.2	80.0 \pm 0.5	78.6 \pm 1.2	82.7 \pm 2.8
CCD-16	15.7 \pm 0.2	12.1 \pm 0.4	11.1 \pm 1.0	13.7 \pm 0.4

NOTE: Cells were treated with Ad-GFP (100 vp/cell) for 3 hours, followed by sulindac at the indicated concentrations for 24 hours. Percentages of transduction efficiency were determined by flow cytometry.

* $P < 0.05$ compared with Ad-GFP treatment alone. No other differences between the groups shown was significant.

Immunofluorescence Assay

Cells (1×10^4) were seeded in two-well chamber slides (Fisher Scientific, Pittsburgh, PA) and treated with PBS, Ad-mda7 (3,000 vp/cell), PBS plus sulindac (0.5 mmol/L), or Ad-mda7 plus sulindac (0.5 mmol/L). At 48 hours after the start of treatment, the cells were washed with PBS and fixed in PBS-buffered 4% paraformaldehyde for 30 minutes at room temperature. The cells were then permeabilized with 0.1% Triton X-100 and 0.1% sodium citrate for 10 minutes at room temperature, followed by incubation with normal goat serum. At 30 minutes after the start of the incubation, cells were washed with PBS and incubated with rabbit polyclonal anti-human MDA7 antibody (Introgen Therapeutics Inc., Houston, TX) for 1 hour at 37°C. The cells were then washed thrice with PBS and incubated for 1 hour with goat anti-rabbit FITC-tagged secondary antibody (Vector Laboratories, Burlingame, CA), washed three times in PBS, mounted with a coverslip, and observed for MDA-7 protein expression using a Nikon fluorescence microscope (Nikon, Melville, NY). Photomicrographs were obtained at high-power magnification.

Proteasome Activity Assay

Proteasome activity assays were done as previously described (43). Briefly, H1299 cells were seeded in six-well plates (2×10^5 cells/well) and treated with Ad-mda7, Ad-mda7 plus sulindac, or Ad-mda7 plus MG132 (5 μ M). The sulindac concentrations tested were the same as those in the other assays. At 24 hours after the start of treatment, the cells were lysed in proteasome buffer [10 mmol/L Tris-HCl (pH 7.5), 1 mmol/L EDTA, 20% glycerol, 5 mmol/L ATP, and 4 mmol/L DTT], sonicated, and then centrifuged at $1,300 \times g$ at 4°C for 10 minutes. The upper supernatant phase was collected and the protein concentration of cell lysates was determined as previously described (5). To assay the chymotrypsin-like activity of the proteasome, the fluorogenic substrate succinyl-leucyl-leucyl-valine-tyrosine-7-amino-4-methylcoumarin (Chemicon International, Inc., Temecula, CA) was used. Twenty-microgram total protein from each treatment group described above was diluted to 100 μ L in reaction buffer [25 mmol/L HEPES (pH 7.5), 0.5 mmol/L EDTA, 0.05% NP40, and 0.001% SDS]. Fluorogenic substrate was added to each sample and incubated at 37°C for 1 hour. The intensity of fluorescence in each sample solution was measured using a fluorescence plate reader (Dynatech Laboratories, Chantilly, VA) at 360 nm excitatory and 460 nm emission wavelengths. All readings were standardized using the fluorescence intensity of an equal volume of free 7-amino-4-methylcoumarin solution (50 μ M). The values were expressed as percentages for control greater than the internal positive control percentages provided by the supplier.

Real-time Quantitative Reverse Transcription-PCR

H1299 cells seeded in six-well plates (5×10^5 /well) were treated with Ad-mda7 (3,000 vp/cell) or Ad-mda7 plus sulindac (0.125, 0.25, or 0.5 mmol/L). Untreated cells served as controls in these experiments. At 48 hours after the start of treatment, the cells were washed in PBS, trypsinized, and resuspended in 1.0 mL PBS. The cell

suspension was transferred into 1.5 mL Eppendorf tubes and centrifuged for 5 minutes at 10,000 rpm at 4°C. The supernatant was discarded and total RNA from the cell pellet was extracted using an RNA isolation kit as described by the manufacturer (Ambion Corp., Austin, TX). The isolated RNA was then treated with DNase I to remove residual DNA and subsequently quantitated using a spectrophotometer at 260 and 280 nm wavelengths. Total RNA (0.1 µg) from each sample was reverse transcribed using a SuperScript reverse transcriptase kit (Invitrogen, Carlsbad, CA). Quantification of *mda-7* mRNA was done using real-time quantitative reverse transcription-PCR. Briefly, quantitative PCR was done in 20 µL volumes consisting of 1 µL total RNA, 10 µL PCR Supermix (PE Applied Biosystems, Foster City, CA), 0.2 µM *mda-7*-specific primers, and 0.1 µM fluorescent probe. The resulting relative increase in reporter and quencher fluorescent dye emission was monitored in real time during PCR amplification using a 7,700 sequence detector (PE Applied Biosystems). The two-step PCR cycling was carried out as follows: 2 minutes at 50°C, 10 minutes at 95°C, 40 cycles of 15 minutes at 95°C, and 1 minute at 60°C. The human *GAPDH* housekeeping gene was used as internal control in the amplification reactions and the primers provided by the supplier (PE Applied Biosystems).

The oligonucleotide sequences used in the assays described above are as follows: *mda-7* 5'-primer, CCC-GTAATAAGCTTGGTACCG; and *mda-7* 3'-primer, TAAATTGGCGAAAGCAGCTC; probe, FAM-TGGAATTCGGCTTACAAGACATGACTGTG-TAMRA.

All reactions were done in triplicate. After the cycling reaction was complete, a standard curve, the threshold cycling (C_t) value of each sample, and its corresponding starting quantity based on the standard curve were determined using the 7,700 sequence detector system software (PE Applied Biosystems). The differences in *mda-7* mRNA expression among various treatment groups were expressed as the change in values over glyceraldehyde-3-phosphate dehydrogenase.

Half-Life Assay

H1299 cells were seeded at a density of 2×10^5 cells in a 60-mm-diameter tissue culture dish. The next day, the cells were infected with Ad-*mda7* (3,000 vp/cell). At 48 hours after infection, sulindac (1 mmol/L) was either added or not added and the incubation continued. Two hours later, the protein synthesis inhibitor cycloheximide (10 µg/mL) was added to the cells and the incubation continued. Cells were harvested at 0, 3, 6, 9, 11, and 13 hours after cycloheximide treatment; cell lysates were then prepared and analyzed for MDA-7 protein expression by Western blot analysis as previously described (5, 6).

Western Blot Analysis

Cells treated with PBS, Ad-*mda7*, Ad-p53, Ad-luc, sulindac, sulindac sulfone, or a combination of Ad-luc, Ad-p53, or Ad-*mda7* with sulindac or sulindac sulfone was subjected to Western blot analyses as previously described (5, 6). The following primary antibodies were used for detection: caspase-3 and poly (ADP-ribose) polymerase

(PARP, BD PharMingen, San Diego, CA); caspase-9, pJNK, and pp38 MAPK (Cell Signaling Technology, Inc., Beverly, CA); PKR, Bax, Bak, Bcl-2, Bcl-x_L, COX-2, p53, and ubiquitin (Santa Cruz Biotechnology, Santa Cruz, CA); β -actin (Sigma); and MDA-7 (Introgen Therapeutics). The proteins were detected using appropriate horseradish peroxidase-conjugated secondary antibodies, and visualized on enhanced chemiluminescence film (Hyperfilm, Amersham, Arlington Heights, IL) by application of Amersham's enhanced chemiluminescence Western blotting detection system. The results were verified by repeating the experiments at least twice. The protein band intensity was semiquantitatively determined as previously described (5).

In vivo Analysis

To determine whether sulindac enhances Ad-*mda7*-mediated tumor growth inhibition of xenograft tumors *in vivo*, H1299 lung tumor cells (5×10^6) were injected s.c. into the lower right flank of athymic BALB/c female nude mice ($n = 48$). When the tumor reached 50 to 100 mm³, the animals were divided into groups and treated as follows: PBS ($n = 8$), sulindac ($n = 8$), Ad-luc ($n = 8$), Ad-*mda7* ($n = 8$), Ad-luc plus sulindac ($n = 8$), or Ad-*mda7* plus sulindac ($n = 8$). The mice were treated with Ad-luc or Ad-*mda7* intratumorally (3×10^9 vp/dose) thrice a week. In mice receiving sulindac, 40 mg/kg was given i.p. daily. Animals were weighed weekly to determine the body weight. Tumor growth was monitored and measured thrice a week as described previously (13, 21). At 22 to 25 days after initiation of the treatment, all animals were killed via CO₂ inhalation, and the tumors were removed for histopathologic examination and Western blot analysis. Experiments were done twice for reproducibility and twice for statistical significance.

Statistical Analysis

Student's *t* test and ANOVA were used to calculate the statistical significance of the experimental results. A value of $P < 0.05$ was considered statistically significant.

Results

Sulindac Enhances Ad-*mda7*-Mediated Growth Inhibition in Lung Cancer Cells

Because previous studies have shown that sulindac exerts cytotoxic effects on cancer cells (33), we conducted preliminary experiments to determine the minimum cytotoxic dose of sulindac against non-small cell lung cancer (A549 and H1299) cells and normal (CCD-16) cells. Treatment of these cells with sulindac at various concentrations (0.062, 0.12, 0.25, 0.5, 1, and 2 mmol/L) showed growth inhibition, with an IC₅₀ of 0.58 ± 0.01 , 0.61 ± 0.07 , and 0.94 ± 0.04 mmol/L in A549, H1299, and CCD-16 cells, respectively (data not shown). At higher doses (1 and 2 mmol/L), cell proliferation was inhibited in both tumor and normal cells resulting in apoptosis (data not shown). However, the inhibitory effect on tumor cell proliferation was higher (>90%) than in normal cells (60%). On the basis of these results, we tested sulindac at concentrations of

<0.5 mmol/L in subsequent experiments. To investigate whether sulindac in combination with Ad-mda7 can inhibit cell proliferation and induce apoptosis, A549, H1299, and CCD-16 were treated with PBS, Ad-luc, and Ad-mda7, alone and in combination with sulindac (0.125, 0.25, or 0.5 mmol/L). Analysis of cells 72 hours after treatment showed that the combination of sulindac and Ad-mda7 significantly inhibited tumor cell proliferation compared with cells that were treated with Ad-mda7 or sulindac alone ($P = 0.001$; Fig. 1A). The growth inhibitory effects produced by this combination therapy were also significant compared with the other treatment groups and were sulindac dose dependent. In contrast, no significant growth inhibitory effects were observed in normal fibroblast cells treated with Ad-mda7 plus sulindac at any concentration tested compared with the other treatment groups. These results indicate that sulindac enhances Ad-mda7-mediated inhibitory activity in tumor cells but not in normal cells.

To further evaluate whether treatment with Ad-mda7 plus sulindac induces apoptosis, tumor and normal cells were analyzed 72 hours after treatment for apoptotic changes by FACS analysis. The number of cells in sub-G₀-G₁ phase, an indicator of apoptotic changes, was significantly higher in tumor (H1299 and A549) cells treated with Ad-mda7 alone or in combination with sulindac than in normal cells subjected to these treatments ($P = 0.001$; Fig. 1B). However, the number of apoptotic cells among the tumor cells treated with Ad-mda7 plus sulindac was significantly greater than that among tumor cells treated with Ad-mda7 alone ($P < 0.01$) and was sulindac dose-dependent. The numbers of apoptotic cells among cells treated with Ad-luc alone or in combination with sulindac were not significantly higher than the number of apoptotic cells among PBS-treated cells. However, among A549 tumor cells, the number of apoptotic cells was significantly increased ($P = 0.01$) at the highest concentration of sulindac (0.5 mmol/L) when combined with Ad-luc treatment compared with PBS-treated cells. Treatment of CCD-16 cells with Ad-mda7 or Ad-mda7 and sulindac even at the highest sulindac concentration (0.5 mmol/L) yielded no significant difference in the number of apoptotic cells compared with control cells (Fig. 1B). Similar enhanced growth inhibitory effects were also observed when lung cancer cells were treated with Ad-mda7 in combination with sulindac sulfone (data not shown). These results show that lung tumor but not normal cells undergo apoptosis when treated with Ad-mda7 and sulindac or sulindac sulfone. Furthermore, the growth inhibitory effects mediated by Ad-mda7 and sulindac are independent of the p53 status given that they occurred in p53-null H1299 and p53 wild-type A549 tumor cell lines. However, the contribution of other genetic factors in the sensitization of these two cell lines to Ad-mda7 and sulindac is not known now and is beyond the scope of the present study.

Sulindac Does Not Increase Adenoviral Transduction

The ability of therapeutic agents to enhance adenovirus transduction efficiency has previously been reported (45). Based on this report, we determined whether sulindac

enhances adenoviral transduction. For this purpose, tumor and normal cells were infected with Ad-GFP at 100 vp/cell and treated with sulindac at various concentrations (Table 1). Cells were transduced with Ad-GFP at low particle numbers because >80% of cells are transduced at a higher virus-particle number, making it difficult to determine the effects of sulindac on transduction. At 24 hours after treatment, the cells were analyzed by flow cytometry. No significant difference in the transduction

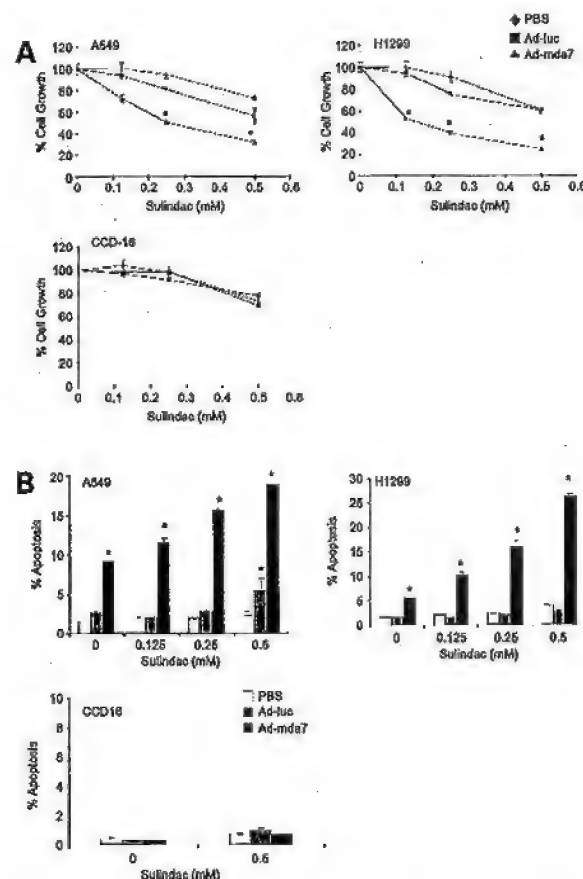


Figure 1. Sulindac enhances Ad-mda7-mediated growth inhibition and apoptosis. **A**, tumor (A549 and H1299) and normal (CCD-16) cells were treated with PBS, Ad-luc, or Ad-mda7 for 3 h. After treatment, cells were incubated with sulindac at the indicated concentrations. After 72 h, cell viability was determined using the trypan blue exclusion assay method. Percentages of cell growth were calculated as the average of cell counts for each group and expressed relative to the each sample treated with PBS, Ad-luc, or Ad-mda7 alone (set to 100%). Tumor but not normal cells treated with Ad-mda7 plus sulindac were significantly inhibited compared with PBS and Ad-luc treatments ($P = 0.001$). The inhibitory effects mediated by sulindac were dose dependent. Bars, SE. **B**, analysis of apoptotic cells by FACS. Tumor cells (A549 and H1299) and normal (CCD-16) cells were treated with PBS, Ad-luc, or Ad-mda7 in the presence of various doses of sulindac. Cells were harvested at 72 h after treatment, stained with propidium iodide, and subjected to FACS analysis. The percentages of apoptotic cells were determined by quantifying cells in the sub-G₁ phase. Columns, mean of duplicate samples; bars, SE. Similar results were observed in at least two independent experiments.

efficiency was observed between cells treated with Ad-GFP plus sulindac and cells treated with Ad-GFP alone (Table 1). However, transduction was increased in A549 cells that had been treated with 0.5 mmol/L sulindac compared with other groups treated with sulindac at lower concentrations ($P = 0.001$).

Sulindac Increases Ectopic MDA-7 Expression

To identify the mechanism by which sulindac enhances Ad-mda7-mediated growth inhibition and apoptosis in lung cancer cells, we first examined ectopic MDA-7 protein expression by Western blotting. All three cell lines (H1299, A549, and CCD-16) were treated with Ad-mda7 and sulindac for 48 hours and analyzed for MDA-7 expression. In Ad-mda7-treated A549 and H1299 cells, sulindac markedly increased the levels of ectopic MDA-7 in a dose-dependent manner (Fig. 2A); endogenous MDA-7 expression was not detected in cells treated with either PBS or sulindac alone. MDA-7 protein expression was increased 2 to 4.5 times in the tumor cells treated with Ad-mda7 plus sulindac compared with cells treated with Ad-mda7 alone. In contrast, in normal CCD-16 cells treated with Ad-mda7, sulindac only slightly increased ectopic MDA-7 protein expression. The level of MDA-7 protein increase in CCD-16 cells after Ad-mda7 plus sulindac treatment was <2-fold compared with cells treated with Ad-mda7 alone.

To evaluate subcellular localization of MDA-7 protein, immunofluorescence studies were done. Consistent with our Western blot data, MDA-7 expression was significantly elevated in cells treated with Ad-mda7 and sulindac compared with cells treated with Ad-mda7 alone (Fig. 2B). Furthermore, the subcellular localization of MDA-7 was not altered by sulindac treatment (Fig. 2B). MDA-7 expression was not detectable in cells treated with PBS or sulindac alone. Expression was also not detectable when cells were stained with an isotypic FITC-labeled antibody, indicating specificity. These results show that sulindac increases ectopic MDA-7 expression in a dose-dependent manner and suggest that this increase contributes to increased apoptotic activity.

To test whether the ability to increase ectopic protein expression was unique to sulindac, experiments were also carried out using sulindac sulfone. Treatment of H1299 cells with Ad-mda7 and sulindac sulfone showed increased ectopic MDA-7 expression compared with cells treated with Ad-mda7 alone (Fig. 2C). The level of induction, however, was observed to be less than that seen with sulindac. MDA-7 expression was not detected in cells that were treated with PBS or sulindac sulfone. These results show the ability of sulindac and its metabolites to increase ectopic protein expression. We next tested whether sulindac specifically increased only MDA-7 protein expression. For this purpose, H1299 tumor cells were treated with Ad-p53 (50 vp/cell) or Ad-p53 and sulindac and analyzed for p53 protein expression and apoptotic cells. Note that cells were treated with 50 vp/cell as these cells are very sensitive to Ad-p53 at higher concentrations. Sulindac increased

the levels of ectopic p53 protein expression in tumor cells treated with Ad-p53 that resulted in increased cell killing (Fig. 2D). Sulindac also increased ectopic GFP protein expression. However, increased GFP protein expression did not result in cell killing (data not shown). These results show that sulindac enhanced ectopic expression of a wide-variety of transgenes (MDA-7, p53, and GFP) and is not specific to Ad-mda7. However, the enhanced killing effect is only observed when sulindac is combined with Ad-mda7 or Ad-p53.

Sulindac Enhances Ad-mda7-Mediated Apoptotic Signaling

We previously reported that induction of Ad-mda7-mediated apoptosis in lung cancer cells was associated with activation of the caspase cascade, including cleavage of caspase-9, caspase-3, and PARP (5, 6). To determine whether treatment with Ad-mda7 and sulindac affects the caspase cascade, we analyzed tumor and normal cells for these molecular markers. Tumor (A549 and H1299) cells treated with Ad-mda7 alone or in combination with sulindac showed cleavage of caspase-9, caspase-3, and PARP, which are indicators of activation of the caspase cascade (Fig. 3A). The expression of cleaved caspase-9, caspase-3, and PARP corresponded to both the concentration of sulindac and the level of MDA-7 expression. Activation of caspase-9, caspase-3, and PARP was also observed in A549 (but not H1299) cells that had been treated with Ad-luc plus the highest concentration of sulindac (0.5 mmol/L) and was consistent with the increased apoptotic fraction revealed in these cells by FACS analysis (Fig. 1B). However, the level of activation was significantly lower than that in A549 cells treated with Ad-mda7 plus sulindac. The caspase cascade was not activated in either A549 or H1299 cells that were untreated or treated with sulindac alone. In CCD-16 cells, the caspase cascade was not activated in cells that were treated with Ad-mda7 alone or in combination with sulindac compared with cells that were untreated or treated with sulindac alone, Ad-luc alone, or a combination of Ad-luc plus sulindac (Fig. 3B). These results show that sulindac selectively enhances caspase cascade activation in tumor but not normal cells. We next examined additional effector molecules upstream of the caspase cascade that are modulated by Ad-mda7 and sulindac treatments. Previous studies have shown PKR, p38MAPK, and pJNK to be important in Ad-mda7-induced apoptosis in lung cancer cells (14, 15, 18). Similarly, regulation of the Bcl-2 family (Bax, Bak, Bcl-2, and Bcl-x_L) proteins has been shown to be critical for sulindac-induced apoptosis and independent of p53 status (46, 47). On the basis of these reports, we evaluated the expression of PKR, pJNK, pp38MAPK, and several Bcl-2 family members in A549 and H1299 cells after treatment with Ad-mda7 and sulindac. Expression of PKR, pJNK, and pp38MAPK was increased in cells treated with Ad-mda7 alone or in combination with sulindac compared with untreated, sulindac-treated, and Ad-luc-treated cells (Fig. 3C). PKR was also slightly increased in cells

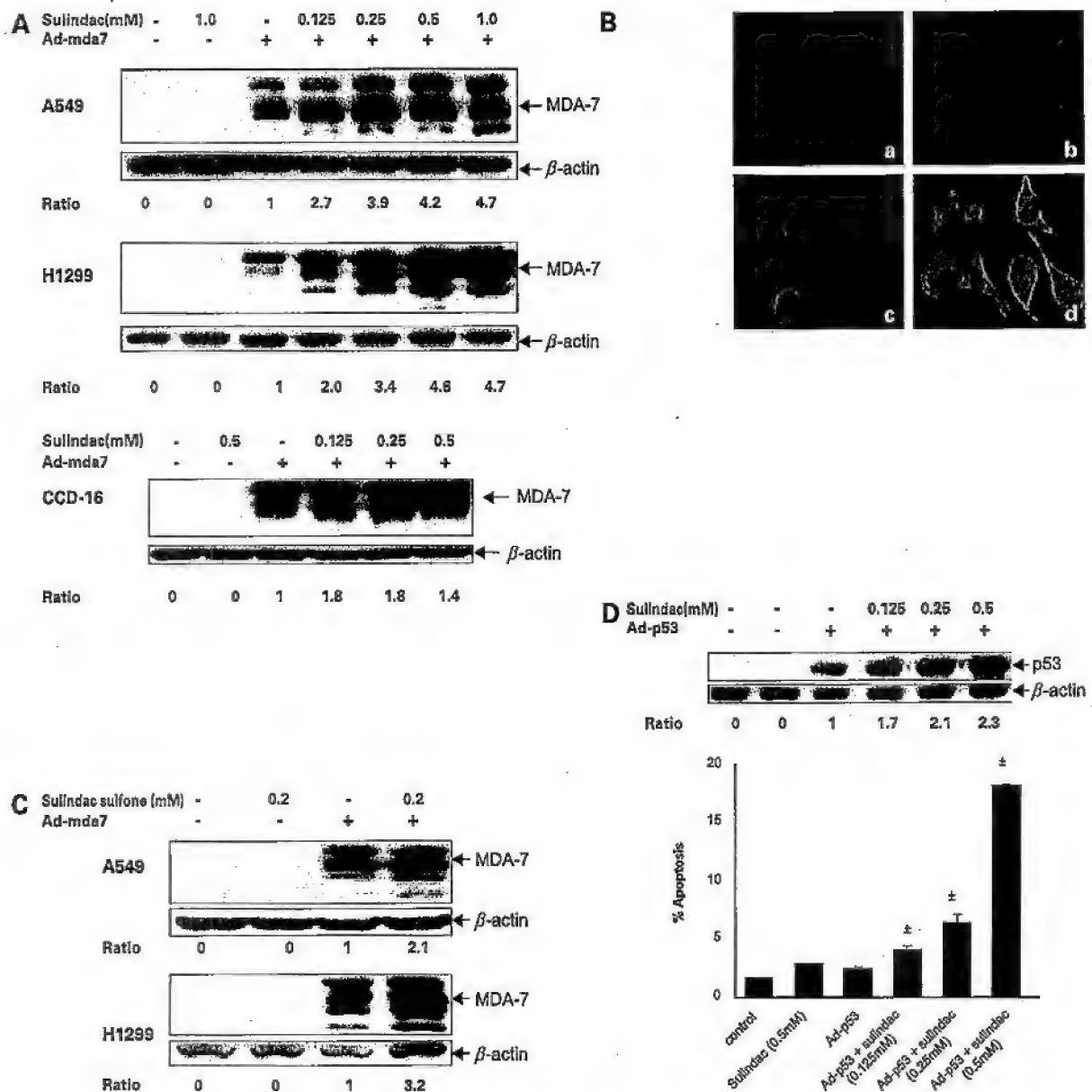


Figure 2. Sulindac increases MDA-7 protein expression. **A**, tumor (A549 and H1299) and normal (CCD-16) cells were treated with PBS or Ad-mda7, followed by treatment with sulindac at the indicated concentrations. At 48 h after infection, the cells were harvested and immunoblotted for MDA-7. Increased MDA-7 protein expression was observed in cells that were treated with Ad-mda7 and sulindac compared with cells that were treated with Ad-mda7. MDA-7 expression was not observed in untreated or sulindac-treated cells. The difference in the level of MDA-7 protein expression was semiquantitatively determined by densitometry and expressed as a ratio. β -actin was used as a protein loading control. **B**, H1299 cells were treated with PBS (a), sulindac (b), Ad-mda7 (c), or with a combination of Ad-mda7 plus sulindac (d). At 48 h after treatment, cells were subjected to immunofluorescence staining for MDA-7 protein as described in Materials and Methods. Cytoplasmic MDA-7 expression was observed in cells treated with Ad-mda7 or Ad-mda7 plus sulindac. However, MDA-7 protein expression was significantly increased in cells treated with Ad-mda7 plus sulindac compared with Ad-mda7-treated cells. MDA-7 protein expression was not detected in cells treated with PBS or sulindac. Original magnification, $\times 400$. **C**, A549 and H1299 cells were treated with PBS or Ad-mda7 in the presence or absence of sulindac sulfone and analyzed for MDA-7 expression. Increased MDA-7 expression was observed in cells treated with Ad-mda7 and sulindac sulfone compared with cells that were treated with Ad-mda7. MDA-7 expression was not observed in PBS or sulindac sulfone-treated cells. The difference in the level of MDA-7 protein expression was semiquantitatively determined by densitometry and expressed as a ratio. β -actin was used as a protein loading control. **D**, H1299 cells were treated with low dose of Ad-p53 (50 vp/cell) or Ad-p53 and sulindac, and analyzed for p53 protein expression and apoptotic cells as described in Materials and Methods. Increased p53 protein was observed in Ad-p53- and sulindac-treated cells that correlated with increased apoptotic cells compared with cells that were not treated or treated with Ad-p53. Bars, SE.

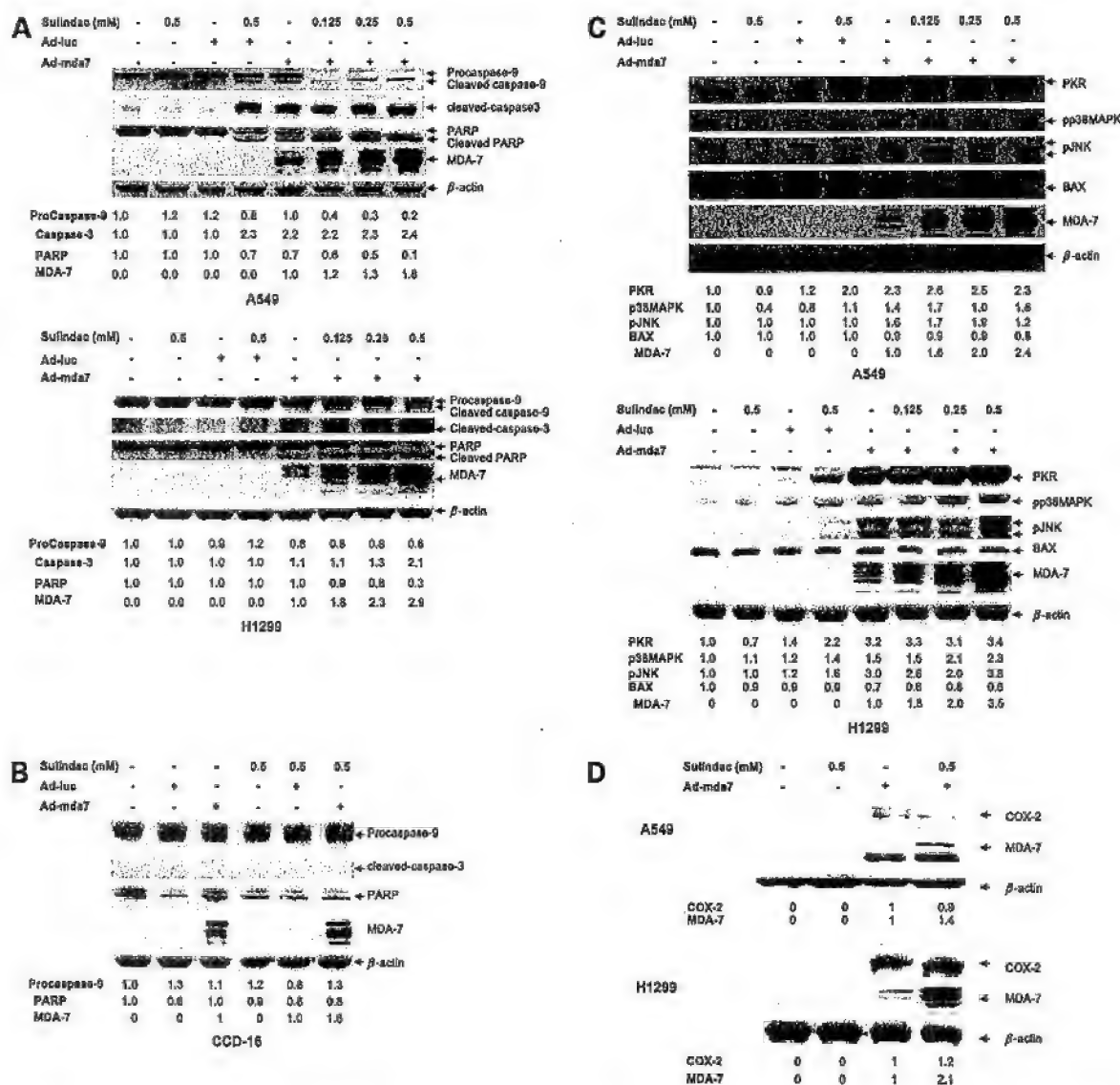


Figure 3. Sulindac increases Ad-mda7-mediated apoptotic signaling. Tumor A549 and H1299 cells [A] and normal (CCD-16) cells [B] were either untreated or treated with Ad-luc or Ad-mda7, alone or in combination with sulindac, at the indicated concentrations. At 72 h after treatment, cells were harvested and lysed, and activation of caspase-9 and caspase-3 and cleavage of PARP was determined by Western blot analysis. The difference in the level of protein expression was semiquantitatively determined by densitometry and expressed as a ratio. β -actin was used as a protein loading control. C, A549 and H1299 cells were treated as described above for 48 h and analyzed by Western blot analysis for various molecular effectors of apoptosis. The difference in the level of protein expression was semiquantitatively determined as described above. D, analysis for COX-2 expression in A549 and H1299 cells treated with Ad-mda7 or Ad-mda7 and sulindac. COX-2 expression was increased in Ad-mda7 and Ad-mda7 plus sulindac-treated cells compared with cells that were treated with PBS or sulindac. However, no significant change in COX-2 expression was observed in Ad-mda7-treated cells compared with Ad-mda7- and sulindac-treated cells. Changes in protein levels were determined semiquantitatively as described above. β -actin served as internal loading control.

treated with Ad-luc plus sulindac compared with untreated, Ad-luc-treated, and sulindac-treated cells. However, the PKR levels in the cells treated with Ad-luc plus sulindac were lower than those observed in cells treated with Ad-mda7 plus sulindac. The increase in PKR, pJNK, and pp38MAPK was associated with the

expression levels of MDA-7 induced by sulindac. No change in the expression levels of Bax, an inducer of apoptosis, was detected in any of the treatment groups (Fig. 3C). The expression level of Bcl-2 or Bcl-x_L, two inhibitors of apoptosis, was also not significantly changed in any of the treatment groups (data not shown). These

Table 2. Cell cycle distribution in lung cancer cells treated with sulindac, Ad-mda 7, or both

Treatment	A549 (%)			H1299 (%)		
	G ₁	S	G ₂ -M	G ₁	S	G ₂ -M
Untreated control medium	68.6 ± 0.7	26.4 ± 0.21	6.9 ± 0.14	58.8 ± 0.98	28.5 ± 0.41	12.8 ± 0.49
Control + sulindac 0.125 mmol/L	64.8 ± 0.14	28.9 ± 0.35	6.4 ± 0.56	66.4 ± 0.42	22.3 ± 0.28	11.4 ± 0.63
Control + sulindac 0.5 mmol/L	75.6 ± 0.14	18.5 ± 0.14	6.0 ± 0.07	74.6 ± 1.7	13.0 ± 1.34	12.7 ± 0.42
Ad-mda7	41.3 ± 0.63	31.6 ± 0.63	27.2 ± 0.07	44.2 ± 0.98	13.5 ± 0.7	42.5 ± 0.77
Ad-mda7 + sulindac 0.125 mmol/L	35.6 ± 0.14	31.8 ± 0.7	32.7 ± 0.36	46.9 ± 1.2	14.0 ± 0.28	39.2 ± 0.91
Ad-mda7 + sulindac 0.5 mmol/L	43.4 ± 0.21	42.6 ± 0.07	12.3 ± 2.4	49.2 ± 0.7	18.4 ± 0.6	32.4 ± 6.9
Ad-luc	73.8 ± 1.5	17.1 ± 1.9	7.1 ± 0.63	78.3 ± 3.5	9.8 ± 1.4	11.9 ± 0.56
Ad-luc + sulindac 0.5 mmol/L	70.0 ± 8.1	18.5 ± 6.3	11.5 ± 1.6	70.4 ± 1.5	9.7 ± 0.30	20 ± 0.14

NOTE: Cells were treated with PBS, Ad-luc, or Ad-mda7 alone, or in combination with 0.5 mmol/L sulindac for 72 hours followed by FACS analysis. The percentage of cells in each cell cycle phase was determined by analysis of the DNA content histogram. Values are the means of duplicate samples ± SD. Similar results were observed in at least two independent experiments.

results support the idea that the induction of apoptosis by Ad-mda7 plus sulindac primarily depends on the ability of sulindac to enhance ectopic MDA-7 expression.

The possibility that enhanced tumor cell killing with Ad-mda7 plus sulindac treatment was due to COX-2 inhibition was next investigated in A549 and H1299 cells. Increased COX-2 expression was observed in cells treated with Ad-mda7 and Ad-mda7 plus sulindac (Fig. 3D). However, there was no significant difference in COX-2 expression levels between the two treatment groups. COX-2 expression was not observed in cells that were treated with PBS or sulindac.

Effects of Sulindac and Ad-mda7 Treatment on Cell Cycle

Previous studies have shown that sulindac induces cell cycle arrest at G₁ (48), and that Ad-mda7 induces cell cycle arrest at G₂-M (5–7). On the basis of these reports, we investigated by FACS analysis the combined effects of sulindac and Ad-mda7 treatment on cell cycle regulation. Tumor cells were either untreated or treated with sulindac, Ad-luc, Ad-mda7, or Ad-mda7 plus sulindac for 72 hours. As previously reported, Ad-mda7 but not Ad-luc treatment increased the number among the G₂-M phase of cell cycle in both A549 (27.2%) and H1299 (42.5%) cells (Table 2). Sulindac treatment alone increased the number of cells in the G₁ phase. In both tumor cell lines, the number of G₁-phase cells was markedly increased at 0.5 mmol/L compared with 0.125 mmol/L sulindac (75.6% versus 64.8% in A549 and 74.6% versus 66.4% in H1299 cells, respectively). Treatment with sulindac and Ad-mda7 abrogated Ad-mda7-induced G₂-M arrest. The effect was more pronounced among cells treated with 0.5 mmol/L sulindac in combination of Ad-mda7, resulting in a decrease in the number of G₂-M-phase cells, from 27.2% to 12.3% in A549 and from 42.5% to 32.4% in H1299 cells, respectively. Abrogation of Ad-mda7-induced G₂-M-phase arrest by sulindac was also observed at 48 hours after treatment (data not shown). These results show that sulindac and Ad-mda7 affect different phases of the cell cycle and that sulindac-enhanced Ad-mda7 tumor cell killing does not occur via increased G₂-M arrest.

Because the killing effect and regulation of proapoptotic molecules in Ad-mda7- and sulindac-treated H1299 and A549 tumor cells were similar, we narrowed our focus in studying the underlying mechanism in only one cell line. Subsequent studies were carried out in H1299 cells as described below.

Sulindac Delays Ectopic MDA-7 Protein Degradation

To assess the mechanism by which sulindac increases ectopic MDA-7 protein, we examined the effect of sulindac on transcriptional activity and MDA-7 protein degradation in H1299 cells. To determine the effect of sulindac on the transcriptional activity of Ad-mda7, we did quantitative real-time PCR analysis of RNA samples extracted from cells that were untreated or that were treated with Ad-mda7 alone or with sulindac at various concentrations. No significant difference in mRNA levels was observed in the cells treated with Ad-mda7 plus sulindac compared with untreated and Ad-mda7-treated cells (Fig. 4A). To evaluate whether sulindac treatment regulates MDA-7 protein degradation, H1299 cells were treated with Ad-mda7 alone or in combination with sulindac for various durations, and the half-life of MDA-7 protein was determined. The MDA-7 protein levels in the Ad-mda7-treated control cells decreased over time (Fig. 4B); protein degradation was complete at 11 hours. In contrast, the degradation of MDA-7 protein in the cells treated with Ad-mda7 plus sulindac was delayed as shown by substantial levels of detectable protein at 13 hours. Semiquantitative analysis of the protein levels indicated that at 0 to 13 hours, the MDA-7 protein level was 8 to 15 times higher in the cells treated with Ad-mda7 plus sulindac than in the Ad-mda7-treated cells (Fig. 4C). These results show that the increase in ectopic MDA-7 protein expression in cells treated with Ad-mda7 plus sulindac is a result of a sulindac-mediated delay of MDA-7 protein degradation.

Sulindac-Enhanced MDA-7 Expression Is Not Due to Inhibition of Proteasome Activity

Given that recent studies have shown that some NSAIDs inhibit proteasome activity (44, 49), we sought

to determine whether the enhanced MDA-7 protein expression mediated by sulindac is due to its ability to inhibit proteasome activity. For this purpose, the effects of sulindac were compared with those of MG132, a known proteasome inhibitor (50) by Western blotting, ubiquitin degradation assay, and proteasome enzymatic activity assay. Western blotting showed that sulindac or MG132 treatment for 12 hours in combination with Ad-mda7 enhanced MDA-7 protein expression compared with cells treated with Ad-mda7 alone (Fig. 5A). However, sulindac enhanced total MDA-7 protein levels, which included both nascent unglycosylated protein and MDA-7 proteins that were glycosylated at different levels, as indicated by multiple bands. In contrast, MG132 enhanced the level of nascent MDA-7 protein, albeit less strongly than did sulindac, and one glycosylated form of MDA-7 protein. Similar results were obtained at 6 and 24 hours after treatment (data not shown). Thus, the mechanisms by which sulindac and MG132 enhance MDA-7 protein seem to differ.

We next determined the ability of sulindac to inhibit proteasome activity. Western blot analysis for total ubiquitinated proteins, an indicator of inhibition of the proteasome pathway, showed ubiquitinated proteins in MG132-treated cells but not in sulindac-treated cells (Fig. 5B). These results show that sulindac, unlike MG132, does not inhibit proteasome activity or the proteasome pathway. Consistent with these findings are the results of the proteasome activity assay in which treatment with Ad-mda7 alone or with sulindac did not inhibit the proteasome activity compared with untreated control cells (Fig. 5C). In contrast, treatment with Ad-mda7 plus MG132 resulted in significant inhibition of proteasome activity ($P = 0.01$). These results suggest that sulindac-enhanced MDA-7 protein expression is not due to inhibition of proteasome activity.

Sulindac Enhances Ad-mda7-Mediated Lung Tumor Growth Suppression *In vivo*

To determine whether Ad-mda7 plus sulindac treatment enhances tumor growth suppression, pilot *in vivo* experiments were conducted using a lung tumor xenograft model. Compared with mice treated with PBS, sulindac, Ad-luc, Ad-mda7, or Ad-luc plus sulindac, mice treated with Ad-mda7 plus sulindac showed a significant growth suppression ($P = < 0.001$; Fig. 6A). A significant tumor inhibition was also observed in mice that were treated with Ad-mda7 alone or Ad-luc plus sulindac compared with PBS- and Ad-luc-treated mice ($P = 0.03$). No significant growth inhibition was observed in sulindac-treated mice compared with PBS-treated mice. Furthermore, treatment-related toxicity as evidenced by morbidity, loss of body weight, and death was not observed in mice treated with Ad-mda7 plus sulindac, suggesting that the treatments were well tolerated (data not shown).

Analysis of s.c. tumors 24 hours after the last treatment with sulindac revealed that MDA-7 protein levels were 3 to 12 times higher in the tumors from mice treated with Ad-mda7 plus sulindac than in the tumors from the mice treated with Ad-mda7 (Fig. 6B). Some faint protein bands

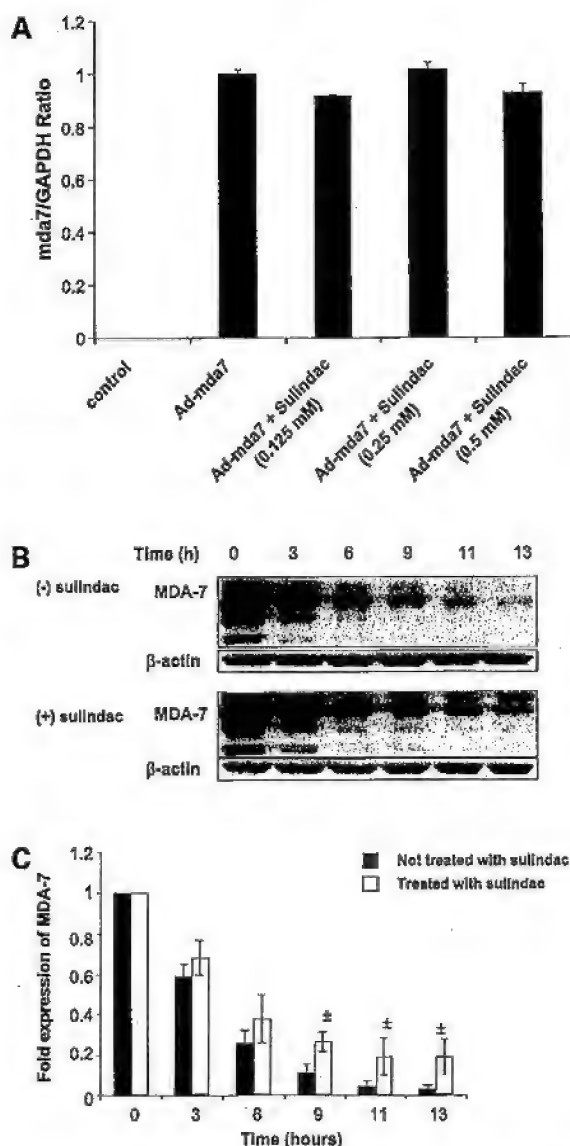


Figure 4. Sulindac delays MDA-7 protein degradation. **A**, H1299 cells were treated with PBS (control), Ad-mda7 alone, or Ad-mda7 in combination with sulindac at the indicated concentrations for 48 h. RNA extraction and quantitative real-time PCR were done as described in Materials and Methods. The results were expressed as a ratio of *mda-7* mRNA/glyceraldehyde-3-phosphate dehydrogenase. No substantial difference in the *mda-7* mRNA levels was observed between the cells treated with Ad-mda7 plus sulindac and the cells treated with Ad-mda7 alone. **B**, H1299 cells were treated with Ad-mda7 for 48 h. After a 2-h incubation in medium without sulindac (–) or with 1 mmol/L sulindac (+), cells were incubated for the indicated periods with 10 μ M cycloheximide, a known protein synthesis inhibitor. Cell lysates were prepared at the indicated time points and analyzed by Western blot analysis for MDA-7 protein levels. Treatment with sulindac delayed the degradation of MDA-7 protein. β -actin was used as an internal loading control. **C**, MDA-7 protein expression levels between H1299 cells not treated with sulindac and sulindac-treated H1299 cells were semiquantitatively determined using ImageQuant software (Molecular Dynamics/Amersham Pharmacia Biotech, Piscataway, NJ). Columns, mean of two independent experiments; bars, SE.

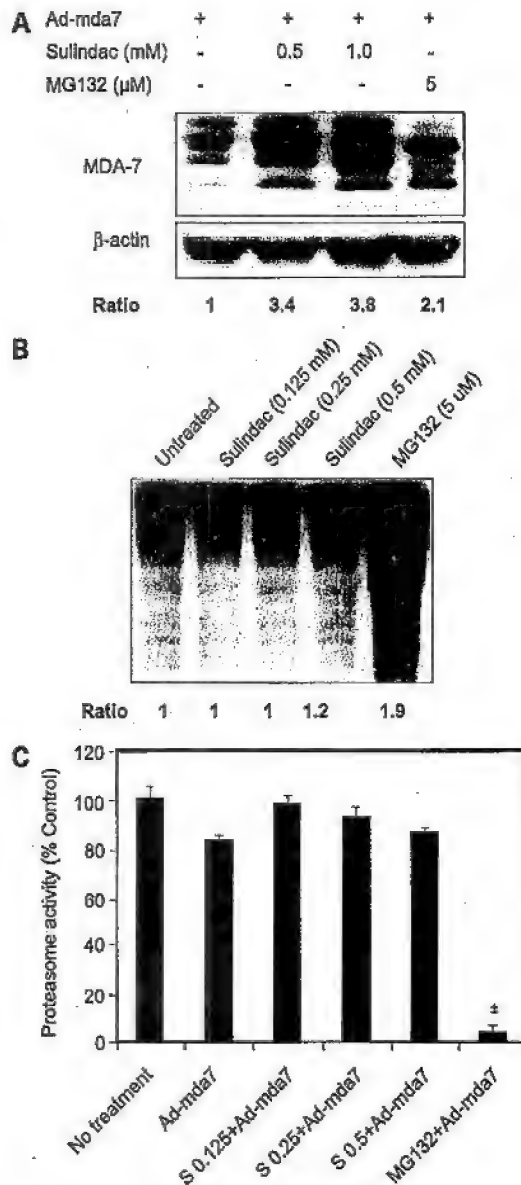


Figure 5. Sulindac does not inhibit proteasome activity. **A**, H1299 cells were treated with Ad-mda7 for 48 h, followed by treatment either with sulindac at the indicated concentrations or with 5 μmol/L MG132 for 12 h. Western blot analysis of whole cell lysates was done for MDA-7. Protein expression levels were semiquantitatively determined by densitometry and expressed as a ratio. β-actin was used as an internal loading control. **B**, H1299 cells were incubated either with sulindac at the indicated concentrations or with 5 μmol/L MG132 for 24 h. Untreated cells served as a control. Whole cell lysates were analyzed for ubiquitinated proteins by Western blot analysis. Ubiquitinated protein was detected in MG132-treated cells but not in sulindac-treated cells. Total protein levels were semiquantitatively determined as described above. **C**, H1299 cells were grown in medium (control), in Ad-mda7 in combination with sulindac at the indicated concentrations for 48 h, or in 5 μM MG132 for 24 h. Proteasome activity was analyzed as described in Materials and Methods. Columns, mean of triplicate samples; bars, SE. MG132, but not sulindac, inhibited proteasome activity in Ad-mda7-treated cells.

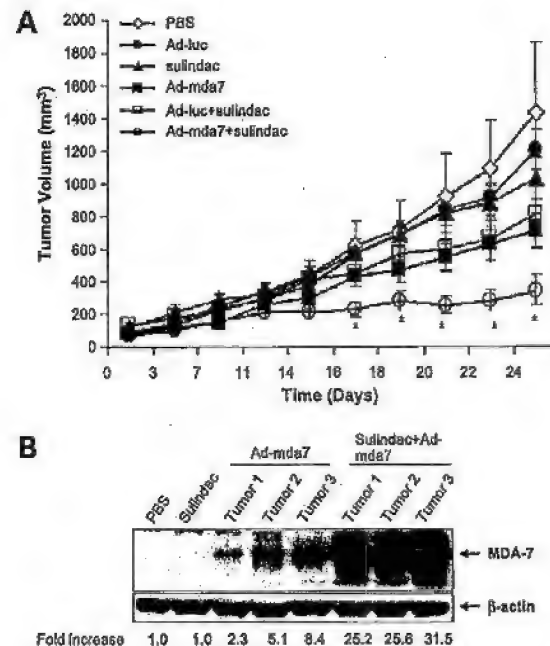


Figure 6. Sulindac enhances Ad-mda7-mediated tumor growth inhibition *in vivo*. **A**, s.c. H1299 tumor-bearing nude mice were divided into groups ($n = 8/\text{group}$). Animals treated with Ad-mda7 plus sulindac showed significant tumor growth inhibition compared with animals treated with PBS, sulindac, Ad-luc, Ad-mda7, or Ad-luc plus sulindac. Ad-mda7 or Ad-luc (3×10^8 vp) was administered by i.t. injection thrice a week and sulindac (40 mg/kg) by i.p. injection daily. Points, mean tumor volume for each group per time point; bars, SE. **B**, MDA-7 expression in s.c. tumor tissues receiving various treatments as described above. MDA-7 expression was increased in tumors from mice treated with Ad-mda7 and sulindac compared with tumors from mice treated with Ad-mda7 alone. MDA-7 protein expression levels were semiquantitatively determined by densitometry and expressed as a ratio. β-actin was used as a protein loading control.

were also observed in the tumors of mice treated with PBS, sulindac, and Ad-luc plus sulindac. However, we believe that these bands were nonspecific or cross-reacting with mouse tissue proteins because the corresponding assay using anti-MDA-7 antibody revealed no endogenous MDA-7 protein in the parental H1299 tumors and murine normal cells (data not shown). These results show that treatment of lung tumors with Ad-mda7 plus sulindac enhances growth suppression in parallel to enhanced MDA-7 protein expression, a finding consistent with our *in vitro* results.

Discussion

We found that treatment of human non-small cell lung cancer cells with Ad-mda7 in combination with sulindac results in significant growth suppression and apoptosis both *in vitro* and *in vivo*. Furthermore, the inhibitory effects are selective for tumor but not normal cells. The ability to inhibit growth of both H1299 (p53-null) and A549 (p53 wild type) cells suggests that this treatment

combination strategy is applicable for human cancers that are defective in p53, which account for >50% of human cancers (51). However, the efficacy of treatment with Ad-mda7 plus sulindac on tumor cells that have defects in other genes or pathways is not known and needs to be tested. Our results also reveal a mechanism by which sulindac enhances Ad-mda7-mediated tumor killing. Preliminary experiments showed that sulindac, in a dose-dependent manner, increased the expression of ectopic MDA-7 protein in Ad-mda7-treated cells, suggesting that the enhanced killing was due to increased MDA-7 protein expression. However, the mechanism by which sulindac increased ectopic protein expression is not known. Previous studies from several laboratories have shown the ability of various drugs to enhance adenoviral transduction efficiency (45). Such findings suggested that the increased MDA-7 protein expression observed in cells treated with Ad-mda7 plus sulindac was due to increased Ad-mda7 transduction that was mediated by sulindac. However, sulindac, unlike the various other drugs, did not enhance adenovirus transduction efficiency. Sulindac also increased ectopic p53 protein expression in cells that were treated with Ad-p53 plus sulindac that resulted in enhanced cell killing. These results suggest that the ability of sulindac to increase ectopic protein expression is not restricted to MDA-7 alone but is applicable to other adenoviral-encoded proteins. Similarly, the ability to increase MDA-7 protein was not unique to sulindac as increased protein expression was also observed in sulindac sulfone-treated cells. Although sulindac also increased MDA-7 protein expression in normal cells, the expression levels were significantly lower than those in the tumor cells; the reason for this difference in normal cells is unclear and should be investigated. We also assessed, after treatment, the molecular effectors that are known to mediate tumor cell inhibition and apoptosis. We and others have previously shown that Ad-mda7 treatment of lung cancer cells results in a G₂-M-phase arrest and induces apoptosis via activation of the caspase cascade and PKR (5-7, 14). Furthermore, Ad-mda7-mediated apoptosis in lung cancer cells is independent of Bax, Bak, and Bcl-2 (5, 6). A requirement for Bax in Ad-mda7-mediated killing, however, has been shown in mesothelioma cells (9). Sulindac, unlike *mda-7*, induces G₁-phase arrest, up-regulates Bax and Bak expression, and inhibits COX-2 expression (46). More recently, Bax was shown to be necessary for sulindac-induced apoptosis in Bax-deficient colorectal cancer cells (52). Another study showed sequential decrease in Bcl-2 expression and increased apoptosis in an intestinal tumor model after treatment with sulindac (47). In the present study, sulindac abrogated Ad-mda7-mediated G₂-M-phase arrest and this abrogation was more pronounced in A549 than in H1299 cells. Additionally, increased expression of PKR, pJNK, and p38MAPK (but not Bak and Bax) that correlated with MDA-7 expression was observed in cells treated with Ad-mda7 plus sulindac. Associated with increased expression of PKR,

pJNK, and p38MAPK were the increase in caspase-9 and caspase-3 expression and activation. Previous studies in colon cancer cells have shown regulation of Bak, Bax, Bcl-2, and COX-2 by sulindac (46-52). Interestingly, in lung cancer cells, we did not find any significant change in the expression levels of these effector molecules by sulindac or Ad-mda7 or the combination. The increased levels of effector molecules that are regulated by Ad-mda7 (PKR, p38MAPK, and pJNK) but not by sulindac suggests that the increased tumor cell killing is merely due to a sulindac-mediated increase in ectopic MDA-7 protein expression. Additional evidence for this claim comes from our study where cells treated with increasing the dose of Ad-mda7 viral particles such that the endogenous MDA-7 protein levels equaled to the levels achieved with Ad-mda7 and sulindac resulted in similar level of tumor cell killing.⁶ However, additional molecules/pathways (cyclic guanosine 3',5'-monophosphate-phosphodiesterase, protein kinase G, and β -catenin) that have previously been reported to be affected by sulindac and its metabolites were not examined in the present study. It is possible that sulindac, when used at high concentrations that induce apoptosis, regulates the expression of some of these molecules. However, in the present study, we used sulindac at concentrations below its IC₅₀ value that does not induce apoptosis. In support of these observations are the findings that treatment of H1299 cells with Ad-p53 plus sulindac resulted in increased ectopic p53 expression and enhanced cell death. Because the effect of Ad-mda7 and sulindac on H1299 and A549 tumor cells were the same, we narrowed our focus on studying the underlying mechanism for enhanced killing using only H1299 cells as described below. We next investigated the mechanism by which sulindac increased MDA-7 protein expression. As described above, the possibility that sulindac increases transduction efficiency was ruled out by the results of flow cytometry assays using GFP reporter. Alternative explanations for increased MDA-7 protein levels included increased transcriptional activity, increased protein half-life, and increased antiproteasome activity. That sulindac did not affect transcriptional activity was shown by real-time quantitative reverse transcription-PCR. The major determinant for protein half-life is the presence of degradation signals contained in the protein. Degradation of most cellular proteins is rapidly done by the proteasome/ubiquitination system, both to eliminate misfolded or denatured polypeptides and to regulate the concentration of components critical for control of cell cycle and metabolism (53-55). Furthermore, recent studies have shown that NSAIDs can inhibit proteasome activity (44). On the basis of these studies, we examined the effect of sulindac on protein half-life and proteasome activity. Sulindac increased the half-life of ectopic MDA-7

⁶ Unpublished data.

protein, as well as the half-life of endogenous proteins, such as p53 (data not shown). The ability of sulindac to increase protein half-life is an unexpected and novel finding. Although the half-life of MDA-7 protein was increased, it is still possible that increased MDA-7 protein levels is partly due to an effect of sulindac on the proteasome/ubiquitin pathway. To test this possibility, we compared sulindac with the proteasome inhibitor MG132 (50). Sulindac, unlike MG132, did not inhibit the proteasome pathway directly or indirectly. Lack of direct inhibitory activity of sulindac on proteasomes was shown by the proteasome activity assay; on the other hand, lack of indirect inhibitory activity was shown by the absence of total ubiquitinated proteins in sulindac-treated cells. The discrepancy between our results from those previously reported is not clear (43, 44). One possibility is that the concentration of sulindac used in the present study was much lower than that used in the studies previously reported. Alternatively, the inhibition of proteasome activity by sulindac may be tumor-type dependent. We are currently investigating these possibilities in the laboratory.

The ability of sulindac and its metabolites to increase the half-life of therapeutic proteins, such as MDA-7 or p53, has immediate clinical implications in that repeated vector injections may be minimized but still achieve the same therapeutic effect. Phase I clinical trials have been completed for Ad-mda7 and for sulindac and its metabolites; these studies have indicated that these agents have no significant toxic effects and are well tolerated when used alone (23, 24, 56). However, combination therapy using Ad-mda7 plus sulindac and its metabolites has not yet been tested; our animal study did not show any enhanced toxicity due to the combination of Ad-mda7 plus sulindac compared with individual treatments. Therefore, additional preclinical studies evaluating the therapeutic effect of Ad-mda7 and sulindac or its metabolites on tumor cells are warranted before testing of this therapy in humans.

Finally, our animal experiments, which were to test whether sulindac enhances Ad-mda7-mediated tumor cell killing *in vivo*, revealed significant tumor growth inhibition in the mice treated with Ad-mda7 plus sulindac compared with the control treatment groups. These inhibitory effects were due to increased MDA-7 protein expression in the tumors consistent with our *in vitro* results. Although we have shown proof-of-principle using s.c. tumor xenografts, additional studies evaluating the therapeutic effects on a spectrum of human xenograft tumors are warranted. Furthermore, the effect of Ad-mda7 and sulindac combination therapy on disseminated lung cancer has not been tested and, compared with localized disease, is more relevant to cancer therapy in clinical settings. We are currently conducting these experiments in our laboratory. In conclusion, we have shown, for the first time, that sulindac enhances Ad-mda7-mediated tumor growth inhibition and apoptosis in non-small cell lung cancer both *in vitro* and *in vivo*.

Furthermore, we have identified a novel mechanism of action of sulindac. Our results form a basis for additional preclinical studies using Ad-mda7 and sulindac for treatment of human lung cancer.

Acknowledgments

We thank Kate Ó Súilleabháin for editorial assistance, Alma Vega for assistance in the preparation of the manuscript, and Xiao Cao and Gitanjali Jayachandran for assistance with real-time PCR experiments.

References

- Wang M, Tan Z, Zhang R, Kotenko SV, Liang P. Interleukin 24 (MDA-7/MOB-6) signals through two heterodimeric receptors, IL-22R1/IL-20R2 and IL-20R1/IL-20R2. *J Biol Chem* 2002;277:7341–7.
- Chada S, Sutton BR, Ekmekcioglu S, et al. MDA-7/IL-24 is a unique cytokine-tumor suppressor in the IL-10 family. *Int Immunopharmacol* 2004;4:649–67.
- Jiang H, Lin JJ, Su ZZ, Goldstein NI, Fisher PB. Subtraction hybridization identifies a novel melanoma differentiation associated gene, *mda-7*, modulated during human melanoma differentiation, growth and progression. *Oncogene* 1995;11:2477–86.
- Su ZZ, Madireddi MT, Lin JJ, et al. The cancer growth suppressor gene *mda-7* selectively induces apoptosis in human breast cancer cells and inhibits tumor growth in nude mice. *Proc Natl Acad Sci U S A* 1998;95:14400–5.
- Saeki T, Mhashilkar A, Chada S, Branch C, Roth JA, Ramesh R. Tumor suppressive effects by adenovirus-mediated *mda-7* gene transfer in non-small cell lung cancer *in vitro*. *Gene Ther* 2000;7:2051–7.
- Mhashilkar AM, Schrock RD, Hindi M, et al. Melanoma-differentiation associated gene-7 (*mda-7*): a novel anti-tumor gene for cancer gene therapy. *Mol Med* 2001;7:271–82.
- Ekmekcioglu S, Ellerhorst J, Mhashilkar AM, et al. Down-regulated melanoma differentiation associated gene (*mda-7*) expression in human melanomas. *Int J Cancer* 2001;94:54–8.
- Jiang H, Su ZZ, Lin JJ, Goldstein NI, Young CS, Fisher PB. The melanoma differentiation associated gene *mda-7* suppresses cancer cell growth. *Proc Natl Acad Sci U S A* 1996;93:9160–5.
- Cao XX, Mohiuddin I, Chada S, et al. Adenoviral transfer of *mda-7* leads to BAX up-regulation and apoptosis in mesothelioma cells, and is abrogated by over-expression of BCL-X_L. *Mol Med* 2002;12:869–76.
- Gopalan B, Sharma S, Litwack V, et al. Gene therapeutic approach for treatment of human ovarian cancer using *mda-7/IL-24*. *Proc Am Assoc Cancer Res* 2003;44:331.
- Saito Y, Mhashilkar AM, Roth JA, Chada S, Ramesh R. Selective induction of apoptosis of cell cycle arrest and apoptosis in human prostate cancer cells through adenoviral transfer of the melanoma differentiation associated 7 (*mda-7*) gene. *Proc Am Assoc Cancer Res* 2003;44:247.
- Yacoub A, Mitchell C, Brannon J, et al. MDA-7 (interleukin-24) inhibits the proliferation of renal carcinoma cells and interacts with free radicals to promote cell death and loss of reproductive capacity. *Mol Cancer Ther* 2003;2:623–32.
- Saeki T, Mhashilkar A, Swanson X, et al. Inhibition of human lung cancer growth following adenovirus mediated *mda-7* gene expression *in vivo*. *Oncogene* 2002;21:4558–66.
- Pataer A, Vorburger SA, Barber GN, et al. Adenoviral transfer of the melanoma differentiation-associated gene 7 (*mda-7*) induces apoptosis of lung cancer cells via up-regulation of the double-stranded RNA-dependent protein kinase (PKR). *Cancer Res* 2002;62:2239–43.
- Kawabe S, Nishikawa T, Munshi A, Roth JA, Chada S, Moyn RE. Adenovirus-mediated *mda-7* gene expression radiosensitizes non-small cell lung cancer cells via TP53-independent mechanisms. *Mol Ther* 2002;6:637–44.
- Mhashilkar AM, Stewart AL, Sieger K, et al. MDA-7 negatively regulates the β -catenin and PI3K signaling pathways in breast and lung tumor cells. *Mol Ther* 2003;8:207–19.
- Sieger K, Mhashilkar AM, Stewart A, et al. The tumor suppressor activity of MDA-7/IL-24 protein is mediated by intracellular protein expression in NSCLC cells. *Mol Ther* 2004;9:355–67.

18. Sarker D, Su ZZ, Lebedeva IV, et al. *mda-7* (IL-24) mediates selective apoptosis in human melanoma cells by inducing the coordinated overexpression of the GADD family of genes by means of p38 MAPK. *Proc Natl Acad Sci U S A* 2002;99:10054–9.
19. Ramesh R, Ito I, Gopalan B, Saito Y, Mhashilkar AM, Chada S. Ectopic production of MDA-7/IL-24 inhibits invasion and migration of human lung cancer cells. *Mol Ther* 2004;9:510–8.
20. Ellerhorst J, Prieto VG, Eckmekcioglu S, et al. Loss of MDA-7 expression with progression of melanoma. *J Clin Oncol* 2002;20:1069–74.
21. Ramesh R, Mhashilkar AM, Tanaka F, et al. Melanoma differentiation-associated gene 7/interleukin (IL)-24 is a novel ligand that regulates angiogenesis via the IL-22 receptor. *Cancer Res* 2003;63:5105–13.
22. Caudell EG, Mumm JB, Poindexter N, et al. The protein product of the tumor suppressor gene, melanoma differentiation-associated gene 7, exhibits immunostimulatory activity and is designated IL-24. *J Immunol* 2002;168:8041–6.
23. Cunningham C, Chada S, Merritt JA, et al. Clinical and local biological effects of an intratumoral injection of *mda-7* (IL-24;INGN 241) in patients with advanced carcinoma: a phase I study. *Mol Ther* 2005;11:149–59.
24. Tong AW, Nemunaitis J, Chada S, et al. Intratumoral injection of INGN 241, a nonreplicating adenovector expressing the melanoma-differentiation associated gene-7 (*mda-7*/IL-24): Biologic outcome in advanced cancer patients. *Mol Ther* 2005;11:160–72.
25. Nishikawa T, Ramesh R, Munshi A, Chada S, Meyn R. Adenovirus mediated *mda-7* gene therapy suppresses angiogenesis and sensitizes NSCLC xenograft tumors to radiation. *Mol Ther* 2004;9:818–28.
26. Yacoub A, Mitchell C, Lister A, et al. Melanoma differentiation-associated 7 (interleukin 24) inhibits growth and enhances radiosensitivity of glioma cells *in vitro* and *in vivo*. *Clin Cancer Res* 2003;9:3272–81.
27. Su Z, Lebedeva IV, Gopalakrishnan RV, et al. Combinatorial approach for selectively inducing programmed cell death in human pancreatic cancer cells. *Proc Natl Acad Sci U S A* 2001;98:10332–7.
28. McKenzie T, Liu Y, Fanale M, Swisher SG, Chada S, Hunt KK. Combination therapy of Ad-*mda-7* and trastuzumab increases cell death in Her-2/neu-overexpressing breast cancer cells. *Surgery* 2004;136:437–42.
29. Vane JR, Bakhle YS, Botting RM. Cyclooxygenases 1 and 2. *Annu Rev Pharmacol Toxicol* 1998;38:97–120.
30. Williams CS, Mann M, DuBois RN. The role of cyclooxygenases in inflammation, cancer, and development. *Oncogene* 1999;18:7908–16.
31. Lancaster T, Silagy C. Aspirin and neoplasia of the digestive tract: is there a chemopreventive effect? *Dig Dis* 1994;12:170–6.
32. Ahnen DJ. Colon cancer prevention by NSAIDs: what is the mechanism of action? *Eur J Surg Suppl* 1998;582:111–4.
33. Piazza GA, Alberts DS, Hixson LJJ, et al. Sulindac sulfone inhibits azoxymethane-induced colon carcinogenesis in rats without reducing prostaglandin levels. *Cancer Res* 1997;57:2909–15.
34. Sanchez-Alcazar JA, Bradbury DA, Pang L, Knox AJ. Cyclooxygenase (COX) inhibitors induce apoptosis in non-small cell lung cancer through cyclooxygenase independent pathways. *Lung Cancer* 2003;40:33–44.
35. Thompson HJ, Jiang C, Lu J, et al. Sulfone metabolite of sulindac inhibits mammary carcinogenesis. *Cancer Res* 1997;57:267–71.
36. Molina MA, Sitja-Arnau M, Lemoine MG, Frazier ML, Sinicrope FA. Increased cyclooxygenase-2 expression in human pancreatic carcinomas and cell lines: growth inhibition by nonsteroidal anti-inflammatory drugs. *Cancer Res* 1999;59:4356–62.
37. Lim JT, Piazza GA, Han EK, et al. Sulindac derivatives inhibit growth and induce apoptosis in human prostate cancer cell lines. *Biochem Pharmacol* 1999;58:1097–107.
38. Piazza GA, Rahm AL, Krutzsch M, et al. Antineoplastic drugs sulindac sulfide and sulfone inhibit cell growth by inducing apoptosis. *Cancer Res* 1995;55:3110–6.
39. Tøgeer I, Pfeilschifter J, Geisslinger G. Cyclooxygenase-independent actions of cyclooxygenase inhibitors. *FASEB J* 2001;15:2057–72.
40. Thompson WG, Piazza GA, Li H, et al. Exisulind induction of apoptosis involves guanosine 3',5'-cyclic monophosphate phosphodiesterase inhibition, protein kinase G activation, and attenuated β -catenin. *Cancer Res* 2000;60:3338–42.
41. Soriano AF, Helfrich B, Chan DC, Heasley LE, Bunn PA Jr, Chou TC. Synergistic effects of new chemopreventive agents and conventional cytotoxic agents against human lung cancer cell lines. *Cancer Res* 1999;59:6178–84.
42. Chan DC, Earle KA, Zhao TL, et al. Exisulind in combination with docetaxel inhibits growth and metastasis of human lung cancer and prolongs survival in athymic nude rats with orthotopic lung tumors. *Clin Cancer Res* 2002;8:904–12.
43. Gupta RA, DuBois RN. Combinations for cancer prevention. *Nat Med* 2000;6:974–5.
44. Choi HJ, Kim HH, Lee HS, et al. Lactacystin augments the sulindac-induced apoptosis in HT-29 cells. *Apoptosis* 2003;8:301–5.
45. Lin T, Gu J, Zhang L, et al. Enhancing adenovirus-mediated gene transfer *in vitro* and *in vivo* by addition of protamine and hydrocortisone. *J Gene Med* 2003;5:868–75.
46. Yang K, Fan K, Kurihara N, et al. Regional response leading to tumorigenesis after sulindac in small and large intestine of mice with Apo mutations. *Carcinogenesis* 2003;24:605–11.
47. McEntee MF, Chiu CH, Whelan J. Relationship of β -catenin and Bcl-2 expression to sulindac-induced regression of intestinal tumors in Min mice. *Carcinogenesis* 1999;20:635–40.
48. Piazza GA, Alberts DS, Hixson LJ, et al. Sulindac sulfone inhibits azoxymethane-induced colon carcinogenesis in rats without reducing prostaglandin levels. *Cancer Res* 1997;57:2909–15.
49. Huang YC, Chuang LY, Hung WC. Mechanisms underlying nonsteroidal anti-inflammatory drug-induced p27(Kip1) expression. *Mol Pharmacol* 2002;62:1515–21.
50. He Q, Huang Y, Sheikh MS. Proteasome inhibitor MG132 upregulates death receptor 5 and cooperates with Apo2L/TRAIL to induce apoptosis in Bax-proficient and -deficient cells. *Oncogene* 2004;23:2554–8.
51. Levine AJ, Momand J, Finlay CA. The p53 tumor suppressor gene. *Nature* 1991;351:453–8.
52. Zhang L, Yu J, Park BH, Kinzler KW, Vogelstein B. Role of BAX in the apoptotic response to anticancer agents. *Science* 2000;290:989–92.
53. Adams GM, Crotchett B, Slaughter CA, DeMartino GN, Gogol EP. Formation of proteasome-PA700 complexes directly correlates with activation of peptidase activity. *Biochemistry* 1998;37:12927–32.
54. Coux O, Tanaka K, Goldberg AL. Structure and functions of the 20S and 26S proteasomes [review]. *Annu Rev Biochem* 1996;65:801–47.
55. Dantuma NP, Masucci MG. Stabilization signals: a novel regulatory mechanism in the ubiquitin/proteasome system. *FEBS Lett* 2002;529:22–8.
56. Bunn PA Jr, Chan DC, Earle K, Zhao TL, Helfrich B, Kelly K. Preclinical and clinical studies of docetaxel and exisulind in the treatment of human lung cancer. *Semin Oncol* 2002;29:87–94.

Development of an Orthotopic Model to Study the Biology and Therapy of Primary Human Lung Cancer in Nude Mice

Amir Onn,^{1,2} Takeshi Isobe,² Satoshi Itasaka,^{2,3}
Wenjuan Wu,² Michael S. O'Reilly,^{2,3}
Waun Ki Hong,¹ Isaiah J. Fidler,² and
Roy S. Herbst^{1,2}

Departments of ¹Thoracic/Head and Neck Medical Oncology, ²Cancer Biology, and ³Radiation Oncology, The University of Texas M. D. Anderson Cancer Center, Houston, Texas

ABSTRACT

Purpose: This study was conducted to develop biologically relevant animal models of human lung cancer that are reproducible, inexpensive, and easy to perform.

Experimental Design: Human lung adenocarcinoma (PC14PE6), bronchioloalveolar carcinoma (NCI-H358), squamous cell carcinoma (NCI-H226), poorly differentiated non-small cell lung cancer (NCI-H1299 and A549), or small cell lung cancer (NCI-H69) cells in Matrigel were injected percutaneously into the left lungs of nude mice. The growth pattern of the different lung cancer tumors was studied. For PC14PE6 and NCI-H358, the growth pattern in the subcutis and the response to paclitaxel were also studied.

Results: As is observed for human primary lung cancer, tumors formed from a single focus of disease and progressed to a widespread and fatal thoracic process characterized by diffuse dissemination of lung cancer in both lungs and metastasis to intra- and extrathoracic lymph nodes. When the lung cancer cell lines were implanted s.c., systemic therapy with paclitaxel induced tumor regression. However, only a limited therapeutic response to paclitaxel was observed when the same cells were implanted orthotopically into the lung. Immunohistochemical analysis of tumor tissue revealed increased expression of the proangiogenic factors interleukin 8, basic fibroblast growth factor, and vascular endothelial growth factor/vascular permeability factor.

Conclusions: Our orthotopic models of human lung cancer confirm the "seed and soil" concept and likely pro-

vide more clinically relevant systems for the study of both non-small cell lung cancer and small cell lung cancer biology, and for characterizing novel therapeutic strategies.

INTRODUCTION

Lung cancer is a major health problem worldwide, and the leading cause of cancer related death for both men and women in the United States with an annual mortality rate that exceeds breast, prostate, and colorectal cancers combined (1). In most cases, lung cancer patients are diagnosed with advanced inoperable disease, and the only therapeutic option is systemic chemotherapy. Unfortunately, recent studies have concluded that conventional therapies may have reached a ceiling of clinical impact as evidenced by the 5-year survival for NSCLC⁴ and SCLC, which remains at 14% and 5%, respectively (2). Clearly, a new approach to the therapy of lung cancer is mandatory. Because organ microenvironment influences the phenotype of tumor cells, as originally enunciated by Pagets' "seed and soil" theory (3) and confirmed by others (4-6), the identification of novel therapeutics depends on the availability of biologically relevant *in vivo* models (7).

NSCLC represents 80% of all lung cancer cases, and most research focuses on this subtype, including the development of several orthotopic models of human NSCLC in rodents. These models include implantation of human cancerous tissue obtained surgically (8) and the injection of tumor cells into the rodent airways (9-11), pleural cavity (12, 13), or lung parenchyma after skin incision (14) or thoracotomy (15-17). In contrast, only two reports describe the use of orthotopic models to study SCLC, which comprises 20% of all lung cancer cases (5, 12). Despite their availability, orthotopic models of human lung cancer are not widely used, and most of the research and development of novel therapeutics for lung cancer still relies upon s.c. tumor models, which are potentially less clinically relevant.

In this article, we describe the development of orthotopic models for different primary human lung cancers in athymic nude mice. We have developed models of each of the most common lung cancer histological types including adenocarcinoma, squamous cell, bronchioloalveolar, and small cell. For each tumor type, lesions develop after direct injection of a tumor cell suspension into the thorax of the mouse, making it a reproducible technique to study either NSCLC or SCLC human tumors. The present model recapitulates the local and regional growth pattern seen in lung cancer patients, *i.e.*, from a solitary

Received 5/13/03; revised 7/15/03; accepted 7/21/03.

Grant support: Supported in part by an M. D. Anderson Cancer Center Physician Scientist Program Award (R. S. H.), an ASCO Cancer Development Award (R. S. H.), a NIH grant for Specialized Program of Research Excellence (SPORE) in Lung Cancer (P50 CA70907, to R. S. H.), a grant from the Department of Defense (DAMD 17-02-1-0706, to W. K. H.), and an award from the CRH Foundation (R. S. H.). The costs of publication of this article were defrayed in part by the payment of page charges. This article must therefore be hereby marked advertisement in accordance with 18 U.S.C. Section 1734 solely to indicate this fact.

Requests for reprints: Roy S. Herbst, MD, PhD, The University of Texas M. D. Anderson Cancer Center, 1515 Holcombe Boulevard, Unit 432, Houston, Texas 77030. Phone: (713) 792-6363; Fax: (713) 796-8655; E-mail: rherbst@mdanderson.org.

⁴ The abbreviations used are: NSCLC, non-small cell lung cancer; SCLC, small cell lung cancer; *i.t.*, intrathoracic; FBS, fetal bovine serum; GFP, green fluorescent protein; IHC, immunohistochemistry; bFGF, basic fibroblast growth factor; VEGF, vascular endothelial growth factor; IL, interleukin; VPF, vascular permeability factor.

nodule to a diffuse thoracic disease involving both lungs and the lymph nodes. Furthermore, in contrast to tumors growing s.c., tumors in the lung are less susceptible to treatment with paclitaxel, suggesting that orthotopic models are more relevant to evaluate chemotherapeutics and other therapies for human lung cancer.

MATERIALS AND METHODS

Cell Lines and Tissue Culture Conditions. Six human lung cancer cell lines were studied. NCI-H358 (bronchioloalveolar carcinoma), NCI-H1299 and A549 (poorly differentiated NSCLC), and NCI-H69 (SCLC) were obtained from the American Type Culture Collection (Manassas, VA). PC14PE6 was selected from human adenocarcinoma cell line PC14 to produce pleural effusion when injected into mice (18, 19). NCI-H226 (lung squamous cell carcinoma) was the gift of Dr. John D. Minna, University of Texas Southwestern Medical Center (Dallas, TX; Ref. 20). B16BL6 melanoma cells (21–23) were initially used to determine the feasibility of the orthotopic injection procedure. Floating aggregates of NCI-H69, floating and adherent monolayer cultures of PC14PE6, and adherent monolayer cultures of other cell lines were incubated at 37°C in 5% CO₂-95% air. NCI-H358 was cultured in RPMI 1640 supplemented with 10% FBS, L-glutamine, and penicillin-streptomycin. NCI-H69 cells were cultured in Dulbecco's modified MEM supplemented with 10% FCS and penicillin-streptomycin. All of the other cell lines were cultured in Eagle's MEM supplemented with 10% FBS, sodium pyruvate, nonessential amino acids, L-glutamine, 2-fold vitamin solution, and penicillin-streptomycin mixture (CMEM; Flow Laboratories, Rockville, MD). All of the tumor cell cultures were free of *Mycoplasma*, and the following pathogenic murine viruses: retrovirus type 3, pneumonia virus, K virus, Theiler's encephalitis virus, Sendai virus, minute virus, mouse adenovirus, mouse hepatitis virus, lymphocytic choriomeningitis virus, ectromelia virus, and lactate dehydrogenase virus (assayed by Microbiological Associates, Bethesda, MD).

Animals and Animal Care. Male athymic nude mice (NCR-nu) and C57BL/6 mice were purchased from the Animal Production Area of the National Cancer Institute-Frederick Cancer Research and Development Center (Frederick, MD). The mice were housed and maintained in specific pathogen-free conditions in facilities approved by the American Association for Accreditation of Laboratory Animal Care, and in accordance with current regulations and standards of the United States Department of Agriculture, United States Department of Health and Human Services, and the NIH. The mice were used in accordance with institutional guidelines when they were 6–10 weeks old.

Matrigel and Preparation of Cell Suspension for i.t. Injection. Matrigel is a basement membrane matrix preparation extracted from Engelbreth-Holm-Swarm mouse sarcoma (Becton Dickinson & Co., San Jose, CA; Refs. 14, 16, 17). For all of the experiments a stock solution of 500 µg Matrigel in 1 ml PBS using a dilution factor of approximately ×30 according to compound concentration was used. Cell suspensions for thoracic injections were prepared of equal volumes of cells in PBS and Matrigel stock, giving final dilution factor of approximately

×60. Matrigel was thawed on ice to avoid gel formation, which can rapidly occur at room temperature or above. In accordance with the manufacturer's instructions, all of the cell line suspensions, syringes, and needles were kept on ice before injections. To prepare suspensions of tumor cells in Matrigel, adherent tumor cells were harvested from subconfluent cultures by a brief exposure to 0.25% trypsin and 0.02% EDTA. Trypsinization was stopped with medium containing 10% serum, and the cells were washed once in serum-free medium and resuspended in PBS. Floating cells were collected after centrifugation. Trypan blue staining was used to assess cell viability, and only single-cell suspensions of >90% viability were used for the injections. Both Matrigel matrix and growth factor-reduced Matrigel matrix were used.

i.t. Injection. Mice anesthetized with sodium pentobarbital (50 mg/kg body weight) were placed in the right lateral decubitus position. One-ml tuberculin syringes (Becton Dickinson) with 30-gauge hypodermic needles were used to inject the cell inoculum percutaneously into the left lateral thorax, at the lateral dorsal axillary line, ~1.5 cm above the lower rib line just below the inferior border of the scapula. The needle was quickly advanced 5–7 mm into the thorax and was quickly removed after the injection of cell suspension. After tumor injection, the mouse was turned to the left lateral decubitus position. Animals were observed for 45–60 min until fully recovered.

s.c. Flank Injection. For s.c. flank injections, unanesthetized mice underwent s.c. injection of cells suspended in a volume of 100 µl HBSS (Sigma Chemicals Co., St. Louis, MO) directly into the flank using 1-ml tuberculin syringes (Becton Dickinson) with 30-gauge hypodermic needles. For chemotherapy experiments, mice were injected with tumor cells in 150 µl PBS with Matrigel. The cell suspension was prepared as described above for i.t. injection. Mice were then examined daily for evidence of tumor development.

In Vivo Selection of Cell Lines for Increased Tumorigenicity. Using the i.t. injection technique described above, NCI-H226 cells were injected into the lungs of nude mice. The mice were killed when moribund, and the largest thoracic tumors were harvested by aseptic techniques, dissociated mechanically using pipetting, and placed into culture for three to five passages (24). The cells were then reinjected into the lungs of nude mice.

In Vitro Selection for Increased Tumorigenicity: Growth in Semisolid Agarose. NCI-H69 *in vitro* selection for increased invasive properties *in vivo* was accomplished using agarose, as described previously (25, 26). Briefly, agarose (Sigma Chemical Co.) was dissolved in distilled water and autoclaved. Base layers of Eagle's MEM with tryptose phosphate broth, 10% FBS, and 0.6% agarose were set in six-well plastic dishes. Over this bottom layer, a second layer of medium containing agarose and a suspension of 1×10^6 single tumor cells was laid. The concentration of agarose in the top layer was 0.9%. After the top layer gelled, 1–2 ml of CMEM medium with 10% FBS was added. Colonies formed from single cells were harvested and expanded by growth as monolayer cultures for *in vivo* injection.

GFP Transfection Protocol. For GFP transfection, cultures of PC14PE6 and NCI-H358 at 70% confluency were transfected with pEGFP-C1 plasmid (Clontech Laboratories Inc.,

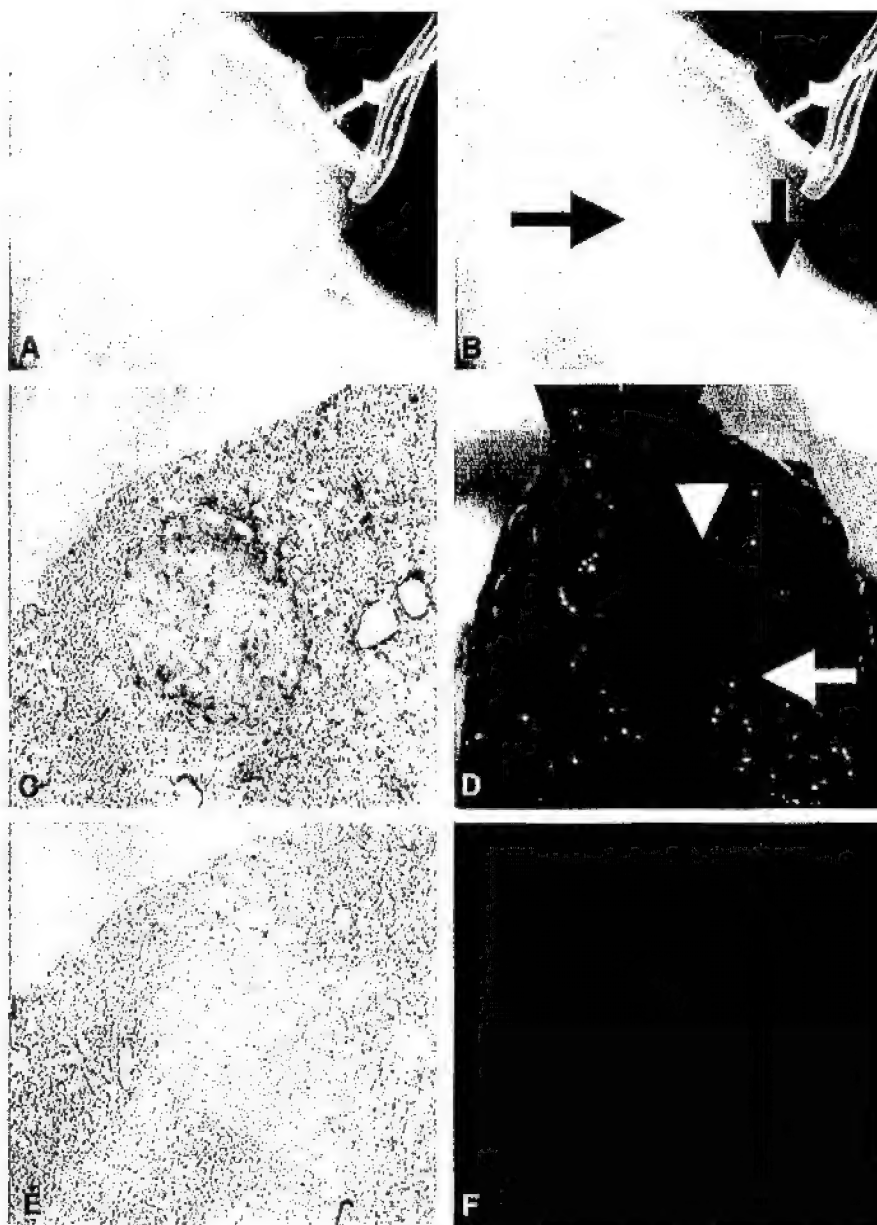


Fig. 1 *A*, to demonstrate fluid spreading after injection into the thorax, a 27.5-gauge needle was inserted into the left lung of a nude mouse (Faxitron X-ray image). *B*, the image was taken immediately after an injection of 75 μ l of iodhexol (omnipaque), an iodinated contrast agent. The fluid blunted the tip of the needle in the lung parenchyma and accumulated in the pleura according to gravity forces (arrows). *C*, the solitary nodules surrounded by a normal lung developed several days after injection of tumor cells with Matrigel, which anchored them and prevented cell suspension spread. PC14PE6 (adenocarcinoma) tumor, 9 days after tumor implantation. *D*, diffuse thoracic disease involving the injected site, the contralateral lung, and lymph nodes. Note the heart (arrowhead) and the small portion of the lung (arrow). *E*, IHC staining revealed that lung cancer in this system expressed bFGF from an early stage of disease. *F*, to study the sequence of metastasis we transfected two cell lines with GFP. The lesion is a microscopic left lung tumor on day 4 after injection of PC14PE6 cells with Matrigel. At this time, we found metastasis in the regional lymph nodes and the right lung.

Palo Alto, CA) using FuGene VI transfection reagents (Roche Molecular Biochemicals, Indianapolis, IN) according to the manufacturer's protocol. After 48 h, the cells were harvested by a 0.25% trypsin-0.02% EDTA solution and placed at a ratio of 1:15 into selective medium containing 800 μ g/ml G418 (Life Technologies, Inc., Gaithersburg, MD) and plated. Neomycin-resistant clones were isolated with cloning cylinders by trypsin-EDTA. For *in vivo* studies, clones with high-intensity GFP fluorescence and stability were pooled. PC14PE6 cells (0.5×10^6) or NCI-H358 cells (1×10^6) in Matrigel were injected into

the lungs of 10 mice. The mice (2/group) were killed at sequential time points thereafter.

Chemotherapy Studies. Therapeutic effects of paclitaxel were determined using NCI-H358 tumors implanted i.t. (1×10^6 cells in 75 μ l) or s.c. (2.5×10^6 cells in 150 μ l), or for PC14PE6 i.t. tumors (0.5×10^6 cells in 75 μ l) or s.c. (1.5×10^6 cells in 150 μ l). All of the cell suspensions were prepared in Matrigel. Four experiments were carried out with NCI-H358 i.t. tumors: one with s.c. tumors, one with PC14PE6 i.t., and two s.c. In all of the experiments, mice were randomized on day 7

Table 1 Production of thoracic tumors

Titration of human NSCLC and SCLC cell lines was conducted to determine the best number of cells needed to repeatedly produce orthotopic thoracic tumors in nude mice. Cells were injected in Matrigel into the left lung, as described in the text. Tumors metastasized to thoracic lymph nodes and the contralateral lung.

Cell line	Histology	Cell number	Tumor development	Survival (days)	Rt. lung metastases/ Lymph node metastases
PC14PE6	Adenocarcinoma ^a	0.5×10^6	10/10	26–30	+/+
		1×10^6	10/10	18–23	+/+
		2×10^6	10/10	14–18	+/+
NCI-H358	Bronchioloalveolar carcinoma	0.5×10^6	8/10	70–80	+/+
		1×10^6	9/10	56–63	+/+
		2×10^6	10/10	42–49	+/+
NCI-H226	Squamous	1.5×10^{6b}	10/10	63–70	+/+
		2×10^6	6/10	3.5–4 mo	+/+
NCI-H1299	Poorly diff NSCLC	1×10^6	10/10	32–40	+/+
A549	Poorly diff NSCLC	1×10^6	10/10	50–60	+/+
NCI-H69	SCLC	1.5×10^{6c}	9/10	50–56	+/+
		2×10^6	1/20	up to 4 mo	–/–

^a PC14PE6 tumors were associated with pleural effusion. The amount of effusion collected was inversely related to number of cells injected as described in "Results."

^b NCI-H226 cells were selected three cycles *in vivo* in the lung to improve tumor uptake and shorten survival time.

^c NCI-H69 cells were selected on agarose for a more tumorigenic clone.

after tumor implantation to a control arm (i.p. 200 μ l PBS/single dose/week) or a treatment arm [i.p. 200 μ l paclitaxel, dosages ranged from 100–200 μ g (4–8 mg/kg)/single dose/week]. For each of the cell lines, the experiment was terminated when i.t. control mice became moribund. Thus, all of the i.t. and s.c. mice for a particular cell line had the same number of chemotherapy cycles and, simultaneously, they were killed, autopsied, and tumor tissues were harvested.

Necropsy, Tissue Preparation, and IHC Staining. Mice were killed with a lethal dose of sodium pentobarbital (100 mg/kg body weight). Subsequent to a laparotomy, the thoracic cavity was inspected through the diaphragm for evidence of pleural effusion. Any pleural effusion was collected, and the thoracic organs were then removed enblock, including all of the lymph nodes and tumors. After dissection and removal of the heart, the lung and tumor mass were washed in cold PBS and weighed. Other visceral organs were removed and inspected for presence of metastases. Subcutis tumors were removed, washed in PBS, and weighed. For IHC and H&E staining procedures, one part of the tumor was fixed in formalin and embedded in paraffin, and another part was embedded in OCT compound (Miles, Inc., Elkhart, IN), rapidly frozen in liquid nitrogen, and stored in -80°C . IHC determination of bFGF, VEGF/VPF, and IL-8 were performed as described previously (27).

Microscopy and Imaging. For studies of tumor cells transfected with GFP, a Leica (model MZ FLIII) fluorescence dissecting stereomicroscope was used to visualize fluorescent metastases. The microscope was equipped with a 100-W, mercury vapor lamp power source and fitted with a GFP filter set. Images were processed using Image Pro Plus (version 4.0; Media Cybernetics, L.P., Silver Spring, MD) and Adobe Photoshop (version 5.5; Adobe Systems Inc., San Jose, CA). Digitalized imaging was performed using Faxitron specimen radiography system model MX-20 (Faxitron X-Ray Corp., Wheeling, IL). Energy was set to 26 kV, time to 10 s.

RESULTS

Formation of Lung Tumors. In the initial set of experiments, we determined the volume of tumor cell inoculum necessary to produce lung lesions without leading to immediate toxicity. For this purpose we used the highly metastatic B16BL6 melanoma cells, which were implanted into the lungs of syngeneic C57BL/6 mice. We selected the injection volume of 75 μ l Matrigel containing suspended tumor cells. The necessity of Matrigel as an anchor to tumor cells, to avoid diffuse spread in the thorax, is demonstrated in Fig. 1, A and B. Injection of tumor cells in saline resulted in spread according to gravity forces, whereas injection of tumor cells with Matrigel formed a solitary lesion as an initial focus of disease. Four NSCLC cell lines (PC14PE6, NCI-H1299, NCI-H358, and A549) suspended in Matrigel were injected into the left lung and produced solitary lesions that progressed to diffuse thoracic disease.

The characteristics of tumor development and metastasis for the various human lung cancer cell lines are summarized in Table 1. The adenocarcinoma (PC14PE6) was the most rapidly growing tumor. Typically, 9 days after injection, solitary lesions could be detected in sections of lung (Fig. 1C). Diffuse thoracic growth (Fig. 1D) lead to death by 2.5–4.5 weeks after injection, depending on the number of cells injected. At the time of death, lymph node metastasis (bilateral axilla and neck) was evident. An inverse ratio was found between the number of tumor cells injected and production of pleural effusion. The injection of 0.5×10^6 cells yielded 8 lung nodules sized 1–2 mm with 0.8 ml bloody pleural effusion. The injection of 1×10^6 cells produced larger tumors that occupied 80% of the thorax with 0.2 ml bloody pleural effusion, and the injection of 2×10^6 cells produced rapid death from extensive tumor with no pleural effusion. In all of the cases, the formation of pleural effusion was associated with pleural seeding by tumor cells. NCI-H12999 (poorly differentiated NSCLC) also produced rapidly growing tumors, and the mice died with diffuse disease 5 weeks

Table 2 Paclitaxel therapy of bronchioloalveolar (NCI-H358) and adenocarcinoma (PC14PE6) i.t. and s.c. tumors

Cells were implanted orthotopically in the lungs or subcutis as described in the text. In all experiments, paclitaxel therapy began on day 7 after tumor implantation. For each of the cell lines, the experiment was terminated when i.t. control mice became moribund. More pronounced effect was noticed in the subcutis tumor in comparison to the thoracic tumors, suggesting that paclitaxel had limited effect on the thoracic tumors in this system.

	Control			Paclitaxel		
	Lung and tumor weight (g)			Lung and tumor weight (g)		
	Incidence ^a	Median	Range	Incidence	Median	Range
Bronchioloalveolar thoracic tumors						
Study 1	10/10	0.307	0.219–0.515	10/10	0.266	0.192–0.342
Study 2	9/9	0.319	0.256–1.240	10/10	0.271	0.229–0.305
Study 3	9/9	0.345	0.266–1.313	9/9	0.215	0.171–0.338
Study 4 ^b	9/9	0.340	0.190–0.399	8/9	0.248	0.180–0.329
Bronchioloalveolar subcutis tumors						
Study 1 ^c	5/5	0.412	0.225–0.662	5/5	0.085	0.025–0.220
Adenocarcinoma thoracic tumors						
Study 1	5/5	0.320	0.298–0.350	5/5	0.231	0.192–0.300
Adenocarcinoma subcutis tumors						
Study 1 ^c	5/5	0.550	0.380–0.850	5/5	0.098	0.015–0.320
Study 2 ^{c,d}	5/5	1.728	0.950–1.950	5/5	0.542	0.132–1.700

^a Number of positive mice/number of mice survived the experiment.

^b Paclitaxel dosage was 200 µg/mouse/week in all experiments except study 4 of NCI-H358 thoracic tumors in which it was 100 µg/mouse week.

^c Tumor weight only reported.

^d In the PC14PE6 subcutis experiments, 1.5×10^6 cells were injected in the first study and 2×10^6 cells in the second study.

after injection. NCI-H358 (bronchioloalveolar carcinoma) cells produced tumors with an intermediate growth rate as compared with the other cell lines that were studied. Solitary nodules were found 2 weeks after injection of 1×10^6 cells, and mice died of progressive disease 8–9 weeks later. A549 (poorly differentiated NSCLC) cells formed slow-growing tumors leading to cachexia characterized by wasting of the interscapular muscles. None of the mice studied became cyanotic, and mice were killed on the development of labored mouth breathing.

Tumorigenicity in Orthotopic and Ectopic Organs. Two human NSCLC cell lines suspended in saline or Matrigel were injected s.c. into the right flank of 5 mice/group. The rate of tumor development was similar in all of the mice. NCI-H358 cells developed s.c. tumors in 80% of mice injected with 2.5×10^6 cells, whereas 100% of mice injected i.t. with 2×10^6 cells developed lung tumors. PC14PE6 cells produced s.c. tumors in 80% of mice injected with 1×10^6 cells, whereas all of the mice injected i.t. with 0.5×10^6 cells developed lung tumors. Thoracic tumors were fatal in all of the mice, whereas s.c. tumors were not associated with mortality when tumors reached maximal permissible size.

Serial *In Vivo* Passages for Selection of Cells with Increased Tumorigenicity. The squamous cell carcinoma cell line NCI-H226 produced slow-growing tumors with no pleural effusion. Injection of 0.5×10^6 or 1×10^6 cells did not form visible tumors up to 4 months after tumor implantation. Six of 10 mice injected i.t. with 2×10^6 cells developed a thoracic tumor and became moribund 3.5–4 months after tumor injection. The largest tumors were harvested and established *in vitro*. Viable cells were harvested and reinjected into the lungs of nude mice. After three such selection cycles, a cell line with an increased tumorigenicity was isolated (Table 1).

***In Vitro* Agarose Selection Enhanced the *In Vivo* Tumorigenicity of NCI-H69 Cells.** The injection of human SCLC NCI-H69 (0.5×10^6 , 1×10^6 , and 2×10^6 cells) into the lungs of nude mice did not form tumors. In 1 mouse injected i.t. with 2×10^6 cells, a 2-mm tumor was found 12 weeks after injection. To enhance the invasive potential of the parental NCI-H69 cell line, a method of *in vitro* selection using anchorage-independent growth of cells in agarose (25, 26) was used. The selection process was twice repeated using higher concentrations of top layer agarose from 0.9% to 1.2% (Table 1). After two cycles of selection in agarose, tumor cells formed lung tumors in all of the mice injected i.t.

Lung and Lymphatic Metastasis of NSCLC Tumor Cells After i.t. Injection. To study tumor progression and metastasis, adenocarcinoma (PC14PE6) and bronchioloalveolar carcinoma (NCI-H358) cells were transfected with GFP. Ten mice were injected with either 0.5×10^6 or 1×10^6 cells in Matrigel, into the left lung as described above. Two mice were killed at 4–7-day intervals. All of the mice injected developed microscopic tumors identified by fluorescence microscopy (Fig. 1F). PC14PE6 progressed to mediastinal lymph nodes and spread to the right lung on day 4 after tumor implantation. In NCI-H358 tumors, lymph node and right lung lesions were detected on day 28 after injection.

Chemotherapy Study. We studied the effect of paclitaxel on NCI-H358 (bronchioloalveolar carcinoma) and PC14PE6 (adenocarcinoma) tumors, growing in the lungs or the subcutis. In all of the experiments, therapy began on day 7 after tumor inoculation. We conducted several experiments using 100 or 200 µg (4 or 8 mg/kg)/dose paclitaxel. Therapy was administered for up to five cycles or until control mice became moribund. Mice injected with NCI-H358 were treated for five cycles and killed 7.5–9 weeks after tumor injection. Mice injected with PC14PE6 cells, a more aggres-

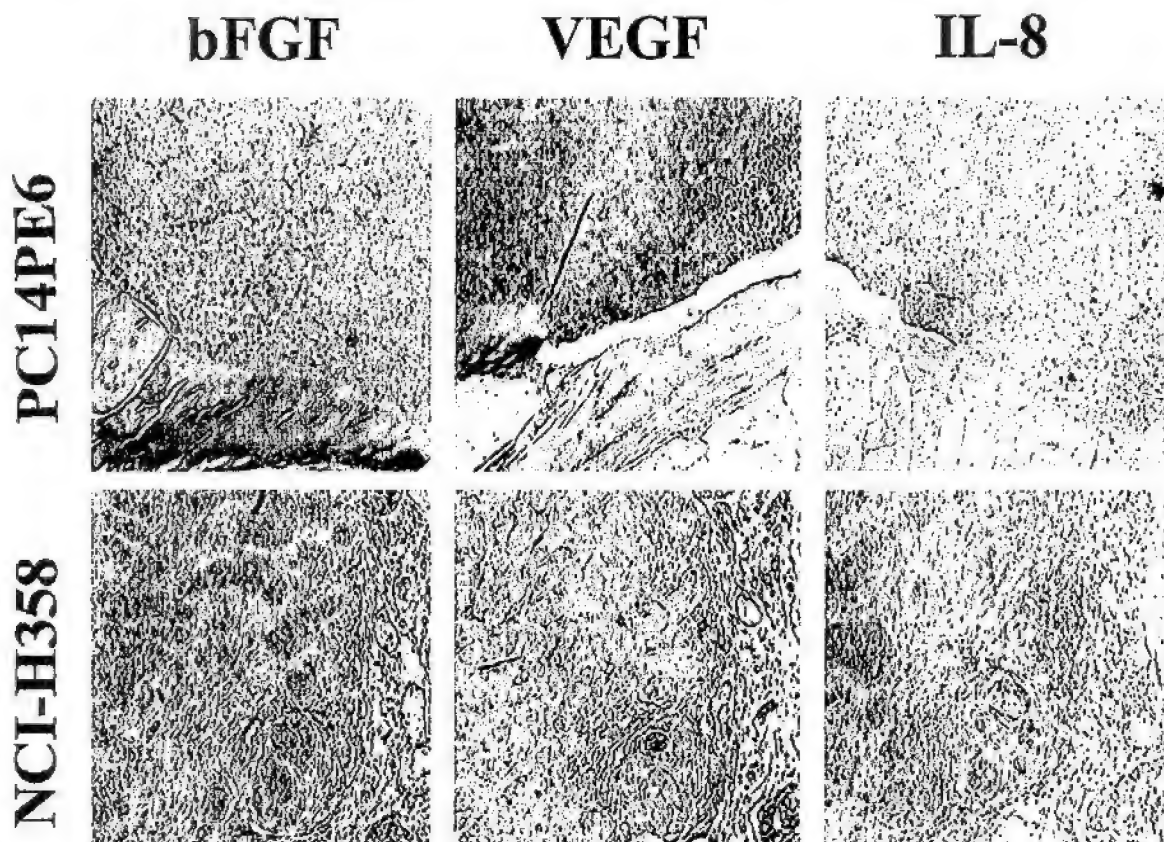


Fig. 2 IHC staining for bFGF, VEGF/VPF, and IL-8 of PC14PE6 and NCI-H358 orthotopic tumors. Although all of the factors were expressed by the two tumors, VEGF/VPF expression was prominent in PC14PE6 tumor, an adenocarcinoma that produces pleural effusion.

sive cell line, were treated for four cycles and were killed 4 weeks after tumor implantation. Control mice in the s.c. injected groups did not have evidence of morbidity at the end of the experiment. All of the mice in all of the groups tolerated therapy well, as assessed by similar median body weights in control *versus* treatment groups (data not shown). The results of all of these experiments suggest that whereas paclitaxel is efficacious in controlling tumor growth in the lungs, it is much more effective for treating s.c. tumors (Table 2). The treatment results of the thoracic tumors did not vary significantly when using 100 or 200 μ g/dose paclitaxel. Similarly, the drug effect did not change significantly when by 7.5 or 9 weeks after tumor implantation.

Immunohistochemical Analysis of Thoracic Tumors. Thoracic tumors were examined for expression of several proangiogenic factors including bFGF, IL-8, and VEGF/VPF. These factors were expressed at an early stage of tumor progression, as noted by positive staining for bFGF in PC14PE6 tumors on day 9 after injection (Fig. 1B). A differential pattern of expression for each growth factor was noted between the different types of lung cancer. The pleural effusion producing adenocarcinoma (PC14PE6) tumors expressed higher levels of VEGF/VPF as compared with IL-8 and bFGF. These three factors were also

expressed by the bronchioloalveolar tumors (NCI-H358), although to similar degree (Fig. 2). The NCI-H358 tumor had low expression of E-cadherin and high expression of matrix metalloproteinase 2 (data not shown).

DISCUSSION

We have developed reliable and reproducible orthotopic nude mouse models of lung cancer in a stepwise fashion. First, we verified the feasibility of thoracic injection and the development of regional metastasis using the pigmented B16BL6 melanoma cell line in syngeneic mice. Next, four different human lung tumor lines were injected into the lung of nude mice: PC14PE6, a pleural effusion producing adenocarcinoma, NCI-H358 bronchioloalveolar carcinoma, and NCI-H1299 and A549 poorly differentiated NSCLC lines. Two additional tumor lines developed tumors after selection for more aggressive and invasive clones: NCI-H226 squamous cell carcinoma was selected *in vivo* in the lung using our model, and NCI-H69 small cell lung carcinoma was selected on agarose *in vitro*. For each of the lung cancer cell lines studied, tumors formed as a single focus at the site of injection into the lung. Tumors then grew progressively within the injected lung and spread to regional and

extrathoracic lymph nodes, and the contralateral lung. The pattern of spread of lung cancer within the thorax is similar to that observed clinically in patients with lung cancer, suggesting that the model is clinically relevant. The absence of clinically apparent distant metastasis is most likely due to the aggressive pattern of locoregional spread of cancer cells with mice dying of diffuse thoracic disease before development of significant distant metastasis. To overcome this potential limitation, complementary models of metastatic disease (*i.e.*, brain, liver, and bone models) are now being developed for each of the lung cancer types.

This model validates the orthotopic principle that tumor cells grow better in their tissue of origin and that more clinically relevant studies can be performed using the orthotopic site of tumor growth. The importance of orthotopic models to study the biology and therapy of cancer had been demonstrated for other neoplasms (4, 7). Chen *et al.* (28) studied the interaction between NSCLC tumors and macrophages in surgical specimens and in cell lines, and found that the importance of tumor cell and microenvironment interaction holds also for the lung. They suggested that this interaction up-regulated the expression of IL-8 by the tumor. Furthermore, high-density infiltration of tumor by macrophages was correlated with increased tumor angiogenesis and adverse outcome in NSCLC patients. Moreover, our model closely resembles human lung cancer in its partial response to chemotherapy. Although treated mice had shown a reduction in tumor burden in response to paclitaxel (as assessed by lung and tumor weight), a more dramatic response was noted in s.c. tumors. This effect of paclitaxel on s.c. implanted tumors may in part explain the difficulty with the translation into a clinical reality of dramatic responses to therapy that have been observed for anticancer agents in preclinical studies that rely solely on s.c. tumor xenografts (6). Therefore, it may be prudent to first screen novel anticancer agents in s.c. tumor models and to then screen active agents in orthotopic models before the initiation of clinical trials.

To date, several orthotopic rodent models have been developed to study human lung cancer. Different techniques have been used to introduce tumors including intrabronchial implantation of a tumor cell inoculum (9–11) with resultant tumor formation in the center of the thorax in 35–95% of animals. However, intrabronchial techniques necessitated irradiation and tracheostomy or laryngoscopy and were associated with operative mortality of >5%. Alternatively, intrapleural implantation of a tumor cell inoculum without Matrigel has been used (12, 13), which resulted in the development of extrathoracic tumors and an operative mortality of 5–10%. Tumors can also be implanted in the lung parenchyma after skin incision (14) or thoracotomy and surgical exploration of the pleura (15–17). The skin incision model was associated with low operative mortality yet was much more time consuming and laborious, whereas the thoracotomy model was associated with mortality of about 5%. Another common technique used surgical human cancerous specimens, which were implanted into the lungs (8). However, in this system the number of tumor cells varies between surgical specimens. To date, none of these models had been widely accepted, and most research is still done using s.c. models.

The models of lung cancer that we describe complement those that have been developed previously and may overcome

some of the limitations associated with them. We have developed orthotopic models of each of the common types of lung cancer, which should lead to an improved understanding of the influence of tumor histology on response to existing and emerging therapies. The techniques needed for our models are reproducible, can be performed quickly (*i.e.*, each mouse can be injected in under 15 s), and are easily taught. It is associated with virtually no procedure related animal mortality. Whereas pneumothorax may occur, as shown in 3 of 10 treated mice studied with X-ray imaging (Faxitron; data not shown), death within 72 h of the thorax puncture is <1%. Matrigel is used to provide a reproducible anchor, which fixes the tumor cells to the site of injection and avoid cell dispersion. In most experiments we used growth factor-reduced Matrigel. It contains limited amounts of growth factors, which are additionally diluted in the process of cell suspension preparation. Overall tumor cell implantation with its addition results in a reproducible tumor size, which enables therapeutic experiments as demonstrated with paclitaxel as well as study of tumor biology and metastasis.

Of special interest is the expression of proangiogenic factors by the implanted lung tumors. The significance of bFGF, VEGF/VPF, and IL-8 in human NSCLC had been studied extensively, and their expression had been shown to correlate with poor outcome in human lung cancer patients (29). These factors are important for tumor progression and the formation of the angiogenic phenotype from an early stage disease. In our model of lung adenocarcinoma, bFGF was expressed by early and locally advanced human lesions in the lungs of nude mice. These data are consistent with what has been observed in the clinic, because bFGF was shown to play a key role in human lung cancer progression (30) and was expressed even in small tumors (≤ 2 cm) growth (31). Taken together, the data suggest that it may be prudent to target bFGF for lung adenocarcinoma using anti-bFGF therapies such as low dose-daily IFN (32). In our model of bronchioloalveolar carcinoma (NCL-H358), tumors were found to have low expression of E-cadherin (associated with cell-to-cell cohesion and adhesion) and high expression of matrix metalloproteinase 2 (associated with invasion). This proportion had been found to correlate with increased human lung cancer tumor aggressiveness (33), which substantiates the metastatic behavior of this tumor. Interestingly, VEGF/VPF expression was higher in lung adenocarcinomas (PC14PE6) than for other lung cancer histologies, which may be related to production of pleural effusion by PC14PE6 tumors. Indeed, Senger *et al.* (34) had identified this molecule by its ability to induce vascular leaking and named it vascular permeability factor. Yano *et al.* (19) had found the relation between VEGF/VPF and PC14PE6 tumors in a metastatic tumor and, as far as we know, our finding is the first in an orthotopic model.

In summary, we have developed *in vivo* models of primary lung cancer for both human NSCLC and human SCLC, which are reproducible, well tolerated, feasible, and straightforward to perform. These lung cancer models closely mimic the patterns observed for the natural progression of primary lung cancer from a single nodule to disseminated disease, and enables study of novel therapeutics and better understanding of lung cancer metastasis.

ACKNOWLEDGMENTS

We thank Bich Tran for her assistance in the preparation of this manuscript.

REFERENCES

- Jemal, A., Murray, T., Samuels, A., Ghafoor, A., Ward, E., and Thun, M. J. Cancer statistics, 2003. *CA. Cancer J. Clin.*, 53: 5-26, 2003.
- Carney, D. N. Lung cancer—time to move on from chemotherapy. *N. Engl. J. Med.*, 346: 126-128, 2002.
- Paget, S. The distribution of secondary growths in cancer of the breast. 1889. *Cancer Metastasis Rev.*, 8: 98-101, 1989.
- Wilhanns, C., Fan, D., O'Brian, C. A., Bucana, C. D., and Fidler, I. J. Orthotopic and ectopic organ environments differentially influence the sensitivity of murine colon carcinoma cells to doxorubicin and 5-fluorouracil. *Int. J. Cancer*, 52: 98-104, 1992.
- Kuo, T. H., Kubota, T., Watanabe, M., Furukawa, T., Kase, S., Tanino, H., Saikawa, Y., Ishibiki, K., Kitajima, M., and Hoffman, R. M. Site-specific chemosensitivity of human small-cell lung carcinoma growing orthotopically compared to subcutaneously in SCID mice: The importance of orthotopic models to obtain relevant drug evaluation data. *Anticancer Res.*, 13: 627-630, 1993.
- Killion, J. J., Radinsky, R., and Fidler, I. J. Orthotopic models are necessary to predict therapy of transplantable tumors in mice. *Cancer Metastasis Rev.*, 17: 279-284, 1998.
- Fidler, I. J. Critical factors in the biology of human cancer metastasis: Twenty-eighth G. H. A. Clowes memorial award lecture. *Cancer Res.*, 50: 6130-6138, 1990.
- Hoffman, R. M. Orthotopic metastatic mouse models for anticancer drug discovery and evaluation: a bridge to the clinic. *Investig. New Drugs*, 17: 343-359, 1999.
- McLemore, T. L., Liu, M. C., Blacker, P. C., Gregg, M., Alley, M. C., Abbott, B. J., Shoemaker, R. H., Bohlman, M. E., Litterst, C. C., and Hubbard, W. C. Novel intrapulmonary model for orthotopic propagation of human lung cancers in athymic nude mice. *Cancer Res.*, 47: 5132-5140, 1987.
- Howard, R. B., Chu, H., Zeligman, B. E., Marcell, T., Bunn, P. A., McLemore, T. L., Mulvin, D. W., Cowen, M. E., and Johnston, M. R. Irradiated nude rat model for orthotopic human lung cancers. *Cancer Res.*, 51: 3274-3280, 1991.
- Hastings, R. H., Burton, D. W., Quintana, R. A., Biederman, E., Gujral, A., and Deftos, L. J. Parathyroid hormone-related protein regulates the growth of orthotopic human lung tumors in athymic mice. *Cancer (Phila.)*, 92: 1402-1410, 2001.
- McLemore, T. L., Eggleston, J. C., Shoemaker, R. H., Abbott, B. J., Bohlman, M. E., Liu, M. C., Fine, D. L., Mayo, J. G., and Boyd, M. R. Comparison of intrapulmonary, percutaneous intrathoracic, and subcutaneous models for the propagation of human pulmonary and nonpulmonary cancer cell lines in athymic nude mice. *Cancer Res.*, 48: 2880-2886, 1988.
- Kraus-Berthier, L., Jan, M., Guilbaud, N., Naze, M., Pierre, A., and Atassi, G. Histology and sensitivity to anticancer drugs of two human non-small cell lung carcinomas implanted in the pleural cavity of nude mice. *Clin. Cancer Res.*, 6: 297-304, 2000.
- Doki, Y., Murakami, K., Yamaura, T., Sugiyama, S., Misaki, T., and Saiki, I. Mediastinal lymph node metastasis model by orthotopic intrapulmonary implantation of Lewis lung carcinoma cells in mice. *Br. J. Cancer*, 79: 1121-1126, 1999.
- Wang, H. Y., Ross, H. M., Ng, B., and Burt, M. E. Establishment of an experimental intrapulmonary tumor nodule model. *Ann. Thorac. Surg.*, 64: 216-219, 1997.
- Miyoshi, T., Kondo, K., Ishikura, H., Kinoshita, H., Matsumori, Y., and Monden, Y. SCID mouse lymphogenous metastatic model of human lung cancer constructed using orthotopic inoculation of cancer cells. *Anticancer Res.*, 20: 161-163, 2000.
- Boehle, A. S., Dohrmann, P., Leuschner, L., Kalthoff, H., and Henne-Bruns, D. An improved orthotopic xenotransplant procedure for human lung cancer in SCID bg mice. *Ann. Thorac. Surg.*, 69: 1010-1015, 2000.
- Yano, S., Nokihara, H., Hanibuchi, M., Parajuli, P., Shinohara, T., Kawano, T., and Sone, S. Model of malignant pleural effusion of human lung adenocarcinoma in SCID mice. *Oncol. Res.*, 9: 573-579, 1997.
- Yano, S., Herbst, R. S., Shinohara, H., Knighton, B., Bucana, C. D., Killian, J. J., Wood, J., and Fidler, I. J. Treatment for malignant pleural effusion of human lung adenocarcinoma by inhibition of vascular endothelial growth factor receptor tyrosine kinase phosphorylation. *Clin. Cancer Res.*, 6: 957-965, 2000.
- Levitt, M. L., Gazdar, A. F., Oie, H. K., Schuller, H., and Thacher, S. M. Cross-linked envelope-related markers for squamous differentiation in human lung cancer cell lines. *Cancer Res.*, 50: 120-128, 1990.
- Fidler, I. J. Selection of successive tumour lines for metastasis. *Nat. New Biol.*, 242: 148-149, 1973.
- Nicolson, G. L., Brunson, K. W., and Fidler, I. J. Specificity of arrest, survival, and growth of selected metastatic variant cell lines. *Cancer Res.*, 38: 4105-4111, 1978.
- Fidler, I. J. Rationale and methods for the use of nude mice to study the biology and therapy of human cancer metastasis. *Cancer Metastasis Rev.*, 5: 29-49, 1986.
- Myers, J. N., Holsinger, F. C., Jasser, S. A., Bekalo, B. N., and Fidler, I. J. An orthotopic nude mouse model of oral tongue squamous cell carcinoma. *Clin. Cancer Res.*, 8: 293-298, 2002.
- Cifone, M. A., and Fidler, I. J. Correlation of patterns of anchorage-independent growth with *in vivo* behavior of cells from a murine fibrosarcoma. *Proc. Natl. Acad. Sci. USA*, 77: 1039-1043, 1980.
- Li, L., Price, J. E., Fan, D., Zhang, R. D., Bucana, C. D., and Fidler, I. J. Correlation of growth capacity of human tumor cells in hard agarose with their *in vivo* proliferative capacity at specific metastatic sites. *J. Natl. Cancer Inst.*, 81: 1406-1412, 1989.
- Baker, C. H., Solorzano, C. C., and Fidler, I. J. Blockade of vascular endothelial growth factor receptor and epidermal growth factor receptor signaling for therapy of metastatic human pancreatic cancer. *Cancer Res.*, 62: 1996-2003, 2002.
- Chen, J. J., Yao, P. L., Yuan, A., Hong, T. M., Shun, C. T., Kuo, M. L., Lee, Y. C., and Yang, P. C. Up-regulation of tumor interleukin-8 expression by infiltrating macrophages: its correlation with tumor angiogenesis and patient survival in non-small cell lung cancer. *Clin. Cancer Res.*, 9: 729-737, 2003.
- Onn, A., and Herbst, R. S. Angiogenesis, metastasis, and lung cancer: An overview. In: B. Driscoll (ed.), *Molecular Pathology Methods and Review 1*, pp. 329-348. Totowa: Humana Press, 2002.
- Volm, M., Koomagi, R., Mattern, J., and Stämmler, G. Angiogenic growth factors and their receptors in non-small cell lung carcinomas and their relationships to drug response *in vitro*. *Anticancer Res.*, 17: 99-103, 1997.
- Ito, H., Oshita, F., Kameda, Y., Suzuki, R., Ikehara, M., Arai, H., Mitsuda, A., Saito, H., Yamada, K., Noda, K., and Nakayama, H. Expression of vascular endothelial growth factor and basic fibroblast growth factor in small adenocarcinomas. *Oncol. Rep.*, 9: 119-123, 2002.
- Slaton, J. W., Perrotte, P., Inoue, K., Dinney, C. P., and Fidler, I. J. Interferon- α -mediated down-regulation of angiogenesis-related genes and therapy of bladder cancer are dependent on optimization of biological dose and schedule. *Clin. Cancer Res.*, 5: 2726-2734, 1999.
- Herbst, R. S., Yano, S., Kuniyasu, H., Khuri, F. R., Bucana, C. D., Guo, F., Liu, D., Kemp, B., Lee, J. J., Hong, W. K., and Fidler, I. J. Differential expression of E-cadherin and type IV collagenase genes predicts outcome in patients with stage I non-small cell lung carcinoma. *Clin. Cancer Res.*, 6: 790-797, 2000.
- Senger, D. R., Galli, S. J., Dvorak, A. M., Perruzzi, C. A., Harvey, V. S., and Dvorak, H. F. Tumor cells secrete a vascular permeability factor that promotes accumulation of ascites fluid. *Science (Wash. DC)*, 219: 983-985, 1983.

Epidermal Growth Factor Receptor Tyrosine Kinase Inhibitor Does Not Improve Paclitaxel Effect in an Orthotopic Mouse Model of Lung Cancer

Amir Onn,^{1,2} Takeshi Isoke,¹ Wenjuan Wu,¹
Satoshi Itasaka,^{1,3} Tomoaki Shintani,^{1,3}
Keiko Shibuya,^{1,3} Yokoi Kenji,¹
Michael S. O'Reilly,^{1,3} Isaiah J. Fidler,¹ and
Roy S. Herbst^{1,2}

Departments of ¹Cancer Biology, ²Thoracic/Head and Neck Medical Oncology, and ³Radiation Oncology, The University of Texas M. D. Anderson Cancer Center, Houston, Texas

ABSTRACT

Purpose: The purpose is to evaluate whether inhibition of epidermal growth factor receptor (EGFR) activation by PKI166, an EGFR-tyrosine kinase inhibitor, affects growth of human lung cancer implanted orthotopically into the lungs of nude mice.

Experimental Design: Lungs of mice were injected with NCI-H358 human bronchioloalveolar cancer cells. In three experiments, groups of mice ($n = 10$ per group) were randomized 7 days after tumor implantation to receive one of the following treatments: i.p. paclitaxel 100 or 200 μ g (4 or 8 mg/kg) once per week, oral PKI166 100 or 200 mg/kg three times per week, paclitaxel plus PKI166, or i.p. saline and oral PKI166-vehicle (control) for 5 weeks. Mice were killed 6.5 to 8 weeks after tumor implantation. The experiments were repeated with PC14PE6 human lung adenocarcinoma cells to assess effect on survival.

Results: Immunohistochemical analyses revealed the expression and phosphorylation of EGFR in the growing tumors. Treatment with PKI166 alone or in combination with paclitaxel diminished activation of EGFR on tumor cells, yet maximal therapeutic effect was observed in mice treated with paclitaxel alone. Activated mitogen-activated protein kinase and basic fibroblast growth factor expression

were similar in all treatment groups. Survival in mice treated with the combination of paclitaxel and PKI166 was shorter than in those treated with paclitaxel alone.

Conclusions: Our results suggest that concurrent administration of EGFR-tyrosine kinase inhibitor and chemotherapy is equivalent and may indeed be inferior to chemotherapy alone, even if EGFR is functional and its phosphorylation effectively inhibited. Our data show that the interaction of EGFR-TKIs and chemotherapy is complex and suggest that other growth factors may activate the downstream signaling events.

INTRODUCTION

Non-small-cell lung cancer (NSCLC) is the most common form of lung cancer and the leading cause of cancer-related death in the world (1). Systemic chemotherapy is the main treatment for the majority of patients with NSCLC because most are diagnosed with advanced inoperable disease. However, recent studies have shown that modern chemotherapeutics may have reached the ceiling of their clinical efficacy, and the 5-year survival rate for NSCLC has plateaued at 14% (2). These findings show that a new approach to the therapy of lung cancer is mandatory.

Targeting the epidermal growth factor receptor (EGFR) is one appealing strategy for the treatment of lung cancer because the EGFR plays a pivotal role in tumor cell proliferation, survival, adhesion, migration, differentiation, and angiogenesis (3). Indeed, increased expression of EGFR, one of the earliest and most frequently detected abnormalities in the bronchial epithelium of heavy smokers (4), is pronounced in the majority of NSCLC cases (5, 6). However, the relationship between EGFR expression and the prognosis of NSCLC patients is still not well established, and retrospective studies of EGFR expression in stage I disease have yielded conflicting results (7). Several approaches to block EGFR-mediated signaling pathways are under evaluation, including using monoclonal antibodies (MAbs) against the ligand or receptor, ligand-toxin conjugates, antisense oligonucleotides, and receptor tyrosine kinase inhibitors (8). A recent phase II trial of monotherapy with the anti-EGFR-tyrosine kinase inhibitor gefitinib (Iressa, ZD1839, AstraZeneca Pharmaceuticals, Wilmington, De) showed tumor response rate of 10%, a stable disease of 30%, and a symptom response rate of 40% (9, 10) for lung cancer patients. Paez *et al.* (11) and Lynch *et al.* (12) recently studied EGFR mutation status in patients treated with gefitinib and found that somatic mutations in tyrosine kinase site characterize responders to therapy.

The clinical effects of several EGFR-tyrosine kinase inhibitors were studied intensively both *in vitro* and *in vivo*, either alone or in combination with diverse chemotherapeutics. Ciardiello *et al.* (13) and Sirotnak *et al.* (14) studied the effect

Received 6/25/04; revised 9/3/04; accepted 9/23/04.

Grant support: An M. D. Anderson Cancer Center Physician Scientist Program Award (R. Herbst), an American Society of Clinical Oncology Clinical Research Career Development Award (R. Herbst), NIH Specialized Program of Research Excellence in Lung Cancer Grant P50 CA70907 (R. Herbst), and an award from the CRH Foundation (R. Herbst).

The costs of publication of this article were defrayed in part by the payment of page charges. This article must therefore be hereby marked advertisement in accordance with 18 U.S.C. Section 1734 solely to indicate this fact.

Requests for reprints: Roy S. Herbst, The University of Texas M. D. Anderson Cancer Center, 1515 Holcombe Boulevard, Unit 432, Houston, TX 77030. Phone: (713) 792-6363; Fax: (713) 796-8655; E-mail: rherbst@mdanderson.org.

©2004 American Association for Cancer Research.

of gefitinib in combination with different chemotherapeutics. PKI166 (Novartis, Switzerland) was studied by Bruns *et al.* (15) in an orthotopic model of human pancreatic cancer in nude mice and by Kim *et al.* (16) and Weber *et al.* (17) in models of human prostate cancer and renal cell cancer growing in the bones of nude mice. In these models, therapy with PKI166 was associated with decreased tumor growth and metastasis, and the anti-tumor effect was enhanced by chemotherapy. We recently developed an orthotopic lung cancer model (18). In this system, human lung cancer cells were injected into the left lung of nude mice. Tumors formed from a single focus of disease and progressed to a widespread and fatal thoracic process, characterized by diffuse dissemination of lung cancer in both lungs and metastasis to intra- and extrathoracic lymph nodes.

The purpose of the present study was to evaluate whether inhibition of EGFR activation by PKI166 affects tumor growth and metastasis of human lung cancer implanted orthotopically into the lungs of nude mice. We studied human bronchioloalveolar cancer (NCI-H358) and lung adenocarcinoma (PC14PE6), which both express the EGFR and the activated EGFR. The results of these studies show that therapy with PKI166 either alone or in combination with paclitaxel inhibited EGFR activation for lung cancer cells growing in the lung. However, the therapeutic efficacy of the regimen of concurrent PKI166 and paclitaxel was inferior to that of paclitaxel alone. These results are similar to those of recent human clinical trials with gefitinib (19, 20), which demonstrated that gefitinib showed no added benefit compared with standard chemotherapy alone in patients with advanced lung cancer. Our data strongly suggest that other growth factors may bypass the EGFR blockade and activate the downstream signaling events.

MATERIALS AND METHODS

Cell Lines and Tissue Culture Conditions. Bronchioloalveolar lung carcinoma cells (NCI-H358) were obtained from the American Type Culture Collection (Manassas, VA). A variant (PC14PE6) of the lung adenocarcinoma cell line PC14 that was selected to produce pleural effusion when injected into mice had been described previously (21, 22). Human bladder cancer (253J-BV), a cell line that highly expresses EGFR and activated EGFR (23), was used as a positive control for the *in vitro* studies. Adherent monolayer cultures of NCI-H358 and 253J-BV cells and floating and adherent monolayer cultures of PC14PE6 cells were incubated at 37°C in 5% CO₂-95% air. NCI-H358 cells were cultured in RPMI 1640 supplemented with 10% fetal bovine serum, L-glutamine, and penicillin-streptomycin, and 253J-BV cells were maintained in DMEM supplemented with 5% fetal bovine serum, sodium pyruvate, nonessential amino acids, L-glutamine, 2-fold vitamin solution (Life technologies, Inc., Grand Island, NY), and a penicillin-streptomycin mixture (Flow Laboratories, Rockville, MD). The tumor cell cultures were free of *Mycoplasma* and the following pathogenic murine viruses: retrovirus type 3, pneumonia virus, K virus, Theiler's encephalitis virus, Sendai virus, minute virus, mouse adenovirus, mouse hepatitis virus, lymphocytic choriomeningitis virus, ectromelia virus, and lactate dehydrogenase virus (assayed by Microbiological Associates, Bethesda, MD).

Reagents. PKI166, an EGFR-tyrosine kinase inhibitor, was synthesized and provided by Novartis Pharma AG (Basel, Switzerland). For *in vivo* administration, PKI166 was dissolved in DMSO/0.5% Tween 80 and then diluted 1:20 in HBSS (15, 16); paclitaxel (Taxol) was purchased from Bristol-Myers Squibb (Princeton, NJ) and dissolved in water for i.p. injections; Matrigel Matrix Growth Factor Reduced was purchased from Becton Dickinson & Co. (San Jose, CA; ref. 18); all antibodies were purchased as listed; (a) rabbit anti-basic fibroblast growth factor-2 (bFGF), rabbit anti-EGF, and rabbit anti-EGFR were purchased from Santa Cruz Biotechnology (Santa Cruz, CA); (b) rabbit anti-phospho-EGFR (activated EGFR; Tyr⁸⁴⁵), rabbit polyclonal phospho-p44/42 mitogen-activated protein kinase (MAPK; Thr²⁰²/Tyr²⁰⁴) were purchased from Cell Signaling Technology, Inc. (Beverly, MA); and (c) the enhanced chemiluminescence detection system was purchased from Amersham, Inc. (Arlington Heights, IL).

Animals and Animal Care. Male athymic nude mice (NCI-nu) were purchased from the Animal Production Area of the National Cancer Institute-Frederick Cancer Research and Development Center (Frederick, MD). The mice were housed and maintained in specific pathogen-free conditions in facilities approved by the American Association for Accreditation of Laboratory Animal Care and in accordance with current regulations and standards of the United States Department of Agriculture, United States Department of Health and Human Services, and the NIH. The mice were used in accordance with institutional guidelines when they were 6 to 10 weeks old.

Western Blot Analysis of EGFR, EGFR Phosphorylation of Lung Cancer Cell Lines, and Response to Treatment with PKI166. Serum-starved NCI-H358 cells were studied for the expression of EGFR and activated EGFR, with or without the stimulation of 40 ng/mL recombinant human EGF for 15 minutes. Serum-starved NCI-H358 cells were then treated with PKI166 (0, 0.5, 1, 2.5, and 5 μ mol/L) for 60 minutes and then incubated with or without 40 ng/mL recombinant human EGF for 15 minutes, washed, scraped into PBS containing 5 mmol/L EDTA and 1 mmol/L sodium orthovanadate, and centrifuged. The pellet was resuspended in lysis buffer [20 mmol/L Tris-HCl (pH 8.0), 137 mmol/L NaCl, 10% glycerol, 2 mmol/L EDTA, 1 mmol/L phenylmethylsulfonyl fluoride, 20 μ mol/L leupeptin, and 0.15 unit/mL aprotinin], sonicated, and centrifuged to recover insoluble protein. Immunoprecipitation was done with monoclonal antibody anti-EGFR (clone EGF-R1) as described previously (15-17). Immunoprecipitates were analyzed on 7.5% SDS-PAGE and transferred onto 0.45- μ m nitrocellulose membranes. The filters were blocked with 3% BSA in TBS [20 mmol/L Tris-HCl (pH 7.5) and 150 mmol/L NaCl], probed with either polyclonal sheep antihuman EGFR (1:1000) or monoclonal anti-phospho-tyrosine (monoclonal antibody 4G10; 1:2000) in TTBS (0.1% Tween 20 in TBS), and incubated with horseradish peroxidase-conjugated donkey antisheep IgG (1:2000; Sigma, St. Louis, MO) or sheep antimouse IgG (1:2000), respectively, in TTBS. Protein bands were visualized by the enhanced chemiluminescence detection system.

Preparation of Cell Suspension and Orthotopic Implantation of Tumor Cells. Cells were injected with Growth Factor Reduced Matrigel, which anchors the tumor cells, thereby preventing their diffusion into the thorax. For all experiments, a

stock solution of 500 μ g of Matrigel in 1 mL of PBS was used. Suspensions were prepared of equal volumes of cells in PBS and Matrigel stock. Matrigel was thawed on ice, and all cell line suspensions, syringes, and needles were kept on ice before the injections. Suspensions of tumor cells in Matrigel were prepared as described previously (18). For intrathoracic injection, mice were anesthetized with sodium pentobarbital (50 mg/kg body weight) and placed in the right lateral decubitus position. Cell inoculum was injected percutaneously into the left lung with 1-ml tuberculin syringes (Becton Dickinson & Co.) with 30-gauge hypodermic needles.

Therapy for Established Human Lung Cancer Tumors Growing in the Lung of Athymic Nude Mice. In the initial set of experiments, the presence of microscopic tumor lesions was determined for each of the cell lines. Three mice, who received injections of NCI-H358 bronchioloalveolar cells (1×10^6 cells in 75 μ L in Matrigel), and three mice, who received injections of PC14PE6 adenocarcinoma cells (0.5×10^6 cells in 75 μ L in Matrigel), were killed, and histologic examination confirmed the lesions to be actively growing lung cancer 9 days (in case of PC14PE6 tumor cells) or 14 days (in case of NCI-H358 tumor cells) after tumor implantation. Mice were then injected orthotopically into the lung with NCI-H358 tumors (1×10^6 cells in 75 μ L in Matrigel). Seven days after implantation, the mice were randomized into the following treatment groups ($n = 10$): once-per-week i.p. administration of paclitaxel (100 or 200 μ g; 4 or 8 mg/kg), three times-per-week oral administration of PKI166 (100 or 200 mg/kg), and a combination of paclitaxel and PKI166 (same dosages and frequencies of each of the drugs given alone). Control mice received the oral vehicle solution for PKI166 (DMSO/0.5% Tween 80 diluted 1:20 in HBSS) and i.p. HBSS (15–17). Three separate experiments were carried out with NCI-H358 tumors for a total of 5 weeks of therapy. The experiments were terminated when the control mice became moribund, and all mice were then simultaneously killed, autopsied, and their tumor tissues were harvested.

Using similar methodologies, the therapy experiment was repeated with PC14PE6 human lung adenocarcinoma cells with overall survival as an end point. Mice were implanted with PC14PE6 cells into the lung and were randomized to the four treatment groups ($n = 10$) on day 7. The mice were killed and necropsied when they became moribund. Survival was evaluated by the Kaplan-Meier method (24).

Necropsy and Tissue Preparation. Mice were killed with a lethal dose of sodium pentobarbital (100 mg/kg body weight). After a laparotomy, the thoracic cavity was inspected through the diaphragm for evidence of pleural effusion. Pleural effusions were collected, and the thoracic organs were then removed en block, including all lymph nodes and tumors. After dissection and removal of the heart, the lung and tumor mass were washed in cold PBS and weighed. Other visceral organs were removed and inspected for the presence of metastases. For immunohistochemical and H&E-staining procedures, one part of the tumor was fixed in formalin and embedded in paraffin.

Immunohistochemical Determination of EGFR, Activated EGFR, bFGF, and Activated MAPK. Paraffin-embedded tissues were used to identify EGFR, activated EGFR, bFGF, and phosphorylated MAPK. Immunohistochemical pro-

cedures for EGFR, activated EGFR, and bFGF were performed as described previously (15–17, 25). Activated MAPK was determined as described by Albanell *et al.* (26). Briefly, tissue sections (4 to 6 μ m) were mounted on positively charged Superfrost slides (Fisher Scientific Co., Houston, TX) and dried overnight. The sections were deparaffinized in xylene, treated with a graded series of alcohol [100, 95, and 80% etomidate/double distilled H_2O (v/v)], and then rehydrated in PBS (pH 7.5). For antigen retrieval, sections used for the activated EGFR and activated MAPK analyses were prepared in 10 mmol/L ethylene diamine tetraacetic acid buffer (pH 8) for 10 minutes in a microwave oven at 600 W. To determine EGFR, slides were prepared by pepsin digestion for 10 minutes. Before being stained for bFGF, the tissues were treated with pepsin for 20 minutes at 37°C and washed with PBS. The tissues were incubated with primary antibodies overnight at 4°C at the following dilutions: EGFR 1/200, activated EGFR 1/1000, activated MAPK 1/80, and bFGF 1/100. Control samples exposed to a secondary antibody alone showed no staining.

Quantification of Immunohistochemical Studies. To quantify the intensity of the immunohistochemical reaction, the absorbance of 100 bFGF- and activated MAPK-positive cells in 10 random 0.039-mm² fields at $\times 200$ of treated tumor tissues was measured with Optimas Image Analysis software (15–17, 25). The samples were not counterstained; therefore, the absorbance was attributable solely to the product of the immunohistochemical reaction. bFGF and activated MAPK cytoplasmic immunoreactivity were evaluated by computer-assisted image analysis and expressed as the ratio of tumor cell expression to normal pancreatic gland expression multiplied by 100 (27, 28).

RESULTS

EGFR Is Expressed and Activated in Human Lung Cancer Cells, and the Activation of EGFR Is Blocked by PKI166. In the first set of experiments, we determined that the NCI-H358 tumor cells express the EGFR and the activated EGFR. A Western blot analysis showed that NCI-H358 tumor cells express the EGFR protein constitutively. The activated EGFR protein was found after stimulation with the ligand EGF. Tumor cells incubated for 15 minutes in medium free of serum but containing EGF exhibited the activated EGFR (M_r 170,000 band), as detected by antisera on Western blot analyses of anti-EGFR immunoprecipitated cell lysates. We next determined that *in vitro* treatment of the cell lines with PKI166 inhibited EGF-stimulated tyrosine phosphorylation of the EGFR. Pretreatment of cells with PKI166 for 1 hour followed by a 15-minute treatment with EGF inhibited the phosphorylation in a dose-dependent manner (0 to 5 μ mol/L). The identity of the M_r 170,000 band was confirmed by Western blot analysis with anti-EGFR antisera (Fig. 1). Similar results were noted with PC14PE6 cells (data not shown).

Inhibition of NSCLC Tumor Growth and Metastasis. Athymic nude mice were injected into their left lungs with NCI-H358 cells in three separate experiments. The mice were killed 6.5 to 8 weeks after tumor implantation, when the control mice became moribund. In all three experiments, oral PKI166 decreased the median lung and tumor weight of the treated mice as compared with that of the control mice but was less effective

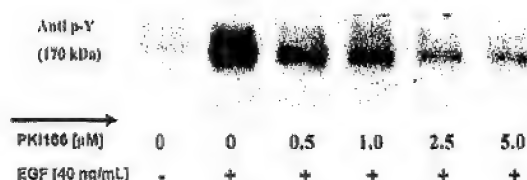


Fig. 1 Inhibition of EGF-induced autophosphorylation of EGFR: NCI-H358 NSCLC cells growing *in vitro* in serum-free medium were stimulated for 15 minutes with EGF (40 ng/mL) in the presence or absence of PKI166 (0 to 5 μ M/L). The cells were washed and lysed, and insoluble proteins in the lysate were immunoprecipitated with an anti-EGFR monoclonal antibody, separated by 7.5% SDS-PAGE, transferred to nitrocellulose, and sequentially probed with antisera to phosphotyrosine (Anti-p-Y) and EGFR (see Materials and Methods). The immunoreactive proteins were detected by incubating the blot with the corresponding peroxidase-conjugated IgG and visualized with the enhanced chemiluminescence system. Densitometric quantitation of the ratio between the M_r 170,000 phospho-tyrosine-specific and the M_r 170,000 EGFR-specific bands was compared in each case with the untreated cells, whose ratio was defined as 1.0.

than weekly paclitaxel alone. The antitumor effects observed in the mice treated with the combination of PKI166 and paclitaxel were equivalent or inferior to those observed in the mice treated with paclitaxel alone (Table 1). Treatment with PKI166 alone or in combination with paclitaxel was well tolerated, as evidenced by maintenance of body weight (data not shown).

For the survival studies, we used the same therapeutic model with human lung adenocarcinoma cells (PC14PB6) injected into the left lungs of 10 mice in each group. The mice were killed and necropsied when they became moribund. As in the therapeutic studies in NCI-H358 cells, results of the studies in PC14PB6 cells showed that the survival of mice treated with a combination of PKI166 and paclitaxel were equivalent to or inferior to the survival of mice treated with paclitaxel alone. The survival data are presented in Fig. 2. A detailed necropsy revealed that all of the mice had thoracic tumors.

Histology and Immunohistochemical Analysis. The NCI-H358 tumor specimens were processed for routine histology and immunohistochemical analyses. Immunohistochemistry with specific anti-EGFR, activated EGFR, bFGF, and activated MAPK showed differences in the level of expression for the different treatment groups. The lesions did not show differences

in the expression of EGFR; yet, the expression of activated EGFR was diminished in the groups treated with PKI166 alone or in combination with paclitaxel (Fig. 3). The expression of bFGF and activated MAPK was determined. Activated MAPK expression was decreased in PKI166-treated tumors, whereas bFGF level was elevated in PKI166 or paclitaxel-treated tumors and even higher in tumors treated with concurrent PKI166 and paclitaxel (Fig. 4).

DISCUSSION

The effects of EGFR-tyrosine kinase inhibitors in combination with chemotherapy on subcutaneous ectopic tumors have been extensively studied. Ciardiello *et al.* (13), with gefitinib on human cancer lines that co-expressed EGFR and its ligand transforming growth factor α , observed an increased antitumor effect and potentiation of cytotoxic drugs both *in vitro* and *in vivo* for s.c. xenografts. Sirotin *et al.* (14) also showed a potentiation of cytotoxic treatment with coadministration of gefitinib for s.c. xenografts, but the effects did not correlate with the level of EGFR expression by the target tumor. However, the level of the activated EGFR, which is the presumptive actual target for gefitinib, was not tested in these studies. Furthermore, the relevance of s.c. tumor growth in animal models to that in human studies has to be carefully ascertained because experimental preclinical results frequently cannot be translated to the clinic. One reason for this is that lower doses of chemotherapy agents often used in animal models to benefit from a synergy with biological therapies (29). Another limitation of animal models is related to tumor implantation. The use of ectopic tumors does not adequately take into account the interaction between the specific organ environment and tumor cells (*i.e.*, lung cancer cells interacting with the lung microenvironment; refs. 30–32) and may therefore alter the tumor response to therapy. Indeed, we have recently shown that paclitaxel is more effective in treating s.c. NSCLC tumors than in orthotopic ones, suggesting that the orthotopic model may be more suitable for the study of lung cancer (18).

In the present study, we examined the clinical and biological effects of targeted therapy against the EGFR alone and in combination with chemotherapy in orthotopic lung cancer models. Our data showed that concurrent therapy with an EGFR-tyrosine kinase inhibitor and paclitaxel in two human lung

Table 1 PKI166 and paclitaxel therapy of NCI-H358 (human NSCLC) tumors

	Control			PKI166			Paclitaxel			PKI166 + paclitaxel		
	Incidence*	Median	Percentage†	Incidence*	Median	Percentage†	Incidence*	Median	Percentage†	Incidence*	Median	Percentage†
Study 1	9/9	0.319	100%	9/10	0.318	99%	10/10	0.271	85%	10/10	0.287	90%
Study 2	9/9	0.345	100%	9/9	0.217	63%	9/9	0.215	62%	9/10	0.226	65%
Study 3‡	9/9	0.340	100%	10/10	0.297	87%	8/9	0.248	73%	9/9	0.245	72%

NOTE. Weight (grams) designates lung and tumor weight.

* Number of positive mice/number of treated mice.

† Percentage of control mice weight.

‡ NCI-H358 human NSCLC cells (1×10^6) were injected into the left lung of nude mice. Seven days later, groups of mice were treated with once-a-week i.p. paclitaxel [studies 1 and 2: 200 μ g (8 mg/kg); study 3: 100 μ g (4 mg/kg)], three times-a-week oral administration of PKI166 [studies 1 and 2: 200 mg/kg; study 3: 100 mg/kg], and combination of paclitaxel and PKI166. Control mice received oral vehicle solution for PKI166 and i.p. injections saline for a total of five weekly courses of therapy. All mice were killed on 6.5 to 8 weeks after tumor injection when control mice became moribund.

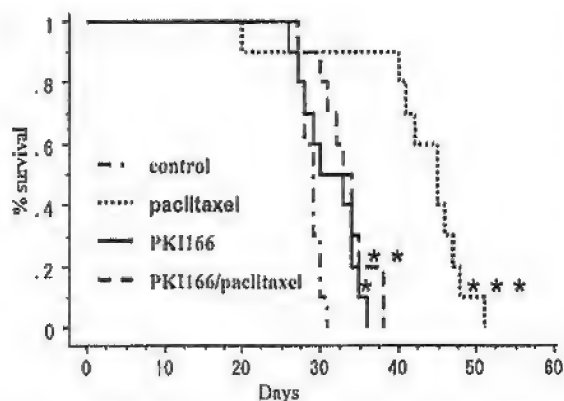


Fig. 2 Therapeutic effects of EGFR blockade and paclitaxel: percentage of cumulative survival. PC14PB6 adenocarcinoma cells were implanted in the lungs of nude mice. The mice were randomized into the above four treatment groups ($n = 10$) and were killed when moribund. Survival analysis was computed by the Kaplan-Meier method. * $P = 0.1$; ** $P = 0.004$; *** $P = 0.001$. Compared to the control, PKI166 alone improved survival by 2.5 days, combination PKI166 and paclitaxel by 4.5 days, and paclitaxel alone by 13.8 days.

cancers growing orthotopically in mice is equivalent to or inferior to therapy with paclitaxel alone, although therapy with PKI166 inhibited EGFR phosphorylation. Our studies were among the first to show the discrepancy between biological activity and clinical results in an orthotopic model of human lung cancer in nude mice. Both lung cancer models studied expressed the EGFR, the presumed target for therapy.

Our data were consistent with those from the clinical trials of EGFR-tyrosine kinase inhibitors and chemotherapy for the treatment of lung cancer. Recent phase III clinical trials of gefitinib or erlotinib in combination with chemotherapy in patients with advanced NSCLC showed that concurrent gefitinib or erlotinib and chemotherapy did not improve overall survival or other efficacy as compared with chemotherapy alone (19, 20, 33, 34). The lack of improved efficacy in the combination groups was observed with different combinations of chemotherapy (carboplatin/paclitaxel or gemcitabine/cisplatin) and with two dosages of gefitinib (250 or 500 mg/day). Similar clinical results have been observed for erlotinib (35).

Two recent studies suggested that response to monotherapy with gefitinib was associated with EGFR mutations. In these important reports, the authors suggested that patients whose tumors express EGFR mutations were likely to respond to gefitinib, whereas patients whose tumors did not express the mutations did not show response (11, 12). Our cell lines did not express EGFR mutations (data not shown). We propose that other mechanisms may be involved in response or resistance to EGFR-tyrosine kinase inhibitors. In our orthotopic lung model, the expression of bFGF by lung tumors was increased in all of the treatment groups with a trend of higher level in tumors treated with the combination of PKI166 and paclitaxel. Furthermore, the expression and activation of MAPK were lower in tumors treated with PKI166, as shown in prior studies with gefitinib (26). MAPK

can be activated by bFGF (36), and our data suggested that the effects of EGFR blockade could possibly be offset by downstream signaling events mediated by bFGF and other growth factors, thereby promoting tumor cell survival. Combination therapy of bFGF signaling inhibitors, *e.g.*, IFNs (37) and anti-EGFR agents, may be warranted. Furthermore, when taken together with the clinical trials, our data suggested that the sequencing of conventional therapy and biological therapy with EGFR-tyrosine kinase inhibitors has to be considered and that concurrent therapy may be detrimental. In this regard, Magne *et al.* (38) recently found differential effect of gefitinib in different combinations with chemotherapy and radiotherapy.

An additional intriguing explanation for the discrepancy between the biological effect and the clinical efficacy of PKI166 was provided by recent studies in animal models that showed a significant response to the combination of PKI166 therapy with

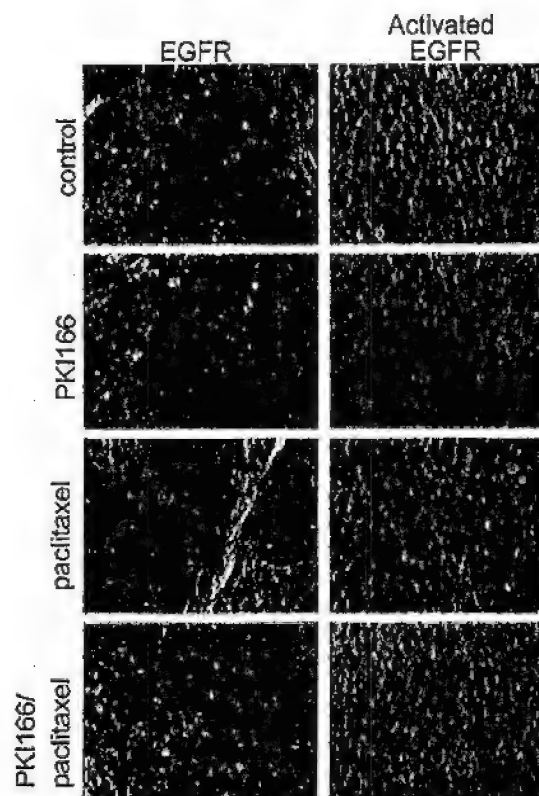


Fig. 3 Representative panels of immunohistochemical determination of EGFR and activated EGFR in lung cancer tumors ($\times 200$ magnification): human NCI-H358 tumors from the lung of nude mice were harvested and processed for histology and immunohistochemical analyses 6.5 to 8 weeks after treatment with once-per-week i.p. paclitaxel (100 to 200 μ g; 4 to 8 mg/kg), three times-per-week oral PKI166 (100 to 200 mg/kg), combination of paclitaxel and PKI166, or control. Tissue sections were stained for expression of tyrosine-phosphorylated, activated EGFR, and total EGFR as described previously (15–17). Tumors from all treatment groups stained positive for EGFR. Only tumors from control mice or mice treated with paclitaxel alone stained positive for activated EGFR.

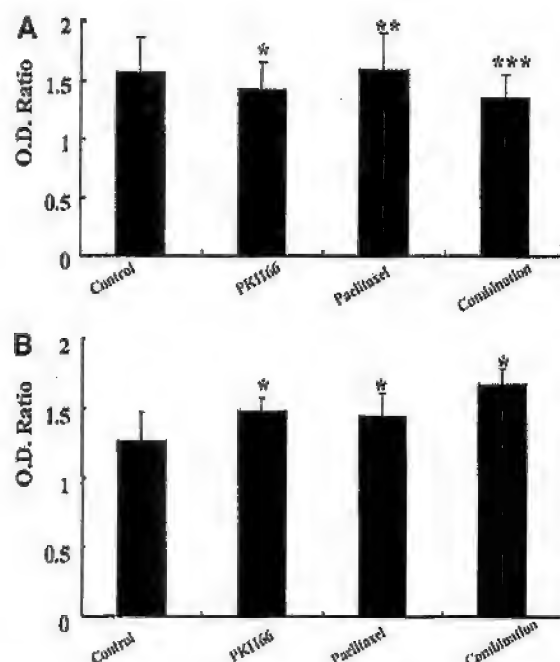


Fig. 4 For quantification of the immunohistochemistry reaction intensity, the absorbance of 100 phosphorylated MAPK-positive cells (A) or bFGF-positive cells (B) from each of the differently treated tumor tissues were measured in 10 random fields at $\times 200$ magnification with the Optimas Image Analysis software (Bioscan). The cytoplasmic immunoreactivity was evaluated by computer-assisted image analysis and was expressed as a ratio of tumor cell expression to normal muscle cell expression multiplied by 100. Student's *t* test was compared the results between control and each of the three different treatment groups. A, **P* = 0.003; ***P* = 0.5; ****P* < 0.00001. B, **P* < 0.00001.

chemotherapy (15–17) in an orthotopic model of pancreatic cancer and an orthotopic model of prostate carcinoma metastasis to the bone. Interestingly, in these studies, both the tumor cells and the tumor-associated blood vessels expressed the target receptor, and the tumor cells expressed the ligand transforming growth factor α (25). In contrast, in our studies of lung cancer, the NCI-H358 and the PC14PE6 tumors did not express transforming growth factor α , and the tumor endothelial cells did not express EGFR (data not shown).

In summary, our data suggest that in lung cancer, EGFR signaling may have an important role, yet it is insufficient to control tumor growth. The combination of several-targeted molecular therapies with conventional chemotherapy may be the basis of future therapy for lung cancer. Future directions for the study of EGFR inhibition in lung cancer should focus on the following topics: identifying the actual target for EGFR-tyrosine kinase inhibitors; identifying the best tumor biological profile that predicts response to therapy with EGFR inhibition, including the role of transforming growth factor α and the expression of EGFR by tumor endothelial cells; and the sequencing of chemotherapy and targeted therapy.

REFERENCES

- Jemal A, Murray T, Samuels A, Ghafoor A, Ward E, Thun MJ. Cancer statistics, 2003. *CA - Cancer J Clin* 2003;53(1):5–26.
- Schiller JH, Harrington D, Belani CP, et al. Comparison of four chemotherapy regimens for advanced non-small-cell lung cancer. *N Engl J Med* 2002;346(2):92–8.
- Huang SM, Harari PM. Epidermal growth factor receptor inhibition in cancer therapy: biology, rationale and preliminary clinical results. *Investig New Drugs* 1999;17:259–69.
- Franklin WA, Vee R, Hirsch FR, Holfrich BA, Bunn PA Jr. Epidermal growth factor receptor family in lung cancer and premalignancy. *Semin Oncol* 2002;29(1 Suppl 4):3–14.
- Hendler FJ, Ozanne BW. Human squamous cell lung cancers express increased epidermal growth factor receptors. *J Clin Invest* 1984;74(2):647–51.
- Onn A, Correa AM, Gilcrease M, et al. Synchronous overexpression of epidermal growth factor receptor and HER2-neu protein is a predictor of poor outcome in patients with stage I non-small cell lung cancer. *Clin Cancer Res* 2004;10(1 Pt 1):136–43.
- Nicholson RI, Gee JM, Harper MB. EGFR and cancer prognosis. *Eur J Cancer* 2001;37(Suppl 4):S9–15.
- Mendelsohn J. Targeting the epidermal growth factor receptor for cancer therapy. *J Clin Oncol* 2002;20(18 Suppl):1S–13S.
- Kris MG, Natale RB, Herbst RS, et al. Efficacy of gefitinib, an inhibitor of the epidermal growth factor receptor tyrosine kinase, in symptomatic patients with non-small cell lung cancer: a randomized trial. *J Am Med Assoc* 2003;290(16):2149–58.
- Fukuoka M, Yano S, Giaccone G, et al. Multi-institutional randomized phase II trial of gefitinib for previously treated patients with advanced non-small-cell lung cancer. *J Clin Oncol* 2003;21(12):2237–46.
- Paez JG, Janne PA, Lee JC, et al. EGFR mutations in lung cancer: correlation with clinical response to gefitinib therapy. *Science* 2004;304(5676):1497–500.
- Lynch TJ, Bell DW, Sordella R, et al. Activating mutations in the epidermal growth factor receptor underlying responsiveness of non-small-cell lung cancer to gefitinib. *N Engl J Med* 2004;350(21):2129–39.
- Ciardiello F, Caputo R, Bianco R, et al. Inhibition of growth factor production and angiogenesis in human cancer cells by ZD1839 (Iressa), a selective epidermal growth factor receptor tyrosine kinase inhibitor. *Clin Cancer Res* 2001;7(5):1459–65.
- Sirotnak FM, Zakowski MF, Miller VA, Scher HI, Kris MG. Efficacy of cytotoxic agents against human tumor xenografts is markedly enhanced by coadministration of ZD1839 (Iressa), an inhibitor of EGFR tyrosine kinase. *Clin Cancer Res* 2000;6(12):4885–92.
- Bruns CJ, Solorzano CC, Harbison MT, et al. Blockade of the epidermal growth factor receptor signaling by a novel tyrosine kinase inhibitor leads to apoptosis of endothelial cells and therapy of human pancreatic carcinoma. *Cancer Res* 2000;60(11):2926–35.
- Kim SJ, Uehara H, Karashima T, Shepherd DL, Killian JJ, Fidler IJ. Blockade of epidermal growth factor receptor signaling in tumor cells and tumor-associated endothelial cells for therapy of androgen-independent human prostate cancer growing in the bone of nude mice. *Clin Cancer Res* 2003;9(3):1200–10.
- Weber KL, Doucet M, Price JB, Baker C, Kim SJ, Fidler IJ. Blockade of epidermal growth factor receptor signaling leads to inhibition of renal cell carcinoma growth in the bone of nude mice. *Cancer Res* 2003;63(11):2940–7.
- Onn A, Isobe T, Itasaka S, et al. Development of an orthotopic model to study the biology and therapy of primary human lung cancer in nude mice. *Clin Cancer Res* 2003;9(15):5532–9.
- Herbst RS, Giaccone G, Schiller JH, et al. Gefitinib in combination with paclitaxel and carboplatin in advanced non-small-cell lung cancer: a phase III trial—INTACT 2. *J Clin Oncol* 2004;22(5):785–94.

20. Giaccone G, Herbst RS, Manegold C, et al. Gefitinib in combination with gemcitabine and cisplatin in advanced non-small-cell lung cancer: a phase III trial—INTACT 1. *J Clin Oncol* 2004;22(5):777–84.
21. Yano S, Nokihara H, Hanibuchi M, et al. Model of malignant pleural effusion of human lung adenocarcinoma in SCID mice. *Oncol Res* 1997;9:573–9.
22. Yano S, Herbst RS, Shinohara H, et al. Treatment for malignant pleural effusion of human lung adenocarcinoma by inhibition of vascular endothelial growth factor receptor tyrosine kinase phosphorylation. *Clin Cancer Res* 2000;6(3):957–65.
23. Dinney CP, Fishbeck R, Singh RK, et al. Isolation and characterization of metastatic variants from human transitional cell carcinoma passaged by orthotopic implantation in athymic nude mice. *J Urol* 1995;154(4):1532–8.
24. Kaplan EL, Meier P. Nonparametric estimation from incomplete observation. *J Am Stat Assoc* 1958;53:457–81.
25. Baker CH, Kednar D, McCarty MF, et al. Blockade of epidermal growth factor receptor signaling on tumor cells and tumor-associated endothelial cells for therapy of human carcinomas. *Am J Pathol* 2002;161(3):929–38.
26. Albanell J, Rojo F, Averbuch S, et al. Pharmacodynamic studies of the epidermal growth factor receptor inhibitor ZD1839 in skin from cancer patients: histopathologic and molecular consequences of receptor inhibition. *J Clin Oncol* 2002;20(1):110–24.
27. Yoneda J, Kuniyasu H, Crispien MA, Price JB, Bucana CD, Fidler IJ. Expression of angiogenesis-related genes and progression of human ovarian carcinomas in nude mice. *J Natl Cancer Inst* (Bethesda) 1998;90(6):447–54.
28. Radinsky R, Risin, Fan, et al. Level and function of epidermal growth factor receptor predict the metastatic potential of human colon carcinoma cells. *Clin Cancer Res* 1995;1(1):19–31.
29. Kerbel RS. What is the optimal rodent model for anti-tumor drug testing? *Cancer Metastasis Rev* 1998–99;17(3):301–4.
30. Morikawa K, Walker SM, Nakajima M, Pathak S, Jessup JM, Fidler IJ. Influence of organ environment on the growth, selection, and metastasis of human colon carcinoma cells in nude mice. *Cancer Res* 1988;48(23):6863–71.
31. Katakai A, Scheid P, Piet M, et al. Tumor infiltrating lymphocytes and macrophages have a potential dual role in lung cancer by supporting both host-defense and tumor progression. *J Lab Clin Med* 2002;140(5):320–8.
32. Glinisky GV, Gliniskii AB, Stephenson AJ, Hoffman RM, Gerald WL. Gene expression profiling predicts clinical outcome of prostate cancer. *J Clin Invest* 2004;113(6):913–23.
33. Gatzemeier U, Pluzanska A, Szczesna E, et al. Results of a phase III trial of erlotinib (OSI-774) combined with cisplatin and gemcitabine chemotherapy in advanced non-small cell lung cancer. *Proc Am Soc Clin Oncol* 2004;23:617.
34. Herbst RS, Prager D, Hermann R, et al. Tribute: a phase III trial of erlotinib HCl (OSI-774) combined with carboplatin and paclitaxel chemotherapy in advanced non-small cell lung cancer. *Proc Am Soc Clin Oncol* 2004;23:617.
35. Akita RW, Sliwkowski MX. Preclinical studies with Erlotinib (Tarceva). *Semin Oncol* 2003;30(3 Suppl 7):15–24.
36. Motamed K, Blake DJ, Angello JC, et al. Fibroblast growth factor receptor-1 mediates the inhibition of endothelial cell proliferation and the promotion of skeletal myoblast differentiation by SPARC: a role for protein kinase A. *J Cell Biochem* 2003;90(2):408–23.
37. Singh RK, Gutman M, Bucana CD, Sanchez R, Llansa N, Fidler IJ. Interferons alpha and beta down-regulate the expression of basic fibroblast growth factor in human carcinomas. *Proc Natl Acad Sci USA* 1995;92(10):4562–6.
38. Magne N, Fischel JL, Tiffon C, et al. Molecular mechanisms underlying the interaction between ZD1839 ('Iressa') and cisplatin/5-fluorouracil. *Br J Cancer* 2003;89(3):585–92.

Suppression of DNA methyltransferase 1 levels in head and neck squamous carcinoma cells using small interfering RNA results in growth inhibition and increase in Cdk inhibitor p21

NOBUHIKO ORIDATE¹ and REUBEN LOTAN

Department of Thoracic/Head and Neck Medical Oncology, The University of Texas
M.D. Anderson Cancer Center, Houston, TX 77030, USA

Received July 9, 2004; Accepted September 23, 2004

Abstract. The ectopic expression of DNA methyltransferase 1 (DNMT 1) can transform mammalian cells, and the inhibition of DNMT1 activity reverses that phenotypic transformation. Therefore, DNMT1 is considered to be an excellent target for therapeutic intervention. Previously, inhibition of DNMT1 was accomplished by using an antagonist or by antisense oligonucleotides. In this study, we examined the ability of the novel approach using small interfering RNA (siRNA) to disrupt the expression of DNMT1 in human non-small cell lung carcinoma A549 cells and the consequences of such an intervention. Transfection of DNMT1 siRNA decreased DNMT1 protein levels specifically and effectively. This decrease was accompanied by suppression of cell proliferation and colony-forming ability. The mechanism of this inhibition may be related to the increased levels of the cyclin dependent kinase inhibitor p21. These results suggest that the siRNA approach can be used to disrupt effectively DNMT1 activity and cancer cell growth.

Introduction

Aberrant patterns of DNA methylation, which occur in parallel with the hyperactivation of DNA methyltransferase (DNMT), have been observed in many cancer cell types (1,2).

DNMT1 is induced by nodal cancer signaling pathways (3-6), and several studies have found that the hyperactivation of DNMT1 leads to oncogenesis (7,8). However, the mechanism by which DNMT1 over-expression induces tumorigenesis remains unknown. One attractive hypothesis is that high levels of DNMT activity lead to the ectopic methylation and inactivation of tumor suppressor genes such as p16 (9). Other studies have shown that the inhibition of DNMT can arrest tumor cell growth (7,8,10). A plausible mechanism underlying this effect is that the inhibition of DNMT results in a stochastic demethylation of a specific site in only a fraction of the cells in each round of replication. An alternative possibility, however, is that the DNMT1 protein might have a direct and immediate effect on the state of cellular growth and transformation (6). The latter hypothesis is based on the observation that the inhibition of the DNMT activity in the human lung cancer cell line A549 by a DNMT antagonist or by anti-sense oligonucleotides induces a rapid up-regulation of the cyclin-dependent kinase inhibitor p21, which does not involve the demethylation of the p21 promoter (11,12).

Current approaches to targeting a specific molecule in mammalian cells have often met limited success. Recently, a new technique that targets specific mRNA molecules for degradation has been developed. This technique takes advantage of post-transcriptional gene silencing (PTGS) induced by the direct introduction of double-stranded RNA (called small interfering RNA or siRNA) that is homologous to the targeted RNA (13,14). siRNA plays a central role in RNA interference (RNAi), and the most effective siRNAs have been reported to be 21 or 22 nucleotides (nt) with 2 nt 3' overhang (15,16). An endonuclease complex uses siRNAs as a guide to cleave the target mRNA of a homologous sequence, decreasing the steady-state levels of the target mRNA. RNAi-mediated PTGS is a potentially powerful way to inhibit cancer cell growth by targeting genes with oncogenic properties.

In this study, we investigated the effects of transfecting DNMT1 siRNA into A549 cells on DNMT1 expression, cell proliferation, colony forming ability, and p21 expression.

Materials and methods

siRNA synthesis. This technique was performed by *in vitro* transcription modified from the method described by Donze

Correspondence to: Dr Reuben Lotan, Department of Thoracic/Head and Neck Medical Oncology, Unit 432, The University of Texas M.D. Anderson Cancer Center, 1515 Holcombe Blvd., Houston, TX 77030-4095, USA
E-mail: rlotan@mdanderson.org

Present address: ¹Department of Otolaryngology-Head and Neck Surgery, Hokkaido University Graduate School of Medicine, Sapporo 060-8638, Japan

Key words: DNA methyltransferase 1, small interfering RNA, p21, cell growth

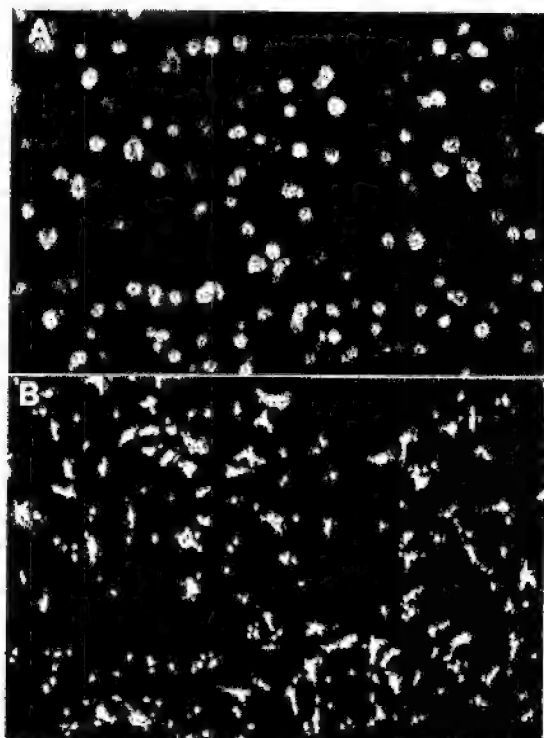


Figure 1. Transfection efficiency of a double-stranded oligonucleotide in non-small cell lung cancer A549 cells. The cells were transfected with a fluorescence-tagged double-stranded oligonucleotide for 24 h, fixed with 10% trichloroacetic acid, and inspected under an inverted fluorescence microscope. (A), A fluorescence image; (B), Phase contrast image of the same field.

and Picard (17). A 39-nt DNA template oligonucleotide was designed to produce 21- or 22- nt siRNAs. The siRNA sequence of the type AAG(N19)CN2 was selected from DNMT1 cDNA, because efficient T7 RNA polymerase initiation requires the first nt of each RNA to be a G (18). The last two nts at the 3' overhang of the siRNA duplex were always UU for the antisense strand (19).

The siRNA sequences used in this study were as follows: DNMT1: 5'-GGAAAAGCACCAGGCAAACCCAC-3'; 3'-UUC CUUUUCGUGGUGCCGUUUGG-5'; mutated DNMT1 (mDNMT1): 5'-GGAAAAGcACCAGcGAAACCCAC-3'; 3'-UUC CUUUUgcUGGUCgcUUUGG-5'.

The mutated sequences did not show significant homology to any human mRNA found in a BLAST database search. For each transcription reaction, a mixture containing 1 nmol of a 39-nt DNA template and an 18-nt T7 promoter oligonucleotide in annealing buffer (10 mM Tris-HCl and 100 mM NaCl) was heated for 5 min at 95°C and then gradually cooled to room temperature to obtain a double-stranded DNA template. *In vitro* transcription was performed overnight using the AmpliScribe T7 High Yield Transcription Kit (Epicentre Technologies, Madison, WI) with 50 pmol of oligonucleotide template in a 20 µl reaction volume, followed by treatment with RNase-free DNase I for 20 min at 37°C. Sense and antisense 22-nt RNAs generated in separate reactions

were annealed by mixing the two crude transcription reactions, heating for 5 min at 95°C, and then cooling slowly to 4°C. An equal amount (42 µl) of 4 M ammonium acetate was added to the mixture, and the siRNA duplex was precipitated with twice the volume of ethanol on ice for 15 min. After centrifugation, the pellet was washed once with 70% ethanol, dried, and re-suspended in 200-250 µl of the annealing buffer. RNA duplexes were identified by co-migration with a chemically synthesized siRNA (Dharmacon, Lafayette, CO) of the same length.

Cell culture and transfection. The human non-small cell lung cancer cell line A549 was obtained from the American Type Culture Collection (Manassas, VA). The cells were maintained in a 1:1 mixture of Dulbecco's modified Eagle's medium:Ham's F12 medium (DMEM:F12) without antibiotics, supplemented with 5% fetal bovine serum (FBS). For transfection of siRNA, cells were plated on dishes on the day before transfection at 50-70% confluency in DMEM:F12 supplemented with 1% FBS. Transfections were performed with siPORTlipid (Ambion, Austin, TX) according to the manufacturer's instructions. The efficiency of transfection was evaluated using a fluorescence-tagged double-stranded oligonucleotide (20). After 24 h of transfection, the cells were fixed with 10% trichloroacetic acid and observed under an inverted fluorescence microscope. The protein expression and the survival of the transfected cells were analyzed 48-72 h after transfection. Cell survival was estimated using a colorimetric sulforhodamine B (SRB) assay using 96-well plates (21,22). At least 3 replicate wells were used for each experimental condition. Anchorage-dependent colony-forming ability was also evaluated by SRB staining as described above, using 6-well plates. The number of colonies was counted using Quantity One software (Bio-Rad Laboratories, Hercules, CA) according to the manufacturer's instructions.

Western blot analysis. The transfected cells were harvested by suspension in lysis-buffer (1 mM dithiothreitol, 0.125 mM EDTA, 5% glycerol, 1 mM phenylmethylsulfonyl fluoride, 1 µg/ml leupeptin, 1 µg/ml pepstatin, 1 µg/ml aprotinin, and 1% Triton X-100 in 12.5 mM Tris-HCl buffer, pH 7.0) on ice. Cell extracts containing 20-50 µg of protein were subjected to electrophoresis using 10% polyacrylamide slab gels in the presence of 0.1% SDS. After electrophoresis, the proteins were transferred electrophoretically to a PDVF membrane in a buffer containing 25 mM Tris-HCl (pH 8.3), 192 mM glycine, and 20% (v/v) methanol. The non-specific binding sites on the membrane were first blocked with 5% (w/v) dried milk in 20 mM Tris-HCl (pH 7.6) containing 0.1 M NaCl and 0.1% (v/v) Tween-20 (TBS-T) for 1 h at room temperature. After three washes with TBS-T, the membrane was incubated with primary antibody diluted 1:1000 in 5% bovine serum albumin in TBS-T for 1 h at room temperature or for overnight at 4°C. The membrane was then washed 3 times in TBS-T and incubated with the corresponding second antibody conjugated with horseradish peroxidase (Amersham Inc., UK) diluted 1:10000 in TBS-T for 1 h at room temperature. The membrane was then washed four times with TBS-T, stained with an enhanced chemiluminescence system (Amersham) according to the

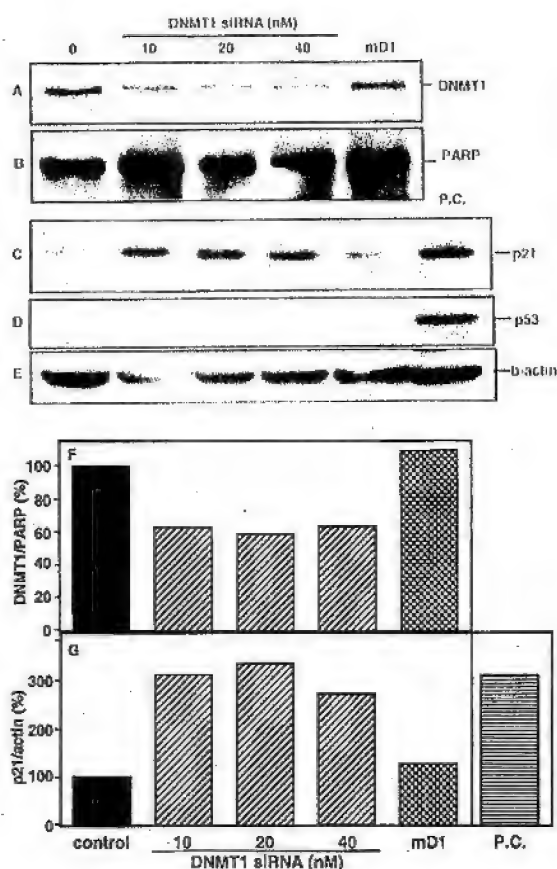


Figure 2. Effects of DNMT1 siRNA transfection on the levels of DNMT1 and p21 in A549 cells. (A-E), A549 cells were transfected with siRNA to DNMT1 using siPORTlipid transfection reagent as described in Materials and methods. After 48 h of transfection, the expression of the indicated genes was evaluated by Western blot analysis. mD1, mDNMT1; P.C., indicates a positive control for p21 and p53. (F and G), The expression of DNMT1 relative to PARP and the expression of p21 relative to β-actin, respectively were determined after densitometric scanning.

supplier's instructions, dried, and exposed briefly to X-ray film. Anti-DNMT1 goat IgG, anti-p21 rabbit IgG, and anti-p53 mouse monoclonal IgG from Santa-Cruz Biotechnology (Santa-Cruz, CA) were used as primary antibodies. The relative expression of the proteins was evaluated using Quantity One software (Bio-Rad Laboratories) according to the manufacturer's instructions.

Results and Discussion

Specific inhibition of DNMT1 expression by siRNA transfection. The transfection efficiency of the A549 cells was evaluated using a fluorescence-tagged double-stranded oligonucleotide and found to exceed 90% (Fig. 1). We then transfected the A549 cells with DNMT1 siRNA and analyzed the effect on the expression of the target gene by Western blotting. DNMT1 levels were decreased after 48 h of transfection (Fig. 2A), whereas the levels of poly(ADP-ribose)

polymerase (PARP) and β-actin used as controls were not affected (Fig. 2B and E, respectively). The effect of siRNA against DNMT1 was apparently specific because cells transfected with the control mutated DNMT1 siRNA (mD1) did not decrease as much as in the DNMT1 siRNA-transfected cells (Fig. 2A). The quantitation of the changes in the levels of the DNMT1 protein after siRNA transfection was performed by scanning and normalization to the level of PARP (Fig. 2F and G). No PARP cleavage was observed in DNMT1 siRNA-treated cells (Fig. 2B), indicating that the decrease in DNMT did not cause caspase 3 activation in A549 cells.

Effect of decreased expression of DNMT1 on the growth of A549. The effect of DNMT1 siRNA on the growth of A549 cells in monolayer culture was examined next. The growth of A549 cells was not affected by siRNA oligonucleotides added to the cells in the absence of the transfection reagent (data not shown). However, when DNMT1 siRNA was introduced at 10, 20 or 40 nM with the transfection reagent, the A549 cells showed about 75 and 65% survival, respectively, compared with the control cells after 48 h of transfection (Fig. 3A). The growth inhibitory effects of the mutated siRNA (mDNMT1) did not exceed 20% indicating the specificity of the DNMT1 siRNA (Fig. 3A).

We also compared the effects of DNMT1 siRNA with those of 5-aza-2-deoxycytidine (5-aza-dC), because experimental inhibition of DNMT has relied for the most part on the 5-aza nucleoside analogs 5-azacytidine (5-azaC) and 5-aza-dC (23). When DNMT1 siRNA was introduced at either 10 or 20 nM with the transfection reagent, the A549 cells showed about 50% survival after 72 h of transfection, while the growth inhibitory effects of 1 and 10 μM 5-aza-dC were 7% and 24% after the 72-h treatment, respectively. To exert its biological effects 5-aza-dC must be incorporated into the DNA, where it covalently trap the bulky 190-kDa DNMT enzyme onto the DNA (24). 5-aza-dC can affect many cellular processes and alter cellular differentiation, even in organisms that do not bear methylated bases in their genomes (25). Experiments in which DNMT has been inhibited by genetic means, such as by targeted disruption of the DNMT gene in mice, resulted in directly opposite effects on gene expression than those observed with 5-aza-dC treatment (26,27). Therefore, the growth inhibitory effect of 5-aza-dC that we have seen here may be because of a change in gene expression caused by mechanisms unrelated to the DNMT inhibition; for example, a modification of the chromatin structure has been suggested (28-30). In any event, the siRNA-mediated specific inhibition of DNMT1 causes stronger and faster inhibition of cell growth than 5-aza-dC treatment.

In addition to the growth in monolayer culture, we also examined the effects of DNMT1 siRNA on colony formation. Fig. 4 shows the effects of treating the A549 cells with siRNA for 48 h followed by harvesting and reseeding at the same cell density, and culturing for additional 6 days. The number of colonies formed by the DNMT1 siRNA-transfected cell suspension was <10%, whereas those from 20 nM mutated siRNA (mDNMT1)-treated cells was 72% of that of the control culture. It should be noted that the maximum effect was obtained at 10 nM of DNMT1 siRNA, suggesting that

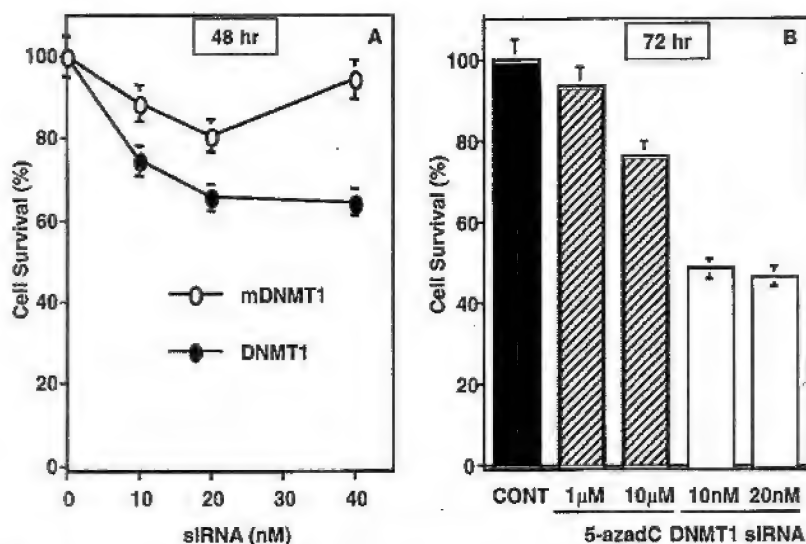


Figure 3. Effect of DNMT1 siRNA transfection on growth of A549 cells. (A), The A549 cells were transfected with different concentrations of DNMT1 or mutated DNMT1 (mDNMT1) siRNAs and analyzed for their survival by SRB assay after 48 h of transfection. (B), The cells were treated with either 5-azadC or DNMT1 siRNA in the presence of the transfection reagent for 72 h. Cell survival was evaluated by the SRB assay. The assays were performed in triplicates and the data are the mean \pm SEM.

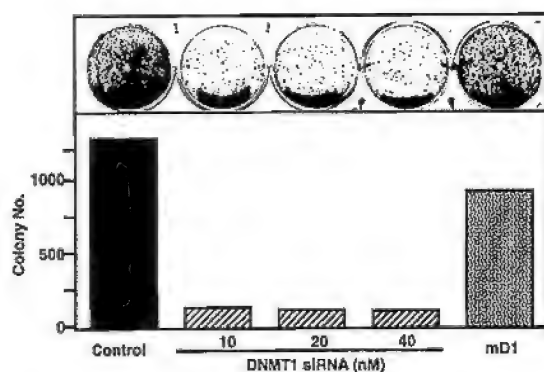


Figure 4. Effect of DNMT1 siRNA introduction on colony forming ability of A549 cells. The cells were treated with different concentrations of DNMT1 or 20 nM mDNMT1 siRNA for 48 h, trypsinized, reseeded at the same cell density, and cultured for 6 days. The adherent colonies were fixed, stained with SRB, photographed (top panel) and counted (lower panel) as described in Materials and methods.

even a partial silencing was sufficient to abolish the colony-forming ability of A549 cells.

Induction of p21 expression by suppression of DNMT1 levels. The inhibition of DNMT activity by a DNMT antagonist or by antisense oligonucleotides in A549 cells was reported to result in a rapid up-regulation of the expression of p21, which was the only one induced among the 16 known tumor suppressors and cell cycle regulators (11,12). Therefore, we examined whether DNMT1 siRNA-transfection changes p21 expression in these cells. We found that the level of p21 expression, but not that of p53, was higher in cells in which

DNMT1 levels were lowered as a result of DNMT1 siRNA transfection (Fig. 2C, D and G). The A549 cells have been reported to harbor the wild-type p53 gene (31). However, the up-regulation of p21 in DNMT1 transfectants was not accompanied by an increase in the level of p53 protein, suggesting that this event does not require p53 activation. p21 controls cell cycle transition at the G1-S boundary by forming a complex with PCNA, cyclin D1, and CDK4 (32). Human DNMT1 competes with p21 for PCNA binding (32). This DNMT1-PCNA complex is found in transformed cells with high levels of DNMT1 but not in non-transformed cells and can be disrupted by p21-derived peptides (33). This competition between DNMT1 and p21 for the same binding site on PCNA may explain the inverse relationship and regulation observed. The elevated levels of DNMT1 compete with and displace p21 from its target PCNA, and the free p21 may be more susceptible to proteolytic degradation than p21 in a complex with PCNA and other proteins. On the other hand, higher levels of p21 would displace DNMT1 from PCNA and lead to its degradation. Thus, the elevated levels of DNMT1 found in transformed cells may effectively regulate proliferation both by reducing cellular p21 levels and by competing directly for the downstream target PCNA (11).

Several studies using an antisense oligonucleotide strategy have shown that DNMT1 is a good target for inhibiting cancer cell growth (7,8,11,12,34). It has been suggested that siRNA may have a better potential clinical activity than antisense RNA or ribozyme approaches in silencing gene expression efficiently and specifically (35). In this study, we found that siRNA-mediated gene silencing can be applied to inhibit the growth of cancer cells. Although siRNA appears to be one of the most promising approaches to suppressing gene expression (13-16), no attempt has been made so far to use this approach to silence DNMT1 in lung cancer cells.

Therefore, we designed this study to test the effect of siRNAs targeting DNMT1. Our findings showed that transfection of siRNA specific to DNMT1 reduced its protein level and that this event was associated with a significant inhibition of cell proliferation. Although the silencing efficacy did not reach 100%, probably because of the positional effects of selected targeted sequences (15), even partial silencing was sufficient to observe growth inhibition by siRNA specific to DNMT1.

Although we found that siRNA-mediated gene silencing could be used to inhibit cancer cell growth in this study, it is obvious that many steps, including providing preclinical data from animal experiments and developing effective siRNA delivery methods, must be completed before this technique can be assessed for clinical potential. Recently, it has been reported that intravenous injection of siRNA specifically reduced target mRNA levels and expression in a mouse model and that the effects persisted without diminution for 10 days (36). Suitable systems that specifically deliver siRNA to the target cells with greater efficiency are expected in the near future.

Acknowledgements

This study was supported by grant DAMD17-02-1-0706-01 from the Department of Defense and by the Irving and Nadine Mansfield and Robert David Leavitt Cancer Research Chair. We thank Dafna Lotan for her excellent technical assistance.

References

1. El-Deiry WS, Nelkin BD, Celano P, Yen RW, Falco JP, Hamilton SR, *et al*: High expression of the DNA methyltransferase gene characterizes human neoplastic cells and progression stages of colon cancer. *Proc Natl Acad Sci USA* 88: 3470-3474, 1991.
2. Baylin SB, Makos M, Wu JJ, Yen RW, De Bustros A, Vertino P, *et al*: Abnormal patterns of DNA methylation in human neoplasia: potential consequences for tumor progression. *Cancer Cells* 3: 383-390, 1991.
3. MacLeod AR, Rouleau J and Szyf M: Regulation of DNA methylation by the Ras signaling pathway. *J Biol Chem* 270: 11327-11337, 1995.
4. Rouleau J, MacLeod AR and Szyf M: Regulation of the DNA methyltransferase by the Ras-AP-1 signaling pathway. *J Biol Chem* 270: 1595-1601, 1995.
5. Slack A, Cervoni N, Pinard M and Szyf M: DNA methyltransferase is a downstream effector of cellular transformation triggered by simian virus 40 large T antigen. *J Biol Chem* 274: 10105-10112, 1999.
6. Szyf M: Targeting DNA methyltransferase in cancer. *Cancer Metastasis Rev* 17: 219-231, 1998.
7. MacLeod AR and Szyf M: Expression of antisense to DNA methyltransferase mRNA induces DNA demethylation and inhibits tumorigenesis. *J Biol Chem* 270: 8037-8043, 1995.
8. Ramchandani S, MacLeod AR, Pinard M, von Hofe E and Szyf M: Inhibition of tumorigenesis by a cytosine-DNA, methyltransferase, antisense oligodeoxynucleotide. *Proc Natl Acad Sci USA* 94: 684-689, 1997.
9. Merlo A, Herman JG, Mao L, Lee DJ, Gabrielson E, Burger PC, *et al*: 5' CpG island methylation is associated with transcriptional silencing of the tumour suppressor p16/CDKN2/MTS1 in human cancers. *Nat Med* 1: 686-692, 1995.
10. Laird PW, Jackson-Grusby L, Fazeli A, Dickinson SL, Jung WE, Li E, *et al*: Suppression of intestinal neoplasia by DNA hypomethylation. *Cell* 81: 197-205, 1995.
11. Fournel M, Sapieha P, Beaulieu N, Besterman JM and MacLeod AR: Down-regulation of human DNA-(cytosine-5) methyltransferase induces cell cycle regulators p16^{ink4a} and p21^{WAF1/Cip1} by distinct mechanisms. *J Biol Chem* 274: 24250-24256, 1999.
12. Milutinovic S, Knox JD and Szyf M: DNA methyltransferase inhibition induces the transcription of the tumor suppressor p21^{WAF1/Cip1}. *J Biol Chem* 275: 6353-6359, 2000.
13. Sharp PA: RNA interference-2001. *Genes Dev* 15: 485-490, 2001.
14. Zamore PD: RNA interference: listening to the sound of silence. *Nat Struct Biol* 8: 746-750, 2001.
15. Elbashir SM, Harborth J, Lendeckel W, Yalcin A, Weber K and Tuschl T: Duplexes of 21-nucleotide RNAs mediate RNA interference in cultured mammalian cells. *Nature* 411: 494-498, 2001.
16. Elbashir SM, Lendeckel W and Tuschl T: RNA interference is mediated by 21- and 22-nucleotide RNAs. *Genes Dev* 15: 188-200, 2001.
17. Donze O and Picard D: RNA interference in mammalian cells using siRNAs synthesized with T7 RNA polymerase. *Nucleic Acids Res* 30: e46, 2002.
18. Milligan JF and Uhlenbeck OC: Synthesis of small RNAs using T7 RNA polymerase. *Methods Enzymol* 180: 51-62, 1989.
19. Hohn JH: RNA interference (RNAi) induction with various types of synthetic oligonucleotide duplexes in cultured human cells. *FEBS Lett* 521: 195-199, 2002.
20. Szyf M: Utilization of antisense oligonucleotides to study the role of 5-cytosine DNA methyltransferase in cellular transformation and oncogenesis. *Methods* 27: 184-191, 2002.
21. Rubinstein LV, Shoemaker RH, Paull KD, Simon RM, Tosini S, Skehan P, *et al*: Comparison of *in vitro* anticancer-drug-screening data generated with a tetrazolium assay versus a protein assay against a diverse panel of human tumor cell lines. *J Natl Cancer Inst* 82: 1113-1118, 1990.
22. Monks A, Scudiero D, Skehan P, Shoemaker R, Paull K, Vistica D, *et al*: Feasibility of a high-flux anticancer drug screen using a diverse panel of cultured human tumor cell lines. *J Natl Cancer Inst* 83: 757-766, 1991.
23. Jones PA: Altering gene expression with 5-azacytidine. *Cell* 40: 485-486, 1985.
24. Juttermann R, Li E and Jaenisch R: Toxicity of 5-aza-2'-deoxycytidine to mammalian cells is mediated primarily by covalent trapping of DNA methyltransferase rather than DNA demethylation. *Proc Natl Acad Sci USA* 91: 11797-11801, 1994.
25. Tamame M, Antequera P, Villanueva JR and Santos T: High-frequency conversion to a 'fluffy' developmental phenotype in *Aspergillus* spp. by 5-azacytidine treatment: evidence for involvement of a single nuclear gene. *Mol Cell Biol* 3: 2287-2297, 1983.
26. Haaf T and Schmid M: 5-Azadeoxycytidine induced undercondensation in the giant X chromosomes of *Microtus agrestis*. *Chromosoma* 98: 93-98, 1989.
27. Efstratiadis A: Parental imprinting of autosomal mammalian genes. *Curr Opin Genet Dev* 4: 265-280, 1994.
28. Hori TA: Induction of chromosome decondensation, sister-chromatid exchanges and endoreduplications by 5-azacytidine, an inhibitor of DNA methylation. *Mutat Res* 121: 47-52, 1983.
29. Lengauer C, Kinzler KW and Vogelstein B: DNA methylation and genetic instability in colorectal cancer cells. *Proc Natl Acad Sci USA* 94: 2545-2550, 1997.
30. Haaf T: The effects of 5-azacytidine and 5-azadeoxycytidine on chromosome structure and function: implications for methylation-associated cellular processes. *Pharmacol Ther* 65: 19-46, 1995.
31. Lehman TA, Bennett WP, Metcalf RA, Welsh JA, Ecker J, Modali RV, *et al*: p53 mutations, ras mutations, and p53-heat shock 70 protein complexes in human lung carcinoma cell lines. *Cancer Res* 51: 4090-4096, 1991.
32. Chuang LS, Iannelli H, Koh TW, Ng HH, Xu G and Li BF: Human DNA-(cytosine-5) methyltransferase-PCNA complex as a target for p21^{WAF1}. *Science* 277: 1996-2000, 1997.
33. Ball KL, Lain S, Fahraeus R, Smythe C and Lane DP: Cell-cycle arrest and inhibition of Cdk4 activity by small peptides based on the carboxy-terminal domain of p21^{WAF1}. *Curr Biol* 7: 71-80, 1997.
34. Knox JD, Araujo FD, Bigey P, Slack AD, Price GB, Zannis-Hadjopoulos M, *et al*: Inhibition of DNA methyltransferase inhibits DNA replication. *J Biol Chem* 275: 17986-17990, 2000.
35. Garber K: Better blocker: RNA interference dazzles research community. *J Natl Cancer Inst* 95: 500-502, 2003.
36. Song E, Lee SK, Wang J, Ince N, Ouyang N, Min J, *et al*: RNA interference targeting Fas protects mice from fulminant hepatitis. *Nat Med* 9: 347-351, 2003.

Research Paper

The Farnesyltransferase Inhibitor Lonafarnib Induces Growth Arrest or Apoptosis of Human Lung Cancer Cells Without Downregulation of Akt

Shi-Yong Sun^{1,*}

Zhongmei Zhou¹

Ruoxiang Wang²

Haian Fu³

Fadlo R. Khuri¹

Departments of ¹Hematology and Oncology, ²Urology and ³Pharmacology, Emory University School of Medicine, Atlanta, Georgia USA

*Correspondence to: Shi-Yong Sun, Winship Cancer Institute, Emory University School of Medicine, 1365-C Clifton Road, NE, Atlanta, Georgia 30322 USA; Tel: 404.778.2170; Fax: 404.778.5520; Email: shi-yong_sun@emoryhealthcare.org

Received 08/03/04; Accepted 08/12/04

Previously published online as a *Cancer Biology & Therapy* E-publication: <http://www.landesbioscience.com/journals/cbt/abstract.php?id=1176>

KEY WORDS

farnesyltransferase inhibitor, Lonafarnib, Akt, growth inhibition, apoptosis, lung cancer

ACKNOWLEDGEMENTS

This work was supported in part by Winship Cancer Institute faculty start-up research fund (to S.-Y. Sun); the Georgia Cancer Coalition Distinguished Cancer Scholar award (to S.-Y. Sun); and Department of Defense Grant DAMD 17-02-1-0706 (to F.R. Khuri).

ABSTRACT

Farnesyltransferase inhibitors (FTIs) have been demonstrated to induce growth arrest or apoptosis independent of Ras mutation. Alternatively, Akt has been proposed as a potential target for the FTI's actions. This study investigated whether Lonafarnib was effective in inhibiting the growth of human non-small cell lung cancer (NSCLC) cells and elucidated the role of Akt in mediating such growth inhibitory effects. Lonafarnib, at clinical achievable concentration ranges, was effective in inhibiting the growth of 10 NSCLC cell lines, particularly after a prolonged treatment, regardless of Ras mutational status. Lonafarnib arrested cells growth at G₁ or G₂/M phase in the majority tested cell lines. However it induced apoptosis when cells were cultured in a low serum (0.1%) medium. The majority of NSCLC cell lines expressed undetectable level of phosphorylated Akt (p-Akt). Lonafarnib at up to 10 μ M did not decrease either total Akt level or p-Akt level in any of the tested cell lines, even after a 48 h treatment. Unexpectedly, Lonafarnib even increased p-Akt level in one cell line, although it was as sensitive as others to Lonafarnib treatment and underwent G₂/M arrest. Bovine serum albumin completely rescued cells from Lonafarnib-induced apoptosis in low serum medium, indicating that proteins rather than cytokines or growth factors in serum masks Lonafarnib's pro-apoptotic effect. Therefore, we conclude that Lonafarnib is effective in inhibiting the growth of NSCLC cells either via growth arrest or induction of apoptosis without downregulation of Akt.

INTRODUCTION

Ras proteins are members of a large superfamily of low molecular-weight GTP-binding proteins and have essential roles in controlling the activity of several crucial signaling pathways that regulate normal cellular proliferation and death.^{1,2} The high frequency of Ras mutation is associated with formation and development of many human cancers including lung cancer, which spurs interest in targeting the Ras pathway for cancer therapy. Because mutational Ras protein requires farnesylation to ensure its cell membrane localization and hence its biological function,^{1,2} farnesyltransferase inhibitors (FTIs) were rationally designed to target the farnesyltransferase enzyme to prevent Ras oncoprotein from farnesylation.^{1,3-5} These agents have shown a remarkable ability to block Ras-mediated oncogenesis,⁶ inhibit the growth of cancer cell lines in culture, or suppress the growth of xenografts, particularly those with H-Ras mutation, in nude mice.⁷ Other studies have shown that these agents exhibit a broader spectrum of activity that includes cancer cells without Ras mutation.^{4,5} In the clinic, FTIs have been shown to be effective against several types of human cancers, especially in combination with taxanes.^{4,5,8} Although these agents were originally designed to be anti-Ras drugs, the Ras-independent antitumor activity of FTIs has been demonstrated.^{4,5} Therefore, the mechanisms underlying FTIs' anticancer activity remain unclear.

One downstream effector pathway of Ras signaling, which mediates cell proliferation and survival, is the phosphoinositide-3'-kinase (PI3K)/Akt cascade.¹ This pathway has recently attracted attention and been considered to be a possible candidate target in mediating FTIs' anticancer effect, particularly their apoptosis-inducing effect.^{1,9} Jiang et al.¹⁰ reported that FTI-277 inhibited the insulin growth factor-1 (IGF-1)- or serum-stimulated PI3K/Akt2 activation in some cancer cell lines and a constitutively active form of Akt2 rescued cancer cells from FTI-277-induced apoptosis. Thus they proposed that FTIs exert their apoptosis-inducing effects through inhibition of PI3K/Akt2-mediated cell survival pathway. Du et al.¹¹ demonstrated that activation of the PI3K/Akt pathway masks the proapoptotic effects of FTIs using Ras-transformed rodent fibroblasts. Chun et al.¹² recently reported that Lonafarnib inhibited Akt activation by decreasing levels of Akt1 and Akt2 in head and neck squamous carcinoma cells and expression of a constitutively active

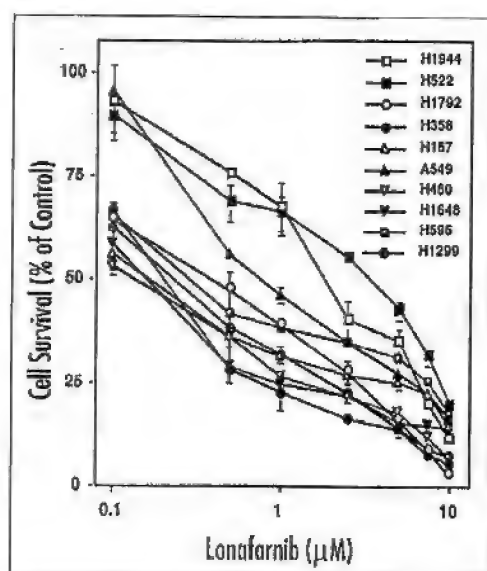


Figure 1. Lonafarnib inhibits the growth of human NSCLC cells. The indicated human NSCLC cell lines were seeded in 96-well plates and treated on the second day with the indicated concentrations of Lonafarnib for five days. Cell numbers were then estimated using the SRB assay. Each point represents a mean \pm SD of four replicate determinations.

form of Akt rescued cells from Lonafarnib-induced apoptosis. Liu et al.¹³ found that Akt1 activation by Ras or epidermal growth factor (EGF) could be disrupted by FTI treatment in COS-7 and MCF-7 cells, respectively. However, they also reported that L-744832 could not suppress basal level activity of endogenous Akt1 in either RhoB^{+/+} or RhoB^{-/-} mouse embryonic fibroblast cells.¹⁴ In another study by Edamatsu et al.,¹⁵ SCH56582 induced apoptosis but did not affect the Akt phosphorylation in LNCaP and PC-3 cells. Therefore, the role of PI3K/Akt pathway in FTI-mediated growth inhibition or apoptosis may vary depending on cell types or FTIs used.

Lonafarnib (also called SCH66336 or Sarasar), a non-peptide tricyclic FTI, was one of the first FTIs to undergo clinical testing and to exhibit significant activity.¹⁶ In vitro, this agent, either alone or in combination with other therapeutic agents, was shown to inhibit the growth or to induce apoptosis of several types of human cancer cells including lung cancer cells.^{12,17-26} In animal models, Lonafarnib demonstrated potent oral activity in a wide array of human tumor xenograft models including tumors of colon, lung, pancreas, prostate, and urinary bladder origin.²¹ When it was combined with other chemotherapeutic agents, enhanced antitumor activity was observed.²⁷ Our recently work demonstrated that a significant clinical activity was seen when the agent was combined with paclitaxel in a phase I trial enrolling individuals with lung or aerodigestive tract cancer.²⁸ Like other FTIs, Lonafarnib was also effective to inhibit the growth of many cancer cell lines without Ras mutation.^{21,27} Thus, it appears that Lonafarnib may exert its antitumor activity through mechanisms beyond suppression of Ras inactivation. Chun et al.¹² recently demonstrated that suppression of Akt activation plays a role in Lonafarnib-induced apoptosis in human head and neck squamous carcinoma cells.

In the present study, we examined the effects of Lonafarnib on the growth of a panel of human non-small cell lung cancer (NSCLC)

Table 1 HISTOLOGY, P53 AND RAS MUTATIONAL STATUS OF HUMAN NSCLC CELL LINES USED IN THIS STUDY AND THEIR RESPONSES TO LONAFARNIB TREATMENT

Cell line	Histology	p53 mutation	Ras mutation ²	Growth inhibition (IC ₅₀ , μ M)		Cell cycle
				3 days	5 days	
H1648	AC ¹	yes	no	5.4	0.15	Sub-G ₁
H522	AC	yes	yes ³	5.5	3.12	G ₂ /M
H1792	AC	yes	yes (K-ras 12)	2.1	0.38	Sub-G ₁
H596	ASC	yes	no	5.8	0.32	G ₂ /M
H157	SCC	yes	yes (K-ras 12)	4.1	0.15	G ₂ /M
H1299	LCC	null	yes (N-ras 61)	5.6	0.32	nt ⁴
H1944	AC	no	unknown	6.2	1.82	Sub-G ₁
H460	LCC	no	yes (K-ras)	5.5	0.14	G ₁
H358	AC	null	yes (K-ras 12)	2.9	0.20	G ₁
A549	AC	no	yes (K-ras)	6.7	0.77	G ₂ /M

Cell numbers were estimated using a SRB assay. ¹AC, adenocarcinoma; SCC, squamous cell carcinoma; LCC, large cell carcinoma; ASC, adenosquamous carcinoma. ²See refs. 32 and 33. ³ATCC data sheet. ⁴nt, not tested.

cell lines with different Ras mutational status and the potential role of PI3K/Akt pathway in mediating such effects. Our results demonstrated that Lonafarnib was effective in inhibiting the growth of NSCLC cells regardless of Ras mutation, particularly after a prolonged exposure. In addition, we demonstrated that the PI3K/Akt pathway was unlikely to be a target for Lonafarnib's growth inhibitory effect in human NSCLC cells.

MATERIALS AND METHODS

Reagents. Lonafarnib was provided by Schering-Plough Research Institute (Kenilworth, NJ). The PI3K inhibitor LY294002 was purchased from Biomol (Plymouth Meeting, PA). They were dissolved in dimethyl sulfoxide (DMSO) at a concentration of 10 mM or 20 mM, and aliquots were stored at -80°C. Stock solutions were diluted to the desired final concentrations with growth medium just before use. Other agents were purchased from Sigma Chemical Co. (St. Louis, MO).

Cell Lines and Cell Culture. All human NSCLC cell lines used in this study were purchased from the American Type Culture Collection (ATCC; Manassas, VA). They were grown in monolayer culture in RPMI 1640 medium supplemented with glutamine and 5% fetal bovine serum (FBS) at 37°C in a humidified atmosphere consisting of 5% CO₂ and 95% air.

Growth Inhibition Assay. Cells were seeded in 96-well cell culture plates and treated on the second day with different concentrations of Lonafarnib. At the end of treatment, cell number was estimated by the sulforhodamine B (SRB) assay as previously described.²⁹

Cell Cycle Analysis. Cells were seeded in 10-cm diameter cell culture dishes and treated on the second day with Lonafarnib alone or combined with other agents. At the end of treatment, cells were trypsinized and single cell suspensions were subjected to staining and subsequent analysis by flow cytometry as described previously.³⁰

Detection of Apoptosis. Formation of sub-G₁ population was primarily used as an indicator of apoptosis, which was measured during cell cycle analysis as described above. In addition, DNA fragmentation was also estimated using a Cell Death Detection ELISA^{plus} kit (Roche Molecular Biochemicals, Indianapolis, IN) according to the manufacturer's instructions. This kit was designed for detecting cytoplasmic histone-associated DNA fragments (mononucleosome and oligonucleosomes) formed during apoptosis.

Western Blot Analysis. The procedures for preparation of whole cell protein lysates and for the Western blotting were described previously.³¹

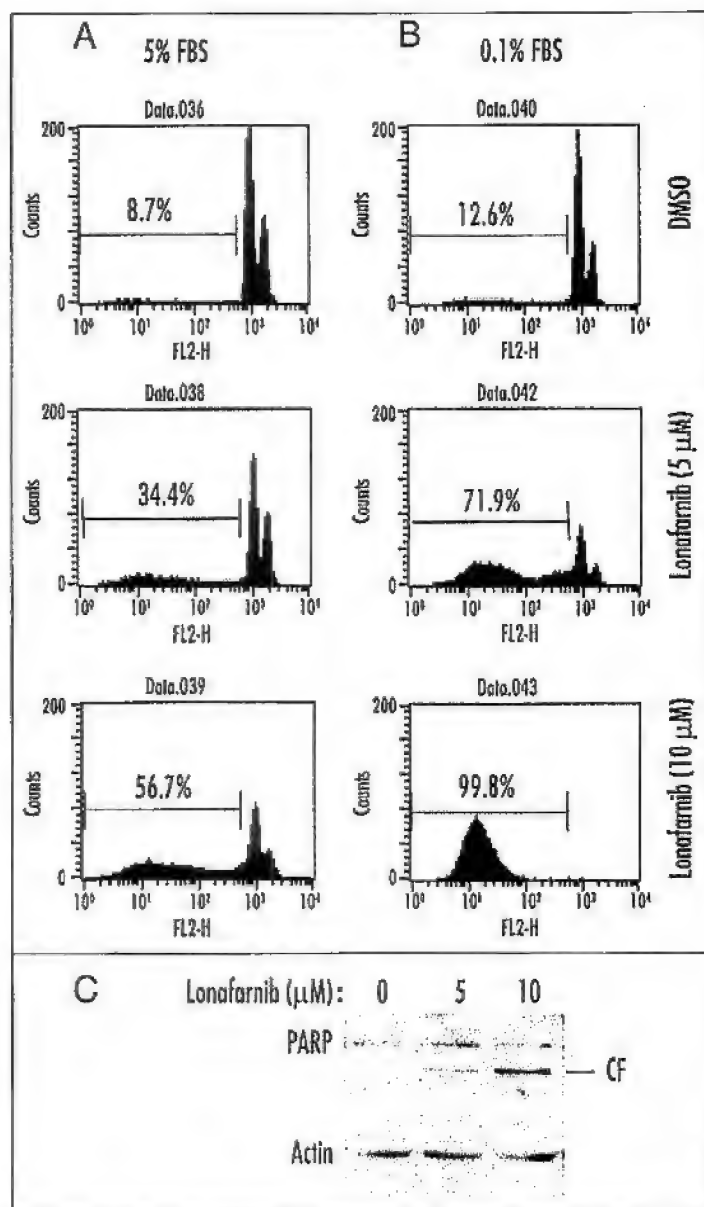


Figure 2. Lonafarnib increases sub-G₁ population (A and B) and induces PARP cleavage (C) in H1792 cells. Cells were treated with the indicated concentrations of Lonafarnib in the medium containing either 5% FBS or 0.1% FBS for 48 h, and then were harvested for sub-G₁ analysis using a flow cytometry (A and B). In addition, partial cells treated in 5% FBS-containing medium were used for preparation of whole cell protein lysates and subsequent analysis of PARP cleavage using the Western blot analysis (C). CF, cleaved fragment.

Whole cell protein lysates (50 μg) were electrophoresed through 10% or 12% denaturing polyacrylamide slab gels and transferred to a PROTRAN pure nitrocellulose transfer membrane (Schleicher & Schuell BioScience, Inc., Keene, NH) by electroblotting. The blots were probed or reprobed with the primary antibodies and then antibody binding was detected using the SuperSignal West Pico Chemiluminescent Substrate (Pierce Biotechnology, Inc., Rockford, IL) according to the manufacturer's protocol. Rabbit polyclonal antibodies against PARP, Akt, phospho-Akt (p-Akt, Ser473), and phospho-GSK-3β (p-GSK-3β, Ser9), respectively, were purchased from Cell Signaling Technology, Inc. (Beverly, MA). Rabbit polyclonal anti-actin antibody was purchased from Sigma Chemical Co.

RESULTS

Lonafarnib Effectively Inhibits the Growth of Human NSCLC Cells. The effects of Lonafarnib, as a single agent, on the growth of NSCLC cells have not been systematically studied. In this study, we used ten human NSCLC cell lines with different histology, p53 status or Ras mutational status (Table 1) to compare the effects of Lonafarnib on their growth. Under normal culture condition (5% FBS), Lonafarnib exhibited a concentration-dependent inhibitory effect on the growth of all tested NSCLC cell lines (Fig. 1). The IC₅₀s, which are the concentrations causing cell number decrease by 50%, for 3-day and 5-day treatments were 2.1 to 9.8 μM and 0.14 to 3.12 μM, respectively (Table 1). Among the ten tested cell lines, only two cell lines (i.e., H522 and H1944) were not as sensitive as other cell lines to Lonafarnib treatment. The IC₅₀s of Lonafarnib for these cell lines were above 1 μM (Table 1). Even though, the growth inhibitory effects of Lonafarnib for a 5-day incubation in these two cell lines were still greatly increased compared with those for a 3-day exposure. Therefore, these results clearly indicate that a prolonged incubation improves Lonafarnib's growth inhibitory effect. We noted that low FBS (0.1%) culture condition further enhanced Lonafarnib's growth inhibitory effect in NSCLC cells (data not shown). Except for H1944, the Ras mutational statuses are known to other NSCLC cell lines (Table 1). However we did not find an association between Ras mutation and cell sensitivity to Lonafarnib in these cell lines. So did to p53 status. Thus, it appears that Lonafarnib inhibits the growth of NSCLC cells independent of p53 or Ras mutation.

Lonafarnib Induces Growth Arrest or Apoptosis in NSCLC Cells Depending on Cell lines or Culture Conditions. To determine how Lonafarnib inhibits the growth of NSCLC cells as demonstrated above, we further analyzed cell cycle distribution of these cell lines after exposure to Lonafarnib using a flow cytometry. We found that the majority of cell lines (seven of nine) underwent either G₁ or G₂/M arrest depending on cell lines when treated with Lonafarnib at up to 10 μM for up to 48 h (Table 1). No significant increase of Sub-G₁ population was detected in these cell lines. However, we were able to detect an increase in the sub-G₁ population in three cell lines (i.e., H1792, H1648 and H1944), indicating that Lonafarnib induces apoptosis in these cell lines. Figure 2A shows an example of results from H1792 cells, in which sub-G₁ population increased from 8.7% (control cells) to 34.4% and 56.7% when treated with 5 μM and 10 μM Lonafarnib, respectively, for 48 h. In agreement, we detected cleaved form of PARP from cells treated with 5 μM or 10 μM Lonafarnib (Fig. 2C).

When cells were cultured in low serum (0.1%) medium, Lonafarnib induced a cytotoxic effect rather than growth arrest by promoting cells to undergo apoptosis. H1792 cells, which primarily underwent apoptosis upon Lonafarnib treatment under normal culture condition, became even more sensitive to Lonafarnib-induced apoptosis. The sub-G₁ population in 0.1% FBS medium after Lonafarnib increased from 12.6% (DMSO control) to 71.9% (5 μM Lonafarnib) or 99.8% (10 μM Lonafarnib) (Fig. 2B) in comparison with an increase in 5% FBS medium from 8.7% (DMSO) to 34.4% (5 μM Lonafarnib) or 56.7% (10 μM Lonafarnib) (Fig. 2A). H157 cells, which primarily underwent G₂/M arrest when exposed to Lonafarnib under the normal culture condition as shown in Figure 3A, exhibited a significant increase of sub-G₁ population from 16.4% (in 5% FBS medium) to 99.8% (in 0.1% FBS medium) after incubation with 10 μM Lonafarnib for 48 h (Fig. 3B). These results indicate that Lonafarnib's effect on cell growth can be converted from cytostatic (growth arrest) to cytotoxic one when cultured in low-serum medium.

Lonafarnib Does Not Decrease Akt or p-Akt Level in Human NSCLC Cells. It has been proposed in some studies that PI3K/Akt may serve as a target for FTI-mediated growth inhibition or apoptosis.¹⁰⁻¹³ Therefore, we next examined whether Lonafarnib exerted any effect on Akt level or activity in human NSCLC cells. Under normal culture conditions, we found that the majority of the NSCLC cell lines (9/10) used in our study expressed basal level of Akt. However, among these cell lines, only H157 expressed high levels of p-Akt, whereas other cell lines expressed very low (A549) or undetectable level of p-Akt (Fig. 4A). The 6 cell lines, when exposed to 5 μ M or 10 μ M Lonafarnib for 24 h, did not apparently show altered expression levels of total Akt (Fig. 4B). In H157 and H1792 cells, Lonafarnib at 5 μ M did not alter the level of Akt even after a 3-day treatment (Fig. 4C). Unexpectedly, we found that Lonafarnib increased p-Akt level (Fig. 4B), indicating that it actually increases Akt activity in H157 cells. This activity was observed at early 4 h after Lonafarnib treatment and sustained for up to 72 h (Fig. 4C). The increase of p-Akt was not observed in other cell lines treated either with 10 μ M Lonafarnib for 48 h (Fig. 4B) or with 5 μ M Lonafarnib for up to 72 h (H1792 in Fig. 4C).

The PI3K Inhibitor LY294002 Enhances Lonafarnib's Apoptosis-Inducing Effect. To further demonstrate the role of PI3K/Akt in Lonafarnib-mediated growth arrest or apoptosis in human NSCLC cells, we examined the effect of Lonafarnib on apoptosis induction in the presence of the PI3K inhibitor LY294002 in H157 cells that express p-Akt. We speculated that suppression of Akt activity by a PI3K inhibitor would enhance cell sensitivity to Lonafarnib-induced apoptosis if PI3K/Akt activation enhances cell resistance to induction of apoptosis. As expected, LY294002 at 10 μ M decreased p-Akt and p-GSK-3 β levels (Fig. 5A, lane 9 vs. lane 1), indicating that it inhibits Akt activity. In the presence of 10 μ M LY294002, Lonafarnib at 1 μ M or 5 μ M failed to increase p-Akt and p-GSK-3 β (Fig. 5A, lanes 6 and 7 vs. lanes 2 and 3), but it at 10 μ M still could do so (Fig. 5A, lane 8 vs. lane 5). Accordingly, the combination of 10 μ M Lonafarnib with 10 μ M LY294002 did not further increase DNA fragmentation (Fig. 5B), whereas 1 μ M or 5 μ M Lonafarnib in combination with 10 μ M LY294002 exhibited augmented induction of DNA fragmentation (Fig. 5B). These results indicate that suppression of Akt activation induced by Lonafarnib augments induction of apoptosis.

Bovine Serum Albumin (BSA) Rescues Cells from Apoptosis Induced by Lonafarnib in Low Serum Medium. Low serum culture makes cells undergo apoptosis upon FTI treatment, which has been demonstrated to be associated with inactivation of PI3K/Akt pathway in some studies.^{11,14} Our results in this study show that Lonafarnib inhibits the growth of human NSCLC cells irrespective of Akt activation. One possibility is that the proteins in serum non-specifically bind to Lonafarnib and thereby may mask its effect on induction of apoptosis by reducing its cellular bioavailability. Therefore, we examined the effect of BSA (the major protein in serum) on Lonafarnib-induced apoptosis in H1792 cells. Lonafarnib induced a dramatic increase in the sub-G₁ population (81.4%) in medium containing 0.1% FBS in comparison with a 17% increase of sub-G₁ population in 5% FBS medium. When cells were cultured in a medium in which 5% FBS was replaced with 0.15% BSA (approximately equals to BSA in 5% FBS), Lonafarnib completely lost its ability to induce apoptosis (Fig. 6A). By measuring DNA fragmentation, a hallmark of apoptosis, we got a similar result in which Lonafarnib markedly increased level of DNA fragments when cells were cultured in 0.1% FBS medium, but only weakly exert such effect in medium containing either 5% FBS or 0.15% BSA (Fig. 6B). Taken together, these results indicate that low serum culture condition allows cells uptake more Lonafarnib resulting in enhanced apoptosis-inducing effect.

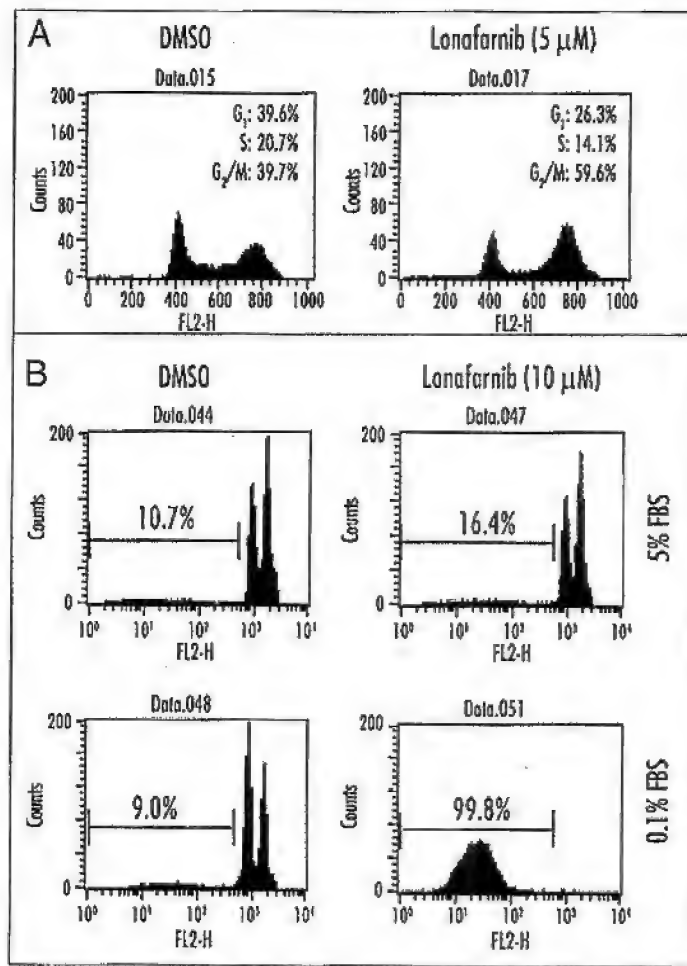


Figure 3. Lonafarnib induces G₀/G₁ arrest (A) or apoptosis in low serum medium (B) in H157 cells. Cells were treated with the indicated concentration of Lonafarnib in the presence of 5% FBS (A) or 0.1% FBS (B) for 48 h, and then subjected to cell cycle and sub-G₁ analysis using a flow cytometry.

DISCUSSION

By examining the effects of the FTI Lonafarnib on the growth of 10 NSCLC cell lines, we have demonstrated that this agent effectively inhibits the growth of NSCLC cells at clinically achievable concentrations. It is worthy pointing out that the growth inhibitory effect of Lonafarnib is time-dependent. In our *in vitro* study, the IC₅₀ of Lonafarnib for a 3-day treatment ranged from 2.1 μ M to 9.8 μ M, which were shifted to a range from 0.14 μ M to 3.12 μ M when incubation time was prolonged for five days, suggesting that continuous, prolonged exposure will improve its efficacy for maximally inhibiting the growth of NSCLC cells. Cell cycle and apoptosis analysis revealed that Lonafarnib primarily exerted a cytostatic effect in the majority of NSCLC cell lines by arresting cells either in G₁ or G₂/M phase under normal culture condition that contained 5% FBS. In a few cell lines, we found that Lonafarnib was cytotoxic and induced apoptosis evidenced by increased sub-G₁ population and PARP cleavage. In agreement with previous findings with other cell types,^{11,14} low serum culture condition made NSCLC cells more sensitive to Lonafarnib-induced apoptosis or converted Lonafarnib's

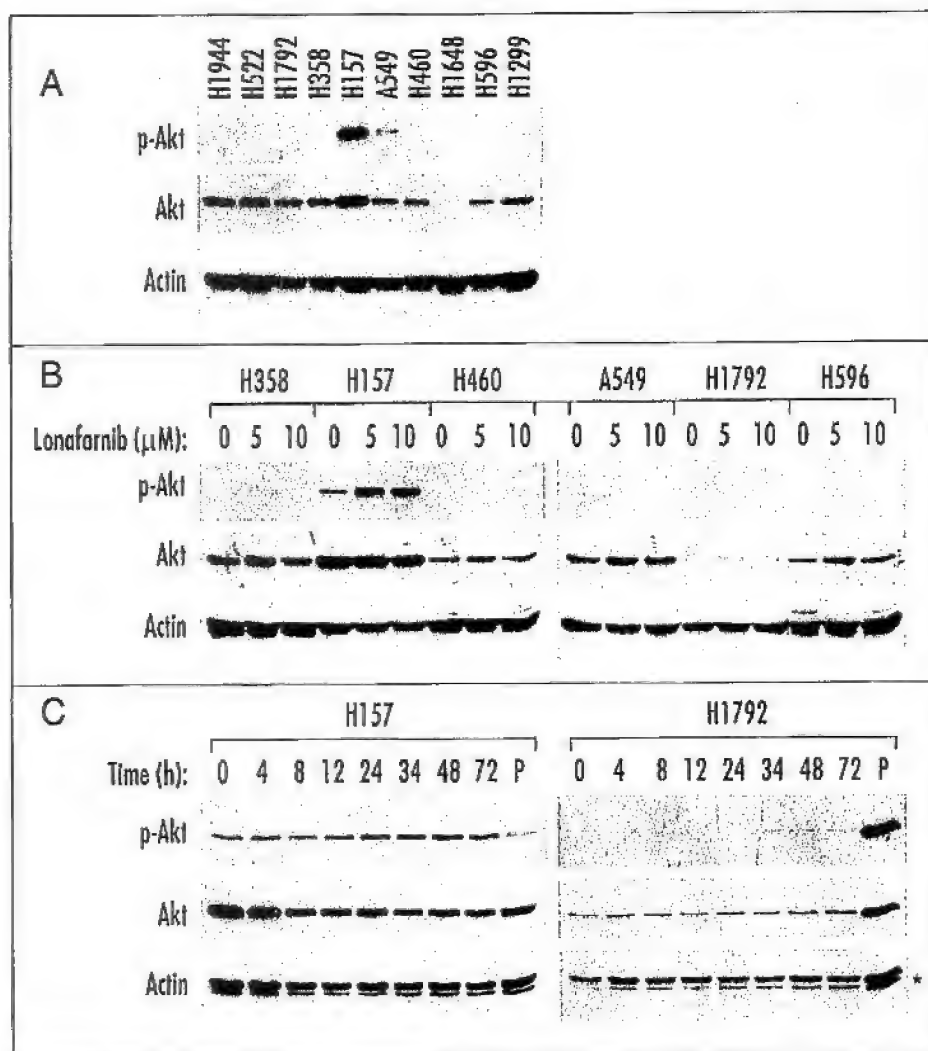


Figure 4. Constitutive expression of p-Akt and total Akt in NSCLC cell lines (A) and effect of Lona-farnib on their expression (B and C). Whole-cell protein lysates prepared from the similar densities of cell lines (A), from the indicated cell lines treated with the indicated concentrations of Lona-farnib for 48 h (B) or from the indicated cell lines treated with 5 μ M Lona-farnib for the indicated times (C) were subjected to Western blot analysis. +, unstripped band; P, positive control lysates prepared from H1155 human NSCLC cells.

effect against the growth of NSCLC cells from growth arrest to apoptosis induction.

FTIs are rationally designed agents that target Ras by blocking its activation.^{1,3-5} However, increased results indicate that FTIs exert their antitumor activity independent of Ras mutational status.^{4,5,9} Most human NSCLC cell lines used in our study have K-Ras mutations. However, we did not find a clear association between Lona-farnib's potencies on growth inhibition and Ras mutational status. In fact, Lona-farnib effectively inhibited the growth of these NSCLC cell lines regardless of Ras mutation, albeit with varying degrees. There was one report demonstrating that human tumor cell lines with wild-type p53 show enhanced sensitivity to Lona-farnib treatment.³⁴ In our study, NSCLC cell lines having wild-type p53 did not exhibit better sensitivity than others with mutant p53 or without p53 to Lona-farnib, indicating that Lona-farnib inhibits the

growth of human NSCLC cells independent of p53 status.

PI3K/Akt is one of the major downstream signaling pathways of Ras oncoprotein and plays a pivotal role in enhancing cell survival.^{1,2} Its activation often confers cell resistance to induction of apoptosis by primarily repressing the function of several proapoptotic proteins such as caspase-9 and Bad.³⁵ Suppression of PI3K/Akt has been proposed to be a mechanism underlying FTI-induced apoptosis in some studies.¹⁰⁻¹³ However, there are other studies that did not demonstrate the importance of PI3K/Akt in FTI-mediated biological function.^{14,15,36} Therefore, even if suppression of PI3K/Akt by FTIs occurs in some cell lines, its role in FTI-mediated biological function may not be universal and is likely to be cell context- or cell type-dependent. In our study, the basal level of p-Akt in the majority of human NSCLC cells (nine out of ten tested cell lines) was either undetectable or very low. This finding appears different from a previous report by Brognard et al,³⁷ in which they demonstrated that human NSCLC cell lines constitutively express active Akt. Because there are only a few cell lines are same in both studies, it is possible that expression levels of the active form of Akt (p-Akt) are cell line-dependent.

Nevertheless, the absence or

low levels of p-Akt in the majority of cell lines used in our study suggest that the PI3K/Akt pathway may not be a critical survival pathway, at least, for these cell lines.

There was a recent study demonstrating that Lona-farnib suppresses p-Akt level by promoting degradation of total Akt protein levels in human head and neck cancer cells.¹² In our study, the majority of NSCLC cell lines constitutively expressed Akt detected by the Western blotting. However, we did not find that Lona-farnib exerted any effect on decreasing either total Akt or p-Akt level in any tested cell line, even at up to 10 μ M or after a longer incubation (48-72 h). Unexpectedly, Lona-farnib in fact increased p-Akt level in H157 cell line that constitutively expresses relatively high level of p-Akt. Interestingly, this cell lines was still as sensitive as others to Lona-farnib treatment and underwent G₂/M arrest upon Lona-farnib treatment. These results clearly indicate that Lona-farnib inhibits the

growth of human NSCLC cells independent of Akt downregulation. In H157 cell line where p-Akt were increased by Lonafarnib, we found that the PI3K inhibitor LY294002 at 10 μ M abrogated p-Akt increase induced by 1 μ M or 5 μ M Lonafarnib accompanied with augmented induction of apoptosis. This result suggests that the increase of p-Akt by Lonafarnib blunts its effect on induction of apoptosis. Therefore, overcome of Lonafarnib-induced p-Akt by PI3K or Akt inhibitors should be a good strategy to increase Lonafarnib's efficacy in patients with NSCLC where p-Akt may be induced during treatment with Lonafarnib.

It is known that PI3K/Akt can be activated in cells exposed to growth factor, hormones, or extracellular matrix components.³⁸ Thus, it was proposed that activation of PI3K/Akt by cytokines and integrins in serum masks the proapoptotic effects of FTIs.¹¹ Therefore, combination of a FTI with a PI3K inhibitor or removal of serum was shown to enhance FTI's effect on apoptosis induction in Ras-transformed rat fibroblasts.¹¹ Since our data do not support a role of the PI3K/Akt pathway in Lonafarnib-mediated growth arrest or apoptosis, we were wondering whether BSA might interfere with Lonafarnib's effect through reducing its intracellular bioavailability. Indeed, we found that simple replacement of 5% FBS with 0.15% BSA in culture medium completely abolished Lonafarnib's effect on apoptosis induction, indicating that BSA alone sufficiently rescues cells from Lonafarnib-induced apoptosis that occurs in low serum medium. Therefore, we believe that the existence of BSA in serum reduces free Lonafarnib concentration that can enter into cells through a non-specific binding mechanism and thus results in decreased biological activity of Lonafarnib. This is also supported by our other finding that Lonafarnib at high concentration (e.g., 15 or 20 μ M) could mimic its effect in low serum medium to induce apoptosis instead of growth arrest (our unpublished data). By simply modulating uptake of Lonafarnib, we can convert Lonafarnib's biological effect from growth arrest (cytostatic) to apoptosis induction (cytotoxic). In this regard, our current finding may have clinical implication for improvement of its efficacy.

In summary, we have demonstrated that Lonafarnib effectively inhibits the growth of human NSCLC cells via either growth arrest or induction of apoptosis, which is independent of Ras mutation and Akt inactivation. Our results warrant further study on its mechanism of action, which may be critical to guide rational usage of Lonafarnib as well as other FTIs as therapeutic agent either alone or in combination with other agents for therapy of NSCLC.

References

- Downward J. Targeting RAS signaling pathways in cancer therapy. *Nat Rev Cancer* 2003; 3:11-22.
- Feig LA, Buchsbaum RJ. Cell signaling: Life or death decisions of ras proteins. *Curr Biol* 2002; 12:R259-61.
- Adjei AA. Blocking oncogenic Ras signaling for cancer therapy. *J Natl Cancer Inst* 2001; 93:1062-74.
- Brunner TB, Hahn SM, Gupta AK, Muschel RJ, McKenna WG, Bernhard EJ. Farnesyltransferase inhibitors: An overview of the results of preclinical and clinical investigations. *Cancer Res* 2003; 63:5656-68.
- Baum C, Kirschmeier P. Preclinical and clinical evaluation of farnesyltransferase inhibitors. *Curr Oncol Rep* 2003; 5:99-107.
- Kohl NE, Mosser SD, deSolms SJ, Giuliani EA, Pompliano DL, Graham SL, et al. Selective inhibition of ras-dependent transformation by a farnesyltransferase inhibitor. *Science* 1993; 260:1934-7.
- Nagasu T, Yoshimatsu K, Rowell C, Lewis MD, Garcia AM. Inhibition of human tumor xenograft growth by treatment with the farnesyl transferase inhibitor B956. *Cancer Res* 1995; 55:5310-4.
- Alsina M, Fonseca R, Wilson EE, Belle AN, Gerbino B, Price-Troska T, et al. Farnesyltransferase inhibitor tipifarnib is well tolerated, induces stabilization of disease, and inhibits farnesylation and oncogenic/tumor survival pathways in patients with advanced multiple myeloma. *Blood* 2004; 103:3271-7.
- Adjei AA. An overview of farnesyltransferase inhibitor and their role in lung cancer therapy. *Lung Cancer* 2003; 41:555-62.

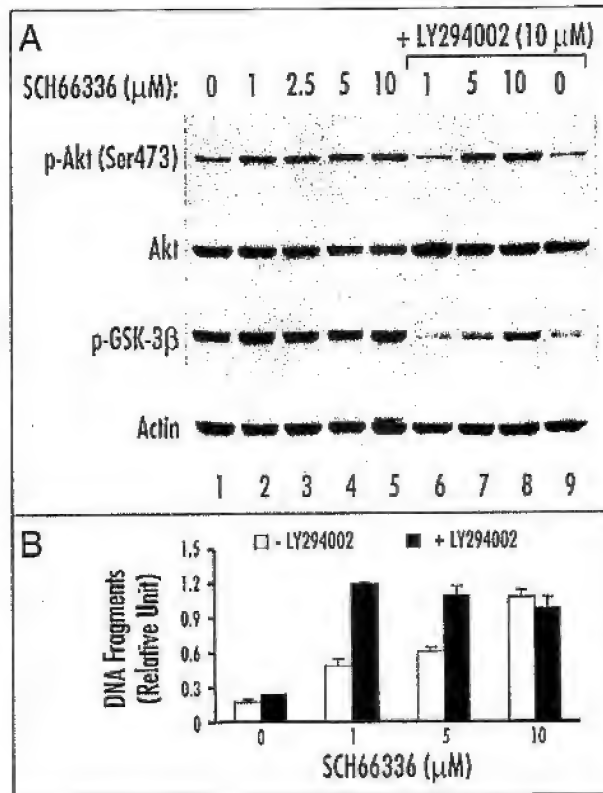


Figure 5. Effect of the Lonafarnib and LY294002 combination on Akt activation (A) and apoptosis induction (B) in H157 cells. Cells were treated with the indicated concentrations of Lonafarnib alone, 10 μ M LY294002 alone, and their combinations for 48 h. p-Akt, Akt and p-GSK-3 β levels were detected using the Western blot analysis (A), whereas apoptosis was measured by monitoring formation of DNA fragments using an ELISA (B). Each column in B represents a mean \pm SD of triplicate determinations.

- Jiang K, Coppola D, Crespo NC, Nicosia SV, Hamilton AD, Sebti SM, et al. The phosphoinositide 3-OH kinase/AKT2 pathway as a critical target for farnesyltransferase inhibitor-induced apoptosis. *Mol Cell Biol* 2000; 20:139-48.
- Du W, Liu A, Prendergast GC. Activation of the PI3K-AKT pathway masks the proapoptotic effects of farnesyltransferase inhibitors. *Cancer Res* 1999; 59:4208-12.
- Chun KH, Lee HY, Hassan K, Khuri F, Hong WK, Lotan R. Inhibition of protein kinase B/Akt and Bcl-2/Bcl-XL suppression by the farnesyl transferase inhibitor SCH66336 in apoptosis induction in squamous carcinoma cells. *Cancer Res* 2003; 63:4796-800.
- Liu A, Prendergast GC. Geranylgeranylated RhoB is sufficient to mediate tissue-specific suppression of Akt kinase activity by farnesyltransferase inhibitors. *FEBS Lett* 2000; 481:205-8.
- Liu A, Du W, Liu JR, Jessell TM, Prendergast GC. RhoB alteration is necessary for apoptotic and antineoplastic responses to farnesyltransferase inhibitors. *Mol Cell Biol* 2000; 20:6105-13.
- Edamatsu H, Gau CL, Nemoto T, Guo L, Tamanoi F. Cdk inhibitors, roscovitine and olomoucine, synergize with farnesyltransferase inhibitor (FTI) to induce efficient apoptosis of human cancer cell lines. *Oncogene* 2000; 19:3059-68.
- Adjei AA, Erlichman C, Davis JN, Cutler DL, Sloan JA, Marks RS, et al. A phase I trial of the farnesyl transferase inhibitor SCH66336: Evidence for biological and clinical activity. *Cancer Res* 2000; 60:1871-7.
- Shi B, Yaremkov B, Hajian G, Terracina G, Bishop WR, Liu M, et al. The farnesyl protein transferase inhibitor SCH66336 synergizes with taxanes in vitro and enhances their antitumor activity in vivo. *Cancer Chemother Pharmacol* 2000; 46:387-95.
- Reichert A, Heisterkamp N, Daley GQ, Griffin J. Treatment of Bcr/Abl-positive acute lymphoblastic leukemia in P190 transgenic mice with the farnesyl transferase inhibitor SCH66336. *Blood* 2001; 97:1399-403.
- Peters DG, Hoover RR, Gerlach MJ, Koh BY, Zhang H, Choe K, et al. Activity of the farnesyl protein transferase inhibitor SCH66336 against BCR/ABL-induced murine leukemia and primary cells from patients with chronic myeloid leukemia. *Blood* 2001; 97:1404-12.
- Glass TL, Liu TJ, Yung WK. Inhibition of cell growth in human glioblastoma cell lines by farnesyltransferase inhibitor SCH66336. *Neuro-oncol* 2000; 2:151-8.

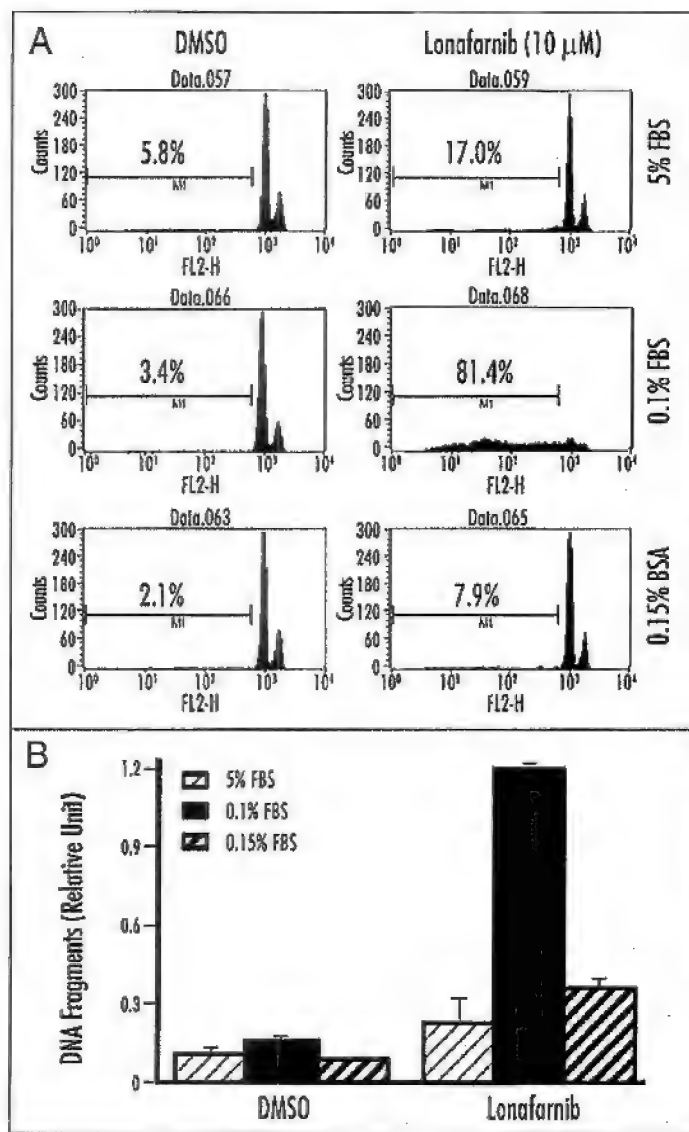


Figure 6. Addition of BSA in medium rescues cells from Lonafarnib-induced apoptosis as evaluated by measuring sub-G₁ population (A) and DNA fragments (B), respectively. H1792 cells were treated with 10 μ M Lonafarnib in the medium containing 5% FBS, 0.1% FBS, or 0.15% BSA for 24 h and then subjected to flow cytometric analysis (A) and EUSA (B), respectively. Each column in B represents a mean \pm SD of triplicate determinations.

- Feldkamp MM, Lau N, Roncari L, Guha A. Isotype-specific Ras GTP-levels predict the efficacy of farnesyl transferase inhibitors against human astrocytomas regardless of Ras mutational status. *Cancer Res* 2001; 61:4425-31.
- Adjaji AA, Davis JN, Brazeal LM, Brichman C, Kaufmann SH. Synergy of the protein farnesyltransferase inhibitor SCH66336 and cisplatin in human cancer cell lines. *Clin Cancer Res* 2001; 7:1438-45.
- Hoover RR, Mahon FX, Melo JV, Daley GQ. Overcoming STI571 resistance with the farnesyl transferase inhibitor SCH66336. *Blood* 2002; 100:1068-71.
- Nakajima A, Tauchi T, Sumi M, Bishop WR, Ohayashi K. Efficacy of SCH66336, a farnesyl transferase inhibitor, in conjunction with imatinib against BCR-ABL-positive cells. *Mol Cancer Ther* 2003; 2:219-24.
- Smalley KS, Eisen TG. Farnesyl transferase inhibitor SCH66336 is cytostatic, pro-apoptotic and enhances chemosensitivity to cisplatin in melanoma cells. *Int J Cancer* 2003; 105:165-75.
- Loprevite M, Favoni RE, De Cupis A, Scolari T, Semino C, Mazzanti P, et al. In vitro study of farnesyltransferase inhibitor SCH 66336, in combination with chemotherapy and radiation, in non-small cell lung cancer cell lines. *Oncol Rep* 2004; 11:407-14.
- Lin M, Bryant MS, Chen J, Lee S, Yaremkov B, Lipari P, et al. Antitumor activity of SCH 66336, an orally bioavailable tricyclic inhibitor of farnesyl protein transferase, in human tumor xenograft models and vav-ras transgenic mice. *Cancer Res* 1998; 58:4947-56.
- Khuri FR, Glisson BS, Kim BS, Stratkevich P, Thall PF, Meyers ML, et al. Phase I study of farnesyltransferase inhibitor (FTI) SCH66336 with paclitaxel in solid tumors. *Clin Cancer Res* 2004; 10:2968-76.
- Sun SY, Yue P, Dawson MI, Michel S, Lamph WW, Heyman RA, et al. Differential effects of synthetic nuclear retinoid receptor-selective retinoids on the growth of human non-small cell lung carcinoma cells. *Cancer Res* 1997; 57:4931-9.
- Sun SY, Yue P, Shroot B, Hong WK, Lotan R. Induction of apoptosis in human non-small cell lung carcinoma cells by the novel synthetic retinoid CD437. *J Cell Physiol* 1997; 173:279-84.
- Sun SY, Yue P, Wu GS, El-Deiry WS, Shroot B, Hong WK, et al. Mechanisms of apoptosis induced by the synthetic retinoid CD437 in human non-small cell lung carcinoma cells. *Oncogene* 1999; 18:2357-65.
- Mitsudomi T, Steinberg SM, Nau MM, Carbone D, D'Amico D, Bodner S, et al. p53 gene mutations in non-small-cell lung cancer cell lines and their correlation with the presence of ras mutations and clinical features. *Oncogene* 1992; 7:171-80.
- Crespo NC, Delarue F, Ohkanda J, Carrico D, Hamilton AD, Sefti SM. The farnesyltransferase inhibitor, FTI-2153, inhibits bipolar spindle formation during mitosis independently of transformation and Ras and p53 mutation status. *Cell Death Differ* 2002; 9:702-9.
- Ashar HR, James L, Gray K, Carr D, McGuirk M, Maxwell B, et al. The farnesyl transferase inhibitor SCH66336 induces a G(2) \rightarrow M or G(1) pause in sensitive human tumor cell lines. *Exp Cell Res* 2001; 262:17-27.
- Franke TB, Hornik CB, Segev L, Shostak GA, Sugimoto C. PI3K/Akt and apoptosis: Sino matters. *Oncogene* 2003; 22:8983-98.
- Suzuki N, Usano J, Tamanoi F. Farnesyltransferase inhibitors induce cytochrome c release and caspase 3 activation preferentially in transformed cells. *Proc Natl Acad Sci USA* 1998; 95:15356-61.
- Brognaud J, Clark AS, Ni Y, Dennis PA. Akt/protein kinase B is constitutively active in non-small cell lung cancer cells and promotes cellular survival and resistance to chemotherapy and radiation. *Cancer Res* 2001; 61:3986-97.
- Datta SR, Bruner A, Greenberg ME. Cellular survival: A play in three Acts. *Genes Dev* 1999; 13:2905-27.

Myristoylation of the Fus1 Protein Is Required for Tumor Suppression in Human Lung Cancer Cells

Futoshi Uno,¹ Jiichiro Sasaki,¹ Masahiko Nishizaki,¹ Giovanni Carboni,¹ Kai Xu,¹ Edward N. Atkinson,² Masashi Kondo,³ John D. Minna,³ Jack A. Roth,¹ and Lin Ji¹

¹Section of Thoracic Molecular Oncology, Department of Thoracic and Cardiovascular Surgery, and ²Department of Biomathematics, The University of Texas M. D. Anderson Cancer Center, Houston, Texas; ³Department of Internal Medicine and Pharmacology, Hamon Center for Therapeutic Oncology Research, The University of Texas Southwestern Medical Center, Dallas, Texas

Abstract

FUS1 is a novel tumor suppressor gene identified in the human chromosome 3p21.3 region that is deleted in many cancers. Using surface-enhanced laser desorption/ionization mass spectrometric analysis on an anti-Fus1-antibody-capture ProteinChip array, we identified wild-type Fus1 as an N-myristoylated protein. N-myristoylation is a protein modification process in which a 14-carbon myristoyl group is cotranslationally and covalently added to the NH₂-terminal glycine residue of the nascent polypeptide. Loss of expression or a defect of myristoylation of the Fus1 protein was observed in human primary lung cancer and cancer cell lines. A myristoylation-deficient mutant of the Fus1 protein abrogated its ability to inhibit tumor cell-induced clonogenicity *in vitro*, to induce apoptosis in lung tumor cells, and to suppress the growth of tumor xenografts and lung metastases *in vivo* and rendered it susceptible to rapid proteasome-dependent degradation. Our results show that myristoylation is required for Fus1-mediated tumor-suppressing activity and suggest a novel mechanism for the inactivation of tumor suppressors in lung cancer and a role for deficient posttranslational modification in tumor suppressor-gene-mediated carcinogenesis.

Introduction

Tumor suppressor genes (TSGs) play a major role in the pathogenesis of human lung and other cancers. Lung cancer cells harbor mutations and deletions in multiple known oncogenes and TSGs; however, genetic alterations and allelic losses on the short arm of chromosome 3 are among the most frequent and earliest cancer abnormalities detected in the pathogenesis of lung cancers and have been shown to occur in 96% of non-small cell lung cancers (NSCLCs) and in 78% of preneoplastic lung lesions (1). The frequent and early loss of heterozygosity and the overlapping homozygous deletions observed in the 3p21.3 region in lung and breast cancers suggest a critical role of one or more 3p21.3 genes as "gatekeepers" in the molecular pathogenesis of these cancers (2, 3).

The novel *FUS1* TSG is one of the candidate TSGs that have been identified in a 120-kb homozygous deletion region in human chro-

sosome 3p21.3 (2, 4, 5). The cloned cDNA of *FUS1* (GenBank accession no. AF055479) is 333 bp in length and encodes a protein of 110 amino acid residues (Fig. 1A). However, the *FUS1* gene does not show homology with any known genes and proteins in databases. We have previously demonstrated that exogenous expression of the wild-type (wt) *FUS1* by plasmid- or adenoviral vector-mediated gene transfer significantly inhibits tumor cell growth, induces apoptosis, and alters cell cycle kinetics in 3p21.3-deficient NSCLC cells *in vitro* and efficiently suppresses tumor growth and inhibits tumor progression and metastases in various human lung cancer xenograft mouse models (4-6). However, the mechanisms involved in the inactivation of the *FUS1* gene in primary human cancers and in *FUS1*-mediated tumor suppression remain unknown. On the basis of our findings reported here, we hypothesize that loss of expression, haploinsufficiency, and deficiency of posttranslational modification of Fus1 protein may lead to loss of its tumor-suppression function and play an important role in lung cancer development.

Materials and Methods

Cell Lines and Cell Culture. The human NSCLC cell lines A549, NCI-H1299, NCI-H358, NCI-H226, NCI-H322, and NCI-H460, with various 3p21.3 and *p53* gene status as described previously (7, 8), and a normal human lung fibroblast cell line, WI-38, were used for *in vitro* and *in vivo* experiments. The A549 line was maintained in Ham's F12 medium supplemented with 10% FCS. The H1299, H358, H226, H322, and H460 lines were maintained in RPMI 1640 supplemented with 10% FCS and 5% glutamine. Normal fibroblast WI-38 cells were cultured in MEM supplemented with 10% FCS and 5% glutamine.

Tumor Cell-Induced Clonogenicity Assay. To analyze the effect of myristoylation of Fus1 protein on tumor cell-derived clonogenicity *in vitro*, we transfected H1299 cells (1×10^5) with various *FUS1*-expressing and control plasmid vector DNAs, using FUGEN 6 *in vitro* transfection reagent (Roche Molecular Biochemicals, Indianapolis, IN). Four μ g of each test plasmid DNA were cotransfected with 1 μ g of the neomycin-resistant gene-containing pcDNA3.1 vector (Invitrogen, Carlsbad, CA); the pcDNA3.1 (1 μ g) vector alone and the pcDNA3.1 plus wt-*p53* plasmid were used as negative and positive controls, respectively. Twenty-four h after transfection, cells were harvested, stained with trypan blue, and counted. Five thousand cells were replated on a 100-mm tissue culture dish in triplicate and grown in 5% fetal-bovine-serum-supplemented RPMI 1640 containing 400 μ g/ml G418 for 2-3 weeks. The numbers of G418-resistant colonies were counted after staining with Crystal Violet.

Immunohistochemical Analysis. Samples of human lung tumor and parallel normal tissues were obtained from patients with informed consent through the Lung SPORE program at the University of Texas Southwestern Medical Center and at the M. D. Anderson Cancer Center. Expression of the Fus1 protein in tissue samples was analyzed by immunohistochemical staining with anti-Fus1 peptide polyclonal antibodies and a VECTASTAIN Elite ABC kit (Vector Laboratories Inc., Burlingame, CA). Briefly, the rabbit anti-Fus1 polyclonal antibodies used for immunohistochemical staining, raised against a synthetic oligopeptide derived from NH₂-terminal amino acid sequence of Fus1 protein, were affinity-purified by use of custom immunochemistry ser-

Received 11/26/03; revised 2/23/04; accepted 3/3/04.

Grant support: Partially supported by grants from the National Cancer Institute, the NIH (Grants SPORE CA70970 and CA71618); a W. M. Keck Gene Therapy Career Development grant (L. Ji); grants from the Department of Defense BESCT (Grant DAMD17-01-1-0689) and TARGET (Grant DAMD17-02-1-0706) Lung Cancer Programs; gifts to the M. D. Anderson Cancer Center Division of Surgery Core Laboratory Facility from Teaneco and Exxon; the M. D. Anderson Cancer Center Support Core Grant (CA16672); a grant from the Tobacco Settlement Funds as appropriated by the Texas State Legislature; and a sponsored research agreement with Introgen Therapeutics, Inc. (SR93-004-1).

The costs of publication of this article were defrayed in part by the payment of page charges. This article must therefore be hereby marked advertisement in accordance with 18 U.S.C. Section 1734 solely to indicate this fact.

Note: F. Uno, J. Sasaki, and M. Nishizaki contributed equally to this work.

Requests for reprints: Lin Ji, Department of Thoracic and Cardiovascular Surgery, Box 445, The University of Texas M. D. Anderson Cancer Center, 1515 Holcombe Boulevard, Houston, TX 77030. Phone: (713) 745-4530; Fax: (713) 794-4901; E-mail: lji@mdanderson.org.

vices provided by Bethyl Laboratories, Inc. (Montgomery, TX). The formalin-fixed, paraffin-embedded tissue sections were incubated with horseradish peroxidase-conjugated rabbit anti-Fus1 antibodies (0.1–2.0 µg/ml in PBS-BSA), and immunostaining was performed with the Vectastain Elite ABC kit according to manufacturer's instruction. Subsequently, the sections were counterstained with Harris hematoxylin. Samples were examined under a microscope, and immunohistochemical images were recorded with an equipped digital camera.

Laser-Capture Microdissection (LCM) and Protein Preparation for Surface-Enhanced Laser Desorption/Ionization Mass Spectrometry (SELDI-MS) Analysis. Frozen tissue sections were rapidly removed from –80°C storage and immersed in or flooded with 70% alcohol for ~1 min, followed by H&E staining. The tumor cells and adjacent normal cells were precisely identified by microscopic examination. LCM was performed with the PixCell LCM microscope (Arcturus Engineering, Mountain View, CA). Approximately 500–1000 microdissected cells were then transferred to a thermoplastic film mounted on optically transparent LCM caps and incubated with 50 µl of protein lysis buffer containing 1% NP40, 0.5% sodium deoxycholate, 0.1% SDS, 1% DTT, and 1× complete protease inhibitors (Roche Biochemicals) in PBS on ice for 15 min. Cell samples were sonicated in a Transonic 700H sonication water bath (Lab-Line Instruments, Melrose Park, IL) at 4°C for 3 min, and protein lysate was cleared by centrifugation for 5 min at 13,000 rpm at 4°C. The protein lysates were either used immediately or stored at –80°C.

Antibody-Capture ProteinChip Array (ACPA) with SELDI-MS. The endogenous or exogenous wt-Fus1 or mutant Fus1 proteins were captured with affinity-purified rabbit Fus1 polyclonal antibodies from cultured cells or LCM-separated and enriched human primary lung tumor and noninvolved normal cells. Five µl (~10 µg) of protein lysate were spotted on a Fus1 antibody-coated preactivated surface (PS20) ProteinChip array and analyzed by SELDI-MS in the presence of CHCA matrix solution; both internal and external standards were used for mass/charge (*m/z*) calibration (Ciphergen Biosystems, Fremont CA). ACPA and SELDI-time-of-flight (TOF)-MS analysis were performed according to the manufacturer's instructions and procedures described in detail elsewhere (9–11).

Animal Studies. All animals were maintained and animal experiments were performed under NIH and institutional guidelines established for the Animal Core Facility at the University of Texas M.D. Anderson Cancer Center. Procedures for H1299 s.c. tumor inoculations in *nude* mice have been described previously (8). When tumors reached an average of ~0.5 cm in diameter (~2 weeks after tumor inoculation), *N*-[1-(2,3-dioleoyloxy)propyl]-*N,N,N*-trimethylammoniummethyl sulfate-cholesterol-complexed wt-*FUS1* or myristoylation-mutant (*myr-mt*)-*FUS1* plasmid vectors (*FUS1* lipoplex) were injected into the tumors three times within a week at a dose of 25 µg of plasmid DNA and 10 nmol liposome/tumor in 100 µl of 5% dextrose in water. PBS and *LucZ* were used as mock and negative controls, respectively. Tumor sizes were measured twice a week, and tumor volume was calculated using the equation $V(\text{mm}^3) = a \times b^2/2$, where *a* is the largest diameter and *b* is the smallest dimension.

To evaluate the effect of systemic administration of *FUS1* lipoplex on development of A549 experimental lung metastases in nude mice, we injected various lipoplexes every 2 days (three times/day) i.v. into all animals at a dose of 25 µg of plasmid DNA and 10 nmol of liposome each in 100 µl of 5% dextrose in water per animal. Each treatment group consisted of 10 animals. Lungs were harvested 2 weeks after the last injection, and metastatic colonies on the surfaces of lung were stained with Indian ink. Tumor colonies on lung surfaces were counted under a dissecting microscope without knowledge of the treatment groups, and the lung tissues were sectioned for further pathological and immunohistochemical analysis and for *in situ* apoptosis analysis with terminal deoxynucleotidyl transferase (Tdt)-mediated nick end labeling (TUNEL) staining (Roche Biochemical).

Results

Loss of Expression of Fus1 Protein in Primary Lung Cancer and Cancer Cell Lines. In a previous study, we examined 40 primary lung cancers and found that mutation of the *FUS1* gene was infrequent and that there were only a few nonsense mutations and a COOH-terminal deletion mutation that arose from aberrant mRNA

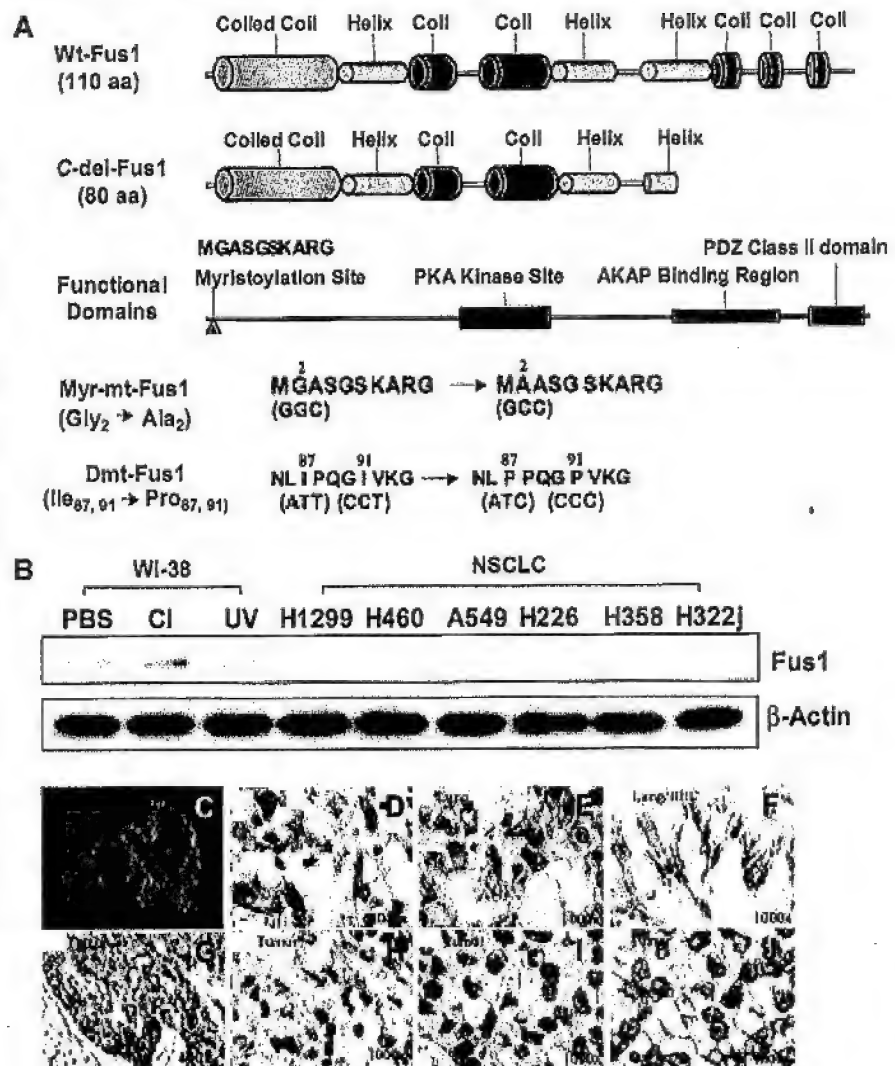
splicing (Fig. 1A; Ref. 5). In addition, we found no evidence for *FUS1* promoter region methylation (data not shown). *FUS1* expression has been detected in various normal human tissues, including brain, heart, pancreas, prostate, kidney, and lung, based on quantification of expressed sequence tags in Unigene clusters, as summarized in GeneCards⁴ by the Crown Human Genomics Center and Yeda Research and Development Co. Ltd. (Rehovot, Israel). Although endogenous Fus1 protein expression could be detected in normal human bronchial epithelial cells and fibroblast cells (WI-38) by immunoblot analysis and *FUS1* mRNA transcription could be seen on Northern blots of RNAs prepared from lung cancer cell lines, we could not detect endogenous Fus1 protein in these lung cancer cell lines on immunoblots using the affinity-purified, anti-Fus1 peptide antibodies we developed (Fig. 1B). In addition, we performed immunohistochemical staining on a set of paired normal lung and lung cancer tissue sections (Fig. 1, C–J). We found that normal lung epithelial cells express Fus1 (Fig. 1, D–F) but that many lung cancers (15 of 20; >70%; Fig. 1, H–J) did not. We also found that even in those tumor samples with Fus1-positive staining, the staining was not uniformly detectable in all tumor cells (Fig. 1G). On the basis of both the lung-cancer-growth-suppressing properties of the Fus1 protein *in vitro* and in animal models and the observed loss of protein expression in primary tumors and tumor-derived cell lines, we hypothesized that *FUS1* would have to act as a TSG in a haploinsufficient manner (because most primary lung cancers experienced allelic loss in this 3p21.3 region; Ref. 12) and that both loss of expression and deficient posttranslational modification of Fus1 protein might lead to loss of its tumor suppression function and to lung cancer development.

Identification of Myristoyl Modification of Fus1 Protein. To test this hypothesis, we first performed computer-based homologous structure modeling and functional domain prediction of Fus1 protein to assess its biochemical and biophysical properties and to obtain possible leads to its biological function (Fig. 1A). The secondary protein structure prediction indicated that the wt-Fus1 protein is a highly hydrophobic protein with extensive helix-coil domain structures lacking transmembrane elements (Fig. 1A). The functional domains of Fus1 protein were predicted by use of a motif-based profile scanning program (13) and showed a potential myristoylation site at the NH₂ terminus, a protein kinase A interaction site, an A kinase-anchoring protein interaction (protein/protein) site, and a PDZ class II domain (Fig. 1A). From these analytical comparisons of Fus1 protein structure and function, we predict that Fus1 is a myristoylated member of the novel cAMP-dependent protein kinase A and A kinase-anchoring protein families, which are associated with many cellular processes, including transcription, signal transduction, metabolism, ion channel regulation, cell cycle progression, and apoptosis (14, 15).

To verify myristoylation of the Fus1 protein, we constructed a plasmid vector expressing either the wt-*FUS1* or a myristoylation-site-deficient mutant (*myr-mt-FUS1*) in which the predicted myristoylation site of glycine (G₂) was replaced with an alanine (A₂; Fig. 1A) by site-directed mutagenesis. A double-mutant (*dmt-FUS1*) in the COOH-terminal region, in which two highly hydrophobic isoleucine residues (I₈₇ and I₉₁) were replaced with two neutral and rigid-conformation-promoting proline residues (P₈₇ and P₉₁; Fig. 1A), was also constructed as another control to confirm the biological significance and specificity of the myristoylation-deficient mutation of Fus1 protein. The wt-Fus1- and mutant-Fus1-expressing plasmid vectors were used to transfect Fus1-deficient human NSCLC NCI-H1299 cells. The expression and posttranslational modification status of these wt and mutant Fus1 proteins were analyzed by SELDI-TOF-MS on an

⁴ <http://bioinfo.weizmann.ac.il/cards-bin/carddisp?FUS1>.

Fig. 1. Predicted secondary structure and functional domains of Fus1 protein and its expression in normal lung and primary lung tumors and tumor-derived cell lines. A, predicted secondary structure and functional domains of wild-type (wt)-Fus1 and C-del-Fus1. The predicted functional elements and domains, including a potential myristoylation site, protein kinase A (PKA) targeting site, a kinase-anchoring protein (AKAP) interface, and a PDZ class II domain are indicated. Mutant *myr-mt-Fus1*, in which the codon GGC for Gly₂ was changed to GCC for Ala₂, and double-mutant *Dmt-Fus1*, in which codon ATT for Ile₈₇ and ATC for Ile₉₁ were changed to CCT for Pro₈₇ and CCC for Pro₉₁, respectively, were constructed by site-directed mutagenesis. C-del-Fus1 is a tumor-related COOH-terminal deletion mutant derived by abnormal mRNA splicing. B, immunoblot analysis of endogenous Fus1 protein expression in normal lung fibroblast WI-38 cells grown in PBS under conditions of contact inhibition (CI) or after exposure of the cells to UV irradiation (100 joules for 5 min) and in non-small cell lung cancer (NSCLC) cells. The same blots were also probed for β -actin to ensure equal loading. C-J, immunofluorescence image analysis in wt-FUS1-transfected H1299 cells with FITC-conjugated rabbit anti-Fus1 antibodies (C) and immunohistochemical analysis of Fus1 protein expression in normal lung cells (D and E), bronchial epithelial cells (F), and primary lung tumor cells (G-J) in formalin-fixed, paraffin-embedded tissue samples. wt-Fus1 has a typical mitochondria/endoplasmic reticulum membrane localization in cytoplasm (C). Expression of Fus1 was detected in cytoplasm in normal lung (D and E) and bronchial epithelia (F); Fus1 expression was also detected in some tumor cells in one primary NSCLC (G) but was undetectable in other primary NSCLC cell lines (H-J) when we used rabbit anti-Fus1 polyclonal antibodies at a 1:2000 dilution. Magnifications: $\times 400$ (G); $\times 1000$ (D-F, H-J).



anti-Fus1 ACPA (Ciphaer Biosystems, Fremont, CA; Fig. 2A). The expressed Fus1 proteins in transfected H1299 cells were specifically captured on the protein chip and detected in the SELDI-TOF-MS spectra (Fig. 2A), but no protein peaks at corresponding mass positions were detected in the spectra with an anti-101F6 (a protein with encoding gene collocated in 3p21.3 region with *FUS1*) antibody-coated chip as a nonspecific control (Fig. 2B). The wt-Fus1 protein was identified as a myristoylated protein based on the detected mass of the captured wt-Fus1 protein (Fig. 2A), which showed a protein peak with a m/z ratio of $12,174 \pm 6.25$ Da compared with the predicted mass of 12,072.98 Da for the nonmyristoylated wt-Fus1 or 12,174.2 Da for the myristoyl-Fus1 protein. The myristoylation-deficient mutant (12,024.6 Da) and the COOH-terminal deletion mutant (8,783.5 Da) of Fus1 protein were also captured and detected on the protein array by SELDI-MS by comparing them with their calculated masses (Fig. 2A). No captured Fus1 proteins were detected in either the untransfected or *pLacZ*-transduced cells (Fig. 2A). On the basis of the 232-Da mass shift between the detected myristoylated Fus1 (12,174 Da) and the predicted nonmyristoylated Fus1 protein (11,942 Da; without the first methionine residue because the methionine residue is removed during myristoylation), we predict that the Fus1 protein is acylated at the G₂ with a 14-carbon myristate (C₁₄H₂₈O₂;

228.4 Da). The myristoylation of Fus1 protein was also confirmed by immunoblot analysis and immunoprecipitation analysis of the ¹⁴C-myristate-labeled and acylated Fus1 protein in the *pFUS1*-transfected cells (Fig. 2S).

Defect of Myristoylation of Fus1 Protein in Primary Lung Cancer. Because mutation of *FUS1* is infrequent and no evidence has been found for methylation or mutation of the *FUS1* promoter region in lung cancers, other factors, such as haploinsufficiency, low expression, abnormal products arising from aberrant mRNA splicing, and posttranslational modification of Fus1, may play important roles in lung tumorigenesis (2, 3). We used ACPA analysis with SELDI-TOF-MS to evaluate the protein expression and myristoylation status in primary lung tumor and uninvolved normal lung tissue samples. Molecular analysis of tumors and their precursor lesions requires the isolation of specific cell subpopulations (normal, preneoplastic, and tumors) from a composite background of multiple cell types in tumor tissue biopsies. This was accomplished with LCM technology (16). To evaluate Fus1 protein expression and posttranslational modifications in human lung tumors and noninvolved tissues, we used LCM combined with appropriate tissue preparation methods to separate and enrich tumor or noninvolved normal cells, and the resulting separated cell populations (~500–1000 cells) were used for the Fus1-specific

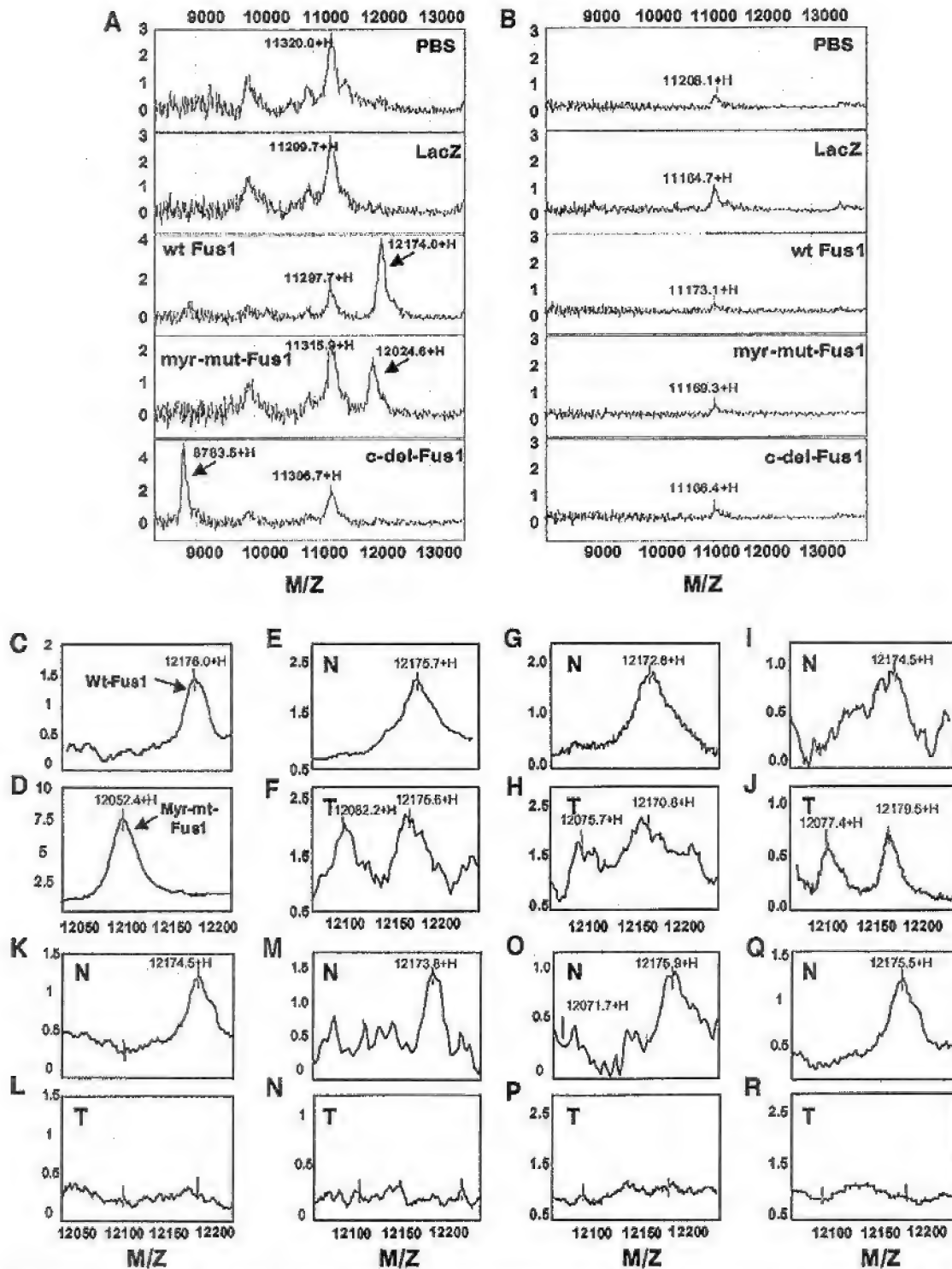


Fig. 2. Detection of myristoylation of Fus1 protein by surface-enhanced laser desorption/ionization time-of-flight mass spectrometry analysis on an anti-Fus1 antibody-capture ProteinChip array (ACPA). A, detection of Fus1 proteins captured on the anti-Fus1 antibody-coated preactivated surface (PS20) chip in wild-type (*wt* *FUS1*) or myristoylated mutant-*FUS1* (*myr-mut-Fus1*)-containing plasmid-transfected H1299 cells. The myristoylated Fus1 proteins are detected as a peak with a mass of 12,174 Da, and the nonmyristoylated Fus1 (*myr-mut-Fus1*) is detected with a mass of 12,024 Da compared with the calculated masses of 12,174 Da for the myristoylated *wt-Fus1* and 12,025 Da for the *myr-mut-Fus1*, respectively. No corresponding proteins were detected in either PBS mock or *LacZ* control cells. B, ACPA assay with PS20 chips coated with nonspecific antibodies (anti-101F6). No Fus1 proteins were detected in these mass spectra when the same protein lysates as in A were applied. C–R, detection of status of Fus1 protein expression and posttranslational modification in laser-capture microdissection-enriched human primary lung tumor (T) and adjacent noninvolved normal (N) cells, shown as representative pairs (pair E and F through pair Q and R) from 15 tissue samples tested by ACPA assay as described in B. The protein lysates prepared from wild-type *FUS1* (*Wt-FUS1*) (C) or myristoylated mutant-*FUS1* (*Myr-mut-FUS1*)-transfected (D) H1299 cells were used as positive controls. A single peak of myristoylated *wt-Fus1* protein with a mass of $12,174 \pm 5.2$ Da was detected in normal cells, whereas two peaks, one with a mass of 12,174 Da, corresponding to the mass expected for the myristoylated *wt-Fus1* protein, and another with a mass of $12,075 \pm 8.5$ Da, corresponding to the mass of the nonmyristoylated *wt-Fus1* protein, were detected in tumor cells. In some tumors, these peaks were not detected. S, Western blot (WB) and

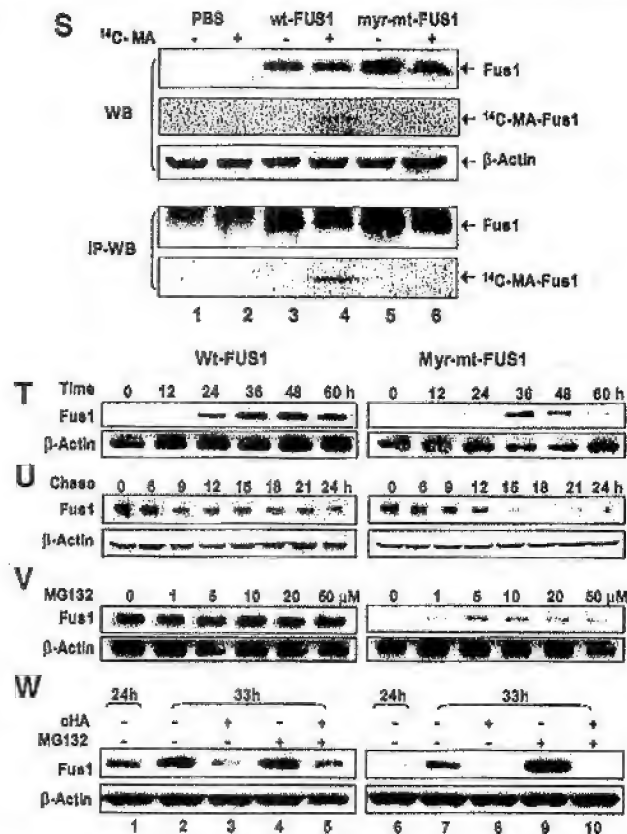


Fig. 2 Continued

ACPA analysis by SELDI-TOF-MS. We found that only myristoylated protein species could be detected in normal cells (13 of 15; $P = 0.0003$, nonparametric 2×2 contingency table; McNemar's χ^2 test) but that both the nonmyristoylated and myristoylated Fus1 protein were detected in tumor cells (5 of 15 samples; $P = 0.0442$) as indicated by detection of a peak corresponding to the Fus1 protein mass on the mass spectra (Fig. 2, C–R). In some tumor samples (7 of 15 samples; $P = 0.0030$), neither form of the Fus1 proteins could be captured (Fig. 2, I, N, P, and R), consistent with the results of the immunohistochemical analyses for these tumor and normal tissue samples. The remaining three samples tested were unresolvable because of the ambiguous spectra (spectra not shown). The difference in the observed Fus1 protein myristoylation status between the normal and the tumor cell populations was significant as indicated by a nonparametric McNemar marginal homogeneity test for the equality of categorical responses from two paired and dependent populations ($P < 0.001$).

Proteasome-Dependent Degradation of Nonmyristoylated Fus1 Protein. To explore the possible mechanism(s) for the involvement of the nonmyristoylated (or demyristoylated) Fus1 protein and the loss of its expression in primary lung cancer, we evaluated the stability of

the exogenously expressed wt-Fus1 and myr-mt-Fus1 proteins in H1299 cells. We found that the duration of transient expression of myr-mt-Fus1 protein was much shorter than that of wt-Fus1. Myr-mt-Fus1 protein expression peaked at 36 h posttransfection and was almost undetectable after 60 h, whereas the wt-Fus1 protein was expressed at high levels beyond 60 h posttransfection (Fig. 2T). The half-life of the myr-mt-Fus1 protein was shorter than that of wt-Fus1 (~6 h for the former and 12 h for the later), as shown by pulse-chase of protein synthesis after treatment with the protein synthesis inhibitor cycloheximide (Fig. 2U). These results suggest that nonmyristoylated Fus1 protein may be degraded more rapidly than the myristoylated form. We therefore investigated the effect of the proteasome inhibitor (17) MG132 on degradation of Fus1 proteins. We found that the nonmyristoylated Fus1 protein levels increased in myr-mt-FUS1-transfected H1299 cells treated with various concentrations of MG132 (Fig. 2V). The MG132-induced recovery of the myr-mt-Fus1 protein could be detected at a very low level (1 μM; Fig. 2V) and was independent of protein synthesis, as demonstrated by significant protein accumulation on treatment with 10 μM of MG132 in the presence or absence of the protein synthesis inhibitor cycloheximide (Fig. 2W), with no effect shown on wt-Fus1 protein under the same experimental conditions (Fig. 2W). These results suggest that myristoylation may stabilize Fus1 protein and that demyristoylation may lead to rapid degradation of Fus1 protein through a proteasome-dependent pathway.

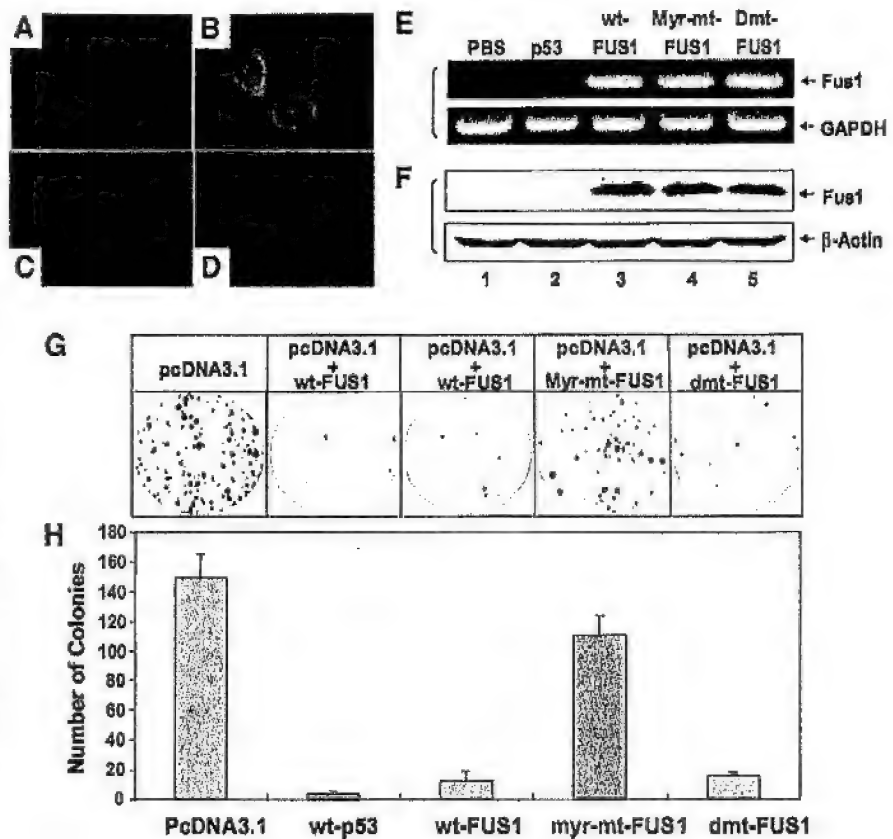
Disrupted Subcellular Localization of Myristoylation-Deficient Mutant of Fus1 Protein. One potential function of protein myristoylation is the facilitation of efficient interactions with cell membranes necessary for correct subcellular localization (18–20). We therefore analyzed the subcellular localization of myristoylation-positive wt-Fus1 and the myristoylation-deficient mt-Fus1 proteins in plasmid-transfected H1299 cells by immunofluorescence image analysis using FITC-conjugated anti-Fus1 antibodies (Fig. 3, A–D). The myr-mt-Fus1 protein lost its characteristic intracellular membrane localization (Fig. 3, C and D), suggesting a critical role for myristoylation in the cellular localization of Fus1 protein.

Myristoylation Is Required for Fus1-Mediated Tumor-Suppressing Activities *in Vitro* and *in Vivo*. To evaluate the biological role of myristoylation in Fus1 protein-mediated tumor suppression, we compared the clonogenicity of the wt-Fus1- and myr-mt-Fus1-expressing H1299 cells *in vitro* (Fig. 3, G and H). The exogenous expression of both the FUS1 genes and proteins in these H1299 transfectants was confirmed by reverse transcription-PCR (Fig. 3E) and by Western blot (Fig. 3F) analysis, respectively. Significant inhibition of clonogenicity was observed in myristoylated wt-Fus1-expressing H1299 cells, but no significant growth inhibition was observed in myr-mt-Fus1-expressing cells compared with the Fus1-nonexpressing controls (Fig. 3, G and H). The COOH-terminal double mutation of Fus1 (dmt-Fus1), which was theoretically expected to severely alter the hydrophobic and conformational properties in this region of Fus1 protein, was still able to significantly inhibit clonogenicity, similar to the effect of wt-Fus1 (Fig. 3, G and H).

We evaluated the effects of wt-Fus1 and myr-mt-Fus1 protein expression on tumor growth in H1299 s.c. tumor xenografts in *nu/nu*

immunoprecipitation Western blot (IP-WB) analyses for verification of myristoylation of Fus1 proteins in H1299 transfectants. H1299 cells were transfected with either wild-type FUS1 (wt-FUS1) or myristoylation-deficient mutant-FUS1 (myr-mt-FUS1) plasmid vectors for 48 h and then incubated with ¹⁴C-labeled myristic acid (MA; American Radiolabeled Chemicals, St. Louis, MO) in a final concentration of 5 μCi/ml for 90 min. Crude protein lysate (80 μg) was loaded in each lane for WB, and 1–2 μg of anti-Fus1 antibodies were used for IP. T and U, effect of myristoylation on Fus1 protein synthesis and stability by WB analysis during a 60-h time course posttransfection (T) and with a 3-h interval pulse chase after treatment with 50 μM of protein synthesis inhibitor cycloheximide (Chexo; U) in wild-type-FUS1 (wt-FUS1) (left panels) or myristoylation-deficient mutant-FUS1 (myr-mt-FUS1)-transfected (right panels) H1299 cells. V and W, effect of proteasome inhibitor MG132 on demyristoylation-induced degradation of Fus1 proteins. H1299 cells were transfected with wt-FUS1 or myr-mt-FUS1 plasmid DNAs for 24 h and then treated with DMSO (Lane 0) and various concentrations (1–50 μM) of MG132 (V), or were treated with 10 μM MG132 in the presence (+) or absence (–) of 50 μM cycloheximide (W). Expression of Fus1 proteins was analyzed by WB with anti-Fus1 antibodies. These experiments were carried at least twice with duplicates for each.

Fig. 3. Effects of myristoylation on Fus1 protein subcellular localization and Fus1-mediated tumor-suppressing activity *in vitro*. **A–D**, immunofluorescence image analysis of Fus1 protein expression and subcellular localization. H1299 cells were transfected with either wild-type Fus1-expressing (**A** and **B**) or myristoylation-deficient mutant-Fus1-expressing (**C** and **D**) plasmid vectors. Fus1 proteins were probed with FITC-conjugated anti-Fus1 antibody (green), and the nucleus was stained with Hoechst dye (blue; Sigma Chemical Co., St. Louis, MO). **E** and **F**, expression of Fus1 genes and proteins in H1299 transfectants were verified by reverse transcription-PCR (**E**) and by Western blot analysis (**F**). *wt-FUS1*, wild-type Fus1; *Myr-mt-FUS1*, myristoylation-deficient mutant-Fus1; *Dmt-FUS1*, double-mutant Fus1; GAPDH, glyceraldehyde-3-phosphate dehydrogenase. **G** and **H**, effect of myristoylation of Fus1 protein on tumor cell-derived clonogenicity *in vitro*. H1299 cells (1×10^5) were transfected with plasmid DNAs *in vitro*. The wild-type (*wt-FUS1*), myristoylation-deficient mutant (*Myr-mt-FUS1*), or hydrophilic double mutant (*dmt-FUS1*) of Fus1-expressing plasmids were cotransfected with the neomycin-resistant gene-containing pcDNA3.1 vector; the pcDNA3.1 vector alone and the pcDNA3.1 plus wt-p53 plasmid were used as negative and positive controls, respectively. The numbers of G418-resistant colonies were counted after staining with Crystal Violet (**G**), and the quantitative analysis is shown in **H**. The experiments were repeated at least three times. The bars represent the SD, and the differences between the pcDNA3.1 vector alone and each testing construct was analyzed statistically by two-tailed Student's *t* test. $P \leq 0.05$ is considered significant.



mice by intratumoral injection of *N*-[1-(2,3-dioleoyloxy)propyl]-*N,N,N*-trimethylammoniummethyl sulfate-cholesterol complexed with either *wt-FUS1* or *myr-mt-FUS1*-expressing plasmid DNAs (*FUS1* lipoplexes; Ref. 21) along with PBS as a mock control and *LacZ* plasmid vector as a negative control (Fig. 4A). The human NSCLC xenograft model, DNA lipoplex preparation, and treatment procedures were as described previously (4, 6, 21). Tumor growth was recorded from the first injection until 31 days after the last injection. Tumor volumes were normalized by calculating the percentage increase in tumor volume after treatment relative to volume at the beginning of treatment in each group. All of the tumors treated with *wt-FUS1* showed significantly suppressed growth ($P < 0.001$) compared with mouse groups treated with PBS or *pLacZ* controls (Fig. 4A). However, the tumor-suppressing activity of the myristoylation-deficient mutant (*myr-mt-FUS1*) of Fus1 protein was significantly reduced compared with *wt-FUS1* ($P < 0.001$), although it retained a small inhibitory effect compared with the PBS and *pLacZ* controls (Fig. 4A).

We also evaluated the effect of the myristoylation of Fus1 protein on development of lung metastases, using the human NSCLC A549 xenograft metastasis mouse model by systemic (i.v.) administration of the *wt-FUS1* or *myr-mt-FUS1* lipoplexes compared with PBS, *pLacZ*, and the lung cancer-originated COOH-terminal deletion mutant of *wt-FUS1* and *dmt-FUS1* plasmid vector controls (4, 6). The development of A549 pulmonary metastases was significantly inhibited ($P < 0.001$), and the numbers of metastatic tumor colonies found on the surfaces of lungs from mice inoculated with A549 cells were reduced >85% in animals treated with *wt-FUS1* compared with those in control treatment groups (Fig. 4B). However, no significant reduction ($P < 0.003$) of metastasis formation was observed in animals

treated with *myr-mt-FUS1*. The formation of metastases was significantly reduced ($P < 0.001$) in animals treated with *dmt-FUS1* compared with those controls treated with either PBS or *LacZ*, but the inhibitory effect was weaker than that observed in the *wt-FUS1*-treated group (Fig. 4B). The size of any remaining metastatic tumor nodules, as shown in H&E-stained sections of mouse lung tissues (Fig. 4C), was reduced in animals treated with *wt-FUS1* but not in those treated with *myr-mt-FUS1*, compared with either PBS or *LacZ*-treated controls. We analyzed the induction of apoptosis in these Fus1-expressing tumor cells by *in situ* apoptosis analysis with FITC-dUTP-labeled TUNEL staining (Roche Biochemicals; Fig. 4, D–J). Induction of apoptosis was detected in the *wt-FUS1*-expressing tumors (Fig. 4E) but not in *myr-mt-FUS1*-expressing (Fig. 4F) or PBS-treated (Fig. 4D) tumors, providing direct evidence for the need for both Fus1 expression and myristoylation in Fus1-mediated tumor suppression and apoptosis *in vivo*.

Discussion

Our studies present the first evidence supporting the biological importance of myristoyl modification of a TSG product and warrant further study of the role of the expression and posttranslational modification of Fus1 protein in the pathogenesis of lung and other human cancers. The N-myristoyl modification of proteins is achieved by a cotranslational linkage of myristic acid via an amide bond to the NH_2 -terminal glycine residues of a variety of cellular and viral proteins in eukaryotic cells (22). Covalent modification of proteins by fatty acids such as myristate and palmitate is now a widely recognized form of protein modification, and ~100 proteins are known to be myristoylated (18, 20). N-Myristoyl proteins play essential roles in

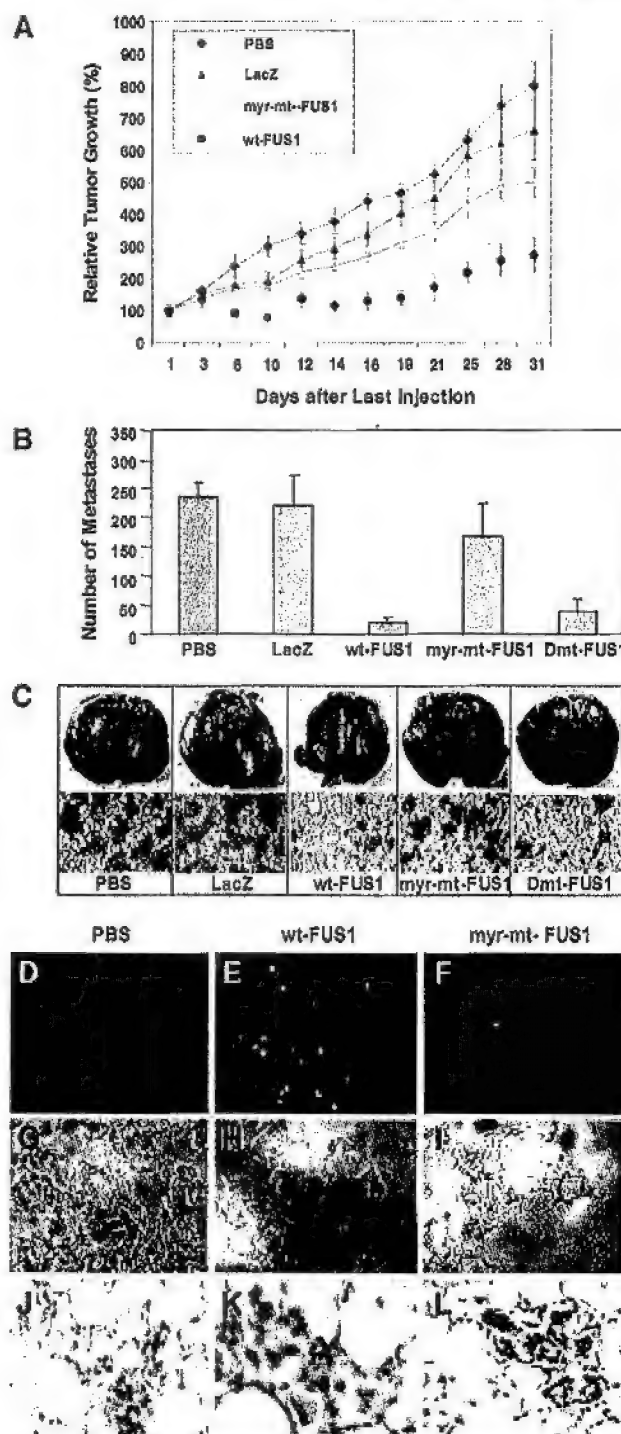


Fig. 4. Effect of myristoylation of Fus1 protein on Fus1-mediated tumor-suppressing activity *in vivo*. **A**, effect on H1299 human tumor xenograft growth in nude mice. Human non-small cell lung cancer H1299 cells were inoculated s.c. in nude mice. When the tumor reached 5–10 mm in diameter (2 weeks after tumor inoculation), *N*-(1-(2,3-dioleoyloxy)propyl)-*N,N,N*-(trimethylammonium)methyl sulfate-cholesterol-complexed wild-type *FUS1* (*wt-FUS1*) or myristoylation-deficient *FUS1* (*myr-mt-FUS1*) plasmid vectors (*FUS1* lipoplex) was injected into the tumors three times within 1 week. PBS and LacZ were used as mock and negative controls, respectively. Results are reported as the mean \pm SD for 5–10 mice in each treatment group. Tumor volumes were normalized by the percentage increase of tumor sizes after treatment relative to those at the beginning of the treatment in each group. The mean tumor volumes \pm SE (bars) from these experiments are shown. ANOVA was performed to determine statistical significance between each treatment group, using Statistica software (StatSoft Inc., Tulsa, OK), and $P \leq 0.05$ was considered significant. **B**, effect of systemic administration of *FUS1* lipoplex on

diverse biological functions, such as regulating cellular structure, directing protein intracellular localization, mediating protein-protein and protein-substrate interactions, and regulating calcium and ion channel activities (18–20, 22). The requirement for myristoylation of the viral p60src protein to mediate its transforming and oncogenic properties demonstrated the biological importance of this hydrophobic myristoyl moiety (23). Recent genetic, biochemical, and cell-biological studies have provided insight into the molecular mechanisms of the regulation of protein myristoylation and explored strategies for modulating this process *in vivo* for therapeutic applications (18–20, 22). Our present evidence that primary lung cancers are deficient for myristoylation of Fus1 protein and that myristoylation is required for Fus1-mediated tumor suppressor activity *in vitro* and *in vivo* also indicates the cancer-preventive and therapeutic potential of positively regulating or reactivating myristoylation for Fus1.

Although the mechanism of demyristoylation is not known, demyristoylation of the myristoylated alanine-rich C-kinase substrate, as shown by electrospray mass spectrometry analyses of the myristoylated and demyristoylated forms of myristoylated alanine-rich C-kinase substrate proteins, has been found in brain (24), and the reduced expression of myristoylated alanine-rich C-kinase substrate has been reported in various cell lines after oncogenic or chemical transformation and in melanoma cells compared with normal choroidal melanocytes (25). The existence of a nonmyristoylated pool of a G protein α subunit (Gpa1p) in yeast has also been reported, and myristoylated Gpa1p is required for specific targeting of the protein to the plasma membrane; however, it is not clear how the nonmyristoylated proteins are generated and maintained (20, 26). Because point mutations of *FUS1* are infrequent, no mutation has been identified in its myristoylation site, and no evidence of epigenetic DNA methylation has been found in the *FUS1* promoter region in lung cancers, the observed reduced or lost expression and the deficient myristoylation of the Fus1 proteins in primary lung tumor cells and tumor-derived cell lines probably results from a deregulated myristoylation process or the accelerated proteasome-dependent degradation of demyristoylated Fus1 proteins.

Because most lung cancers experience allelic loss in this 3p21.3 region, haploinsufficiency may play a critical role in inactivation of Fus1 protein in lung cancer (3). In a diploid organism, each gene exists in two copies, in contrast to haploids, in which each cell contains a single copy of the genome. When one of the alleles is mutated or deleted, there is an $\sim 50\%$ reduction in the level of proteins

development of A549 experimental lung metastases in nude mice. All animals received i.v. injections of various lipoplexes every 2 days (three times) at a dose of 25 μ g of plasmid DNA and 10 nmol of liposome each in 100 μ l of 5% dextrose in water per animal; PBS alone was used as a mock control and LacZ as a negative control. Each treatment group consisted of 10 animals. Lungs were harvested 2 weeks after the last injection, and metastatic colonies on the surfaces of lung were counted without knowledge of the treatment groups. Bars represent SE. A nonparametric *t* test (Wald-Wolfowitz runs test) was performed to determine the statistical significance between each treatment group, using Statistica software (StatSoft Inc.), and $P \leq 0.05$ was considered significant. Significant inhibition of metastasis development was observed in mice treated with wild-type *FUS1* (*wt-FUS1*; $P < 0.001$) and double-mutant *FUS1* (*Dmt-FUS1*; $P < 0.001$) compared with mice treated with PBS or LacZ, but there was no significant inhibition in mice treated with myristoylation-deficient *FUS1* (*myr-mt-FUS1*; $P = 0.892$). The representative Indian ink-stained lungs and H&E-stained formalin-fixed, paraffin-embedded tissue sections in each treatment group are shown in **C**. The white spots on the lung surfaces indicate the metastatic tumor colonies. **D–I**, induction of apoptosis by wt-Fus1 expression *in vivo*. The A549 experimental metastasis tumor-bearing mice were treated with Fus1 lipoplexes three times within 1 week at the same dose as in **B**. Forty-eight h after the last treatment, animals were killed, and the lungs were harvested and freshly frozen. Induction of apoptosis was analyzed using an *in situ* apoptosis detection kit with FITC-dUTP-labeled terminal deoxynucleotidyl transferase (Tdt)-mediated nick end labeling reaction (Roche Biochemicals), and fluorescence images were examined under a fluorescence microscope and recorded with an equipped digital camera (**D–F**). Tumor morphology is shown in photographs **G–I**, taken at the same positions as above **D–F** under a regular optical light source. The hematoxylin-stained tissues from the same samples but in different sections were shown in photographs **J–L**.

synthesized. Generally, the haploinsufficiency occurs when the level of proteins synthesized falls below a threshold level and is insufficient for the onset of some desired biological activity, leading to specific types of diseases or pathological changes. In our case, the haplotype in the 3p21.3 region where the *FUS1* gene is located may lead to a reduction or loss of FUS1 protein synthesis and deficiency of myristoylation, thus inactivating FUS1 and leading to the development of lung cancer. The importance of TSG haploinsufficiency in tumor cell biology has recently drawn increasing attention, and it may have profound effects on gene transcription, protein expression, posttranslational modification, stability, and dose-dependent activity of TSGs because of the resulting decreased genomic stability, unbalanced chromosomal spatial symmetry, increased susceptibility to stochastic delays of gene initiation, altered transcriptional and translational stoichiometry, and interrupted gene expression (27–33). Although point mutations are rarely found in 3p21.3 genes in lung and other cancers, the accumulating evidence strongly argues that the extensive genomic changes (gains or losses of genetic material) collectively known as aneuploidy, which occurs frequently in lung cancer, particularly in adenocarcinoma, may collaborate with intragenic mutations during tumorigenesis and that changes in gene dosage may be modulated by the presence of adjacent genes with antagonistic activities, such as growth promotion and inhibition, a condition referred to as classic linkage disequilibrium (34). These observations raise the possibility that aneuploidy in chromosome 3; mutations of some critical checkpoint genes, such as *p53*, *Rb*, or *Ras*; and inactivation of the adjacent gatekeeper genes, such as *PTPRG*, *FHIT*, or *VHL* in the 3p region may influence the transcription, translation, and posttranslational processing of loss of heterozygosity-associated 3p21.3 genes such as *FUS1* to permit emergence of protumorigenic gene dosage changes or gene product inactivation that may facilitate early tumor development, inhibit cell proliferation, and induce apoptosis.

Our findings point to an essential role for protein myristoylation in human cancer pathogenesis and warrant further studies of alternative mechanisms involved in the inactivation of novel TSGs. Our results also suggest that it may be possible to prevent and delay tumorigenesis by neutralizing the effects of 3p haploinsufficiency before progression of premalignant lesions to invasive cancer and to suppress tumor growth by inducing apoptosis and altering cell cycle processes after tumor onset through wt-*FUS1* gene transfer.

Acknowledgments

We thank Dr. Sandra Hofmann at the University of Texas Southwestern Medical Center, Dallas for critical review of the manuscript; Drs. Nebiyou Bekele and Michael Gilcrease at M. D. Anderson Cancer Center for performing McNemar statistical analyses and for pathological evaluation of immunohistochemically stained human tissue sections, respectively; and Dr. Charlotte Clarke from Ciphergen Biosystems, Inc., for technical assistance with the SELDI-TOF-MS technology.

References

- Lerman MI, Glenn GM, Daniel L, et al. A new polymorphic probe on chromosome 3p: lambda LJB28-77 (D3S1698). *Nucleic Acids Res* 1990;18:205.
- Lerman MI, Minna JD. The 630-kb lung cancer homozygous deletion region on human chromosome 3p21.3: identification and evaluation of the resident candidate tumor suppressor genes. The International Lung Cancer Chromosome 3p21.3 Tumor Suppressor Gene Consortium. *Cancer Res* 2000;60:6116–33.
- Zbarovsky ER, Lerman MI, Minna JD. Tumor suppressor genes on chromosome 3p involved in the pathogenesis of lung and other cancers. *Oncogene* 2002;21:6915–35.
- Ji L, Nishizaki M, Gao B, et al. Expression of several genes in the human chromosome 3p21.3 homozygous deletion region by an adenovirus vector results in tumor suppressor activities in vitro and in vivo. *Cancer Res* 2002;62:2715–20.
- Kondo M, Ji L, Kamibayashi C, et al. Overexpression of candidate tumor suppressor gene FUS1 isolated from the 3p21.3 homozygous deletion region leads to G₁ arrest and growth inhibition of lung cancer cells. *Oncogene* 2001;20:6258–62.
- Ramesh R, Saeki T, Templeton NS, et al. Successful treatment of primary and disseminated human lung cancers by systemic delivery of tumor suppressor genes using an improved liposome vector. *Mol Ther* 2001;3:337–50.
- Fondon JW, Mele GM, Brezinschek RI, et al. Computerized polymorphic marker identification: experimental validation and a predicted human polymorphism catalog. *Proc Natl Acad Sci USA* 1998;95:7514–9.
- Ji L, Pang B, Yen N, Fong K, Minna JD, Roth JA. Induction of apoptosis and inhibition of tumorigenicity and tumor growth by adenovirus vector-mediated fragile histidine triad (FHIT) gene overexpression. *Cancer Res* 1999;59:3333–9.
- Cai H, Wang Y, McCarthy D, et al. BACE1 is the major beta-secretase for generation of A β peptides by neurons. *Nat Neurosci* 2001;4:233–4.
- Davies H, Lomas L, Austen BM. Profiling of amyloid β peptide variants using SELDI ProteinChip arrays. *Biotechniques* 1999;27:1258–61.
- von Beggel B, Davies H, Lomas L, et al. Tissue-specific microdissection coupled with ProteinChip array technologies: Applications in cancer research. *Biotechniques* 2000;29:1066–70.
- Wistuba II, Behrens C, Virmani AK, et al. High resolution chromosome 3p allelotyping of human lung cancer and preneoplastic/preinvasive bronchial epithelium reveals multiple, discontinuous sites of 3p allele loss and three regions of frequent breakpoints. *Cancer Res* 2000;60:1949–60.
- Yaffe MB, Lepore GG, Lal J, Obata T, Volinia S, Cantley LC. A motif-based profile scanning approach for genome-wide prediction of signaling pathways. *Nat Biotechnol* 2001;19:348–53.
- Felicetto A, Gottesman MB, Avvedimento EV. The biological functions of A-kinase anchor proteins. *J Mol Biol* 2001;308:99–114.
- Herberg FW, Maleszka A, Hide T, Vossebein L, Tasken K. Analysis of A-kinase anchoring protein (AKAP) interaction with protein kinase A (PKA) regulatory subunits: PKA isoform specificity in AKAP binding. *J Mol Biol* 2000;298:329–39.
- Maitra A, Wistuba II, Virmani AK, et al. Enrichment of epithelial cells for molecular studies. *Nat Med* 1999;5:459–63.
- Baumeister W, Walz J, Zuhl F, Seemuller B. The proteasome: paradigm of a self-compartmentalizing protease. *Cell* 1998;92:367–80.
- Ames JB, Tanaka T, Stryer L, Ikura M. Portrait of a myristoyl switch protein. *Curr Opin Struct Biol* 1996;6:432–8.
- Ames JB, Ishima R, Tanaka T, Gordon JJ, Stryer L, Ikura M. Molecular mechanics of calcium-myristoyl switches. *Nature (Lond)* 1997;389:198–202.
- Resh MD. Fatty acylation of proteins: new insights into membrane targeting of myristoylated and palmitoylated proteins. *Biochim Biophys Acta* 1999;1451:1–16.
- Templeton NS, Lasic DD, Frederik PM, Stryer L, Roberts DD, Pavlikis GN. Improved DNA: liposome complexes for increased systemic delivery and gene expression. *Nat Biotechnol* 1997;15:647–52.
- Bhatnagar RS, Futterer K, Farazi TA, et al. Structure of N-myristoyltransferase with bound myristoyl-CoA and peptide substrate analogs. *Nat Struct Biol* 1998;5:1091–7.
- Kamps MP, Buss JB, Sefton BM. Mutation of NH₂-terminal glycine of p60src prevents both myristoylation and morphological transformation. *Proc Natl Acad Sci USA* 1985;82:4625–8.
- Manenti S, Sorokine O, Van Dorsselaer A, Taniguchi H. Demyristoylation of myristoylated alanine-rich C kinase substrate. *Biochem Soc Transact* 1995;23:561–4.
- Manenti S, Malecave F, Chap H, Darbon JM. Overexpression of the myristoylated alanine-rich C kinase substrate in human choroidal melanoma cells affects cell proliferation. *Cancer Res* 1998;58:1429–34.
- Song J, Hirschman J, Gunn K, Dohlman HG. Regulation of membrane and subunit interactions by N-myristoylation of a G protein α subunit in yeast. *J Biol Chem* 1996;271:20273–83.
- Celeste A, Petersen S, Romanenko PJ, et al. Genomic instability in mice lacking histone H2AX. *Science (Wash DC)* 2002;296:922–7.
- Cook DL, Gerber AN, Tapscott SJ. Modeling stochastic gene expression: Implications for haploinsufficiency. *Proc Natl Acad Sci USA* 1998;95:15641–6.
- Dworkin J, Losick R. Differential gene expression governed by chromosomal spatial asymmetry. *Cell* 2001;107:339–46.
- McLaughlin MB. Thinking beyond the tumor cell: NF1 haploinsufficiency in the tumor environment. *Cancer Cell* 2002;1:408–10.
- Seidman JG, Seidman C. Transcription factor haploinsufficiency: when half a loaf is not enough. *J Clin Invest* 2002;109:451–5.
- Veitia RA. Exploring the etiology of haploinsufficiency. *Bioessays* 2002;24:175–84.
- Zhu Y, Ghosh P, Charnay P, Burns DK, Parada LF. Neurofibromas in NF1: Schwann cell origin and role of tumor environment. *Science (Wash DC)* 2002;296:920–2.
- Pihan GDS. Mutations and aneuploidy: co-conspirators in cancer? *Cancer Cell* 2003;4:89–94.

Expression of Nucleotide Excision Repair Proteins in Lymphocytes as a Marker of Susceptibility to Squamous Cell Carcinomas of the Head and Neck

Qingyi Wei,^{1,4} Li-E Wang,¹ Erich M. Sturgis,^{1,2} and Li Mao^{3,4}

Departments of ¹Epidemiology, ²Head and Neck Surgery, and ³Thoracic/Head and Neck Medical Oncology, The University of Texas, M.D. Anderson Cancer Center; and ⁴The University of Texas Graduate School of Biomedical Sciences at Houston, Houston, Texas

Abstract

The transcript levels of nucleotide excision repair (NER) genes were shown to be associated with risk of squamous cell carcinomas of the head and neck (SCCHN). However, this association may be biased, because the transcript level does not necessarily reflect the level of protein expression. To address this issue, we did a pilot study to test the hypothesis that the expression of six core NER proteins is associated with risk of SCCHN. We obtained cultured lymphocytes from 57 patients with newly diagnosed SCCHN patients and 63 cancer-free controls. We transfected some of the lymphocytes with both damaged and undamaged plasmid DNA and quantified NER protein levels in these lymphocytes using a reverse-phase protein microarray. The relative NER protein levels in the 63 controls were highly correlated with each other ($P < 0.001$ for all). Compared with the controls, the cases had lower expression levels for all the NER proteins, particularly XPC and XPF, which were reduced by about

25% ($P < 0.01$). When we used the median expression levels of the NER proteins in the controls as cutoff values, we found that a significantly increased risk of SCCHN was associated with low expression of XPA [odds ratio (OR), 2.99; 95% confidence interval (CI), 1.22-7.47], XPC (OR, 2.46; 95% CI, 1.04-5.87), XPD (OR, 3.02; 95% CI, 1.18-7.76), and XPF (OR, 5.29; 95% CI, 2.01-13.9), but not ERCC1 and XPG, after adjustment for age, sex, ethnicity, smoking, alcohol use, and sample storage time. In a multivariate logistic regression model that included all covariates and NER proteins, however, only low expression of XPF remained a significant risk factor for SCCHN (OR, 11.5; 95% CI, 2.32-56.6). These results suggest that XPF may be a crucial rate-limiting factor in DNA repair and that the reverse-protein microarray assay may be a useful tool for measuring protein markers of susceptibility to cancer. (Cancer Epidemiol Biomarkers Prev 2005;14(8):1961-6)

Introduction

Squamous cell carcinomas of the head and neck (SCCHN) are common malignancies, with >500,000 new cases worldwide estimated each year (1). In the U.S. in 2004, there were ~37,200 new cases of and 11,000 deaths from SCCHN (2). Many factors contribute to SCCHN, including tobacco smoking (3), alcohol use (4), viral infection (5), and genetic factors (6). Although smoking and alcohol use have a major role in the etiology of SCCHN, only a fraction of smokers and drinkers develop SCCHN, suggesting interindividual variations in genetic susceptibility to SCCHN in the general population.

Cellular DNA is constantly damaged by various endogenous and exogenous agents, including the recognized DNA adduct-inducing carcinogens contained in tobacco smoke. Sophisticated DNA repair pathways and mechanisms have evolved to maintain genomic integrity after insults from environmental hazards. One of the most important of these DNA repair pathways is nucleotide excision repair (NER; ref. 7).

A number of crucial proteins, including seven core factors (ERCC1, XPA, XPB, XPC, XPD, XPF, and XPG), participate in NER (7). Functional mutations in any one of the seven genes

encoding these core factors can lead to abnormal NER and thereby increase susceptibility to cancer (8). Several rare syndromes are characterized by NER deficiency coupled with high sensitivity to UV light and increased risk of cancer (9). Patients with xeroderma pigmentosum, for example, have mutations in at least one of seven NER genes and are extremely sensitive to sunlight-induced skin damage. Consequently, these patients have very high incidences of non-melanoma skin cancer, melanoma, and other solid tumors (9).

In previous studies, we showed that an increased risk of SCCHN is associated with reduced DNA repair capacity, as measured by the host-cell reactivation assay (10), and with reduced levels of NER mRNA in lymphocytes (11). However, the transcript levels may not accurately reflect the level expression of proteins that perform the repair functions. To test the hypothesis that reduced expression of NER proteins is associated with increased risk of SCCHN, we developed a proteomic microarray assay to measure NER protein expression in lymphocytes from SCCHN patients and cancer-free controls.

Materials and Methods

Sample Procurement. The research protocol for this study as a part of an ongoing large molecular epidemiology of SCCHN was approved by the Institutional Review Board of The University of Texas M.D. Anderson Cancer Center.

We used previously cryopreserved, viable peripheral blood lymphocyte samples from 57 patients in an ongoing case-control study of SCCHN. The sample collection started in 2000 with patients who had newly diagnosed, untreated SCCHN, that was histologically confirmed at The University

Received 2/6/05; revised 5/20/05; accepted 6/6/05.

Grant support: NIH grants R01 ES11740, CA 97007, PO1 CA106451, CA100264, and CA16672, and Department of Defense grant DAMD 17-02-1-0706.

The costs of publication of this article were defrayed in part by the payment of page charges. This article must therefore be hereby marked advertisement in accordance with 18 U.S.C. Section 1734 solely to indicate this fact.

Requests for reprints: Qingyi Wei, Department of Epidemiology, Unit 189, and Li Mao, Department of Thoracic & Head and Neck Medical Oncology, Unit 432, The University of Texas, M.D. Anderson Cancer Center, 1515 Holcombe Boulevard, Houston, TX 77030. Phone: 713-792-3020; Fax: 713-563-0999; E-mail: qwei@mdanderson.org.

Copyright © 2005 American Association for Cancer Research.

doi:10.1158/1055-9965.B71-05-0101

of Texas M.D. Anderson Cancer Center. The 63 cancer-free controls were frequency-matched with cases on age (± 5 years), sex, and ethnicity that were obtained from a structured questionnaire.

We selected those subjects whose cryopreserved samples contained sufficient lymphocytes for cell culture and subsequent transfection with plasmid DNA damaged by benzo(a)pyrene diol epoxide, a tobacco carcinogen we previously used for studying host-cell NER DNA repair capacity as measured by the host-cell reactivation assay (12). The blood sample processing, plasmid preparation, and transfection have been described in detail previously (12). Briefly, lymphocytes were isolated from whole peripheral blood by Ficoll gradient centrifugation, cryopreserved within 24 hours with freezing medium, and stored in a -80°C freezer in 1.5 mL aliquots.

Cell Culture and Protein Preparation. The cryopreserved cells in each vial were quickly thawed and mixed, before the last trace of ice disappeared, with 8.5 mL of thawing medium (50% fetal bovine serum, 40% RPMI 1640, and 10% dextrose; purchased from Sigma Chemical, St. Louis, MO). This thawing method ensured a cellular viability of $>80\%$, as confirmed by exclusion with 0.4% trypan blue (Sigma). After being washed with the thawing medium, the cells were incubated in RPMI 1640 (Life Technologies, Grand Island, NY) supplemented with 20% fetal bovine serum (Life Technologies) and stimulated with 56.25 $\mu\text{g/mL}$ phytohemagglutinin (Murex Diagnostics, Norcross, GA) at 37°C for 72 hours. Only stimulated lymphocytes were expected to uptake the plasmids (13) and have active NER (14, 15).

After stimulation, the cells ($\sim 1 \times 10^6$) were collected and transfected by the DEAE-dextran (Pharmacia Biotech, Piscataway, NJ) method with 0.25 μg of untreated plasmids (as the baseline for comparison) or benzo(a)pyrene diol epoxide-damaged plasmids. In keeping with the protocol for the host-cell reactivation assay, in which the reactivation of the report gene is measured by quantifying the enzyme activity (12). The cells were collected for protein extraction 40 hours after the transfections. This procedure is crucial to ensure that the repair process is activated by the presence of the damaged plasmids, which served as the substrate for the NER enzymes. Thirty microliters of cell suspension ($\sim 1 \times 10^5$ cells) from each patient sample was mixed with 10 μL of $4\times$ SDS sample buffer containing 50 mmol/L Tris-HCl (pH 8.0), 150 mmol/L NaCl, 0.1% SDS, and 1% Triton X-100 supplemented with a protease inhibitor cocktail (Roche Applied Science, Indianapolis, IN). The cell lysate was then boiled for 5 minutes and stored at -80°C .

Construction of Reverse-Protein Microarrays. Proteins were extracted from the cells and were used to construct the microarrays. The extracted protein samples were serially diluted 1:1 with PBS (pH 7.5) to achieve final total protein concentrations ranging from 1 to 0.025 $\mu\text{g}/\mu\text{L}$. The minimum detectable total protein concentration was 0.0525 $\mu\text{g}/\mu\text{L}$. The serial dilutions were applied to FAST slides (Schleicher & Schuell Bioscience, Keene, NH) using a SpotBot microarrayer (TeleChem International, Cupertino, CA). Each sample containing the antigens (the NER proteins) to be detected was spotted in duplicate. Prepared slides were either used immediately or stored at -20°C .

Quantitative Analysis of Protein Levels Using Reverse-Protein Microarrays. We used mouse anti-human monoclonal or anti-goat or anti-rabbit polyclonal antibodies against XPD and XPG (Santa Cruz Biotechnology, Santa Cruz, CA); XPA, XPC, and XPF (Abcam, Cambridge, MA); ERCC1 (Novus Biological, Littleton, CO); and β -actin (Sigma). XPB was not assayed because no commercially available antibodies against XPB were specific enough for this study.

Briefly, the protein-spotted slides were treated with ReBlot (Chemicon, Temecula, CA) for 15 minutes and then washed twice for 10 minutes each with washing buffer containing 300 mmol/L NaCl, 0.1% Tween 20, and 50 mmol/L Tris (pH 7.6). The protein arrays were then blocked with I-Block (Applied Biosystems, Foster City, CA) for 30 minutes at room temperature. The primary antibodies were diluted based on their affinities, which were determined in our preliminary tests (data not shown). The dilution ratios were 1:300 for XPA and ERCC1; 1:500 for XPC, XPD, XPF, and XPG; and 1:100,000 for β -actin. The arrays were incubated with individual antibodies for 1 hour at room temperature. The anti-mouse, anti-goat, and anti-rabbit secondary antibodies (Vector Laboratories, Burlingame, CA) were labeled with biotin, diluted 1:10,000, and added to the slides, which were then incubated at room temperature for 30 minutes. Signals were enhanced using a catalyzed signal amplification system (DAKO, Carpinteria, CA) according to the manufacturer's protocol, except that in the final step, we incubated the slides with Cy5-conjugated streptavidin (1:1,000; Jackson ImmunoResearch Laboratories, West Grove, PA) for 30 minutes. After each incubation step, the arrays were washed thrice for 5 minutes each with the washing buffer described above.

Signals on the protein microarrays were scanned on a ScanArray Lite microarray scanner (Perkin-Elmer Life Sciences, Boston, MA). The signal intensity of each spot and its background signal were analyzed using a ScanArray Express 2.0 microarray analysis system (Perkin-Elmer Life Sciences) running the "Run-easy Quant" protocol. The final data were stored as graphic images for further analysis. Any scan-reading value $<2,000$ was treated as missing data. The median value of the scan-reading data for each dot of a protein on the microarray was used to calculate the means of the duplicates. Scan-reading data for the β -actin were used as a baseline to obtain the relative expression levels for each protein. The coefficient of variation (CV) was calculated as $[(\text{SD} / \text{mean}) \times 100]$.

Statistical Analysis. The mean signal intensity values for the cases and controls for each NER protein were compared with Student's *t* test. The distribution of select variables of the cases and controls were compared with the χ^2 test. The correlation between the expression levels of different proteins was analyzed by the Pearson correlation coefficient. The median protein expression for the controls was used as the cutoff value for calculating the odds ratios (OR) associated with low expression and their 95% confidence intervals (CI). Multivariate logistic regression models were used to calculate the adjusted ORs and 95% CIs with adjustment for age (in years), sex (male versus female), ethnicity (non-Hispanic versus others), and sample storage time (in months). *P* values <0.05 were considered statistically significant. All statistical analyses were performed with SAS software version 8.0e (SAS Institute, Cary, NC).

Results

Protein Microarray Data. We began by testing the reproducibility and linearity of the reverse-protein microarray assay. Four samples of cell extracts from four controls were each diluted 1:1 five times; all 20 aliquots were spotted in triplicate on one slide (a total of 60 spots). We made three such slides for each sample and probed them with antibodies to XPA and XPF (Fig. 1A). The expression levels of XPA and XPF were linear on a log scale at the tested total protein concentrations between 1.0 and 0.0525 $\mu\text{g}/\mu\text{L}$ (Table 1). These results were consistent between all samples and repeated experiments (Fig. 1B). Based on the CVs, however, it seemed that the reproducibility of the results was better at higher protein concentrations (CV as low as 0.8%) than at lower concentrations (CV as high as 24.6%; Table 1).

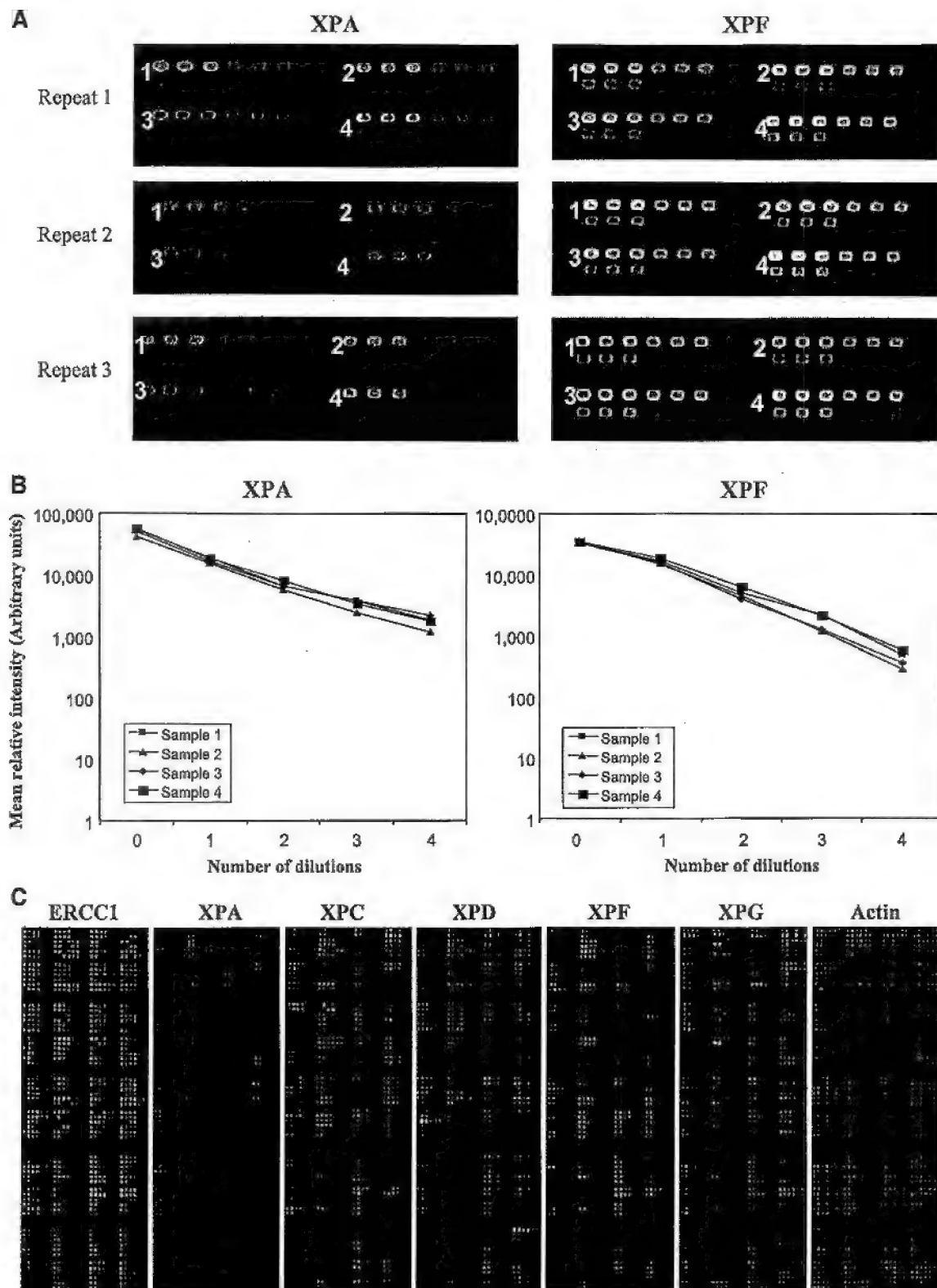


Figure 1. Reproducibility and linearity of reverse-protein microarray assay data. **A.** Serial dilutions of four cell-extract samples (1, 2, 3, and 4) were spotted in triplicate and probed with specific antibodies against XPA and XPF. Each slide was tested three times (repeats 1, 2, and 3). The statistical data are summarized in Table 1. **B.** The mean intensities of the spots in (*A*; in arbitrary units) were plotted on a log scale against the number of dilutions of the cell extract. **C.** Reverse-protein microarray assay of expression of the NER proteins ERCC1, XPA, XPC, XPD, XPF, and XPG. The level of β -actin was used as an internal control for standardization of the expression levels. The statistical data are summarized in Table 3.

Table 1. Reproducibility and linearity of reverse-protein microarray data

XPA				XPF							
Sample 1											
Total protein (μg/μL)		0.96	0.48	0.24	0.12	0.06	0.96	0.48	0.24	0.12	0.06
Signal intensity	R1*	51,787	18,817	8,025	4,641	2,375	36,356	16,923	4,481	2,369	436
(arbitrary units)	R2	54,704	15,702	6,130	3,418	1,797	32,925	16,802	5,574	2,119	476
	R3	49,131	15,106	5,488	3,263	1,461	30,030	16,255	4,969	2,243	553
Mean (SD) [†]		51,874 (2,788)	16,542 (1,993)	6,548 (1,319)	3,774 (755)	1,878 (462)	33,104 (3,167)	16,660 (356)	5,008 (548)	2,244 (125)	488 (60)
CV (%)		5.4	12.1	20.2	20.1	24.6	9.6	2.1	10.9	5.6	12.2
Sample 2											
Total protein (μg/μL)		1	0.5	0.25	0.125	0.0625	1	0.5	0.25	0.125	0.0625
Signal intensity	R1	46,645	18,305	5,724	2,713	1,354	35,249	15,373	4,331	1,054	317
(arbitrary units)	R2	43,944	13,908	5,901	2,513	1,316	37,172	16,418	4,774	1,058	294
	R3	38,014	14,368	5,593	2,118	839	33,349	14,328	4,826	1,473	258
Mean (SD) [†]		42,868 (4,415)	15,527 (2,417)	5,739 (155)	2,448 (303)	1,170 (287)	35,257 (1,912)	15,373 (1,045)	4,644 (272)	1,195 (241)	290 (30)
CV (%)		10.3	15.6	2.7	12.4	24.5	5.4	6.8	5.9	20.2	10.3
Sample 3											
Total protein (μg/μL)		0.88	0.44	0.22	0.11	0.055	0.88	0.44	0.22	0.11	0.055
Signal intensity	R1	58,360	21,799	8,297	4,644	2,511	33,940	17,236	4,507	1,316	374
(arbitrary units)	R2	58,558	18,709	5,318	3,561	1,947	33,720	15,228	3,769	1,327	385
	R3	51,531	17,762	5,931	3,306	2,201	32,877	13,946	3,776	1,193	321
Mean (SD) [†]		56,150 (4,001)	19,423 (2,111)	6,515 (1,573)	3,837 (710)	2,220 (283)	33,512 (561)	15,470 (1,658)	4,017 (424)	1,279 (74)	360 (34)
CV (%)		7.1	10.9	24.2	18.5	12.7	1.7	10.7	10.6	5.8	9.5
Sample 4											
Total protein (μg/μL)		0.84	0.42	0.21	0.105	0.0525	0.84	0.42	0.21	0.105	0.0525
Signal intensity	R1	60,447	22,560	9,560	4,214	2,130	35,167	18,616	6,519	2,119	538
(arbitrary units)	R2	59,055	16,333	7,948	3,163	1,918	34,935	18,613	6,584	1,865	538
	R3	52,017	15,913	6,862	2,828	1,314	34,615	18,931	6,259	2,428	680
Mean (SD) [†]		57,173 (4,519)	18,269 (3,722)	8,123 (1,358)	3,402 (723)	1,787 (423)	34,906 (277)	18,720 (182)	6,454 (172)	2,137 (282)	585 (82)
CV (%)		7.9	20.4	16.7	21.3	23.7	0.8	1.0	2.7	13.2	14.0

*R1-3, repeats 1 to 3.

†Standard deviation of the three experiments.

We next diluted each of the 120 test samples twice, and then spotted them on the arrays in duplicate (Fig. 1C). The means of the duplicate readings were used to calculate the relative protein expression. Because of mechanical problems during the spotting, some protein spots were unreadable on the arrays, consequently, valid readings could not be obtained for up to five samples per protein. Consistent with the results of our reproducibility and linearity tests, the readings from spots with lower protein concentrations had greater variation, whereas the spots with higher protein concentrations produced consistent, strong, and readable signals. We therefore used the latter data (i.e., the original samples without dilution) to calculate the relative expression levels.

We also transfected cells from these samples with either undamaged plasmids or benzo(a)pyrene diol epoxide-damaged plasmids to stimulate DNA repair activity. When we compared the relative expression of NER proteins between the cases and controls, we found that the data from the samples transfected with damaged plasmids were a better predictor of risk of SCCHN (data not shown), although the two data sets were statistically correlated ($P < 0.01$). We therefore used data derived from cells transfected with damaged plasmids in the following experiments.

Subject Characteristics. Our analysis included 57 patients with newly diagnosed SCCHN and 63 cancer-free controls whose cryopreserved lymphocytes were available for culture, transfection, and protein extraction. The cases and controls were frequency-matched on age, sex, and ethnicity. The cases were slightly younger (56.2 versus 57.2 years) and comprised more males and non-Hispanic whites than did the controls, but these differences were not statistically significant (Table 2).

There were more smokers and alcohol drinkers among the cases than among the controls, and these differences were statistically significant (Table 2). Because the cases were recruited before the controls, the duration of lymphocyte storage was also significantly different between the two groups

Table 2. Characteristics SCCHN patients and control subjects

Variable	Cases (n = 57)	Controls (n = 63)	P*
	No. (%)	No. (%)	
Age (y)			
≤55	24 (42)	25 (40)	0.787
>55	33 (58)	38 (60)	
Sex			
Male	43 (75)	39 (62)	0.112
Female	14 (25)	24 (38)	
Ethnic group			
African-American	3 (5)	3 (5)	0.962
Mexican-American	3 (5)	4 (6)	
Non-Hispanic White	51 (90)	56 (89)	
Tobacco use [†]			
Yes	42 (74)	31 (49)	0.006
No	15 (26)	32 (51)	
Alcohol use [‡]			
Yes	43 (75)	33 (52)	0.009
No	14 (25)	30 (48)	

*Calculated using two-sided χ^2 test.

†The question asked was, "Have you ever smoked at least 100 cigarettes in your lifetime?"

‡The question asked was, "Have you ever drunk alcoholic beverages at least once a week for 1 year or more?"

Table 3. Relative expression of NER proteins in SCCHN patients and controls

	n*	Mean \pm SD		Difference (%)	P†
		Cases	Controls		
Age (y)	57/63	56.2 \pm 9.7	57.2 \pm 9.5		0.418
Storage time	57/63	17.7 \pm 11.7	13.2 \pm 6.8		0.013
Relative expression (%)‡					
ERCC1	53/58	1.369 \pm 0.401	1.696 \pm 0.539	-19.3	<0.001
XPA	53/61	0.363 \pm 0.111	0.424 \pm 0.160	-14.4	0.017
XPC	54/62	1.326 \pm 0.650	1.770 \pm 0.923	-25.1	0.003
XPD	52/59	0.947 \pm 0.343	1.137 \pm 0.584	-19.0	0.037
XPF	56/62	0.966 \pm 0.438	1.297 \pm 0.764	-25.5	0.004
XPG	55/60	1.206 \pm 0.453	1.432 \pm 0.628	-15.8	0.028

*Number of cases/controls.

†Calculated using two-sided Student's *t* test.‡Expression level relative to that of β -actin.

(Table 3). We further adjusted for all of these variables in the multivariate logistic regression analysis.

Difference in NER Protein Expression Between the Cases and Controls. We used Student's *t* test to evaluate the differences in NER protein expression between the cases and controls. The expression of all seven NER proteins was significantly lower among the cases than among the controls (Table 3). The greatest reduction was in the relative expression of XPC and XPF, which was reduced by about 25% in the cases compared with the controls. The reduction in the expression of all NER proteins may reflect their association with repair activities, in which certain levels of proteins need to be present. Correlative analysis revealed that the relative expression levels of these NER proteins were all highly correlated ($P \leq 0.001$). For example, the expression of XPC was correlated with that of ERCC1 ($r = 0.706$), XPF ($r = 0.505$), and XPG ($r = 0.715$), and the expression of XPF was correlated with that of XPA ($r = 0.695$), XPD ($r = 0.541$), and XPG ($r = 0.781$). This led us to investigate which protein has the most significant role in the increased risk of SCCHN.

Association Between NER Protein Expression and Risk of SCCHN. We used the median expression level in the control samples as the cutoff values for calculating the ORs for risk of SCCHN. The crude ORs for low compared with high expression of XPA, XPC, XPD, XPF, but not those for ERCC1 and XPG, were significantly increased (Table 4). The ORs remained essentially unchanged after adjustment for age, sex, ethnicity, smoking, alcohol use, and sample storage time. The highest adjusted OR was for XPF (5.29; 95% CI, 2.10-13.92) followed by XPD and XPA. Because the relative expression

levels of these NER proteins were highly correlated with each other, the relative expression levels of all proteins were simultaneously adjusted for each other in the final multivariate logistic regression model containing age, sex, ethnicity, smoking, alcohol use, and sample storage time. The only significant adjusted OR was for XPF (11.5; 95% CI, 2.32-56.6) in the presence of other proteins in the same model (Table 4).

Discussion

Our reverse-protein microarray assay successfully detected the target proteins at a total protein concentration as low as 0.0525 $\mu\text{g}/\mu\text{L}$. However, the measurements seemed to be more reproducible at a total protein concentration $\geq 0.5 \mu\text{g}/\mu\text{L}$. The cell extract from $\sim 1 \times 10^5$ cells (yielding 30 μL of sample) would thus be sufficient for repeated experiments, because each printed spot contained only 0.0033 μL . Using this assay, we showed that the relative expression levels of the six NER proteins (ERCC1, XPA, XPC, XPD, XPF, and XPG) were consistently significantly lower among the SCCHN patients than among the controls. Four of the six NER proteins tested (XPA, XPC, XPD, XPF) were associated with a significantly increased risk of SCCHN.

The data from this study are consistent with those in two of our previously published studies (10, 11). In the first study, we measured DNA repair capacity in 55 newly diagnosed SCCHN patients and 61 controls by the host-cell reactivation assay using a benzo(a)pyrene diol epoxide-damaged reporter gene (10). The mean DNA repair capacity in that study was significantly lower in the cases than in the controls. Those

Table 4. Estimation of SCCHN risk (OR and 95% CI) associated with expression levels of NER proteins

Expression level*		Cases	Controls	Crude OR	Multivariate adjusted†	Multivariate adjusted
		No. (%)	No. (%)	(95% CI)	OR (95% CI)	OR† (95% CI)
ERCC1	high	17 (32)	29 (50)	2.12 (0.98-4.59)	2.18 (0.91-5.24)	0.78 (0.21-2.85)
	low	36 (68)	29 (50)			
XPA	high	15 (28)	30 (49)	2.45 (1.12-5.35)	2.99 (1.22-7.47)	2.01 (0.57-7.14)
	low	38 (72)	31 (51)			
XPC	high	13 (24)	31 (50)	3.15 (1.42-7.01)	2.46 (1.04-5.87)	1.17 (0.31-4.41)
	low	41 (76)	31 (50)			
XPD	high	15 (29)	29 (49)	2.38 (1.09-5.24)	3.02 (1.18-7.76)	1.88 (0.50-7.01)
	low	37 (71)	30 (51)			
XPF	high	13 (23)	31 (50)	3.31 (1.49-7.33)	5.29 (2.01-13.9)	11.5 (2.32-56.6)
	low	43 (77)	31 (50)			
XPG	high	18 (33)	30 (50)	2.06 (0.96-4.38)	1.56 (0.79-3.92)	0.48 (0.13-1.74)
	low	37 (67)	30 (50)			

*Dichotomized based on median values of control subjects.

†Obtained from logistic regression model with adjustment for age, sex, race, smoking status, alcohol use, and lymphocyte storage time.

‡Obtained from logistic regression model with adjustment for age, sex, race, smoking status, alcohol use, lymphocytes.

with DNA repair capacity values in the middle and lowest tertiles had >2-fold and 4-fold increased SCCHN risk, respectively, compared with those whose DNA repair capacity values were in the highest tertile. In the subsequent study, we investigated which NER genes might be responsible for the reduced DNA repair capacity in SCCHN. We previously measured the relative expression of the genes encoding five NER proteins (ERCC1, XPB, XPG, CSB, and XPC) by a multiplex RT-PCR method (11). The relative mRNA expression levels of ERCC1, XPB, XPG, and CSB were significantly lower in the cases than in the controls, and the risk of SCCHN associated with low expression of these genes was higher by 2- to 6-fold (11). In that study, we were not able to measure the expression of XPA, XPD, or XPF because the sequences of the genes were unknown at that time and the high level of sequence homology in the genome for the primers chosen made the assays unreliable.

In the present study, simultaneous adjustment for the expression levels of all proteins and other confounding factors revealed that the relative expression level of XPF was the only independent risk factor for SCCHN. Low compared with high expression of XPF was associated with an SCCHN risk >11-fold higher. Although the estimate was imprecise as evidenced by the wide 95% CI, this finding suggests that XPF may play a role in the repair of carcinogen-damaged DNA. Because ERCC1 needs XPF to form a functional complex (7), it is possible that XPF acts as a rate-limiting modulator. Based on our data, ERCC1 was expressed at higher levels than the other five proteins were, whereas XPF expression was <70% of ERCC1 expression. It is possible that our system was saturated with ERCC1 protein, so the amount of XPF became crucial for modulating the overall DNA repair capacity.

The present study is an extension of our previous studies assessing the best biomarkers of DNA repair capacity for predicting susceptibility to SCCHN. In the present study, we measured the relative expression levels of six of the seven core NER proteins because we did not find an appropriate antibody for XPB. Our data further support the notion that altered NER capacity, at the cellular, mRNA, or protein levels, may contribute to the risk of tobacco-induced SCCHN. More important, our reverse-protein microarray assay of relative protein expression seemed to be the most sensitive, compared with previously reported assays of cellular DNA repair capacity and the mRNA expression levels (10, 11). Further studies are warranted to correlate the expression of these markers in surrogate and target tissues such as oral epithelial cells.

There are several advantages to the reverse-protein microarray assay. First, compared with the host-cell reactivation assay (12), the microarray assay requires significantly (3-fold) fewer viable lymphocytes for protein extraction. Second, compared with the RT-PCR assay, the microarray assay is highly sensitive and reproducible, which is optimal for large-scale screening. Third, the microarray assay has the potential to test virtually any protein involved in NER or other molecular pathways underlying increased cancer risk. Finally, the microarray assay is rapid and cost-effective and produces a large quantity of data. With the availability of antibodies for

specific protein posttranslational modifications, the microarray method may also become a powerful tool to assess functional changes in proteins.

Although the design of this pilot case-control study has inherent limitations of recall and selection biases, the reverse-protein microarray assay may be a powerful tool for future prospective studies if it is technically fine-tuned and the sampling issues resolved (16, 17). For instance, future studies must address the differences in protein concentrations between surrogate and target tissues, between fresh and stored serum samples, and before and after cancer diagnosis and treatment. An improved reverse-protein microarray assay should become a useful tool for future hypothesis-driven molecular epidemiologic studies of cancer.

Acknowledgments

We thank Dr. Margaret R. Spitz for critical review; Margaret Lung and Dr. Peggy Schuber for assistance in recruiting the subjects; Youhong Fan, Zhaozheng Guo, and Yawei Qiao for laboratory assistance; Betty Jean Larson and Joanne Sider for manuscript preparation; and Pierrette Lo for scientific editing.

References

- Pisani P, Parkin DM, Bray F, Ferlay J. Estimates of the worldwide mortality from 25 cancers in 1990. *Int J Cancer* 1999;83:18-29.
- American Cancer Society Inc. *Cancer facts and figures 2003*. Atlanta: American Cancer Society; 2003.
- Johnson N. Tobacco use and oral cancer: a global perspective. *J Dent Educ* 2001;65:328-39.
- Casiglia J, Woo SB. A comprehensive review of oral cancer. *Gen Dent* 2001; 49:72-82.
- Dahlstrom KR, Adler-Storthz K, Etzel CJ, et al. Human papillomavirus type 16 infection and squamous cell carcinoma of the head and neck in never-smokers: a matched pair analysis. *Clin Cancer Res* 2003;9:2620-6.
- Sturgis EM, Wei Q. Genetic susceptibility-molecular epidemiology of head and neck cancer. *Curr Opin Oncol* 2002;14:310-7.
- Sancar A, Lindsey-Boltz LA, Unsal-Kacmaz K, Linn S. Molecular mechanisms of mammalian DNA repair and the DNA damage checkpoints. *Annu Rev Biochem* 2004;73:39-85.
- Friedberg EC. How nucleotide excision repair protects against cancer. *Nat Rev Cancer* 2001;1:22-33.
- Kraemer KH, Lee MM, Andrew AD, et al. The role of sunlight and DNA repair in melanoma and nonmelanoma skin cancer. *Arch Dermatol* 1994;130: 1018-21.
- Cheng L, Eicher SA, Guo Z, Hong WK, Spitz MR, Wei Q. Reduced DNA repair capacity in head and neck cancer patients. *Cancer Epidemiol Biomarkers Prev* 1998;7:465-8.
- Cheng L, Sturgis EM, Eicher SA, Spitz MR, Wei Q. Expression of nucleotide excision repair genes and the risk for squamous cell carcinoma of the head and neck. *Cancer* 2002;94:393-7.
- Wei Q, Cheng L, Amos CI, et al. Repair of tobacco carcinogen-induced DNA adducts and lung cancer risk: a molecular epidemiologic study. *J Natl Cancer Inst* 2000;92:1764-72.
- Cheng L, Wang LE, Spitz MR, Wei Q. Cryopreserving whole blood for functional assays using viable lymphocytes in molecular epidemiology studies. *Cancer Lett* 2001;166:155-63.
- Athas AF, Hedayati M, Matanoski GM, Farmer BR, Grossman L. Development and field-test validation of an assay for DNA repair in circulating human lymphocytes. *Cancer Res* 1991;51:5786-93.
- Barret JM, Calsou P, Salles B. Deficient nucleotide excision repair activity in protein extracts from normal human lymphocytes. *Carcinogenesis* 1995;16: 1611-6.
- Shivji MKK, Kenny MK, Wood R. Proliferating cell nuclear antigen is required for DNA excision repair. *Cell* 1992;69:367-74.
- Cutler P. Protein arrays: the current state-of-the-art. *Proteomics* 2003;3:3-18.

Epidemiology 9: Descriptive Epidemiology and Methodology
Abstract #4051

Building a comprehensive quantitative risk assessment model for lung cancer

Carol J. Etzel, Qing Zhang, Matthew Schabath, Qiong Dong, Xifeng Wu, Qingyi Wei, Margaret Spitz and Christopher I. Amos

UT M. D. Anderson Cancer Ctr., Houston, TX

Introduction: Lung cancer (LC) is still the leading cause of cancer death and the ability to distinguish individuals (smokers and non-smokers) at high risk for LC has significant preventive implications. High-risk smoking subgroups could be targeted for intensive cessation interventions and recruited into chemoprevention and specialized screening trials. The goal of this project was to develop a comprehensive LC risk assessment model that included epidemiologic and nutritional data from 24 hour food frequency questionnaires to identify such high-risk groups. Methods: We constructed our models from data derived from 2768 Caucasian LC cases (recruited through UT MD Anderson Cancer Center) and controls (recruited from a multispecialty physician practice and matched on age, sex and smoking status). Models were constructed for never, former and current smokers using multiple logistic regression. We also completed model diagnostics including identification of multi-collinearities and model goodness-of-fit. Many of the nutritional variants were highly correlated and resulted in model multi-collinearities. When such a situation occurred, we constructed separate models for the correlated variants and compared their ROC values. Results and Conclusions: For never smokers, the epidemiologic model included second-hand smoke (ETS) which was associated with a two-fold risk for LC (ROC=.581). We also obtained three nutritional models with similar yet slightly higher ROC scores as compared to the epidemiologic model: ETS and daily

servings of vegetables (ROC=.635), ETS and proVitamin A carotenoids (ROC=.662) and ETS and beta-Carotene (ROC=.661). For former smokers, a physician's diagnosis of emphysema, asbestos exposure, family history of LC and years since smoking cessation were all independently associated with increased risk of LC while hay fever was protective (ROC=.671). With the inclusion of nutritional variants, we obtained two subsequent models, one including number of different sources of weekly fat intake and daily servings of vegetables (ROC=.688) and the other including amount of saturated fat and total carotenoid intake (ROC=.689). For current smokers, the epidemiologic model included risk factors of emphysema, family history of LC, years smoked and number of cigarettes smoked per day while hay fever was protective (ROC=.711). The nutritional model for current smokers also included number of different sources of weekly fat intake and daily servings of vegetables (ROC=.714). These results show that LC is a complex disease with varying etiology based on smoking history; hence, the development of risk models must account for smoking history. The amount of increase in model prediction afforded by the inclusion of nutritional variants did not justify the time and expense of collecting such data. This project was supported by NCI grants CA55769 and CA093592 (K07) and DAMD17-02-1-07-06.

Epidemiology 15: Biomarkers of DNA Damage and Repair, Exposure, and Phenotype Abstract #5663

Prior respiratory disease, DNA repair capacity, and inflammation-related genotypes modify lung cancer risk.

Matthew B. Schabath, Qingyi Wei, Xifeng Wu and Margaret R. Spitz

University of Texas M. D. Anderson Cancer Center, Houston, TX

Introduction: A prior history of certain non-malignant respiratory diseases, such as emphysema, increases lung cancer (LC) risk. The long-standing inflammatory reaction in the bronchi is accompanied by a continual cycle of injury and repair and therefore could play a key role in lung carcinogenesis. Because of a higher rate of cell turnover, the likelihood increases for propagation of genetic errors and subsequent cancer development. Therefore, we utilized data from an on-going case-control study to examine the interplay between emphysema, DNA repair capacity (DRC), and inflammation-related genotypes for risk of LC. **Methods:** We compared self-reported histories of emphysema in 2,134 LC cases and 2,295 matched healthy controls and incorporated available data on DRC (measured by the *in vitro* host cell reactivation assay) and two biologically relevant polymorphic genes (matrix metalloproteinase-1 [*MMP-1*] and myeloperoxidase [*MPO*]). **Results:** As previously published, cases exhibited a

significantly lower mean DRC compared to controls (8.3 ± 2.8 versus 8.9 ± 3.1 ; $P < .01$); however, there was no difference in DRC between individuals with and without emphysema. When DRC was dichotomized on the median value in controls, individuals with suboptimal DRC ($< \text{median}$) had a 3-fold ($2.4 - 3.6$) increased risk of LC. Overall, a **prior** history of emphysema was associated with 1.5-fold ($1.3 - 1.7$) increased risk of LC, and in "heavy" smokers (≥ 40 pack-years) this risk was substantially elevated to 4.2 ($3.1 - 5.6$). On stratified analysis, the joint effect of emphysema and suboptimal DRC yielded a 5.2-fold ($3.5 - 7.9$) increased risk. In a three-way joint effects analysis, a 6.6-fold ($3.7 - 11.7$) increased risk was noted in the presence of emphysema, heavy smoking, and *efficient* DRC. Yet, the risk was substantially enhanced among emphysemics with *suboptimal* DRC who were moderate (OR = 9.1; $5.6 - 14.9$) or heavy smokers (OR = 11.6; $6.3 - 21.4$). Next, carriers of the "adverse" *MPO* and *MMP-1* alleles with a history of emphysema exhibited 4.9-fold increased risk ($2.8 - 8.6$), which was also modified in separate three-way joint effects analysis that included smoking or DRC. Specifically, emphysema, the adverse alleles, and heavy smoking resulted in a 5.5-fold ($2.5 - 12.2$) risk for LC, while emphysema, the adverse alleles, and suboptimal DRC produced a 8.0-fold ($2.8 - 23.3$) risk. Conclusions: Because cancer is a multifactorial **disease**, a single risk factor may have only a small effect on the **disease** phenotype. However, assessing multiple risk factors including relevant susceptibility markers, history of **respiratory** conditions, and deleterious exposures may reveal a more accurate representation of LC risk and help in the identification of subgroups that are at the greatest risk for developing LC. *Funding support from the Flight Attendant Medical Research Institute, grants CA 55769 and CA 70907 from the NCI and DAMD17-02-1-0706 from the DOD.*

Epidemiology 15: Biomarkers of DNA Damage and Repair, Exposure, and Phenotype Abstract #5661

A novel assay to measure the capacity to repair N7-guanine site- specific DNA damage.

**Luo Wang, Qiuling Shi, Zhaosheng Guo, Yawei Qiao, Margaret R. Spitz and
Qingyi Wei**

UT MD Anderson Cancer Center, Houston, TX

The nitrosamine 4-(methylnitrosamino)-1-(3-pyridyl)-1-butanone (NNK) is a potent inducer of lung adenocarcinoma through the formation of DNA adducts, especially N7-guanine lesions. Our previous research on susceptibility to tobacco-induced carcinogenesis has focused on benzo[a]pyrene diol epoxide (BPDE) as the in vitro mutagen challenge for phenotype assays of DNA repair, but there is no comparable DNA repair assay for NNK-induced damage. Thus, we have developed a new assay to specifically investigate the association between DNA repair capacity (DRC) of NNK-induced N7-guanine damage and lung adenocarcinoma risk. Since NNK and its precursor 4-(acetoxyl)-NNK (NNKOAc) did not induce stable DNA damage lesions, we created specific damage at the N7-site of guanine in DNA of a pCMVluc plasmid by introducing a methyl group with a potent methylating agent (DMS). After confirming that the

introduction of N7-methyl guanine did not alter the apparent conformation of the plasmid DNA, we established damage-repair dose-response curves in three lymphoblastoid cell lines known to be either nucleotide excision repair proficient or deficient and in phytohemagglutinin (PHA)-stimulated normal primary lymphocytes. After establishing the optimal dose, we applied this assay in a pilot study of 48 newly diagnosed lung adenocarcinoma patients and 45 controls matched on age, gender, and smoking status to test the hypothesis that lower capacity for repair of the N7-guanine site-specific lesion is associated with increased risk of lung adenocarcinoma. The cases exhibited a lower mean DRC than did the controls. A nearly three-fold increased risk (odds ratio = 2.87; 95% confidence interval = 1.18 to 7.00) was found in those who exhibited lower DRC. It was more pronounced for older individuals and women. There was no correlation between the N7-guanine site-specific DRC and that measured in parallel with the BPDE assay. On analysis of the joint effects of the two assays, the risk increased to more than 11-fold for those (24/48) who exhibited suboptimal repair for both N7-guanine damage and BPDE damage. We did not explore the detailed repair mechanism involved in this new assay but only indirectly demonstrated that nucleotide excision repair appeared not to be involved in the repair of N7-guanine site-specific damage and that XRCC1-related base excision repair could play a partial role in the repair process. These data suggest that multiple mechanisms may be responsible for the repair of site-specific N7-guanine damage. We conclude that variability in DRC of different tobacco mutagens is a risk factor for lung adenocarcinoma, and that studying both repair pathways in parallel enhances the precision of the risk estimate. Our results provide the proof-of-principle for a new assay that can assess the DRC for NNK-induced damage. [Supported by CA 55769, CA 70907, DMDD17-02-1-0706, Flight Attendant Medical Research Institute, ES11740 and CA100264 [[GenBank](#)]]



AMERICAN SOCIETY OF CLINICAL ONCOLOGY

www.asco.org

Prognostic role of promoter hypermethylation of death-associated protein (DAP) kinase and p16 genes in early-stage non-small cell lung cancer.

Sub-category: Non-Small Cell Lung Cancer

Category: Lung Cancer

Meeting: 2006 ASCO Annual Meeting

Abstract No: 7216

Citation: *Journal of Clinical Oncology*, 2006 ASCO Annual Meeting Proceedings Part I. Vol 24, No. 18S (June 20 Supplement), 2006: 7216

Author(s): C. Lu, I. Wistuba, X. Zhou, B. N. Bekele, J. B. Putnam, A. Correa, L. Mao

Abstract: **Background:** Promoter hypermethylation is an epigenetic mechanism of gene silencing commonly observed in malignancies. Prior studies suggest that hypermethylation of *DAP kinase* and *p16*, genes involved in apoptosis and cell cycle regulation, respectively, are associated with poorer survival in NSCLC patients. In this study we investigate the prognostic role of *DAP kinase* and *p16* promoter hypermethylation in a large cohort of early-stage NSCLC patients. **Methods:** Pathologic stage I and II NSCLC patients who underwent complete surgical resection between 1/97 and 12/01 at our institution and did not receive adjuvant therapy were identified. Formalin-fixed, paraffin-embedded tissue blocks were retrieved, and *p16* and *DAP kinase* promoter methylation status was determined by methylation specific PCR. Two-sided statistical analyses were performed to determine associations between methylation status, clinicopathologic characteristics, and survival. **Results:** *DAP kinase* and *p16* methylation status was observed in 36.3% (97 of 267) and 36.4% (95 of 261) cases, respectively. Subject characteristics: 55% female, 77% former/current smokers, 81% stage I, 19% stage II, 61% adenocarcinoma, 29% squamous carcinoma, 63% performance status (PS) 0, 37% PS 1, 93% < 5% weight loss. Recurrent NSCLC and death occurred in 21.3% and 38% of cases, respectively. No significant associations were observed between *DAP kinase* methylation status and subject characteristics. *P16* methylation was associated with moderate/high grade ($p = 0.03$). A higher frequency of *p16* methylation was observed in ever vs never smokers (39% vs 28%, $p = 0.17$). Preliminary analyses do not demonstrate significant associations between methylation status and overall survival (*p16* $p = 0.13$; *DAP kinase* $p = 0.56$) or disease-free survival (*p16* $p = 0.36$; *DAP kinase* $p = 0.71$). **Conclusions:** In this relatively large cohort of early-stage NSCLC patients, we did not detect significant associations between *p16* and *DAP kinase* promoter methylation and clinical outcome. Further subset analyses stratified by gender and histology will be performed. The prognostic role of these biomarkers in NSCLC remains unclear.

Associated Presentation(s):

1. Prognostic role of promoter hypermethylation of death-associated protein (DAP) kinase and p16 genes in early-stage non-small cell lung cancer.

No presentation available

Meeting: 2006 ASCO Annual Meeting

Presenter: Charles Lu

Session: Lung Cancer (General Poster Session)

Other Abstracts in this Sub-Category

1. ZD6474 versus gefitinib in patients with advanced NSCLC: Final results from a two-part, double-blind, randomized phase II trial.

Meeting: 2006 ASCO Annual Meeting Abstract No: 7000 First Author: R. B. NataleCategory: Lung Cancer - Non-Small Cell Lung Cancer

2. Efficacy and safety of sunitinib in previously treated, advanced non-small cell lung cancer (NSCLC): Preliminary results of a multicenter phase II trial.

Meeting: 2006 ASCO Annual Meeting Abstract No: 7001 First Author: M. A. SocinskiCategory: Lung Cancer - Non-Small Cell Lung Cancer

3. Phase II trial of single-agent sorafenib in patients with advanced non-small cell lung carcinoma.

Meeting: 2006 ASCO Annual Meeting Abstract No: 7002 First Author: U. GatzemeierCategory: Lung Cancer - Non-Small Cell Lung Cancer

More...

Abstracts by C. Lu

1. **Induction chemotherapy (CT) with weekly paclitaxel, carboplatin, and cetuximab for squamous cell carcinoma of the head and neck (HN).**
Meeting: [2006 ASCO Annual Meeting](#). Abstract No: 5520 First Author: [M. S. Kies](#)
Category: [Head and Neck Cancer](#)
2. **Pemetrexed in combination with paclitaxel: A phase I clinical and pharmacokinetic trial in patients with solid tumors.**
Meeting: [2006 ASCO Annual Meeting](#). Abstract No: 2051 First Author: [T. Graefe](#)
Category: [Developmental Therapeutics: Cytotoxic Chemotherapy - Pharmacology/pharmacokinetics](#)
3. **Prognostic role of promoter hypermethylation of death-associated protein (DAP) kinase and p16 genes in early-stage non-small cell lung cancer.**
Meeting: [2006 ASCO Annual Meeting](#). Abstract No: 7216 First Author: [C. Lu](#)
Category: [Lung Cancer - Non-Small Cell Lung Cancer](#)

More...

Presentations by C. Lu

1. **Prognostic role of promoter hypermethylation of death-associated protein (DAP) kinase and p16 genes in early-stage non-small cell lung cancer.**
No presentation available
Meeting: [2006 ASCO Annual Meeting](#)
Presenter: [Charles Lu](#)
Session: [Lung Cancer \(General Poster Session\)](#)
2. **A phase III study of AE-941 with induction chemotherapy (IC) and concomitant chemoradiotherapy (CRT) for stage III non-small cell Lung cancer (NSCLC) (NCI T99-0046, RTOG 02-70, MDA 99-303): An interim report of toxicity and response**
No presentation available
Meeting: [2005 ASCO Annual Meeting](#)
Presenter: [Charles Lu, MD](#)
Session: [Lung Cancer \(General Poster Session\)](#)
3. **Association between glutathione S-transferase (GST) P1 polymorphisms and survival of patients with advanced non-small cell lung cancer (NSCLC).**
Meeting: [2004 ASCO Annual Meeting](#)
Presenter: [Charles Lu, MD](#)
Session: [Lung Cancer I \(Oral Presentation\)](#)



More...

Journal of Clinical Oncology Articles by C. Lu

1. **Phase II Study of a Liposome-Entrapped Cisplatin Analog (L-NDDP) Administered Intrapleurally and Pathologic Response Rates In Patients With Malignant Pleural Mesothelioma.**
J Clin Oncol, United States
Vol 23, No 15 (5/24/2005): pp. 3495-501
2. **Prognostic factors in resected stage I non-small-cell lung cancer: a multivariate analysis of six molecular markers.**
J Clin Oncol, United States
Vol 22, No 22 (11/16/2004): pp. 4575-83
3. **The role of computed tomography of the chest in the management of small-cell lung cancer.**
J Clin Oncol, UNITED STATES
Vol 2, No 12 (12/1/1984): pp. 1359-65

More...

PubMed Articles by C Lu

PubMed



1. **Hydrothermal growth of large-scale micropatterned arrays of ultralong ZnO nanowires and nanobelts on zinc substrate.**
Chem Commun (Camb), England

Vol , No 33 (8/22/2006): pp. 3551-3
PMID: 16921442 [PubMed - In process]

2. Microfluidic chemical cytometry based on modulation of local field strength.

Chem Commun (Camb), England
Vol , No 33 (8/22/2006): pp. 3528-30
PMID: 16921434 [PubMed - In process]

3. COMPARISON OF INTRINSIC CLEARANCE IN LIVER MICROSOMES AND HEPATOCYTES FROM RATS AND HUMANS - EVALUATION OF FREE FRACTION AND UPTAKE IN HEPATOCYTES.

Drug Metab Dispos,
Vol , No (6/23/2006): pp.
PMID: 16790553 [PubMed - in process]

More...

©Copyright 2006 American Society of Clinical Oncology All rights reserved worldwide.

- [Similar articles in this journal](#)
- [Download to citation manager](#)

- [Articles by Wu, X.](#)
- [Articles by Spitz, M. R.](#)

- [Articles by Wu, X.](#)
- [Articles by Spitz, M. R.](#)

Epidemiology 15: Biomarkers of DNA Damage and Repair, Exposure, and Phenotype Abstract #5662

DNA repair and cell cycle control pathways in lung cancer predisposition.

Xifeng Wu, Maosheng Huang, Jian Gu, Christopher I. Amos, Lina Shao, Qing Zhang and Margaret R. Spitz

The University of Texas M.D. Anderson Cancer Center, Houston, TX

DNA repair and cell cycle control pathways are the guardians of genomic stability. In an ongoing lung cancer case-control study of 1908 patients and 1908 matched controls, we applied pathway-based genotypic assays and two phenotypic assays in peripheral blood lymphocytes to examine whether deficient DNA repair capacity and aberrant cell cycle control are predisposing factors for lung cancer. Among 23 SNPs genotyped, *XPA* (A/G at 5' UTR), *CCNH* (*Val270Ala*), *p53* intron 6, and *STK 15* (*Phe31Ile*) exhibited significant main effects in assessing lung cancer risk. Interestingly, we found a significant gene-dosage effect: as the number of unfavorable genotypes increased, the risk increased with a risk of 3.38 (1.78–6.41) in the stratum with the highest number of adverse genotypes (trend test $P < 0.0001$). Additionally, we found a significantly increased risk associated with an increasing number of putative adverse alleles for both pathways. This

observation was only evident in ever smokers but not in never smokers. For example, in ever smokers, for the cell cycle control pathway, compared to the referent group with ≤ 1 adverse allele, the ORs for individuals with 2, 3, and ≥ 4 adverse alleles were 1.61 (0.97–2.69), 1.66 (1.03–2.69), and 1.71 (1.08–2.69), respectively (P for trend: 0.059). We also implemented a statistical approach to cross validate these observations by evaluating the risk associated with each allele in half of the data and validating the results in the other half set. We cross-validated 10 randomly selected samples from the original data set. Classification and regression tree analysis enabled us to identify subsets of individuals with high or low cancer risk, based on distinct combinations of SNPs. We used comet assay to measure DNA damage/repair and found that the mean γ -radiation- and BPDE-induced tail moments, the parameter for DNA damage, were significantly higher in the cases (4.29 and 3.26, respectively) than in the controls (4.03 and 2.83, respectively) ($P < 0.001$). We used flow cytometry to examine cell cycle profiles and found that the mean γ -radiation-induced cell cycle arrest and accumulation in S and G2 phases were significantly lower in the cases (26.98% and 12.89%, respectively) than in the controls (30.31% and 13.87%, respectively) ($P < 0.001$). In addition, we found that shorter G2 delay was associated with higher levels of γ -radiation- and BPDE-induced damage. We also demonstrated significant correlation between the number of unfavorable NER genotypes and both baseline and BPDE induced DNA damage in the controls. Similarly, there was an inverse correlation between the number of unfavorable cell cycle genotypes and G2 and S delay length. In summary, we found that deficient DNA repair capacity and disruption of cell cycle checkpoints assessed by either genotype or phenotype contribute to elevated lung cancer risk. *Supported by NCI CA 55769, CA 70907, CA111646 [GenBank], DAMD17-02-1-0706 and Flight Attendant Medical Research Institute.*

**AACR Meeting
Abstracts Online**

QUICK SEARCH: [advanced]

Author: Keyword(s):

HOME HELP FEEDBACK CME INFORMATION SEARCH

Go

Wu, X

Institution: MD ANDERSON HOSPITAL Sign In as Member or Individual Non-Member

[Proc Amer Assoc Cancer Res, Volume 47, 2006]

Services

▸ [Similar articles in this journal](#)

▸ [Download to citation manager](#)

Google Scholar

▸ [Articles by Wu, X.](#)

▸ [Articles by Spitz, M. R.](#)

PubMed

▸ [Articles by Wu, X.](#)

▸ [Articles by Spitz, M. R.](#)

Epidemiology 1: Genes and Biomarkers in Tobacco-related Cancer Abstract #435

Interplay between mutagen sensitivity and epidemiological factors in modulating lung cancer risk

Xifeng Wu, Jie Lin, Carol J. Etzel, Matthew B. Schabath, Olga Y. Gorlova, Qing Zhang, Qiong Dong, Christopher I. Amos and Margaret R. Spitz

The University of Texas M.D. Anderson Cancer Center, Houston, TX

Increased genetic instability as unmasked by **mutagen sensitivity** has been shown as a promising cancer predisposition factor. This study consisted of 977 lung cancer patients and 977 matched controls to corroborate the role of **mutagen sensitivity** and its **interplay** with selected epidemiological factors in modulating lung cancer risk. **Mutagen sensitivity** was quantified by measuring chromatid breaks in *in vitro* lymphocyte cultures challenged by bleomycin and BPDE. There were significant differences **between** cases and controls for bleomycin **sensitivity** (0.76 vs. 0.62, $P < 0.001$) and BPDE **sensitivity** (0.70 vs. 0.61, $P < 0.001$). **Mutagen sensitivity** showed an increasing trend with age in controls ($P = 0.002$). Current smokers in controls exhibited the lowest breaks per cell as compared to former and never smokers, suggesting DNA damage caused by tobacco carcinogens may stimulate DNA repair. Interestingly, controls with a history of

emphysema showed higher **sensitivity** than those who had no emphysema history (0.72 vs. 0.61, $P=0.02$). Likewise, cases with a history of hay fever showed lower **sensitivity** than those without hay fever history (0.65 vs. 0.72, $P=0.003$). High **mutagen sensitivity** was associated with a significant 2.29-fold increased risk (95% CI: 1.72-3.04). In quartile analyses, when compared to the first quartile with lowest **sensitivity to mutagen**, the ORs for the second, third and fourth quartiles were 1.63(95% CI: 1.03-2.57), 2.73 (95% CI: 1.79-4.16), and 3.25 (95% CI: 2.13-4.95), respectively (P for trend <0.001). We then investigated the interaction **between mutagen sensitivity** and a panel of epidemiological factors, which had significant distribution differences **between** cases and controls (all $P<0.01$). There was a significant interaction **between mutagen sensitivity** with dietary folate intake (P for interaction= 0.02) and wood dust exposure (P for interaction= 0.03). We divided subjects into four categories based on **mutagen sensitivity**, asbestos exposure, history of emphysema, and wood dust exposure. When compared with the reference group without those risk factors, those exposed to one, two and three or more risk factors were at a 1.58-fold (95% CI: 1.08-2.30), 3.60-fold (95% CI: 2.33-5.55) and 13.97-fold (95% CI: 4.85-45.39) increased risk (P for trend <0.001). Finally, the recursive partitioning procedure further identified high and low risk groups. In ever smokers, history of emphysema was the most important predictor, followed by **mutagen sensitivity**, wood dust exposure, family history of lung cancer, history of hay fever, family history of smoking-related cancer, and history of asbestos exposure. This study strongly supports a substantial **interplay between mutagen sensitivity** and epidemiological risk factors in lung cancer development. Supported by NCI CA 55769, CA111646 [GenBank] , CA 70907, DAMD17-02-1-0706 and Flight Attendant Medical Research Institute.

**Epidemiology 1: Genes and Biomarkers in
Tobacco-related Cancer
Abstract #445**

***ATM* haplotype-tagging SNPs
predict non-small cell lung cancer
risk in Caucasians**

**Hushan Yang, Margaret R. Spitz, Jun Liu, Jian Gu, Charles Lu, David J. Stewart
and Xifeng Wu**

The University of Texas M.D. Anderson Cancer Center, Houston, TX

ATM is a crucial tumor suppressor gene implicated in the pathogenesis of Ataxia telangiectasia (AT), a recessive cancer-prone disorder characterized by extremely high radiosensitivity. Genetic alterations of *ATM* have been identified in a variety of human cancers, especially breast cancer. However, the role of common *ATM* polymorphisms in lung cancer risk has largely been unexplored. We employed a strategy of combining algorithm and literature to select 11 *ATM* haplotype-tagging SNPs (htSNPs) in a frequency-matched case-control study in Caucasians patients with non-small cell lung cancer (NSCLC) (cases, n = 556; controls, n = 556). A high degree of linkage disequilibrium (LD) was observed across the gene. When the homozygous wild-type plus heterozygous genotypes were used as the reference group, the homozygous mutant of either rs170548 or rs227060 was associated with elevated NSCLC risk (OR: 1.51; 95%

CI: 0.99-2.31 or OR: 1.55; 95% CI: 1.02-2.35, respectively). Elevated risks were more evident in men, in young onset patients and in former smokers. We then evaluated genotype-phenotype correlations using two phenotypic assays, the comet assay for DNA damage and flow cytometry for cell cycle arrest. Lymphoblastoid cell lines from homozygote mutant carriers of either of the two SNPs exhibited significantly increased DNA damage as evidenced by a higher mean value of the radiation-induced olive tail moment in the comet assay (rs170548: 5.14 ± 0.75 vs. 3.79 ± 0.16 , $P = 0.01$; rs227060: 4.86 ± 0.73 vs. 3.79 ± 0.15 , $P = 0.04$), and reduced cell cycle arrest shown as lower S phase population by flow cytometry (rs170548: $24.21\% \pm 3.16\%$ vs. $31.21\% \pm 0.87\%$, $P = 0.02$; rs227060: $24.78\% \pm 2.99\%$ vs. $31.35\% \pm 0.86\%$, $P = 0.03$), when compared to individuals with at least one wild type allele. Haplotypes and diplotypes of *ATM* were estimated using a Bayesian algorithm. H5 haplotype was significantly associated with reduced NSCLC risk in former smokers (OR: 0.47, 95% CI: 0.22-0.99) compared with the most common H1 haplotype. Diplotype analysis showed that, compared to the most common H1-H2 diplotype, H2-H2 (OR: 1.58; 95% CI: 0.99-2.54) and H3-H4 (OR: 2.29; 95% CI: 1.05-5.00) diplotypes were associated with an increased NSCLC risk. Overall, our study presents the first epidemiologic evidence that *ATM* genetic polymorphisms, as well as haplotypes and diplotypes, are associated with increased risk of NSCLC, and that the causal variant alleles conferring the risk might act through down-regulating the functions of ATM in DNA repair activation and cell cycle checkpoint maintenance. *Supported by NCI CA 111646, CA 55769, CA 70907, DAMD17-02-1-0706 and Flight Attendant Medical Research Institute.*

**Chemistry 7: Proteomic Analysis and Tumor
Cell Biology
Abstract #3099**

**Identification of markers for
squamous metaplasia of bronchial
epithelial cells**

**Seung Wook Kim, Chang Hoon Kim, Kyounga Cheon, Keith Newton,
David Hawke, Ryuji Kobayashi and Ja Seok Koo**

UT M. D. Anderson Cancer Center, Houston, TX

Lung cancer is the leading cause of death among all cancers in the United States. The prognosis is poor, with less than 15% of patients surviving 5 years after diagnosis, and is strongly correlated with the stage of the disease at the time of diagnosis. Therefore, the development of molecular markers that identify early stages of cancer is critically needed. It has been generally accepted that squamous cell carcinoma is the consequence of the malignant progression of normal epithelium to squamous metaplasia, dysplasia, carcinoma in situ, and invasive carcinoma. To identify molecular markers that identify premalignant lesions in the early stage of lung carcinogenesis, apical surface fluid (ASF) from the squamous metaplasia was analyzed by a 2-dimensional polyacrylamide gel electrophoresis (2D-PAGE) method with early-passage normal human tracheobronchial epithelial cells (NHTBE) using a 3-dimensional organotypic culture method known as the

air-liquid interface (ALI) in defined serum-free media supplemented with growth factors and hormones. Under these conditions, the ability of these cells to differentiate into mucous and ciliated cells is maintained under retinoic acid containing media. These cells also differentiated into squamous metaplasia when they were maintained in retinoic acid-deficient media. Total, 174 protein spots were detected as unique proteins in the ASF from metaplastic squamous NHTBE cell cultures when compared to mucociliary differentiated NHTBE cells. Among them, 25-well separated protein spots were analyzed by liquid chromatography-tandem mass spectrometry (LC-MS/MS). The identified protein includes SCCA1, SCCA2, Annexin 1, Annexin 2, S100A8, and S100A9. Further dot blot analysis using the ASF from squamous and mucous NHTBE verified the presence of the identified proteins in the ASF from the squamous NHTBE cells but not in the ASF from mucous NHTBE cells. Moreover, several squamous cell carcinoma but not adenocarcinoma cell lines expressed SCCA1 and SCCA2. These results suggest that expression of SCCA1 and SCCA2 in early abnormal changes in epithelial cells was retained during progression of squamous cell carcinoma and that these protein may hold promise as potential biomarkers for early detection of squamous cell carcinoma in the lung. Supported by Department of Defense, TARGET Grant: DAMD17-02-1-0706

HOME HELP FEEDBACK CME INFORMATION SEARCH

Cancer Research
Cancer Epidemiology Biomarkers & Prevention
Molecular Cancer Research

Clinical Cancer Research
Molecular Cancer Therapeutics
Cell Growth & Differentiation

Copyright © 2005 by the American Association for Cancer Research.

Cellular and Molecular Biology 24: Epigenetic Therapy Abstract #1820

Antineoplastic action of 5-aza-2'-deoxycytidine and suberoylanilide hydroxamic acid (SAHA) on human lung carcinoma cells

Junya Fujimoto, Waun Ki Hong and Reuben Lotan

UT M.D. Anderson Cancer Center, Houston, TX

Lung cancer is the leading cause of cancer death in the United States. The severe morbidity and mortality from lung cancer have not been reduced and the discouraging <15% overall 5-year survival rate, has not been improved despite advancements in treatment modalities. For this reason, the identification of novel approaches to the prevention and treatment of lung cancer are urgently needed. Loss of expression of tumor suppressor genes is one of the hallmarks of cancer development. It occurs after loss of heterozygosity and mutations in tumor suppressor genes. In addition, epigenetic silencing of such genes can occur by aberrant methylation of CpG islands in gene promoter regions and by changes in chromatin structure resulting from alterations in histone acetylation state. Nucleosomes containing unacetylated positively charged histones bind tightly to DNA producing a compact configuration, which inhibits transcription. A recent approach

to reverse the silencing of genes has been the use of the DNA methylation inhibitor, 5-aza-2'-deoxycytidine (5-AZA-CdR), and the histone deacetylase inhibitor suberoylanilide hydroxamic acid (SAHA). Each of these agents can reactivate the expression of certain silenced genes. The objective of this study was to determine combination of these agents, can enhance their antitumor activity. We examined the ability of different concentrations of 5-AZA-CdR alone, SAHA alone and their combinations to induce growth inhibition in non-small cell lung cancer cell lines NCI-H460, NCI-H157, NCI-H1792, SK-MES-1, as well as in immortalized bronchial epithelial cells BEAS-2B and 1799, transformed 1198 cells, and tumorigenic 1170I cells. We also compared the response of the premalignant and malignant cells with the responses of normal bronchial epithelial cells (NHBE) and small airway epithelial cells (SAEC). We used the sulforhodamine B assay to detect inhibition of cell growth. We found that in most cells tested, 5-AZA-CdR and SAHA in combination produced a greater inhibition of cell growth than either agent alone. These results provide a rationale to investigate the combination of 5-AZA-CdR and SAHA in animal models and eventually in patients with lung cancer. Supported by the Samuel Waxman Foundation's David Workman Award and by a Department of Army Grant, DAMD17-02-1-0706.

HOME HELP FEEDBACK CME INFORMATION SEARCH

Cancer Research

Clinical Cancer Research

Cancer Epidemiology Biomarkers & Prevention

Molecular Cancer Therapeutics

Molecular Cancer Research

Cell Growth & Differentiation

Copyright © 2005 by the American Association for Cancer Research.

**Experimental and Molecular Therapeutics 32:
Targeting Multiple Levels in Molecular
Therapeutics
Abstract #3853**

**Valproic acid induces growth
inhibition and apoptosis in head and neck squamous
carcinoma cell lines**

Meiling Zhong, Ann M. Gillenwater and Reuben Lotan

UT MD Anderson Cancer Center, Houston, TX

Histone deacetylase (HDAC) inhibitors are compounds that increase acetylation level of core nucleosomal histones, thereby relaxing the structure of chromatin associated with genes involved in cell **growth**, differentiation and apoptosis, allowing these genes to be expressed. Many HDAC inhibitors can suppress tumor **growth in vivo**. **Valproic acid** (VPA), a commonly used anti-seizure medication, is also a HDAC inhibitor. To determine whether VPA has potential clinical applications for chemoprevention and therapy in patients with head and neck squamous cell carcinoma (HNSCC), we analyzed the effect of VPA on **growth** and apoptosis in nine HNSCC cell lines. VPA suppressed the **growth** of all nine cell lines with IC 50 ranging from 1.73 mM to 15.17 mM after a 3-day treatment. Subsequent study focused on the most sensitive cell line, 17B. Cell cycle analysis revealed an increased percentage of cells in G1 after 16 hrs incubation with VPA

in a dose-dependent manner. TUNEL assay demonstrated that a 16-hr exposure to VPA at concentrations of 2.5, 5 and 10 mM resulted in 15%, 22.1% and 37.5% apoptotic cells, respectively. Western blot analysis showed that VPA indeed increased nuclear content of acetylated histones. To further investigate the mechanisms underlying the effect of **growth** inhibition and apoptosis induction of VPA, Northern and Western blot analyses were performed to study the expression of key genes in **growth** arrest and apoptosis pathways. The levels of p53 mRNA and protein decreased, while the levels of p21WAF1 increased after treatment with VPA, suggesting that VPA exerted the **growth** inhibition effect through a p21-dependent, but p53-independent pathway. The protein levels of procaspases 2, 3, 6 and 9 decreased, accompanied by simultaneous increased levels of cleaved caspases 3 and 9, and cleaved PARP. Addition of a caspase inhibitor Z-VAD-FMK to VPA-treated 17B cells abolished VPA-induced apoptosis, indicating that VPA induced apoptosis through a cascade of caspases. VPA treatment did not change the protein levels of Fas, Bax, Bcl-2 or caspase 8. Together, our data suggest that **Valproic acid** has **growth** inhibitory and apoptosis-inducing activity in HNSCC cells *in vitro* and should be further investigated for therapeutic use in patients with this malignancy.

HOME HELP FEEDBACK CME INFORMATION SEARCH

Cancer Research

Clinical Cancer Research

Cancer Epidemiology Biomarkers & Prevention

Molecular Cancer Therapeutics

Molecular Cancer Research

Cell Growth & Differentiation

Copyright © 2006 by the American Association for Cancer Research.

oral keratinocytes (NHOK) and its immortalized derivative expressing human papillomavirus type 16 E6E7 oncoproteins (HOK16E6E7). Galectin-7 was down-regulated more than 10 fold in immortalized HOK16E6E7 compared to NHOK. Northern blot confirmed the array result. In addition, galectin-7 was not present in other head and neck squamous cell carcinoma. The expression of galectin-7 level was also increased along with increasing passage of NHOK. Telomerase activity assay showed that there was a decrease in later passage of NHOK. Inhibition of RNA (siRNA) leads to extended cellular life span. Overexpression of galectin-7 in squamous cell carcinoma, SCC4 and SCC9, appear to increase apoptosis. These results suggested that galectin-7 may play a role in tumor suppressor function in oral keratinocytes. This work was supported by NIH/NIDCR K23 DE00430 and NIH/RCMI P20 RR11145.

#1050 Prohibitin, a potential tumor suppressor for prostate cancer. Shankar Jagadeesh and Partha Banerjee. *Department of Cell Biology, Georgetown University Medical Center, Washington, DC.*

To control growth of prostate cancer in men there is an urgent need to understand the function of genes that are involved in negative control of cell proliferation. Prohibitin is an intracellular protein that has an anti-proliferative activity in different systems. Up till now, there is no report about prohibitin's role in prostate cancer. In this study, we examined the relative levels of prohibitin in normal human prostate and prostate cancer tissues. Our results show that immunostaining intensity of prohibitin is much higher in normal prostate compared to the prostate cancer. Prohibitin is predominantly expressed in the epithelial cells in both normal and prostate cancer tissues. Human prostate cancer cell lines (LNCaP, PC-3 and DU-145) express prohibitin but the levels vary among these cell lines. Androgen-responsive prostate cancer cell line, LNCaP, showed the highest level compared to the PC-3 cells and lowest level was observed in DU-145 cells. Interestingly, the cell proliferation and thereby growth of these cell lines in vitro correlated with the levels of prohibitin protein present in these cells, as the slowest growth was observed in LNCaP cells and fastest growth was observed in DU-145 cells. To understand the role of prohibitin in prostate cancer cells, we used gain-of-function and loss-of-function analyses by transfecting sense and anti-sense prohibitin expression vectors in DU-145 cells. Several clonal populations of stably transfected cells were obtained that express various levels of prohibitin. Overexpression of prohibitin in DU-145 cells reduced cell proliferation (more than 50%) and colony forming ability (more than 70%) in vitro. Overexpression of prohibitin also altered the phenotype of DU-145 cells (emergence of prominent hexagonal morphology with distinct cell wall) compared to the vector control or non-transfected cells (loss of hexagonal morphology). On the other hand, inhibition of prohibitin expression by antisense-prohibitin transfection vector induced cell death. These results suggest that a minimum level of prohibitin is essential for cell survival, whereas the higher levels of prohibitin inhibit cell proliferation in prostate cancer cells. Therefore, overexpression of prohibitin might act as a tumor suppressor for prostate cancer. (Supported by the start-up fund from the Georgetown University)

#1051 Overexpression of Id-1 in hormone-refractory prostate cancer. Philip E. Ryan, Nancy J. Nesslinger, Xubao Shi, Christopher P. Evans, Colin A. Baron, Jeffrey P. Gregg, Ralph W. deVere White, Hsing-Jien Kung, and Clifford G. Tepper. *University of California, Davis School of Medicine, Sacramento, CA.*

Hormone refractory prostate cancer is the principal cause of mortality due to this neoplasm. To study this we have been utilizing the CWR22 human tumor xenograft model which effectively simulates the clinical course of prostate cancer by exhibiting androgen-dependent growth in male nude athymic mice, regression in response to androgen withdrawal, and relapsed growth of the tumor after several months. In addition, we have characterized a novel androgen receptor mutation in the 22Rv1 cell line and described it as a model of androgen independence and repression. In order to gain insight into the molecular mechanisms underlying the transition to androgen-independence, microarray gene expression profiling was performed on parental CWR22 and relapsed CWR22R xenograft tumors using Affymetrix HG-U95Av2 GeneChip arrays. Hierarchical clustering of the resulting data was performed to identify gene expression patterns associated with particular molecular alterations and phenotypes. This demonstrated that the CWR22R-2152 tumor and its derivative 22Rv1 androgen-independent cell line possessed a unique gene expression signature underscored by markedly elevated expression of Id-1 (Inhibitor of Differentiation/DNA binding-1) in comparison to the parental tumors and the other relapses. Id-1 is a dominant-negative helix-loop-helix protein known to suppress replicative senescence and promote tumor aggressiveness. Quantitative real-time PCR and immunoblot analyses confirmed the microarray findings and demonstrated similarly elevated Id-1 levels in the androgen-independent, p53-mutated DU145 and PC-3 cell lines. In contrast, Id-1 expression was marginally expressed in the LNCaP androgen-dependent cell line. Interestingly, Id-1 expression was up-regulated in LNCaP-p53 mutant sublines harboring p53 gain-of-

function mutant alleles and a p53 loss-of-function allele (P151S), implicating the mutational inactivation of p53 as a basis for Id-1 deregulation. Since the LNCaP-p53^{GOF} sublines, but not LNCaP-p53(P151S), are capable of androgen-independent proliferation, Id-1 expression alone is insufficient to mediate androgen independence. Further analysis showed increased Id-1 expression in primary prostate cancer cell cultures when compared to cultures established from benign prostatic hyperplasia. Id-1 was easily detected in prostate cancer samples in tissue microarrays by immunohistochemical staining and exhibited a punctate, cytoplasmic staining pattern. Our data implicate Id-1 overexpression as a feature of prostate cancers harboring p53 mutations and/or androgen-independent tumors progressing to an androgen-independent and -insensitive phenotype. In cells with p53^{GOF} mutations, elevated Id-1 expression would be expected to suppress the Rb pathway; thus, these tumors would effectively have loss of both tumor suppressor genes combined with the oncogenic attributes of p53^{GOF} mutations.

#1052 PMEPA1, an androgen-regulated NEDD4 binding protein exhibits cell growth inhibitory function and decreased expression during prostate cancer progression. Linda L. Xu, Yinghui Shi, Gyorgy Petrovics, Mazen Makareem, Chen Sun, Wei Zhang, Isabell A. Sesterhenn, David G. McLeod, Leon Sun, Judd W. Moul, and Shiv Srivastava. *Center for Prostate Disease Research, Bethesda, MD, Armed Forces Institute of Pathology, Dept. of Genitourinary Pathology, Washington, DC, and Urology Service, Department of Surgery, Walter Reed Army Medical Center, Washington, DC.*

Serial Analysis of Gene Expression in androgen-treated LNCaP prostate cancer cells has led to the discovery of a novel androgen-regulated gene, *PMEPA1*. The expression of *PMEPA1* is prostate abundant and is restricted to prostatic epithelial cells. *PMEPA1* shows high protein sequence homology to *N4WBP4*, a mouse NEDD4-binding protein with unknown function. A recent study, showing consistent *PMEPA1* overexpression in non-tumorigenic revertants following chromosome 8 transfer into tumor cells, suggests for direct or indirect regulation of *PMEPA1* by chromosome 8, the most frequently altered chromosome in prostate cancer (CaP). In this study, we demonstrate that *PMEPA1* interacts with NEDD4 WW domains through its PY motifs. Mutation of the PY motifs significantly decreased the binding ability of *PMEPA1* to NEDD4. *PMEPA1*-GFP fusion protein localizes to the cis-Golgi matrix compartment but not to the trans-Golgi network in cells transfected with the *PMEPA1*-GFP expression vector. Overexpression of *PMEPA1* in widely used prostate tumor cell lines: DU145, PC3, LNCaP and LNCaP sublines (C4, C4-2 and C4-2B) resulted in significant cell growth inhibition. Laser capture microdissection derived paired normal and primary tumor specimens from 62 prostate cancer patients were analyzed for *PMEPA1* expression by real-time RT-PCR assays. Forty of 62 (64.5%) matched prostate specimens exhibited decreased expression of *PMEPA1* in tumor tissues. Decreased *PMEPA1* expression was significantly associated with higher pathologic stage and higher levels of serum PSA, suggesting that decreased *PMEPA1* function may have some role in prostate tumorigenesis. As an androgen-regulated and prostate-abundant gene, *PMEPA1* appears to have functions in the regulation of prostate cell growth and these functions may be mediated through the interaction of *PMEPA1* with NEDD4 proteins involved in the ubiquitin-proteasome pathway.

#1053 Synergistic inhibition of tumor cell growth by CACNA2D2 and p53 via activation of DAPK pathway in lung cancer. Giovanni I. Carboni, Jianhua Shao, Kai Xu, Boning Gao, Masahiko Nishizaki, Ralph A. Schmid, John D. Minna, Jack A. Roth, and Lin Ji. *University Hospital Bern, Division of General Thoracic Surgery, Berne, Switzerland, UT MD Anderson Cancer Center, Dept. of Thoracic and Cardiovascular Surgery, Houston, TX, and UT Southwestern Medical Center, Dallas, TX.*

The Ca²⁺-channel subunit gene CACNA2D2 (CACN) is located in the human chromosome 3p21.3 homozygous deletion region. We previously showed that enforced expression of wild-type (wt)-CACN by the recombinant adenoviral vector-mediated transfer in CACN-deficient NSCLC cells significantly inhibited cell growth and induced apoptosis in vitro and in vivo. We also observed that the wt-p53-expressing NSCLC cells appeared more sensitive to Ad-CACN-mediated growth inhibition and apoptosis induction, suggesting a possible p53-dependent mechanism for the CACN-mediated function. To explore the molecular mechanism behind the apparent interaction between CACN and p53, we evaluated the combined effect of the Ad-CACN and Ad-p53-mediated gene co-transfer on tumor cell growth and apoptosis and analyzed the potential downstream signaling pathways mediated by these tumor suppressors in NSCLC cells. A significant synergistic inhibition of tumor cell growth was observed in Ad-CACN and Ad-p53-cotransduced H358 and H1299 (p53 null) cells ($p = 0.035$ and $p = 0.046$, respectively) by isobologram modeling and statistical analysis. A similar synergistic effect on induction of apoptosis was also observed, as shown by the significant increase of apoptotic cell populations, 26.3% ($p = 0.03$) in H358 and 20.3% ($p = 0.06$) in

H1299 cotransduced by Ad-CACN and Ad-p53, respectively, compared to the either vector treatment alone. To analyze the effect of CACN on endogenous p53 expression, we performed Western-blot analysis in Ad-CACN-transduced A549 and H460 (p53 wt) cells and found that the ectopic expression of CACN enhanced p53 protein expression, possible due to p53 stabilization, in both cells but with a less degree of increase in H460. Furthermore, we explored the possibility of the involvement of the death associated protein kinase (DAPK), a Ca^{2+} /Calmodulin activated protein kinase that has been shown to induce apoptosis in a p53-dependent mechanism. We found that exogenous CACN expression induces phosphorylation of DAPK in A549 and H358. The H460 cells are deficient of both gene and protein expression due to promoter methylation, as confirmed by methylation-specific PCR, Western blot and RT-PCR analysis. Treatment with the methyltransferase inhibitor 5-Aza-2'-deoxycytidine (AZA) restored DAPK protein expression in H460. Combination treatment with Ad-CACN and AZA synergistically suppressed H460 cell growth and efficiently induced p53 stabilization. Based on these observations, we conclude that exogenous co-expression of CACN and p53 synergistically inhibits tumor cell growth in NSCLC cells and the observed synergy might result from the p53 stabilization through the CACN-mediated DAPK activation and phosphorylation.

#1054 Increased expression of H19, a putative tumor suppressor gene, follows the initiation of hepatocyte proliferation *in vivo* and *in vitro*. Yuji Nishikawa, Youhei Yamamoto, Masayuki Yoshida, Takuya Nishimura, Takuo Tokairin, Yasufumi Omori, and Katsuhiko Enomoto. *Akita University School of Medicine, Akita, Japan.*

H19 is a paternally imprinted gene that is believed to function as a mRNA without being translated into a protein. Decreased gene expression and/or abnormal imprinting status (loss or gain of imprinting) have been noted in some malignant tumors, including Wilms tumor, lung and liver cancers, and suppression of malignant phenotype has been demonstrated in tumor cell lines by transfection of a H19 gene construct. While these data strongly suggest that H19 may be a tumor suppressor gene, its physiological role is largely unknown. In the liver, the gene was expressed at high levels during fetal period, but rapidly downregulated after birth and only a little expression remains in the adult liver. In the present study, to explore the possibility that H19 might participate in the regulation of hepatocyte proliferation in the adult liver, we examined the changes in H19 expression during *in vivo* and *in vitro* hepatocyte growth. Adult male CBA X BALB/c F1 mice and F344 rats were subjected to a two-thirds partial hepatectomy (PH). After various time periods, the livers were perfused with collagenase to isolate hepatocytes for subsequent studies. RT-PCR analysis demonstrated that the expression of H19 was dramatically increased at 4 days (mouse) and 2 days (rat) after PH and then gradually decreased. The increase in H19 gene expression was slightly behind the initiation of hepatocyte proliferation that was estimated by ornithine decarboxylase gene and proliferating cell nuclear antigen (PCNA) expression. A restriction fragment length polymorphism analysis using the reported one-base-pair polymorphism in the exon 1 between CBA and BALB/c mice (Ainscough et al., 1997), showed that paternal imprinting status of H19 gene was strictly maintained during the increase of its mRNA. H19 gene expression was also examined in the rat hepatocytes cultured on positively-charged plastic dishes (Primaria) in the presence of BGF and insulin. In the culture system, in which hepatocytes formed spheroidal aggregates, there was a distinct peak of PCNA expression at 2 to 3 days after plating. H19 gene expression was increased in the spheroids cultured for 5 to 7 days. The increased H19 expression was extinguished when the spheroids were transferred to collagen-coated plastic dishes to facilitate proliferation as monolayers. Our results demonstrated that H19 gene expression is dynamically regulated in adult hepatocytes in close association with their proliferation both *in vivo* and *in vitro*, without changing its imprinting status. Since the increase in H19 mRNA is subsequent to the initiation of hepatocyte proliferation, it might be involved in the negative, rather than positive, regulation of cell growth, which is consistent with the supposed tumor suppressing capacity of H19 gene.

#1055 Suppression of cellular proliferation and enhanced radiation and chemotherapeutic response by the restoration of chromosome 19 in glioma cells. Gaspar J. Kitange, Mark E. Law, Cheryl L. Soderberg, and Robert B. Jenkins. *Mayo Clinic Rochester, Rochester, MN.*

Deletion of the 19 q-arm is observed in more than 50% of human oligodendrogliomas. As a result, chromosome 19 is believed to contain a novel tumor suppressor gene involved in the development of these tumors. Although a minimal region of deletion in primary gliomas has previously been mapped, to date no candidate tumor suppressor gene has yet been identified. To facilitate our cloning effort of the 19q glioma tumor suppressor gene, we have used FISH analysis to screen 19 q-arm deletions in a panel of human glioma cell lines. We identified two cell lines, A172 and U87, which contain deletions encompassing the minimally deleted region in

primary gliomas. To define a functional role of the 19 q-arm candidate tumor suppressor gene, we have used a microcell-mediated chromosome transfer to rescue a normal human 19 in the A172 cell line. So far, we have isolated 13 hybrid (A172/neo19) clones; 11 of which contain an extra whole 19, and 2 an extra portion of 19q. Interestingly, A172 neo19 clones, with either whole 19 or 19q, elicited slower proliferation than control vector-transfected clones. Moreover, A172 neo19 clones were more sensitive to radiation, as evidenced by clonogenic survival analysis. Exposure of A172 neo19 clones to CCNU or BCNU resulted in significantly reduced survival as well as increased cell death compared to vector-transfected clones. Taken together, these findings provide functional evidence that chromosome 19 contains a glioma tumor suppressor gene and that restoration of this gene renders glioma cells more sensitive to radiation and chemotherapy. The A172 neo19 clones should be useful for the identification of candidates for the glioma tumor suppressor gene. Supported in part by CA85799.

#1056 The role of PAX6 in glioblastoma formation: A putative novel suppression pathway. Yi-Hong Zhou, Fang Tan, Yue-Xi Shi, Tricia Glas, Kyle W. Chen, Kenneth R. Hess, Joy Gumin, Frederick Lang, and W.K. Alfred Yung. *M.D. Anderson Cancer Center, Houston, TX.*

Glioblastomas (GBMs) are the most common and malignant primary brain tumors in adults. The PAX6 gene encodes a transcription factor for regulating cell proliferation, migration, and differentiation in the development of the eye and central nervous system. We have reported that PAX6 expression was inversely correlated with the tumorigenicity of glioma cell lines and the grade of gliomas, and a lower value of PAX6 expression was an unfavorable prognostic factor for malignant glioma patients. To substantiate the putative tumor suppression function of PAX6, we introduced a PAX6 expression construct into two human GBM cell lines, U251HF and LN229, and found that ectopic expression of PAX6 suppressed cell invasion *in vitro* in both cell lines. Subcutaneous and intracranial implantation of U251HF and its PAX6 transfectants in nude mice suppressed tumor growth and significantly extended survival. In an attempt to elucidate the suppression mechanism of PAX6, we found that the expression of the gene encoding platelet-derived growth factor receptor alpha (PDGFR α) was repressed in PAX6 transfectants of both U251HF and LN229 cell lines. Furthermore, neutralizing antibodies to PDGFR α suppressed the invasion ability of glioma cells. Thus, a putative mechanism for PAX6 suppression of GBM formation may be inhibiting the invasiveness of cells mediated through the PDGFR α cell signaling pathway.

#1057 Infectious delivery of the 132 kb CDKN2A/CDKN2B genomic DNA region results in suppression of growth in glioma cells. Ryo Inoue, Kaveh Asadi Moghaddam, Moksha Ranasinghe, Yoshinaga Sacki, E. Antonio Chiocca, and Richard Wade-Martins. *Molecular Neuro-Oncology, Massachusetts General Hospital, Charlestown, MA.*

The chromosomal region 9p21.3 spanning the CDKN2A and CDKN2B loci demonstrates complex splicing of overlapping genes. The region encodes up to six proteins involved in cell cycle control, and 9p21.3 deletion is one of the most frequent mutations found in human glioblastomas (GBMs), occurring in ~60% of cases. We recently developed an efficient infectious gene delivery system for large genomic regions, termed the infectious bacterial artificial chromosome, or iBAC, system. The iBAC is based on the herpes simplex virus type 1 (HSV-1) amplicon, an infectious vector with a transgene capacity of ~150 kb, and tropism for neuronal cells. In this study, we wished to evaluate the efficacy of infectious delivery of the complete CDKN2 region to human glioma cells and evaluate restoration of cell cycle regulation. We first screened ten glioma cell lines for homozygous deletions of the p16INK4a, p14ARF and p15INK4b exons, and selected for further study the Gli-33 and Gli-36 cell lines which have deletions of the entire CDKN2 region. Next, we constructed the iBAC-CDKN2 vectors, pHSV-CDKN2 and pHSV-EBV-CDKN2 (a hybrid amplicon including episomal retention elements from Epstein-Barr virus), carrying a fully sequenced 132 kb genomic DNA insert. As a preliminary, we transfected the constructs into Gli-36 cells and verified expression of p16INK4a by immunohistochemistry, and of p16INK4a, p14ARF and p15INK4b, by RT-PCR. We then packaged the iBAC vectors using an improved helper virus-free HSV-1 amplicon packaging system. Following infectious delivery to Gli-36 we confirmed expression of p16INK4a, p14ARF and p15INK4b by RT-PCR. This is the first demonstration of the correct expression of alternative splice forms of a human genomic locus >100 kb following infectious delivery. We then examined if CDKN2A and CDKN2B expression could restore cell cycle control in human glioma cells. We used flow cytometry to sort infected cells, using the iBAC green fluorescent protein (GFP) reporter gene as a marker. GFP positive cells seeded at low density were allowed to divide and were evaluated for growth rate using the WST-1 colorimetric assay. The growth rate of Gli-36 and Gli-33 cells infected with the iBAC-CDKN2 vectors was significantly lower by days 3 and 7, respectively, than that of cells infected with control amplicons. On day 5, Gli-36

infected with the iBAC-CDKN2 cell line, which is undergoing apoptosis, offers a potential and regulate

#1058 Potentially H. Schonhuth, Center, La.

Germline mutation theory of genomic integrity (2) cell cycle. These functional cycles cell cycle. Cells undergo therefore inv. ovarian cystad undergoes crisis by a marked increase in the crisis pl. chromosome act. other. Real-time about a 3-f. at early passage to aneuploid or detected when crisis. These ret. of crisis which

#1059 ATM sequence. David I.

ATM encodes a protein kinase (1-3 kinase) sequence is conserved in all eukaryotes. However, in predominantly localization to discrete fragments of proteins used evidence of signal (NL). Mutation predominantly can facilitate the NES of amino ter.

#1060 Mechanism of HIV-1 infection in patients with HIV-1. Tat, secreted candidate of its genome lymph lymph.

tion, ranging from less than 6 h in PC346 cells till up to approximately 24 h in PC3 cells. The variable effect of wortmannin in the different cell lines could not be attributed to degradation of the drug. In LNCaP and PC346 cells transient increase in p27^{Mp1} mRNA expression correlated with the observed transient FKHL1 activation following wortmannin treatment. PC3 cells displayed a prolonged increase of p27^{Mp1} mRNA expression after PI3K inactivation. However, p27^{Mp1} protein expression in LNCaP, PC346 was not affected by wortmannin. In PC3 cells p27^{Mp1} protein expression slowly accumulated, but no obvious correlation was observed between the kinetics of p27^{Mp1} mRNA and protein accumulation. Taken together we conclude that regulation of p27^{Mp1} mRNA expression via the PI3K/PYEN downstream target FKHL1 does not significantly contribute to regulation of p27^{Mp1} protein expression in prostate cancer cell lines.

#396 The transforming acidic coiled coil proteins are components of multiple protein complexes. Omkaram Gangisetty, Gautam Sridharva, Ananthakrishmy Vethakkorumakankav, Zeenat Jalsani, Brenda Lauffart, and Ivan H. Still. *Roswell Park Cancer Institute, Buffalo, NY.*

Dysregulation of the human TACC genes is thought to be important in the evolution of breast cancer, prostate cancer and multiple myeloma. However, the exact role of the TACC proteins in the oncogenic process is currently unknown. To investigate their potential functions, we have used the yeast two-hybrid system to identify proteins that bind to human TACC1, TACC2 and TACC3. Our analysis indicates that TACC interacting proteins can be divided into two broad categories: 1) proteins with roles in centrosome/mitotic spindle dynamics, and 2) proteins involved in gene regulation, either at the level of transcription, or subsequent RNA processing and translation. Specifically, we demonstrate that each family member directly interacts with the bromodomain-containing histone acetyltransferases (HAT), hGCN5 and pCAF. Significantly, we also show that the human TACC proteins bind to GAS41 and either directly, or indirectly to the INI-1 core component of the SWI/SNF chromatin-remodeling complex. This suggests a more intimate association between the TACC family and the processes involved with the initiation of gene transcription. Thus, as the number of TACC interacting factors grows, it is becoming evident that, similar to BRCA1 and BRCA2, the TACC proteins are present in a diverse set of multiprotein complexes. Thus, dysregulation of TACC family members has the potential to impact several cellular functions, promoting tumorigenesis and progression.

#397 Myristoylation of Fus1 protein is required for Fus1-mediated tumor suppressing activities in human lung cancer. Futoshi Uno, Jilchiro Sasaki, Masahiko Nishizaki, Giovanni Carboni, Kai Xu, John D. Minna, Jack A. Roth, and Lin Ji. *The University of Texas M.D. Anderson Cancer Center, Houston, TX and The University of Texas Southwestern Medical Center, Dallas, TX.*

FUS1 is a novel 3p21.3 candidate tumor suppressor gene which is inactivated in primary lung cancers by a combination of allele loss, rare mutations, and frequent deficiency of protein expression. Re-expression of wild-type (wt)-Fus1 in Fus1-deficient non-small cell lung cancer (NSCLC) cells inhibits tumor cell growth and induced apoptosis in vitro and in vivo. A motif-based profile scanning analysis revealed a potential myristoylation site at the N-terminus of Fus1 protein sequence. Using surface-enhanced laser desorption and ionization-Mass (SELDI-MS) spectrometry analysis on a Fus1-antibody-captured ProteinChip array (ACPA), we identified wt-Fus1 as a myristoylated protein, which was further confirmed by Western-blot and immunoprecipitation analysis of H3-myristate-labeled Fus1 protein. We evaluated Fus1 protein expression and posttranslational modification using ACPA with SELDI-MS in primary uncultured NSCLCs and non-involved lung tissues using Laser Capture Micro-dissection to separate tumor from normal cells. Only myristoylated protein species were detected in normal lung cells but both unmyristoylated and myristoylated Fus1 protein were detected in tumor cells. N-myristoyl-proteins play essential roles in diverse biological functions, such as regulating cellular structure, directing protein intracellular localization, and mediating protein-protein and protein-substrate interactions. Thus, We tested whether myristoylation was required for tumor suppressing activity by transfecting expression plas-

mid vectors containing wt-FUS1 or a myristoylation-deficient mutant (Myr-mut-FUS1) made by site-directed mutagenesis. By immunofluorescence imaging analysis, Myr-mut-Fus1 compared to wt-Fus1 dramatically lost its characteristic intracellular membrane localization in transfected H1299 cells. We then analyzed the effects of the wt-FUS1 and Myr-mut-FUS1 expression on tumor cell-induced clonogenicity in vitro, on the growth of NSCLC (NCI)-H1299 subcutaneous tumor xenografts, and on the development of NSCLC A549 lung metastases in nude mice by intratumoral injection or systemic administration of FUS1-Lipoplexes. Myr-mut-FUS1 compared to wt-FUS1 exhibited significant loss of the ability to inhibit clonogenicity in vitro and suppress xenograft subcutaneous tumor and lung metastasis growth in H1299 tumor-bearing animals. We conclude that posttranslational myristoylation is required for Fus1 tumor suppressing activity and that loss of both protein expression and myristoylation occur in primary human lung cancers.

#398 The WT1 gene regulates prostate cancer cell tumorigenicity in an isoform-specific fashion. Julie M. Carroll, Natalop Sipanatsakul, Joy L. Ware, and Charles T. Roberts. *Oregon Health and Science University, Portland, OR and Virginia Commonwealth University, Richmond, VA.*

The WT1 gene encodes a zinc-finger transcription factor and was originally classified as a tumor suppressor based upon its inactivation in a subset of Wilms' tumors. More recently, however, it has been found that the WT1 gene is expressed in many hematopoietic and solid tumors, as well as tumor cell lines, including those derived from the prostate. The WT1 gene is subject to alternative splicing of exons 5 and 9 that produces four isoforms of the full-length protein. The alternative splicing of exon 9, which produces two isoforms that contain or lack a KTS sequence between zinc fingers 3 and 4, is thought to have the main impact on WT1 function. We have recently demonstrated that the increased tumorigenicity of sublines derived from an SV40 T antigen-immortalized human prostate epithelial cell line was accompanied by increased expression of a novel WT1 transcript comprised of portions of intron 5 and exons 6-10 of WT1, and which is subject to the alternative splicing of exon 9. Collectively, these findings have led us to propose that WT1 may function as an oncogene in advanced prostate cancer, rather than as a classical tumor suppressor. To directly assess the role of full-length WT1 in prostate cancer, we generated stable transfectants of the PC-3 cell line expressing an antisense RNA complementary to WT1 exon 1. Isolated clones were analyzed at early passage (3) for WT1 protein expression by Western immunoblotting and re-examined at passage 8: Three of four clones that exhibited decreased levels of all full-length WT1 isoforms at passage 3 expressed higher levels at passage 8, suggesting that there was selective pressure against decreased WT1 expression during monolayer growth. Nude mice injected s.c. with two clones at passage 3 (expressing 6 and 13 %, respectively, of control levels of WT1) exhibited >90% reduction of tumor volume at 30 and 45 days. Mice injected with a clone at passage 8 that had rebounded from 5 to 30% of control levels of WT1 exhibited increased latency and somewhat decreased tumor volume, while another passage-8 clone that expressed 40% of the control WT1 level behaved similarly to control cells. Thus, modulation of full-length WT1 levels is sufficient to regulate tumorigenesis of prostate cancer cells, and this effect is proportional to the change in WT1 expression. To address the role of novel truncated WT1 proteins, we expressed both exon-9 splice variants in the weakly tumorigenic M2205 prostate cancer cell line. Expression of the -KTS isoform of the truncated WT1 protein increased tumor size in xenografts, while expression of the +KTS isoform inhibited tumor growth. These experiments demonstrate an oncogenic function for WT1 in human prostate cancer cells, and suggest that manipulation of WT1 activity may provide a novel therapeutic strategy for these cancers. Supported by DOD10273 and Lematta Foundation (CTR) and DK52683 and CA58126 (JLW).

Experimental and Molecular Therapeutics 34: Genes, Drugs, and Novel Agents

Abstract #3796

Enhanced sensitivity of tumor cells to chemotherapeutic agents by activation of *FUS1* tumor suppressor gene in lung cancer cells.

Jiichiro Sasaki, Futoshi Uno, John D. Minna, Jack A. Roth and Lin Ji

UT. M.D. Anderson Cancer, Houston, TX and UT Southwestern Medical Center, Dallas, TX.

FUS1 is a novel tumor suppressor gene (TSG) identified in the human chromosome 3p21.3 region that is deleted in many cancers. We previously found that *FUS1* TSG was inactivated in many primary lung cancers and cancer-derived cell lines by either the loss of expression or the deficiency of the posttranslational myristoylation modification of the wild-type (wt)-Fus1 proteins. We also demonstrated that exogenous expression of the wt-*FUS1* by plasmid- or adenoviral vector-mediated gene transfer significantly inhibited tumor cell growth, induced apoptosis, and altered cell cycle kinetics in 3p21.3-deficient lung cancer cells *in vitro* and efficiently suppressed tumor growth and inhibited tumor progression and metastases in human lung cancer xenograft mouse models. Based on these pre-clinical investigations, a phase I clinical trial is now undertaking in advanced non-small cell lung cancer patients using systemic administration of DOTAP-cholesterol-complexed wt-*FUS1*-expressing plasmid DNA (*FUS1*-lipoplex). In this study, we explored the capability of the wt-*FUS1* gene product as a modulator of chemotherapeutic drugs for enhancing chemotherapeutic potency and overcoming drug resistance in lung cancer cells. We found that a transient expression of the wt-Fus1 protein in *FUS1*-expressing plasmid-transfected H1299 cells significantly enhanced the cisplatin-mediated inhibitory effect on tumor cell growth at a low-dose (1 micro molar) of cisplatin

treatment. In addition, a stable expression of the wt-*FUS1* gene, which is under the control of a ponasterone A-inducible promoter, reduced more than 30% of IC₅₀ values of both cisplatin and paclitaxel treatments in H1299 cells, even at a low level of induced Fus1 expression. However, the maximum stable expression of a functionally deficient mutant Fus1 protein (mt-Fus1) in a similar inducible system did not enhance the sensitivity of tumor cells to these drugs. Furthermore, a significant increase in apoptotic cell populations were detected in cells with the induced expression of the wt-Fus1 protein but not in those with induced expression of mt-Fus1, as shown by a FACS analysis with TUNEL reaction. These results suggest that the wt-Fus1 may play a critical role in modulating the sensitivity of tumor cells to the chemotherapeutic agents, especially, to DNA damaging agents such as cisplatin and that a combination treatment with the *FUS1*-lipoplex-mediated molecular therapy and the cisplatin or taxcel-based chemotherapy may be an efficient treatment strategy for lung cancer.

Abstract #4821

Activation of apoptotic signaling pathway by direct interaction between tumor suppressor Fus1 and Apaf-1 proteins in lung cancer cells

Futoshi Uno, Jiichiro Sasaki, Gitanjali Jayachandran, Kai Xu, John D. Minna, Jack A. Roth and Lin Ji

The University of Texas M.D. Anderson Cancer Center, Houston, TX and The University of Texas Southwestern Medical Center, Dallas, TX

FUS1 is a novel tumor suppressor gene identified in a 120-kb overlapping homozygous-deletion region in human chromosome 3p21.3 in lung and breast cancers. We previously demonstrated that enforced expression of the wild-type (wt)-*FUS1* in 3p21.3-deficient non-small cell lung cancer (NSCLC) cells significantly suppressed tumor cell growth by induction of apoptosis and alteration of cell cycle kinetics *in vitro* and *in vivo*. However, the molecular mechanism and signaling pathway involved in the *FUS1*-mediated apoptosis remained unknown. In this study we aimed to identify the potential cellular targets of Fus1 protein to have an insight into the mechanism of Fus1 function. We performed immuno-precipitation (IP) analysis using anti-Fus1 antibodies with protein lysates prepared from Fus1-expressing plasmid-transfected NSCLC H1299 cells to analyze the Fus1-mediated protein-protein interactions. The potential cellular protein targets that directly interact with Fus1 protein were analyzed by SDS-PAGE of the IP complexes and further identified by peptide mapping of the trypsin-digested proteins in the complexes by a surface-enhanced laser desorption and ionization-mass spectrometry on a ProteinChip array. One of the potential Fus1-interacting proteins was predicted by peptide mapping as the apoptotic protease activation factor 1 (Apaf-1). This Fus1-Apaf1 interaction was further confirmed by IP and immuno-blot analysis using either anti-Fus1 or anti-

Apaf1 antibodies, alternatively. We also observed that both the wt-Fus1 and a *N*-myristoylation-deficient mutant Fus1 (myr-mt-Fus1) protein but not the *C*-terminal-deletion (10-20 amino acids) mutants of Fus1 proteins could bind to Apaf-1 protein in H1299 transfectants. A computer-aided structural analysis predicted a PDZ domain in the *C*-termini of the both Fus1 and Apaf1 proteins, suggesting that the Fus1-Apaf-1 interaction might be mediated through these classic PDZ protein-protein interaction motifs. Using an immuno-fluorescence image analysis with Fus1 and Apaf1 antibodies, we detected that the Apaf1 proteins were co-localized with the wt-Fus1 proteins in their typical mitochondria and ER membrane locations but with the myr-mt-Fus1 proteins, which lost its membrane-attachment capability, everywhere in the cytoplasm in the wt-*FUS1* and myr-mt-*FUS1*-transfected H1299 cells, respectively. These results suggest that Fus1 protein may function as a key mediator in Apaf1-mediated mitochondria apoptosis pathway by recruiting and directing cytoplasmic Apaf1 protein to the critical cellular location and activating it *in situ* for the efficient induction of apoptosis.


www.asco.org

Synergistic inhibition of EGFR tyrosine kinase and tumor cell growth in non-small cell lung cancer (NSCLC) by combination treatment with FUS1-nanoparticles and Gefitinib

Sub-category: Non-Small Cell Lung Cancer

Category: Lung Cancer

Meeting: 2005 ASCO Annual Meeting

Abstract No: 7081

Citation: *Journal of Clinical Oncology*, 2005 ASCO Annual Meeting Proceedings. Vol 23, No. 16S, Part I of II (June 1 Supplement), 2005: 7081

Author(s): L. Ji, H. Kawashima, C. Lu, J. Kurie, S. Chada, J. D. Minna, J. A. Roth

Abstract: **Background:** FUS1 is a novel tumor suppressor gene (TSG) identified in the human chromosome 3p21.3 region that functions in the Apaf1-associated apoptotic pathway, and is a potent tumor suppressor. We explored the use of FUS1 for enhancing chemotherapeutic potency of Gefitinib and overcoming Gefitinib-resistance in both Gefitinib-sensitive and resistant NSCLC cells. **Methods and Results:** We found that expression of wt-FUS1 by FUS1-nanoparticle-mediated gene transfer in FUS1-deficient and Gefitinib-resistant NSCLC H1299, H358, and H460 cells significantly sensitized the response to Gefitinib treatment, as demonstrated by a more than additive inhibitory effect on tumor cell growth and a synergistic induction of apoptosis. Enhanced growth inhibition was also observed in the Gefitinib-sensitive HCC827 (EGFR mutant) and H1819 (EGFR amplification) cells co-treated with FUS1-nanoparticles and a low dose of Gefitinib (IC_{10}). A marked inhibition of phosphorylated EGFR protein was also detected in cells treated with FUS1-nanoparticles alone or in combination with Gefitinib, as shown by Western-blot analysis with phospho-EGFR-specific antibodies. A significant inhibition ($P < 0.001$) of tumor growth was detected in animals treated by FUS1-nanoparticles in less than 2 weeks of treatment compared to those untreated or treated by GFP-nanoparticles, as shown by MR imaging and volume analysis. Induction of apoptosis was also detected in tumor cells in mice treated by FUS1-nanoparticles by an in situ apoptosis assay with TUNEL staining in frozen tissue samples. We have an ongoing phase I study of single agent FUS1-nanoparticles given intravenously in stage IV NSCLC patients who have progressed on chemotherapy. The treatment is well-tolerated in seven patients entered to date with a median survival of 17+ months. **Conclusions:** Our results suggest that wt-FUS1 may play a critical role in modulating the sensitivity of tumor cells to protein tyrosine kinase inhibitors. Supported by grants from NIH NCI (SPORE P50CA70907), DOD (TARGET, DAMD17002-1-0706) and Introgen Therapeutics, Inc.

Associated Presentation(s):

1. Synergistic inhibition of EGFR tyrosine kinase and tumor cell growth in non-small cell lung cancer (NSCLC) by combination treatment with FUS1-nanoparticles and gefitinib

No presentation available

Meeting: 2005 ASCO Annual Meeting

Presenter: Lin Ji, PhD

Session: Lung Cancer (General Poster Session)

Other Abstracts in this Sub-Category

1. Randomized phase II/III Trial of paclitaxel (P) plus carboplatin (C) with or without bevacizumab (NSC # 704865) in patients with advanced non-squamous non-small cell lung cancer (NSCLC): An Eastern Cooperative Oncology Group (ECOG) Trial - E4599
Meeting: 2005 ASCO Annual Meeting Abstract No: 4 First Author: A. B. Sandler
Category: Lung Cancer - Non-Small Cell Lung Cancer
2. Paclitaxel and gemcitabine vs carboplatin and gemcitabine. A multicenter, phase III randomized trial in patients with advanced inoperable Non-small cell lung cancer (NSCLC).
Meeting: 2005 ASCO Annual Meeting Abstract No: 7000 First Author: P. A. Kosmidis
Category: Lung Cancer - Non-Small Cell Lung Cancer
3. A randomized phase III trial comparing bexarotene/carboplatin/paclitaxel versus carboplatin/paclitaxel in chemotherapy-naïve patients with advanced or metastatic non-small cell lung cancer (NSCLC)
Meeting: 2005 ASCO Annual Meeting Abstract No: 7001 First Author: G. R. Blumenschein
Category: Lung Cancer - Non-Small Cell Lung Cancer

More...

Abstracts by L. Ji

1. Blood oxygen level dependent (BOLD) contrast MRI and breast cancer chemotherapy response.
Meeting: [2006 ASCO Annual Meeting](#) Abstract No: 10514 First Author: [D. Tripathy](#)
Category: Breast Cancer - [Local-Regional Therapy](#)
2. Synergistic and selective inhibition of NSCLC cell growth via a caspase-independent cell death pathway by tumor suppressor 101F6 nanoparticles plus vitamin C *in vitro and in vivo*.
Meeting: [2006 ASCO Annual Meeting](#) Abstract No: 13086 First Author: [S. Ohtani](#)
Category: Developmental Therapeutics; Molecular Therapeutics - [Gene Therapy/Antisense Strategies](#)
3. Synergistic inhibition of EGFR tyrosine kinase and tumor cell growth in non-small cell lung cancer (NSCLC) by combination treatment with FUS1-nanoparticles and Gefitinib
Meeting: [2005 ASCO Annual Meeting](#) Abstract No: 7081 First Author: [L. Ji](#)
Category: Lung Cancer - [Non-Small Cell Lung Cancer](#)
More...

Presentations by L. Ji

1. Synergistic inhibition of EGFR tyrosine kinase and tumor cell growth in non-small cell lung cancer (NSCLC) by combination treatment with FUS1-nanoparticles and gefitinib
No presentation available
Meeting: [2005 ASCO Annual Meeting](#)
Presenter: [Lin Ji, PhD](#)
Session: [Lung Cancer](#) (General Poster Session)
More...

PubMed Articles by Lin Ji

PubMed



1. Eliminating established tumor in nu/nu nude mice by a tumor necrosis factor-alpha-related apoptosis-inducing ligand-armed oncolytic adenovirus.
Clin Cancer Res, United States
Vol 12, No 17 (9/5/2006): pp. 5224-30
PMID: 16951242 [PubMed - in process]
2. Generation and differentiation of human embryonic stem cell-derived keratinocyte precursors.
Tissue Eng, United States
Vol 12, No 4 (5/6/2006): pp. 665-79
PMID: 16674282 [PubMed - in process]
3. Inhibition of human embryonic stem cell differentiation by mechanical strain.
J Cell Physiol, United States
Vol 206, No 1 (6/21/2005): pp. 126-37
PMID: 15965964 [PubMed - in process]
More...

©Copyright 2006 American Society of Clinical Oncology All rights reserved worldwide.

Abstract #2707

Synergistic inhibition of EGFR tyrosine kinase activity and NSCLC cell growth by combination treatment with FUS1-nanoparticle and gefitinib

Hiroyuki Kawashima, Futoshi Uno, Jonathan Kurie, John D. Minna, Jack A. Roth and Lin Ji

The UT M.D. Anderson Cancer Center, Houston, TX and The UT Southwestern Medical Center, Dallas, TX

New cancer treatments designed to restore functions of defect genes and gene products in tumor suppressing and apoptotic pathways by gene transfer and to target at the specific and frequently occurring molecular alterations in key signaling pathways by "smart drugs" such as protein tyrosine kinase inhibitors (PTKIs) are fundamentally changing cancer therapy and holding a promise for lung cancer treatment. *FUS1* is a novel tumor suppressor gene (TSG) identified in the human chromosome 3p21.3 region that is frequently altered or deleted in many human cancers and has been shown to function as a key mediator in Apaf1-associated apoptotic pathway and as a potent tumor suppressor *in vitro* and *in vivo*. In light of our recent observations on the FUS1-mediated PTK inhibition and the direct interactions of FUS1 with PTK and Apaf1 proteins together with the current findings of activating mutations of EGFR gene in gefitinib-responders in NSCL patients and the role of these mutations in selectively activating cell survival signaling and blocking pro-apoptotic pathway by other researchers, in this study we explored the capability of using the multifunctional FUS1 as a modulator for enhancing chemotherapeutic potency of gefitinib and overcoming gefitinib-resistance by simultaneously inactivating cell survival and proliferation signaling and activating proapoptotic pathways in both gefitinib-sensitive and resistant NSCLC cells. We found that reactivation of wt-

FUS1 by *FUS1*-nanoparticle-mediated gene transfer or treatment with a wt-FUS1-derived peptide (wt-FP) in 3p-deficient and Gefitinib-resistant NSCLC H1299, H358, and H460 cells significantly sensitized these cells' response to Gefitinib treatment, as demonstrated by a more than additive inhibitory effect on tumor cell growth and a synergistic induction of apoptosis. An enhanced growth inhibition was also observed in gefitinib-sensitive HCC827 (with an activating mutation of EGFR) and H1819 (with amplification of EGFR) cells co-treated with FUS1-nanoparticles and a very low dose of gefitinib (at a level of IC_{10}). A marked inhibition on activities of phosphorylated EGFR and Erk proteins was also detected in cells treated by FUS1-nanoparticle or wt-FP alone or in combination with gefitinib, as demonstrated by Western-blot analysis with phospho-EGFR or Erk-specific antibodies. Our results suggest that the wt-Fus1 may play a critical role in modulating the sensitivity of tumor cells to the chemotherapeutic agents such as PTKIs and that a combination treatment of the FUS1-nanoparticle-mediated molecular therapy with these small molecule chemotherapeutics may be an efficient treatment strategy for lung cancer. This abstract is supported by grants of NIH NCI (SPORE P50CA70907) and DOD (TARGET, DAMD17002-1-0706).

Abstract #3516

Synergistic tumor suppression by coexpression of *FUS1* and *p53* concurrences with FUS1-mediated down regulation of MDM2, accumulation of p53, and activation of Apaf1-dependent apoptotic pathway in human NSCLC cells

Wuguo Deng, Futoshi Uno, John D Minna, Jack A. Roth and Lin Ji

UT-MD Anderson Cancer Center, Houston, TX and UT Southwestern Medical Center, Dallas, TX

FUS1 is a novel tumor suppressor gene (TSG) identified in human chromosome 3p21.3 region where allele loss and genomic alterations are frequently found in a wide spectrum of human cancers and occur at the earliest stage of cancer development. Loss of expression and deficiency of posttranslational modification of FUS1 protein have been found in a majority of NSCLCs and in almost all SCLCs. Restoration of wt-FUS1 function in 3p21.3-deficient human lung cancer cells by adenoviral vector- or DOTAP:cholesterol nanoparticle-mediated gene transfer inhibits the growth of these tumor cells by induction of apoptosis and alteration of cell kinetics *in vitro* and *in vivo*. We previously also noticed that the tumor suppression function of *FUS1* as well as several other potential 3p21.3 TSGs were directly or indirectly dependent of p53 activity. In this study, we evaluated the combined effects of FUS1 and p53 on tumor cell growth and apoptosis induction in NSCLC cells co-transfected with *FUS1*- and *p53*-nanoparticles and explored molecular mechanisms of their mutual actions *in vitro*. We found that co-expression of wt-p53 with the wt-FUS1, but not the dysfunctional myristoylation-deficient mutant (mt-FUS1), synergistically inhibited cell proliferation and induced apoptosis in various human NSCLC cells. We also

found that co-expression of FUS1 and p53 enhanced the sensitivities of NSCLC cells to treatments with the DNA-damaging agents γ -radiation and cisplatin. Furthermore, we found that the observed synergistic tumor suppression by FUS1 and p53 concurred with the FUS1-mediated down-regulation of MDM2 expression and the resultant accumulation and stabilization of p53 protein as well as up-regulation of Apaf-1 expression and activation of caspase cascade in Apaf-1-associated apoptotic pathway in human NSCLC cells. Our results therefore revealed a novel molecular mechanism involving FUS1-mediated tumor suppression function and its interaction with other cellular components in the pathways regulating p53 and Apaf-1 activities. Our findings imply that a treatment targeting multiple pathways by combining functionally synergistic tumor suppressors such as *FUS1* and *p53* with chemotherapy or radiotherapy may be an effective therapeutic strategy for NSCLC and other cancers. This abstract is supported by grants of NIH NCI (SPORE P50CA70907) and DOD (TARGET, DAMD17002-1-0706).

Abstract #3345

A novel strategy for suppressing toxicity-mediated by systemic delivery of DNA-nanoparticles

Began Gopalan, Cynthia D. Branch, Clifton L. Stephens, Jack A. Roth and Rajagopal Ramesh

UT M.D. Anderson Cancer Ctr., Houston, TX

Lung cancer remains the leading cause of cancer mortality in the US. Despite the modest improvement in survival for these patients, prognosis remains dismal.

The need for novel approaches remains high and nanoparticle based gene therapy holds promise in this area. Therapeutic responses have been obtained in animal lung tumor models when DOTAP:Cholesterol (DOTAP:Chol) based nanoparticle formulation carrying the *FUS1* tumor suppressor gene (*FUS1*-nanoparticle) was delivered by intravenous injection. Based on our findings we have recently initiated a Phase-I trial for systemic treatment of lung cancer.

However, a major problem associated with systemic delivery of *DNA*-nanoparticles is the induction of acute inflammatory response resulting in dose-limiting toxicity in mice. In this study, we have investigated the molecular signaling pathway responsible for *FUS1*-nanoparticle induced inflammation and the protective effects of the anti-inflammatory drug, naproxen on *FUS1*-nanoparticle associated toxicity. When 100 μ g of *FUS1*-nanoparticles was injected intravenously into immunocompetent female C3H mice, increased TNF- α , IL-6 and IFN- γ production in the serum and organs (lung, liver, and spleen) were observed that resulted in 100% mortality within 48h post treatment. Mortality was not observed in mice injected with empty nanoparticles or *FUS1* plasmid alone. Analysis of the molecular signaling pathway in the lungs, liver and spleen revealed activation of MAP kinases (p38MAPK, and pJNK), NF- κ B and STAT3.

Activation of the signaling molecules occurred earlier in the lungs than in liver and spleen suggesting that the pathways were differentially regulated in various organs and in a time-dependent manner. Administration of single clinically relevant dose of naproxen (15 mg/Kg) prior to systemic injection of *FUS1*-nanoparticles (100 µg) completely protected the mice resulting in 100% survival. Furthermore, naproxen significantly inhibited TNF- α , IL-6 and IFN- γ production in the serum and organs of *FUS1*-nanoparticles treated mice compared to mice that did not receive naproxen treatment. Additionally, naproxen inhibited activation of the signaling molecules (MAPK, NF- κ B, STAT3 and COX-2) that are associated with inflammation. Histopathological analysis of lungs and liver from naproxen treated mice showed reduced focal acute pneumonitis, pulmonary edema, and mild multifocal acute necrosis of the liver, compared to mice that were not treated with naproxen. These results show for the first time the ability of naproxen to effectively inhibit the toxicity induced by systemic delivery of DNA-nanoparticles and thereby deliver higher doses of the therapeutic gene. Our study also provides a strategy for improving the systemic delivery of DNA-nanoparticles for the treatment of non-small-cell lung cancer. This work was supported in part by BESCT Grant (DAMD17-01-1-0689) and TARGET Grant (DAMD17-02-1-0706).

Experimental and Molecular Therapeutics 42: Circumventing Drug Resistance

Abstract #5426

Overcoming gefitinib resistance in NSCLC via inactivation of the PI3K/AKT signaling pathway by a combination of FUS1 nanoparticles and EGFR inhibitors.

Hiroyuki Kawashima, Gitanjali Jayachandran, Wuguo Deng, Kai Xu, John D. Minna, Jack A. Roth and Lin Ji

UT M.D. Anderson Cancer Center, Houston, TX and UT Southwestern Medical Center, Dallas, TX

Gefitinib (Iressa) is an orally active epidermal growth factor receptor (EGFR) tyrosine kinase inhibitor that has been shown to be clinically effective in a subpopulation of non small cell lung cancer (NSCLC) patients. Despite initial responses to gefitinib in some NSCLC patients, cancer eventually progresses by unknown mechanisms of acquired resistance. We explored the use of the novel tumor suppressor FUS1 to enhance the chemotherapeutic potency of gefitinib and overcome gefitinib resistance in NSCLC. We found that reactivation of wild-type FUS1 by FUS1 nanoparticle-mediated gene transfer into FUS1-deficient and gefitinib-resistant NSCLC H1299, H322, H358, and H460 cells significantly ($P < 0.001$) sensitized their response to gefitinib treatment and synergistically induced apoptosis in vitro and in an H322 orthotopic lung cancer mouse model. To understand the mechanism of gefitinib-induced resistance, we established a gefitinib-resistant HCC827GR NSCLC cell line ($IC_{50} = 16 \mu M$) by selecting against gefitinib from the parental HCC827 cells that contain an activating deletion mutation of the EGFR gene and are extremely sensitive to gefitinib treatment ($IC_{50} = 0.016 \mu M$). We found no secondary mutations in the EGFR

gene in the HCC827GR cells, but these cells registered a significantly elevated level of phosphorylated AKT protein. Combination treatment with FUS1 nanoparticles and gefitinib at a dose level of IC_{10} significantly re-sensitized the cells to gefitinib, as demonstrated by synergistically enhanced growth inhibition and apoptosis. FUS1 nanoparticle treatment alone or with gefitinib markedly inactivated EGFR and AKT, as demonstrated by decreased phosphorylation levels of both proteins on Western blots, compared with either agent alone. Cleavage of caspase-3, caspase-9, and PARP was also significantly induced by the combination of FUS1 and gefitinib in HCC872GR and other gefitinib-resistant NSCLC cells. Our results suggest that a combination treatment of FUS1 nanoparticles and gefitinib could overcome drug-induced resistance by simultaneously inactivating EGFR and the AKT signaling pathway and by facilitating apoptosis. This abstract is supported by grants from NCI (SPORE P50CA70907) and DOD (TARGET, DAMD17002-1-0706).

Cellular and Molecular Biology 19: Oncogenic Mutations and Signaling
Activation

Abstract #1460

Interaction of the tumor suppressor FUS1 with
PDGFR β inhibits PDGFR-mediated proliferation of
human lung cancer cells

Guanglin Wu, Wuguo Deng, Gitanjali Jayachandran, John D. Minna, Jack A. Roth and Lin Ji

U.T.M.D.Anderson Cancer Center, Houston, TX and UT Southwestern Medical Center, Dallas, TX

Platelet-derived growth factors (PDGFs) play crucial roles in diverse biological processes like cell migration, proliferation, apoptosis, and survival. PDGFs activate their protein tyrosine kinase (PTK) receptors, PDGFR α and PDGFR β , which subsequently stimulate the downstream targets MEK and ERK to activate PI3-K/Akt signaling, thus promoting cell survival and anti-apoptotic processes in many cell systems. Blocking constitutive oncogenic PDGFRs with selective PTK inhibitors has promoted anti-angiogenesis and suppressed tumor proliferation in vitro and in animal models of human cancers. FUS1 is a novel tumor suppressor gene identified in human chromosome region 3p21.3, where genomic and genetic abnormalities are common and occur early in the development of many types of cancer. We previously found that FUS1 protein expression was deficient in many human primary lung cancer specimens and cell lines and that reactivating FUS1 in 3p21 [PDB] .3-deficient lung cancer cells inhibited their growth and induced apoptosis, in part by inhibiting the activity of oncogenic PTKs such as c-Abl, c-Kit, and PDGFR. Here we examined PDGFR expression in various non-small cell lung cancer (NSCLC) and small cell lung cancer (SCLC) cell lines and found high expression of PDGFR β but not PDGFR α in almost all cell lines tested. Immunoprecipitation and immunoblot analyses showed that

FUS1 protein interacted directly with PDGFR β but not with the PDGF ligands. Forced expression of wt-FUS1 by nanoparticle-mediated gene transfer in the PDGFR β -expressing SCLC H128 and NSCLC H358 cell lines inactivated PDGFR, as evidenced by significant reductions in phospho-PDGFR β relative to untransfected or LacZ-transfected controls. Levels of phospho-PI3-K and phospho-AKT proteins, downstream targets of the PDGF/PDGFR signaling pathway, were markedly reduced as well. Finally, combined treatment with FUS1-nanoparticles and the PTK inhibitor imatinib (Gleevec) synergistically inhibited growth and induced apoptosis in SCLC and NSCLC cell lines that contained highly activated phospho-PDGFR β . Our results suggest that the interaction of the FUS1 protein with PDGFR β can interrupt PDGF/PDGFR oncogenic signaling, block PDGFR-mediated tumor cell survival, and inhibit proliferation by promoting apoptosis in lung cancer cells. These findings also indicate that combination treatments with a pro-apoptotic tumor suppressor FUS1 and selective PTK inhibitors may be a useful therapeutic strategy for human lung cancer. This work was supported by grants from the NCI (P50 CA70907) and Department of Defense (TARGET, DAMD17002-1-0706).

Abstract #3527

The spatial distribution and etiology of genomic instability in organotypic bronchial epithelial cell cultures

Walter N. Hittelman, Guiying Wang, Ja Seok Peter Koo and Tao Lu

UT M. D. Anderson Cancer Ctr., Houston, TX

Chromosome in situ hybridization and molecular genetic analyses of bronchial biopsies of smokers demonstrate genetic instability and clonal/subclonal bronchial cell outgrowths that continue despite tobacco cessation. To better understand the molecular underpinnings of genomic instability in the lungs of former smokers, an organotypic culture model was established whereby bronchial epithelial cells at different stages of lung tumorigenesis were plated onto transwell-clear culture filter inserts, allowed to reach confluence, and an air-liquid interface created. The cell types utilized included normal human bronchial epithelial cells (NHBE), NHBE cells immortalized (Jerry Shay) with hTERT and cdk4 (HccBE), NHBE cells immortalized (Klein-Szanto) with Ad12/SV40 (Beas2B), and immortalized (1799), transformed (1198), and tumorigenic (1170I) carcinogen-treated Beas2B cells. These cultures evolved into multi-layer cultures resembling normal (NHBE and HccBE) or dysregulated stratified bronchial epithelium (Beas2B, 1799, 1198, 1170I). Confocal microscopy of cultures after BrdU pulse labeling or phospho-histone H3 (P-H3) immunostaining demonstrated that NHBE cells preferentially undergo DNA synthesis and mitosis at the basal layer, HccBE cells proliferate at the basal and peribasal layers, whereas more advanced bronchial epithelial cells proliferate throughout the multi-layer cultures. Examination of anaphase cells in these populations by propidium iodide staining and confocal microscopy demonstrated that NHBE cells showed less than 2%

anaphases with either lagging chromosomes or chromosome bridges compared to more than 10% in other cell types. Visualization of mitotic figures with P-H3 immunostaining demonstrated that P-H3 staining was strong at metaphase and uniformly disappeared during anaphase in cells at the basal layer, whereas P-H3 staining was not uniform in cells dividing away from the basal layer with lagging chromosomes and chromosome bridges differentially P-H3-positive in late anaphase. To determine when the chromosome regions involved in aberrations had been replicated, cultures were pulse-labeled with BrdU, harvested at various times following the pulse label; and analyzed for BrdU staining patterns of the lagging chromosomes and chromosome bridges. More than 90% of the aberrant chromosome regions were labeled in cells harvested 3-4 hours after BrdU labeling (i.e., replicated in late S phase) whereas less than 60% were labeled at 9-10 hours after BrdU labeling (i.e., replicated in early-mid S phase). These results suggest that proliferation away from the basal layer in these organotypic cultures is associated with increased genomic instability, possibly associated with dysregulated cell cycle control and abnormal mitotic progression. Supported in part by DAMD 17-02-1-0706 and W81XWH-04-1-01-42, and NIH/NCI P01 CA-91844 and EDRN CA-86390.

[Back](#)

Abstract Number: 4511

Assessment of subclonal evolution in human bronchial epithelial cell lines progressing toward malignancy by fluorescence inter-simple sequence repeat PCR

Tao Lu, Walter N. Hittelman. UT MD Anderson Cancer Center, Houston, TX.

Tumors of the aerodigestive tract reflect a field cancerization process whereby carcinogen-exposed tissue progresses through a multistep process of clonal evolution driven by genetic instability and chronic wound healing. Prior chromosome in situ hybridization studies on bronchial biopsies of current and former smokers demonstrated the presence of chromosome changes throughout the exposed epithelial field. Spatial chromosome and molecular analyses of the bronchial epithelium suggested that with chronic tobacco exposure, the lung become a mosaic of clones and subclones, the extent of which is related to the degree and duration of tobacco exposure. These clones/subclones remain for years following smoking cessation. Because a high frequency of subclonal outgrowths are found in normal and premalignant epithelium adjacent to lung tumors, it is postulated that an assessment of the degree of genetic instability and clonal outgrowth in the bronchial epithelium of smokers may provide a risk marker for lung cancer development. We sought a quantitative technique with sufficient dynamic range that could be used to probe bronchial epithelium for the frequency of clonal/subclonal outgrowths. Fluorescence inter-simple sequence repeat PCR (ISSR-PCR) is a DNA fingerprinting technique whereby unique sequences between simple sequence repeat segments are amplified leading to a series of bands on a DNA sequencing gel. Genetic changes such as deletions, insertions, and rearrangements in the unique sequences lead to changes in the number and locations of bands. The numbers of bands changed from normal reflect the accumulated numbers of clonal alterations. To test the feasibility of this approach for quantifying clonal changes during malignant development, we applied ISSR-PCR (using two sets of fluorescence-labeled oligo primers with two anchor nucleotides at the 3' end of a (CA)₈-repeat) to four sequentially evolved lung cell lines derived from large T-antigen immortalized normal human bronchial epithelial cells (Beas-2B), grown in vivo (1799), treated with cigarette smoke condensate (1198), and evolved to cancer (1170I). We observed 7 altered bands from Beas-2B to 1799, 3 additional bands to 1198, and 3 additional bands to 1170I. For comparison of dynamic range, we carried out a preliminary microsatellite LOH analyses using 5 primer pair sets (2 for chromosome (Chr) 3p14, 2 for Chr 9p21, and 1 for Chr 13q14) and found a total of 2 changes between Beas-2B and 1170I cells. These results suggest that ISSR-PCR has promise for quantifying the extent of subclonal outgrowth in cell populations and may prove useful in the assessment of lung cancer risk when applied to the analysis of bronchial epithelium. Supported in part by DAMD17-02-1-0706, CA-68437, CA70907, and EDNRN NCI CA-86390.

Presenter: Walter N. Hittelman

Affiliation: UT MD Anderson Cancer Center, Houston, TX . Email: whittelm@mail.mdanderson.org

Copyright © 2003 American Association for Cancer Research. All rights reserved.

Citation for abstracts scheduled for publication: Proceedings of the AACR, Volume 44, 2nd ed., July 2003.

Citation for abstracts not scheduled for publication: Proceedings of the AACR, Volume 44, 1st ed., March 2003.

Regulated Gap Junction-Cytoskeletal Associations in Rat Alveolar Epithelial Cells*

Yihai Guo, PhD, Gawa-Martinez-Williams, and
D. Eugene Bannels, PhD

(CHEST 2004; 125:1105)

Abbreviations: Cx = connexin; GJ = gap junction

Connexin 43 (Cx43) is a predominant gap junction (GJ) protein that is expressed by pulmonary alveolar epithelial cells, both *in vivo* and in primary culture. Cx43 expression increases with culture time, as type II cell isolates assume a more type I cell-like phenotype. In these cell populations, Cx trafficking, assembly, and turnover are regulated by diverse pathways, including those that involve integrin-mediated cell-extracellular matrix interactions and/or elements of the cytoskeleton. Immunocytochemical double labeling demonstrates the association of microtubules with the cellular internalization of Cx43-positive GJ plaques. Antibodies against the $\alpha 5$ integrin subunit block cell-extracellular matrix interactions, with little effect on tubulin expression. In contrast, the inhibition of mitogen-activated protein kinase kinase by PD98059 reduces tubulin expression, based either on direct immunostaining or on Western blot analysis. To examine the association of microtubules with GJ plaques, day 3 cells were exposed with colchicine (0.5 to 24 h). The drug disassembled the microtubules within 60 min, whereas Western blot showed no change in tubulin abundance. Colchicine caused a parallel redistribution of immunopositive Cx43 from the plasma membrane to the cytosol. These data are consistent with the conclusion that in alveolar epithelial cells, the direct association of cytoskeletal proteins with GJs plays a role in the regulation of Cx43 expression and intracellular distribution via integrin-mediated signal transduction pathways.

*From the Department of Cellular & Molecular Physiology, The Pennsylvania State University College of Medicine, Hershey, PA. This study was supported by grants HL61632, HL10358 from the National Institutes of Health, and AHA 0150244N from the American Heart Association. Reproduction of this article is prohibited without written permission from the American College of Chest Physicians (e-mail: permissions@chestnet.org).

Correspondence to: D. Eugene Bannels, PhD, Department of Cellular and Molecular Physiology (C4900D), The Pennsylvania State University College of Medicine (H166), 500 University Dr, Hershey, PA 17033-0850; e-mail: ebannels@psu.edu

Improvement and Application of Fluorescence Inter-Simple Sequence Repeat Polymerase Chain Reaction for the Study of Subclonal Growths in Lung Epithelial Cell Populations*

Tao Lu, PhD, and Walter N. Hittelman, PhD

(CHEST 2004; 125:1105-1115)

Abbreviations: FISSR = fluorescent dye-labeled primers for the inter-simple sequence repeat; PCR = polymerase chain reaction

Chromosome *in situ* hybridization and loss of heterozygosity analyses on bronchial biopsy specimens of current and former smokers have demonstrated the presence of clonal and subclonal outgrowths throughout the exposed lung epithelium. Since high frequencies of clonal outgrowths have been detected in the normal/premalignant epithelium adjacent to lung tumors, it is postulated that the frequency of subclonal outgrowths may provide a risk marker for lung cancer development. We therefore examined a quantitative technique with sufficient dynamic range (ie, inter-simple sequence repeat polymerase chain reaction [PCR]) for its ability to detect subclonal outgrowths in lung epithelial cell populations.

To improve the reproducibility and quantitative aspects of this method, we used fluorescent dye-labeled primers for the inter-simple sequence repeat (FISSR)-PCR reaction, separated and quantified the PCR products on a sequencer (model ABI 377), and analyzed the results using computer software (GeneScan, Foster City, CA). To test the reproducibility of the sequencer, aliquots of single FISSR-PCR reactions were run in separate lanes and were shown to give reproducible band patterns. To test the reproducibility of the FISSR-PCR reaction, we carried out triplicate reactions with the same DNA source and showed reproducible band patterns. To determine its sensitivity for detecting clonal evolution during lung tumorigenesis, we quantified the number of genetic alterations detected by FISSR-PCR in a bronchial epithelial cell progression model system consisting of four evolved lung cell lines, including large T-antigen immortalized normal human bronchial epithelial cells (BEAS-2B cells), grown *in vivo* (1799 cells), treated with cigarette smoke condensate (1198 cells), and evolved to cancer (1170 cells) originally

*From the Department of Experimental Therapeutics, University of Texas MD Anderson Cancer Center, Houston, TX. This research was supported in part by grants DAMD17-02-1-0706, CA-58437, and CA70907.

Reproduction of this article is prohibited without written permission from the American College of Chest Physicians (e-mail: permissions@chestnet.org).

Correspondence to: Tao Lu, PhD, Department of Experimental Therapeutics, Box 19, University of Texas MD Anderson Cancer Center, 1515 Holcombe Blvd, Houston, TX 77030; e-mail: lu@mdanderson.org

derived by Klein-Szanto et al¹). Using two groups of primers, we identified nine alterations between the BEAS2B and 1799 cells, 8 additional changes to the 1198 cells, and 4 additional changes to tumorigenic 1170f cells. To determine the ability to detect subclonal populations, we isolated single-cell clones from the BEAS2B and 1170f populations, and demonstrated the presence of distinct subclones. To determine the sensitivity of this technique for detecting subclones, we carried out mixing experiments of subclonal fractions, and demonstrated a quantitative relationship between relative peak height and subclonal fraction.

These results suggest that FISSR-PCR has promise for quantifying the extent of subclonal outgrowth in cell populations, and that it may prove useful in the assessment of lung cancer risk when applied to the analysis of the bronchial epithelium of current and former smokers.

REFERENCE

1. Klein-Szanto AJP, Hsiao T, Momiki S, Carella-Piazza L, Casanueva J, Metzall B, Walsh J, Harris CC. A tobacco-specific N-nitrosamine or cigarette smoke condensate causes neoplastic transformation of xenotransplanted human bronchial epithelial cells. *Proc Natl Acad Sci U S A* 1992; 89:6693-6697.

Sprouty 2 Gene in Mouse Lung Tumorigenesis*

George Minowada, MD, and York F. Miller

(CHEST 2004; 125:1115)

Abbreviations: NSCLC = non-small cell lung cancer; *Spry* = *Sprouty*.

Members of the *Sprouty* (*Spry*) gene family encode novel proteins that function as intracellular antagonists of the Ras signaling pathway. Loss of *Spry* function would be predicted to enhance Ras signaling.

Several mechanisms appear to increase Ras signaling in the most common type of human lung cancer, non-small cell lung cancer (NSCLC). Epidermal growth factor receptor members and/or one of their ligands are expressed in most NSCLCs. Similarly, fibroblast growth factor-2 is expressed in many NSCLCs, if not most. Alternatively, 15

to 20% of NSCLCs have activating mutations in the *KRAS* gene. It remains unclear what role Ras signaling may play in the pathogenesis of NSCLC, but at least one consequence appears to be increased proliferation. In a mouse model of lung cancer, the chemical carcinogen urethane causes activating mutations in *K-ras* and induces lung tumors. Thus, perturbations that would be predicted to enhance Ras signaling appear to play a key role in the pathogenesis of some types of NSCLC. Such perturbations also appear to be markers of a more biologically aggressive cancer since patients with these tumors do worse.

Of the four members of the *Spry* family of genes, *Spry 2* is expressed in the lung epithelium, the cell type from which NSCLC arises. We hypothesized that the Ras signaling antagonist *Spry 2*, which is expressed in the lung epithelium, modulates susceptibility to and/or the biological behavior of lung cancer. To begin to test this hypothesis, we have compared urethane-induced lung tumor development in *Spry 2* lung-specific overexpressing mice (13 mice) with their littermate controls (14 mice). Consistent with the hypothesis, the mean tumor multiplicity and diameter were lower in the overexpressor mice (13.5 vs 18.7 tumors per mouse, respectively; 0.78 vs 0.88 mm per tumor, respectively).

Gene Expression Patterns, Prognostic and Diagnostic Markers, and Lung Cancer Biology*

Nafali Kaminski, MD, and Meir Kripisky, MD

(CHEST 2004; 125:1115-1155)

Key words: array comparative genomic hybridization; early detection; microarrays; non-small cell lung cancer; surrogate markers.

Lung cancer is a common malignancy and is the major determinant of overall cancer mortality in developed countries.¹ Extensive prospective epidemiologic data clearly have established cigarette smoking as the major cause of lung cancer.² Tragically, despite an impressive

*From the University Hospitals of Cleveland, Case Western Reserve University, Denver VAMC, University of Colorado Health Sciences Center.

Reproduction of this article is prohibited without written permission from the American College of Chest Physicians (e-mail: permissions@chestnet.org).

Correspondence to: George Minowada, MD, Division of Pulmonary and Critical Care Medicine, Case Western Reserve University School of Medicine, University Hospitals of Cleveland, 2109 Adelbert Rd, RBB-10th Floor, Rm 1023, Cleveland, OH 44106; e-mail: gmin45@case.edu.

*From the Dorothy P. & Richard P. Simmons Center for Interstitial Lung Disease (Dr. Kaminski), Pulmonary, Allergy and Critical Care Medicine, University of Pittsburgh Medical Center, Pittsburgh, PA; and the Institute of Respiratory Medicine and Physiology (Dr. Kripisky), Sheba Medical Center, Sheba, Israel. Dr. Kaminski's work was partly supported by the Tel-Aviv Chapter of the Israel Lung Association.

Reproduction of this article is prohibited without written permission from the American College of Chest Physicians (e-mail: permissions@chestnet.org).

Correspondence to: Nafali Kaminski, MD, Dorothy P. & Richard P. Simmons Center for Interstitial Lung Disease, Pulmonary, Allergy and Critical Care Medicine, University of Pittsburgh Medical Center, NW 628 MUII, 3459 5th Ave, Pittsburgh, PA 15261; e-mail: kaminski@upmc.edu.

[Back](#)

Abstract Number: 2925

Quantitative fluorescence inter-simple sequence repeat PCR (FISSR-PCR) for subclonal analysis of bronchial cell populations

Tao Lu and Walter N. Hittelman. *The Univ. of Texas MD Anderson Cancer Center, Houston, TX.*

Tumorigenesis is a process of cumulative clonal and subclonal cell expansion in a field of epithelial cells driven by genetic instability. Quantitative assessment of the frequency and complexity of clonality in pre-malignant tissues may therefore provide cancer risk information. Inter-Simple Sequence Repeat PCR (ISSR-PCR) is a DNA fingerprinting technology that has proven useful for quantifying clonal changes in human tumors. FISSR-PCR involves the same technology as ISSR-PCR except that fluorescence-dye labeled oligonucleotide primers are utilized and the PCR products are analyzed using the ABI 377 DNA Sequencer. We previously demonstrated that FISSR-PCR could distinguish clonal outgrowths of bronchial epithelial clones derived from single cells. The purpose of this study was to determine the sensitivity of FISSR-PCR to detect subclonal variation in populations of bronchial epithelial cells. To this end, DNA of single cell clones with gains and losses at known loci, previously isolated from lung epithelial Beas 2B and 11701 cell lines, were mixed together in different proportions at 10% increments to mimic cell populations with different degrees of subclonal variation. Following gel separation and fluorescence quantitation of size (i.e., migration) and relative amount (peak size) of the resultant PCR fragments, the DNA band profiles were aligned on the basis of the largest cluster of common bands. The scans derived from the various cell mixtures were then compared on the basis of normalized peak heights. For common peaks between variant cell populations, the standard deviation was found to be less than 10% of the absolute mean value (data from triplicates of 11 population mixture reactions). On the other hand, the relative peak height of known variant bands varied linearly with the relative ratio of cell mixtures (linear regression analysis, $R^2 > 0.98$). Based on these studies, a change in relative peak height of 20% was sufficient to detect the presence of a subclonal variant. This suggests that FISSR-PCR may provide a sensitive technique for quantifying clonal variation in bronchial epithelial cell populations and may prove useful for cancer risk assessment. Supported in part by DAMD17-02-1-0706, CA-68437, and CA70907.

Presenter: Tao Lu

Affiliation: The Univ. of Texas MD Anderson Cancer Center, Houston, TX; E-mail: llu@mail.mdanderson.org

Copyright © 2004 American Association for Cancer Research. All rights reserved. Citation information: Proceedings of the AACR, Volume 45, March 2004.

Detection of clonal and subclonal outgrowths in the upper aerodigestive tract of current and former smokers with lung cancer

Tao Lu, Ignacio I. Wistuba and Walter N. Hittelman

UT M. D. Anderson Cancer Ctr., Houston, TX

Our prior results using chromosome in situ hybridization suggested the existence of genetic instability and clonal/subclonal mosaicism in the bronchial epithelium of current and former smokers without cancer. To verify these results by an independent methodology and to develop an assay system to quantitatively detect clonal/subclonal variations with high sensitivity and dynamic range, we adapted and modified the technique of fluorescence simple-sequence repeat PCR (FISSR-PCR) so that as little as 500 cell groups could be analyzed. We microdissected groups of cells from the stroma (from 1 to 8 regions per case), adjacent bronchial epithelium (from 1 to 10 regions per case), and tumor (from 1 to 12 regions per case) from frozen tissue sections of resected lung cancer specimens from 11 patients with a history of tobacco exposure. Genomic DNA was extracted from the microdissected cells and subjected to FISSR-PCR analysis using a Fam-(CA)₈RG primer. Lung tumor regions exhibited a relatively high degree of clonal/subclonal alterations (median, 7.2; range, 2 to 25 DNA band changes) and heterogeneity when compared to normal stromal regions. Bronchial epithelial cells in the field of lung tumors also showed evidence of clonal/subclonal outgrowths, albeit fewer than that observed in the lung tumor regions (median, 2.5; range, 0 to 7 DNA band changes). Of interest, there was a correlation between the number of band changes in the tumor and bronchial epithelium within individual lung tumor specimens (linear regression analysis, R^2

= 0.56). In some cases, a common subset of band changes was observed in the bronchial epithelium and associated lung tumor, suggesting a precursor-tumor relationship. In other cases, distinct band changes were observed in the adjacent epithelium that were not present in the associated tumor regions, suggesting multifocality of initiated clones. Significantly, we also detected clonal/subclonal populations in the lung stroma, albeit at a lower frequency than that observed in the bronchial epithelium (median, 1.8; range, from 0 to 4 DNA band changes). These results provide further support to the prior finding of clonal and subclonal outgrowths in tobacco-exposed lung. These results also suggest the extent of the multifocal changes can be quantified by FISSR-PCR analysis and might be exploited in the future for assessing lung cancer risk in current and former smokers. Supported in part by DAMD17-02-1-0706, NIH/NCI CA-91844, and EDNRN NCI CA-86390.

Existence of clonal and subclonal outgrowths in the bronchial epithelium and stroma of current smokers

Tao Lu, Ignacio I. Wistuba and Walter N. Hittelman

UT MD Anderson Cancer Center, Houston, TX

The identification of individuals at high risk for lung cancer is critical for individualized clinical management and is important for the identification of suitable subjects for chemoprevention trials. Using chromosome in situ hybridization (CISH) technology, we previously demonstrated the presence of chromosomal instability and multifocal clonal/subclonal outgrowths in the bronchial epithelium of current and former smokers. We also verified the presence of these clonal/subclonal outgrowths in normal-appearing bronchial epithelium in lung cancer resections using fluorescence inter-simple sequence repeat PCR (FISSR-PCR) analysis, a DNA fingerprinting methodology. To evaluate and compare FISSR-PCR and CISH technologies for accessing genetic instability and clonal/subclonal outgrowth, we subjected frozen bronchial biopsies obtained prior to entry onto a chemoprevention trial to FISSR-PCR analysis from sixteen (16) current smokers without lung cancer. The group of biopsies from these same individuals have previously been analyzed by CISH and exhibited a wide range of chromosomal changes. Multiple regions (i.e., 1-4 areas each) of bronchial epithelium and stroma were microdissected, and purified genomic DNA was analyzed by FISSR-PCR using three sets of primers ((CA)₈RG, (CA)₈RY, and (AGC)₄Y), providing a maximum of 350 informative DNA bands of varying lengths. Overall, we detected from 0 to 55 total band changes per microdissected epithelial region (median = 1.6 per 100 DNA bands). Different regions within the same bronchial biopsies showed both common and distinct DNA band changes, suggesting subclonal variations even within a single biopsy. We also detected

from 0-20 total band changes per microdissected stromal region (median = 1.0 per 100 DNA bands), suggesting the presence of clonal outgrowths even in the stroma. Interestingly, bronchial biopsies with high clonal frequencies showed increased clonal change in the associated stroma ($p = 0.04$, two-tailed chi square). Importantly, bronchial biopsies from individuals showing high clonal changes by FISSR-PCR also showed evidence of high clonal change by CISH ($R^2 = 0.3$). These results confirm the existence of clonal/subclonal outgrowths in both the bronchial epithelium and stroma of smokers. With future improvements in microdissection, automated genomic DNA extraction, and DNA sequencing, FISSR-PCR has potential to be a sensitive method with high dynamic range to detect clonal/subclonal outgrowths in lung tissue. Such a methodology may be of use in identifying individuals at high risk for developing lung cancer. Supported in part by DAMD17-02-1-0706, NIH/NCI CA-91844, and EDNRN NCI CA-86390.

**AACR Meeting
Abstracts Online**[HOME](#) [HELP](#) [FEEDBACK](#)[CME INFORMATION](#)[SEARCH](#)**QUICK SEARCH:** [advanced]

Author: Keyword(s):

Go Institution: MD ANDERSON HOSPITAL [Sign In as Member or Individual Non-Member](#)

[Proc Amer Assoc Cancer Res, Volume 46, 2005]

Services

- ▶ [Similar articles in this journal](#)
- ▶ [Download to citation manager](#)

Google Scholar

- ▶ [Articles by Shibuya, K.](#)
- ▶ [Articles by O'Reilly, M. S.](#)
- ▶ [Articles citing this Article](#)

PubMed

- ▶ [Articles by Shibuya, K.](#)
- ▶ [Articles by O'Reilly, M. S.](#)

Experimental and Molecular Therapeutics 48: Antiangiogenesis and Antivascular Agents Abstract #5828

Combined blockade of VEGFR and EGFR with ZD6474 enhances the antitumor and antivascular effects of radiation therapy in an orthotopic mouse model of human lung cancer

Keiko Shibuya, Ritsuko Komaki, Tomoaki Shintani, Wenjuan Wu, Satoshi Itasaka, Takeshi Isobe, Anderson J. Ryan, Roy S. Herbst and Michael S. O'Reilly

University of Texas, Houston, TX and AstraZeneca, Macclesfield, United Kingdom

Chemoradiotherapy is considered to be the standard treatment for locally advanced NSCLC, but its therapeutic success is limited. ZD6474 targets two key pathways in tumor growth by selectively inhibiting VEGFR and EGFR tyrosine kinase activity. We evaluated the feasibility of combining ZD6474 with radiation therapy (RT), and compared this with chemoradiation, in an orthotopic model of human NSCLC. The left lungs of nude mice ($n = 8$ per group; experiment repeated twice) were injected with human lung adenocarcinoma cells (NCI-H441) and after 8 days of tumor growth, mice were randomized to one of six treatment regimens: low-dose ZD6474 (15 mg/kg daily p.o.); RT (4 Gy fractions 3 times/week to 20 Gy); paclitaxel (Pac; 200 μ g weekly i.p.); ZD6474 + RT; Pac + RT; or vehicle. The experiment was terminated when the control group began to show signs of morbidity. Tumor burden was assessed by lung and tumor weight, and pleural effusion volume. Tumor and adjacent tissues were analyzed by immunohistochemical staining for CD-31, VEGF, VEGFR-2, EGF, EGFR, MMP2, MMP9 and bFGF. Lung and tumor weight (mg) of mice treated with vehicle, RT, Pac, Pac + RT, ZD6474, or ZD6474 + RT was 840 ± 220 , 437 ± 49.6 , 518 ± 100 , 356 ± 37.3 , 371 ± 59.7 and 271 ± 12.4 ($P=0.032$ vs Pac + RT), respectively. Pleural effusion (μ l) in mice treated with vehicle, RT, Pac + RT or ZD6474 + RT was 745 ± 112 , 565 ± 99.4 , 246 ± 69.4 and 14.2 ± 4.8 , respectively. Compared with vehicle, combined therapy with ZD6474 + RT enhanced tumor (12 ± 4.1 vs $1.3 \pm 0.2\%$) and endothelial cell (9.4 ± 2.3 vs $0.3 \pm 0.3\%$) apoptosis, and suppressed tumor (8.8 ± 1.2 vs $33 \pm 3.8\%$) and endothelial cell (5.4 ± 3.0 vs $27 \pm 3.5\%$) proliferation. Microvessel density of lung primary tumors in vehicle, RT, Pac + RT, and ZD6474 + RT treated groups was 55 ± 3.3 , 52 ± 7.3 , 31 ± 3.5 and 16 ± 1.9 , respectively. Expression of VEGF and EGF significantly decreased after ZD6474 treatment ($P<0.0001$ and <0.001 vs vehicle, respectively). Expression of VEGFR-2 significantly increased after RT ($P<0.0001$ vs vehicle),

but this was offset by combined treatment with ZD6474. Expression of EGFR increased after RT or Pac treatment, but not after ZD6474 treatment. A marked increase in expression of β FGF was observed after RT or Pac, but the RT-induced increase was offset by administration of ZD6474. Expression of MMP2 and MMP9 was induced by Pac, but not RT, and the Pac-induced increase was reduced by ZD6474. Targeted inhibition of VEGFR and EGFR with low-dose ZD6474 significantly enhances the antiangiogenic, antivascular and antitumor effects of RT for human lung cancer growing orthotopically in mice. Furthermore, low-dose ZD6474 + RT showed greater antitumor and antivascular effects than Pac + RT. These data strongly suggest that it will be prudent to include certain targeted agents in the multimodality management of lung cancer.

HOME	HELP	FEEDBACK	CME INFORMATION	SEARCH
	Cancer Research		Clinical Cancer Research	
	Cancer Epidemiology Biomarkers & Prevention		Molecular Cancer Therapeutics	
	Molecular Cancer Research		Cell Growth & Differentiation	

Copyright © 2005 by the American Association for Cancer Research.

AACR Meeting Abstracts Online

[HOME](#)
[HELP](#)
[FEEDBACK](#)
[CME INFORMATION](#)
[SEARCH](#)
QUICK SEARCH: [advanced]

Author: Keyword(s):

 Institution: MD ANDERSON HOSPITAL [Sign In as Member or Individual Non-Member](#)

[Proc Amer Assoc Cancer Res, Volume 46, 2005]

Services

[Similar articles in this journal](#)
[Download to citation manager](#)
[Google Scholar](#)
[Articles by Shintani, T.](#)
[Articles by O'Reilly, M. S.](#)
[Articles citing this Article](#)
[PubMed](#)
[Articles by Shintani, T.](#)
[Articles by O'Reilly, M. S.](#)

Experimental and Molecular Therapeutics 48: Antiangiogenesis and Antivascular Agents Abstract #5844

ZD6474 inhibits human lung cancer bone metastases in a murine model by targeting both the tumor and its vasculature

Tomoaki Shintani, Valerae O. Lewis, Ritsuko Komaki, Wenjuan Wu, Anderson J. Ryan, Roy S. Herbst and Michael S. O'Reilly

University of Texas, Houston, TX and AstraZeneca, Macclesfield, United Kingdom

The vascularization and growth of primary and metastatic lung cancer is influenced by tumor microenvironment. We have previously shown that ZD6474, a selective inhibitor of VEGFR and EGFR tyrosine kinase activity, was effective alone and with paclitaxel (Pac) chemotherapy in an orthotopic model of human lung cancer. The purpose of the current study was to evaluate and characterize therapy against VEGFR and/or EGFR, alone and in combination with Pac, in a human lung cancer bone metastasis model that mimics clinical patterns. To develop the model, human lung adenocarcinoma (PC14) cells were injected into the tibias of nude mice. Digitized radiographic imaging (Faxitron) of the legs was performed weekly. When lytic bone lesions were observed, mice (7-9 per group) were randomized to one of six treatment regimens: ZD6474 (25 mg/kg daily p.o.); gefitinib (50 mg/kg daily p.o.); Pac (200 µg weekly i.p.); concomitant ZD6474 + Pac; concomitant gefitinib + Pac; or vehicle (Table). Therapy was continued until signs of the onset of morbidity were observed in controls. Analysis of tumor (TUNEL) and endothelial (TUNEL/CD31) apoptosis demonstrates that ZD6474 ± Pac induced comparable tumor cell apoptosis, while endothelial cell apoptosis was maximal in ZD6474 (12.6 ± 3.7%) vs ZD6474 + Pac treated tumors (2.9 ± 1.4%, $P < 0.001$). Tumor cells expressed EGFR, but not activated EGFR. Both the tumor and endothelial cells expressed VEGFR-2, and ZD6474 significantly inhibited VEGFR-2 activation ($P < 0.01$). In a repeat experiment, different sequences of ZD6474 and Pac administration (concurrent or ZD6474 before or after Pac for 2 weeks) were compared in the bone metastasis model. The antagonism of the antitumor effect of ZD6474 by Pac was independent of their sequence of administration. In summary, we have developed a murine model to study the biology and therapy of lung cancer bone metastasis, and show that ZD6474 can effectively treat lung cancer bone metastases by targeting both the tumor and its associated vasculature. Surprisingly, our data in this tumor model show that Pac can antagonize these effects of ZD6474 in the bone microenvironment, and

that this antagonism is independent of their sequence of administration.

Effect of treatments						
Parameter	Vehicle	ZD6474	ZD6474 + Pac	Gefitinib	Gefitinib + Pac	Pac
Tumor weight (% of control)	—	22	59	101	101	74
Tumor volume (% of control)	—	14	49	67	81	57
Microvessel density	33 ± 1.5	14 ± 1.6	24 ± 4.0	32 ± 3.2	26 ± 1.8	30 ± 3.8
Tumor cell proliferation (PCNA)	113 ± 5.2	74 ± 5.8	86 ± 5.2	115 ± 6.5	105 ± 7.2	110 ± 6.2

HOME	HELP	FEEDBACK	CME INFORMATION	SEARCH
		Cancer Research		Clinical Cancer Research
		Cancer Epidemiology Biomarkers & Prevention		Molecular Cancer Therapeutics
		Molecular Cancer Research		Cell Growth & Differentiation
Copyright © 2005 by the American Association for Cancer Research.				

**AACR Meeting
Abstracts Online**[HOME](#) [HELP](#) [FEEDBACK](#)[CME INFORMATION](#)[SEARCH](#)Institution: MD ANDERSON HOSPITAL [Sign In as Member or Individual Non-Member](#)

QUICK SEARCH: [advanced]

Author: Keyword(s):

Go

[Proc Amer Assoc Cancer Res, Volume 45, 2004]

Services

- ▶ [Similar articles in this journal](#)
- ▶ [Download to citation manager](#)

Google Scholar

- ▶ [Articles by Isobe, T.](#)
- ▶ [Articles by Herbst, R. S.](#)
- ▶ [Articles citing this Article](#)

PubMed

- ▶ [Articles by Isobe, T.](#)
- ▶ [Articles by Herbst, R. S.](#)

Cellular, Molecular, and Tumor Biology 109: Preclinical Science and Imaging in Cancer Models

Abstract #5136

Biology and therapy of human small cell lung cancer (SCLC) in novel orthotopic nude mouse models

Takeshi Isobe, Amir Onn, Wenjuan Wu, Tomoaki Shintani, Satoshi Itasaka, Keiko Shibuya, Waun K. Hong, Michael S. O'Reilly and Roy S. Herbst

UT M. D. Anderson Cancer Center, Houston, TX

SCLC is one of the most aggressive phenotypes of human lung cancer and conveys a poor prognosis due to the limited efficacy of existing treatment strategies. To provide clinically relevant strategies for studying new therapeutics and tumor biology, we developed three orthotopic models of human SCLC in nude mice. Three different human SCLC cell lines (H69A, a variant of the NCI-H69 cell line selected for invasiveness in vitro on semisolid agarose; NCI-H187; and NCI-N417) were studied. Tumor cells (1.5×10^6 cells in growth factor reduced Matrigel) were injected into the left lung of anesthetized nude mice. Tumors developed within 8 to 12 weeks and new cell lines were established from the lung tumors (H69ALu, H187Lu, and N417Lu) to select for a reproducible growth pattern for the orthotopic tumors and to minimize variation of tumor size. For each model, tumors started as a solitary mass in the left lung tumor that then spread to mediastinal and axillary lymph nodes, and to the right lung in a pattern similar to that observed in the clinic. N417Lu and H187Lu formed a 100 mm^3 left lung mass within 30-40 days of injection, and mice were moribund within 50 to 60 days of injection. H69ALu tumors reached a volume of 100 mm^3 within 60 days of injection and mice became moribund within 4 to 6 months. All tumors larger than 100 mm^3 expressed the proangiogenic factors bFGF and IL-8 (at the tumor periphery), and VEGF/VPF (tumor center and periphery). To compare the efficacy of different chemotherapeutic agents in each of our models, groups of mice ($n = 5$) were randomized to weekly i.p. treatment with saline (control), 6 mg/kg/mouse of cisplatin (CDDP), 50 mg/kg/mouse of paclitaxel, 125 mg/kg/mouse of irinotecan (CPT-11), or 40 mg/kg/mouse of etoposide. Therapy was initiated on day 10 (H187Lu and N417Lu) or day 20 (H69ALu) after tumor injection coincident with the formation of microscopic lesions. Therapy was well tolerated and mice were killed after five (H187Lu and N417Lu) or seven (H69ALu) weeks of therapy. Tumor burden was assessed by lung and tumor weight (g) and primary tumor volume (mm^3). CPT-11 significantly inhibited the growth and progression of N417Lu

tumors as compared to control (lung and tumor weight 0.23 ± 0.01 vs. 0.62 ± 0.15 , $p = 0.02$; tumor volume 0.3 ± 0.1 vs. 364 ± 156 , $p = 0.03$) and CDDP significantly inhibited the growth and progression of H69ALu tumors as compared to control (tumor volume 0.3 ± 0.1 vs. 100 ± 0.01 , $p = 0.04$). The development of our orthotopic models of SCLC provides a better understanding the biology of this disease and will enable evaluation of novel therapeutic strategies (supported by a grant from the Department of Defense (DAMD 17-02-1-0706 to W.K.H.).

HOME	HELP	FEEDBACK	CME INFORMATION	SEARCH
	Cancer Research		Clinical Cancer Research	
	Cancer Epidemiology Biomarkers & Prevention		Molecular Cancer Therapeutics	
	Molecular Cancer Research		Cell Growth & Differentiation	

Copyright © 2004 by the American Association for Cancer Research.



Keynote lectures

P14

ZD6474 ENHANCES THE ANTICANCER EFFICACY OF PACLITAXEL IN HUMAN LUNG CANCER MODELS

Wenjuan Wu, Amir Onn, Tomoaki Shintani, Michael S. O'Reilly & Roy S. Herbst

Department of Cancer Biology, Radiation Oncology, and Thoracic/Head and Neck Medical Oncology, The University of Texas MD Anderson Cancer Center, Houston, Texas, USA

Background: Vascular endothelial growth factor (VEGF) and epidermal growth factor (EGF) are critical survival factors for tumour-associated endothelial cells and tumour cells, respectively. ZD6474 is a small molecule inhibitor of VEGFR-2 tyrosine kinase with additional activity against EGFR tyrosine kinase that has shown antitumour efficacy in a broad range of tumour models. **Materials and Methods:** The effect of ZD6474 plus paclitaxel was assessed *in vitro* using human lung adenocarcinoma cells, NCI-H441, and mouse lung endothelial cells (MLECs). *In vivo* assessments were performed using an orthotopic NCI-H441 mouse model, which closely mimics the patterns of growth and metastasis observed in the clinic. Treatment with ZD6474 alone (12.5 mg/kg, p.o. daily), paclitaxel alone (150 µg/mouse, i.p. weekly), or a combination of the two agents was initiated on day 5 post-implantation. **Results:** *In vitro*, the presence of VEGF or EGF decreased paclitaxel-induced apoptosis in NCI-H441 and MLECs. ZD6474 treatment prevented this effect and decreased the IC₅₀ of paclitaxel twofold. *In vivo*, the most significant antitumour effects were seen in animals receiving combined ZD6474 and paclitaxel therapy. The lung weights in control, ZD6474, paclitaxel, and combined treatment groups were 0.46 ± 0.07 , 0.18 ± 0.04 , 0.29 ± 0.06 and 0.02 ± 0.001 g, respectively. Similar results were seen for pleural effusion, with 287 ± 77 , 12 ± 12 , 141 ± 107 and 0 ± 0 µl in these groups, respectively. Pleural invasion was also most significantly reduced in the combination group. Immunohistochemical staining demonstrated that combined ZD6474/paclitaxel therapy induced more extensive tumour and endothelial cell apoptosis than either treatment alone. **Conclusions:** These data suggest that the combination of ZD6474 and paclitaxel results in significant enhancement of antitumour and antivascular effects, which translate into significant therapeutic benefits *in vivo*.

Shibuya K, Komaki R, Wu W, Shintani T, Itasaka S, Isobe T, Ryan A, Herbst RS, O'Reilly MS. **Targeted therapy against VEGFR and EGFR signaling with ZD6474 enhances the therapeutic efficacy of irradiation in an orthotopic mouse model of human non-small cell lung cancer.** *International Journal of Radiation Oncology, Biology, Physics* 2004;60(1 Suppl S):S149-50, Abs 35 (46th Annual Meeting of the American Society for Therapeutic Radiology and Oncology, Atlanta, GA, USA, 3-7 October 2004)

Abstract

The effectiveness of ZD6474 and radiotherapy for the treatment of human non-small cell lung cancer was compared with that of chemoradiation in an animal study involving an orthotopic nude mouse model and an in vitro study using the human lung adenocarcinoma NCI-H441 cell line. Cell proliferation and levels of sublethal damage were assessed in irradiated NCI-H441 cells which had or had not been treated with ZD6474 in a clonogenic assay. In vivo, mice which had received injections of NCI-H441 cells to the left lung were randomized to receive ZD6474, paclitaxel, radiation, ZD6474 plus radiation, paclitaxel plus radiation or vehicle from day 8 until days 24-26 after injection. Tumor burden and immunohistochemical changes were then recorded. It was found that cell proliferation of H441 cells occurred 72-96 h after irradiation. Cell growth was suppressed by ZD6474 by 55% for 4 h prior to irradiation and 72 h after irradiation. The radioresponse was increased by a factor of 1.37 in the clonogenic assay. ZD6474 was found to suppress sublethal damage repair completely for 4 h split time. Recovery ratios were found to be 1.34 and 1.04 in the control and ZD6474 groups, respectively. In the mouse model, the greatest inhibition of tumor growth and metastasis was observed in the ZD6474 plus radiation group. Increases in lung weight of 330%, 200%, 155%, 147% and 110% were noted in mice treated with vehicle, radiation, ZD6474, paclitaxel plus radiation and ZD6474 plus radiation, respectively. The total weights of disseminated lesions were found to be 197, 160, 53.9, 47.5 and 17.2 in control, radiation, ZD6474, paclitaxel plus radiation and ZD6474 plus radiation-treated mice, respectively. The formation of pleural effusion was inhibited to a greater extent by ZD6474 plus radiation than paclitaxel plus radiation (14.2 and 246 mcl, respectively). A significant increase in tumor cell apoptosis was noted in mice which were treated with ZD6474 plus radiation. In lung primary tumors, microvessel density was found to be 55, 52, 13, 42, 31 and 16 in mice treated with vehicle, radiation, ZD6474, paclitaxel, paclitaxel plus radiation and ZD6474 plus radiation, respectively. The authors conclude that significant anti-angiogenic, anti-vascular and anti-tumor effects were observed with ZD6474 plus radiation treatment in vivo and in vitro.

Blocking VEGF and EGF receptor signalling with ZD6474 sensitizes human non-small cell lung cancer to chemotherapy with paclitaxel

W Wu, T Shintani, MS O'Reilly, and RS Herbst

Departments of Cancer Biology, Radiation Oncology, and Thoracic/Head and Neck Medical Oncology, University of Texas MD Anderson Cancer Center, Houston, Texas, USA

Introduction

- Lung cancer is the leading cause of human cancer death worldwide and treatment options, including chemotherapy for patients with advanced disease, are limited.
- VEGF and EGF receptor signalling pathways are critical for tumour growth and angiogenesis. VEGF and EGF are critical survival factors for tumour-associated endothelial cells and tumour cells, and are responsible for activating the Akt pathway and up-regulating anti-apoptotic molecules.
- ZD6474 (Figure 1) is a novel, orally active agent that selectively targets both VEGFR2 and EGF receptor tyrosine kinases, two key effectors of signalling pathways that are central to tumour growth. This novel agent has been shown to inhibit angiogenesis and tumour growth in a wide range of xenograft models.¹
- In this study, we examined the role of VEGFR and EGFR signalling in determining the sensitivity of human lung cancer cells to treatment with paclitaxel in an orthotopic lung cancer model.

Figure 1. Structure of ZD6474



Methods

Cell lines and reagents

- NCI-H460 lung adenocarcinoma cells were obtained from the ATCC, and mouse lung adenocarcinoma (MLEC) were supplied by Dr Lingling for our department. ZD6474 was synthesized by AstraZeneca, Macclesfield, UK. Paclitaxel was obtained from Bristol-Myers Squibb, Princeton, NJ, USA. Paclitaxel was obtained from Bristol-Myers Squibb, Princeton, NJ, USA.

Cell proliferation assay

- NCI-H460 or MLEC (5×10^3 per well) cells were plated in 96-well plates and incubated overnight. The cells were then washed and cultured in drug-containing medium. Cell proliferation was measured by RTT after 72 hours.

Apoptosis assay

- Cells were treated with growth factors, ZD6474 and paclitaxel for 48 hours in 2% FBS medium and were incubated with 50 mg/ml propidium iodide and 100 units/ml RNase. Apoptosis was analysed by flow cytometry.

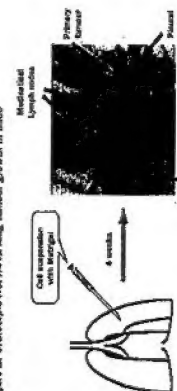
Immunohistochemistry

- CD31 expression was determined in frozen tissue sections using rat anti-mouse CD31 Mab (Pharmingen, San Diego, CA, USA). IHC was performed on formalin-fixed, paraffin-embedded tissue sections using mouse anti-HER2 (DAKO, Carpinteria, CA, USA).

In vivo orthotopic lung cancer model

- A suspension of 5×10^5 NCI-H460 cells mixed with 10% Matrigel was injected into the left lobe of nude mice (Figure 2).² Treatment with ZD6474 (12.5 mg/kg/day p.o.) and/or paclitaxel (150 µg/week i.p.) was initiated 5 days after tumour injection. Mice were sacrificed 4 weeks after tumour cell inoculation, and lung weight, pleural effusion and general inspection were assessed. Mice were monitored daily and sections were taken at the site of tumour with evident.

Figure 2. Orthotopic NCI-H460 lung tumour growth in mice



Statistical analysis

- The data were analysed by Student's *t*-test (two-tailed) and chi-square test.³

Results

In vitro evaluation

- ZD6474 enhances the anti-proliferative effects of paclitaxel in NCI-H460 and MLEC (Figure 3).
- ZD6474 treatment antagonizes the protective effect of EGF or VEGF against apoptosis of NCI-H460 and MLEC, induced by paclitaxel (Figure 4).

Figure 3. Effect of ZD6474 on paclitaxel-induced growth inhibition of a. MLEC and b. NCI-H460 cells in vitro

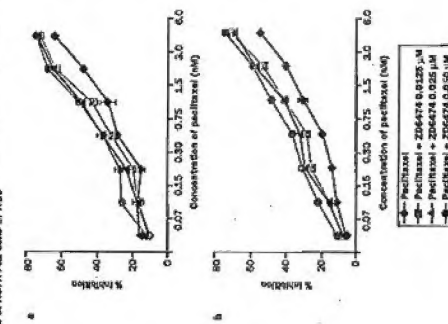
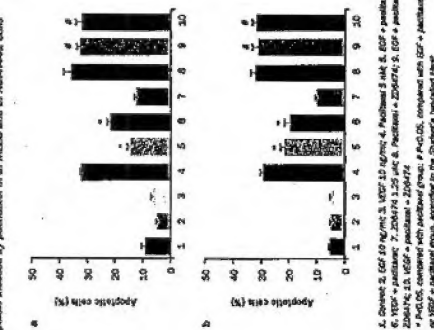


Figure 4. ZD6474 antagonizes the protective effect of EGF or VEGF against apoptosis induced by paclitaxel in a. MLEC and b. NCI-H460 cells



In vivo evaluation

- ZD6474 therapy resulted in significant tumour growth inhibition and reduced pleural effusion. The most significant tumour effects were seen in animals receiving combined ZD6474 and paclitaxel therapy (Table 1).
- Combination of ZD6474 and paclitaxel significantly prolonged survival by 200% relative to vehicle (Figure 5).
- Combination of ZD6474 and paclitaxel impaired lung cancer angiogenesis and resulted in reduced cell proliferation (HER2) and enhancement in apoptosis of both tumour cells and endothelial cells, compared with chemotherapy alone (Figure 6).

Table 1. Treatment of NCI-H460 human lung adenocarcinoma growing in lungs of nude mice with ZD6474 and/or paclitaxel

Group	Lung tumour	Pleural effusion	Pleural invasion	Lymph node metastases
	Weight (mg)	Incidence	Volume (µl)	Incidence
Vehicle	0.60 (0.35-0.72)	8/8	21.5 (0-50.0)	0/8
Paclitaxel	0.37 (0.04-0.54)	5/8	29.0 (0-50.0)	7/8
ZD6474	0.17 (0.04-0.38)	9/9	10 (0-30)	6/8
ZD6474 + paclitaxel	0.05 (0.05-0.05)	0/8	0 (0-0)	1 (0-8)

a. 5×10^5 NCI-H460 cells were injected into the lobe of lung (normal lung weight is about 0.275 g). Treatment with ZD6474 (12.5 mg/kg, daily p.o.) and/or paclitaxel (150 µg/week, intraperitoneal, i.p.) was initiated 5 days after tumour injection. Mice were sacrificed 4 weeks after tumour cell inoculation, and lung weight, pleural effusion and general inspection were assessed. Mice were monitored daily and sections were taken at the site of tumour with evident.

Figure 5. Combination of ZD6474 and paclitaxel prolongs survival² of mice bearing NCI-H460 lung tumours

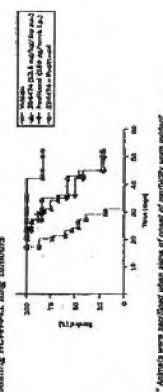
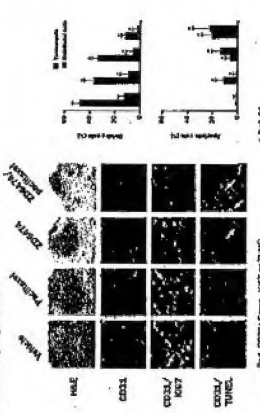


Figure 6. Immunohistochemical analysis of NCI-H460 lung tumours treated with ZD6474 and/or paclitaxel



Conclusions

- ZD6474 targets multiple pathways that are critical for tumour progression, metastasis and angiogenesis, including proliferation and survival of tumour and endothelial cells.
- ZD6474 significantly sensitizes established orthotopic lung adenocarcinomas to paclitaxel, and suppresses tumour growth, pleural effusion and metastasis.
- ZD6474 alone has direct effects upon the existing tumour vasculature and in combination with paclitaxel enhances apoptosis and inhibits proliferation of tumour, and tumour-associated, endothelial cells.
- The substantial antiangiogenic, endothelial and antitumour effects of ZD6474 combined with paclitaxel provide a basis for the design and clinical evaluation of this approach in lung cancer patients.

References

- Wu W, et al. Cancer Res 2002;62:4645-4655.
- Lin A, et al. Clin Cancer Res 2003;9:3532-3539.

AACR Meeting Abstracts Online

[HOME](#) [HELP](#) [FEEDBACK](#)

[CME INFORMATION](#)

[SEARCH](#)

QUICK SEARCH: [advanced]

Author: Keyword(s):

Go

Institution: MD ANDERSON HOSPITAL [Sign In as Member or Individual Non-Member](#)

[Proc Amer Assoc Cancer Res, Volume 45, 2004]

Services

- ▶ [Similar articles in this journal](#)
- ▶ [Download to citation manager](#)

Google Scholar

- ▶ [Articles by Wu, W.](#)
- ▶ [Articles by Herbst, R. S.](#)
- ▶ [Articles citing this Article](#)

PubMed

- ▶ [Articles by Wu, W.](#)
- ▶ [Articles by Herbst, R. S.](#)

Experimental and Molecular Therapeutics 41: Angiogenesis Abstract #4551

ZD6474, a small molecule targeting VEGF and EGF receptor signaling, inhibits lung angiogenesis and metastasis and improves survival in an orthotopic model of non-small cell lung cancer

Wenjuan Wu, Takeshi Isobe, Satoshi Itasaka, Tomoaki Shintani, Robert R. Langley, Amir Onn, Jill C. Hansen, Michael S. O'Reilly and Roy S. Herbst

MD Anderson Cancer Center, Houston, TX

Vascular endothelial and epidermal growth factor receptors (VEGFR, EGFR) are critical regulators of tumor and endothelial cells. To further understand the role of VEGFR and EGFR signaling in human lung cancer progression, we investigated the antiangiogenic and antimetastatic activity of ZD6474 (a selective small molecule inhibitor of VEGFR-2 tyrosine kinase with additional activity against the EGFR tyrosine kinase) using *in vitro* and *in vivo* systems. In the human lung cancer cell line NCI-H441 (which we determined to express VEGF, TGF- α , VEGFR-2 and EGFR) and mouse lung endothelial cells (MLECs), ZD6474 inhibited EGFR phosphorylation, VEGFR-2 phosphorylation and subsequently downstream Akt phosphorylation. ZD6474 treatment of both NCI-H441 and MLECs decreased proliferation and colony formation, induced apoptosis and inhibited migration and invasion. These *in vitro* data suggest that ZD6474 targets multiple events that are important for both angiogenesis and metastasis. ZD6474 also inhibited *in vivo* angiogenesis formation, demonstrated by a decrease in microvessel density (MVD) in subcutaneously implanted gelfoam-agarose sponges. To better characterize the effect of ZD6474 in human lung cancer, an orthotopic model using NCI-H441 cells was developed that closely mimics the patterns of growth and metastasis observed in the clinic. Treatment was evaluated at different stages of tumor progression (early, middle and late) with ZD6474 initiated on day 5, 10 or 15 after tumor injection, respectively. ZD6474 (25 mg/kg and 50 mg/kg) impaired pleural effusion formation and pleural invasion at every stage. Daily oral dosing with 25 or 50 mg/kg ZD6474 (initiated on day 5 following tumor inoculation) resulted in the almost complete suppression of the growth, invasion and metastasis of established lung tumors, when compared with controls ($P < 0.001$). Therapy with 50 mg/kg ZD6474 initiated on day 15 after tumor injection significantly prolonged survival by >300% relative to the control (25 days vs 80 days, the time of experiment termination,

$P < 0.001$). Immunohistochemical staining demonstrated an increase in endothelial cell apoptosis, and a reduction in MVD and proliferating cell nuclear antigen in the tumor specimens. We conclude that the combined inhibition of both VEGFR and EGFR with ZD6474 induces significant antivasculature and antitumor effects that translate into significant therapeutic benefits *in vivo*, providing a basis for the design of clinical trials in human lung cancer patients.

HOME	HELP	FEEDBACK	CME INFORMATION	SEARCH
	Cancer Research		Clinical Cancer Research	
	Cancer Epidemiology Biomarkers & Prevention		Molecular Cancer Therapeutics	
	Molecular Cancer Research		Cell Growth & Differentiation	

Copyright © 2004 by the American Association for Cancer Research.

Wu W, Isobe T, Onn A, Shintani T, Itasaka S, Shibuya K, Langley RR, Hansen JC, Fidler IJ, Ryan AJ, Herbst RS, O'Reilly MS. **Targeted therapy against VEGF and EGF receptor signaling with ZD6474 blocks angiogenesis and inhibits the growth and dissemination of orthotopic human lung cancer in mice.** *Clinical Cancer Research* 2003;9(16 Pt 2 Suppl S):6143s, Abs B15 (AARC-NCI-EORTC International Conference, Boston, MA, USA, 17-21 November 2003).

Abstract

The aim of this study was to investigate the role of the vascular endothelial growth factor receptor (VEGFR) and the epidermal growth factor receptor (EGFR) signaling in human lung cancer progression by examining the anti-angiogenic, antivascular and antitumor effects of ZD6474 both in human and mouse endothelial cells and in 2 murine orthotopic models of human non-small cell lung cancer. EGF and VEGF-induced proliferation, EGFR phosphorylation and VEGFR-2 phosphorylation were inhibited by ZD6474 treatment in both pulmonary artery endothelial cells and in murine lung microvascular endothelial cells (MLEC). These results correlated with decreased expression and decreased phosphorylation of mitogen-activated protein kinase and Akt. In addition, an increase in DNA fragmentation and caspase-3 activation (endothelial cell apoptosis indicator) was reported following treatment of MLECs with ZD6474 which also resulted in inhibition of tubule formation and extracellular matrix attachment. Altogether, these results suggest that ZD6474 targets multiple pathways that are critical for angiogenesis. In the second part of the study, the effects of ZD6474 in human lung cancer were characterized using several orthotopic human lung adenocarcinoma (PCI4PE6 and NCI-H441) models. Administration of ZD6474 once daily orally to mice induced nearly complete suppression of the growth and invasion of established lung tumors. In addition, lung weight was almost normal in ZD6474-treated mice in both lung adenocarcinoma models, compared with the 300% increase observed in untreated controls. Moreover, ZD6474 treatment was able to completely prevent pleural effusion formation and to inhibit chest wall invasion by > 85%. In contrast, no change in lung cancer progression was observed following systemic weekly therapy with paclitaxel. ZD6474 treatment also almost completely suppressed angiogenesis in lung tumors. The authors conclude that "the combined targeting of VEGFR and EGFR with ZD6474 induces a significant antivascular effect that translates into significant therapeutic benefits in vivo, providing a basis for the design of clinical trials in human lung cancer patients".